UNIVERSIDAD PERUANA
CAYETANO HEREDIA
ESCUELA DE POSGRADO

DEVELOPMENT OF A TEST ASSOCIATED WITH MAGNETIC NANOPARTICLES FOR THE DIAGNOSIS OF TUBERCULOSIS.

TESIS PARA OPTAR EL GRADO DE DOCTOR EN CIENCIAS DE LA VIDA.

NANCY LEÓN JANAMPA

LIMA - PERU

2019

THESIS DIRECTORS

PERUVIAN DIRECTOR

Patricia SHEEN CORTAVARRIA, PhD. MSc. MHS
Departamento de Ciencias Celulares y Moleculares
Laboratorio de Bioinformática
Facultad de Ciencias y Filosofía
Universidad Peruana Cayetano Heredia (Lima-Perú)

FRENCH DIRECTOR

Magali SZLOSEK-PINAUD, PhD.
Group ‘‘Catalysis, Synthesis and Health’’ (CSH)
Institut des Sciences Moléculaires,
UMR CNRS N° 5255, Université de Bordeaux (Bordeaux-France)

Acknowledgments / Agradecimientos

This doctoral thesis is the sum of effort and perseverance, which would not have been possible without the support of the people who were by my side during these years. For this reason, I want to thank:

- *To my thesis directors and my professors:*

I deeply thank my doctoral thesis directors, Dr. Patricia SHEEN of the Laboratory of Bioinformatics and Molecular Biology (LBB) of the Peruvian University Cayetano Heredia (UPCH) and Dr. Magali SZLOSEK of the Catalysis, Synthesis and Health (CSH) group of the Institut des Sciences Moléculaires of the University of Bordeaux. Thank you very much for trusting me, for having always supported me during the development of the doctoral thesis, for allowing me to be part of your team, for your wise teachings and for your valuable time invested in my professional and personal development.

I thank Dr. Svitlana SHINKARUK of Bordeaux Sciences Agro and Dr Mirko ZIMIC of LBB-UPCH, for helping me during the planning and development of the research, for being committed to me, and for making me feel like family during these years. I hope someday to be able to follow suit and demonstrate the same conviction that you show every day to your students.

To Dr. Eric FOUQUET for accepting me at the ISM, I am very grateful for your trust.

I also thank Dr. Didier ASTRUC for helping me with the procedures for my enrollment in the doctoral school and for his time and consideration invested in me, thank you very much.

- *To my collaborators:*

Without them this investigation would not have been possible to complete. To all my collaborators, thank you very much for your time and have had a lot of patience with me. Additionally, I thank everyone for their collaboration in the review of the published article, product of this research.

I thank Dr. Quispe-Marcatoma of the Center for Technological, Biomedical and Environmental Research (CITBM) of the Faculty of Physical Sciences, Universidad Nacional Mayor de San Marcos, for his collaboration in the measurements of X-ray Diffraction and in the magnetometry of nanoparticles synthesized

To Dr. Gutarra of the Nanostructured Materials Laboratory of the National University of Engineering (UNI), for having supported me in the thermogravimetry analysis of bio-conjugated nanoparticles.

To Dr. Gwénaëlle Le Bourdon of the Institut des Sciences Moléculaires of the University of Bordeaux, for her collaboration in the analysis of Diffuse reflectance infrared fourier transform spectroscopy for the analysis of the chemical nature of the surface of the nanoparticles.

To Dr. Gayot of PLACAMAT, CNRS-Université Bordeaux, for his support in the analysis of nanoparticles using the Transmission Electronic Microscopy (TEM).

To PhD (c) Kate Changanaqui and Dr Falcon of the Faculty of Science of the National University of Engineering for their collaboration in the measurement of Dynamic Light Scattering (DLS) of magnetic nanoparticles.

- *To my jurors:*

A particular thanks to Dr BABIN for having agreed to be the president of my thesis jury. To Dr. VALDERRAMA and Dr. MONNIER for having been my jurors and at the same time my thesis reporters, thank you very much for validating my thesis for defense. To Dr AREVALO for being part of my juries. To Dr MILON for not only being my jury but also for having thoroughly reviewed my manuscript after my defense.

Thank you all for your comments for the constant improvement of my manuscript, my work and especially my person.

- *To my colleagues and friends:*

I am very grateful to Murielle BERLANDE and Frédéric CHANTAGREL because they have always made me feel like family, they have supported me in what

they have been able and they have always given me their unconditional friendship during these years.

To my friends in the laboratory Nicholas, Julien, Obinna, Charlotte, Alexis, Laura and all those who are part of the CSH team of the Institut des Sciences Moléculaires.

To my friends from the Laboratory of Bioinformatics and Molecular Biology (LBB) of the Cayetano Heredia Peruvian University (UPCH), Katherine Vallejos, Elisa Roncal, Ricardo Antiparra, Sueline, Emily, Hugo Alcantara, Hugo Valdivia , Adriana del Valle, Nicole Sheen, Erika, and all the other members of the laboratory, with whom I have shared memorable moments and research gatherings.

I also want to thank the members of the ISM Administration and those responsible for international students (Stephanie DANAUX, Violeta PEREZ and Rebeca CALDAS) for helping me to make possible my cotutelle-contract between both universities and in the paperwork during my years of study.

- *A mi familia:*

A mis padres, Fredy LEON y Marcelina JANAMPA, por haberme inculcado muchos valores, por confiar en mí todos los días y animarme siempre en ir detrás de mis sueños. A mi hermana Deicy por ser como una madre para nosotros, a mi hermano Jefferson por ayudarme en los trámites de la tesis en Perú, y a mi hermano Robert por su apoyo moral. A mis tías(os) (Otilia, Santa, Pedro, Vicente, Juanita, Flor) y primas(os) por su amor y ejemplo de unidad familiar.

Surely there are many people that I have not mentioned, but from the bottom of my heart thank you very much for having accompanied me in this crazy, anguishing and fun story of my doctoral thesis.

Financial supports: I am grateful for the Peruvian government for the financial support received from Scholarship Program at the Franco-Peruvian Doctoral School in Life Sciences (FONDECYT), Universidad Peruana Cayetano Heredia and University of Bordeaux (France). In addition, I thank the support of ‘Unraveling the resistance mechanism of pyrazinamide, the unique - sterilizing drug against tuberculosis’ project financed for Wellcome Trust organization.

TABLE OF CONTENTS

IMAGE INDEX

Figures Chapter I.

Figures Chapter II.

Figures Chapter III.

Figures Chapter IV.

TABLE INDEX

Chapter II Tables.

Chapter III Tables.

Chapter IV Tables.

Table IV.4: Laboratory results of patients positive for TB. The sputum samples from confirmed patients (13) were collected, processed and stored at -20 ℃ until their use. Also, sputum samples from patients suspected for TB (7), but with negative laboratory diagnosis, were also considered as negative control (data not shown). **Pag. 244**

LIST OF ABBREVIATIONS AND SYMBOLS

APTES: (3-aminopropyl) triethoxysilane.

BSA: Bovine Albumin Serum.

CMD : Carboxymethyl-dextran.

DLS: Dynamic light scattering.

DRIFTS: Diffuse reflectance infrared Fourier transform spectroscopy.

EDC: *N*-(3-Dimethylaminopropyl)-*N'*-ethylcarbodiimide hydrochloride.

EDTA: Ethylenediaminetetraacetic acid.

ELISA: Enzyme-linked immunosorbent assay.

ELISA-MNP: ELISA associated with magnetic nanoparticles.

HCl: Hydrochloric acid.

HRP: Horseradish peroxidase.

IPTG: Isopropyl β-D-1-thiogalactopyranoside.

GST: Glutathione S-transferase

LB: Luria-Bertani medium

MNP: Magnetic nanoparticles.

MTB: *Mycobacterium tuberculosis.*

MTC: *Mycobacterium tuberculosis* complex.

MNP: Magnetic nanoparticles

MNP@Si@ab: Magnetic nanoparticles funcionalized with polyclonal antibodies.

MNP@Si@ab-ag: Antigen detected for an antibody immobilized on modified MNP surface.

MNP@Si@NH_2: Magnetic nanoparticles amine-silanized.

MNP@Si@BSA: Magnetic nanoparticles functionalized with Bovine Serum Albumin,

MNP@Si@anti-Hsp16.3: Magnetic nanoparticles functionalized with polyclonal antibodies anti-Hsp16.3.

MNP@Si@NH_2: Magnetic nanoparticles amine-silanized.

MS : Mössbauer spectroscopy.

MW : Molecular weight.

NHS: N-Hydroxysuccinimide.

OD : Optic density.

ON : Overnight

OPD: o-phenylenediamine dihydrochloride

PBS: Phosphate Buffered Saline.

PPD: Purified protein-derived tuberculin test.

PCR: Polymerase chain reaction.

RT: Room temperature.

SDS: Sodium dodecyl sulfate.

SDS-PAGE: sodium dodecyl sulfate polyacrylamide gel electrophoresis

sELISA-MNP@Si@ab: **S**andwich ELISA associated to magnetic nanoparticles.

TEOS: Tetraethyl orthosilicate.

TEM Transmission electron microscopy.

TGA: Thermogravimetry analysis.

XRD: X-ray powder diffraction.

RESUMEN

Mycobacterium tuberculosis causa una de las enfermedades con la tasa más alta de mortalidad y morbilidad en las Américas y en todo el mundo. En países en vías de desarrollo, el diagnóstico de tuberculosis (TB) se basa en microscopía de frotis y cultivos bacteriológicos. El primer método tiene baja sensibilidad y el segundo toma varias semanas para llegar a un diagnóstico confirmatorio. La falta de un diagnóstico rápido compromete los esfuerzos para controlar la TB, lo que favorece su transmisión a la población susceptible. Actualmente, las nanopartículas magnéticas (MNP) funcionalizadas con biomoléculas se han utilizado en biomedicina, debido a las propiedades magnéticas, eléctricas y ópticas. De esta manera, aplicando campos magnéticos externos, se utilizan MNP bio-funcionalizadas para detectar y concentrar células y biomoléculas a partir de muestras biológicas.

En este trabajo presentamos la síntesis, caracterización y bio-funcionalización de las nanopartículas magnéticas para desarrollar un ensayo ELISA sándwich usando MNPs para detectar antígenos de *M. tuberculosis*. Para este propósito, las nanopartículas magnéticas fueron sintetizadas por el método de co-precipitación. La superficie de MNP fue amino-silanizada (MNP@Si@NH_2) y se caracterizada por métodos físico y químicos.

Los antígenos de MTB evaluados en este estudio fueron: Hsp16.3, CFP10, ESAT6, MTC28, MPT64, proteína de 38 kDa, Ag85B y MoeX. La clonación y la expresión de las proteínas recombinantes se realizaron en el sistema de *E. coli* BL21 (DE3) pLysS. Se produjeron anticuerpos policlonales en conejos de Nueva Zelanda y ratones BALB/C, inmunizados previamente con antígenos recombinantes purificados. Se inmovilizaron anticuerpos específicos (ab) en las superficies de MNP amino-silanizadas (MNP@Si@ab). El MNP@Si@ab fue utilizado en un ensayo ELISA sándwich colorimétrico para capturar y detectar antígenos de MTB nativos en muestras de esputo.

La XRD, espectroscopia de Mössbauer, la potencial zeta, TEM y FTIR demostraron la preparación exitosa de los MNP, el cual mostró un diámetro de difracción del cristal de ~ 12.5 nm (10.48 ± 2.56 nm), carga neta superficial de ζ: +23.57 ± 2.87 mV, patrones característicos de magnetita y una estructura esférica. Además, una saturación de magnetización de 37.06 $emu.g^{-1}$ fue observada. Para la funcionalización de superficies de nanopartículas con anticuerpos, se utilizó el método del éster activo para la formación de enlaces peptídicos. Parámetros tales como el tiempo de incubación, la concentración de los agentes de acoplamiento y el nivel de saturación de la superficie de las MNPs amino-silanizadas (MNP@Si@NH_2) fueron estandarizadas.

Finalmente, se usaron MNP funcionalizados con anticuerpos para capturar y detectar antígenos nativos y recombinantes de *M. tuberculosis* en una prueba sándwich de ELISA-MNP@Si@ab en un tiempo de reacción <4 h. Los antígenos ESAT6 y CFP10 se discriminaron mejor en las muestras de esputo de los pacientes con TB (*fold value* ~ 1,8). El uso de MNP@Si@ab mejoró la detección de antígenos de MTB en muestras biológicas con respecto a un sELISA convencional. Nuestros resultados son alentadores, pero el ensayo requiere evaluaciones adicionales, como determinar reacciones cruzadas con muestras de esputo de pacientes con otras infecciones, realizar la prueba con esputo frescos de pacientes con TB y determinar la sensibilidad y especificidad clînica del método.

Palabras claves: Tuberculosis activa, prueba ELISA tipo sándwich, nanopartículas magnéticas amino-silanizadas, proteínas recombinantes, anticuerpos policlonales.

ABSTRACT

Mycobacterium tuberculosis causes one of the diseases with the highest mortality and morbidity rate in the Americas and around the world. In developing countries, the diagnosis of tuberculosis (TB) is based on smear microscopy and bacteriological cultures. The first method has low sensitivity, and the second take several weeks to reach a confirmatory diagnosis. The lack of a rapid diagnosis compromises the efforts to control TB, favoring its transmission to the susceptible population. Currently, magnetic nanoparticles (MNPs) functionalized with biomolecules have been used in biomedicine, due the magnetic, electrical and optical properties. In this way, applying external magnetic fields, bio-functionalized MNPs are used to detect and concentrate cells and biomolecules from biological samples.

In this work we present the synthesis, characterization and bio-functionalization of magnetic nanoparticles to develop a sandwich ELISA assay using MNPs to detect antigens from *M. tuberculosis*. For this purpose, magnetic nanoparticles were synthesized by the co-precipitation method. The MNP surface was amine-silanized (MNP@Si@NH_2) and characterized by physical and chemical methods.

The MTB antigens evaluated in this study were: Hsp16.3, CFP10, ESAT6, MTC28, MPT64, 38 kDa protein, Ag85B and MoeX. Cloning and expression of recombinant proteins were expressed in *E. coli* BL21 (DE3) pLysS system. Polyclonal antibodies were produced in New Zealand rabbits and BALB/C mice, previously immunized with purified recombinant antigens. Specific antibodies (ab) were immobilized in the amine-silanized MNP surfaces (MNP@Si@ab). The MNP@Si@ab were used in a colorimetric sandwich ELISA assay to capture and detect native MTB antigens from sputum samples.

The XRD, Mössbauer spectroscopy, zeta potential, TEM and FTIR demonstrated the successful preparation of the MNPs showing a diffraction crystal diameter of ~12.5 nm (10.48 ± 2.56 nm), superficial net charge of ζ: +23.57 ± 2.87 mV, characteristic patterns of magnetite and a spherical structure. Additionally, a magnetization saturation of 37.06

emu.g^{-1} was observed. For the functionalization of nanoparticle surfaces with antibodies, an active ester method was used for peptide bond formation. Parameters such as time of incubation, concentration of coupling agents and surface saturation level of amine-silanized MNPs (MNP@Si@NH_2) were standardized.

Finally, antibody functionalized on MNPs were used to capture and detect recombinant and *native M. tuberculosis* antigens in an ELISA-MNP@Si@ab sandwich test in a reaction time <4 h. The ESAT6 and CFP10 antigens were better discriminated in sputum pooles from patients with TB (fold value ~ 1.8). The use of MNP@Si@ab improved the detection of MTB antigens in biological samples with respect to conventional sELISA. Our results are encouraging, but the essay requires additional evaluations such as determining cross-reactions with sputum samples from patients with other infections, performing the test with fresh sputum of TB patients, and determining the clinical sensitivity and specificity of the method.

Key words: Active tuberculosis, sandwich ELISA assay, amine-silanized magnetic nanoparticles, recombinant proteins, polyclonal antibodies.

RESUME

Mycobacterium tuberculosis provoque l'une des maladies qui présentent le taux de mortalité et de morbidité le plus élevé des Amériques et du monde. Dans les pays en développement, le diagnostic de la tuberculose (TB) repose sur la microscopie des frottis et des cultures bactériologiques. La première méthode a une faible sensibilité et la seconde met plusieurs semaines à atteindre un diagnostic de confirmation. L'absence de diagnostic rapide compromet les efforts de lutte contre la tuberculose, favorisant ainsi sa transmission à la population vulnérable. Actuellement, les nanoparticules magnétiques (MNP) fonctionnalisées par des biomolécules sont utilisées en biomédecine, en raison de leurs propriétés magnétiques, électriques et optiques. De cette manière, en appliquant des champs magnétiques externes, les MNP bio-fonctionnalisées sont utilisées pour détecter et concentrer les cellules et les biomolécules à partir d'échantillons biologiques.

Dans ce travail, nous présentons la synthèse, la caractérisation et la bio-fonctionnalisation de nanoparticules magnétiques afin de développer un test ELISA sandwich en utilisant des MNPs, afin de détecter les antigènes de *M. tuberculosis.* À cette fin, des nanoparticules magnétiques ont été synthétisées par une méthode de co-précipitation. La surface des MNP a été amino-silanisée (MNP@Si@NH_2) et caractérisée par des méthodes physiques et chimiques.

Les antigènes MTB évalués dans cette étude étaient: Hsp16.3, CFP10, ESAT6, MTC28, MPT64, protéine de 38 kDa, Ag85B et MoeX. Le clonage et l'expression de protéines recombinantes ont été réalisés dans le système de E. coli BL21 (DE3) pLysS. Des anticorps polyclonaux ont été produits chez des lapins Nouvelle-Zélande et des souris BALB/C, préalablement immunisés avec des antigènes recombinants purifiés. Des anticorps spécifiques (ab) ont été immobilisés sur les surfaces des MNP amino-silanisées (MNP@Si@ab). Les MNP@Si@ab ont été utilisées dans un test ELISA sandwich colorimétrique pour capturer et détecter les antigènes natifs du MTB à partir d'échantillons d'expectorations.

La XRD, la spectroscopie Mössbauer, le potentiel zêta, la TEM et le FTIR ont validé l'obtention des MNP montrant un diamètre de cristal de diffraction de ~ 12,5 nm (10,48 ± 2,56 nm), une charge nette superficielle de +23,57 ± 2,87 mV, des profils caractéristiques de magnétite et une structure sphérique. De plus, une saturation en aimantation de 37,06 emu.g-1 a été observée. Pour la fonctionnalisation des surfaces de nanoparticules avec des anticorps, une méthode via l'utilisation d'ester activé a été utilisée pour la formation de liaisons peptidiques. Des paramètres tels que le temps d'incubation, la concentration des agents de couplage et le niveau de saturation de surface des MNP amines silanisées (MNP@Si@NH_2) ont été standardisés.

Enfin, des anticorps fonctionnalisés sur des MNP ont été utilisés pour capturer et détecter les antigènes recombinants et natifs de *M. tuberculosis* dans un test sandwich ELISA-MNP@Si@ab dans un temps de réaction <4 h. Les antigènes ESAT6 et CFP10 ont été mieux différenciés dans les expectorations des patients atteints de tuberculose (fold value ~ 1,8). L'utilisation de MNP@Si@ab a amélioré la détection des antigènes du MTB dans des échantillons biologiques par rapport au sELISA conventionnel. Nos résultats sont encourageants, mais des évaluations supplémentaires sont nécessaire telles que la détermination de réactions croisées avec des échantillons d'expectorations provenant de patients atteints d'autres infections, la réalisation du test avec les expectorations fraîches de patients tuberculeux et la détermination de la sensibilité et de la spécificité clinique de la méthode.

Mots clés: Tuberculose active, test ELISA en sandwich, nanoparticules magnétiques amines silanisées, protéines recombinantes, anticorps polyclonaux.

Resúmen de disertación.

La tuberculosis (TB) es una de las enfermedades con las tasas más altas de mortalidad y morbilidad en las Américas y el mundo. La ausencia de un diagnóstico rápido, efectivo y económico contribuye a la permanencia de la TB, favoreciendo así su transmisión a las poblaciones vulnerables.

Actualmente, las nanopartículas magnéticas (MNP) son ampliamente estudiadas en biomedicina, para detectar y enfocar células y biomoléculas de muestras biológicas. En este trabajo, las MNP se han sintetizado y caracterizado. Además, la superficie de estas MNP se ha recubierto con biomoléculas (anticuerpos) capaces de detectar marcadores (proteínas) característicos de *M. tuberculosis.* Posteriormente, estas nanopartículas funcionalizadas se incubaron con muestras de esputo de pacientes con tuberculosis. Una prueba colorimétrica determinó si las nanopartículas eran capaces de capturar y detectar proteínas de la mycobacteria contribuyendo así al diagnóstico de tuberculosis.

Dissertation summary.

Tuberculosis (TB) is one of the diseases with the highest mortality and morbidity rates in the Americas and the world. The absence of a rapid, effective and inexpensive diagnosis contributes to the permanence of TB, thus favoring its transmission to vulnerable populations.

Currently, magnetic nanoparticles (MNPs) are widely studied in biomedicine to detect and focus cells and biomolecules from biological samples. In this work, MNPs have been synthesized and characterized. In addition, the surface of these MNPs has been coated with biomolecules (antibodies) capable of detecting markers (proteins) characteristic of *M. tuberculosis.* Subsequently, these functionalized nanoparticles were incubated with sputum samples from patients with tuberculosis. A colorimetric test determined whether nanoparticles were capable of capturing and detecting mycobacterial proteins, thus contributing to the diagnosis of tuberculosis.

Résumé de thèse vulgarisé.

La tuberculose (TB) est une des maladies qui présente le taux de mortalité et de morbidité le plus élevé des Amériques et du monde. L'absence de diagnostic rapide, efficace et peu coûteux contribue à la permanence de la TB, favorisant ainsi sa transmission aux populations vulnérables.

Actuellement, les nanoparticules magnétiques (MNPs) sont largement étudiées en biomédecine pour détecter et concentrer des cellules et des biomolécules à partir d'échantillons biologiques. Dans ce travail, des MNPs ont été synthétisées et caractérisées. De plus, la surface de ces MNP a été recouverte de biomolécules (anticorps) capables de détecter des marqueurs (protéines) caractéristiques de *M. tuberculosis.* Par la suite, ces nanoparticules fonctionnalisées ont été incubées avec des échantillons d'expectorations de patients atteints de tuberculose. Un test colorimétrique a permis de déterminer si les nanoparticules étaient capables de capturer et de détecter les protéines mycobactériennes, contribuant ainsi au diagnostic de la tuberculose.

Introduction

Tuberculosis (TB) is an infectious disease caused by *Mycobacterium tuberculosis* (MTB), transmitted orally-respiratory and mainly affects the lungs, leading to an intense cough, fever and chest pains (Fogel, 2015). TB is one of the most serious and complex problems in the public health, especially in developing countries. TB spreads in poor, crowded and poorly ventilated environments and mainly affects the most vulnerable populations, such as people with low economic resources and some individuals with other health conditions such as HIV, diabetes, drug or alcohol addictions (WHO, 2016).

Adequate treatment of the disease requires early diagnosis, as well as determination of microbial susceptibility. Although more than a hundred years have passed since the identification of TB (1882), there is still no rapid or low-cost diagnostic assay with high sensitivity and specificity. Anti-tuberculosis treatment is no longer appropriate when they are delivered without having an early diagnosis or a result of the susceptibility of the mycobacteria to drugs (Bonilla, 2008). It makes in vain the efforts to control this disease and generates substantial economic losses by the state. The main drawbacks in the rapid diagnosis are due to the use of traditional MTB detection methods, which can take weeks and even months to report the result, and it is associated with a rising mortality and drug resistance rate (Bonilla, 2008).

Around the world, the TB diagnostic assays more used are sputum smear microscopy (10^4 bacilli/ml) and culture (10^1 - 10^2 bacilli/ml in Lowestein-Jensen medium). Although the first is fast and inexpensive, it has a low sensitivity and specificity. The culture is considered as the 'gold standard' method for TB diagnosis (Ugarte-Gil *et al*., 2008). Currently, there are different types of MTB cultures, capable to discriminate growth and antibiotic bacteria resistance. For example, the test of susceptibility to drugs by microscopic observation (MODS), is a type of culture where the sputum samples are decontaminated and grown in a liquid media (Middlebrook 7H9) supplemented with

rifampicin and isoniazid. This method is effective, but it takes at least one week to have a result (Caviedes *et al*., 2000; Ugarte-Gil *et al*., 2008).

Consequently, molecular tests as the polymerase chain reaction (PCR) and its variants, have been used for being faster and have a high sensitivity and specificity (95 and 92% respectively). However, quantitative PCR shows low sensitivity in samples from patients with low MTB load (Albuquerque *et al.*, 2014). In general, there are different amplified markers; 16SrDNA, cyp141, and others; but the most used is the insertion sequence 6110 (IS6110) (Farzam *et al*., 2015, Tsai *et al*., 2013). It is found in multicopy in the genome of the bacterium, and it is exclusive to the *M. tuberculosis* complex (MTBC) (Farzam *et al*., 2015). Despite the advantages of these methods, their main limitations are the low sensitivity in patients with low bacillary load, sophisticated equipment is required and as well as the trained personnel, making their implementation expensive (Tsai *et al*., 2013).

Therefore, the current challenge is to develop diagnostic tests with high sensitivity and specificity that can be applied directly in clinical samples without costly equipment or complex procedures. Most commercial methods are based on the antibody detection; but they have failed because the complex and still not understood human immune response towards the bacterium (Steingart *et al*., 2007). This means that these methods are non-specific to discriminate a patient with active TB, a patient who has already completed anti-tuberculosis treatment or a patient who has only been exposed to MTB; because in all cases the patients have produced antibodies against MTB (Daniel and Debanne, 1987; Fujita *et al.*, 2005). In this context, it is a priority to identify and characterize the main abundant bacteria antigens able to act as a biomarker of the disease. In this sense, these MTB antigens can be identified directly in clinical samples from TB suspected patients.

In recent years, different strategies have been developed to identify MTB antigens from culture and TB patient samples. For example, to detect the secretory protein CFP10, surface plasmon resonance spectroscopy (SRP spectroscopy) and the detonation nanodiamonds/ matrix-assisted laser desorption/ionization mass spectrometry (DND MALDI-TOF MS,

with sensitivity of 97.4% and specificity of 100%) methods, were developed. In the case of ESAT6 detection, immune-electrochemical biosensor and strategies associated to gold nanoparticles to identify CFP10/ESAT6, were reported (Diouani *et al*., 2017; He *et al*., 2016; Soo *et al*., 2015; Hong *et al*., 2011; Wu *et al*., 2010). Other examples are MPT64 detection using sandwich ELISA (Ji *et al*., 2014), Ag85B detection using gold nanorods/ silica-coated quantum dots (Kim *et al*., 2017), and MoeX detection using Mass spectrometry (López-Hernández *et al.*, 2016; Pollock *et al*., 2013). Although these are accurate and sensitive methods, they are very expensive, and therefore economic alternatives are required.

In the last decades, the technology in nanometer scale (nanotechnology) have been widely applied in studies of molecular interactions of the cell, platforms for drug delivery, molecular diagnosis, cancer treatment, bio-separation, environmental biosensors, etc. A clear example is the diagnostic tests using magnetic nanoparticles (MNP) to increase its speed and sensitivity (Jesse *et al.*, 2015).

Our study proposes to develop a sandwich ELISA assay using magnetic nanoparticles to capture and detect antigens from *M. tuberculosis*, comparing it with the liquid culture MODS test. For this purpose, specific antibodies were immobilized on modified magnetic nanoparticles. Recombinant and native antigens would be recognized and separated using the magnetic properties of the functionalized nanoparticles. This MNP-antibody-antigen complex was coupled to a colorimetric sandwich ELISA assay to discriminate a positive or negative reaction. This strategy could contribute in the fast and accurate diagnosis of TB, utilizing sputum samples from suspected patients. Also, it can be used in low-income areas where the prevalence of tuberculosis remains high and the implementation of a rapid diagnosis tests is fundamental.

Chapter I: Tuberculosis and magnetic nanoparticles.

Chapter I

Tuberculosis and magnetic nanoparticles.

I.1. Generalities on tuberculosis.

I.1.1. Introduction

Tuberculosis (TB) is caused by *Mycobacterium tuberculosis* (MTB), and severe cough (3 weeks or more), chest pain, coughing up blood or sputum (phlegm that comes from the bottom of the lungs) are the main symptoms (Bonilla *et al.;* 2008).

TB is the first cause of death due to preventable infectious disease around the world (WHO, 2019). Although not all people exposed to *M. tuberculosis* develop the disease (although they reach a latent infection state), it has been observed that between 5 and 10% of those exposed may develop the disease at some point in their lifetime (Narasimhan *et al*., 2013). This estimation may be influenced by a number of factors that alter the individual immunological system (Fogel, 2015). In 2017 it has been reported in the world: 10 million cases of TB (1.6 million deaths, including 0.3 million among co-infections associated with HIV), and 558,000 new cases with resistance to rifampicin in multidrug-resistant TB (WHO, 2018).

Early diagnosis and treatment are necessary pillars to reduce the TB burden worlwide. Inadequate strategies to strengthen these pillars can increase TB transmission and severity of illness (**Figure I.1**).

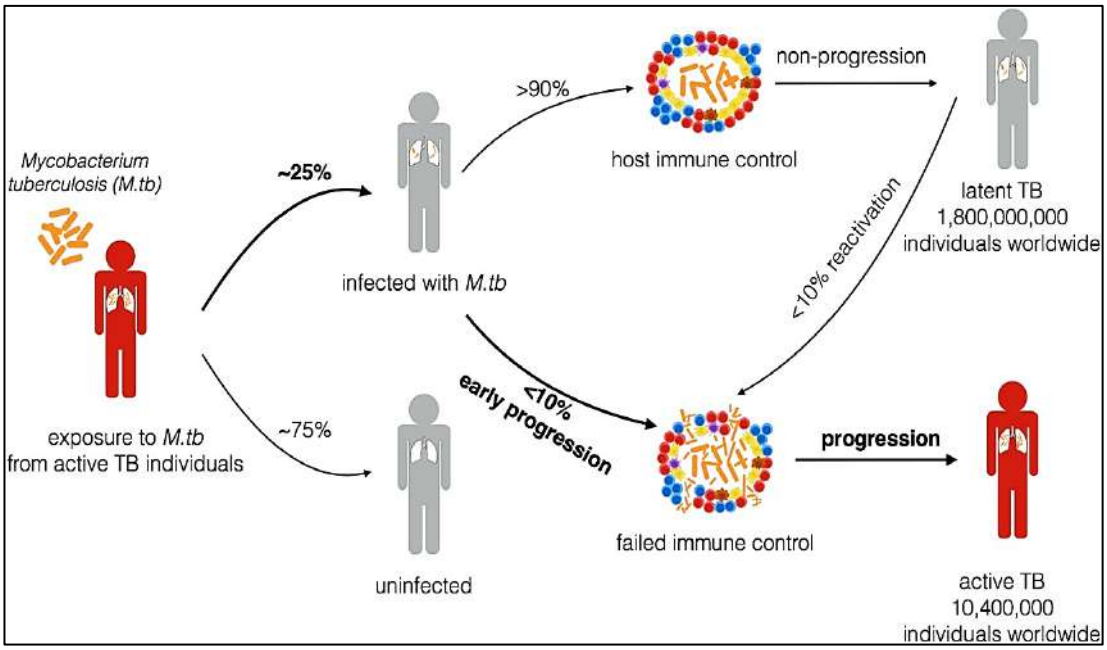

Figure I.1: Pathophysiology of TB (WHO, 2017) (Luo *et al.*, 2018).

In the last decade, significant progress has been made in the new TB diagnosis technology, entering in an era of molecular detection that provides faster methods to diagnose and confirm drug resistance (Lawn, 2015). However, many of them are expensive, not practical to use in field or not accessible to people with limited economic resources. In this regard, antigen detection from non-invasive samples (sputum) is a promising tool for early diagnosis of TB disease.

I.1.2. *Mycobacterium tuberculosis*.

Mycobacterium genus is characterized by a complex envelope of the cell wall (presence of alpha-alkyl and beta-hydroxy fatty acids) which is responsible for the low permeability and its differential coloration (Zhiel-Neelsen). Mycobacterium genus is divided into fast-growing species (opportunistic or non-pathogenic bacteria) and slow-growing species (MTB complex, etiological agents of TB) (Forrellad *et al.*, 2013). MTB complex refers to a group of species that are genetically very similar (*M tuberculosis, M. canettii, M. africanum, M. microti, M. bovis, M. caprae* and *M. pinnipedii*), where MTB is

the most known because it infects more than one-third of the world's population, and it is also capable of infecting animals that have had contact with infected humans (Forrellad *et al*., 2013). *M. canettii* and *M. africanum*, can also cause human TB and are usually isolated from African patients (Forrellad *et al*., 2013). *M. bovis* presents the widest range of host infection, affecting humans, domestic and wild cattle, and goats (Forrellad *et al*., 2013). In humans, *M. bovis* causes similar symptoms of TB and may include fever, night sweats and weight loss (Forrellad *et al*., 2013). *M. caprae* affects only goats. *M. microti* is a rodent pathogen, usually isolated from mice (microtus genus), but may affect immunocompromised individuals. Finally, *M. pinnipedii* infects seals (Cousins *et al*., 2003).

It is believed that MTB complex has evolved from a common ancestor which through successive deletions and insertions has resulted in mycobacterium speciation with differences in pathogenicity (Forrellad *et al.*, 2013). The complete genome of the H37Rv strain has approximately 4,000 genes in 4.41 Mb and grouped into 14 differential regions (RD1-14). The genetic sequence information of this strain is centralized in *TubercuList* online support (http://www.pasteur.fr/Biol/Tu bercuList/).

The *Mycobacterium tuberculosis* specie is an aerobic facultative intracellular pathogen that can persist within the host through a reduced metabolism state and start the replication in a chronic lung infection (Kruh *et al*., 2010). In addition, this bacterium has a predilection for oxygenated tissues as well as lungs and lobes of kidney (Kruh *et al*., 2010). *In vitro* studies have hypothesized the environment within an infected lung, defining the bacterial response to pH, salivation and hypoxia (Kruh *et al*., 2010). However, *in vivo* studies of combined effects are required, to evaluate the environmental factors and mycobacterial responses (Kruh *et al*., 2010). High percentage of lipids in the cell wall is an important feature of these bacilli. It represents 60% of the dry weight, protecting them against bactericidal activity of complement and macrophage digestion (Cambier CJ, Takaki KK, Larson RP, Hernandez RE, Tobin DM, Urdahl KB, 2017). In this way, the bacterial cell

wall lipids increase the bacillus survival in a expectorated dry sputum (López-Hernández *et al*., 2016). The treatment of tuberculosis is difficult and requires long treatment with various antibiotics, where rifampicin and isoniazid are the most used **(Figure I.2)** (Figure from National Institute of Allergy and Infectious Diseases).

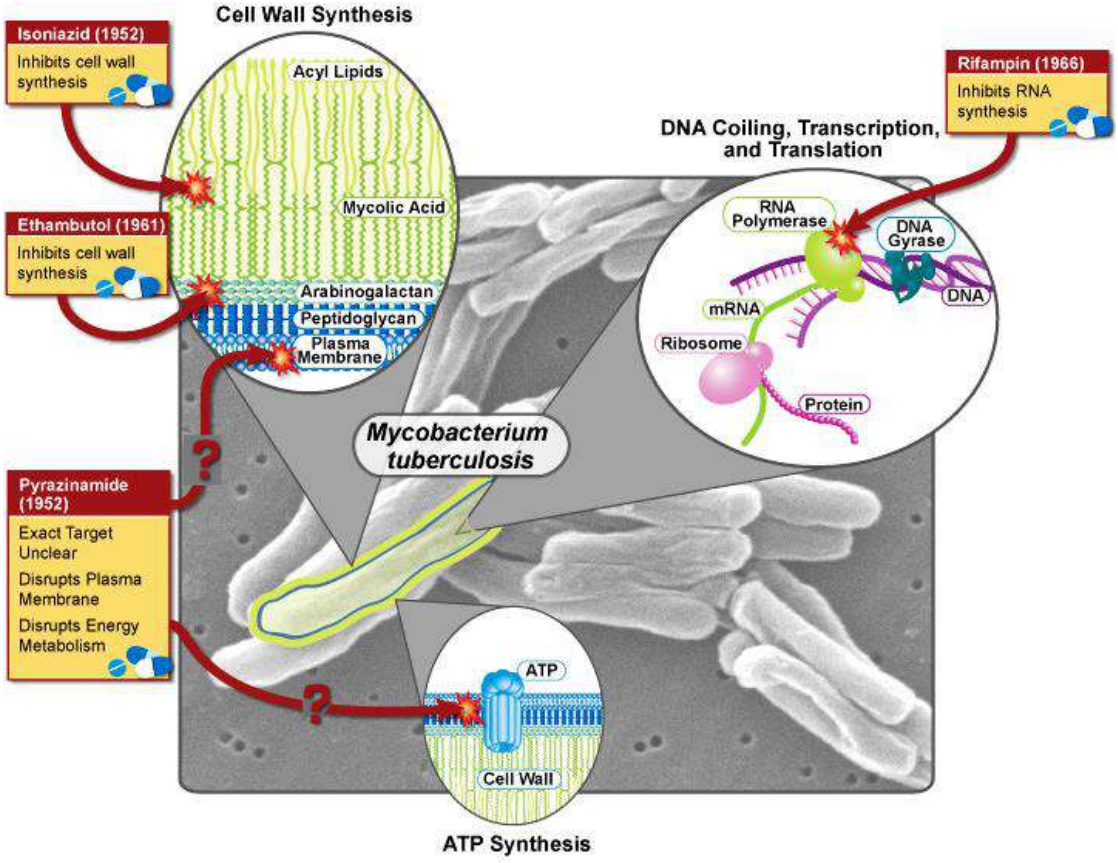

Figure I.2: *Mycobacterium tuberculosis* and the more used antibiotics against this bacterium. (Figure from National Institute of Allergy and Infectious Diseases).

I.1.3. TB infection.

MTB can remain dormant in the human body for decades only progressing to active disease in 5 to 10% of immunocompromised individuals (Murray *et al*., 2013). The bacillus is transmitted through aerosols and enters the lungs through inhalation (Murray *et al*., 2013). The susceptibility and the environment of the receiver are some of the factors that influence the transmission (Murray *et al*., 2013)

The initial infection is usually asymptomatic and localized mainly in the lungs, although this may affect other tissues, producing a broad spectrum of disease (Davis JM and Ramakrishnan, 2011; Krishnan *et al*., 2010; López-Hernández *et al*., 2016). In the lung, the bacillus may reside within the alveolar macrophage triggering the aggregation of immune cells and the formation of a granuloma (**Figure I.3)** (Pai *et al*., 2016)**..** Alveolar macrophages ingest and destroy the bacillus (Kirby *et al*., 2013). This action will depend on the intrinsic microbicidal capacity of the host phagocytes and the virulence of the strain (Volkman *et al.*, 2004). Dendritic cells play an important role in the early stages by activating T cells, which have the ability to present antigens (García-Romo *et al.*, 2004). The bacteria survive to this multiply attack and cause lysis of the macrophage (Bozzano *et al*., 2014). At this time, monocytes and other inflammatory cells are recruited into the lung, and allow the survival of the bacteria (Piccini *et al.*, 2014). In this symbiotic state, the mycobacteria grow logarithmically, and produce small tissue damage (Piccini *et al.*, 2014). Approximately three weeks later, cell-mediated immunity is developed, containing growing bacteria (Piccini *et al.*, 2014). Granulomatous lesions appear, and as a result the infection may remain latent or progress and spread to the rest of the body (Hernandez-Pando *et al*., 1995; Volkman *et al*., 2004). Although the main defense mechanism is the cellular immune response, evidence suggests that antibodies can mediate different actions against the bacillus, mainly in the first hours after infection (López *et al.*, 2009).

During infection, granulomas play two roles: they serve as a niche for invasion of the bacteria, protecting the host from active disease. The granulomas population in infected host, consists of primary and post-primary lesions. Primary granulomas contain the original inhaled strain which are morphologically different from post-primary granulomas that have developed through disseminated infection. Leading to a heterogeneous population of bacilli (Kaplan G, Post FA, Moreira AL, Wainwright H, Kreiswirth BN, Tanverdi M, Mathema B, Ramaswamy SV, Walther G, Steyn LM, Barry III CE, 2003; Kruh *et al*., 2010; McMurray, 2003).

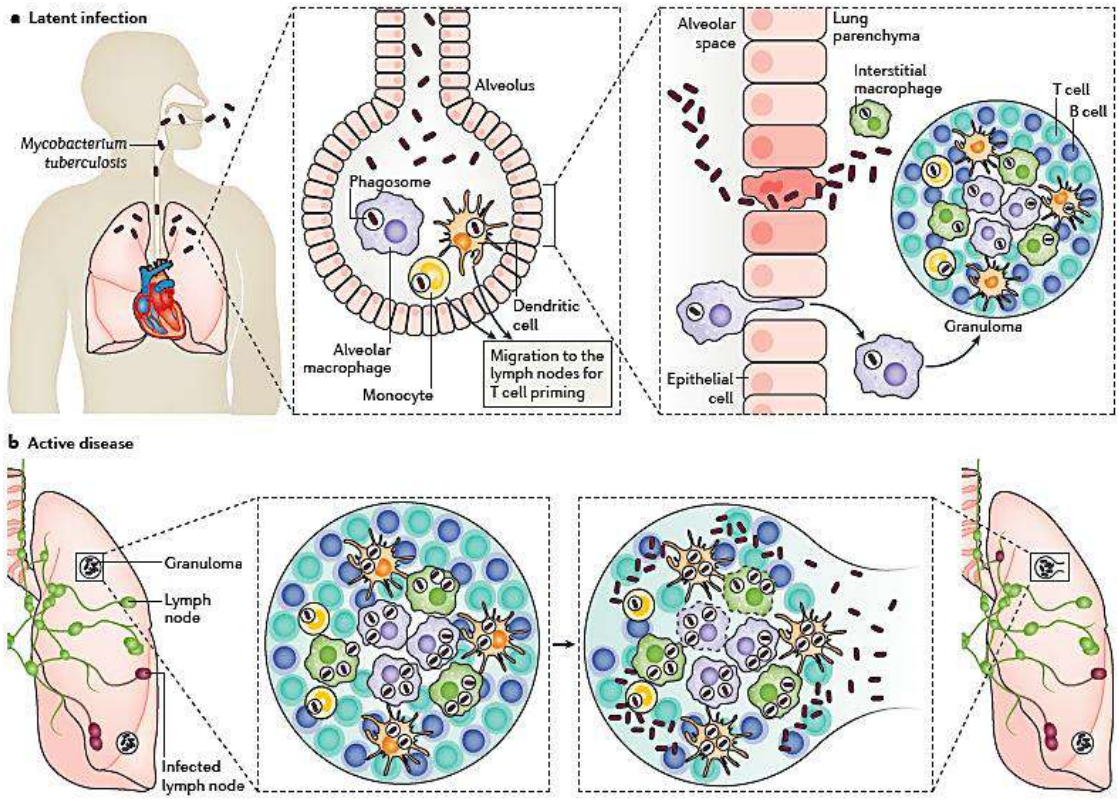

Figure I.3: TB infection (Pai *et al*., 2016).

I.1.4. Epidemiology of TB.

Although new techniques for TB diagnosis have been reported worldwide, traditional methods that identify and isolate the bacteria still dominate (Ali, 2014; Narasimhan *et al*., 2013). They turn limited for low bacterial load samples and this becomes a problem when rapid diagnosis is urgent, especially in multidrug, extensively or totally resistant TB patients (Albuquerque *et al*., 2014; Narasimhan *et al*., 2013).

According to World Health Organization, 2018, an estimation of 23% of the world's population (1.7 billion people) have a latent TB infection, and they can develop an active TB in a part of their lifetime (**Figure I.4)** (WHO, 2018)**.** In 2017, approximately 10.0 million people (range, 9.0–11.1 million) developed TB, which caused an estimated 1.3 million deaths (range, 1.2–1.4 million) among HIV-negative people and 300 000 deaths (range, 266 000–335 000) among HIV-positive people (WHO, 2018). Being 90% adults

(aged ≥15 years), 9% people with HIV (72% in Africa) and two thirds were detected mainly in eight countries: India (27%), China (9%), Indonesia (8%), the Philippines (6%), Pakistan (5%), Nigeria (4%), Bangladesh (4%) and South Africa (3%)(WHO, 2018). Only 6% of global cases were European (3%) and the Americas (3%) regions (WHO, 2018).

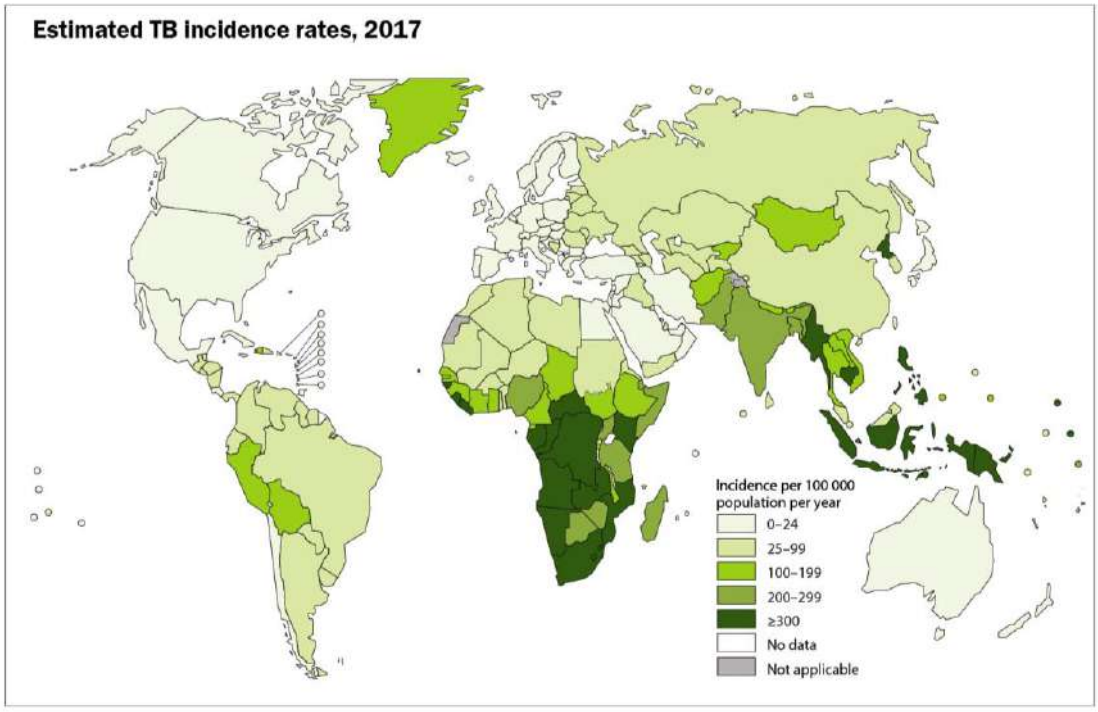

Figure I.4: Worlwide TB incidence, 2017 (WHO, 2018).

Additionally, the drug-resistant TB continue being a serious public health around the world (WHO, 2018)**.** In 2017, an estimation of 558 000 people (range, 483 000–639 000) were positive for rifampicin resistant-TB (RR-TB), 82% of them become multidrug-resistant TB (MDR-TB) (WHO, 2018). Almost half of MDR/RR-TB world's cases are in: India (24%), China (13%) and the Russian Federation (10%). Also, 8.5% of MDR-TB developed the extensively drug-resistant TB (XDR-TB) **(Figure I.5)** (WHO, 2018).

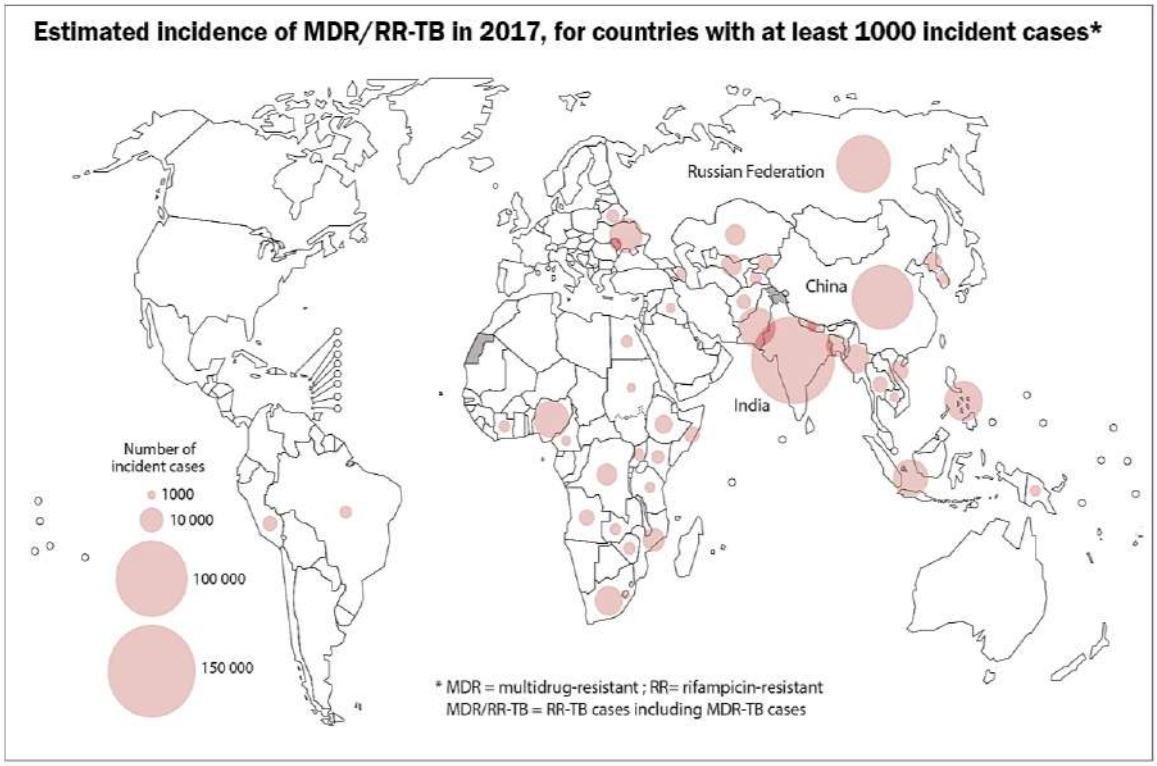

Figure I.5: Resistant TB incidence around the world, 2017 (WHO, 2018).

I.1.5. TB diagnosis.

Among the most commonly used conventional methods **(Figure I.6)** for diagnosing TB we have:

A. Smear microscopy.

It is a simple, fast and inexpensive method where stained mycobacteria are observed directly from a clinical sample using a microscope. The classic staining is the Ziehl-Nielsen (ZN) used mostly in sputum samples from suspected TB patients (Laszlo, 1999). Currently this method is considered a gold standard for the diagnosis of TB. However, the method is not very sensitive (34-80% positive cultures) and occasionally it is negative in low bacillary loads (paucibacillary) because it needs 10^4 bacilli/ml or more for detection (Laszlo, 1999; López-Hernández *et al*., 2016; Reji *et al.*, 2013). Auramine and fluorescence detection of the bacillus is another staining method, allowing a faster

analysis of multiple samples (Slim-Saidi *et al*., 2015). This technique is more sensitive (increases by 10%) than the ZN, and is justified in laboratories with high demand (Slim-Saidi *et al*., 2015).

B. Culture.

The MTB culture is the conventional 'gold standard' for TB diagnosis. Although this method is sensitive (limit of detection ~ 10-100 CFU/ml sputum sample), requires 6-9 weeks to visualize the growth of mycobacteria (Rodriguez *et al*., 2014). This is because their growth is very slow, replicating every 18 hours compared with the most bacteria that requires 1 h or less to replicate (Rodriguez *et al*., 2014). Solid or liquid methods can be used to incubate the bacteria at 37 °C in 10% CO_2 for 6-8 weeks. The most commonly used solid media are: Lowestein Jensen, Middlebrook 7H10, 7H11 and selective agar 7H11; and the liquid media are: Middlebrook 7H9 and radiometric BACTEC 12B, used to reduce the growth time of bacteria (Laszlo, 1999; Laverdiere et al., 2000; López-Hernández *et al*., 2016; Ugarte-Gil *et al*., 2008). Their main disadvantages are the high risk of contamination and the inability to distinguish the morphology of different mycobacteria strains (López-Hernández *et al*., 2016). Also, the treatment of the sputum sample is a critical step and requires a biosafety laboratory level 3 (Reed et al., 2017; Rodriguez et al., 2014; Zyl-smit et al., 2011).

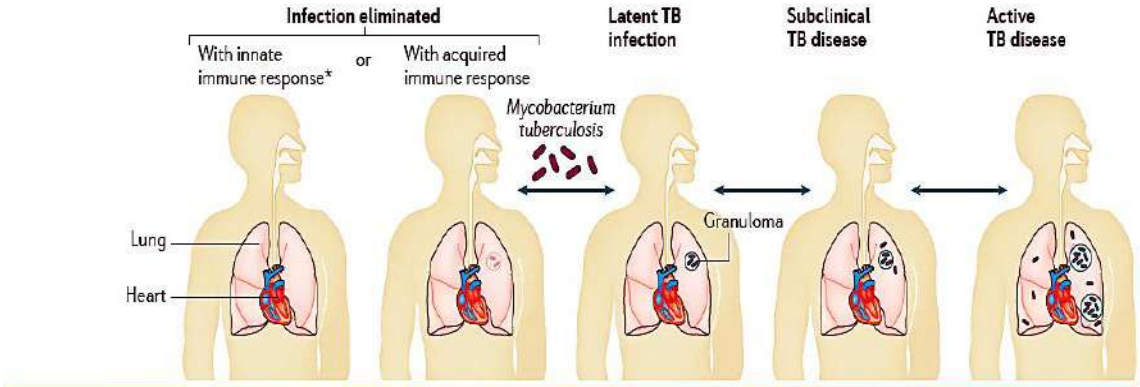

TST	Negative	Positive	Positive	Positive	Usually positive
IGRA	Negative	Positive	Positive	Positive	Usually positive
Culture	Negative	Negative	Negative	Intermittently positive	Positive
Sputum smear	Negative	Negative	Negative	Usually negative	Positive or negative
Infectious	No	No	No	Sporadically	Yes
Symptoms	None	None	None	Mild or none	Mild to severe
Preferred treatment	None	None	Preventive therapy	Multidrug therapy	Multidrug therapy

Figure I.6: Behavior of TB in the different diagnostic methods, from infection by Mycobacterium tuberculosis to active tuberculosis (pulmonary) disease (Pai *et al.*, 2016)**.**

C. Microscopic Observation Drug Susceptibility (MODS).

It is a method based on the observation of *Mycobacterium tuberculosis* microcolonies growth using an inverted microscope (Caviedes *et al.*, 2000). MTB morphology in the liquid culture looks like a specific cord pattern. Therefore it is useful for the diagnosis and to determine resistance to isoniazid (INH) and rifampicin (RMP) (Caviedes *et al.*, 2000; Moore *et al.*, 2006). Since the creation of MODS, many studies on its performance and applicability have been published worldwide (Moore *et al.*, 2006). In a meta-analysis study, nine studies performed on the efficacy of MODS in the diagnosis of rifampicin (RMP) resistance showed a sensitivity of 98.0% (95% CI 94.5-99.3) and a specificity of 99.4% (95.7-99.9). For isoniazid (INH) resistance it showed 97.7% (94.4-99.1) of sensitivity and 95.8% (88.1-98.6) of specificity (Minion *et al.*, 2010). Likewise, they estimated the mean response time of 9.9 days (95% CI 4.1-15.8); and it was 11 times

less expensive than the Genotype MTBDR plus® method used to determine drug resistance at the National Institute of Health - Peru (Solari *et al.*, 2011).

D. Molecular methods.

- **Polymerase chain reaction (PCR).**

PCR can detect small amounts of DNA from mycobacteria. The insertion sequence 6110 (IS6110), identified by Thierry *et al* in the early 1990, is a genetic sequence of insertion detectable only in the genomes of the *Mycobacterium tuberculosis* complex where it is present in multiple copies (Thierry *et al.*, 1990). IS6110 based PCR is a rapid technique (Thabet and Souissi, 2017), sensitive and specific for the diagnosis of MTB (Hwang *et al*., 2015). In addition, MPT64 amplification is more sensitive than IS6110 PCR when it is desired to detect extrapulmonary TB with negative sputum or TB of the central nervous system (Sethi *et al.*, 2012); however, in multiplex it is useful to detect osteoarticular TB (Bekmurzayeva *et al*., 2013).

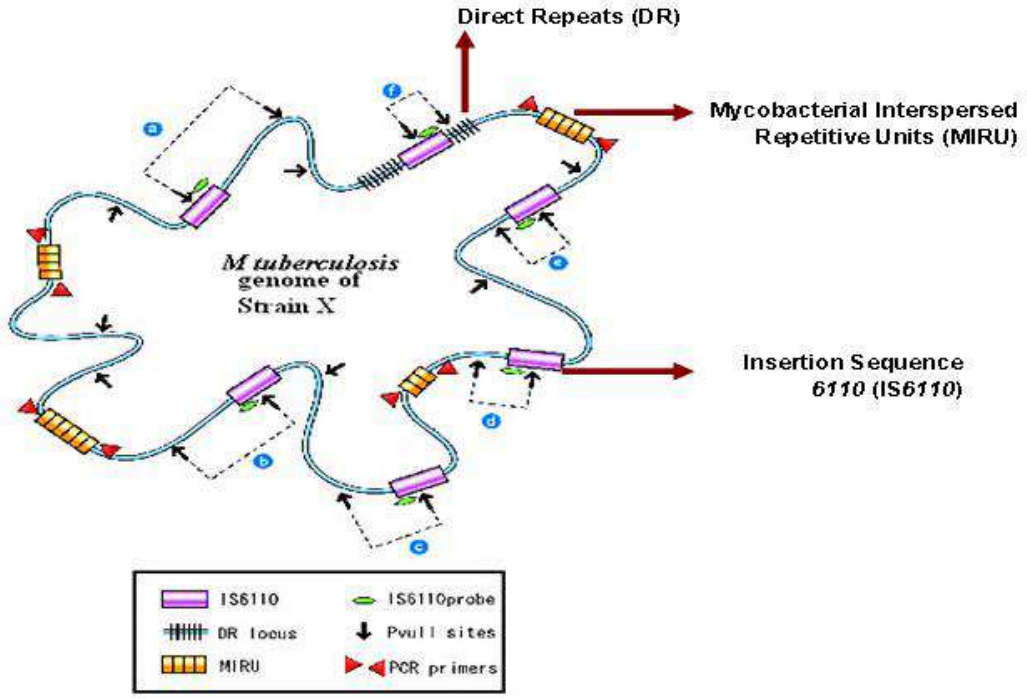

Figure I.7: Polymorphic repetitive sequence IS6110 in hypothetical MTB genome (Ali, 2014).

- **Fingerprinting.**

Restriction Fragment Length Polymorphism (RFLP) or the Spoligotyping technique are also highly effective in typing mycobacteria and determining the genotypes of clinical isolates. The molecular typing of human tuberculosis is achieved by the use of the insertion sequence IS6110 (Cave *et al.*, 1991).

E. Serological methods.

The purified protein-derived tuberculin test (**PPD**) is a non-recommended test for the diagnosis of active TB because it is positive in people who have antibodies against the bacterial antigens (individuals with active TB, recent vaccinations with BCG or TB-cured patients) but this does not mean that the person is positive for active TB (Chaudhary *et al.*, 2010; Bekmurzayeva *et al.*, 2013). In addition, immunosuppressed persons may give false negatives. Basically, the test involves inoculating under the skin a small amount of a mixture of antigens derived from heat inactivated MTB and wait 3-4 days to visualize a hypersensitivity reaction if it is positive (forms an erythema and/or vesiculation) (Bekmurzayeva *et al.*, 2013). The test cannot differentiate active TB from latent TB, and may be positive even if the individual has been infected and/or exposed to another species of mycobacteria (Bekmurzayeva *et al.*, 2013).

Similarly, the Interferon-Gamma Release Assay (**IGRA**) does not provide information on the clinical features of TB (Steingart *et al.*, 2007; Chaudhary *et al.*, 2010).

So serological tests have not presented a satisfactory profile due to their low specificity and sensitivity (López-Hernández et al., 2016; Steingart *et al.*, 2007).

F. Others.

Additionally, there are other methods that have been evaluated but are not yet widely used:

- **Skin patch with MPT4.**

A skin patch based on MPT64 has been developed taking advantage of its property of differentiating immune response in people with active TB. It was observed that the test did not cross-react with: patients who had received the BCG vaccine, patients infected with other mycobacteria and patients who had been cured of TB (Bekmurzayeva *et al.*, 2013). In studies conducted in Japan and the Philippines, the test showed 98% sensitivity and 100% specificity (Chaudhary *et al.*, 2010). In addition, this test is simple, laboratory or trained professionals are not necessary to performed it (Bekmurzayeva *et al.*, 2013; Chaudhary *et al.*, 2010)

- **Immunochromatographic tests (ICAs).**

ICAs are able to detect antigens or antibodies (Bekmurzayeva *et al.*, 2013). Samples (blood/ serum or culture of bacteria) flow laterally in a single device, where positive reactions show colored bands (Bekmurzayeva *et al.*, 2013). ICAs are commercially available to detect IgG and IgM against MTB antigens (Bekmurzayeva *et al.*, 2013). There are three ICAs based on the detection of MPT64, the Capilia rapid test (Tauns Laboratories Inc., South Korea) being the most used to confirm MTB in solid and liquid positive cultures. The limitations of ICAs are false negatives due to mutations of the genes encoding the proteins that the test recognizes (Bekmurzayeva *et al.*, 2013)

- **Immunohistochemistry (IHC).**

IHC is a test that detects antigens in sections of tissues and uses polyclonal and monoclonal antibodies (Ramos-Vara, 2005). For example, there is an IHC that recognizes MPT64 in formalin-fixed or paraffin-embedded biopsies (Bekmurzayeva *et al.*, 2013), showing a sensitivity of 89-93% and specificity of 95-98% in patients with abdominal TB or tuberculous lymphadenitis (Purohit *et al.*, 2007). In addition, this test can detect $5x10^5$ - $1x10^6$ organisms per gram of tissue, and has been successfully used in lymph node aspirates, cerebrospinal fluid and pleural effusions (effusions) (Purohit *et al.*, 2007). Finally, Baba *et al* developed an IHC based on MPT64 to diagnose pleural TB and showed

81% of sensitivity and 100% of specificity (Baba *et al*., 2008). One of the main limitations of the IHC is the cost and time required to collect and treat the sample.

- **ELISA-MPT64.**

Lu *et al* developed a sandwich ELISA to detect the MPT64 antigen and showed that the test was able to detect 0.01 mg/l of the protein with a sensitivity of 97.3% and a specificity of 100% comparing it a PCR that amplify MPT64 gene and shows a sensitivity of 98.2% and a sensitivity of 100% (Liu *et al.*, 2009).

- **Biosensors.**

Biosensors are analytical devices that integrate a biological sensing element and a transducer to quantify a biological event (Bhalla *et al*., 2016). To detect TB, an optical biosensor platform based on light waves has been designed for the direct detection of three specific biomarkers of TB: liparabinomannan (LAM), ESAT6 and Ag85 (Mukundan *et al*., 2012). The entire system is based on a sandwich immunoassay: a biotinylated capture antibody and a detection antibody labeled with a fluorophore located on the surface of the sensor. The proposed sensor has a detection limit of 0.5 pM for ESAT6, 100 pM for Ag85 and 1 pM for LAM (Mukundan *et al.*, 2012). However, poor antibody stability reduces the use of this assay in clinical samples (Mukundan *et al*., 2012). Another group has developed an immunoassay based on surface plasmon resonance (SPR) spectroscopy that targets CFP10 (Hong *et al.*, 2011). Here, the detection interface is constructed by immobilizing CFP10 on a gold surface of the Surface Plasmon Resonance (SPR) chip, then blocking the void spaces with cystamine (Hong *et al.*, 2011). The detection limit of this assay has been reported at 100 ng/ml with a linear relationship between the displacement of the SPR angle and the CFP10 concentrations of 0.1 to 1 mg/ml protein (Hong *et al*., 2011).

I.2. Biomarkers of the *Mycobacterium tuberculosis*.

I.2.1. Main biomarkers from MTB.

A biomarker is a biomolecule that can be measured as an indicator of normal or altered biological processes, and these can usually be molecules derived from the host or pathogen (Bekmurzayeva *et al.*, 2013; McNerney *et al.*, 2010). In the case of TB, identifying and validating biomarkers for sensitive and specific diagnostic tests is a challenge because these molecules must be at detectable levels in different types of samples, such as sputum, plasma and urine (McNerney *et al.*, 2010). In addition, they should be able to discriminate between infected and uninfected individuals and should return to baseline levels during treatment for reproducible clinical predictions (Bekmurzayeva *et al*., 2013).

MTB filtered proteins are candidates for biomarkers, since they represent the most abundant secretory proteins of MTB. Lee *et al* (2006) have evaluated the production of secretory proteins in MTB culture, and have found that these proteins were increasing over the weeks (1: 2.6 μg/ml, 2: 5.4 μg/ml, 3: 25.5 μg/ml, 4: 74.5 μg/ml, 5: 264 μg/ml, 6: 331 μg/ml, 7: 479 μg/ml and 8: 549 μg/ml) (Lee *et al*., 2006). Also, they successfully purified the native proteins Ag85B KDa (0.56 mg) and MTB12 (1.81 mg) from 1l of the 6-week filtered culture, which contained 307.81 mg of MTB filtered culture protein H37Rv (Lee *et al*., 2006). Some important MTB biomarkers are described below:

a. MTC28 protein.

MTC28 is one of the major secreted and specific antigens of the MTB complex, with a molecular weight of 28 kDa and rich in proline and alanine residues. MTC28 structure contains ten β strands and three α helices. The β strands are forming a structure similar to a sandwich (β sandwich pattern) where seven antiparallel β strands are stacked between α1, α2 on one side and between α3 on the other side. Also, on MTC28 surface is observed a V-shaped cleft, which is positively charged because it is surrounded by Arg107, Arg111, Arg229 and His231 positive aminoacids (**Figure I.8**) (Kundu *et al.*, 2016). MTC28, also known as Rv0040c, is only conserved in pathogenic strains of mycobacteria (Kundu *et al.*, 2016). The specificity of the immune response can be attributed to the lack of cross-

reactivity with T-cell and B-cell epitopes of environmental mycobacterial species such as *M. avium* (Manca *et al.*, 1997). Previous studies showed that, when MTC28 is used individually in ELISA assay to detect antibody, a sensitivity and specificity of 72.4% and 71.4%, respectively were observed (Wu *et al.*, 2010). MTC28 is considered as a potential candidate for vaccine design and immunodiagnosis of TB (Manca *et al.*, 1997). According to a bioinformatic prediction, 5 potential epitopes were identified: **89**QRPHGFKALD**98**, **102**PMPPRWTQVPDPNVPD**117**, **124**DRLGNSVYTS**143**, **178**PSSIIEGTYRENDMTL**194**, and **220**LSQAVTDGPATDA**232** (Kundu *et al.*, 2016; Manca *et al.*, 1997). According to Kundu *et al.*, 2016, the most reactive peptides of MTC28, against pulmonary tuberculosis patient sera, were **128**ALDITLPMPPR**137** and **138**WTQVPDPNVPDAFVVIADR**156** (Kundu et al., 2016).

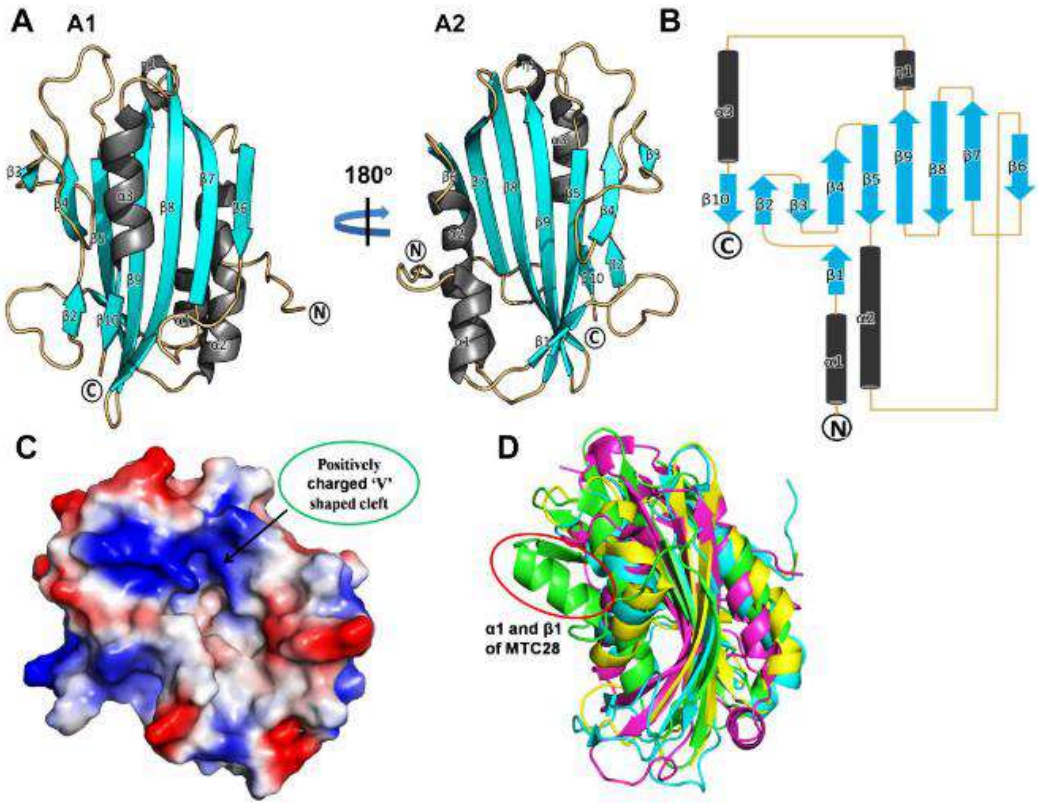

Figure I.8: MTC28 structure. **A**, MTC28 showing the characteristic β sandwich pattern (A1) and 180° rotation (A2). **B**, MTC28 topology. **C,** Surface electrostatic potential of MTC28 showing a positively charged V-shaped. **D**, Comparison of MTC28 (green) with

three other structural homologs. The α1 and β1 structures of MTC28 are unique (extracted from Kundu *et al.*, 2016).

b. SA5k protein.

SA5k is an 8.3 kDa protein secreted into the extracellular environment by MTB and *M. bovis* BCG in culture filtrate and is overexpressed during intracellular growth of MTB and in the lung of patients, being found in the sputum of patients (Bottai *et al.*, 2003). In addition, it is believed that SA5k is involved in the intracellular survival mechanisms of MTB (Bottai *et al.*, 2003). This protein is also known as Rv1174c or TB8.4.

c. 38kDa protein.

38kDa antigen is an extracellular lipoprotein, detected almost solely in MTB and the most potent immunogen of the mycobacteria (Chang *et al*., 1994). This protein is known as pab, antigen 5, antigen 78 or PstS-1 or Rv0934; and represents 1.81% of the total filtered MTB culture proteins (Lee *et al.*, 2006). Although, 38kDa antigen is actively secreted, the lipid tail of surface mycobacterial cell attaches the protein binding carbohydrate residues on 38kDa (Harboe and Wiker, 1992). 38kDa antigen is capable of inducing immune response involving B and T cells with high specificity for MTB infection (Marín *et al.*, 2015; Steingart *et al*., 2007).

d. Hsp16.3 protein.

A small heat shock (Hsp) 16.3 protein from *Mycobacterium tuberculosis*, also known as Acr1, HspX, 16-kDa Antigen, and Rv2031c, is an immuno-dominant antigen and the major membrane protein. It is a protein that is secreted during the growth of MTB, and it is an important component that facilitates the survival of MTB during latent human infection but is not present under conditions of logarithmic growth (Meng *et al.*, 2014). The protein is overexpressed under stress conditions as elevated temperatures (Kennaway

et al., 2005). *In vitro*, Hsp16.3 exists as nanomers and forming polymers (dissociation/re-association) in solutions (**Figure I.9**) (Kennaway *et al*., 2005; Zhang et al., 2015, 2005).

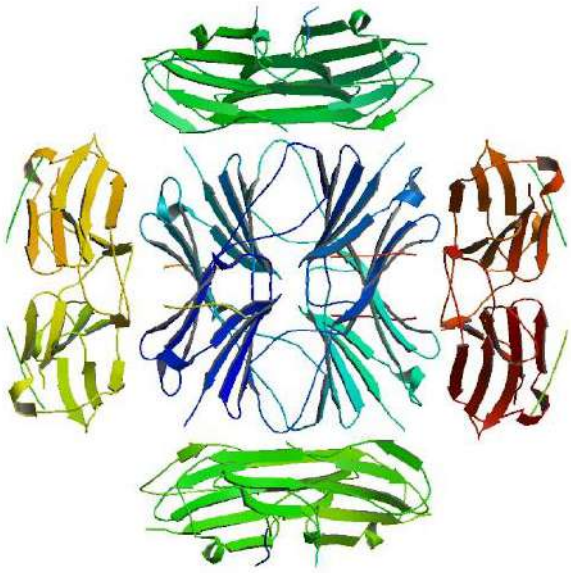

Figure I.9: Dodecameric structure of the Hsp16.3 from *Mycobacterium tuberculosis* (extracted from kennaway *et al.,* 2005)

e. Lipoarabinomanan (LAM).

It is a major antigen evaluated as a biomarker. Assays such as sandwich ELISAs have been developed for the detection of LAM in samples of sputum (10^4 bacteria/ml) and urine (Peter *et al.*, 2012; Sarkar *et al.*, 2014).

f. MoeX protein.

MoeX antigen was identified in urine samples from active TB patients by mass spectroscopy (Pollock *et al.*, 2013). The putative molybdopterin biosynthesis protein MoeX/MoeA is coded by *Rv1681* gene (Pollock *et al.*, 2013). It is a specific protein only for the MTB complex (no homologues have been found in databases), and was clinically validated as a diagnostic biomarker for active pulmonary TB (Pollock *et al.*, 2013).

g. Ag85B protein.

Immunodominant and major secretory protein of actively replicating MTB, Ag85B protein represents 3.25% of the total filtered MTB culture proteins. The Ag85 complex is involved in biological processes as well as cell wall biosynthesis and immunogenic responses (Anderson *et al.*, 2001). This complex comprises Ag85 A, B and C, which are encoded by separate genes. They are generally expressed in the ratio of 2:3:1 but may vary according to changes in their environment (Druszczynska *et al.*, 2017). Although Ag85 B (30kDa) is of higher expression, C is 8 times more biologically active than B; but all three are necessary to evade the immune response (Anderson *et al.*, 2001; Armitige *et al.*, 2000; Bekmurzayeva *et al*., 2013). Ag85 proteins are secreted and can be found in the phagosome, in the outer layer of the cell wall of the bacterium and in the blood (Armitige *et al.*, 2000; Bekmurzayeva *et al*., 2013). Also, the Ag85 complex has been shown to bind fibronectin of plasma, an extracellular matrix glycoprotein, or IgG, altering the host immune response. This interaction appears to reduce MTB phagocytosis, thereby promoting infection (Bentley-hibbert *et al.*, 1999). Expression of Ag85 is essential for the intracellular survival of MTB within the macrophage. Additionally, the complex possesses mycolyl transferase activity, catalyzing the synthesis of trehalose 6,6-dimicolate (cord factor) **(Figure I.10)**, one of the most abundant glycolipid on the cell wall of mycobacteria (Bekmurzayeva *et al*., 2013; Belisle *et al.*, 2016). This protein is also known as Rv1886c or fbpB.

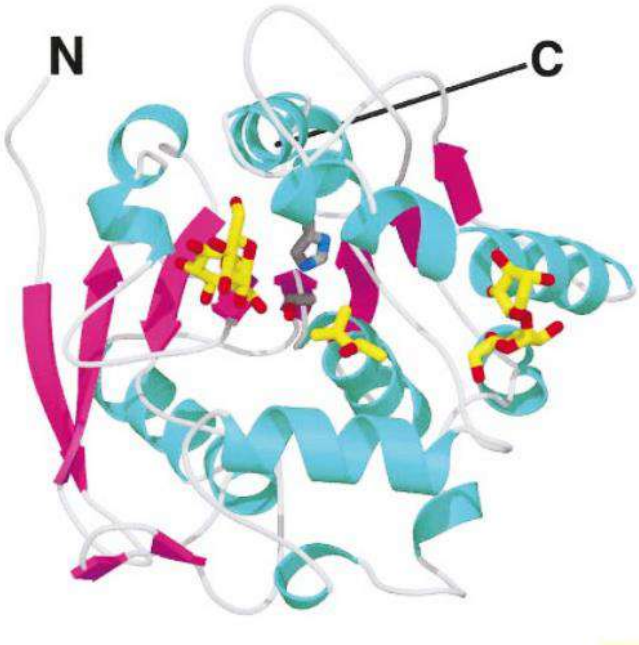

Figure I.10: Structure of Ag85B from MTB, with trehalose. The protein present α-helices, β-strands, coil and turn regions (extracted from Anderson *et al.*, 2001).

h. MPT64 protein.

MPT64 is a secretory immunodominant protein, also known as MBP64 or Rv1980c, identified in high levels in the filtered MTB culture. MPT64 represents 8% of the total protein found in an MTB filtered culture and is one of the predominant proteins actively secreted during MTB growth and is expressed early when MTB is in active cleavage (Wang *et al*., 2007). Molecular weights have been reported in the literature from 22.3 kDa to 28 kDa (Bekmurzayeva *et al*., 2013; Roche *et al*., 1996). Also, MPT64 multimers, covalently connected through disulfide bonds were evidenced by western blot. In the MPT64 structure was observed a composition of 2.2% α-helix, 50.9% β-sheet, 19.5% turn, and 27.4% random coil **(Figure I.11)** (Chu and Yuann, 2011; Wang *et al*., 2007).

In patients with early MTB infections, T cells recognize several MTP64 epitopes, for which this protein has been extensively used for the diagnosis of TB, as well as for vaccine candidate (Roche *et al*., 1996). It is believed that MPT64 has an anti-apoptotic effect on granulomas and promotes the persistence of MTB-infected macrophages (Roche *et al*.,

1996). Additionally, MPT64 is a highly specific protein of the MTB complex, and is not found in non-tuberculous mycobacteria (Kumar *et al.*, 2011). MPT64 is found in one of 11 differential regions (RD) of MTB, and absent in certain BCG strains. The loss of MPT64 in RD2 implies a decrease in virulence in animal models of infection (Forreland *et al.*, 2013).

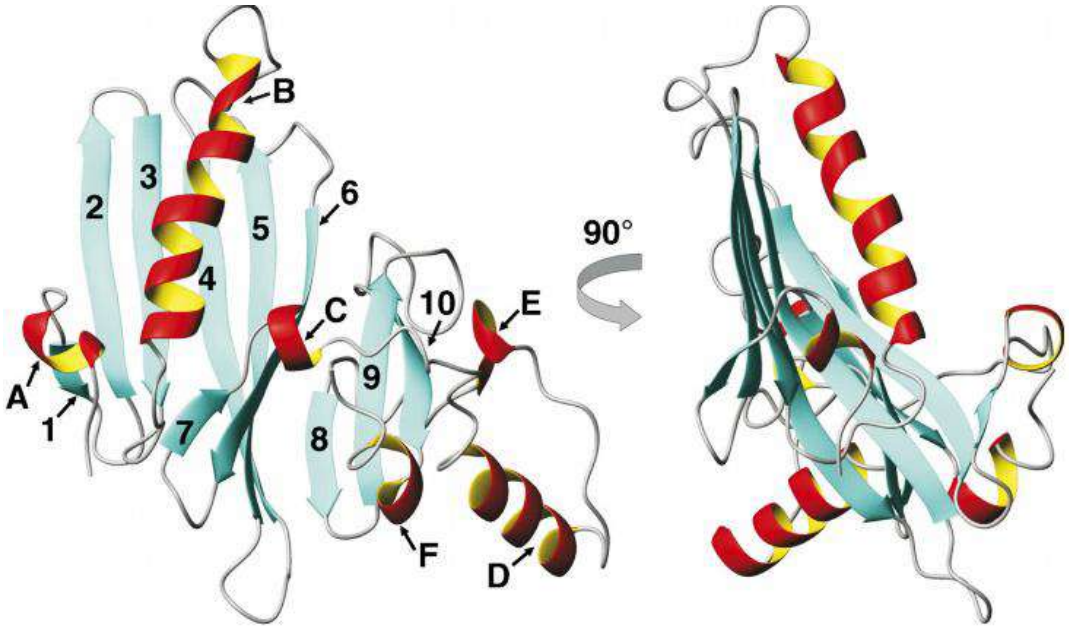

Figure I.11: MPT64 antigen from MTB. MPT64 structure rotated 90°. Representation of β-strands (numbers) and α-helices (letters), proceeding from N to C terminus (Extracted from Wang *et al*., 2007).

i. ESAT6/CFP10.

ESAT6/CFP10 are the most abundant secretory proteins of the filtered MTB culture, with 6 and 10 kDa of molecular weight, respectively. They are absent in *M. bovis* BCG or in most nontuberculous mycobacteria (Kaufmann *et al*., 2005). These proteins are included in RD1, which plays a role in virulence and is absent in BCG. ESAT6/CFP10 are secreted actively in a specialized transport system product of several flanking genes (Scherrer *et al.;* 2019). In addition, the C-terminal end of CFP10 forms a flexible arm, important for engaging the cell surface (Renshaw *et al.*, 2005). ESAT6 and CFP10 form a heterodimeric

four-helix complex **(Figure I.12),** without hydrophobic faces, suggesting that these two proteins probably do not form a transmembrane structure (Kaufmann *et al*., 2005).

Approximately one-third of all TB patients are seronegative for a single antigen; that is why the combination of proteins either separately or fused have been studied. Ag85B-Esat6, Ag85B-TB10.4 and Mtb10.4-HspX are vaccine candidates, where the first two combine proteins secreted early, while the third is based on dormant protein and early secretion (Bekmurzayeva *et al*., 2013).

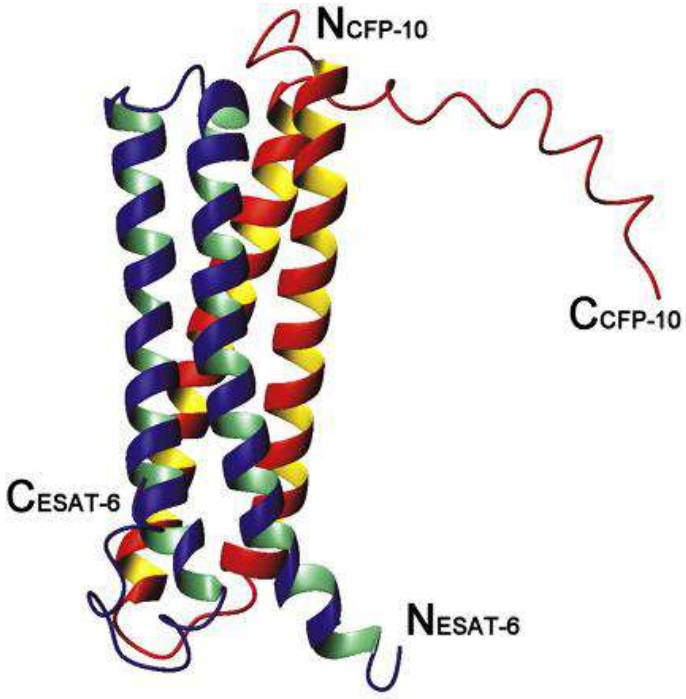

Figure I.12: Topology of CFP10/ESAT6 complex. The structure shows two helix-turn-helix hairpins formed by CFP10 and ESAT6 (extracted from Kaufman *et al*., 2005).

I.3. Application of magnetic nanoparticles in biomedicine.

I.3.1. Magnetic Nanoparticles (MNPs).

Nanotechnology means development of technologies in nanometer scales. It is a multidisciplinary domain (physics, engineering, biology and medicine) with application in a wide range of areas. Nanomaterials used in biological and biomedical fields applications require nanoparticles with more stablished structure and complex design. In addition,

nanotechnology allows to improve the diagnostic techniques that result in high-performance screening (Smit, 2018). Nanotechnology has been widely used in biomedical applications, especially in focused treatments and in the improvement of biomolecules detection (Ito *et al*., 2005). For example, to capture biomolecules from infectious agents doing more efficient and faster the diagnostic methods (Jesse *et al*., 2015). In this sense, magnetic nanoparticles (MNPs) have demonstrated to have several applications in medicine, biotechnology and tissue bioengineering due to their magnetic, electrical and optical properties (Ali *et al*., 2016; Unsoy *et al*., 2015).

The nanoparticles are structures in nanoscale, their operation improves when their size is between 10-20 nm (Smit, 2018). Nanoparticles have been widely studied because they have unique properties compared to bulk (Gatoo *et al.,* 2005). These properties are determined by the size, structure, and physical-chemical composition of the surface and its core (Smit, 2018). A disadvantage of magnetic nanoparticle is its aggregation, reducing its specific surface area, its functionalization efficiency and its performance. In addition, the magnetic nanoparticles based in metals (Fe, Co or Ni) are chemically very active, oxidizing easily, generating a loss of magnetism and scattering capacity.

Iron oxides, γ-Fe_2O_3 (maghemite), Fe_3O_4 (magnetite) and the rest of the ferrites are widely used. Magnetite and maghemite have a closed cubic structure and are the most studied due to their electrical and magnetic properties for use in biological applications (Smit, 2018). However, it is magnetite that shows stronger magnetic properties; therefore, it has been used in more biomedical applications (He *et al*., 2015; Smit, 2018). Fe^{2+} containing iron oxides readily oxidize to Fe^{3+}, so they are chemically stabilized with organic species such as surfactants or polymers or coated with a layer of silica or carbon (Katia Caamaño, 2016). In this way, the nanoparticles can be protected from oxidation, their agglomeration is reduced and a subsequent functionalization is facilitated (Katia Caamaño, 2016).

A. Magnetic property of magnetic nanoparticles.

Magnetic effects are caused by movements of particles that have both mass and electric charges. These particles are electrons, holes, protons, and positive and negative ions. For example, in the case of magnetite, the dynamic states of Fe^{2+} to Fe^{3+}, and vice versa, are due to the movement of electrons in their orbitals, and this generates an electric charge in the particle. In this way, a rotating electric charge particle is generated, which at the same time creates a magnetic dipole, called a magneton. In the case of ferromagnetic materials, magnetons are associated in domains, where a magnetic domain refers to a volume of ferromagnetic material in which all magnets are aligned in the same direction by the exchange forces. Consequently, we have that when the size of a ferromagnetic material is reduced below a critical value, it becomes a single domain. This is because the free energy state is lower in ferromagnetic particles that are below a certain critical size, producing a uniform magnetization (single domain) for the particles and a non-uniform magnetization (multidomain) for larger particles (Akbarzadeh *et al.*, 2012).

The behavior of ferromagnetic materials in an applied magnetic field is described in a hysteresis loop, characterized by: remanence and coercivity. Where the 'thickness' of the curve determines the coercivity. In the case of very fine magnetic particles, coercivity depends mainly on the size of the material, and coercivity is the property of greatest interest. In the F**igure I.13** is observed that as the particle size is reduced, the coercivity increases to a maximum and then decreases towards zero. This happens when the size of the single domain particles decreases further below a critical diameter. Such particles become superparamagnetic (coercivity is zero). The superparamagnetism depends on the temperature, it means that in superparamagnetic particles, the thermal fluctuations are able to spontaneously demagnetize a set of previously saturated particles (zero coercivity and they do not present hysteresis). So, the nanoparticles become magnetic in the presence of an external magnet but return to a non-magnetic state when the external magnet is removed. This avoids an "active" behavior of the particles when there is no applied field. It means

that there is no magnetic remanence. This behavior is important when magnetic particles are introduced into living systems, where the particles must have a magnetic behavior only in the presence of a magnetic field. There is a series of crystalline materials that exhibit ferromagnetism, among others Fe, Co or Ni. Since ferrite-magnetite oxide (Fe_3O_4) is the most magnetic of all natural minerals in the earth, it is widely used in the form of superparamagnetic nanoparticles for all kinds of biological applications (Akbarzadeh *et al.*, 2012; Chamé, 2013; Rockenberger *et al*., 1999).

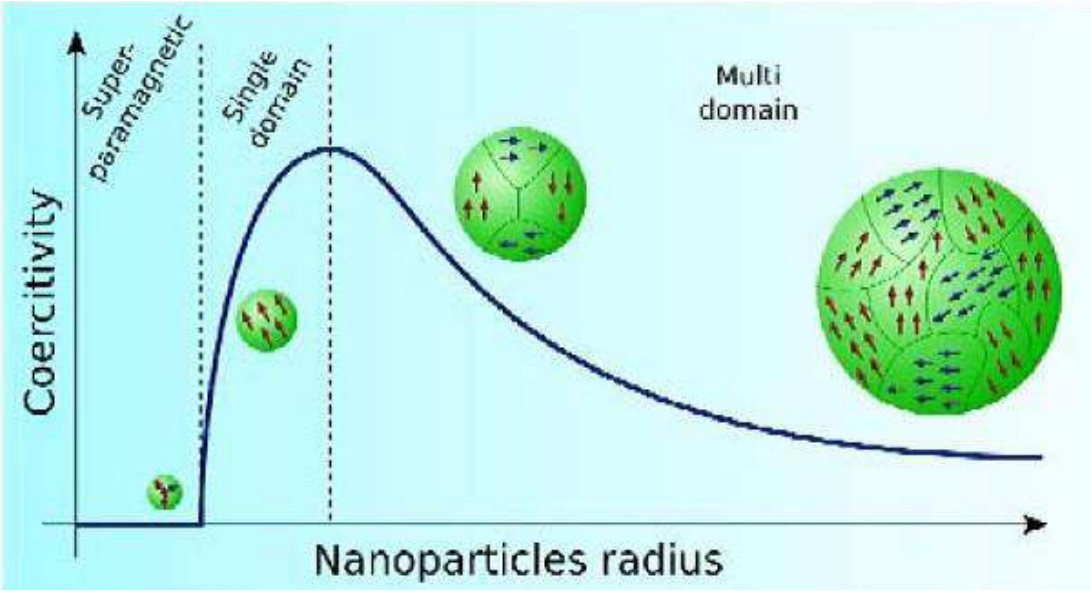

Figure I.13: Coercivity-size relations of small particles (extracted from Akbarzadeh *et al.*, 2012).

Materials are classified by their response to an externally applied magnetic field. There are different basic types of magnetism, according to the behavior of the orientations of the magnetic domains:

- *Diagmagnetism:* In the presence of an externally applied magnetic field, the atomic current loops created by the orbital motion of the electrons respond to oppose the applied field. All materials show this kind of weak repulsion to a magnetic field known as diamagnetism. However, diamagnetism is very weak and, therefore, any other form of magnetic behavior of the material can

overcome the effects of current loops (Akbarzadeh *et al.*, 2012). The magnetic moments are in an antiparallel way canceling the magnetism. They are non-magnetizable materials, not attracted but slightly repelled by a magnetic field (Chamé, 2013).

- *Paramagnetism:* Materials that have ferromagnetism have aligned atomic magnetic moments of equal magnitude, and their crystalline structures allow direct coupling interactions between moments, which can greatly increase the flux density (for example, Fe, Ni and Co). In addition, the moments aligned in ferromagnetic materials can confer a spontaneous magnetization in the absence of an applied magnetic field. Materials that retain permanent magnetization in the absence of an applied field are known as hard magnets (Akbarzadeh *et al.*, 2012). The paramagnetic materials are weakly attracted by a magnetic field and have a small tendency to magnetization. Among them we have: Aluminum, magnesium, molybdenum, lithium, chromium, platinum, copper sulphate, tin, potassium, and others (Chamé, 2013).
- *Ferromagnetism:* Electrons interact through an exchange mechanism in the case of metals (metal oxides), causing a strong increase in magnetic flux density. Ferromagnetic materials are easily magnetized, strongly attracted by a magnetic field and able to retain their magnetization after the magnetizing force has been removed (hard magnets). Among them we have: iron, nickel, cobalt, gadolinium, most steels, cobalt and nickel alloys, and copper, manganese and aluminum alloys (Katia Caamaño, 2016).
- *Superparamagnetism:* Magnetic moments are easily oriented in the presence of a magnetic field, but immediately lose their orientation by eliminating the field (eliminating a remaining magnetization) (Chamé, 2013).

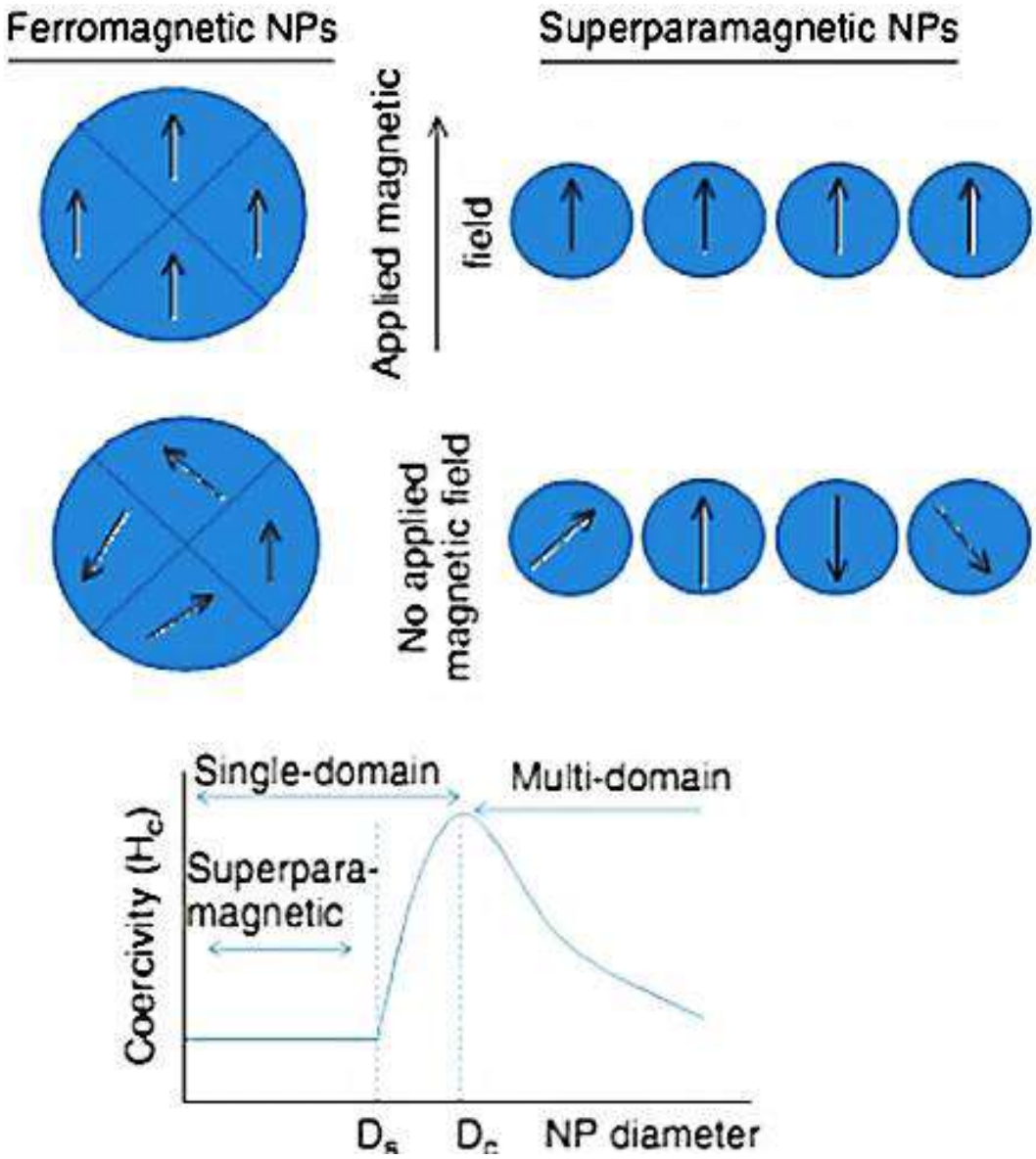

Figure I.14: Magnetization behavior of ferromagnetic and superparamagnetic MNPs under an external magnetic field. Ds: superparamagnetism threshold, and Dc: critical size threshold (extracted from Akbarzadeh *et al*., 2012).

The **Figure I.14** shows that under an external magnetic field, domains of a ferromagnetic nanoparticles align with the applied field. The magnetic moment of single domain superparamagnetic nanoparticle aligns with the applied field. In the absence of an external field, ferromagnetic nanoparticles will maintain a net magnetization, whereas superparamagnetic nanoparticles will exhibit no net magnetization due to rapid reversal of

the magnetic moment. In addition, the curve shows the relationship between nanoparticle size and the magnetic domain structures (Akbarzadeh *et al*., 2012).

B. Synthesis of magnetic nanoparticles.

The synthesis of magnetic nanoparticles are developed with the aim of obtaining a uniform material, predictable reproducibility and control of their properties based on the manipulation of the parameters of the synthesis. The synthesis techniques can be divided into processes that produce particles from solutions (precipitations, coprecipitations, microemulsions and polyol), from aerosol/vapor phases (pyrolysis by pulverization and pyrolysis by laser), and those that produce compounds of nanoparticles consisting of magnetic particles surrounded by organic and inorganic matrices. One of the most important factors during the synthesis of nanoparticles is the control of the particle size, the size distribution and the reduction of particle agglomeration (Warren, 2013).

- Precipitation.

Precipitation is a method to synthesize uniform particles, where there are two stages: nucleation and growth of the particle nuclei. It is observed that in a homogeneous precipitation, nucleation is rapid when the solute concentration reaches a critical point of supersaturation. Subsequently, the formed nuclei grow uniformly by diffusion of the solute from the solution to the surface. According to the model presented by LaMer and Dinegar, particles with a uniform size distribution are obtained, if the nucleation and growth process are separated **(Figure I.15)** (LaMer and Dinegar, 1950).

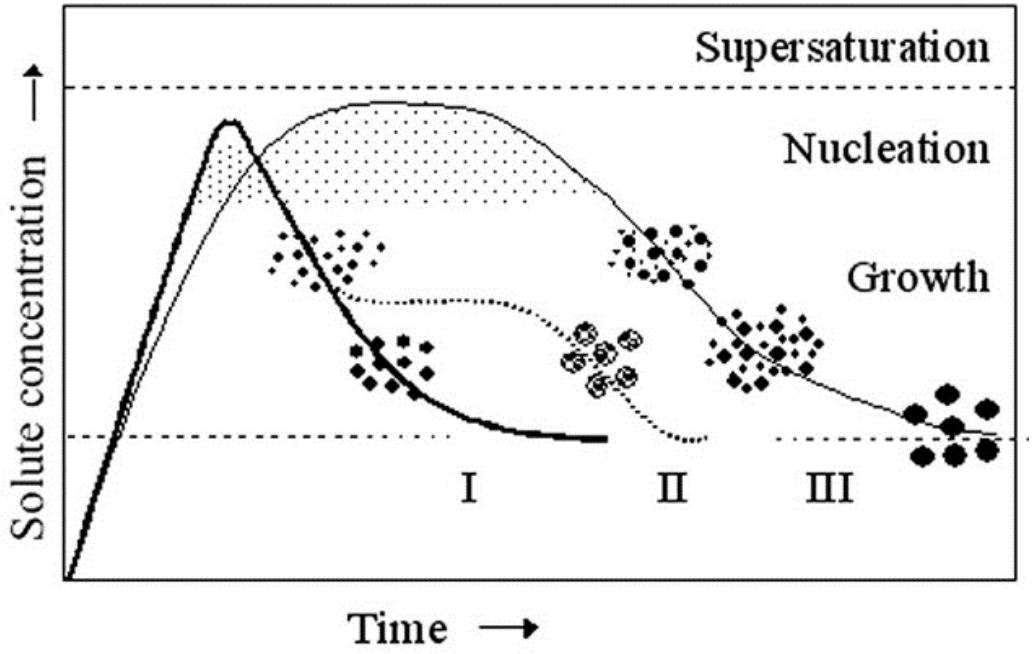

Figure I.15: LaMer and Dinegar model of particles nucleation and growth (LaMer and Dinegar, 1950).

The **Figure I.15** indicates that nucleation occurs in a very short period; then the solute must be supplied slowly for growth of the particle, without it oversaturating the solution, to avoid additional nucleation (curve I). Another way is by placing the newly formed cores in a solution containing solute below the critical point of supersaturation (curve II). On the other hand, the formation of larger particles can occur at the expense of the smaller particles (curve III) (LaMer and Dinegar, 1950; Warren, 2013). This is known as the maturation of Oswald, where the molecules on the surface are less stable than those in the interior, generating a difference in energy. But the system will try to decrease its total energy, causing the atoms on the surface to leave the largest particle. As a result, the solution becomes saturated with the small particles, and these are re-deposited on the surface of the larger particles. This behavior of contraction and growth of the particles generates larger diameter particles averaged. Over time, the particles become a large particle to minimize the total surface area. This means that there is an indirect relation between the particle size and the proportion of atoms on the surface of the particles (**Figure**

I.16) (Cambier, 2006; Warren, 2013). Thus, larger particles promote a lower energy state of the solution. Therefore, the solution will decrease its total energy because the smaller particles are bonded to the surface of the larger particles. Finally, a solution with a relatively homogeneous particle size distribution will be obtained; however, this also generates an agglomeration of the particles. This may occur during synthesis, drying or post-synthesis processing. Therefore, it is important to use a compound that covers the surface of the particles (shell) to avoid agglomeration. For example, surfactants can be used during synthesis to increase repulsive forces between particles (Warren, 2013).

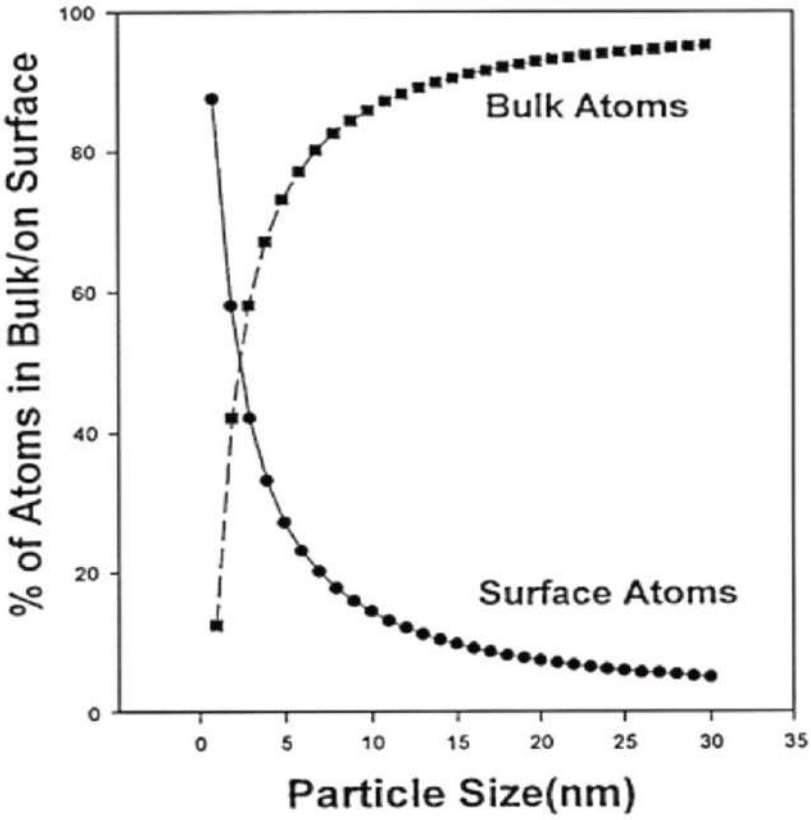

Figure I.16: Indirect relation between particle size (nm) and percentage of atoms on particle surface (Cambier, 2006).

- **Co-precipitation.**

Coprecipitation is a simple, economical and effective method for the synthesis of magnetic nanoparticles of iron oxide. This method consists in a stoichiometric mixture of

ferrous and ferric salts in an aqueous alkaline solution. According to the thermodynamic energy of the reaction, the complete precipitation of Fe_3O_4 occurs at a pH between 8 and 14, in a non-oxidizing environment. The stability of size and shape of the nanoparticles obtained depending on the type of salt used, the ratio of ferric and ferrous ions, reaction temperature, pH values, ionic strength of the medium and other reaction parameters such as, the agitation speed and the rate of addition of the basic solution (Katia Caamaño, 2016; Sánchez Paradinas, 2013). It has been shown that by adjusting the pH and the ionic strength of the reaction solution, it is possible to control the average particle size from 2 nm to 15 nm. This is because by increasing the pH and the ionic strength of the reaction solution, there is a general trend in the reduction of the nanoparticle size. This can be explained because the pH and the ionic strength affect the composition of the surface and the surface charge of the particles (Thapa *et al.*, 2004; Warren, 2013).

$$Fe^{2+} + 2Fe^{3+} + 8OH^- \rightarrow Fe_3O_4(\downarrow) + 4H_2O$$

MNP synthesis under nitrogen or argon gas is important because exposure to the ambient atmosphere causes the surface of the Fe_3O_4 nanoparticles to be often covered with a multilayer of α-Fe_2O_3 (hematite) and monolayers of surface hydroxyl and water physically adsorbed (Ali *et al.*, 2016; Smit, 2018; Unsoy *et al.*, 2015).

- **Thermal decomposition.**

This type of reaction is based on decomposition processes of compounds in organic solvents at high temperatures. In order to increase the size of these nanoparticles, higher boiling solvents can be used, which can reach up to 20 nm of core size (Katia Caamaño, 2016).

C. Stabilization of Magnetic Particles.

Size stabilization of the nanoparticles is a very important factor to avoid their aggregation, and thus be able to be used in biological applications. However, other factors like the type and concentration of salts, ionic strength of media, reaction temperature, can influence the size, the shape and the magnetic properties of MNPs (Unsoy *et al*., 2015). Stabilizing particles means balancing the forces of attraction and repulsion. Stabilization can be easily achieved by exploiting these forces by encapsulating the particles in organic and inorganic matrices (Warren, 2013). In order to avoid destabilization due to the formation of aggregates, or attraction forces between the magnetic nanoparticles, the iron oxide cores must have a suitable surface coating (ligands or biocompatible polymers). However, in some cases the saturation magnetism becomes weaker when a shell is used. The most commonly used coatings in the preparation of biocompatible iron oxide suspensions are polymers such as polyethylene glycol (PEG), carboxymethylated dextran, dextran, arabinogalactan, glycosaminoglycan, polyvinyl alcohol, polyoxamines, alkoxy silanes, etc (Demin et al., 2013; Makovec et al., 2015). In the case of the dextran coating, it is suggested that the main mechanism of adsorption is the formation of multiple hydrogen bonds between the hydroxyl groups of the dextran molecule and the surface of the iron oxide particles (Rodríguez, 2014).

On the other hand, to control the reactivity of the iron nanoparticles with the air (pyrophoric), the nanoparticles have been alloyed with a less reactive metal layer, to serve as an oxygen barrier. For example, iron-platinum nanoparticles or iron particles coated with gold, gadolinium and magnesium. Although gold is ideal because of its inertia towards oxidation and its ability to easily functionalize a variety of thiol groups on the surface; it has been observed that iron nanoparticles coated with gold are magnetically weak (Lin *et al.*, 2001).

On the surface of the iron nanoparticles the hydroxyl functional groups can be observed with two pairs of isolated electrons together with a dissociable hydrogen atom, allowing an

'acid-base' behavior of the particles. This means that the iron particles are amphoteric, therefore it is important to know the surface charge for the stabilization of the particles, as well as their reactivity with other ligands (Tamura *et al.*, 1999).

The charged surface of the hydrodynamic layer surrounding a nanoparticle has two parts: internal region (Stern layer), with strong bonds between the ions; external region (diffuse), with ion-free binding. However, there is a limit inside the diffuse layer where the ions of the particles stabilize. It means, that the ions move within this limit when the nanoparticles move in the solution. Ions that are above the limit tend to stay behind in the bulk fluid. The potential in this limit is called zeta potential; which predicts the stability of the colloidal system **(Figure I.17).** For example, in a particle suspension a high negative or positive zeta potential prevents the nanoparticles from aggregation and/or precipitating. An important factor that affects the zeta potential in iron oxides in solution is pH. The zero-charge point (isoelectric point) (pH range 6-10) of an iron oxide is equal to the pH at which the charge at the surface is zero. It means that at this pH there is an equilibrium between the adsorbed compounds with positive charge and with a negative charge on particle surface. In this sense, at a pH lower than the point of zero charge, the $FeOH^{2+}$ group will predominate on the surface of the particle; but when the pH increases the FeO^{-} groups increase. At the zero charge point, the $FeOH^{2+}$ number will be equal to the FeO^{-} number (Shaw, 1992).

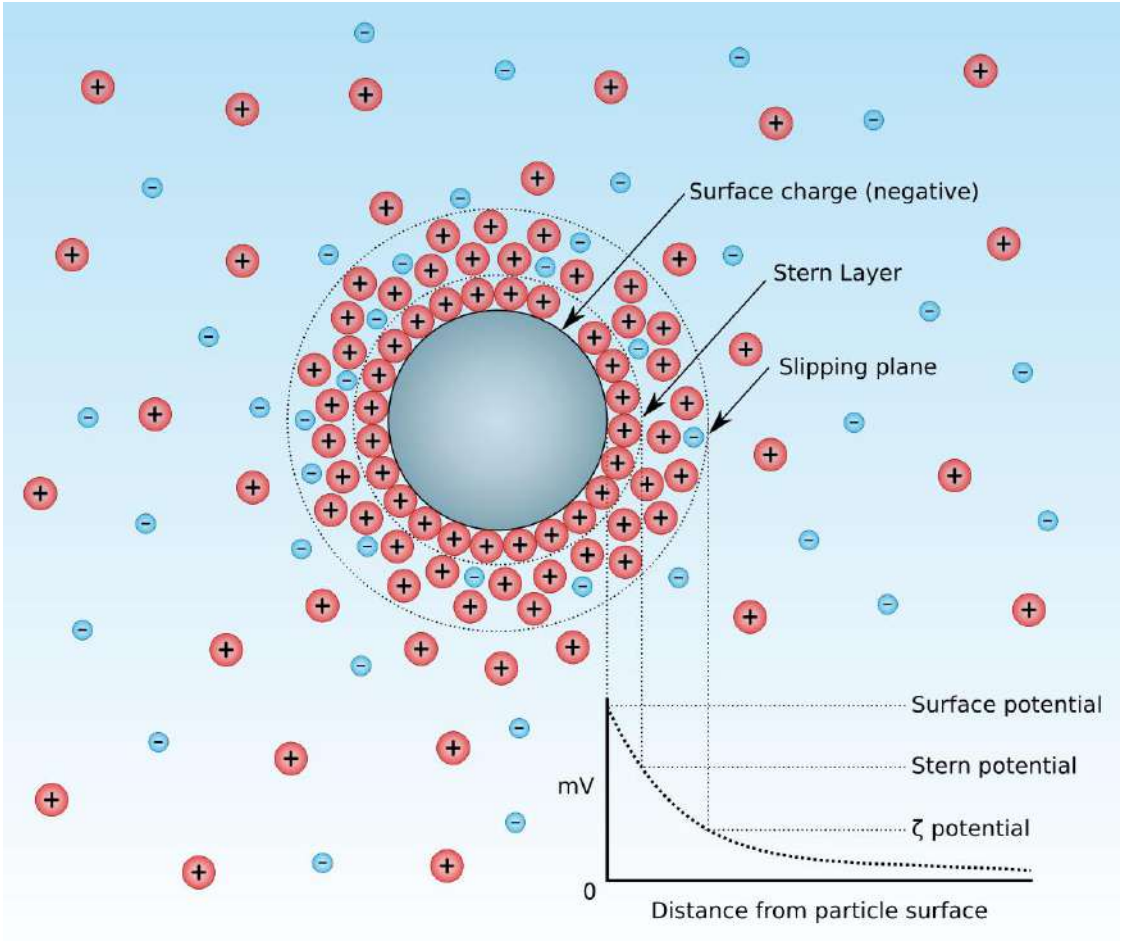

Figure I.17: Zeta potential of magnetic nanoparticles surface.

The inorganic and organic coatings of the surface of the particles, allows to produce particles with important properties that the uncoated particles lack. The polymers with opposite charge to the surface of the nanoparticles, can be gradually adsorbed to form a layer-by-layer accumulation on the particles. Polymer coatings prevent aggregation of the particles, protect the surface from oxidation and reduce toxicity. The coatings can be made during the synthesis (*in situ*) or after the synthesis.

At the same time, the iron oxide particles have been coated with inorganic compounds that make them more stable in solution and allows the immobilization of biological ligands to the surface of the particle. For example, by using silane groups on the particle surface, many specific ligands (bio-molecules) can be coupled. This is because

silane groups improve chemical stability and also provide protection against toxicity. For the amino-silanization, the (3-aminopropyl) tri-etoxysilane compound (APTES) is mostly used, since it allows the coupling of silanes, and exposes amino groups on the surface of the magnetic iron oxide nanoparticles. This allows a broad use of these nanoparticles in biological applications, such as bioseparation, in diagnosis as an MRI contrast agent, in the transport of magnetically controlled drugs and in hyperthermia. In this sense, knowing and controlling the characteristics and physical-chemical properties of nanoparticles is of great importance (Ito *et al*., 2005; Liu *et al.*, 2013). The coating of the particles with silica can be carried out by hydrolysis and condensation of a precursor (tetra-ethyl-orthosilicate, TEOS) (Strober method). On the other hand, a silicic acid solution can be used for the deposition of silica on the surface. Finally, micelles can also be used to confine and control the coating of the iron nanoparticles with silica (Barnakov *et al.*, 2005; Warren, 2013).

Liu *et al* (2013), reported that although the kinetics of the formation of layers of the Fe-O-Si bond between the nanoparticles is relatively simple, precise control of the formation of layer quality has been a difficult task. Silane binding can exist in physisorption, hydrogen bonding or electrostatic binding, or covalent binding. In addition, one or more layers can be formed on the surface, and this can influence the binding of biomolecules (Acres *et al*., 2012).

The general silanization sequence follows by the hydrolysis of the triethoxyl groups into trihydroxyl groups and then the polycondensation of the hydroxyl groups with the surface hydroxyl groups of the MNP surface. However, different reactions can occur that generate heterogeneous layers on the surface of the nanoparticles **(Figure I.18)**. For example, after hydrolysis, the silanol groups can react with the hydroxyl groups on the surface, leading to silanization of the surface. The ligands immobilized on the surface are then condensed with neighboring silanol groups which form a monolayer or a highly branched polycondensed structure. This can be controlled by using different solvents in the

silanization reaction, as well as different temperatures in a slow incubation process (Liu *et al*., 2013).

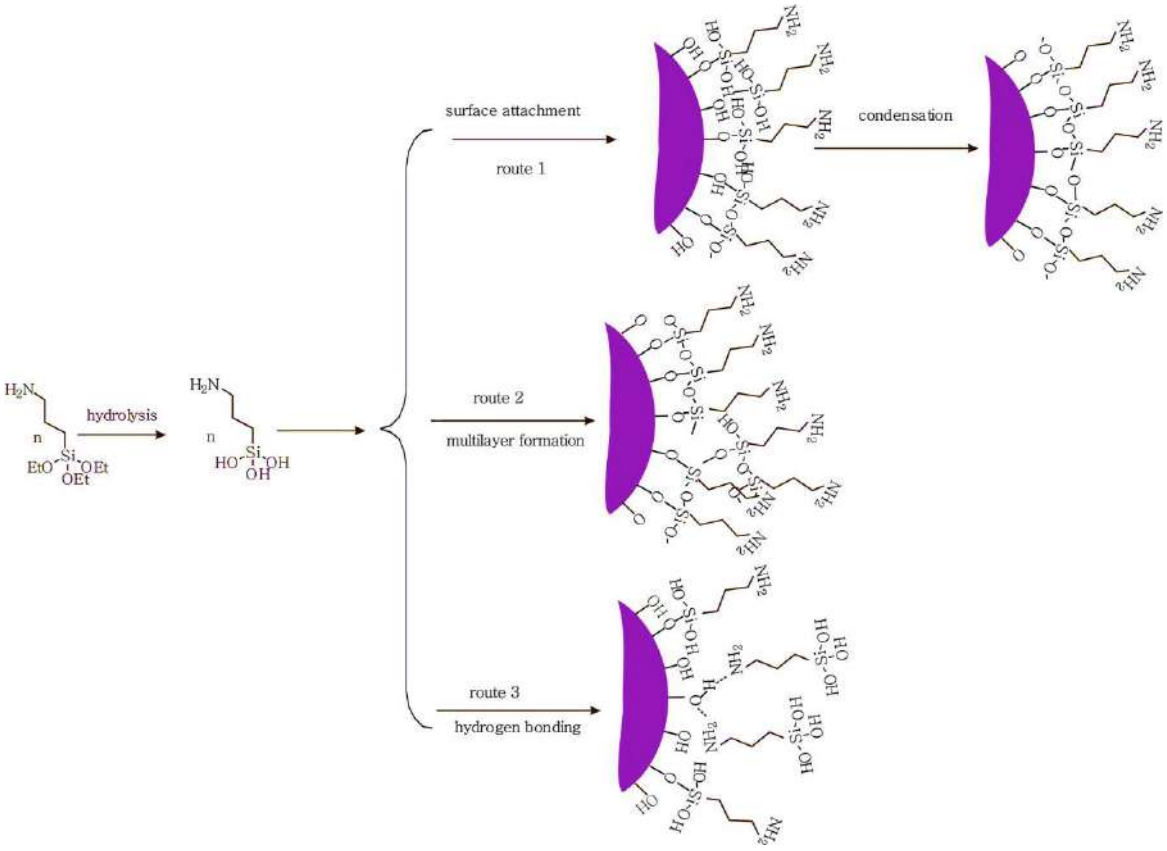

Figure I.18: Possible reaction routes of amine- silanization using APTES on magnetic nanoparticle surfaces (extracted from Liu *et al*., 2013).

I.3.2. Biomedical applications.

A. Drug delivery.

Studies of drug administration to a specific target have increased dramatically in recent years **(Figure I.19)**. The iron nanoparticles loaded with the drug in combination with an external magnetic field are transported to the specific organ and / or tissue. At the local site, the media is released and acts locally (magnetic orientation of medicines). This can eliminate side effects as well as reduce the dose of the medication (Gupta *et al*., 2007).

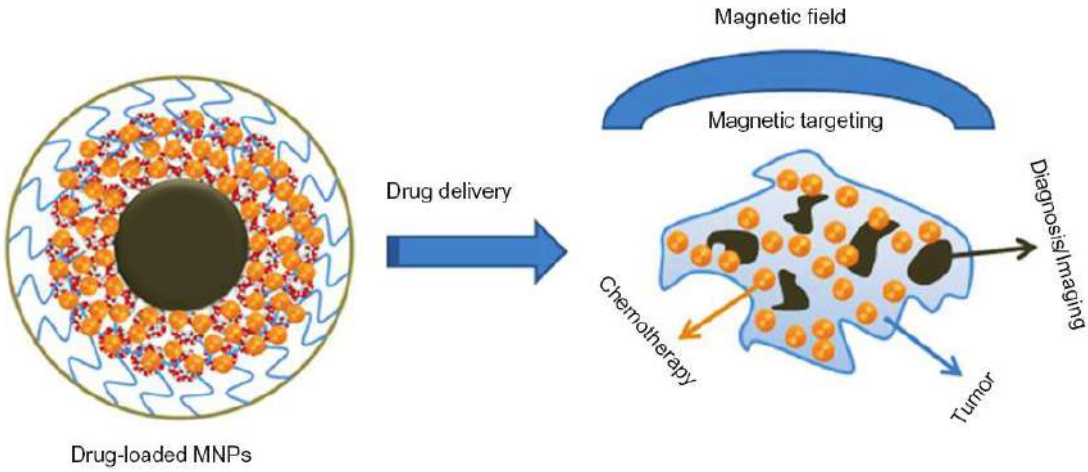

Figure I.19: Applications of drug-loaded MNP in tumor tissue (Yallapu *et al.*, 2012).

B. Hyperthermia.

It consists in the manipulation of the magnetic field of the superparamagnetic iron oxide to allow the transfer of magnetic energy in the form of heat, generating for example an increase in the temperature of tumor tissues to destroy pathological cells by hyperthermia. The principle is that tumor cells are more sensitive to temperature rise than healthy cells (Behrouzkia *et al.,* 2016). The advantage of magnetic hyperthermia is its focused action to the tumor area. In addition, nanoparticles (single domain) are preferable to microparticles (multidomain), because the former absorbs much more energy and does not have magnetic remanence (Kim *et al.*, 2006).

C. Magnetic Resonance Imaging (MRI).

Magnetic resonance imaging (MRI) is a powerful tool used for noninvasive molecular and cellular imaging. MNPs have been examined extensively as MRI contrast agents to improve the detection, diagnosis, and therapeutic management of solid tumors (Conroy *et al*., 2008)

There are three groups of contrast agents: T1 agents provide positive contrast (bright signal) by shortening the longitudinal relaxation time of surrounding water molecules, T2 agents (black signal) shorten the transverse relaxation time of water protons, and the chemical exchange saturation transfer (CEST) (Mao *et al*., 2017).

In addition, the biocompatibility and versatility of the chemistry that can be carried out on its surface of the MNPs, are added advantages. The contrast agent with enhancement in T2 is the most used in MRI, darkening the tissues in which they accumulate (Cheng *et al*., 2015; Herranz *et al.*, 2014). However, the black signal it provides is, in many cases, complicated to identify in the presence of hypointense signals (bleeding, presence of Ca^{2+}, etc.). For this reason, contrast agents with T1 enhancement are gaining popularity (Bhavesh *et al*., 2015).

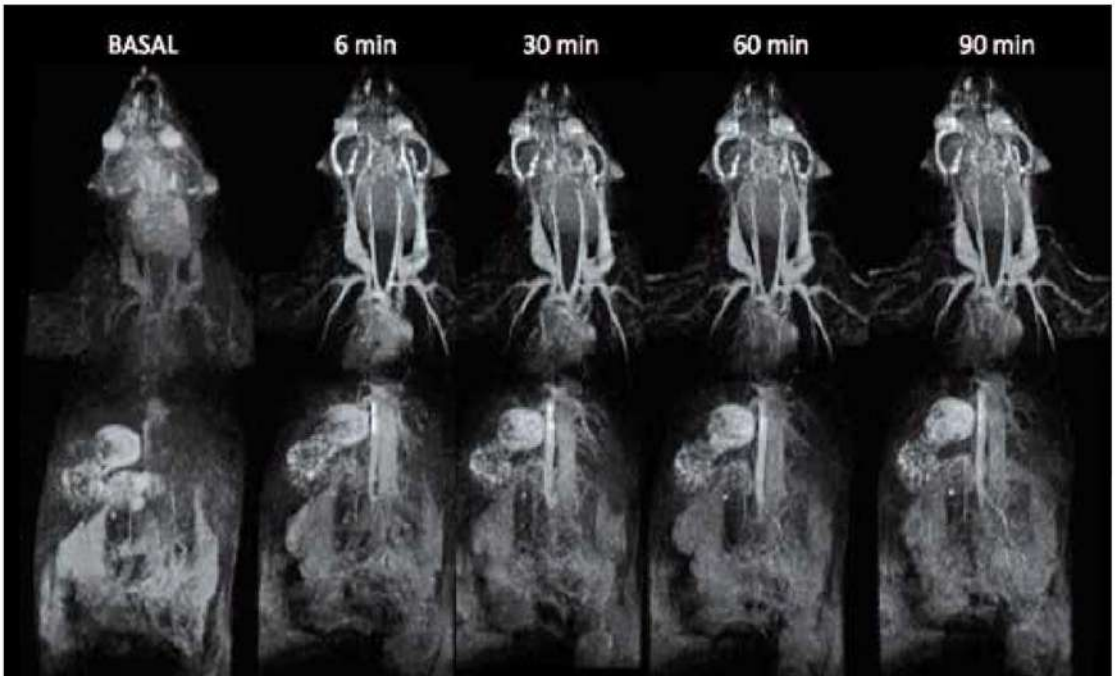

Figure I.20: Magnetic resonance angiography in mice before and several times after the injection of iron oxide nanoparticles as T1 contrast agents (Bhavesh *et al.*, 2015).

Bhavesh *et al*. (2015) reported fluorescein-labeled extremely-small iron oxide nanoparticles (fdIONP) for cell labeling and T1-MRI. The small nanoparticles coated with

FITC-CM Dextran (4 kDa) were produced in a single step using fast microwave assisted method (Bhavesh *et al*. 2015). The nanoparticle synthesized (TEM: 2.5 ± 0.2 nm and DLS: 21.5 nm) had a negative surface charge (−15.8 mV) and magnetite and maghemite in their composition. These fdIONP were used for *in vivo* positive contrast MRI in mice **(Figure I.20)**, demonstrating to be efficient due their small size and biocompatible surface coating (Bhavesh *et al*., 2015).

Similarly, hybrid nanoparticles have been developed in recent years, as well as liposomes conjugated with contrast agents to improve MRI (Mao *et al.;* 2017).

D. Bio-separation.

This application is widely used for the separation of specific biomolecules (DNA, proteins, viruses and cells) from their native environment. For this application it is preferred to use superparamagnetic colloids because it has no magnetic remanence, allowing the transport of biomolecules with a magnetic field. One of the trends is magnetic separation using antibodies to specifically capture their corresponding antigens on the surface of the target species (Maximilien *et al.*, 2015; Jesse *et al.*, 2015) **(Figure I.21)**.

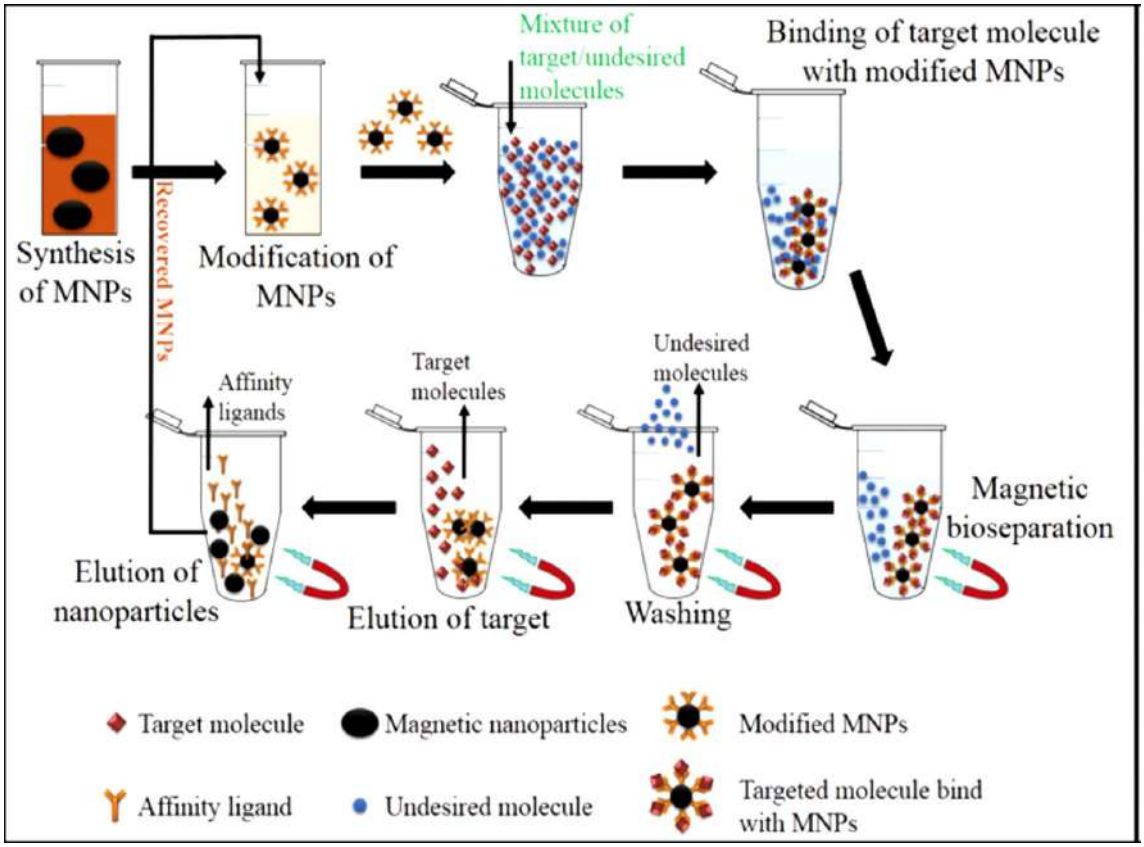

Figure I.21: Bio-separation of biomolecules using magnetic nanoparticles (Hira and Kyo-seon, 2017).

Magnetic bioseparation has been widely researched for biomedical applications, since the method is simple, robust and versatile, in addition to the important properties of MNP, such as low toxicity, biocompatibility and large surface to volume ratios (Maximilien *et al.*, 2015). On the other hand, the whole process can take place in a single test tube, it is enough to use functionalized nanoparticles and a magnetic force that allows the separation of specific molecules (Hira and Kyo-seon, 2017).

I.3.3. Applications of magnetic nanoparticles in tuberculosis diagnosis.

Currently, MNPs have been introduced in different strategies to improve TB diagnosis. However, many of these methods have not yet been massively implemented because more field studies are required or that technique implementation demands a higher cost due to the technology used for these assays (Lawn, 2015).

Cheon *et al*., 2019 reported a specific DNA-aptamer to recognize an antibody (Cheon *et al*., 2019). They developed a colorimetric biosensing system to capture the anti-MPT64. The strategy is based on the immobilization of a specific single stranded (ss) DNA-type aptamer, capable to detect anti-MPT64, on MNP surfaces (diameter: 13 nm). After, a solution containing anti-MPT64 was incubated with MNP-aptamer. The anti-MPT64 hijacks the specific DNA aptamer, exposing the Fe_3O_4 core of MNPs, which can oxidize a peroxidase substrate (ABTS + H_2O_2). The reactions were measured at 417 nm UV-vis absorbance **(Figure I.22)**. In general, because the aptamer covered the core surface of the MNP, the oxidation of the substrate was reduced (weak color signal). But when the MNP-aptamer was incubated with the antibody, by competition the anti-MPT64 entrained the aptamer leaving the surface of the MNP naked. Consequently, this allowed a greater oxidation of the peroxidase substrate (strong color signal) (Cheon *et al.*, 2019).

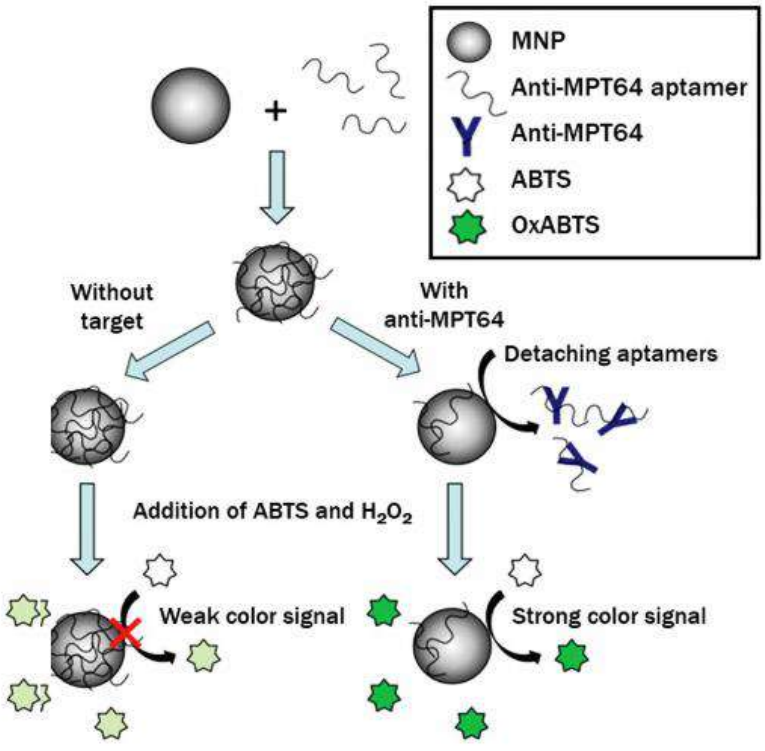

Figure I.22: Schematic illustration of the colorimetric detection of antiMPT64 based on an aptamer adsorbed MNPs. **ABTS:** 2,2′-azino-bis(3-ethylbenzo-thiazoline-6-sulfonic acid. (extracted from Cheon *et al*., 2019).

Bhusal *et al* 2019, reported a nanoparticle-based colorimetric biosensing assay (NCBA) to detect acid-fast bacilli (AFB) in decontaminated sputum samples (Bhusal *et al* 2019). Basically, the strategy was to isolate AFB from decontaminated sputum samples using the glycan-coated magnetic nanoparticles (GMNP). The GMNP-AFB complex was separated using a magnet. The complex was stained and observed under a light microscope **(Figure I.23).** The GMNP captures MTB cells through glycan-glycoprotein interaction, because the MTB cell envelope is rich in complex carbohydrates and glycoproteins that bind with the GMNP. Although glycan-glycoprotein interaction is not specific only to pulmonary TB, it is observed that environmental and non-pathogenic mycobacteria are usually absent in TB sputum samples. The method was able to detect 10^2 CFU/mL. Also, NCBA was validated with 500 sputum samples from TB patients, with an accordance of 100 % of sensitivity with the Xpert system. (Bhusal *et al*., 2019).

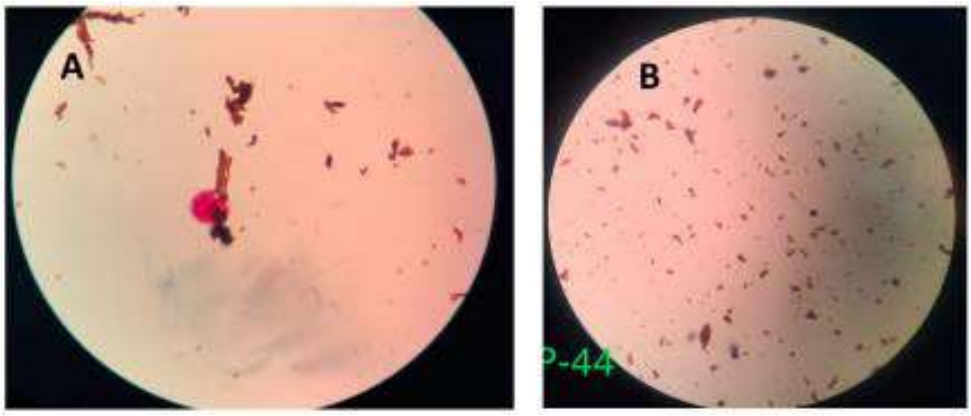

Figure I.23: Detection of MTB using MNP. TB positive sample: GMNP-AFB complex (corded and agglomerated) **(A)**. TB negative sample: Dispersed brown GMNP **(B)** (extracted from Bhusal *et al* 2019).

Another example is the magnetophoretic immunoassay (MPI) designed to capture CFP10 antigens using gold and magnetic nanoparticles. For antigen recognition, two specific monoclonal anti-CFP10 (G2 and G3) were immobilized on the nanoparticle surface. The gold NPs (diameter: 55 nm) were used for signaling, and the gold clusters on magnetic nanoparticles were used for separation **(Figure I..24).** The detection limit of the

method was 0.3 pM, and it was able to detect specifically CFP10 in MTB culture from day 3. The method had sensitivity and specificity of 88.4%, and 80.9%, respectively. However, this method showed cross reaction with CFP10-like proteins present in non-tuberculous mycobacterial clinical isolates, resulting in false-positives (Kim *et al*., 2017).

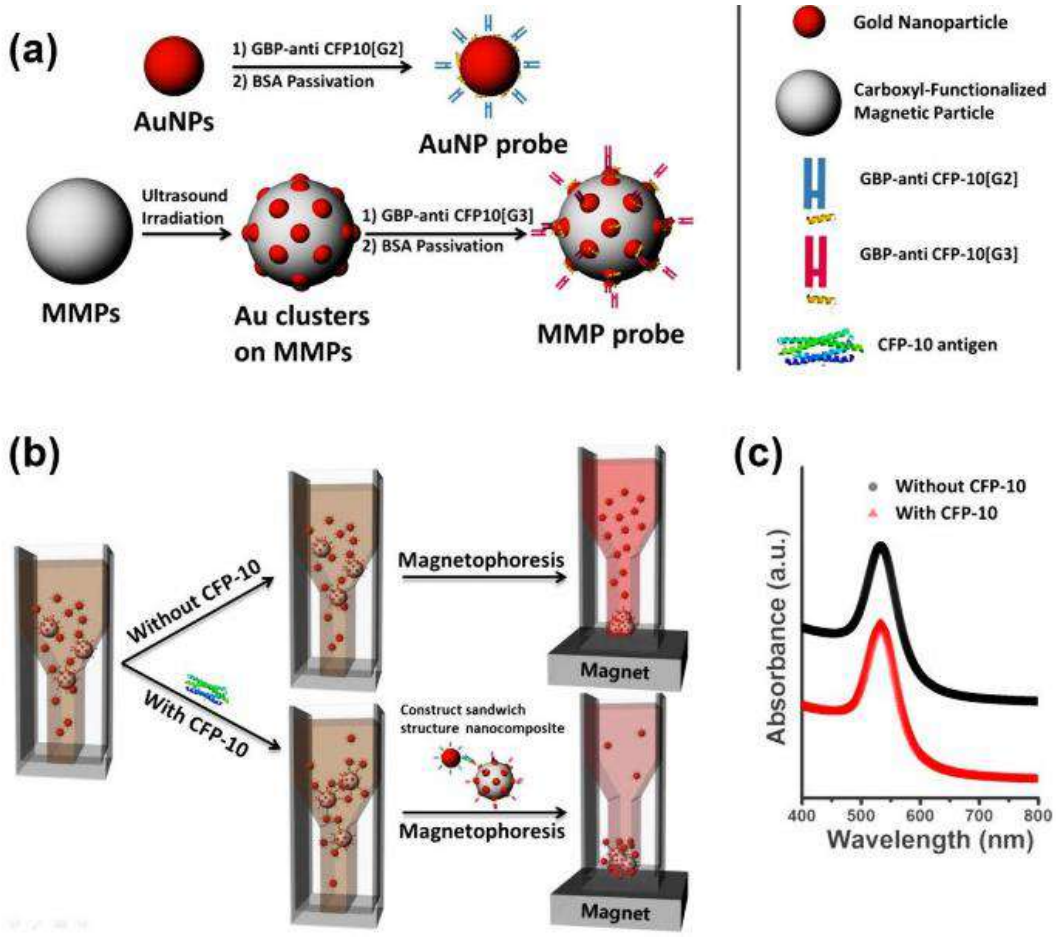

Figure I.24: Magnetophoretic immunoassay for TB diagnosis. Preparation of two different probes: Au NPs were conjugated with anti-CFP10[G2] while Au cluster on MMPs were conjugated with anti-CFP10[G3] **(A)**. Antigen detection strategy: CFP10 was detected for both probes, forming a plasmonic sandwich immunocomplex. Using a magnet, the structures are captured. In CFP10 absence, no interactions occur between the two probes, therefore only MMP probes are removed **(B)**. Measurement of remnant Au NP probes: Concentration of the colorimetric gold nanoparticles-anti-CFP10[G2] present in the supernatant is quantified using UV-Vis spectrophotometry **(C)** (extracted from Kim *et al.*, 2017).

In summary, there are several studies where nanoparticles have been used in different strategies to improve the diagnosis of TB. In many cases, the results proved promising, so the application of nanotechnology to improve the sensitivity of infectious diseases diagnosis is effective. However, there are still many other methods and MTB biomarkers that have not yet been evaluated with nanoparticles, and which are described in this study.

I.4. Hypothesis and objectives of the research.

I.4.1. Hypothesis.

The coupling of functionalized magnetic nanoparticles with polyclonal antibodies would improve the ability of a sandwich ELISA to detect secretory antigens of *M. tuberculosis* from sputum samples of TB patients.

I.4.2. Objectives.

General Objective.

Develop a sandwich ELISA associated with magnetic nanoparticles to capture and detect recombinant and native *M. tuberculosis* antigens from sputum samples of patients with tuberculosis.

Specific Objectives.

i. Select, clone, express and purify superficial and secretory recombinant antigens of *Mycobacterium tuberculosis*, in the bacterial system *Escherichia coli* BL21 (DE3) pLysS.

ii. Produce specific polyclonal antibodies for *M. tuberculosis* recombinant antigens in New Zealand rabbits and BALC/C mice and evaluate the antibodies production in a direct colorimetric ELISA assay.

iii. Synthesize, amine-silanize and characterize the physical-chemical properties of modified iron magnetic nanoparticles (MNPs) using Transmission Electronic Microscopy (TEM), X Ray Diffraction (XRD), Dynamic Light Scattering (DLS), Vibrating-Sample Magnetometry (VSM), Fourier-transform infrared spectroscopy (FTIR), Mössbauer Spectroscopy (MS) and Thermogravimetric analysis (TGA).

iv. Bio-functionalize the magnetic nanoparticle surfaces using Bovine Serum Albumin (BSA) and specific polyclonal antibodies, to develop a sandwich ELISA associated with MNPs to bio-recognize MTB antigens (recombinant proteins, negative and positive sputum pools from confirmed patients).

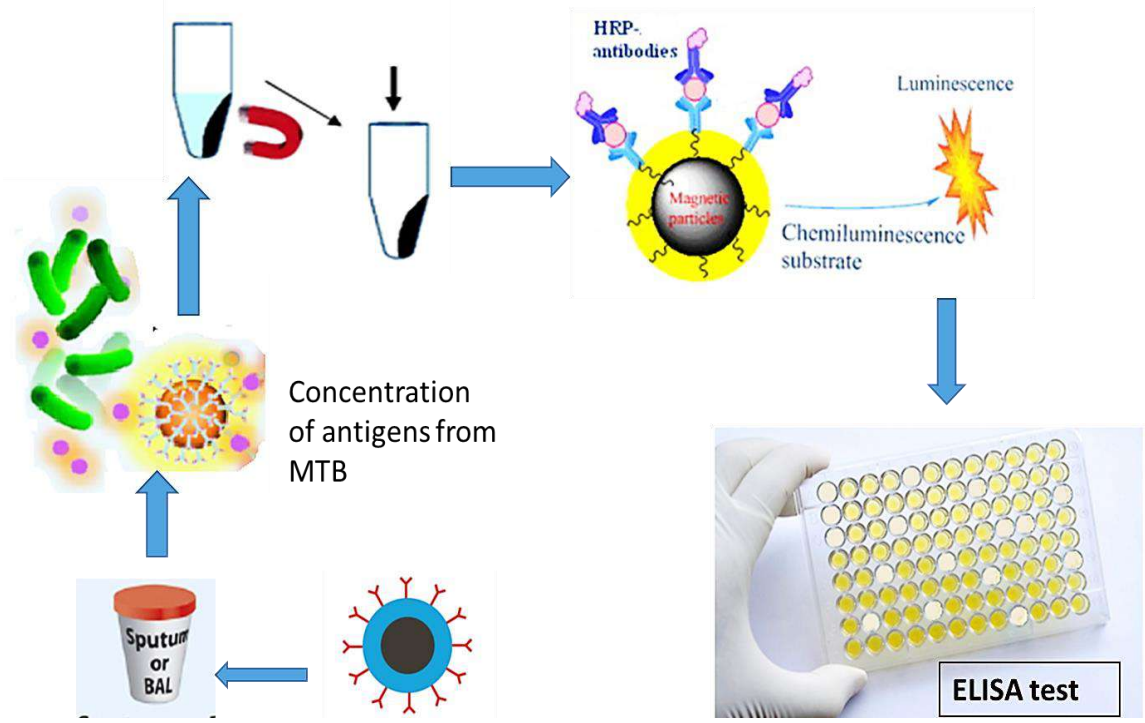

Figure I.25: Development of an ELISA assay associated with magnetic nanoparticles (MNPs) to detect *Mycobacterium tuberculosis* (MTB) antigens from sputum samples of patients with TB. The nanoparticles are functionalized with specific antibodies, which will capture MTB antigens. Using a magnet, the detected antigens will be concentrated, which

through a colorimetric assay (ELISA) will determine the presence (change of color) or absence of MTB antigens in the biological samples.

NOTE:

The doctorate is part of a collaboration program (cotutelle) between the Peruvian University Cayetano Heredia (UPCH) and the University of Bordeaux (UBx). Due to the domains covered in this research, and in compliance with the guidelines of both universities, the doctoral thesis presents a structure with the objective that it can be easily understood by professionals from different scientific fields.

Each chapter has been divided into 4 subchapters: narrative description, experimental section (methodology), results and discussion. The structure of narrative description - experimental section is a format widely used in the domain of chemical sciences, while the structure of methodology - results - discussion is a standard format in the area of biology. In each chapter, the narrative description shows merged results and discussion. The experimental section (methodology) describes the materials and methods used in this chapter. The results and discussion sections have the same content as the previously described narrative description, but they are separated. This means that reading the narrative description - experimental section (methodology) is the equivalent of reading experimental section - results - discussion.

Despite the redundancy of information between narrative section and results – discussion, this format is justified for easy understanding for chemists (narrative section - experimental section) and biologists (experimental section - results - discussion).

Chapter II: Selection, cloning, expression of recombinant MTB antigenic proteins and production of polyclonal hyperimmune antibodies.

Chapter II

Selection, cloning, expression of recombinant MTB antigenic proteins and production of polyclonal hyperimmune antibodies.

Abstract:

Introduction: Secretory and superficial MTB proteins, which have not been evaluated in sputum samples yet, were considered in this study. The selected recombinant proteins from *M. tuberculosis* were: rHsp16.3, rMPT64, rMTC28, rMoeX, r38 kDa protein, rAg85B, rESAT6, and rCFP10.

Methodology: Recombinant MTB proteins were selected, amplified, cloned and expressed in *E. coli* BL21 (DE3) pLysS, using as inductor IPTG. Almost all proteins were induced at 37 °C, overnight (ON), however rHsp16.3 and rCFP10 proteins were expressed at room temperature (RT), ON, while rESAT6 was expressed at 37 °C for 4 h. The IPTG concentration was 0.5 mM, except in MTC28 (0.6 mM), rAg85B, rMoeX and rESAT6 (0.65 mM) and in r38kDa (0.8 mM). The expressed proteins, tagged with 6xHis, were purified by affinity chromatography using HisTag columns. Purified recombinant MTB proteins were used for the immunization of New Zealand rabbits and BALC/C mice to produce polyclonal hyperimmune antibodies. The elicited antibodies over time were evaluated by an indirect ELISA. The sera dilution standardization was performed in an indirect ELISA and in a sandwich ELISA to evaluate the capacity of detecting the selected proteins.

Results: All recombinant proteins were successfully produced in *E. coli*. A production of high titers of polyclonal antibodies for each purified recombinant antigen was observed. In the case of antibody evaluation using the sandwich ELISA assay, different folds were obtained. In CFP10 and ESAT6 low folds (< 2.0) were observed. The Hsp16.3, MTC28

and 38 kDa presented folds > 2.28. In the case of the specific sera for MoeX, Ag85B and MPT64, the highest folds were observed (> 5.0).

Discussion: The selected proteins: rHsp16.3, rMPT64, rMTC28, rMoeX, r38 kDa protein, rAg85B, rESAT6, and rCFP10, presented promising conditions to be considered as potential antigens for the diagnosis of TB. A high production of polyclonal antibodies was observed in the experimental animals, demonstrating the high immunogenicity of the recombinant proteins. On the other hand, in the sandwich ELISA assays varied folds were observed for each pair of antibodies (rabbit-mouse).

Conclusion: The selected proteins were successfully produced in the bacterial system. The recombinant proteins were immunogenic, elicitating antibodies in both immunized experimental animals.

NOTE:

This chapter has been divided into 4 subchapters: narrative description (**II.1**), experimental section (methodology, **II.2**), results (**II.3**) and discussion (**II.4**). The structure of narrative description - experimental section is a format widely used in the domain of chemical sciences, while the structure of methodology - results - discussion is a standard format in the area of biology. In this chapter, the narrative description shows merged results and discussion. The experimental section describes the materials and methods used in this chapter. The results and discussion sections have the same content as the previously described narrative description, but they are separated. This means that reading the narrative description - experimental section is the equivalent of reading experimental section - results - discussion. Despite the redundancy of information between narrative section (**II.1**) and results – discussion (**II.3** and **II.4**), this format is justified for easy understanding for chemists (narrative section - experimental section) and biologists (experimental section - results - discussion).

II.1. NARRATIVE DESCRIPTION.

II.1.1 Selection of MTB antigens.

The MTB life cycle could be separated into three main stages: latent, reactivating, and active TB (Ottenhoff, 2012). In each stage, a differential MTB gene expression is observed (Zhang *et al.,* 2015). MTB antigens selected in this study are listed in **Table II.1.** To select specific MTB biomarkers inclusion and exclusion criteria were considered:

Inclusion criteria:

- Secretory and non-secretory antigens that have been previously used in diagnostic tests were included, either for the detection of antigens or antibodies.
- Abundant secretory proteins, which are specific for the complex of *Mycobacterium tuberculosis* (MTBC), were included.
- Antigens that have been used in more than two publications related to TB diagnosis were considered.

Exclusion criteria:

- Antigens that have been proven to cross-react with mycobacteria that are not part of the MTBC were excluded.
- Antigens expressed in mycobacteria that are not part of MTBC were excluded.
- Antigens that have not been used in any type of diagnostic method were excluded.

At least one diagnostic test for all selected TB antigens has been described. Most of the tests used for the diagnosis were immunological assays (ELISA) to detect specific human anti-MTB antibodies. However, assays to detect DNA and antigens present in MTB are also described.

Table II.1: MTB selected proteins used in this study.

Protein	Detection	Assay*	Sensitivity and specificity	Ref.
Hsp16.3	Antibody	ELISA,	63.33% and 88.04%	(Zhang *et al.*, 2015)
MPT64	Antibody Antibody Antigen DNA	ELISA, Colorimetric biosensing system, ELISA, PCR	80.5% and 74% Not reported 100% and 100% 74% and 100%	(Wu *et al.*, 2010) (Cheon *et al.*, 2019) (Ji *et al.*, 2014) (Sethi *et al.*, 2012)
MTC28	Antibody	ELISA,	72.4% and 71.4%	(Wu *et al.*, 2010)
MoeX	Antigen Antigen	ELISA MoexX/MoeA Mass spectrometry	Not reported Not reported	(Pollock *et al.*, 2013) (López-Hernández *et al.*, 2016)
38 kDa	Antibody Antibody Antibody	ELISA, Piezoelectric Immunosensors, ELISA ESAT-6/14KD/38KD	79.5% and 74% Not reported 77.6% and 84.3%	(Wu *et al.*, 2010) (Marín *et al.*, 2015) (Zhang *et al.*, 2013)
Ag85B	Antigen Antibody Antibody	AuNRs/SiQDs ELISA, ELISA	Not reported 72.9% and 72.9%, 63.33% and 80.43%	(Kim *et al.*, 2017) (Wu *et al.*, 2010) (Zhang *et al.*, 2015)
ESAT6	Antigen Antigen Antibody	IEB, Au-IDE/CFP10-ESAT6 aptamer/DNA-AuNPs MSPQC, ELISA.	Not reported Not reported 82.9% and 64.1%	(Diouani *et al.*, 2017) (He *et al.*, 2016) (Wu *et al.*, 2010)
CFP10	Antigen Antigen Antibody	DND MALDI-TOF MS, SPR spectroscopy, ELISA	97.4% and 100% Not reported 65.2% and 79.2%	(Soo *et al.*, 2015) (Hong *et al.*, 2011) (Wu *et al.*, 2010)

*Assay:

- ELISA: enzyme-linked immunosorbent assay.
- PCR: polymerase chain reaction
- AuNRs-Ag85B-SiQDs: gold nanorods-Ag85B-silica-coated quantum dots.
- IEB: immune-electrochemical biosensor.
- Au-IDE/CFP10-ESAT6 aptamer/DNA-AuNPs MSPQC: gold-interdigital electrode/CFP10-ESAT6 aptamer/DNA-gold nanoparticles multiple channel of the series piezoelectric quartz crystal.
- DND MALDI-TOF MS: detonation nanodiamonds (DNDs) and matrix-assisted laser desorption/ionization mass spectrometry (MALDI-TOF MS).
- SPR spectroscopy: surface plasmon resonance spectroscopy.

II.1.2. Cloning and expression of recombinant proteins from MTB.

Although some antigens, as lipoarabinomannan (LAM), have already been described in biological samples from TB patients (Pereira Arias-Bouda *et al.*, 2000), others secretory and superficial MTB proteins have not been evaluated in sputum samples yet. In this study, **rHsp16.3, rMPT64, rMTC28, rMoeX, r38 kDa protein, rAg85B, rESAT6,** and **rCFP10,** from *M. tuberculosis* were expressed in the *E. coli* bacterial system.

The coding DNA sequences of selected proteins were amplified with the conditions described in the methodology **(Section II.2, page 107)**.

Figure II.1 shows the amplified DNA with specific primers **(Table II.6)** in a PCR, using genomic MTB DNA. The bands observed in the electrophoresis gel correspond to the coding DNA sequences of selected MTB proteins: Ag85B (994 nt), MTC28 (950 nt), MPT64 (701 nt), MoeX (1010 nt), Hsp16.3 (446 nt), 38 kDa (1139 nt) and ESAT6 (302).

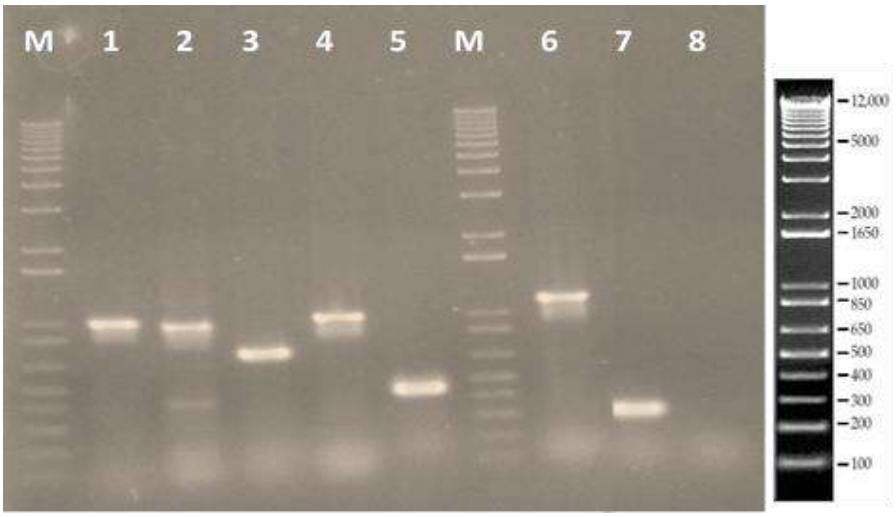

Figure II.1: Electrophoresis on 1.2% agarose gel of coding DNA sequences. **Lane 1:** Ag85B (994 nt), **2**: MTC28 (950 nt), **3:** MPT64 (701 nt), **4:** MoeX (1010 nt), **5:** Hsp16.3 (446 nt), **6:** 38 kDa (1139 nt), **7:** ESAT6 (302 nt), **8:** blank. Molecular weight marker 1 kb (Invitrogen). The shadows in the lower part of the lanes could be attributed to an excess of nucleotides.

In all cases an adequate digestion of the coding sequences and the plasmids is confirmed **(Figure II.2).** In lane 1, corresponding to the sequence of MoeX, a slight shadow

is observed that can be a consequence of DNA degradation by the restriction enzymes. This did not affect the cloning.

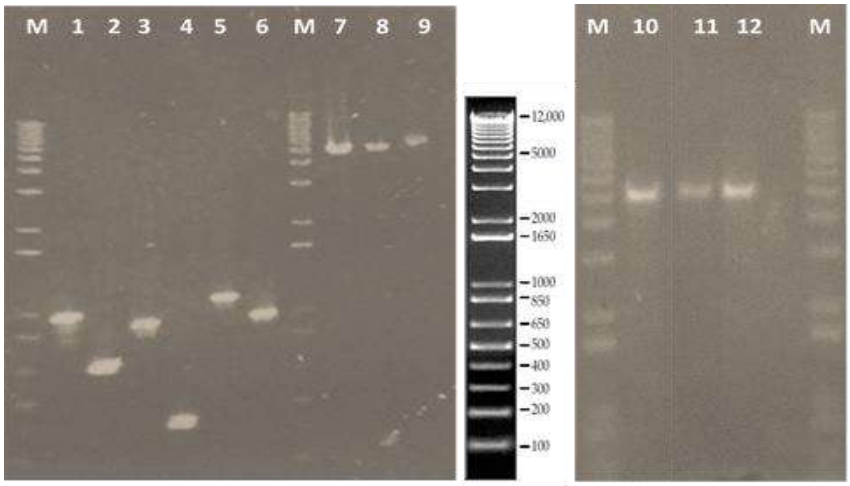

Figure II.2: Electrophoresis of digested DNA product and plasmids observed on a 1.2% agarose gel. **1:** MoeX, **2:** MPT64, **3:** MTC28, **4:** Hsp16.3, **5:** 38 kDa, **6:** Ag85B, **7:** pET28a (NcoI/XhoI), **8:** pET28a (NcoI/HindIII), **9:** pET28a undigested, **10:** pGEX4T1 (BamHI/EcoRI), **11:** pGEX4T1 (EcoRI), **12:** pGEX4T1 (EcoRI/XhoI). Molecular weight marker 1 kb (Invitrogen).

After amplification and cloning of coding DNA sequences, the recombinant proteins (rHsp16.3, rMPT64, rMTC28, rMoeX, r38 kDa protein, rAg85B, rESAT6 and rCFP10) were produced successfully in the *E. coli* bacterial system. All proteins were induced to an optic density (OD) of 0.6-0.8, corresponding to a logarithmic phase culture. Most of them were induced at 37 °C, ON, but rHsp16.3 and rCFP10 proteins were expressed at RT, ON. Additionally, rESAT6 was expressed at 37 °C, 4 h. The IPTG concentration was 0.5 mM, except for MTC28 (0.6mM), rAg85B, rMoeX and rESAT6 (0.65 mM) and for r38kDa (0.8 mM). Most of the recombinant proteins were found in the insoluble fraction, however rESAT6, rHsp16.3 and rCFP10 proteins were found in the soluble fraction of the induced culture.

Recombinant proteins were purified by affinity chromatography. All recombinant antigens, except ESAT6, presented an additional 1 kDa because of the 6xHis tag added.

Eluted recombinant proteins formed peaks at different imidazole concentrations. Most of them eluted between 100 - 300 mM Imidazole in 20 mM phosphate buffer, pH 7.4. The cloning and expression protocol of each specific MTB antigen is described in detail below.

- **Cloning and expression of rHsp16.3**.

Hsp16.3 is the most abundant *M. tuberculosis* secreted protein during latent stage (non-replicative), but it is reduced when the bacteria is in the logarithmic growth phase (Sutherland *et al*., 2013). It plays an important role in the survival of the mycobacteria and in the immune response of the host to the infection (Meng *et al.,* 2014). In addition, Hsp16.3 is frequently recognized in the TB patient sera (Kennaway *et al.,* 2005). These findings make the Hsp16.3 protein a potential biomarker for the TB diagnosis.

Cloning of Hsp16.3:

In our study, Hsp16.3 amplicon presented a length of 459 bp including the histidine tail (6xHis); and it was inserted between the restriction sites NcoI and XhoI **(Appendix 1.1, page 269).**

The coding sequence of Hsp16.3 was successfully ligated into the plasmid pET28a (+). **Figure II.3** shows that all 6 clones selected for screening, pET28a-Hsp16.3 (5565 bp) **(Appendix 1.1, page 269)**, presented a slight size difference (~196 bp) comparing to the plasmid pET28a alone (5369 bp). This is observed in the electrophoresis on 1.2% agarose gels (lanes 1-3 *vs* lane 4, and lanes 6-8 *vs* lane 5, **Figure II.3**).

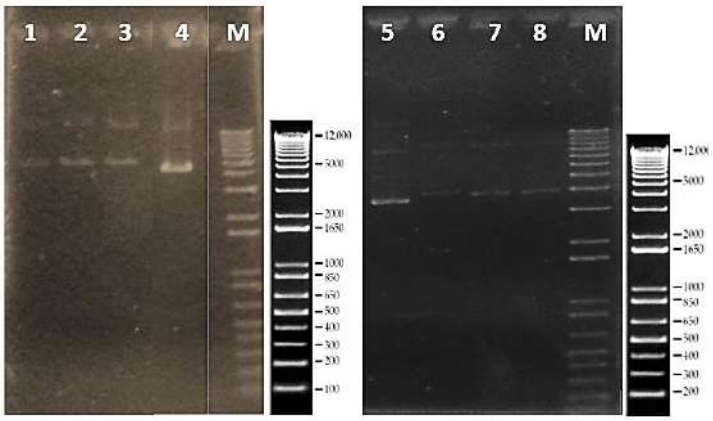

Figure II.3: Electrophoresis on 1.2% agarose gel showing pET28a (+) plasmid with inserted Hsp16.3 sequence. **lanes 1-3** and **6-8**: clones pET28a-Hsp16.3; **lanes 4,5**: plasmid pET28a (+), **M**: Molecular weight marker 1 kb (Invitrogen).

The cloning was corroborated by sequencing **(Appendix 1.2, page 270)**. The clones 1 and 2 contained the Hsp16.3 sequence inserted appropriately into the pET28a plasmid.

Expression and purification of rHsp16.3:

Kennaway *et al.,* 2005 reported a soluble Hsp16.3 from MTB, subcloned in pET8a (without 6xHis) and expressed in *E. coli* BL21 (DE3) Star (Novagen) at 37 °C, with 1 mM IPTG for 4 h.

In our case, expression of rHsp16.3 was performed in *E. coli* BL21 (DE3) and *E. coli* BL21 (DE3) pLysS. The expression conditions were: 0.5mM IPTG, at 37 °C and at RT (improved the protein solubility) for 16 h of induction. The rHsp16.3 was found both in soluble and insoluble fractions (**Figure II.4)**.

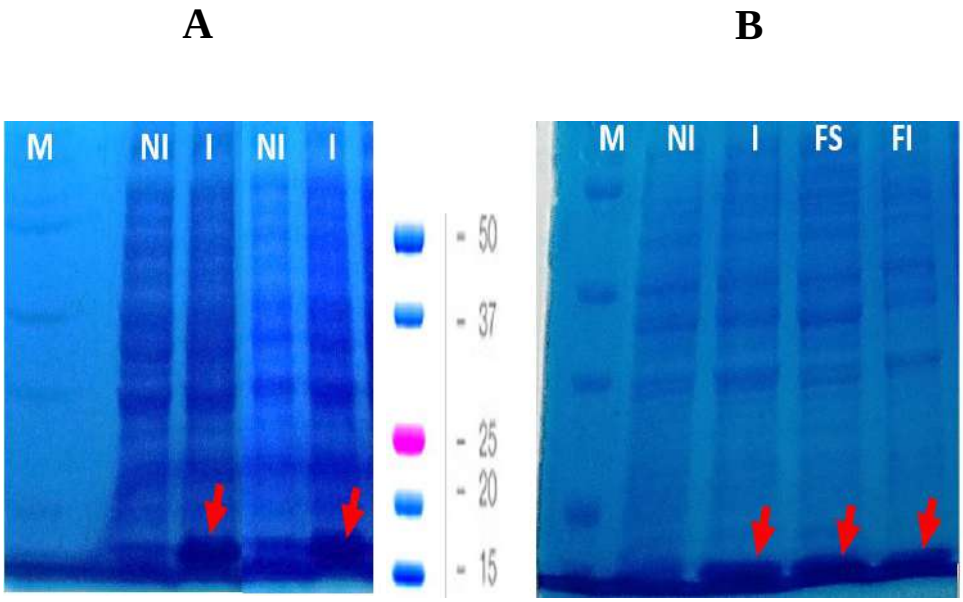

Figure II.4: SDS-PAGE (15%) of proteins. rHsp16.3 expression in the *E. coli* BL21 (DE3) (**A**) and *E. coli* BL21 (DE3) pLysS (**B**) systems at 37 °C for 16 h. **NI:** Not Induced, **I:** induced, **FS:** Soluble Fraction, **FI:** Insoluble Fraction and **M:** Molecular weight marker in kDa (Dual color BioRad).

Both soluble fraction and insoluble fractions of Hsp16.3 were purified separately by affinity chromatography. The soluble fraction was eluted at 300-500 mM Imidazole (**Figure II.5**); while the insoluble fraction eluted at 100 mM Imidazole (**Figure II.6**). The soluble fraction had a large amount of Hsp16.3, but the protein tended to precipitate when stored at -20 °C.

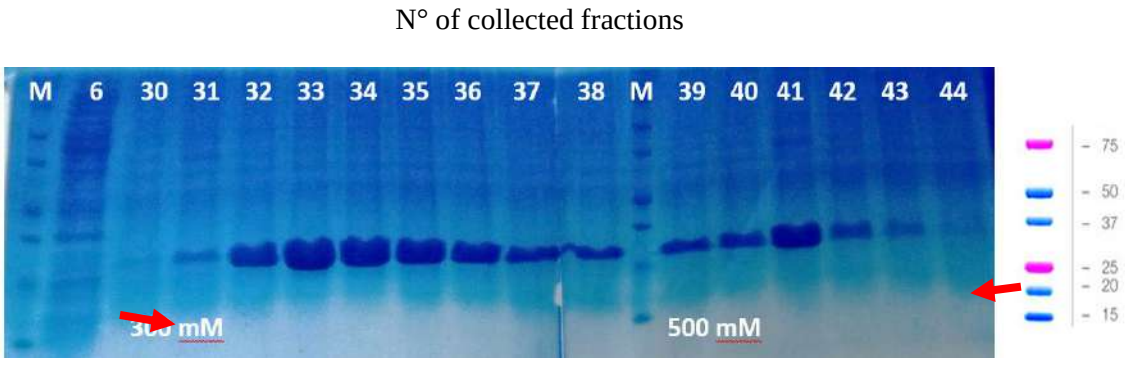

Figure II.5: SDS-PAGE (15%) of proteins, showing the purification of soluble fraction of rHsp16.3 by affinity chromatography. The protein elutes between 300-500 mM

Imidazol. **M:** Molecular weight marker in kDa (Dual color BioRad). In red narrows are indicated the bands of rHsp16.3.

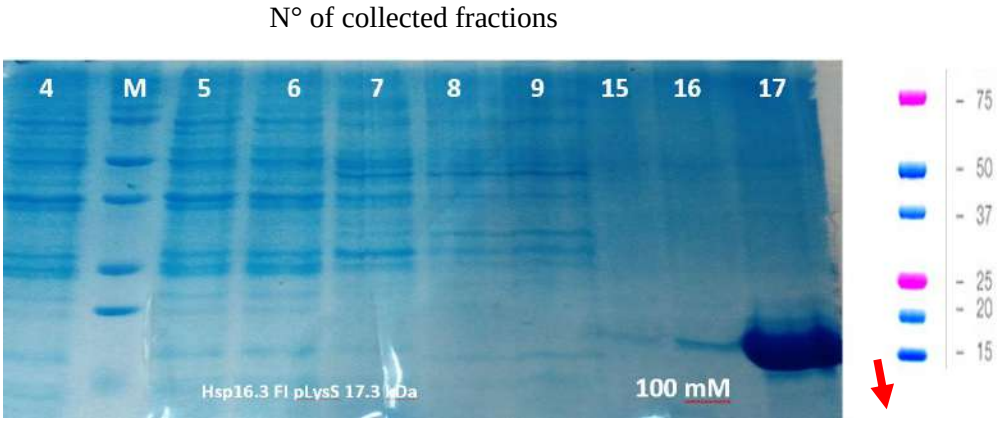

Figure II.6: SDS-PAGE (15%) of proteins, showing the purification of insoluble fraction of rHsp16.3 by affinity chromatography. The protein elutes in 100 mM Imidazole. **M:** Molecular weight marker in kDa (Dual color BioRad). In red narrow is indicated the band of rHsp16.3.

Figure II.7 shows the amino acid (aa) sequence and the dodecameric structure of rHsp16.3 produced. The monomer unit was expressed in our experiment because the molecular weight (~16.3 kDa) is corresponded. However, these proteins were self-polymerized in the process.

Hsp16.3 is part of an HSP (Heat Shock Protein) family and they share a conserved central domain called α-crystallin domain (~90 aa, with divergent extensions in NH_2 and *COOH* terminal regions). In general, the structure of HSP is a dimer formed by interactions between conserved α-crystalline domains. However, Abulimiti *et al.,* 2003 reported that Hsp16.3 of MTB can form polymers of trimers in solution. Polymerization of Hsp16.3 (previously reported) could explain why proteins were precipitated over time (Kennaway *et al.*, 2005).

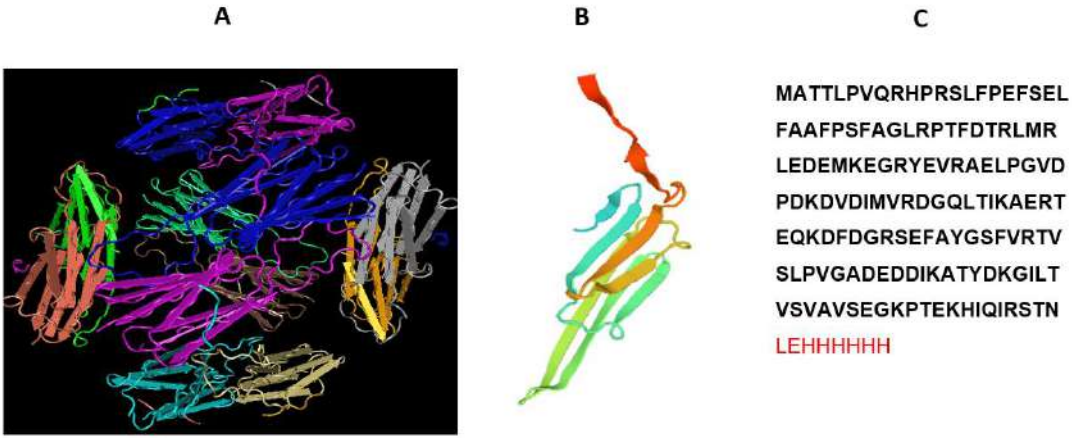

Figure II.7: Structure and sequence of the Hsp16.3 protein. Dodecameric structure of the small heat shock protein Acr1 from *Mycobacterium tuberculosis*, crystal structure of the complete protein **(A).** Monomer rHsp16.3 modeled by homology with (3w1z.1, Heat shock protein 16.0 from *Schizosaccharomyces pombe*) (https://swissmodel. expasy.org/interactive/qawtYd/templates/) **(B)**. Amino acid sequence of the protein, in red the additional amino acids added to the protein **(C).**

On the other hand, Kennaway *et al.* (2005) reported that Hsp16.3 forms a single set tetrahedral dodecameric assembled from dimers, being compatible with the original structural properties of the family of HSPs (Kennaway *et al.*, 2005).

In a phylogenetic analysis (**Appendix 1.3 and 1.4, both in page 271**) is observed that the amino acid sequence of Hsp16.3 of MTB differs from HSP of other mycobacteria, showing high specificity for the MTB complex.

- **Cloning and expression of rMPT64.**

MPT64 (~23 kDa) is a secreted protein restricted to members of the *Mycobacterium tuberculosis* complex (MTBC). It is able to induce T cell responses and cutaneous reactions in TB infected animals (Roche *et al.*, 1996).

Previously, the expression of MPT64from MTB was reported by Chu and Yuann (2011), they inserted the coding DNA sequence in pET23a(+) and expressed the protein in E. coli BL21 system. The MPT64 analysis was performed to study the pathogenicity of MTB, in order to develop a vaccine based on MPT64 (Chu and Yuann, 2011).

In our study, a rMTP64 from MTB is cloned and expressed to be used for polyclonal antibodies production and ELISA tests.

Cloning of rMPT64:

A slight size difference of the purified plasmids pET28a-MPT64 (lanes 1-3) compared with pET28a alone (lane 4) is observed in **Figure II.8**. It indicates a successfully insertion of MPT64 coding sequence into the pET28a (+) plasmid. Also, *in silico* was observed that the sequence of MPT64 was correctly ligated between the restriction sites NcoI and XhoI, corresponding to a total size of 714 pb including the nucleotides of 6xHis tag (**Appendix 1.5, page 272**).

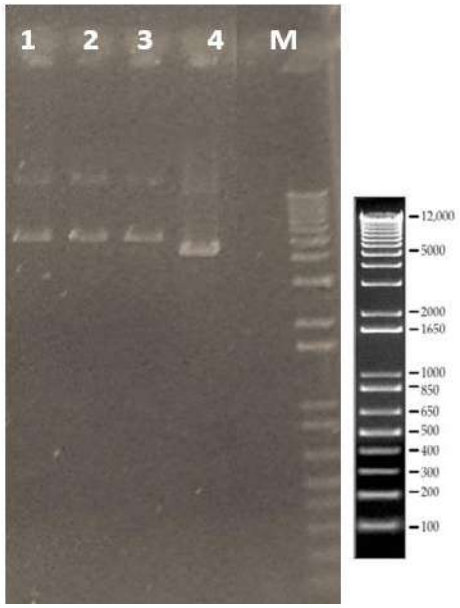

Figure II.8: Electrophoresis of DNA on 1.2% agarose gel, showing pET28a (+) plasmid with inserted MPT64 sequence. **Lanes 1-3:** clones pET28a-MPT64; **lane 4:** pET28a (+) plasmid, **M:** molecular weight marker 1 kb (Invitrogen).

The sequencing corroborated the previous results, variation or mutation in the sequence were not observed (**Appendix 1.6, page 273**).

Expression and purification of MPT64:

In addition, Chu and Yuann (2011) reported an expression protocol of MTP64. Unlike traditional protocols, in which proteins are expressed at 37 °C, MPT64 was better expressed at 20 °C with 10 mM IPTG for 22 h. The protein concentration was increased in the time (24 h). MPT64 expressed at 37 °C and 30 °C (under the same conditions) were lower than at 20°C. The protein was insoluble, but after refolding it was aggregated to become tetramers. High concentrations of β-mercaptoethanol (8%–20%) decreased the tetrameric and dimeric structures. However, the aggregation was very stable suggesting an intermolecular covalent interaction between MTP64 subunits with disulfide bonds (Chu and Yuann, 2011).

In our case, the MPT64 protein was slightly larger (26 kDa), and it was evaluated in *E. coli* BL21 (DE3) pLysS and in *E. coli* BL21 DE3 systems (**Figure II.9).** The parameters considered were 0.5 mM IPTG, at 37 °C, for 16 h of induction. A reduced production of the recombinant protein was observed, and it was found only in the insoluble fraction, as previously reported.

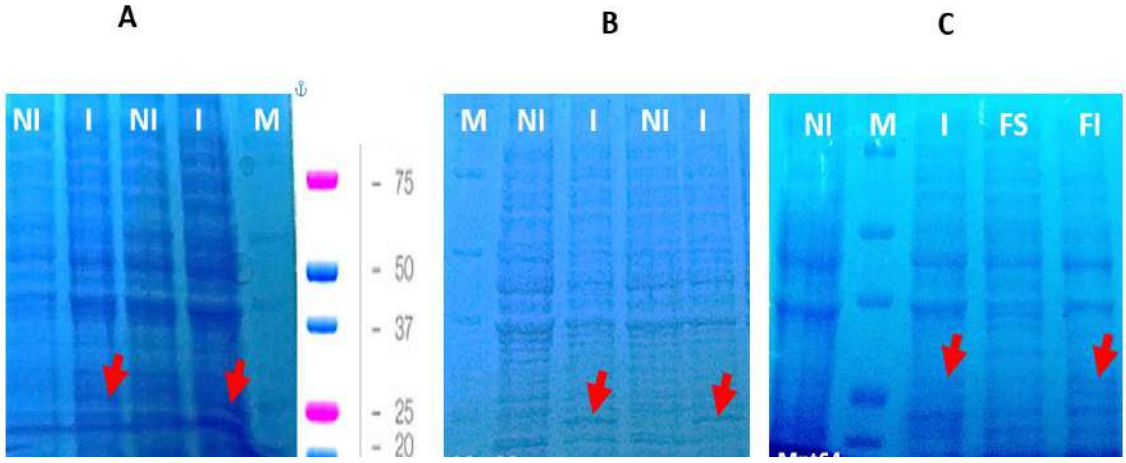

Figure II.9: SDS-PAGE (15%) of proteins after the expression of rMPT64 at 37 °C for 16 h (indicated with red arrows). Expression in *E. coli* BL21 (DE3) pLysS system **(A)**; Expression in *E. coli* BL21 (DE3) (**B and C).** The recombinant protein MPT64 is found and slightly observed in the insoluble fraction (Figure C). **NI:** Not Induced, **I:** Induced, **FS:**

Soluble Fraction, **FI:** Insoluble Fraction and **M:** Molecular weight marker in kDa (Dual color BioRad).

The rMPT64 expressed in the *E. coli* BL21 (DE3) system was purified from insoluble fraction by affinity chromatography increasing concentration of Imidazol: 40, 60, 80, 100, 200, 300 and 500 mM. The protein rMPT64 eluted at 100 mM Imidazole (**Figure II.10**), and it was not refolded.

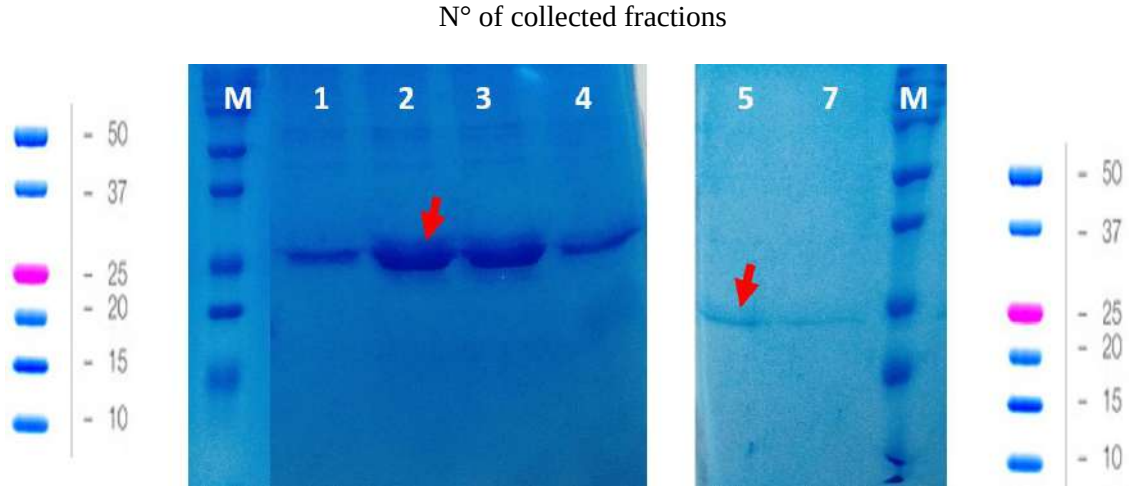

Figure II.10: SDS-PAGE (15%) of fractions purified by affinity chromatography of rMPT64 expressed in *E. coli* BL21 (DE3) pLysS system. The protein is eluted at 100 mM Imidazole. **M:** Molecular weight marker in kDa (Dual color BioRad).

MPT64 protein structure is composed mostly of β-sheet strands and tetrameric aggregates can be observed, suggesting strong protein–protein interactions *via* disulfide bonds between MPT64 subunits. Due to strong interactions, important properties related to Mycobacterium virulence, can be attributed to MPT64 protein (Chu and Yuann, 2011). The amino acid sequence and the modeled structure of rMPT64 is observed in **Figure II.11.** It is corresponded to MPT64 previously reported for MTB. Phylogenetic analysis shows a high specificity of MPT64 protein for the MTB complex (**Appendix 1.7 And 1.8, pages 274 and 275 respectively).**

A **B**

MVRIKIFMLVTAVVLLCCSGVATAAPKTYC
EELKGTDTGQACQIQMSDPAYNINISLPSY
YPDQKSLENYIAQTRDKFLSAATSSTPREA
PYELNITSATYQSAIPPRGTQAVVLKVYQN
AGGTHPTTTYKAFDWDQAYRKPITYDTLW
QADTDPLPVVFPIVQGELSKQTGQQVSIAP
NAGLDPVNYQNFAVTNDGVIFFFNPGELLP
EAAGPTQVLVPRSAIDSMLALEHHHHHH

Figure II.11: Structure and sequence of the MPT64 protein. Structure of MPT64 modeled by homology with 2hhi.1, antigen MPT64 from *Mycobacterium tuberculosis* (https://swissmodel.expasy.org/interactive/qawtYd/templates/) **(A).** Amino acid sequence of the rMPT64, in red the additional amino acids added to the protein **(B).**

- **Cloning and expression of rMTC28.**

MTC28 (28 kDa) is an extracellular protein and actively secreted by MTB. MTC28 is found in the early culture filtrate of MTB and like many of the MTB extracellular proteins, it elicits immune responses in guinea pigs immunized with live mycobacteria (Manca *et al*., 1997).

Cloning of rMTC28:

The coding sequence of MTC28 was successfully inserted into the plasmid pET28a (+). **Figure II.12** shows the clones with the pET28a-MTC28 construct inside, run on 1-3 and 5-6 lanes. In the electrophoresis of DNA (1.2 % agarose gel) the clones 1-3 and 6-7 present the coding MTC28 sequence inserted into the plasmid. A difference size (800 bp) was observed between the plasmid without insert (5369 bp) and the clones pET28a-MTC28 (6169 bp) (**Appendix 1.9, page 275**).

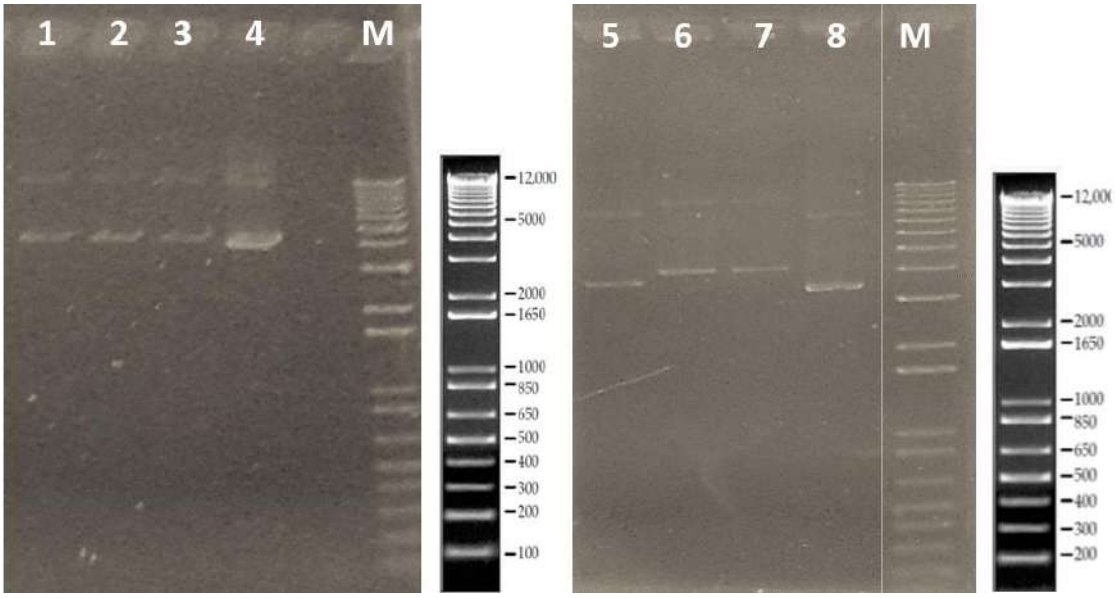

Figure II.12: Electrophoresis on 1.2% agarose gel of pET28a-MTC28 and pET28a (+) plasmids**. Lanes 1-3 and 6-7:** clones pET28a-MTC28; **lanes 4,5**: plasmids pET28a (+), **lane 8:** a clone with the plasmid without MTC28 inserted; **M**: Molecular weight marker 1 kb.

An alignment (**Appendix 1.10, page 277**) of sequencing clones shows that clone pET28a-MTC28, run on lane 6, has a better performance. It could be due to better quality of the plasmid DNA (without impurities). So, it presents less ambiguities and it is identical to theoretical MTC28 sequence. The sequence of a clone (lane 7) has undefined nucleotides (N), not presenting a 100% correspondence with the theoretical MTC28 sequence. Consequently, this clone (lane 7) was excluded, using only the clone run on lane 6.

Expression and purification of rMTC28:

The protein rMTC28 (33 kDa) was evaluated in two expression systems. A higher expression was observed in *E. coli* BL21 DE3 compared with *E. coli* BL21 (DE3) pLysS. The expression parameters were 0.5-0.65 mM IPTG (there was no variation in expression) at 37 °C, for 16 h of induction. An SDS-PAGE of the induced and non-induced culture shows the expression of the rMTC28 protein (**Figure II.13)**. After, rMTC28 was purified by affinity chromatography from insoluble fraction, the target protein is observed in the

fraction N° 23 with the apparent molecular weight between 25-37 kDa marker bands on SDS-PAGE (**Figure II.14).**

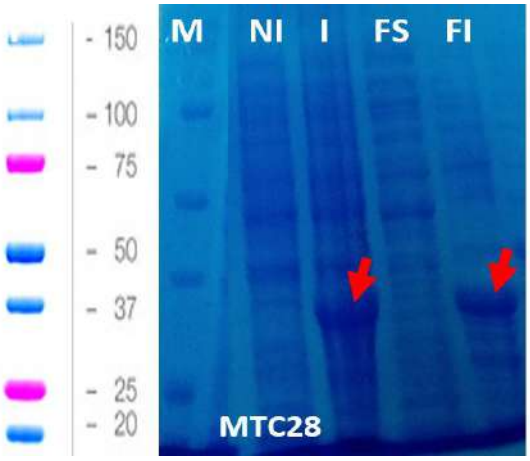

Figure II.13: SDS-PAGE (15%) of rMTC28 expressed in *E. coli* BL21 (DE3) system (IPTG: 0.6mM) (indicated with red arrows). The rMTC28 is observed in the insoluble fraction. **NI:** Non-induced, **I:** induced, **FS:** Soluble Fraction, **FI:** Insoluble Fraction and **M:** Molecular weight marker in kDa (Dual color BioRad).

N° of collected fractions

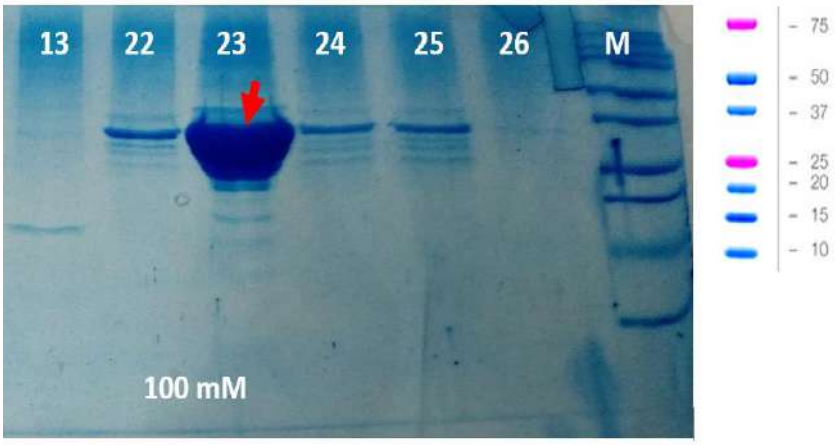

Figure II.14: SDS-PAGE (15%) of fractions purified by affinity chromatography of rMTC28 expressed in *E. coli* BL21 (DE3) system. The protein is eluted at 100 mM Imidazole. **M:** Molecular weight marker in kDa (Dual color BioRad).

Yamaguchi *et al.* (1989) reported that the abnormally slow migration in SDS-PAGE, is a common property of proline-rich MTC28 (Yamaguchi *et al.,* 1989). It could

explain some variations in the protein molecular weight migration observed in some SDS-PAGE (data not shown). Manca *et al.* (1997) observed that a MTC28 (28.66 kDa) protein migrated in SDS-PAGE with an apparent molecular mass of 49 kDa (Manca *et al.*, 1997). It could be attributed to the rigidity and reduced mobility of proline-rich stretches. Also, a low electrophoretic mobility of MTC28 obtained both from MTB (native) and from *E. coli* system (recombinant), is observed, discarding the effect of post translational modifications, such as glycosylation (Dobos *et al.*, 1996)

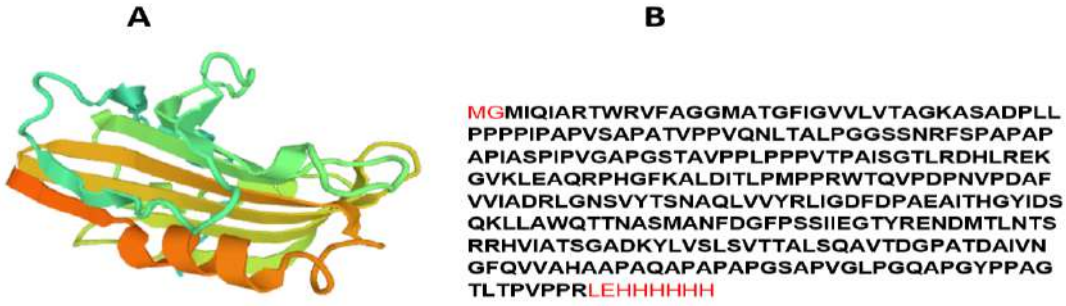

Figure II.15: Structure and sequence of rMTC28 protein. Structure of MTC28 modeled by homology with 4ol4.1, crystal structure of secreted proline rich antigen MTC28 (Rv0040c) from *Mycobacterium tuberculosis* (https://swissmodel.expasy.org/interactive/qawtYd/templates/) **(A).** The amino acid sequence of the protein, in red the additional amino acids added to the protein **(B).**

The amino acid sequence and the structure of rMTC28 is shown in **Figure II.15.** MTC28 is a protein with high proline content in the NH_2-terminal (34%) and *COOH*-terminal (30%) regions. In addition, a putative 32 aa secretion signal peptide in the NH_2-terminal is observed, and an extracytoplasmic mature region of 278 aa (Manca *et al.*, 1997). Phylogenetic analysis shows a high specificity of MTC28 protein for the MTBC (**Appendix 1.11 and 1.12, pages 278 and 279, respectively).**

- **Cloning and expression of MoeX**.

MoeX is a specific protein of MTBC, validated as a biomarker of active TB (Pollock *et al.*, 2013). This biomarker has not yet been reported in MTB identification

assays, so its diagnostic potential is explored in this study for the first time. The cloning and expression of rMoeX are described below.

Cloning of MoeX:

The insertion of MoeX into the pET28a (+) plasmid was successfully performed. **Figure II.16** shows that only clones 1 and 3 (6229 bp, **Appendix 1.13, page 279)** are longer than the plasmid without insert (5369 bp), showing a slight size difference (~ 860 bp). The sequences of these clones were identical to the theoretical MoeX sequence, except for an undefined nucleotide (N) of clone 1 (**Appendix 1.14, page 281).**

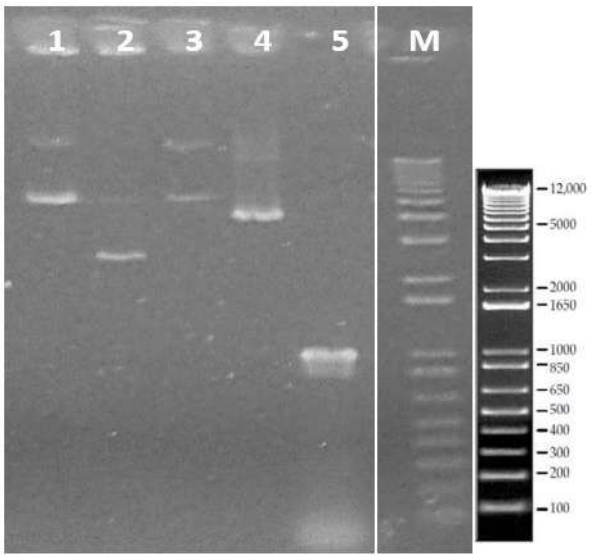

Figure II.16: DNA electrophoresis on 1.2% agarose gel of pET28a-MoeX and pET28a (+) plasmids**. Lanes 1 and 3:** clones pET28a-MoeX; **lane 2:** a clone with the plasmid without MoeX inserted; **lane 4:** plasmid pET28a(+); **lane 5:** MoeX amplicon; **M:** Molecular weight marker 1 kb (Invitrogen).

Expression and purification of rMoeX:

The rMoex protein (36.6 kDa) was expressed in both *E. coli* BL21 (DE3) pLysS and *E. coli* Lemo 21 systems, with 0.5-0.8 mM IPTG (variation in the expression was not observed) at 37 °C for 6 - 16 h of induction. In both systems the protein was found in insoluble fraction (**Figure II.17**).

A greater amount of protein was obtained from induced *E. coli* BL21 (DE3) pLysS culture. The rMoeX was purified at 100-300 mM imidazole, especially in the fractions N° 18-20 (**Figure II.18**).

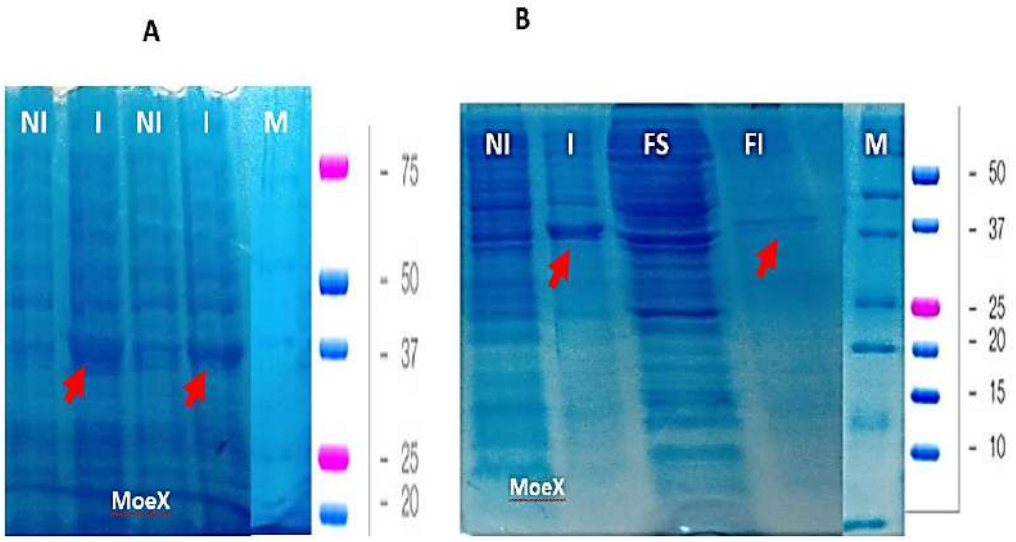

Figure II.17: SDS-PAGE (15%) of the expression of rMoeX at 37 °C for 16 h, in *E. coli* BL21 (DE3) pLysS system **(A**) and in *E. coli* Lemo 21 (**B**). The recombinant protein MoeX is observed in the insoluble fraction (indicated with red arrows). **NI:** Non-Induced, **I:** Induced, **FS:** Soluble Fraction, **FI:** Insoluble Fraction and **M:** Molecular weight marker in kDa (Dual color BioRad).

Previously, MoeX was identified in urine samples from TB patients. Three discrete protein bands of 75, 50, and 32 kDa corresponding to MoeX were identified in urine samples. According Pollock *et al.,* bands of 50 kDa and 75 kDa might represent a polymerization because MoeX contains 8 cysteine residues, or MoeX could be complexed with other proteins (Pollock *et al.*, 2013). In our study, the protein rMoeX presented a MW of ~37 kDa (theorical 36.6 kDa), aggregation was not observed because the protein was initially found in the insoluble fraction and it was solubilized in a denaturating solution (8 M urea).

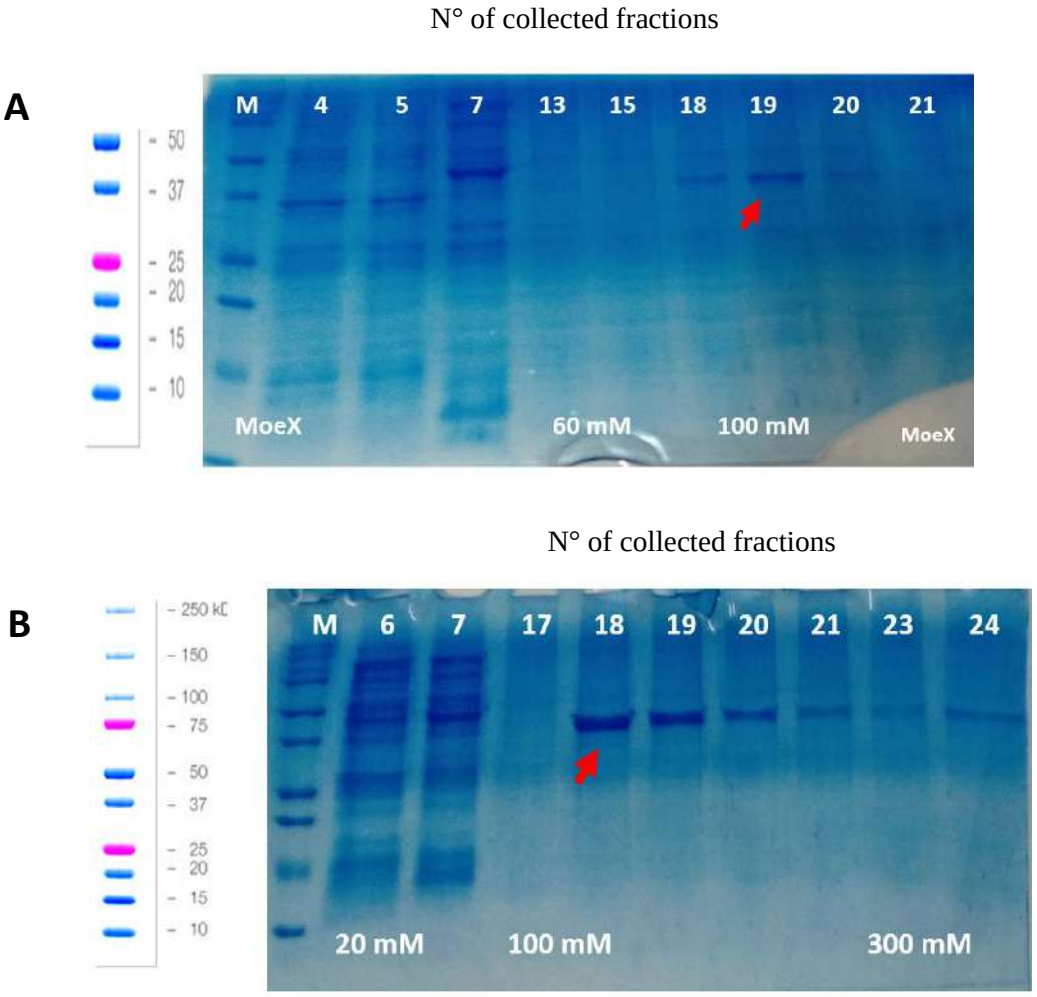

Figure II.18: SDS-PAGE (15%) of fractions purified by affinity chromatography of rMoex expressed in the *E. coli* Lemo21 (**A**) and *E. coli* BL21 (DE3) pLysS (**B)** systems. In the first case, the protein is eluted in a small amount at 100 mM Imidazole, while in the second, a greater amount of protein eluted between 100-300 mM of Imidazole is observed. **M:** Molecular weight marker in kDa (Dual color BioRad).

The amino acid sequence and the structure of modeled rMoeX is shown in **Figure II.19**.

The specificity of MoeX for MTBC was corroborated with phylogenetic analysis of its amino acid sequence compared to the proteins reported in the database (**Appendix 1.15 and 1.16, pages 282 and 283, respectively).**

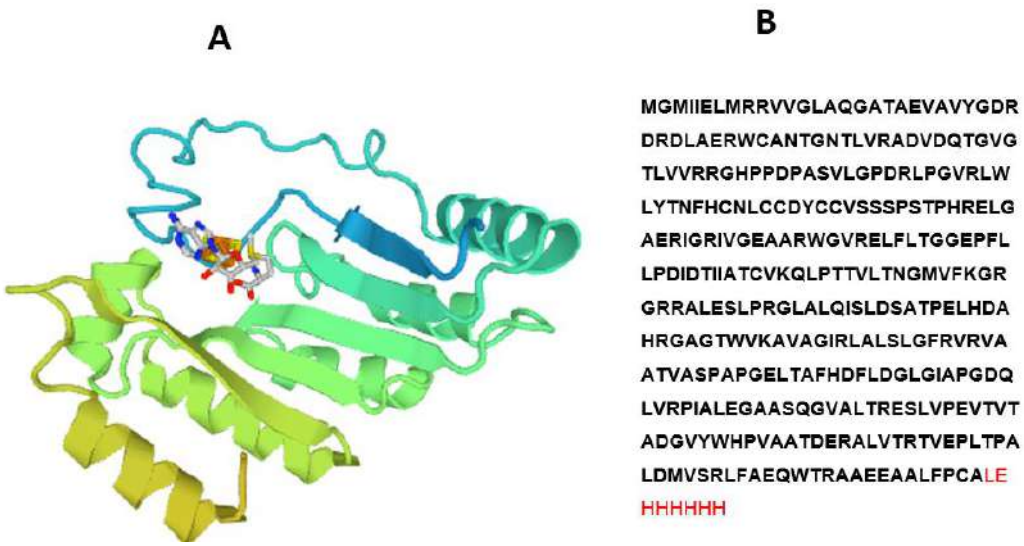

Figure II.19: Modeled structure of the MoeX protein. MoeX structure constructed by homology with Molybdenum cofactor biosynthesis protein A (2fb2.1.A) (https://swissmodel.expasy.org/interactive/qawtYd/templates/) **(A).** rMoeX sequence, in red the additional amino acids added to the protein **(B).**

- **Cloning and expression of r38 kDa protein**.

38 kDa protein is actively secreted and it is considered as one of the most important MTB antigens, because it is a major constituent of MTB culture fluid (in synthetic Sauton medium) (Harboe and Wiker, 1992). Due to these properties, this protein has been widely studied in different MTB diagnostic methods. In our study we report the cloning and expression of r38kDa, which was subsequently used for the production of polyclonal antibodies.

Cloning of 38 kDa protein.

The coding sequence of 38 kDa was successfully ligated in the plasmid pET28a (+). The clones pET28a-38kDa (6358 bp) (lanes 1-3) show a size difference (989 pb) comparing to plasmid without insert (5369 bp) (lane 4), indicating the insertion of coding DNA sequence of 38 kDa into the plasmid (**Figure II.20)** (**Appendix 1.17, page 283**). In the alignment (**Appendix 1.18, page 285)** the clones 1 and 2 are identical to the theoretical 38kDa sequence, so it corroborates that the cloning of this gene was successful.

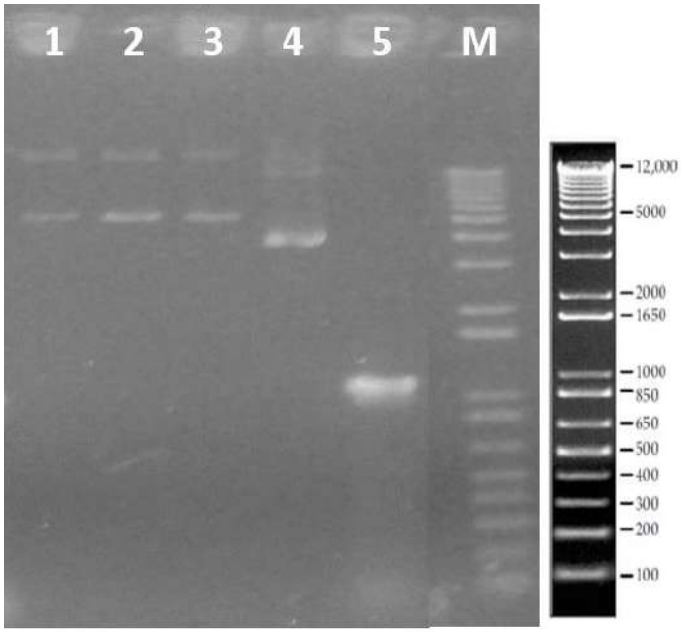

Figure II.20: DNA electrophoresis on 1.2% agarose gel of pET28a-38kDa and pET28a (+) plasmids. **A. Lanes 1-3:** clones pET28a-38kDa; **lane 4:** plasmid pET28a (+); **Lane 5:** 38kDa amplicon; **M:** Molecular weight marker 1 kb (Invitrogen).

Expression and purification of r38 kDa:

Previously, Chang *et al.*, 1994 reported a truncated 38kDa antigen from MTB. It was expressed successfully in *E. coli* BL21 (DE), with 0.2 mM IPTG, ON. The recombinant 38kDa was observed in both soluble and insoluble fractions (Chang *et al*., 1994).

In our case, the r38kDa protein (39.4 kDa) was successfully expressed in *E. coli* BL21 (DE3) pLysS and in *E. coli* BL21 (DE3). In both systems, the parameters were: 0.8 mM IPTG at 37 °C for 16 h of induction. However, the protein was found only in the insoluble fraction and solubilized with urea (**Figure II.21)**. A higher amount of r38 kDa (collected fractions N° 1-2 and 13) expressed in *E. coli* BL21 (DE3) pLysS was purified by affinity chromatography, compared to the other collected fractions (**Figure II.22)**.

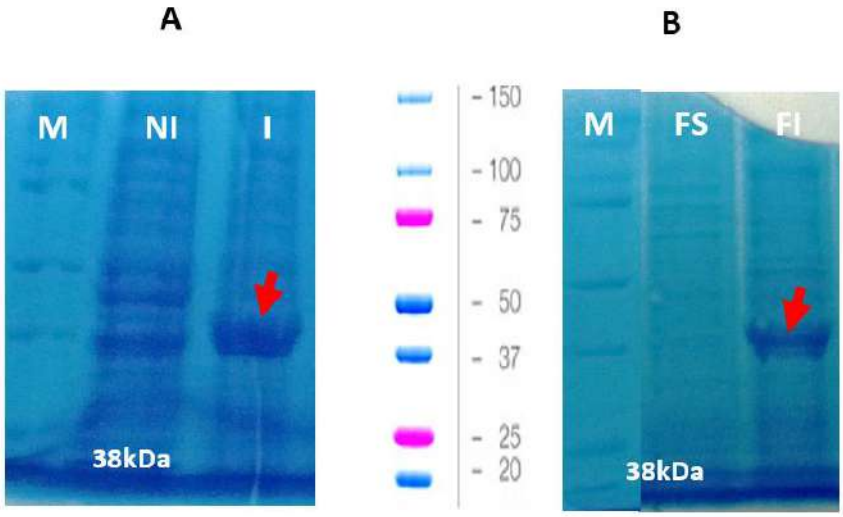

Figure II.21: SDS-PAGE (15%) of r38kDa expressed in *E. coli* BL21 (DE3) system **(A and B)** at 37 °C for 16 h. The recombinant protein 38kDa (indicated with red arrows) is observed in the insoluble fraction. **NI:** Non-Induced, **I:** Induced, **FS:** Soluble Fraction, **FI:** Insoluble Fraction and **M:** Molecular weight marker in kDa (Dual color BioRad).

Choudhary *et al.* (1994) reported the crystallization of 38kDa using a pure recombinant form of the protein. They demonstrated that 38kDa protein acts binding phosphate using a mechanism like phosphate-binding protein localized in the periplasm of *E. coli*. In this way, the structure of the protein and its similarity to an extracellular phosphate transporter justifies the function of 38kDa, but its role not completely elucidated (Choudhary *et al.*, 1994). The amino acid sequence and the modeled r38 kDa protein based on extracellular phosphate ABC transport receptor are described in **Figure II.23**.

In addition, a phylogenetic analysis was made to corroborate the high specificity of 38kDa protein for the MTB complex (**Appendix 1.19 and 1.20, both in page 286).**

A

N° of collected fractions

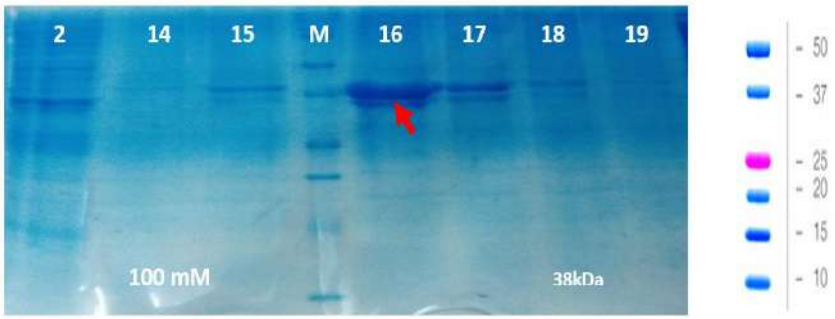

B

N° of collected fractions

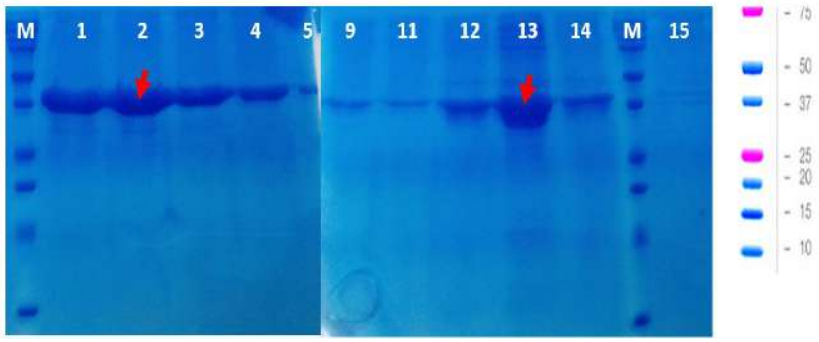

Figure II.22: SDS-PAGE (15%) of purified fractions of r38kDa, expressed in the *E. coli* BL21 (DE3) (**A**) and *E. coli* BL21 (DE3) pLysS (**B)** systems. In the first case, the protein elutes in a small amount at 100 mM Imidazole, while in the second, a greater amount of protein eluted between 80-300 mM of Imidazole is observed. **M:** Molecular weight marker in kDa (Dual color BioRad).

A **B**

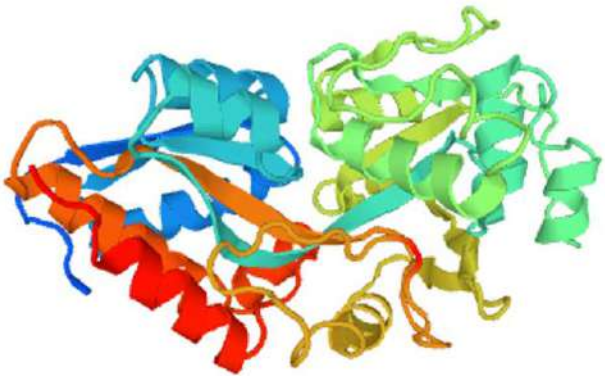

MVKIRLHTLLAVLTAAPLLLAAAGCGSKPPSG
SPETGAGAGTVATTPASSPVTLAETGSTLLYPL
FNLWGPAFHERYPNVTITAQGTGSGAGIAQAA
AGTVNIGASDAYLSEGDMAAHKGLMNIALAIS
AQQVNYNLPGVSEHLKLNGKVLAAMYQGTIKT
WDDPQIAALNPGVNLPGTAVVPLHRSDGSGDT
FLFTQYLSKQDPEGWGKSPGFGTTVDFPAVP
GALGENGNGGMVTGCAETPGCVAYIGISFLDQ
ASQRGLGEAQLGNSSGNFLLPDAQSIQAAAA
GFASKTPANQAISMIDGPAPDGYPIINYEYAIVN
NRQKDAATAQTLQAFLHWAITDGNKASFLDQ
VHFQPLPPAVVKLSDALIATISSLEHHHHHH

Figure II.23: Structure and sequence of the r38kDa protein. Structure modeled by homology with 1pc3.1, crystal structure of the extracellular phosphate ABC transport receptor (PstS-1) and immunodominant antigen of *M. tuberculosis* (https://swissmodel. expasy.org/interactive/qawtYd/templates/) **(A**). The amino acid sequence of the protein is shown, in red the additional amino acids added to the protein (**B**).

- **Cloning and expression of rAg85B**.

Ag85B is the major secretory protein of MTB, it was able to activate the protective immunity of Ag85B-vaccinated guinea pigs against aerosol MTB exposure (Zarif *et al.,* 2013). Due to these and other previously described characteristics, the rAg85B antigen was selected, cloned and expressed in this study.

Zarif *et al.* (2013) reported an Ag85B cloned in pET101/D and transformed in *E. coli* BL21 strain. The recombinant antigen (33 kDa) was expressed at 37 °C with 2 µL/mL of IPTG. After 12 h of induction the recombinant Ag85B was abundant and insoluble (present in inclusion body) (Zarif *et al*., 2013).

Cloning of rAg85B:

In our case, the rAg85B was cloned in pET28a. The coding DNA sequence of Ag85B was successfully inserted in the plasmid. The clones pET28a-Ag85B (6229 bp) (lanes 1 and 2) were longer than the plasmid without insert (5369 bp) (lane 4) (**Figure II.24)**. Additionally, it is observed *in silico* that the Ag85B sequence is correctly ligated

between the restriction sites NcoI and HindIII (**Appendix 1.21, page 287**). **Appendix 1.22, page 288,** shows that the clones 1 and 2 are identical to the theoretical Ag85B sequence, corroborating a successful insertion f Arg85B in the plasmid.

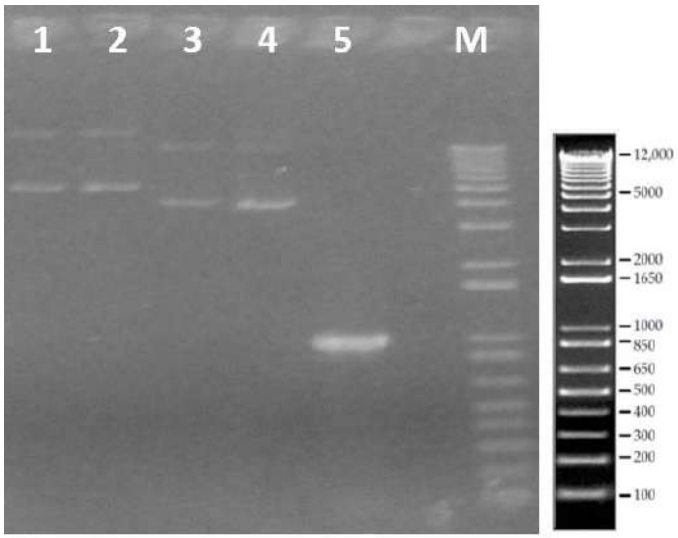

Figure II.24: DNA electrophoresis on 1.2% agarose gel of pET28a-Ag85B and pET28a (+) plasmids**. Lanes 1-2:** clones pET28a-Ag85B; **lane 3:** a clone with the plasmid without Ag85B inserted; **lane 4:** plasmid pET28a(+); **lane 5:** Ag85B amplicon; **M:** Molecular weight marker 1 kb (Invitrogen).

The protein rAg85B (36.3 kDa, PI: 6.29) was successfully expressed in *E. coli* BL21 (DE3) pLysS and in *E. coli* BL21 (DE3). Expression parameters were: 0.5-0.7 mM IPTG (there was no variation in expression, 0.65 mM IPTG was used) at 37 °C for 16 h. In both expression systems, the protein was found in insoluble fraction (**Figure II.25)**.

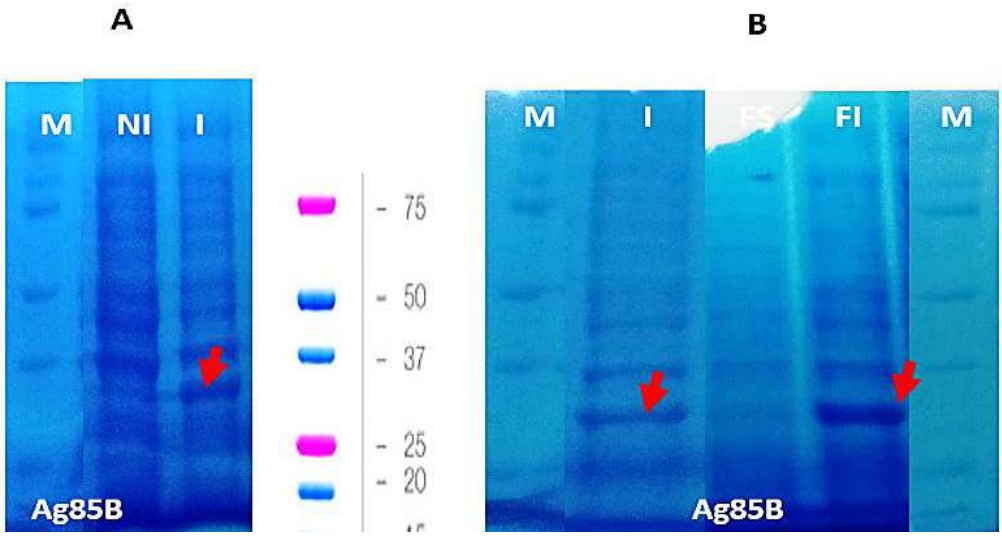

Figure II.25: SDS-PAGE (15%) of rAg85B at 37 °C for 16 h (indicated in red narrows). **NI:** Not Induced, **I:** induced, **FS:** Soluble Fraction, **FI**: Insoluble Fraction and **M:** Molecular weight marker in kDa (Dual color BioRad). **A and B:** Expression in *E. coli* BL21 (DE3), showing that the recombinant protein Ag85B is in the insoluble fraction.

The insoluble fractions of rAg85B expressed in the system *E. coli* BL21 (DE3) pLysS and in *E. coli* BL21 (DE3), were purified. In both cases, rAg85B was eluted at 80-300 mM Imidazole. The purification was improved when a buffer battery with more dilute imidazole was used: 20, 40, 60, 80, 100, 200, 300 and 500 mM of Imidazole (**Figure II.26)**.

Phylogenetic analysis shows a high specificity of Ag85B protein for the MTB complex (**Appendix 1.23 and 1.24, pages 289 and 290, respectively).**

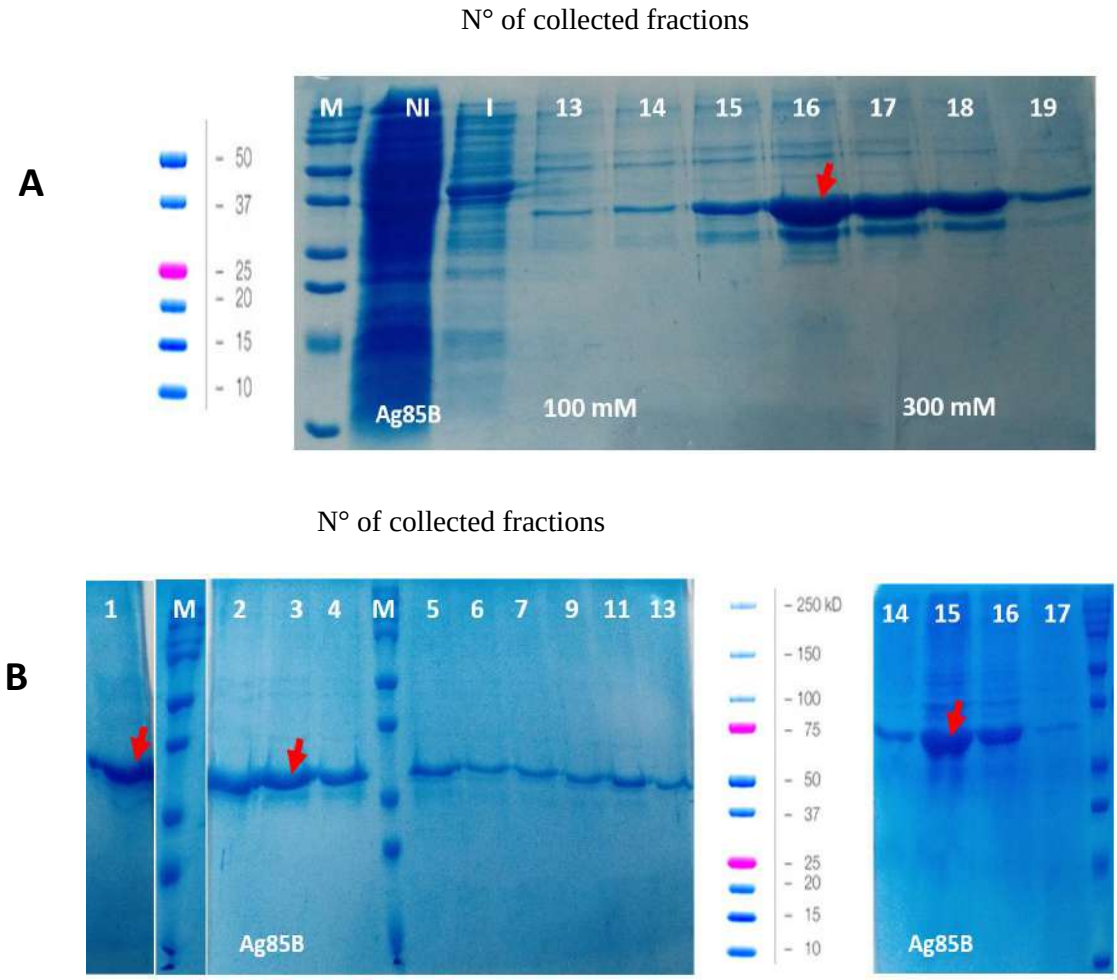

Figure II.26: SDS-PAGE (15%) of fractions purified by affinity chromatography of rAg85B, expressed in the *E. coli* BL21 (DE3) (**A**) and *E. coli* BL21 (DE3) pLysS (**B)** systems. In the first case, rAg85B elutes with non-specific proteins at 100-300 mM Imidazole, while in the second case, a greater amount of protein eluting between 80-300 mM of Imidazole is observed. **M:** Molecular weight marker in kDa (Dual color BioRad).

Ag85B is closely related to a mycolyl transferases, and associated with two other forms Ag85A and Ag85C, contributing to build the bacterial cell wall. In a crystal previously reported, a molecule of trehalose was linked in two sites at opposite ends of the active-site cleft (Anderson *et al*., 2001).

In this sense, the modeled structure presents a central region in the form of a pocket, which could correspond to the active site of the protein (**Figure II.27).**

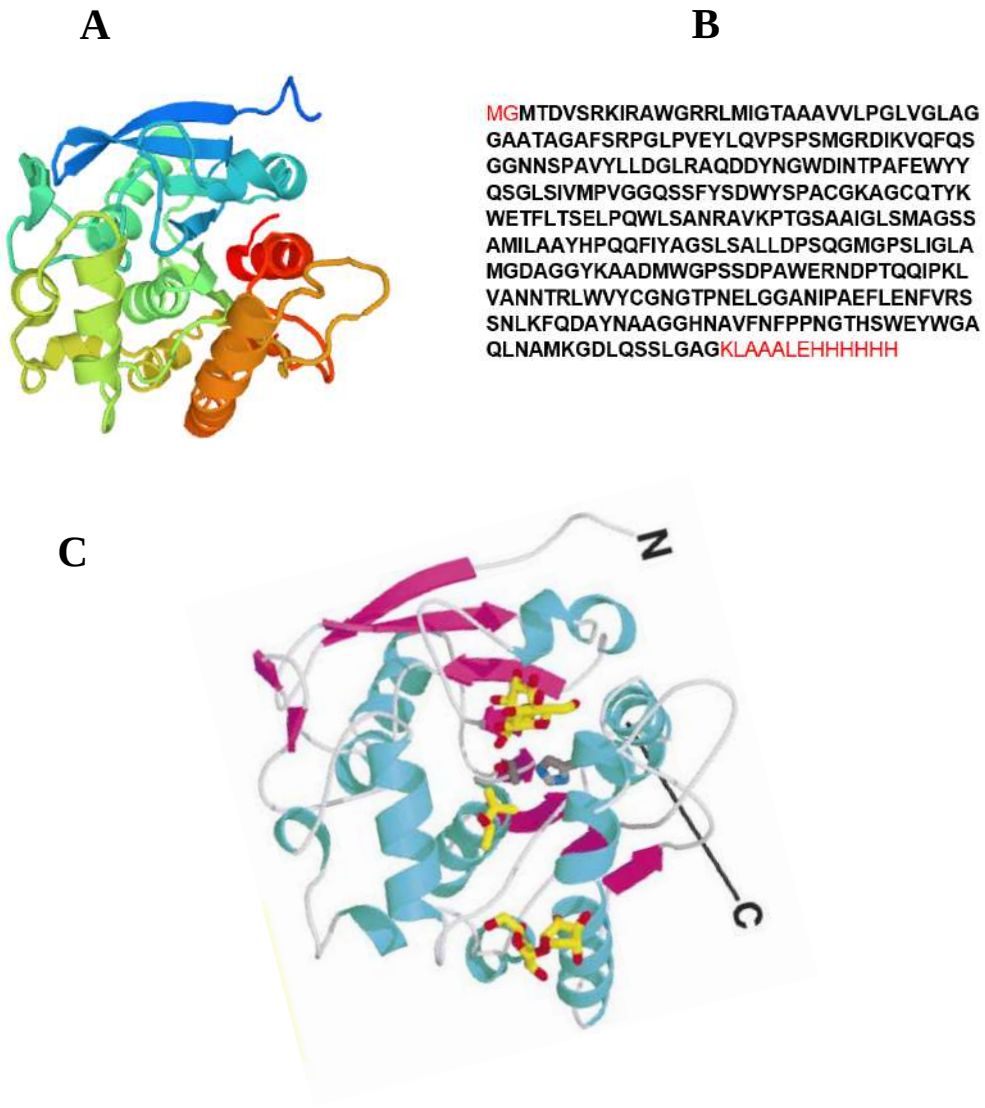

Figure II.27: Structure and sequence of Ag85B protein. Structure modeled by homology with 1f0n.1, crystal structures of the *Mycobacterium tuberculosis* 30 kDa major secretory protein (Antigen 85B), to mycolyl transferase (https://swissmodel.expasy.org/ interactive/qawtYd/templates/) **(A**). Amino acid sequence of rAg85B is shown, in red the additional amino acids added to the protein **(B).** Ribbon diagram of trehalose-bound Ag85B, trehalose is indicated in yellow (extracted from Anderson *et al.*, 2001).

- **Cloning and expression of rESAT6**.

ESAT6 and CFP10 are the most important virulence factors and they are recognized over 70% of TB patients (Skjot *et al.*, 2000). Mahmoudi *et al.*, 2013 reported a ESAT6 cloned in the vector pET32a (+) and transformed into *E. coli* BL21 DE3. The expression

parameters were: 1mM IPTG, at 37 °C for 4 h of time induction. Most of the protein was found in the soluble fraction (Mahmoudi *et al.,* 2013).

Cloning of ESAT6:

In our study the protein was cloned in a Phusion plasmid pGEX4T1 in order to improve the solubilization of the protein. In the DNA electrophoresis on 1.2 % agarose gel is observed that clones pGEX4T1-ESAT6 have a longer length than pGEX4T1 without insert (**Figure II.28)**. Therefore, the ESAT6 coding sequence was successful inserted into the plasmid pGEX4T1. Besides, *in silico* cloning is observed that ESAT6 sequence is correctly ligated between the BamHI and EcoRI restriction sites (**Appendix 1.25, page 290**), corresponding to a total size of 1002 bp including the GST (Glutathione S Transferase) tag. A slight size difference (282 bp) between pGEX4T1-ESAT6 (5251 bp) and pGEX4T1 plasmid (4969 bp) is observed.

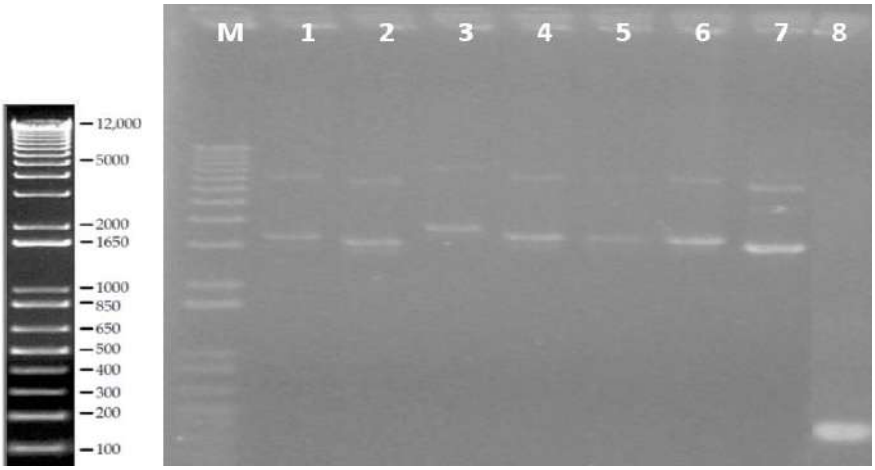

Figure II.28: DNA electrophoresis on 1.2% agarose gel of pGEX4T1-ESAT6 and pGEX4T1 plasmids**. Lanes 1, 4-6:** clones pGEX4T1-ESAT6; **lane 2:** a clone with the plasmid without ESAT6 inserted; **lane 3**: a clone with apparently two copies of ESAT6 inserted; **lane7:** plasmid pGEX4T1; **lane 8:** ESAT6 amplicon; **M:** Molecular weight marker 1 kb (Invitrogen).

In the alignment (**Appendix 1.26, page 291)** the clone 6 is identical to the theoretical ESAT6 sequence, except for one variation at the beginning and at the end of the sequence.

Expression and purification of rESAT6:

The protein rESAT6-GST (37.7 kDa, PI: 5.58) was expressed successfully in *E. coli* BL21 (DE3) pLysS and in *E. coli* BL21 (DE3). The expression parameters were: 0.65 mM IPTG, at 37 °C and at RT. The room temperature favored the expression of the soluble fraction of the protein, for 16 h of induction. A fraction of the protein was soluble, and another fraction was insoluble. For the purification an affinity chromatography was performed using the soluble fraction in a column packed with a resin coated with Glutathione. The SDS-PAGE analysis of expressed and purified rESAT6 is shown in **Figure II.29**.

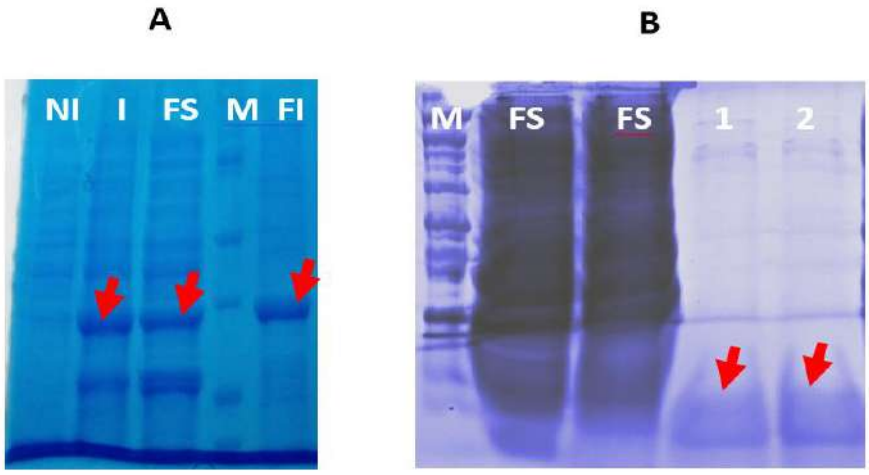

Figure II.29: SDS-PAGE (15%) of rESAT6-GST protein expressed in *E. coli* BL21 (DE3) system. The protein was found in in soluble and insoluble fractions (**A**). Purified rESAT6 (lanes 1 and 2) (**B**). **NI:** Not Induced, **I:** induced, **FS:** Soluble Fraction, **FI**: Insoluble Fraction and **M:** Molecular weight marker in kDa (Dual color BioRad).

Both CFP10 and ESAT6 proteins are secreted forming a four-helix bundle structure. In the **Figure II.30** only the structure of the rESAT6 protein and the sequence of rESAT-GST are shown. Also, phylogenetic analysis shows a high specificity of ESAT6 protein for the MTB (**Appendix 1.27 and 1.28, page 291 and 292, respectively).**

A **B**

MSPILGYWKIKGLVQPTRLLLEYLEEKYEEHLYERDEGDKWRNK
KFELGLEFPNLPYYIDGDVKLTQSMAIIRYIADKHNMLGGCPKERA
EISMLEGAVLDIRYGVSRIAYSKDFETLKVDFLSKLPEMLKMFEDR
LCHKTYLNGDHVTHPDFMLYDALDVVLYMDPMCLDAFPKLVCFK
KRIEAIPQIDKYLKSSKYIAWPLQGWQATFGGGDHPPKSDLVPRG
SMTEQQWNFAGIEAAASAIQGNVTSIHSLLDEGKQSLTKLAAAW
GGSGSEAYQGVQQKWDATATELNNALQNLARTISEAGQAMAST
EGNVTGMFAEFPGRLERPHRD

Figure II.30: Structure of the rESAT6, and sequence of the rESAT6-GST protein. ESAT6 structure was modeled by homology with 1wa8.1, solution structure of the CFP10-ESAT6 complex, major virulence determinants of pathogenic mycobacteria (https://swissmodel .expasy.org/interactive/qawtYd/templates/) (**A**). Amino acid sequence of the rESAT6-GST protein is shown, in red the additional amino acids added to the protein, in purple the GST sequence, in green the cutting site for the enzyme thrombin and in black the amino acid sequence of ESAT6 (**B**).

- **Expression of rCFP10.**

Similarly to ESAT6, Mahmoudi *et al*. (2013) reported a soluble CFP10 cloned in pET32a(+) and expressed in *E. coli* BL21 (DE3), with 1mM IPTG, at 37 °C for 4 h (Mahmoudi *et al.,* 2013). In our case, the pET28a-CFP10 plasmid was purchased from a company (GenScript). The gene was inserted between NcoI and BamHI (**Appendix 1.29, page 292**).

The protein rCFP10 (11.6 kDa, PI: 5.59) was successfully expressed in *E. coli* BL21 (DE3) pLysS at 0.5 mM IPTG at 37 °C for 4 h of induction. The protein was found in the soluble fraction (**Figure II.31**).

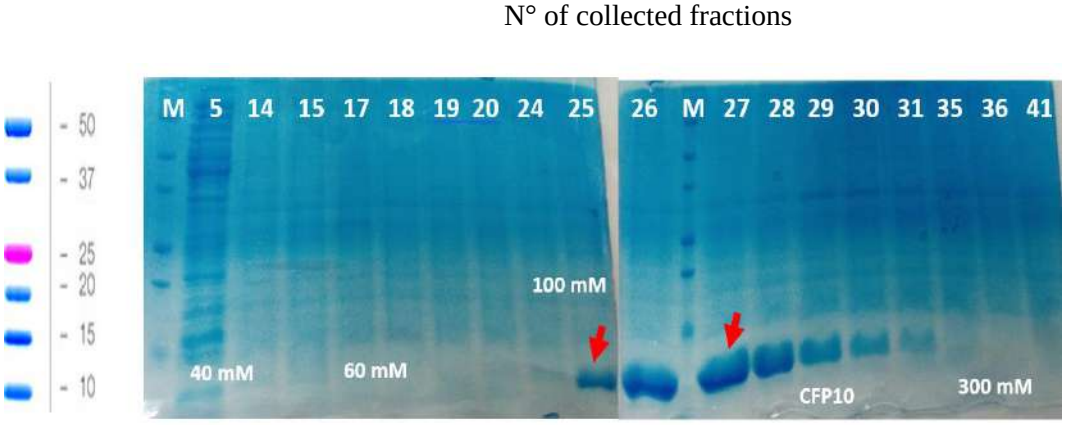

Figure II.31: SDS-PAGE (15%) of fractions purified by affinity chromatography of rCFP10, expressed in *E. coli* BL21 (DE3) pLysS system. The protein is eluted at 100 mM Imidazole. **M:** Molecular weight marker in kDa (Dual color BioRad).

Phylogenetic analysis, using the amino acid sequence of the MTB CFP10 protein, as well as the sequences of other mycobacteria, showed that the CFP10 protein was specific for MTB (**Appendix 1.30 and 1.31, both in page 293).** The amino acid sequence and the modeled structure of rCFP10 are showed in **Figure II.32.**

Figure II.32: Structure and sequence of the rCFP10 protein. Structure of CFP10 modeled by homology with a structure of the CFP10-ESAT6 complex from *Mycobacterium tuberculosis* (3fav.2) (**A**) (https://swissmodel.expasy.org/interactive/qawtYd/templates/). Also, the amino acid sequence of the protein is shown, in red the additional amino acids added to the protein (**B**).

Table II.2 summarize the main parameters used for the expression of recombinant MTB proteins selected in this study.

Table II.2: Conditions for the expression and purification of recombinant proteins.

Protein	Bacterial system	IPTG (mM)	T (°C)	Fraction	Induction time	Imidazol (mM)
rHSP16.3	*E. coli* BL21 DE3 pLysS	0.5	RT	soluble	16 h	300-500
		0.5	37 °C	insoluble	16 h	100
rMPT64	*E. coli* BL21 DE3	0.5	37 °C	insoluble	16 h	100
rMTC28	*E. coli* BL21 DE3	0.6	37 °C	insoluble	16 h	100
rMoeX	*E. coli* BL21 DE3 pLysS	0.65	37 °C	insoluble	16 h	100-300
r38 kDa	*E. coli* BL21 DE3 pLysS	0.8	37 °C	insoluble	16 h	80-300
rAg85B	*E. coli* BL21 DE3 pLysS	0.65	37 °C	insoluble	16 h	80-300
rESAT6	*E. coli* BL21 DE3	0.65	RT	soluble	16 h	-
rCFP10	*E. coli* BL21 DE3 pLysS	0.5	37 °C	soluble	4 h	100

II.1.3. Polyclonal anti-MTB antibodies production.

- **Polyclonal antibody production over time.**

Purified **rHsp16.3, rMPT64, rMTC28, rMoeX, r38 kDa protein, rAg85B, rESAT6,** and **rCFP10** proteins were used for the immunization of New Zealand rabbits and BALC/C mice to produce polyclonal hyperimmune antibodies.

The antibody elicitation over time and the sera dilution standardization in sandwich ELISA were evaluated. Considering the folds values in the analysis and graphics of ELISA assays, calculated as indicated below.

Fold values (**positive/negative ratio = average of positive OD/ average of negative OD**)

Some ELISA curves to evaluate the production of polyclonal antibodies over time, were not performed with all sera after each dose of immunization. This is because the amount of serum extracted was not enough (especially in mice) or they were hemolyzed in the transport or storage process.

Polyclonal anti-rHsp16.3 production:

In the case of immunization with recombinant Hsp16.3, 4 doses were used in rabbits and 3 doses in mice. In the **rabbit** model (the curve is plotted only until the third dose), we obtained **a fold of 8.25** after the first dose, and subsequently the antibody titer remained stable with **a fold of 6.75 and 6.50** after the second and third doses, respectively. In the case of **mice,** the increase in antibody titer was progressive, reaching **a fold of 13.25** produced by the second dose, and ending with **a fold of 12.50** after the third dose (**Figure II.33**).

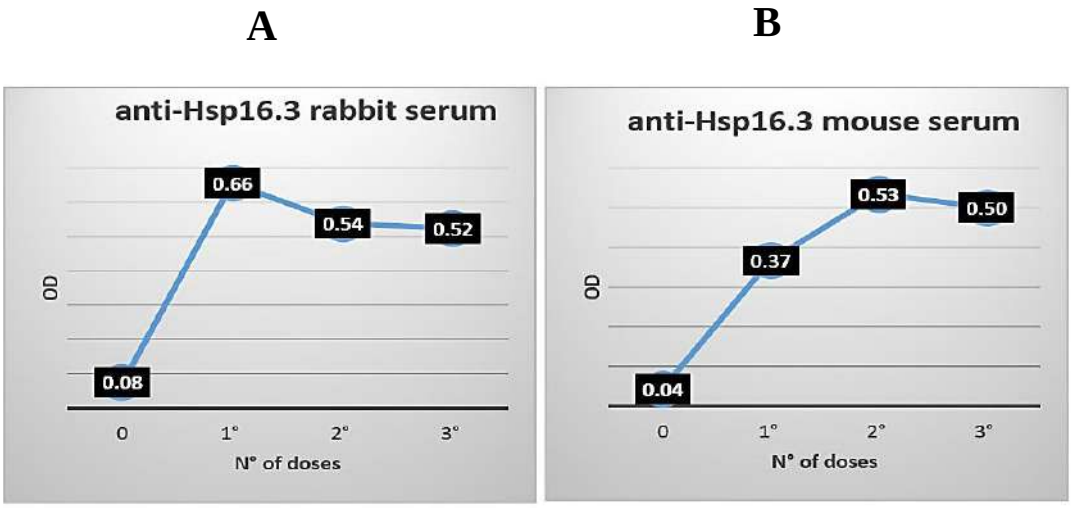

Figure II.33: Evaluation of rabbit (**A**) and mouse (**B**) polyclonal anti-Hsp16.3 production over time (1° dose: 1 day, 2° dose: 14 days, 3° dose: 21 days), using an ELISA test. **OD:** Absorbance 492 nm.

Polyclonal anti-rMPT64 production:

In the case of immunization with recombinant MPT64, 4 doses were used in rabbits and 3 doses in mice. In the curve of ODs obtained for **rabbit sera** (the curve is plotted only

until the third dose)**,** a **fold of 3.13** produced by the second dose can be observed, and it decreases slightly to **a fold of 3.00** after the third dose, remaining generally stable. In the case of **mouse sera**, there is a slight increase in the antibody titers after the first dose, and it increased rapidly after the second dose. For the third dose the titer remains stable with a **fold of 9.2 (Figure II.34).**

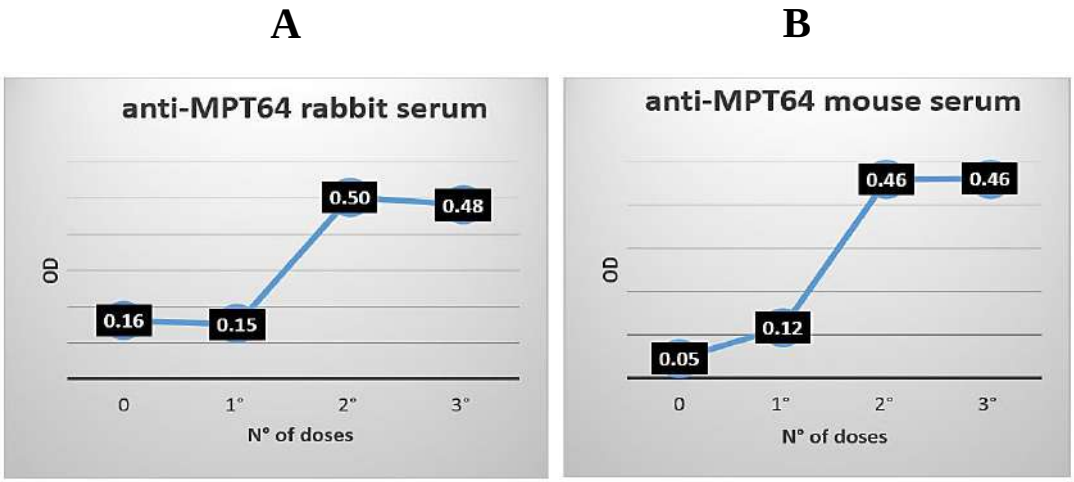

Figure II.34: Evaluation of rabbit (**A**) and mouse (**B**) polyclonal anti-MPT64 production over time (1° dose: 1 day, 2° dose: 14 days, 3° dose: 21 days), using an ELISA test. **OD:** Absorbance 492 nm.

Polyclonal anti-rMTC28 production:

In the case of immunization with recombinant MTC28, 4 doses were used in rabbits and mice. In both models, the curves are plotted only until the third dose. In the **rabbit** model an overproduction of antibody is observed after the first dose with a **fold of 10.25,** this is kept stable after the second dose with **a fold of 8.63-8.75.** Additionally, in the case of **mice** we have an increase in antibody titer after the second dose with **a fold of 15.5**, settling to **a fold of 14.5** after a third dose (**Figure II.35).**

A **B**

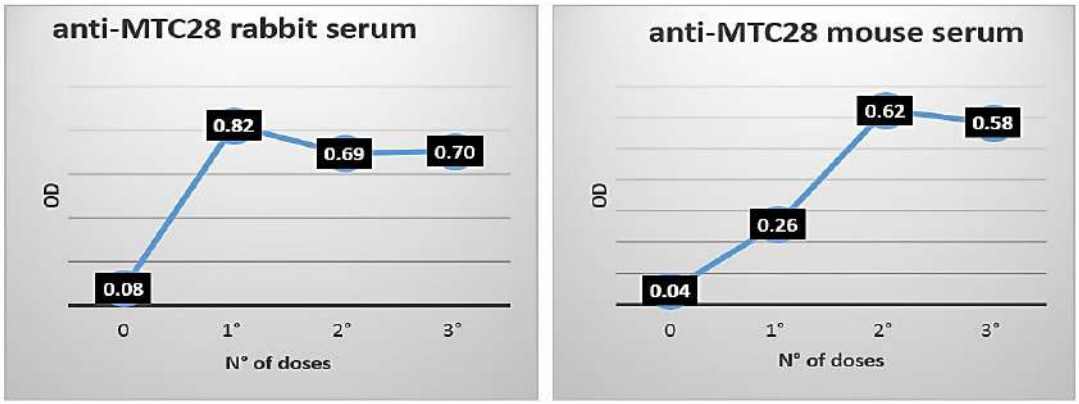

Figure II.35: Evaluation of rabbit (**A**) and mouse (**B**) polyclonal anti-MTC28 production over time (1° dose: 1 day, 2° dose: 14 days, 3° dose: 21 days), using an ELISA test. **OD:** Absorbance 492 nm.

Polyclonal anti-rMoeX production:

In the case of immunization with recombinant MoeX, 3 doses were used in rabbits and 4 doses in mice. The production of polyclonal antibodies in rabbits is constant after the second and third doses with **a fold of 5.73**. In **mice** (the curve is plotted only until the second dose), the increase of polyclonal antibodies is done progressively, observing a fold **of 10.40** after the second dose of immunization (**Figure II.36).**

A **B**

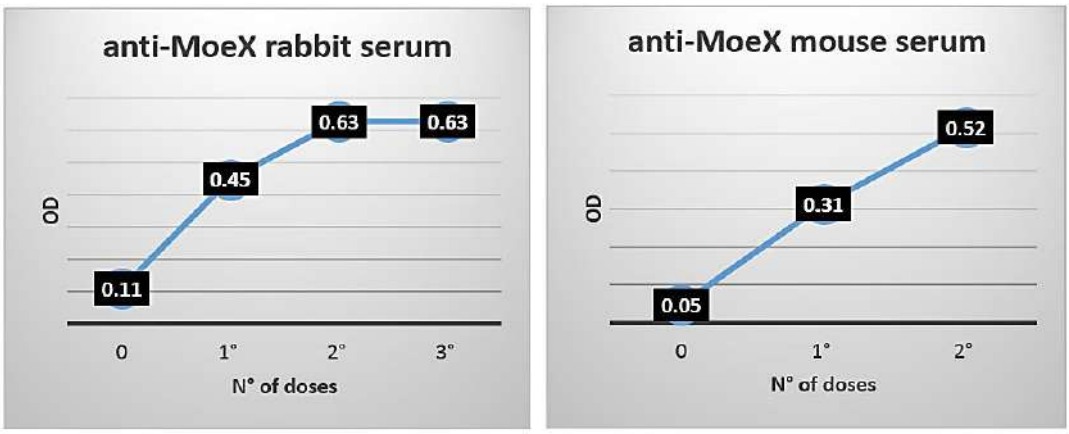

Figure II.36: Evaluation of rabbit (**A**) and mouse (**B**) polyclonal anti-MoeX production over time (1° dose: 1 day, 2° dose: 14 days, 3° dose: 21 days), using an ELISA test. **OD:** Absorbance 492 nm.

Polyclonal anti-r38 kDa protein production:

In the case of immunization with recombinant 38kDa, 4 doses were used in rabbits and 3 doses in mice. The sera collected after each dose were pre-absorbed with *E. coli* antigens before performing the ELISA assay. In **rabbits** (the curve is plotted only until the third dose), a rapid production of antibodies was observed after the first dose with **a fold of 9.60**, remaining stable after the second and third doses **(folds 9.20-9.00).** In the case of **mice sera**, we have an overproduction of antibodies with **a fold of 11.50** after the third dose (**Figure II.37)**.

A **B**

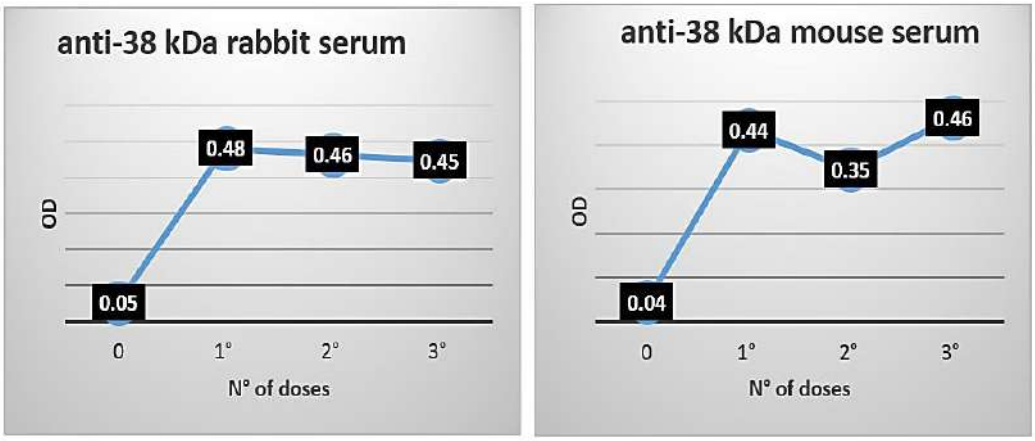

Figure II.37: Evaluation of rabbit (**A**) and mouse (**B**) polyclonal anti-38kDa production over time (1° dose: 1 day, 2° dose: 14 days, 3° dose: 21 days), using an ELISA test. **OD:** Absorbance 492 nm.

Polyclonal anti-rAg85B production:

In the case of immunization with recombinant Ag85B, 4 doses were used in rabbits and 3 doses in mice. A progressive increase in the antibody titer was observed in **rabbit** (the curve is plotted only until the third dose), reaching **a fold of 2.59**; where the OD of the pre-immune serum had a reading of 0.27, which is very high, probably requires a pre-absorption. A fourth dose was considered to increase the antibody production (data not shown). In the case of **mice,** a pre-absorption with *E. coli* antigen was performed before doing the ELISA test. According to the ODs, we have a remarkable increase in the production of antibodies after the second dose, with **a fold of 9.80**, decreasing **to 7.40 after the third dose (Figure II.38).**

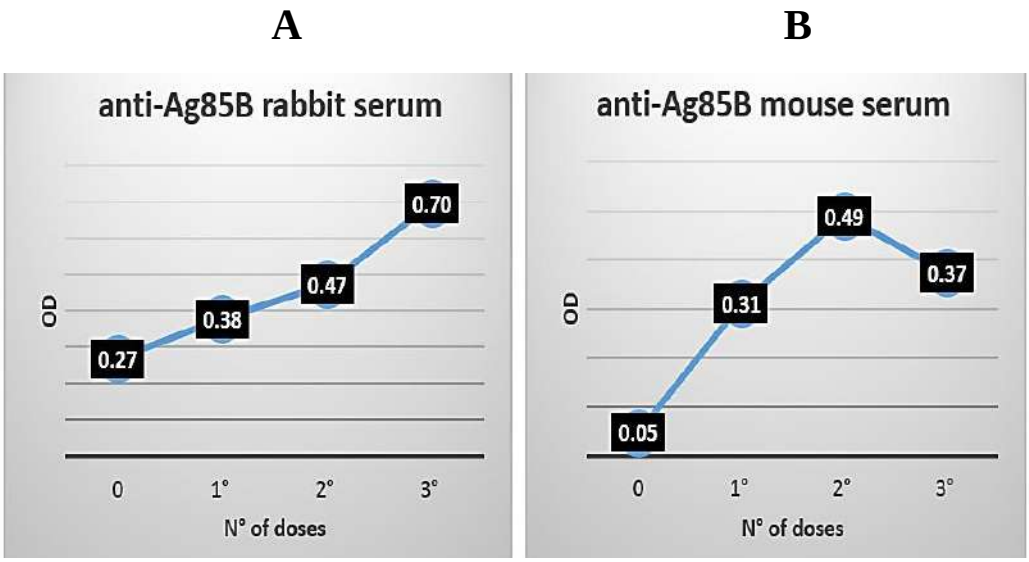

Figure II.38: Evaluation of rabbit (**A**) and mouse (**B**) polyclonal anti-Ag85B production over time (1° dose: 1 day, 2° dose: 14 days, 3° dose: 21 days), using an ELISA test. **OD:** Absorbance 492 nm.

Polyclonal anti-rESAT6 production:

In the case of immunization with recombinant ESAT6, 3 doses were used in rabbits and mice. In the case of **rabbits** (the curve is plotted only until the second dose)**,** we have a significant increase of antibodies after the second dose with **a fold of 13.80**. Otherwise, it is observed in **mice**, where only **a fold of 2.25** is obtained after the second dose. Therefore, the third dose was continued (data not shown) and a fourth dose was not performed because there was not enough of the recombinant protein (**Figure II.39).**

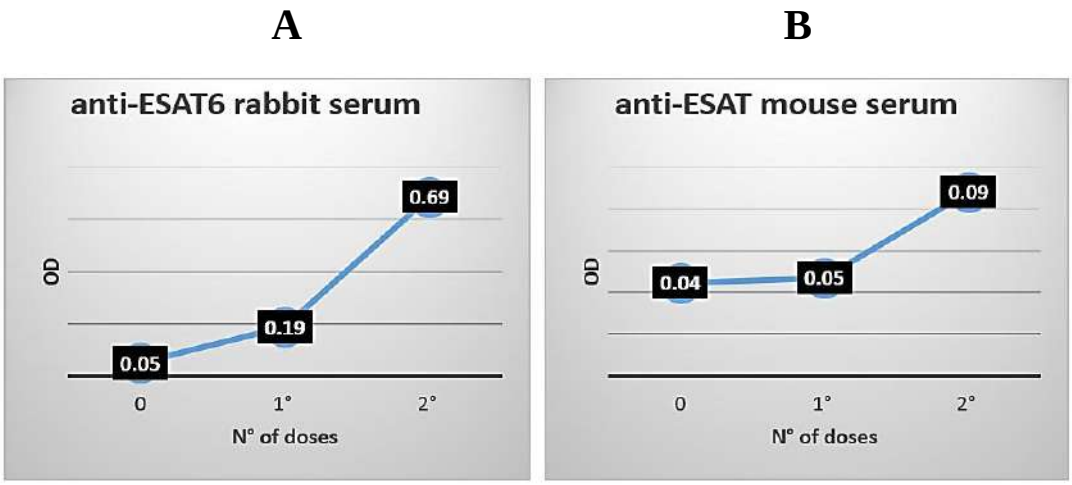

Figure II.39: Evaluation of rabbit (**A**) and mouse (**B**) polyclonal anti-ESAT6 production over time (1° dose: 1 day, 2° dose: 14 days), using an ELISA test. **OD:** Absorbance 492 nm.

Polyclonal anti-rCFP10 production:

In the case of immunization with recombinant CFP10, 3 doses were used in rabbits and mice. After 3 sera collected to perform the assay, a remarkable increase in antibody titer was observed from the second dose, with **a fold of 11.00 and 10.75 in rabbit and mouse**, respectively.

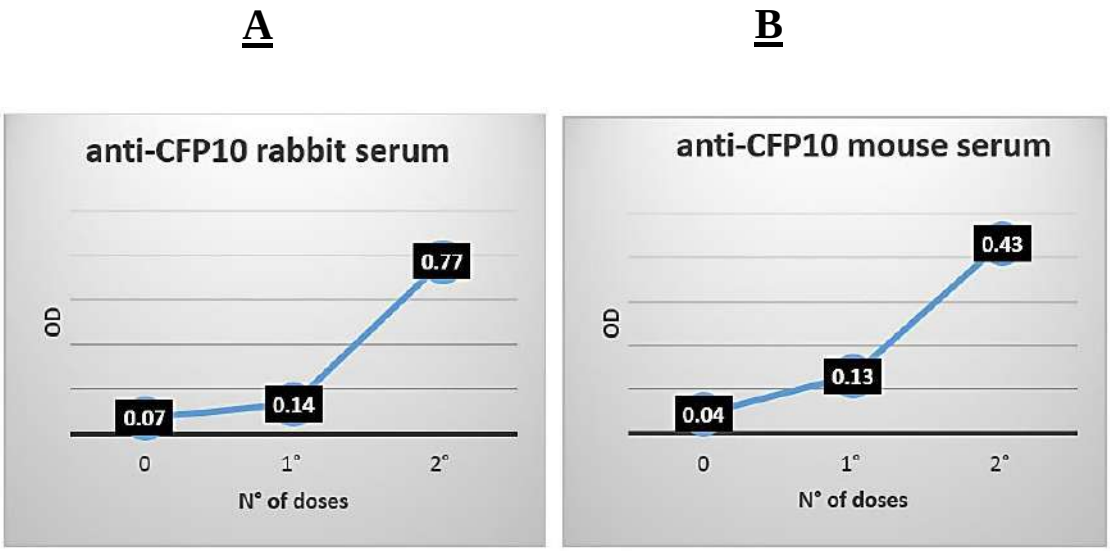

Figure II.40: Evaluation of rabbit (**A**) and mouse (**B**) polyclonal anti-CFP10 production over time (1° dose: 1 day, 2° dose: 14 days), using an ELISA test. **OD:** Absorbance 492 nm.

Table II.3 shows that the polyclonal antibodies were successfully produced in each animal model. In the case of rabbits, after the first dose (7 days) of immunization the antibody titer was raised; except in anti-MPT64, anti-Ag85B and anti-CFP10, which were increased after the second dose (14 days) of immunization. In most cases, the production of polyclonal antibodies was stabilized after the third dose (21 days) (data not shown). But in anti-Hsp16.3 was observed that the production of polyclonal antibodies was stabilized from the second dose, both in rabbits and in mice. In some cases, four doses (28 days) were considered in the immunization protocol.

Table II.3: Summary of the folds obtained during the evaluation of polyclonal antibody production in both rabbits and mice. ELISA protocol (2 days): 1µg antigen/well, 1/250 sera dilution, 1/5000 anti IgG HRP (KPL).

Evaluation of antibody production over time.				
	Rabbits sera		**Mice sera**	
Immunization protein	**N° of Doses**	**Folds**	**N° of Doses**	**Folds**
rHsp16.3	0, 1°, **2°**, 3°	8.25/ **6.75/ 6.50**	0, 1°, **2°**, 3°	9.25/ **13.25**/ 12.50
rMPT64	0, 1°, 2°, **3°**	0.94/ **3.13/ 3.00**	0, 1°, 2°, **3°**	2.40/ 9.20/ **9.20**
rMTC28	0, 1°, 2°**, 3°**	10.25/ **8.63/ 8.75**	0, 1°, **2°,** 3°	6.50/ **15.5**/ 14.5
rMoeX	0, 1°, 2°, **3°**	4.09/ **5.73/ 5.73**	0, 1°, **2°**	6.20/ **10.40**
r38kDa	0, **1°**, 2°, 3°	**9.60/ 9.20/ 9.00**	0, 1°, 2°, **3°**	11.00/ 8.75/ **11.50**
rAg85B	0, 1°, 2°, **3°**	1.41/ 1.74/ **2.59**	0, 1°, **2°**, 3°	6.20/ **9.80**/ 7.40
rESAT6	0, 1°, **2°**	3.80/ **13.80**	0, 1°, **2°**	1.25/ **2.25**
rCFP10	0, 1°, **2°**	2.00/ **11.00**	0, 1°, **2°**	3.25/ **10.75**

- **Evaluation of polyclonal antibody titers produced in rabbits and mice.**

Currently there are many diagnostic tests based on the capture of specific antibodies for TB antigens. However, the detection of human anti-MTB does not determine the diagnosis of active TB, because cross-reactions are observed with sera from people exposed to MTB, people vaccinated against TB, or in people who had TB and have already been cured (Steingart *et al.*, 2011). For this reason, many efforts are focused on developing diagnostic tests to directly detect MTB antigens.

On the other hand, there are highly specific antigens that have been proven to be effective in discriminating infectious mycobacteria from non-pathogenic mycobacteria (Meier *et al.*, 2018). These antigens have been studied and evaluated in diagnostic tests to detect specific antibodies.

Caccamo *et al.* (2010) reported that immune responses to ESAT6/CFP10 and Ag85B from MTB, were significantly higher in active TB than in latent TB infection (LTBI) (Caccamo *et al.*, 2010). In this way, Zhang *et al*. (2015), reported an ELISA to detect anti-Ag85B-Hsp16.3. In the case of active TB, the sensitivity and specificity reported were 61.67% and 95.65%, respectively. In LTBI, theses parameters were 60.00% and 73.91%, respectively (Zhang *et al.*, 2015).

In order to improve the detection efficiency, additional assays combining the antigens were made. The optimal antigen combination to diagnose active TB was Ag85B-Hsp16.3/ESAT6 with a specificity and sensitivity of 93.33% and 92.39%, respectively. In the case of LTBI, it was Hsp16.3/ESAT6, with a specificity and sensitivity of 75.0% and 76.67%, respectively (Zhang *et al.*, 2015).

These studies with human sera from patients with TB and LTBI indicate that the proteins selected for MTB diagnosis are very immunogenic.

Evaluation of anti-rHsp16.3 titers:

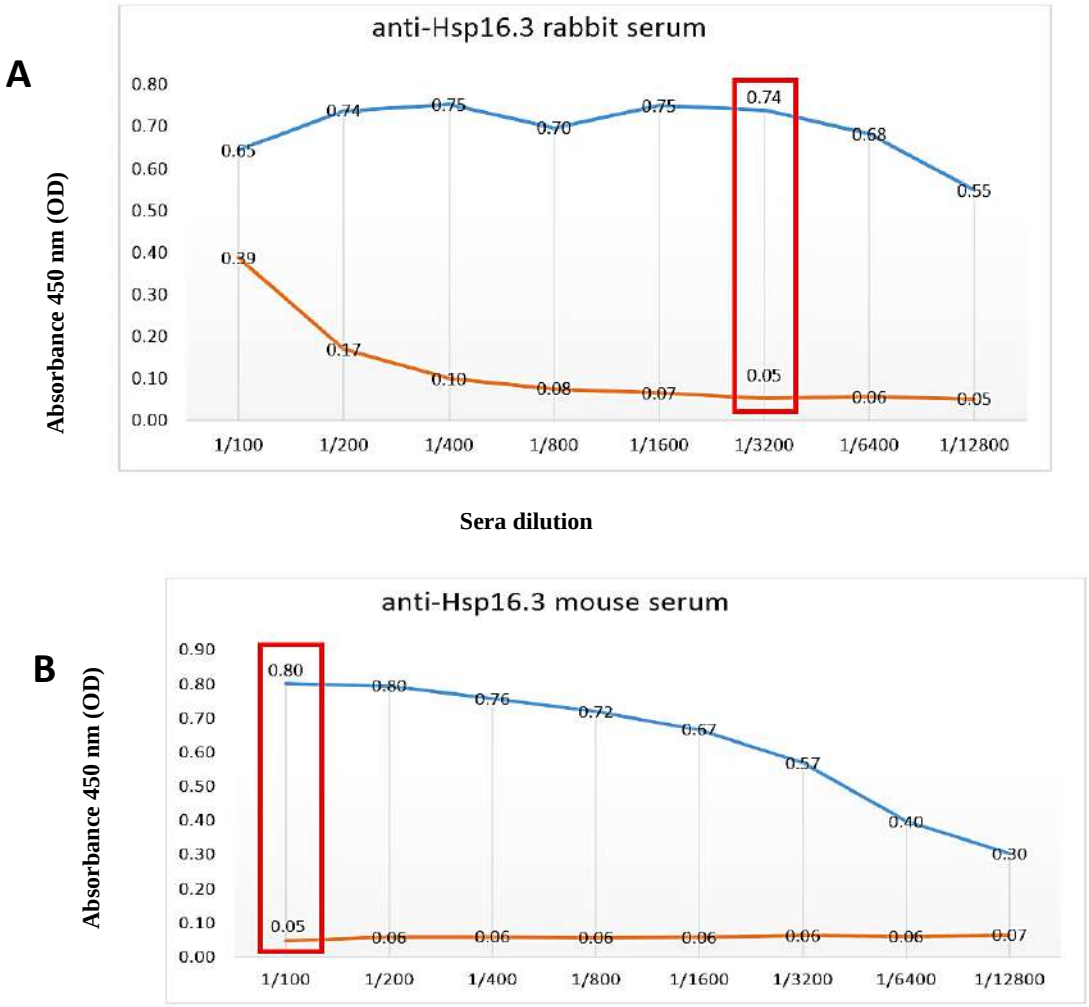

Figure II.41: Evaluation of the **anti-Hsp16.3** antibody titre produced in **rabbit (A)** and **mice (B)**. The orange curve indicates the OD values of the pre-immune serum (negative), while the blue curve shows the OD values of the serum immunized. In red, the highest fold **(14.80)** is observed in a dilution of **1/3200 (rabbit)** and a fold of **16.00** in the **1/100** dilution (**mice**).

In the case of Hsp16.3, the small heat shock protein protects the MTB through an association of the protein with MTB membrane (Zhang *et al.*, 2005). This could explain why this antigen is found in large quantities in the TB serum. Zhang *et al.*, 2015, reported

an ELISA to capture anti-Hsp16.3 for detecting TB antibody response in humans. In the case of active TB, the sensitivity and specificity reported were 63.33% and 88.04%, respectively. But in LTBI, theses parameters were 53.33% and 88.04%, respectively (Zhang *et al.*, 2015).

In our work, a high fold was observed for the anti-Hsp16.3 produced in rabbits and mice, at dilutions of 1/3200 and 1/100 respectively (**Figure II.41).**

Evaluation of anti-rMPT64 titers.

MPT64 antigen is a major secretory protein of MTB (specific for MTBC), and it is not expressed in non-pathogenic mycobacteria. Ji *et al.* (2014) reported a sandwich ELISA to detect MPT64 protein using monoclonal antibodies. The assay showed a lower detection limit of 2.1 ng/mL and 1.7×10^4 CFU/mL of MTB. Using 389 clinical MTB culture suspensions, the sensitivity and specificity were calculated, obtaining 100% for both parameters (Ji *et al.*, 2014).

A disadvantage of the previously described study was that the clinical samples had to be previously cultured before applying them to the MPT64 sandwich ELISA. Consequently, this method took a longer time for the TB diagnosis.

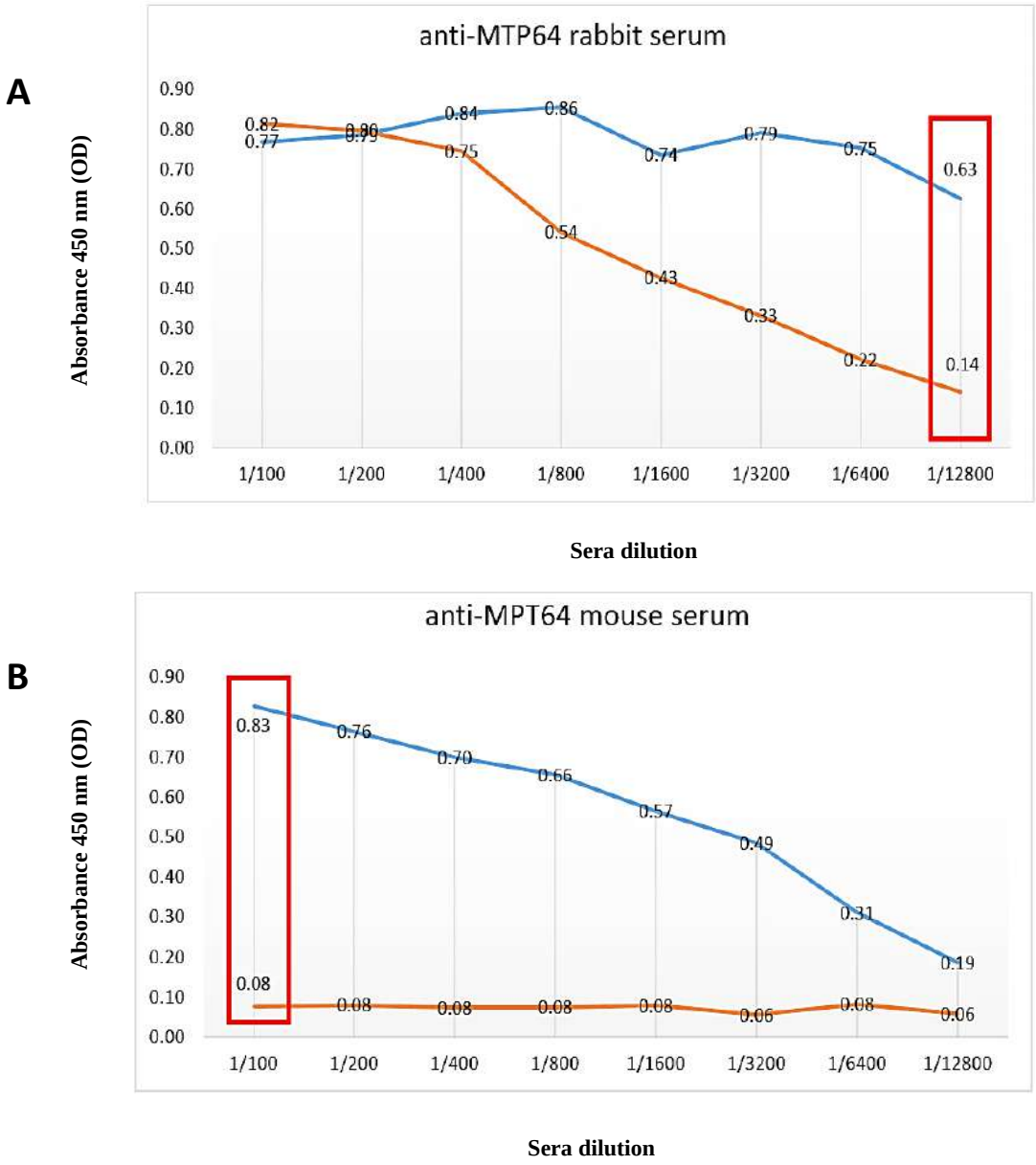

Figure II.42: Evaluation of the dilution of **anti-MPT64** antibody produced in rabbit (**A**) and mice (**B**). The orange curve indicates the OD values of the pre-immune serum (negative), while the blue curve shows the OD values of the serum immunized. In red, the highest **fold (4.5**) is observed in a dilution of **1/12800 (rabbit**) and a fold **of 10.34 in the 1/100 dilution (mice**).

In our study, we introduce magnetic nanoparticles in a sandwich ELISA to improve the MTP64 antigen detection and thus reduce the time of the TB diagnosis process. For this purpose, the standardization of the dilution of anti-MPT64 previously produced in rabbits

and mice is important. In the **Figure II.42** a **fold of 4.50** is observed in a dilution of **1/12800 for anti-MPT64 produced in rabbit** and a fold **of 10.34 in the 1/100 dilution for anti-MPT64 mice serum**.

Evaluation of anti-rMTC28 titers.

MTC28 is a component immunologically active of the MTB culture filtrate. MTC28 elicited strong immune responses in immunized guinea pigs comparable with immunodominant secreted antigens (MPT64 and 38kDa antigen) (Manca *et al*., 1997). Lim *et al*., 1995 reported that ~ 25% of patients with active TB showed a strong antibody response to MTC28. This strong immunological activity of MTC28 is associated with specificity for MTC (Lim *et al.*, 1995).

This high specificity makes the MTC28 protein an excellent diagnostic candidate. In our case, the immunogenicity of rMTC28 was corroborated by producing polyclonal antibodies in rabbits and mice. In addition, a high dilution of the serum was observed to detect the recombinant antigen (**Figure II.43**). A fold of **9.33** is observed in a dilution of **1/400 in rabbit serum** and a fold of **10.20 in the 1/50** dilution in mice.

A

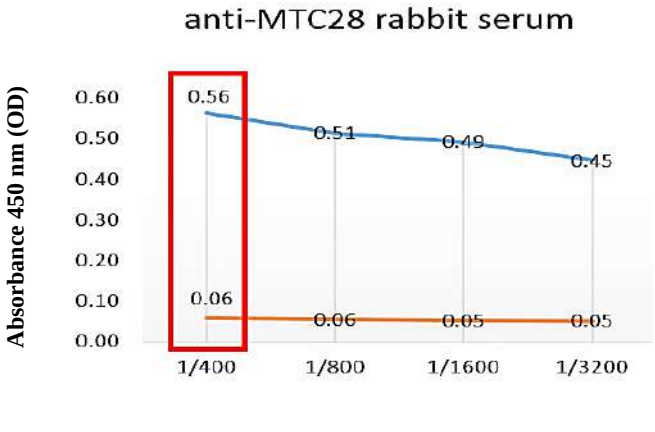

B

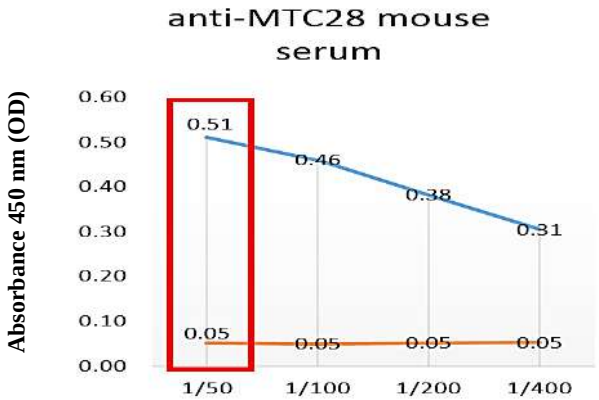

Figure II.43: Evaluation of the **anti-MTC28** antibody dilution in rabbit (**A**) and mice sera (**B**). The orange curve indicates the OD values of the pre-immune serum (negative), while the blue curve shows the OD values of the serum immunized. In red, the highest fold (**9.33**) is observed in a dilution of **1/400 (rabbit**) and a fold of **10.20 in the 1/50** dilution (mice).

Evaluation of anti-rMoeX titers.

In the case of MoeX, this protein was reported as specific antigen for MTBC. Also, this protein was described as an attractive candidate for the development of a highly sensitive and specific urine MTB antigen detection test (Pollock *et al.*, 2013). This is one of the reasons why the protein was selected for this study. The standardization of the anti-MoeX dilution produced in rabbits and mice is required to verify the antigenicity of the protein as well as the production of the antibodies.

Figure II.44 shows that anti-MoeX produced in **rabbit** has a fold of **8.00** in a sera dilution of **1/12800.** In the **mice,** the fold is **9.20** in a sera dilution of **1/50.**

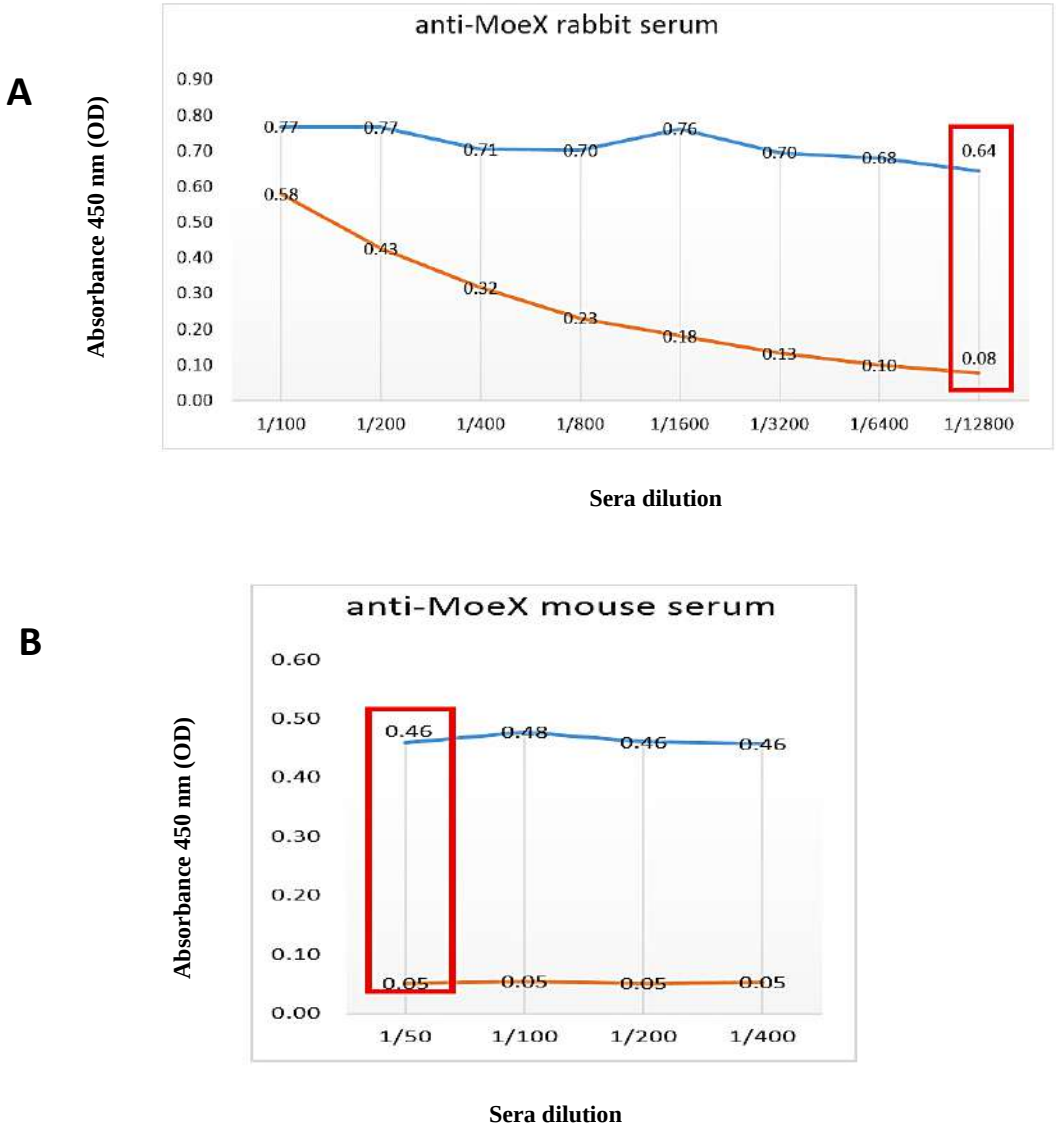

Figure II.44: ELISA using lyophilized **anti-MoeX** polyclonal sera extracted from rabbits (**A**) and mice (**B**). The orange curve indicates the OD values of the pre-immune serum (negative), while the blue curve shows the OD values of the serum immunized. **In rabbit a fold of 8.00 (1/12800) and in mice 9.20 (1/50)** is observed.

Evaluation of anti-r38 kDa protein titers.

B and T cell responses are induced by 38 kDa protein with high specificity for TB infection. It could be due to its extracellular localization (Harboe and Wiker, 1992). Tiwari

et al. (2014) reported an ELISA test standardized for the major protein antigens (6, 27, 30, 38 and 64 kDa) obtained from MTB culture filtrated proteins (antigens not described). An enhanced sensitivity (~98.67 %) and specificity (~98.06 %), compared with commercial ELISA assays, were found for the mixture proteins (Tiwari *et al.*, 2014).

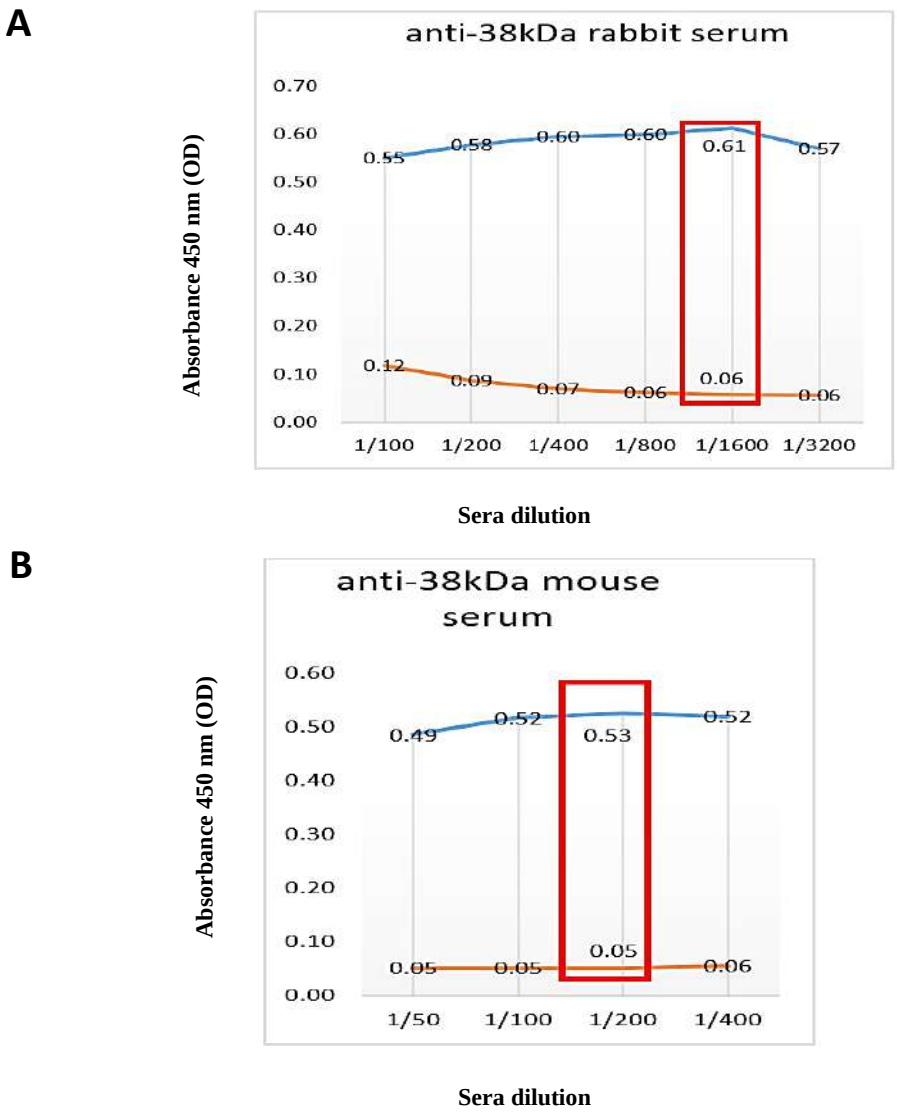

Figure II.45: ELISA using lyophilized **anti-38kDa** polyclonal sera extracted from rabbits (**A**) and mice (**B**). The orange curve indicates the OD values of the pre-immune serum (negative), while the blue curve shows the OD values of the serum immunized. In **rabbit a fold of 10.17 (1/1600) and in mice 10.60 (1/200)** is observed.

This indicates that the 38kDa protein, like the others studied, activates the immune response of the host, allowing the production of antibodies. This was corroborated with the ELISAs performed with the anti-38kDa produced in rabbits and mice. **Figure II.45** shows a fold of **10.17** for **1/1600** dilution of sera obtained from immunized **rabbit**, and a fold of **10.60** for **1/200** dilution from **mice** sera.

Evaluation of anti-rAg85B titers.

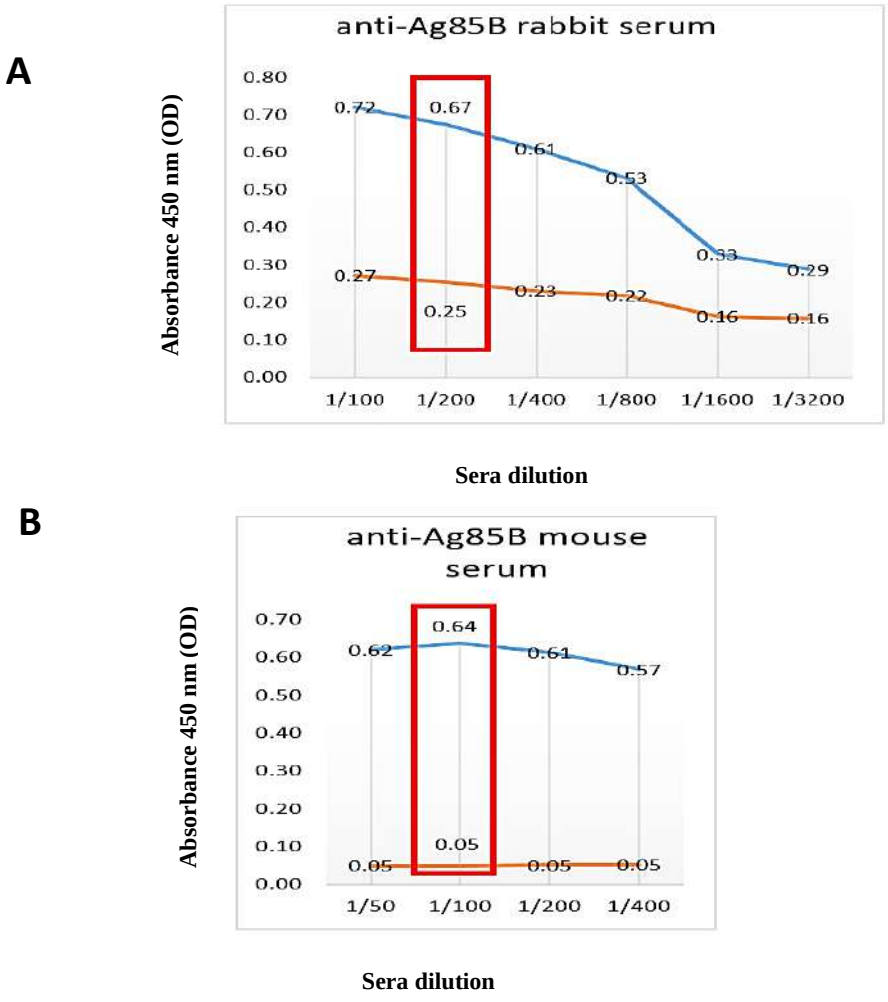

Figure II.46: ELISA using lyophilized **anti-Ag85B** polyclonal sera extracted from rabbits and mice. The orange curve indicates the OD values of the pre-immune serum (negative), while the blue curve shows the OD values of the serum immunized. In **rabbit** a fold of **2.68 (1/200)** and in **mice 12.80 (1/100)** is observed.

Ag85B protein is the most abundant protein secreted by MTB and it is a potent immunoprotective antigen (Anderson *et al.*, 2001). Zhang *et al*., 2015, reported an ELISA to capture anti-Ag85B for detecting TB antibody response in humans. In the case of active TB, the sensitivity and specificity were 53.33% and 97.83%, respectively; in LTBI, theses parameters were 60.00% and 88.04%, respectively (Zhang *et al.*, 2015). In this sense, the Ag85B protein proved to be highly immunogenic, and this was corroborated by our results of immunization process of rabbits and mice. **Figure II.46** shows a fold of **2.68** in a dilution of **1/200** for anti-Ag85B produced in **rabbit**, and a fold of **12.80** for a dilution **1/100** in **mice** sera.

Evaluation of anti-rESAT6titers.

In the case of ESAT6, Feng *et al*., 2013 reported that the sensitivity of ESAT6 antigen to detect antibodies in TB patients varies from 5% to 76% with a specificity ranging of 51% to 100% (Feng *et al.*, 2013). Therefore, a careful standardization of the method for this marker was carried out by other research groups. For example, Zhang *et al*. (2015) reported an ELISA to capture anti-ESAT6 for detecting TB antibody response in humans. In the case of active TB, the sensitivity and specificity reported were 86.67% and 95.65%, respectively. But in LTBI, theses parameters were 60.00% and 84.78%, respectively (Zhang *et al*., 2015). As the protein was able to produce antibodies in TB patients, the rESAT6 was used and used for the immunization of rabbits and mice in this study.

Figure II.47 shows a fold of **10.80** in anti-ESAT6 dilution of **1/400 (mice).** Data from the evaluation of rabbit serum titers are not shown because there was not enough antigen available for the ELISA assay.

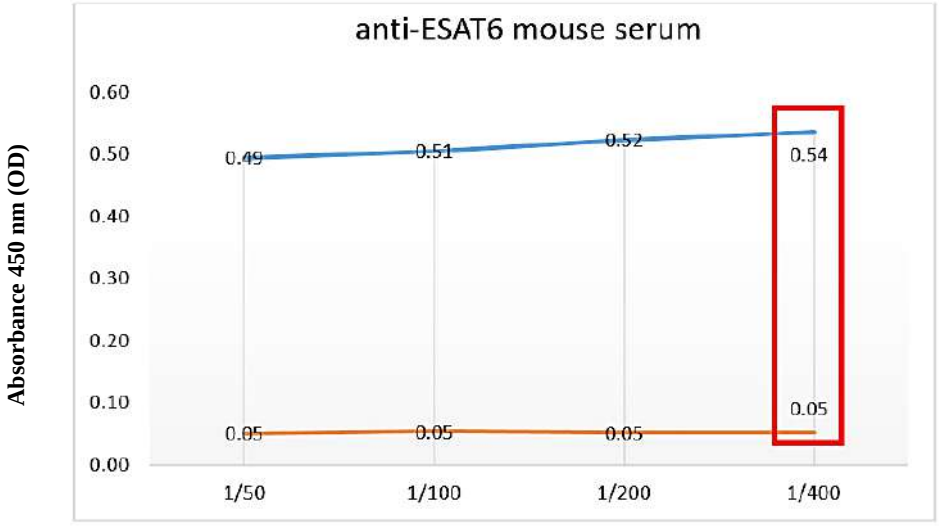

Figure II.47: ELISA using lyophilized **anti-ESAT6** polyclonal sera extracted from mice. The orange curve indicates the OD values of the pre-immune serum (negative), while the blue curve shows the OD values of the serum immunized. A fold of **10.80 (1/400)** is observed.

Evaluation of anti-rCFP10 titers.

In the case of CFP10, Parkash *et al*. (2009) reported that the sensitivity of ELISA using CFP10 to detect antibodies in TB patients varies from 9% to 78% with a specificity ranging of 55% to 100%. This variation in sensitivity and specificity may be due to the conditions and the type of test or protocol performed for the immunodiagnostic (Parkash *et al*., 2009).

Zhang *et al.* (2015) reported an ELISA to capture anti-CFP10 for detecting TB antibody response in humans. In the case of active TB, the sensitivity and specificity reported were 80.00% and 80.43%, respectively. But in LTBI, theses parameters were 73.33% and 69.57%, respectively (Zhang *et al.* 2015). This last study indicates the antigenic capacity of the protein. **Figure II.48** shows the dilution standardization for anti-CFP10 produced in **rabbit** (fold of **11.57**, dilution of **1/200**) and in **mice** (fold of **14.33**, dilution of **1/100**).

A

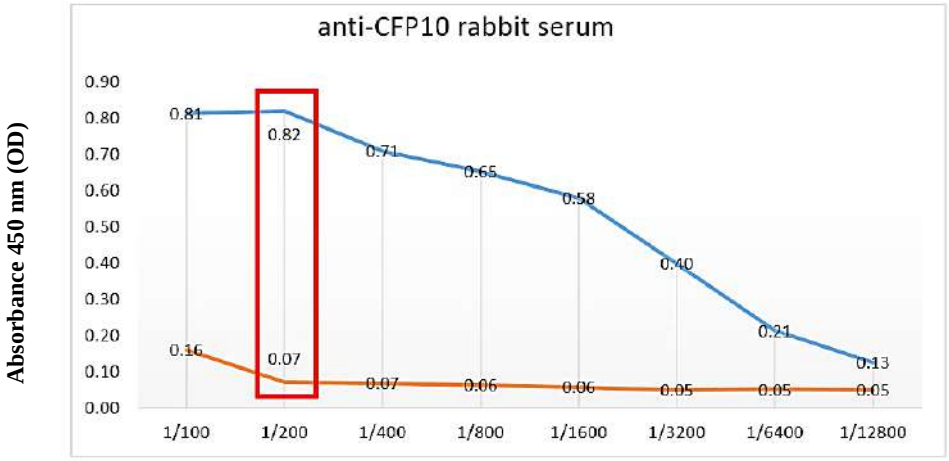

B

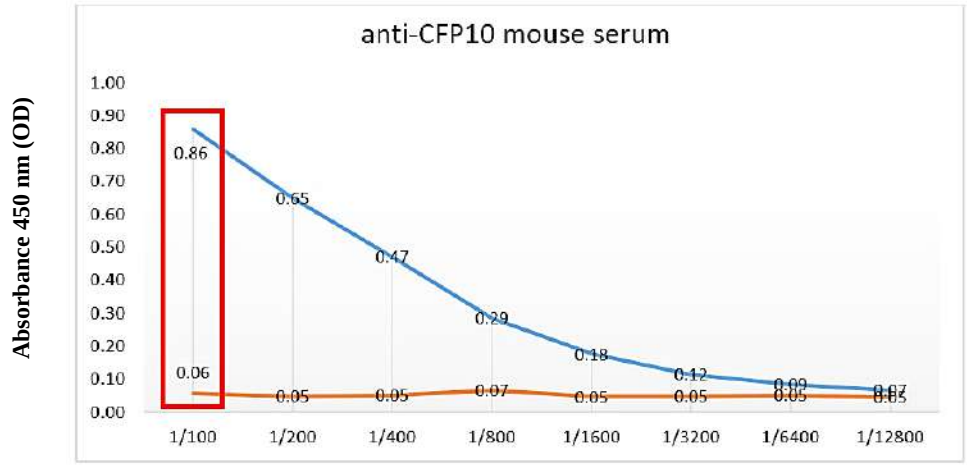

Figure II.48: ELISA using lyophilized **anti-CFP10** polyclonal sera extracted from rabbits (**A**) and mice (**B**). The orange curve indicates the OD values of the pre-immune serum (negative), while the blue curve shows the OD values of the serum immunized. In **rabbit** a fold of **11.57 (1/200)** and in **mice 14.33 (1/100)** is observed.

The best conditions evaluated to detect MTB antigens during the standardization of specific sera dilution, are summarized in the **Table II.4**.

Table II.4: Optimized conditions for the evaluation of the titer of antibodies produced in rabbits and mice immunized with the recombinant *M. tuberculosis* antigens. ELISA test performed in a protocol of 2 days.

Protein	Antigen/ well	Blocking solution	anti-IgG HRP	Rabbit serum	FOLD	Mouse serum	FOLD
rHsp16.3	1 µg	Milk	1/5000 KPL	1/ 3200	14.80	1/ 100	16.00
rMPT64	1 µg	Milk	1/5000 KPL	1/12800	4.50	1/ 100	10.34
rMTC28	0.25 µg	Casein	1/1500 Thermo	1/400	9.33	1/50	10.20
rMoeX*	1 µg and 0.25 µg	Milk and casein	1/5000 KPL and 1/1500 Thermo	1/12800	8.00	1/50	9.20
r38kDa	0.25 µg	Casein	1/1500 Thermo	1/1600	10.17	1/200	10.60
rAg85B	0.25 µg	Casein	1/1500 Thermo	1/200	2.68	1/100	12.80
rESAT6	0.25 µg	Casein	1/1500 Thermo	-	-	1/400	10.80
rCFP10	1 µg	Milk	1/5000 KPL	1/200	11.57	1/100	14.33

*1 µg, milk and 1/5000 anti-IgG HRP KPL for ELISA using rabbit serum and 0.25 µg, casein and 1/1500 anti-IgG HRP Thermo for ELISA using mouse serum.

- **Standardization of antibody titers for a sandwich ELISA using antibodies produced in rabbits and mice.**

In contrast to the previously described assays, where rabbit and mouse antibodies were evaluated separately, in this section rabbit and mouse antibody titres are evaluated in the same sandwich ELISA assay to detect the recombinant MTB antigen (protocol describe in **Section II.2, page 115**). **Table II.5** summarizes the optimized dilutions of sera from rabbits and mice for the sandwich ELISA.

The CFP10 and ESAT6 proteins have low folds (<2), which would indicate that the amount of immunocomplexes formed during the assay is very low. These results could be due to non-optimal conditions of the recombinant proteins (low amounts and slight precipitation).

The Hsp16.3, MTC28 and 38 kDa proteins presented folds > 2.28. In the case of MPT64, MoeX and Ag85B, folds greater than 5.0 were obtained. About the specific sera for MoeX, Ag85B and MPT64, the highest folds were observed.

Table II.5: Summary of the optimized experimental conditions for the antibodies dilution standardization in sandwich ELISA tests.

Protein	**Rabbit serum**	**blocking**	**Mouse serum**	**Antigen/ well**	**Anti-IgG HRP**	**FOLD**	**time**
rHsp16.3	1/400	casein	1/1600	100 ng	1/1500 Thermo	3.26	2 days
rMPT64	1/1600	milk	1/200	250 ng	1/5000 KPL	6.25	2 days
rMTC28	1/800	casein	1/400	250 ng	1/1500 Thermo	3.60	2 days
rMoeX	1/800	casein	1/800	100 ng	1/1500 Thermo	5.00	2 days
r38kDa	1/3200	milk	1/200	250 ng	1/5000 KPL	2.28	2 days
rAg85B	1/3200	milk	1/200	250 ng	1/5000 KPL	6.39	2 days
rESAT6	1/800	milk	1/200	250 ng	1/5000 KPL	1.77	2 days
rCFP10	1/3200	milk	1/400	250 ng	1/5000 KPL	1.93	2 days

II.2. EXPERIMENTAL SECTION (METHODOLOGY).

II.2.1. Selection of MTB biomarkers.

Secretory and non-secretory antigens, abundant and specific for the MTB complex, and that have been previously published and tested in TB diagnostics (for the detection of antigens or circulating antibodies) were selected. An exhaustive review of the main MTB antigens was carried out (**Table II.1).** In this study, **rHsp16.3, rMPT64, rMTC28, rMoeX, r38 kDa protein, rAg85B, rESAT6,** and **rCFP10,** from *M. tuberculosis* were selected. An important selection criterion was that the selected antigens have been described in at least one diagnostic method. Most of the diagnostic tests were immunological assays (ELISA) to detect specific human anti-MTB antibodies.

On the other hand, assays to detect DNA and antigens are also described. For the detection of antigens, more sophisticated methods have been developed, including SPR spectroscopy, Mass spectrometry, nanoparticles-based biosensors among others.

II.2.2. Cloning and expression of recombinant proteins from *M. tuberculosis* in *E. coli* system.

Cloning and expression of the recombinant antigens were made in *E. coli* system using the pET28(a+) and the pGEX4T1 vectors, as it is described below.

- **Primers design.**

Primers (5'→3') were designed using Primer3Plus (http://www.bioinformatics.nl/cgi-bin/primer3plus/primer3plus.cgi), Primer Blast (https://www.ncbi.nlm.nih.gov/tools/primer-blast/), and OligoAnalyzer 3.1 (https://eu.idtdna.com/calc/analyzer) softwares; and specific sites for restrictions enzymes of the vector pET28a(+) (Merck, Darmstadt, Germany) and pGEX4T1 (GE Healthcare Life Sciences) were included (**Table II.6).**. Using the SnapGene software (http://www.snapgene.com), the correct alignments of the primers in the target sequences have been verified.

Table II.6: Sequences of the designed primers (**5 '→ 3'**) to clone and express the recombinant proteins of MTB, in the *E. coli* system. Underlined the restriction enzymes sequences.

Primer name	5'→ 3'	Restriction enzymes	Fragment (pb)
MTC28_F	TTT**CCATGG**GGATGATCCAGATCGCGCGCACCT	NcoI	950
MTC28_R	TTT**CTCGAG**GCGCGGCGGGACTGGTGTCA	XhoI	
MPT64_F	TTT**CCATGG**TGCGCATCAAGATCTICATGCTGG	NcoI	701
MPT64_R	TTT**CTCGAG**GGCCAGCATCGAGTCGATCGCGGAA	XhoI	
MoeX_F	TTT**CCATGG**GGATGATCATAGAGCTGATGCGCCGGGTGG	NcoI	1010
MoeX_R	TTT**CTCGAG**CGCACACGGGAACAACGCGGCCTCTT	XhoI	
38kDa_F	TTT**CCATGG**TGAAAATTCGTTTGCATACGCTGTTGG	NcoI	1139
38kDa_R	TTT**CTCGAG**GCTGGAAATCGTCGCGATCAA	XhoI	
Ag85B_F	TAC**CATGG**GCATGACAGACGTGAGCCGAAA	NcoI	994
Ag85B_R	CGC**AAGCTT**GCCGGCGCCTAACGAAC	HindIII	
CFP10_F	TTT**CCATGG**CAGAGATGAAGACCGATGCCGCTAC CC	NcoI	321
CFP10_R	TTT**GGATCC**TCAGTGATGGTGGTGATGATGGAAG CCCATTTGCGAGGACAGCGCCT	BamHI	
ESAT6_F	TAA**GGATCC**ATGACAGAGCAGGAGTG	BamHI	302
ESAT6_R	GC**GAATTC**TGCGAACATCCCAGTG	EcoRI	
Hsp16.3_F	TTT**CCATGG**CCACCACCCTTCCCGTTCAGCGCC	NcoI	446
Hsp16.3_R	TTT**CTCGAG**GTTGGTGGACCGGATCTGAATGTG	XhoI	

- **Construction of the recombinant plasmids.**

Total DNA was extracted from the *Mycobacterium tuberculosis* H37Rv culture using phenol-chlorofom method (Sigma-Aldrich, Saint Louis, USA). DNA quality and concentration were determined using the spectrophotometer Nanodrop ND 2000 (Thermo Scientific, Delaware, USA). The coding sequences**: CFP10, ESAT6, MTC28, MPT64, 38 kDa protein, Hsp16.3, Ag85B** and **MoeX** from *M. tuberculosis* DNA were amplified using 'Phusion Flash High-Fidelity PCR Master Mix' (Thermo Fisher Scientific, Vilnius,

Lithuania) by a conventional PCR reaction (1.25 µM _F, 1.25 µM _R, 150 ng ADN in a final volume of 200 µl). The cycling PCR program profile was: 98 °C for 10 seconds for initial activation; 30 cycles of 98 °C for 1 second, 60 °C for 5 seconds, 72 °C for 15 seconds; and a final extension of 72 °C for 5 minutes, according to the manufacturer's instructions. The amplification products were visualized on a 1.2% agarose gel.

The amplified coding sequences from *M. tuberculosis* were purified using QIAquick® PCR Purification Kit (QIAGEN, Center Mainz, Germany). Subsequently, amplicons and plasmids were digested with their respective restriction enzymes (10U of enzyme/µg of DNA, in a final volume of 120 µL) at 37 °C for 16 hours. The digested products were again purified using QIAquick® PCR Purification Kit and observed on an agarose gel.

Purified digested coding sequences and the digested plasmid were ligated with T4 DNA ligase (New Englands Biolab, Ipswich, England) for 16 h at 16 °C, in a proportion 3:1 (150 ng coding DNA: 50 ng plasmid). A volume of 5 µL of plasmid ligated with the coding sequence was used to transform competent *E. coli* Novablue™ cells (Novagen®, Madison, USA) by heat shock: 30 min on ice, 1 min at 42 °C, 2 min on ice. To reconstitute the bacterial cell wall, 500 µL of Luria-Bertani (LB) liquid medium was added, and incubated for 3 h at 37 °C. The pellet obtained by centrifugation was resuspended in 100 µL LB. Using the drigalsky loop, 50 µL of the bacterial suspension was seeded in a solid medium supplemented with antibiotics. Transformed bacterial clones containing the pET28a plasmid were selected by kanamycin resistance (40 µg/mL) while the clones with pGEX4T1 plasmid by Carbanicilin resistance (100 µg/mL), in LB agar cultured at 37 °C for 16 h.

- **Verification of the correct insertion of the MTB coding sequences in the selected plasmids.**

Six clones of each plate of transformed clones were seeded in 6 quadrants of an LB plate supplemented with antibiotics. Plasmid DNA was extracted using alkaline-lysis method. A well-loaded bacterial was resuspended in 150 µL of elution buffer (**buffer I or**

cell suspension solution: 50 mM glucose, 10 mM EDTA, 25 mM Tris pH 7.5), then 200 µL of lysis buffer (**buffer II or lysis buffer:** 0.2 N NaOH, 1% SDS w/v) was added. The mixture was incubated by 5 minutes at RT, 250 µL of binding buffer (**buffer III our neutralization buffer:** 3 M potassium acetate, pH 5.2) was added and incubated for 5 minutes on ice, the tubes were centrifuged at 13000 rpm for 8 min, the supernatant was separated in a clean tube and 600 µL of cold absolute ethanol were added and incubated at -70 °C for 30 min, then centrifuged at 13000 rpm for 5 min. The supernatant was discarded and 1 ml of cold 70% ethanol was added into the tube. The tubes with precipitated DNA were centrifuged at 13000 rpm for 5 min, the supernatant was discarded, and the pellet was dried at 60 °C for 10 min, the plasmid DNA was resuspended with 200 µL elution buffer.

To verify the coding sequence insertion in the plasmid, electrophoresis in a 1.2% agarose gel was made to evaluate a size difference between the plasmid-sequence and the plasmid without coding sequence. Additionally, PCR and sequencing (Macrogen) was made to corroborate the results.

- **MTB protein expression.**

The selected transformed clones were grown in LB culture supplemented with antibiotic. The vector with inserted gene was purified with QIAprep Spin Miniprep kit (QIAGEN, Valencia, CA) and used to transform *E. coli* BL21 (DE3) pLys competent cells (Novagen, Madison, WI, USA) by heat shock.

Transformed cells were used to express the recombinant protein using 0.5 - 0.8 mM Isopropyl β-D-1-thiogalactopyranoside, or IPTG (Sigma-Aldrich, Mannheim, Germany) inductor, at a bacterial optical density of 0.6-0.8, ON, at RT or 37 °C depending of protein (Table II.2).

- **Purification and quantification of recombinant protein.**

The purification of recombinant protein was carried out by affinity chromatography using columns HisTrap HP histidine-tagged protein purification columns (GE Healthcare Life Sciences, Uppsala, Sweden). The proteins were eluted at different concentrations of

imidazole (20, 40, 60, 100, 300 and 500 mM) in phosphate buffer (20 mM phosphate buffer, 500 mM NaCl, pH 7.4). The protein was concentrated by the Amicon ultrafiltration system (Millipore Corporation, Bedford, USA), where the imidazole concentration was reduced with serial washings with the same phosphate buffer. In the case of the ESAT6 protein, it is fused at the *N*-terminus, with the glutathione *S*-transferase (GST) protein. For its purification a column coated with glutathione substrate (Glu-Cys-Gly) was used, the washes were done with phosphate buffer pH 7.4, and then the thrombine enzyme was added and the mixture was incubated for 16 h at RT. The purified ESAT6 was collected in clean eppendorf tubes and stored at -20 °C. The purified recombinant protein was quantified by Bradford assay (BioRad).

II.2.3. Production of hyperimmune polyclonal antibodies in rabbit and mice.

The protocols used in experimental animals were approved by the Institutional Ethics-Animal Committee of the Universidad Peruana Cayetano Heredia (UPCH). In all cases, the experimental animals were acclimated for a period of two weeks before starting the immunization. The immunization protocol is summarized in **Table II.7** and is described below:

- **Rabbit Immunization.**

Nine New Zealand rabbits 1.0 - 1.5 months old and weighting between 1.8 and 2.3 kg were used and obtained from the National Institute of Health (INS) of Peru. Rabbits were immunized with previously expressed recombinant proteins. The immunization was subcutaneous and included 3-4 doses, using Quil-A® adjuvant (InvivoGen, California, USA). Before immunization, the pre-immune serum was obtained (1 ml of venous blood from a marginal vein). Similarly, the post-immune serum was obtained periodically before each immunization in an approximate volume of 1 ml of venous blood (marginal vein), 14 days after the first immunization and at 7-day intervals after the second and third doses. In some cases, described below, a fourth dose was used. To collect venous blood

aseptically, ethanol 70 % was used. A local lidocaine ointment was applied to the skin of the ear at least 15 minutes before taking a blood sample. After the last immunization, final bleeding was performed under anesthesia (5 mg/kg intramuscular Ket-A-Xyl® Vetanis, Ate, Perú) to collect 50 ml of blood by cardiac puncture. The serum was separated and stored at -20 °C for later evaluation. After bleeding, the anesthetized rabbits were sacrificed with an overdose of Halatal at 70 mg/kg administered intramuscularly.

- **Immunization of mice.**

BALB/C male mice of 3-4 weeks old were used. Groups of five mice were used for immunization with each antigen. Like rabbits, mice were acclimated for 14 days before immunization. Each dose contained the diluted recombinant protein and Quil-A® adjuvant in a total volume of 0.1 ml. The concentration of each protein used for the immunization protocol is described in the Table II.7. To evaluate antibody production over time. a few drops of blood were extracted from the terminal region of the tail before and during immunization, in the same timing as for the rabbits. The serum was separated by centrifugation (5000 g for 20 min at 4 °C) and stored at -20 °C.

Table II.7: Immunization protocol in rabbits and mice. A 2-week acclimatization of the experimental animals was performed before the beginning of the immunization.

Immunization protocol in rabbits						
Protein	**day 1 (1° dose)**	**day 14 (2° dose)**	**day 21 (3° dose)**	**day 28 (4° dose)**	**day 35**	**Antibobies production**
MTC28	400 µg	400 µg	400 µg	400 µg	Total bleeding	++
MoeX	450 µg	450 µg	450 µg	0	Total bleeding	++
MPT64	500 µg	500 µg	500 µg	500 µg	Total bleeding	+
Hsp16.3	500 µg	500 µg	500 µg	500 µg	Total bleeding	++
Ag85B	500 µg	500 µg	500 µg	500 µg	Total bleeding	+
38kDa	500 µg	500 µg	500 µg	500 µg	Total bleeding	++
CFP10	300 µg	150 µg	150 µg	0	Total bleeding	+++
ESATt6	900 µg	700 µg	300 µg	0	Total bleeding	++++
Immunization protocol in mice						
Protein	**day 1 (1° dose)**	**day 14 (2° dose)**	**day 21 (3° dose)**	**day 28 (4° dose)**	**day 35**	**Antibobies production**
MTC28	60 µg	60 µg	60 µg	60 µg	Total bleeding	+++
MoeX	22 µg	22 µg	22 µg	14.4 µg	Total bleeding	+++
MPT64	36 µg	36 µg	36 µg	0	Total bleeding	+++
Hsp16.3	36 µg	36 µg	36 µg	0	Total bleeding	+++
Ag85B	96 µg	96 µg	96 µg	0	Total bleeding	+
38kDa	14.4 µg	14.4 µg	14.4 µg	0	Total bleeding	+++
CFP10	15.6 µg	15.6 µg	15.6 µg	0	Total bleeding	+++
ESATt6	50 µg	50 µg	50 µg	0	Total bleeding	+/-

- **Evaluation of antibody production over time.**

The production of antibodies over time in rabbits and in mice, was followed by an ELISA assay. For antigen binding, the recombinant protein was diluted until 10 ng/µL of concentration. A volume of 100 µL (1 µg of antigen) was fixed in each well of the ELISA

plate for 16 h at 4 °C. Subsequently, each well was blocked with 250 µL of 5% milk (Difco) at 37 °C for 1 h. The pre-immune serum and post-immune sera collected (1st, 2nd, 3rd and 4th doses in some cases) were incubated in a titer of 1/25, 16 h at 4 °C. Subsequently, it was incubated with anti-IgG labeled with HRP (1/5000) for 1 h at 37 °C. The wells were washed and revealed with *o*-phenylenediamine dihydrochloride (OPD, ThermoFisher) and the reaction was stopped with 0.5 M HCl.

Fold values of OD (**mean OD using post-immune sera)/ (mean OD using pre-immune sera**), were calculated.

- **Evaluation of polyclonal antibodies titers produced in rabbits and mice.**

Similarly as in the evaluation of antibodies production over time, indirect ELISAs were used to measure antibody titers (rHsp16.3, rMTP64, rMoeX and rCFP10) elicited during immunization: 1 µg/ well of antigen was coated in an ELISA plate (16 h at 4 °C), washed and blocked with 120 µL of milk 5% (Difco) at 32 °C for 3 h. Both the pre-immune serum and the serum obtained after the final puncture were incubated in the titre of 1/100 - 1/12800, 16 h at 4 °C. Subsequently, the immunocomplexes were incubated with anti-IgG labeled with HRP (1/5000) for 3 h at 37 °C. It was revealed with OPD and the reaction was stopped with 0.5 M HCl (**Figure II.49).**

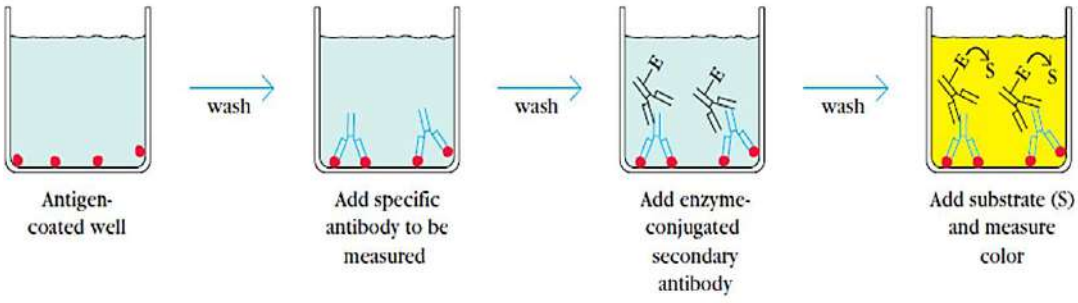

Figure II.49: Indirect ELISA used to evaluate of the titer of polyclonal antibodies produced in rabbits and mice.

Antibodies not previously evaluated (rMTC28, rMoeX, r38kDa, rAg85B and rCFP10), were lyophilized and transported to the University of Bordeaux (France). ELISAs were

performed to determine antibody titers. The protocol was similar to the previous one, but with the following modifications:

- The sera of rabbits were previously pre-absorbed (with *E. coli* antigens*) and lyophilized for transport at room temperature.
- The sera of mice, due to its small volume, were only lyophilized.
- The sera were hydrated at the same original volume, with PBS 1x (pH 7.4).
- 250 ng/ well of recombinant antigens were evaluated.
- The blocking solution used was casein.

* To obtain *E. coli* antigens, the pellet of a bacterial culture (250 mL of LB, 37 °C, ON) was resuspended in 50 mL of PBS 1x pH 7.4 and lysed by thermal shock and sonication.

- **Standardization of the antibody titers for a sandwich ELISA.**

The ELISA sandwich protocol is described below: fix capture antibody (rabbit serum) in a plate with protein affinity, at different dilutions 1/ 50 - 1/ 3200 for 16 h at 4 °C. Subsequently, block 1 h at 37 °C and incubate with 250 ng/ well of antigen for 16 h at 4 °C. Wash and incubate with detection antibody (mouse serum) in dilutions of 1/100 - 1/400. To identify the immuno-complex formed, anti IgG HRP (KPL) was used in a dilution of 1/2500 and 1/5000 for 1 h at 37 °C. The reactions were revealed with OPD and stopped with 0.5 M HCl (**Figure II.50).**

As negative control, we used the readings from the wells where the rabbit serum was not incubated (PBS 1x pH7.4 was placed instead), therefore, neither the antigen nor the mouse serum should have been bound to the ELISA plate, giving as reading 0.

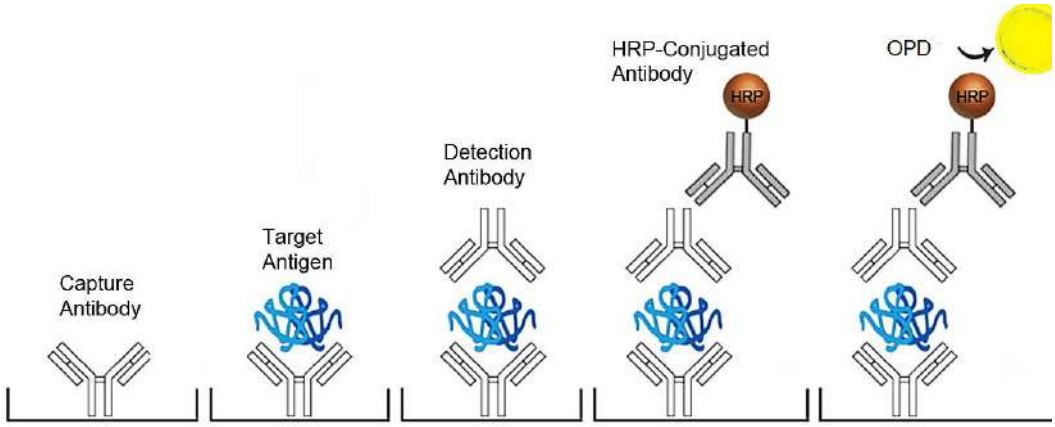

Figure II.50: sandwich ELISA used to evaluate of the titer of polyclonal antibodies produced in rabbits and mice.

II.3. RESULTS.

II.3.1. Cloning and expression of recombinant proteins from MTB.

The coding DNA sequences (**Figure II.1)** of selected proteins were amplified with the conditions described in the methodology (**Section II.2, page 107**).

Figure II.1 shows the amplified DNA with specific primers (**Table II.6**) in a PCR, using genomic MTB DNA. The bands observed in the electrophoresis gel correspond to the coding DNA sequences of selected MTB proteins: Ag85B (994 nt), MTC28 (950 nt), MPT64 (701 nt), MoeX (1010 nt), Hsp16.3 (446 nt), 38 kDa (1139 nt) and ESAT6 (302).

In all cases an adequate digestion of the coding sequences and the plasmids is confirmed (**Figure II.2**). In lane 1, corresponding to the sequence of MoeX, a slight shadow is observed that can be a consequence of DNA degradation by the restriction enzymes. This did not affect the cloning.

After amplification and cloning of coding DNA sequences, the recombinant proteins were produced successfully in the *E. coli* bacterial system. All proteins were induced to an OD of 0.6-0.8, corresponding to a logarithmic phase culture. Most of them were induced

at 37 °C, ON. However, the rHsp16.3 and rCFP10 proteins were expressed at RT, ON, and found in the soluble fraction of the induced culture. Additionally, rESAT6 was expressed in a time of 4 h. The IPTG concentration was 0.5 mM, except in MTC28 (0.6mM), rAg85B, rMoeX and rESAT6 (0.65 mM) and in r38kDa (0.8 mM).

Recombinant proteins were purified by affinity chromatography. All recombinant antigens, except ESAT6, presented an additional 1 kDa because of the 6xHis tag added. Eluted recombinant proteins formed peaks at different imidazole concentrations. Most of them eluted between 100 - 300 mM Imidazole in 20 mM phosphate buffer pH 7.4. The cloning and expression protocol of each specific MTB antigen is described in detail below.

- **Cloning and expression of rHsp16.3**.

In our study, Hsp16.3 amplicon presented a length of 459 bp including the histidine tail (6xHis); and it was inserted between the restriction sites NcoI and XhoI (**Appendix 1.1, page 269**).

The coding sequence of Hsp16.3 was successfully ligated into the plasmid pET28a (+). **Figure II.3** shows that all 6 clones selected for screening, pET28a-Hsp16.3 (5565 bp) (**Appendix 1.1, page 269**), presented a slight size difference (~196 bp) comparing to the plasmid pET28a alone (5369 bp). This is observed in the electrophoresis on 1.2% agarose gels (lanes 1-3 *vs* lane 4, and lanes 6-8 *vs* lane 5, **Figure II.3**). The cloning was corroborated by sequencing (**Appendix 1.2, page 270**). The clones 1 and 2 contained the Hsp16.3 sequence inserted appropriately into the pET28a plasmid. The clones 1 and 2 contained the Hsp16.3 sequence inserted appropriately into the pET28a plasmid.

The expression of rHsp16.3 was performed in *E. coli* BL21 (DE3) and *E. coli* BL21 (DE3) pLysS. The expression conditions were: 0.5mM IPTG, at 37 °C and at RT (improved the protein solubility) for 16 h of induction. The rHsp16.3 was found both in soluble and insoluble fractions (**Figure II.4).** The soluble fraction and the insoluble fraction of Hsp16.3 were purified separately. The soluble fraction was eluted from 300-500 mM Imidazole

(**Figure II.5)**; while the insoluble fraction eluted at 100 mM Imidazole (**Figure II.6)**. The soluble fraction had a large amount of Hsp16.3, but the protein tended to precipitate when stored at -20 °C.

Figure II.7 shows the sequence and the dodecameric structure of rHsp16.3 produced. The monomer unit was expressed in our experiment; but it was self - polymerized in the process.

In a phylogenetic analysis (**Appendix 1.3 and 1.4, both in page 271**) is observed that the amino acid sequence of Hsp16.3 of MTB differs from HSP of other mycobacteria, showing high specificity for the MTB complex.

- **Cloning and expression of rMPT64.**

In this study, a rMTP64 from MTB is cloned and expressed to be used for polyclonal antibodies production and ELISA tests.

A slight size difference of the purified plasmids pET28a-MPT64 (lanes 1-3) compared with pET28a alone (lane 4) is observed in **Figure II.8**. It indicates a successful insertion of MPT64 coding sequence into the pET28a (+) plasmid. Also, *in silico* is observed that the sequence of MPT64 is correctly ligated between the restriction sites NcoI and XhoI, corresponding to a total size of 714 pb including the nucleotides of 6xHis tag (**Appendix 1.5, page 272**). The sequencing corroborated the previous results, variation or mutation in the sequence were not observed (**Appendix 1.6, page 273**).

MPT64 protein (26 kDa) was expressed in *E. coli* BL21 (DE3) pLysS and in *E. coli* BL21 DE3 systems (**Figure II.9).** The parameters considered were 0.5 mM IPTG, at 37 °C, for 16 h of induction. A reduced production of the recombinant protein was observed, and it was found only in the insoluble fraction, as previously reported.

The rMPT64 expressed in the *E. coli* BL21 (DE3) system was purified from insoluble fraction using purification buffers with 40, 60, 80, 100, 200, 300 and 500 mM Imidazol. The protein rMPT64 eluted at 100 mM Imidazole (**Figure II.10**), and it was not refolded.

The amino acid sequence and the modeled structure of rMPT64 is observed in **Figure II.11.** Phylogenetic analysis shows a high specificity of MPT64 protein for the MTB complex (**Appendix 1.7 and 1.8, pages 274 and 275, respectively).**

- **Cloning and expression of rMTC28.**

The coding sequence of MTC28 was successfully inserted into the plasmid pET28a (+). **Figure II.12** shows the clones 1-3 and 5-6 with the pET28a-MTC28 construct inside. In the electrophoresis of DNA (1.2 % agarose gel) the clones 1-3 and 6-7 presented the coding MTC28 sequence inserted into the plasmid. A difference size (800 bp) was observed between the plasmid without insert (5369 bp) and the clones pET28a-MTC28 (6169 bp) (**Appendix 1.9, page 275**).

An alignment (**Appendix 1.10, page 277**) of sequencing clones shows that clone 6 pET28a-MTC28 has a better performance. It could be due to better quality of the plasmid DNA (without impurities). So, it presents less ambiguities and it is identical to theoretical MTC28 sequence. The sequence of clone 5 has undefined nucleotides (N), not presenting a 100% correspondence with the theoretical MTC28 sequence.

The protein rMTC28 (33 kDa) was evaluated in two expression systems. A higher expression was observed in *E. coli* BL21 DE3 compared with *E. coli* BL21 (DE3) pLysS.

The expression parameters were 0.5-0.65 mM IPTG (there were no variation in expressions) at 37 °C, for 16 h of induction. An SDS-PAGE of the induced and non-induced culture shows the expression of the rMTC28 protein (**Figure II.13**). After, rMTC28 was purified from insoluble fraction, the purified protein is observed in the fraction N° 23 (**Figure II.14)**

The amino acid sequence and the structure of rMTC28 is observed in **Figure II.15.**

According the phylogenetic analysis a high specificity of MTC28 protein for the MTBC is observed (**Appendix 1.11 and 1.12, page 278 and 279, respectively).**

- **Cloning and expression of MoeX**.

The insertion of MoeX into the pET28a (+) plasmid was successfully performed. **Figure II.16** shows that only clones 1 and 3 (6229 bp, **Appendix 1.13, page 279**) are longer than the plasmid without insert (5369 bp), showing a slight size difference (~ 860 bp).

Appendix 1.14, page 281, shows that the sequence of clones 1 and 3 were identical to the theoretical MoeX sequence, except for an undefined nucleotide (N) of clone 1.

The rMoex protein (36.6 kDa) was expressed in *E. coli* BL21 (DE3) pLysS and in *E. coli* Lemo 21 systems, with 0.5-0.8 mM IPTG (variation in the expression was not observed) at 37 °C for 6 - 16 h of induction. In both systems the protein was found in insoluble fraction (**Figure II.17**).

A greater amount of protein was obtained from induced *E. coli* BL21 (DE3) pLysS culture. The rMoeX was purified at 100-300 mM imidazole, especially in the fractions N° 18-20 (**Figure II.218**).

The amino acid sequence and the structure of modeled rMoeX is show in **Figure II.19**.

The specificity of MoeX for MTBC was corroborated with phylogenetic analysis of the amino acid sequence of the protein compared to the proteins reported in the database (**Appendix 1.15 and 1.16, pages 282 and 283, respectively).**

- **Cloning and expression of r38 kDa protein**.

The coding sequence of 38 kDa was successfully ligated in the plasmid pET28a (+). The clones pET28a-38kDa (6358 bp) (lanes 1-3) show a size difference (989 pb) comparing to plasmid without insert (5369 bp) (lane 4), indicating the insertion of coding DNA sequence of 38 kDa into the plasmid (**Figure II.20)** (**Appendix 1.17, page 283**).

In the alignment (**Appendix 1.18, page 285)** the clones 1 and 2 are identical to the theoretical 38kDa sequence, so it corroborates that the cloning of this gene was successful.

r38kDa protein (39.4 kDa) was successfully expressed in *E. coli* BL21 (DE3) pLysS and in *E. coli* BL21 (DE3). In both systems, the parameters were: 0.8 mM IPTG at 37 °C for 16 h of induction. However, the protein was found in the insoluble fraction and solubilized with urea (**Figure II.21**). A higher amount of r38 kDa (collected fractions N° 1-2 and 13) expressed in *E. coli* BL21 (DE3) pLysS was purified (**Figure II.22**). The expressed r38kDa was purified only from the insoluble fraction at 80 - 300mM Imidazole solutions.

The amino acid sequence and the modeled r38 kDa protein like to extracellular phosphate ABC transport receptor are described in **Figure II.23.**

In addition, a phylogenetic analysis was made to corroborate the high specificity of 38kDa protein for the MTB complex (**Appendix 1.19 and 1.20, both in page 286).**

- **Cloning and expression of rAg85B**.

rAg85B was cloned in pET28a. The coding DNA sequence of Ag85B was successfully inserted in the plasmid. The clones pET28a-Ag85B (6229 bp) (lanes 1 and 2) were longer than the plasmid without insert (5369 bp) (lane 4) (**Figure II.24)**. Additionally, it is observed *in silico* that the Ag85B sequence is correctly ligated between the restriction sites NcoI and HindIII (**Appendix 1.21, page 287**).

Appendix 1.22, page 288, shows that the clones 1 and 2 are identical to the theoretical Ag85B sequence, corroborating a successful insertion f Arg85B in the plasmid.

The protein rAg85B (36.3 kDa, PI: 6.29) was successfully expressed in *E. coli* BL21 (DE3) pLysS and in *E. coli* BL21 (DE3). Expression parameters were: 0.5-0.7 mM IPTG (there was no variation in expression, 0.65 mM IPTG was used on a larger scale) at 37 °C for 16 h. In both expression systems, the protein was found in insoluble fraction (**Figure II.25**).

The insoluble fraction of rAg85B expressed in the system *E. coli* BL21 (DE3) pLysS and in *E. coli* BL21 (DE3), were purified. In both cases, rAg85B was eluted at 80-300 mM

Imidazole. The purification was improved when a buffers battery with more dilute imidazole was used: 20, 40, 60, 80, 100, 200, 300 and 500 mM of Imidazole (**Figure II.26**).

The amino acid sequence and the modeled structure of rAg85B (**Figure II.27).**

Phylogenetic analysis shows a high specificity of Ag85B protein for the MTB complex (**Appendix 1.23 and 1.24, pages 289 and 290, respectively).**

- **Cloning and expression of rESAT6**.

In our study the protein was cloned in a Phusion plasmid pGEX4T1 in order to improve the solubilization of the protein.

In the DNA electrophoresis on 1.2 % agarose gel is observed that clones pGEX4T1-ESAT6 have a longer length than pGEX4T1 without insert (**Figure II.28).** Therefore, the ESAT6 coding sequence was successful inserted into the plasmid pGEX4T1. Besides, *in silico* cloning is observed that ESAT6 sequence is correctly ligated between the BamHI and EcoRI restriction sites (**Appendix 1.25, page 290**), corresponding to a total size of 1002 bp including the GST (Glutathione S Transferase) tag. A slightly size difference (282 bp) between pGEX4T1-ESAT6 (5251 bp) and pGEX4T1 plasmid (4969 bp) is observed.

In the alignment (**Appendix 1.26, page 291)**, the clone 6 is identical to the theoretical ESAT6 sequence, except for one variation at the beginning and at the end of the sequence.

The protein rESAT6-GST (37.7 kDa) was expressed successfully in *E. coli* BL21 (DE3) pLysS and in *E. coli* BL21 (DE3). The expression parameters were: 0.65 mM IPTG, at 37 °C and at RT. The RT favored the expression of the soluble fraction of the protein, for 16 h of induction. A fraction of the protein was soluble, and another fraction was insoluble. For the purification an affinity chromatography was performed using the soluble fraction in a column packed with a resin coated with Glutathione. The expressed and purified rESAT6 is observed in **Figure II.29.**

The amino acid sequence and the modeled structure of rESAT6 are showed in **Figure II.30.** Phylogenetic analysis shows a high specificity of ESAT6 protein for the MTB (**Appendix 1.27 and 1.28, pages 291 and 292, respectively).**

- **Expression of rCFP10.**

The pET28a-CFP10 plasmid, was purchased from a company (GenScript). The gene was inserted between NcoI and BamHI (**Appendix 1.29, page 292**). The protein rCFP10 (11.6 kDa, PI: 5.59) was successfully expressed in *E. coli* BL21 (DE3) pLysS at 0.5 mM IPTG at 37 °C for 4 h of induction. The protein was found in the soluble fraction (**Figure II.31).** Phylogenetic analysis, using the amino acid sequence of the MTB CFP10 protein, as well as the sequences of other mycobacteria, showed that the CFP10 protein was MTB specific (**Appendix 1.30 and 1.31, both in page 293)**. The amino acid sequence and the modeled structure of rCFP10 are showed in **Figure II.32.**

Table II.2 summarizes the expression conditions of recombinant MTB proteins, with the main parameters used in the process.

II.3.2. Polyclonal anti-MTB antibodies production.

- **Polyclonal antibody production over time.**

Purified **rHsp16.3, rMPT64, rMTC28, rMoeX, r38 kDa protein, rAg85B, rESAT6,** and **rCFP10** proteins were used for the immunization of New Zealand rabbits and BALC/C mice to produce polyclonal hyperimmune antibodies.

The antibody elicitation over time and the sera dilution standardization in sandwich ELISA were evaluated. Considering the folds values in the analysis and graphics of ELISA assays, calculated as indicated below.

Fold values (**positive/negative ratio = average of positive OD/ average of negative OD**)

Some ELISA curves to evaluate the production of polyclonal antibodies over time, were not performed with all sera after each dose of immunization. This is because the

amount of serum extracted was not sufficient (especially in mice) or they were hemolyzed in the transport or storage process.

Polyclonal anti-rHsp16.3 production:

In the case of immunization with recombinant Hsp16.3, 4 doses were used in rabbits and 3 doses in mice. In the **rabbit** model (the curve is plotted only until the third dose), we obtained **a fold of 8.25** after the first dose, and subsequently the antibody titer remained stable with **a fold of 6.75 and 6.50** after the second and third doses, respectively. In the case of **mice,** the increase in antibody titer was progressive, reaching **a fold of 13.25** produced by the second dose, and ending with **a fold of 12.50** after the third dose (**Figure II.33**).

Polyclonal anti-rMPT64 production:

In the case of immunization with recombinant MPT64, 4 doses were used in rabbits and 3 doses in mice. In the curve of ODs obtained **rabbit sera** (the curve is plotted only until the third dose)**,** a **fold of 3.13** produced by the second dose can be observed, and it decreases slightly to **a fold of 3.00** after the third dose, remaining generally stable. In the case of **mouse sera**, there is a slight increase in the antibody titers after the first dose, and it increased rapidly after the second dose. For the third dose the titer remains stable with a **fold of 9.2 (Figure II.34).**

Polyclonal anti-rMTC28 production:

In the case of immunization with recombinant MTC28, 4 doses were used in rabbits and mice. In both models, the curves are plotted only until the third dose. In the **rabbit** model an overproduction of antibody is observed after the first dose with a **fold of 10.25,** this is kept stable after the second dose with **a fold of 8.63-8.75.** Additionally, in the case of **mice** we have an increase in antibody titer after the second dose with **a fold of 15.5**, settling to **a fold of 14.5** after a third dose (**Figure II.35**).

Polyclonal anti-rMoeX production:

In the case of immunization with recombinant MoeX, 3 doses were used in rabbits and 4 doses in mice. The production of polyclonal antibodies in rabbits is constant after the second and third doses with **a fold of 5.73**. In **mice** (the curve is plotted only until the second dose), the increase of polyclonal antibodies is done progressively, observing a fold **of 10.40** after the second dose of immunization (**Figure II.36**).

Polyclonal anti-r38 kDa protein production:

In the case of immunization with recombinant 38kDa, 4 doses were used in rabbits and 3 doses in mice. The sera collected after each dose were pre-absorbed with *E. coli* antigens before performing the ELISA assay. In **rabbits** (the curve is plotted only until the third dose), a rapid production of antibodies was observed after the first dose with **a fold of 9.6**, remaining stable after the second and third doses **(folds 9.20-9.00).** In the case of **mice sera**, we have an overproduction of antibodies with **a fold of 11.5** after the third dose (**Figure II.37**).

Polyclonal anti-rAg85B production:

In the case of immunization with recombinant Ag85B, 4 doses were used in rabbits and 3 doses in mice. A progressive increase in the antibody titer was observed in **rabbit** (the curve is plotted only until the third dose), reaching **a fold of 2.59**; where the OD of the pre-immune serum had a reading of 0.27, which is very high, probably requires a pre-absorption. A fourth dose was considered to increase the antibody production (data not shown). In the case of **mice,** a pre-absorption with *E. coli* antigen was performed before doing the ELISA test. According to the ODs, we have a remarkable increase in the production of antibodies after the second dose, with **a fold of 9.8**, decreasing **to 7.4 after the third dose (Figure II.38).**

Polyclonal anti-rESAT6 production:

In the case of immunization with recombinant ESAT6, 3 doses were used in rabbits and mice. In the case of **rabbits** (the curve is plotted only until the second dose)**,** we have a significant increase of antibodies after the second dose with **a fold of 13.80**. Otherwise,

it is observed in **mice**, where only **a fold of 2.25** is obtained after the second dose. Therefore, the third dose was continued (data not shown) and a fourth dose was not performed because there was not enough of the recombinant protein (**Figure II.39**).

Polyclonal anti-rCFP10 production:

In the case of immunization with recombinant CFP10, 3 doses were used in rabbits and mice. Although only 3 sera collected were used to perform the assay, a remarkable increase in antibody titer was observed from the second dose, with **a fold of 11.00 and 10.75 in rabbit and mouse**, respectively (**Figure II.40**).

Table II.3 shows that the polyclonal antibodies were successfully produced in each animal model. In the case of rabbits, after the first dose (7 days) of immunization the antibody titer was raised; except in anti-MPT64, anti-Ag85B and anti-CFP10, which were increased after the second dose (14 days) of immunization. In most cases, the production of polyclonal antibodies was stabilized after the third dose (21 days) (data not shown). But in anti-Hsp16.3 was observed that the production of polyclonal antibodies was stabilized from the second dose, both in rabbits and in mice. In some cases, four doses (28 days) were considered in the immunization protocol.

- **Evaluation of polyclonal antibody titers produced in rabbits and mice.**

In the case of anti-rHsp16.3 titers, high folds were observed among the anti-Hsp16.3 produced in rabbits and mice, at dilutions of **1/3200 (14.80)** and **1/100 (16.00)**, respectively (**Figure II.41**).

In the **Figure II.42** a **fold of 4.50** is observed in a dilution of **1/12800 for anti-MPT64 produced in rabbit** and a fold **of 10.34 in the 1/100 dilution for anti-MPT64 mice serum**.

In the case of anti-rMTC28 titers, a high dilution of the serum was observed to detect the recombinant antigen (**Figure II.43**). A fold of **9.33** is observed in a dilution of **1/400 in rabbit serum** and a fold of **10.20 in the 1/50** dilution in mice.

Figure II.44 shows that anti-MoeX produced in **rabbit** has a fold of **8.00** in a sera dilution of **1/12800.** In the **mice,** the fold is **9.20** in a sera dilution of **1/50.**

For the evaluation of anti-r38 kDa protein titers, the **Figure II.45** shows a fold of **10.17** for **1/1600** dilution of sera obtained from immunized **rabbit**, and a fold of **10.60** for **1/200** dilution from **mice** sera.

Figure II.46 shows a fold of **2.68** in a dilution of **1/200** for anti-Ag85B produced in **rabbit**, and a fold of **12.80** for a dilution **1/100** in **mice** sera.

In the case of anti-rESAT6 titers, **Figure II.47** shows a fold of **10.80** in anti-ESAT6 dilution of **1/400 (mice).** Data from the evaluation of rabbit serum titers are not shown because there was not enough antigen available for the ELISA assay.

About anti-rCFP10 titers, **Figure II.48** shows the dilution standardization for anti-CFP10 produced in **rabbit** (fold of **11.57**, dilution of **1/200**) and in **mice** (fold of **14.33**, dilution of **1/100**).

- **Standardization of antibody titers for a sandwich ELISA using antibodies produced in rabbits and mice.**

In contrast to the previously described assays, where rabbit and mouse antibodies were evaluated separately, in this section rabbit and mouse antibody titres are evaluated in the same sandwich ELISA assay to detect the recombinant MTB antigen.

Table II.5 summarizes the titers obtained for the dilutions of sera from rabbits and mice during the standardization process of the sandwich ELISA. The CFP10 and ESAT6 proteins have low folds (<2), which would indicate that the amount of immunocomplexes formed during the assay is very low. The Hsp16.3, MTC28 and 38 kDa proteins presented folds > 2.28. In the case of MPT64, MoeX and Ag85B, folds greater than 5.0 were obtained. In the case of the specific sera for MoeX, Ag85B and MPT64, the highest folds were observed.

II.4. DISCUSSION.

II.4.1. Cloning and expression of recombinant proteins from MTB.

Although some antigens, as lipoarabinomannan (LAM), have been already described in biological samples from TB patients (Pereira Arias-Bouda *et al.*, 2000), others secretory and superficial MTB proteins have not been evaluated in sputum samples yet.

- **Cloning and expression of rHsp16.3**.

Hsp16.3 is the most abundant *M. tuberculosis* secreted protein during latent stage (non-replicative), but it is reduced when the bacteria is in the logarithmic growth phase (Kennaway *et al.*, 2005). This means that this protein is a good diagnostic candidate for latent TB.

It plays an important role in the survival of the mycobacteria and in the immune response of the host to the infection. In addition, Hsp16.3 is frequently recognized in the TB patient sera (Kennaway *et al.*, 2005). These findings make the Hsp16.3 protein a potential biomarker for TB detection.

In our study we modeled the rHsp16.3 from MTB by homology, and this was consistent with the HSP (Heat Shock Protein) model described in the literature. Hsp16.3 is part of an HSP family and they share a conserved central domain called α-crystallin domain (~90 aa, with divergent extensions in *N*- and *C*- terminal regions). In general, the structure of HSP is a dimer formed by interactions between conserved α-crystalline domains. So, Hsp16.3 protein forms a single set tetrahedral dodecameric assembled from dimers, being compatible with the original structural properties of the family of HSPs (Kennaway *et al.*, 2005).

On the other hand, Abulimiti *et al.*, 2003 reported that Hsp16.3 of MTB can form polymers of trimers in solution, causing protein aggregation (Abulimiti *et al.*, 2003). This would explain the protein precipitation observed in our experiments.

- **Cloning and expression of rMPT64.**

There are many reasons why MPT64 is a potential TB diagnostic candidate. MPT64 (~23 kDa) is a secreted protein restricted to members of the *Mycobacterium tuberculosis* complex (MTBC). It is able to induce T cell responses and cutaneous reactions in TB infected animals (Roche *et al.*, 1996)

Chu and Yuann (2011) reported an expression protocol of MTP64 from MTB. The MPT64 analysis was performed to study the pathogenicity of MTB, in order to develop a vaccine based on MPT64. Unlike traditional protocols, in which proteins are expressed at 37 °C, MPT64 was better expressed at 20 °C with 10 mM IPTG for 22 h. The protein concentration was increased in the time (24 h). MPT64 expressed at 37 °C and 30 °C (under the same conditions) were lower than at 20°C. The protein was insoluble, but after refolding it was aggregated to become tetramers. High concentrations of β-mercaptoethanol (8%–20%) decreased the tetrameric and dimeric structures. However, the aggregation was very stable suggesting an intermolecular covalent interaction between MTP64 subunits with disulfide bonds (Chu and Yuann, 2011). In our case, the MPT64 protein was slightly larger (26 kDa), and it was evaluated in *E. coli* BL21 (DE3) pLysS and in *E. coli* BL21 DE3 systems (**Figure II.9).** A reduced production of the recombinant protein was observed, and it was found only in the insoluble fraction, as previously reported.

MPT64 protein structure is composed mostly of β-sheet strands and tetrameric aggregates can be observed, suggesting strong protein–protein interactions *via* disulfide bonds between MPT64 subunits. Due to strong interactions, important properties related to Mycobacterium virulence, can be attributed to MPT64 protein (Chu and Yuann, 2011).

The amino acid sequence and the modeled structure of rMPT64 by homolgy is observed in **Figure II.11.** It is corresponded to MPT64 previously reported for MTB.

- **Cloning and expression of rMTC28.**

The MTC28 protein was selected due to its characteristics that makes it a potential candidate for TB diagnosis. MTC28 antigen (28 kDa) is an extracellular protein and actively secreted by MTB. MTC28 is found in the early culture filtrate of MTB and it elicits immune responses in guinea pigs immunized with live mycobacteria, like many of the MTB extracellular proteins (Manca *et al*., 1997). Also, our phylogenetic analysis showed a high specificity of MTC28 protein for the MTC (**Appendix 1.11 and 1.12, page 278 and 279, respectively).**

Yamaguchi *et al.* (1989) reported that the abnormally slow migration in SDS-PAGE, is a common property of proline-rich MTC28 (Yamaguchi *et al.*, 1989). Manca *et al.* (1997) observed that a MTC28 (28.66 kDa) protein migrated in SDS-PAGE with an apparent molecular mass of 49 kDa (Manca *et al.,* 1997). It could be attributed to the rigidity and reduced mobility of proline-rich stretches. Also, a low electrophoretic mobility of MTC28 obtained both from MTB (native) and from *E. coli* system (recombinant), is observed, discarding the effect of post translational modifications, such as glycosylation (Dobos *et al.,* 1996). This phenomenon would explain some variations in the electrophoretic runs of rMTC28 during our experiments.

The amino acid sequence and the modeled structure of rMTC28 is observed in **Figure II.12.** The structure of MTC28 modeled by homology corresponds to those previously reported in the literature. MTC28 is a protein with high proline content in the NH_2-terminal (34%) and *COOH*-terminal (30%) regions. In addition, a putative 32 aa secretion signal peptide in the NH_2-terminal is observed, and an extracytoplasmic mature region of 278 aa (Manca *et al.*, 1997).

- **Cloning and expression of MoeX**.

MoeX is a specific protein of MTBC, validated as a biomarker of active TB (Pollock *et al.,* 2013). This biomarker has not yet been reported in MTB identification assays, so its diagnostic potential was explored in this study. Previously, MoeX was identified in urine samples from TB patients. Three discrete protein bands of 75, 50, and 32 kDa corresponding to MoeX were identified in urine samples. According Pollock *et al*., bands of 50 kDa and 75 kDa might represent a polymerization because MoeX contains 8 cysteine residues, or MoeX could be complexed with other proteins (Pollock *et al.,* 2013). In our study, the protein rMoeX presented a MW of ~37 kDa (theorical 36.6 kDa), aggregation was not observed because the protein, initially found in the insoluble fraction, was solubilized in a denaturating solution (8 M urea).

- **Cloning and expression of r38 kDa protein**.

38 kDa protein is actively secreted and it is considered one of the most important MTB antigens, because it is a major constituent of MTB culture fluid (in synthetic Sauton medium) (Harboe and Wiker, 1992). Due to these properties, this protein has been widely studied in different MTB diagnostic methods. In our study we report the cloning and expression of r38kDa, which was used to produce polyclonal antibodies.

Previously, Chang *et al.,* 1994 reported a truncated 38kDa antigen from MTB. It was expressed successfully in *E. coli* BL21 (DE), 0.2 mM IPTG, ON. The recombinant 38kDa was observed in both soluble and insoluble fractions (Chang *et al*., 1994).

In our case, the r38kDa protein (39.4 kDa) was successfully expressed in *E. coli* BL21 (DE3) pLysS and in *E. coli* BL21 (DE3).

Choudhary *et al. (*1994) reported the crystallization of 38kDa using a pure recombinant form of the protein. They demonstrated that 38kDa protein acts binding phosphate using a mechanism like phosphate-binding protein localized in the periplasm of *E. Coli* (Choudhary *et al.*, 1994). In this way, the structure of the protein and its similarity to an

extracellular phosphate transporter justifies the function of 38kDa. It is corroborated with the modeled r38 kDa protein (**Figure II.23**) like to extracellular phosphate ABC transport receptor.

- **Cloning and expression of rAg85B**.

Ag85B is the major secretory protein of MTB, it was able to activate the protective immunity of Ag85B-vaccinated guinea pigs against aerosol MTB exposure (Zarif *et al.*, 2013). Due to these and other previously described characteristics, the rAg85B antigen was selected, cloned and expressed in this study.

Zarif *et al.* (2013) reported an Ag85B cloned in pET101/D and transformed in *E. coli* BL21 strain. The recombinant antigen (33 kDa) was expressed at 37 °C with 2 µL/mL of IPTG. After 12 h of induction the recombinant Ag85B was abundant and insoluble (present in inclusion body) (Zarif *et al*., 2013). In our case, rAg85B (36.3 kDa) was successfully expressed in *E. coli* BL21 (DE3) pLysS and in *E. coli* BL21 (DE3), with 0.65 mM IPTG at 37 °C for 16 h. Similarly, in both expression systems, the protein was found in insoluble fraction (**Figure II.24**).

Ag85B is closely related to a mycolyl transferases, and associated with both Ag85A and Ag85C, contributing to build the bacterial cell wall. In a crystal previously reported, a molecule of trehalose was linked in two sites at opposite ends of the active-site cleft (Anderson *et al*., 2001). In this sense, the modeled structure presents a central region in the form of a pocket, which could correspond to the active site of the protein (**Figure II.27**)

- **Cloning and expression of rESAT6/rCFP10**.

ESAT6 and CFP10 are the most important virulence factors and they are recognized over 70% of TB patients (Skjot *et al.*, 2000).

Mahmoudi *et al*., 2013 reported cloning and expression protocols for ESAT6 and CFP10. Both proteins were cloned in the vector pET32 a (+) and transformed into *E. coli*

BL21 DE3. The expression parameters were: 1mM IPTG, at 37 °C for 4 h of time induction. Most of the proteins were soluble (Mahmoudi *et al.*, 2013).

In our case, the protein rESAT6-GST (37.7 kDa) was expressed successfully in *E. coli* BL21 (DE3) pLysS and in *E. coli* BL21 (DE3). The RT favored the expression of the soluble fraction of the protein, which was used for purification in a column packed with a resin coated with Glutathione. On the other hand, the protein rCFP10 (11.6 kDa) was successfully expressed in *E. coli* BL21 (DE3) pLysS at 0.5 mM IPTG at 37 °C for 4 h of induction, being in the soluble fraction.

The proteins CFP10 and ESAT6 are secreted forming a four-helix bundle structure. In the **Figure II.30 and Figure II.32** the modeled structures of the rESAT6 and rCFP10 proteins are shown.

II.4.2. Polyclonal anti-MTB antibodies production.

Currently there are many diagnostic tests based on the capture of specific antibodies for TB antigens. However, the detection of anti-MTB does not determine the diagnosis of active TB, because cross-reactions are observed with sera from people exposed to MTB, people vaccinated against TB, or in people who had TB and have already been cured. For this reason, many efforts are focused on developing diagnostic tests to directly detect MTB antigens.

On the other hand, there are highly specific antigens that have proven effective in discriminating infectious mycobacteria from non-pathogenic mycobacteria. These antigens have been studied and evaluated in diagnostic tests to detect specific antibodies.

Caccamo *et al.* (2010) reported that immune responses to ESAT6/CFP10 and Ag85B from MTB, were significantly higher in active TB than in latent TB infection (LTBI) (Caccamo *et al.*, 2010). In this way, Zhang *et al*. (2015), reported an ELISA to detect anti-Ag85B-Hsp16.3. In the case of active TB, the sensitivity and specificity reported were

61.67% and 95.65%, respectively. In LTBI, theses parameters were 60.00% and 73.91%, respectively (Zhang *et al.*, 2015). In addition, assays combining the antigens were tested. The optimal antigen combination to diagnose active TB was Ag85B-Hsp16.3/ESAT6 with a specificity and sensitivity of 93.33% and 92.39%, respectively. In the case of LTBI, it was Hsp16.3/ESAT6, with a specificity and sensitivity of 75.0% and 76.67%, respectively (Zhang *et al.*, 2015). The literature with human sera from patients with TB and LTBI indicates that in our study the proteins selected for MTB diagnosis are very antigenic.

In general, all produced antibodies after immunization showed high folds in the indirect ELISA tests, indicating high antibody production in experimental animals. The highest folds were observed in anti-MTP64 and anti-Ag85B, indicating the high capacity of capture and recognition of antigens by these antibodies.

Considering that the amount of rESAT and rCFP10 expressed and purified were low, and that the antibodies were lyophilized and then hydrated for transport, in the case of sandwich ELISA, the anti-ESAT6 and anti-CFP10 titers did not show high folds, possibly because the antibodies or proteins used were probably not in optimal conditions.

Evaluation of anti-rHsp16.3 titers:

The small heat shock protein, Hsp16.3, protects the MTB through an association of the protein with MTB membrane (Zhang *et al*., 2005). This could explain why this antigen is found in large quantities in the TB serum. Zhang *et al.*, 2015, reported an ELISA to capture anti-Hsp16.3 for detecting TB antibody response in humans. In the case of active TB, the sensitivity and specificity reported were 63.33% and 88.04%, respectively. But in LTBI, theses parameters were 53.33% and 88.04%, respectively. In our experiments, the folds obtained in sera of rabbits (>6.50) and mice (>12.50) were high. However, a fold of 3.26 was observed when the antibodies were evaluated (in triplicate) in the sandwich ELISA assay.

Evaluation of anti-rMPT64 titers.

MPT64 antigen is a major secretory protein of MTB (specific for MTBC), and it is not expressed in non-pathogenic mycobacteria. Ji *et al.* (2014) reported a sandwich ELISA to detect MPT64 protein using monoclonal antibodies. The assay showed a lower detection limit of 2.1 ng/mL and 1.7×10^4 CFU/mL of MTB. Using 389 clinical MTB culture suspensions, the sensitivity and specificity were calculated, obtaining 100% for both parameters (Ji *et al.,* 2014). A disadvantage of the previously described study was the culture that the clinical samples required before applying them to the MPT64 sandwich ELISA. Consequently, this method took a longer time for the TB diagnosis. In our study, we introduced magnetic nanoparticles in a sandwich ELISA to improve the MTP64 antigen detection and thus reduce the time of the TB diagnosis process. For this purpose, the evaluation of antibody production was made. The folds obtained in sera of rabbits (>3.00) and mice (>9.2) were slightly high. In the same way, a fold of 6.25 was observed when the antibodies were evaluated (in triplicate) in the sandwich ELISA assay.

Evaluation of anti-rMTC28 titers.

MTC28 is a component immunologically active of the MTB culture filtrate. MTC28 elicited strong immune responses in immunized guinea pigs comparable with immunodominant secreted antigens (MPT64 and 38kDa antigen) (Manca *et al*., 1997). Lim *et al*., 1995 reported that ~ 25% of patients with active TB showed a strong antibody response to MTC28. This strong immunological activity of MTC28 is associated with specificity for MTBC (Lim *et al.,* 1995).

This high specificity makes the MTC28 protein an excellent diagnostic candidate. In our case, the immunogenicity of rMTC28 was corroborated by producing polyclonal antibodies in rabbits and mice. However, a fold of 3.6 was observed when the antibodies were evaluated (in triplicate) in the sandwich ELISA assay.

Evaluation of anti-rMoeX titers.

In the case of MoeX, this protein was reported as specific antigen for MTBC. Also, this protein was described as an attractive candidate for the development of a highly sensitive and specific urine MTB antigen detection test (Pollock *et al.*, 2013). This is one of the reasons why the protein was selected for this study. The standardization of the anti-MoeX dilution produced verified the antigenicity of the protein as well as the production of the antibodies. In our experiments, the folds obtained in sera of rabbits (5.73) and mice (10.40) were high. In the sandwich ELISA assay, a fold of 5.00 was observed when the antibodies were evaluated (in triplicate).

Evaluation of anti-r38 kDa protein titers.

According Harboe and Wiker (1992), B and T cell responses are induced by 38 kDa protein with high specificity for TB infection. It could be due to its extracellular localization (Harboe and Wiker, 1992). Tiwari *et al*. (2014) reported an ELISA test standardized for the major protein antigens (6, 27, 30, 38 and 64 kDa) obtained from MTB culture filtrated proteins (antigens not described). An enhanced sensitivity (~98.67 %) and specificity (~98.06 %), compared with commercial ELISA assays, were found for the mixture proteins (Tiwari *et al.*, 2014).

This indicates that the 38kDa protein, like the others studied, activates efficiently the immune response of the host, allowing the production of antibodies. This was corroborated with the ELISAs performed with the anti-38kDa produced in rabbits and mice. However, a fold of 2.28 was observed when the antibodies were evaluated (in triplicate) in the sandwich ELISA assay.

Evaluation of anti-rAg85B titers.

Ag85B protein is the most abundant protein secreted by MTB and it is a potent immunoprotective antigen (Anderson *et al.*, 2001). Zhang *et al*., 2015, reported an ELISA to capture anti-Ag85B antibodies for detecting TB humoral response in humans. In the case of active TB, the sensitivity and specificity reported were 53.33% and 97.83%, respectively. But in LTBI, theses parameters were 60.00% and 88.04%, respectively

(Zhang *et al.*, 2015). In our study, the Ag85B protein proved to be highly immunogenic, and this was corroborated in the immunization process of rabbits and mice. In the same way, a fold of 6.39 was observed when the antibodies were evaluated (in triplicate) in the sandwich ELISA assay.

Evaluation of anti-rESAT6 titers.

In the case of ESAT6, Feng *et al*., 2013 reported that the sensitivity of ESAT6 antigen to detect antibodies in TB patients varies from 5% to 76% with a specificity ranging of 51% to 100% (Feng *et al.,* 2013). Therefore, a careful standardization of the method for this marker was carried out by other research groups.

Zhang *et al*. (2015), reported an ELISA to capture anti-ESAT6 for detecting TB antibody response in humans. In the case of active TB, the sensitivity and specificity reported were 86.67% and 95.65%, respectively. But in LTBI, theses parameters were 60.00% and 84.78%, respectively (Zhang *et al*., 2015). I this way, the ESAT6 protein was able to induce a high level of antibodies in TB patients. In our case, considerable amounts of anti-rESAT6 antibodies were produced in rabbits and mice. However, in the ELISA sandwich test a very low fold (1.77) was observed.

Evaluation of anti-rCFP10 titers.

In the case of CFP10, Parkash *et al*. (2009) reported that the sensitivity of ELISA using CFP10 to detect antibodies in TB patients varies from 9% to 78% with a specificity ranging of 55% to 100%. This variation in sensitivity and specificity may be due to the conditions and the type of test or protocol performed for the immunodiagnostic, as well as the conditions of the antigens and the samples of patients with TB (Parkash *et al*., 2009).

Zhang *et al.* (2015) reported an ELISA assay to capture anti-CFP10 for detecting TB antibody response in humans. In the case of active TB, the sensitivity and specificity reported were 80.00% and 80.43%, respectively. But in LTBI, theses parameters were 73.33% and 69.57%, respectively (Zhang *et al.* 2015). Our study confirms the antigenic

capacity of this protein. As anti-rESAT6, in the ELISA sandwich test, a low fold (1.93) was observed. Probably, the conditions of the protein were not optimal (low amounts and slight precipitation).

II.5. CONCLUSION.

The recombinant proteins (Hsp16.3, CFP10, ESAT6, MTC28, MPT64, 38 kDa protein, Ag85B and MoeX) successfully expressed in *E. coli* were able to elicit a high amount of polyclonal antibodies in rabbits and mice, that were specific to recognize the purified recombinant proteins. Elevated antibody titers were observed in experimental animals during the different immunization doses. In the sandwich ELISA, the folds were greater in the anti-MPT64 and anti-Ag85B. However, the other antibodies also demonstrated efficiency in recognizing and capturing specific recombinant antigens.

Chapter III: Synthesis, amine-silanization and physical-chemical characterization of magnetic nanoparticles.

Chapter III

Synthesis, amine-silanization and physical-chemical characterization of magnetic nanoparticles.

Abstract:

Introduction: This chapter describes the synthesis, coating and physical and chemical properties of iron oxide magnetic nanoparticles (MNPs).

Methodology: The magnetite core was synthesized using co-precipitation method. In general, Fe^{2+} and Fe^{3+} ions were co-precipitated using alkaline conditions (ammonium hydroxide), with a stoichiometric ratio of Fe^{3+}/Fe^{2+} = 2:1 at pH range between 10 and 12. The surface was coated with amine-silane groups (TEOS and APTES in two steps) to stabilize the MNPs. For the characterization of chemical and physical properties, different techniques were used and analyzed: Transmission Electronic Microscopy (TEM), X Ray Diffraction (XRD), Dynamic Light Scattering (DLS), Vibrating-Sample Magnetometry (VSM), Fourier-Transform Infrared Spectroscopy (FTIR), Mössbauer Spectroscopy (MS) and Thermogravimetric analysis (TGA).

Results: High amount of nanoparticles were synthesized by coprecipitation method. The most important physico-chemical properties of nanoparticles were a diffraction crystal diameter of ~12.5 nm (10.48 ± 2.56 nm), superficial net charge of ζ: +23.57 ± 2.87 mV, characteristic patterns of magnetite and a spherical structure. Additionally, a magnetization saturation of 37.06 $emu.g^{-1}$ was observed.

Discussion: Co-precipitation is a simple and economical method due to the large gram-scale product that can be formed. The pH and the ionic strength affected the surface composition, as well as the surface charge of the particles. The nitrogen blanket gas was an important parameter because MNPs have the tendency to become maghemite due to instability and susceptibility to O_2. After oxidation occurs, the magnetic properties decrease

considerably. In addition, the amine-silanization surround the iron particle surface was a crucial step to prevent its oxidation and the subsequent loss of magnetic properties.

Conclusion: All the nanoparticles reported in this study were synthesized successfully by the co-precipitation methodology, following different protocols. Similarly, the surface of the nanoparticles was efficiently silanized in two steps (TEOS/APTES). The characterization demonstrated the presence of magnetite in the core of the synthesized MNPs

NOTE:

This chapter has been divided into 4 subchapters: narrative description (**III.1**), experimental section (methodology, **III.2**), results (**III.3**) and discussion (**III.4**). The structure of narrative description - experimental section is a format widely used in the domain of chemical sciences, while the structure of methodology - results - discussion is a standard format in the area of biology. In this chapter, the narrative description shows merged results and discussion. The experimental section describes the materials and methods used in this chapter. The results and discussion sections have the same content as the previously described narrative description, but they are separated. This means that reading the narrative description - experimental section is the equivalent of reading experimental section - results - discussion.

Despite the redundancy of information between narrative section (**III.1**) and results – discussion (**III.3** and **III.4**), this format is justified for easy understanding for chemists (narrative section - experimental section) and biologists (experimental section – results - discussion).

III.1. NARRATIVE DESCRIPTION.

To evaluate the different MNP coverage agents (dextran, APTES, TEOS/APTES), the synthesis of the nanoparticles varied according to the type of coverage agent used, as well as the type of solvent evaluated (**Chapter III.1**). But in general, the MNP synthesis protocols corresponded to the co-precipitation method. All protocols described below were previously reported. To determine the MNP with better characteristics to immobilize proteins on its surface, a general protein conjugation test was performed.

The protocol that generated the nanoparticle with the best characteristics to immobilize proteins is described in **Chapter III.2**. Likewise, a complete physicochemical characterization was performed on these nanoparticles.

The standardization of the immobilization of BSA and IgG on the surface of these characterized nanoparticles is described in **Chapter IV.**

III.1. 1. Evaluation of conditions for the coating of magnetic nanoparticles.

This section describes the previously evaluated conditions before determining the best methodology for the synthesis and coating of the MNPs.

- **<u>Condition N° 1</u>: MNP coating using CMD.**

After the synthesis, the naked MNPs must be covered to avoid degradation, aggregation and oxidation, especially with metals such as iron. A shell layer allows to increase the chemical stability and integrity of the MNP (Fields *et al*., 2016). Before choosing the amino groups for the coating of the MNPs, the Carboxymethyl-dextran (CMD) was evaluated, because this polymer was used in previous studies in biomedicine (Han *et al.*, 2010).

The CMD is a polysaccharide commonly used due to its negative charged carboxylic groups and its hydrophilicity, avoiding the agglomeration of MNP-CMD (Li *et al*., 2011). Han *et al.*, 2010 reported a MNP-CMD conjugated to Octreotide, which is a synthetic somatostatin analogue that specifically targets somatostatin receptors, for MRI applications

on pancreatic and colon cancer cells (Han *et al.*, 2010). Also, Li *et al*., 2011 reported a MNP-CMD able to conjugate covalently anti-BSA in their surface. After incubation with BSA, the antigen was efficiently dissociated and the regenerated antibody covered MNP-CMD was repeatedly used *(Li et al.*, 2011).

In our study, we evaluated three previously reported protocols: Protocol 1 (Han *et al*., 2010), protocol 2 (Makovec *et al.*, 2015) and protocol 3 (Li *et al*., 2011), where CMD was successfully coated on the surface of the MNPs. However, in our results the process of MNP coating with CMD generated nanoparticles with low magnetism, and consequently they were not efficient to immobilize proteins on their surface (data not shown). The high reduction of magnetism could be explained because the CMD is a complex and large polymer, and probably it is generating an interference between the surface and the magnetic domains of the MNPs.

The **Table III.1** shows the main visible characteristics of the MNP-CMD after the synthesis.

Table III.1: General properties of the MNP-CMD synthesized in the three protocols previously described (P1, P2 and P3).

MNP	color	magnetism (powder)	magnetism (liquid)	agglomeration
MNP@CMD P1	brown	-	++	-
MNP@CMD P2	black	+++	++	-
MNP@CMD P3	black	+++	++	-
MNP	brown	-	++	-

Iron nanoparticles are characterized by having a blackish color. In our case, we obtained brown and black MNPs. In addition, the magnetism varied according to the state of the MNP, the magnetization was faster when the black MNP was in powder (+++) and the brown (oxidized) did not show magnetization. However, a medium magnetization (++) was observed when the brown MNP was dispersed. Finally, no agglomeration of the nanoparticles was observed.

In general, the CMD option was discarded to conjugate biomolecules due to its instability in its magnetization, which could be due to the interference of the CMD exerted on its surface. Consequently, amino-silane groups were used to cover the surface of the MNPs.

- **Condition N° 2: MNP coating using APTES at RT.**

Silica is a popular election for the inorganic coating of MNPs. It is because the silanization process is not complex, is effective, has low cytotoxicity, inertia to redox reactions, stability in acidic conditions and a great number of different functional groups associated to commercial silanes are available (Fields *et al*., 2016). In general, the initial silanization is a very fast process, but the saturation progress is very slow, involving adsorption, chemical sorption, and chemical diffusion processes (Liu *et al.*, 2013).

Jesse *et al.*, 2015 reported a modified protocol to synthesize nanoparticles with APTES; and conjugate specific antibodies covalently for the bio-separation of begomovirus (Jesse *et al*., 2015).

In our results, the silanized MNP with APTES at RT, presented a high polydispersity (29.5%) in DLS measurements, this means that there was a heterogeneity of MNPs with different measures. The hydrodynamic diameter was elevated (285,2 nm ± 9,5 nm) compared to 25 nm (d_H) reported by Jesse *et al.,* 2015 (**Figure III.1A**).

The magnetic hysteresis is a characteristic where MNPs retain a remaining magnetism, although the magnetic field no longer exists. The hysteresis curve shows the behavior of the magnetism of a material to different levels of magnetic intensity (Oe) applied. At certain point, the magnetization is proportional (linear zone) until reaching the point of saturation induction. This means that although a greater magnetic force is induced to the material, it will no longer magnetize (Ahmadzadeh *et al*., 2018).

Our silanized MNPs showed a hysteresis of 10.87 Oe. This is because by subjecting the silanized MNPs to an alternating magnetic field, their domains were oriented according

to the sense of the magnetic field. But when the intensity of the field decreased, most of the domains returned to their initial position. However, others did not reach it, possibly due to molecular friction between them. Therefore, these domains retained part of their forced orientation, persisting a remnant magnetism that manifests as a small level of magnetic induction (**Figure III.1 C**)

The positive zeta potential demonstrated a correct silanization of the MNP surface (**Figure III.1 B**). However, previous studies reported that a high temperature for the silanization process, can improve an homogeneous monolayer structure of the amine-silane groups on MNP surfaces.

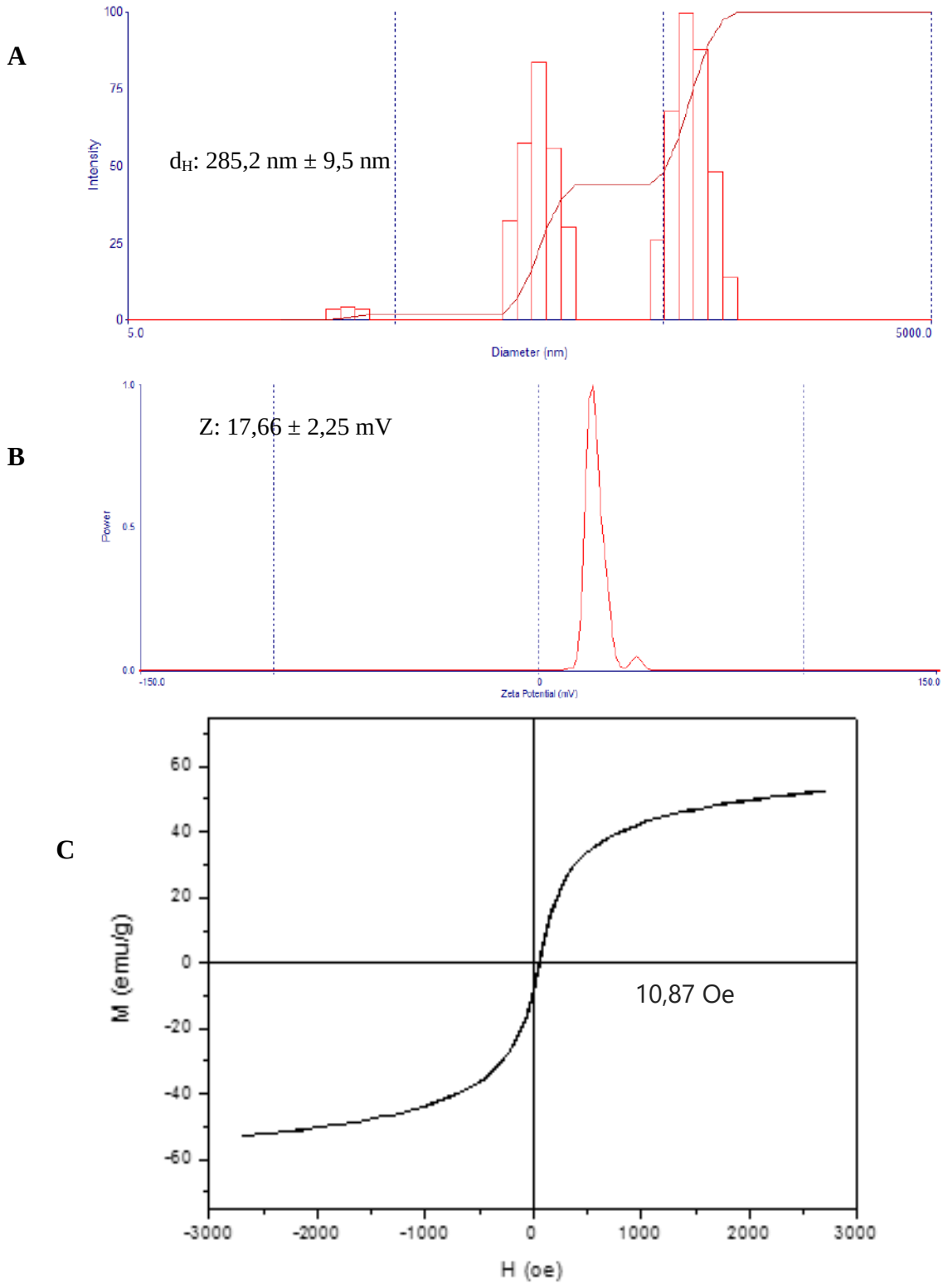

Figure III.1: Characterization of nanoparticles synthesized with the aqueous solvent at room temperature. Silanized MNPs have a hydrodynamic diameter of 285.2 nm (**A**), a positive surface charge, indicating the amine groups of the surface (**B**) and a hysteresis of 10.87 Oe (**C**).

- **<u>Condition N° 3</u>: MNP coating using APTES at 70°C using different solvents.**

The silane groups are activated by hydrolysis, subsequently a condensation between the Si-OH (silanol) and OH- (MNP surface) groups, is made by forming stable bonds on the surface. However, the different types of solvents in the silanization process could influence the formation of homogenous or heterogeneous layers of silane groups on the MNP surfaces (Liu *et al*., 2013). This could have an impact on the immobilization of biomolecules on the surface of the nanoparticles. In this way, silanized MNPs with different solvents were identified and their effect on protein conjugation was evaluated.

In this case, the amine-silanization was made only with APTES, using as solvents water, ethanol/water and methanol/toluene. Characteristics of the nanoparticles with and without APTES were evaluated, such as the zeta potential values and the hydrodynamic diameter.

Amino-silanization of nanoparticles using water as solvent.

Figure III.2 shows nanoparticles with and without APTES in water as solvent (APTES-water), both has a negative surface charge, indicating that probably the OH groups are the predominant ones on the surface. It means that the functionalization with the amino groups is scarce or null.

In **Figure III.3** the hydrodynamic diameter of the nanoparticles synthesized is observed. The MNP silanized with APTES-water is greater than the nanoparticles without APTES, indicating that there is no stabilization of the nanoparticles by APTES.

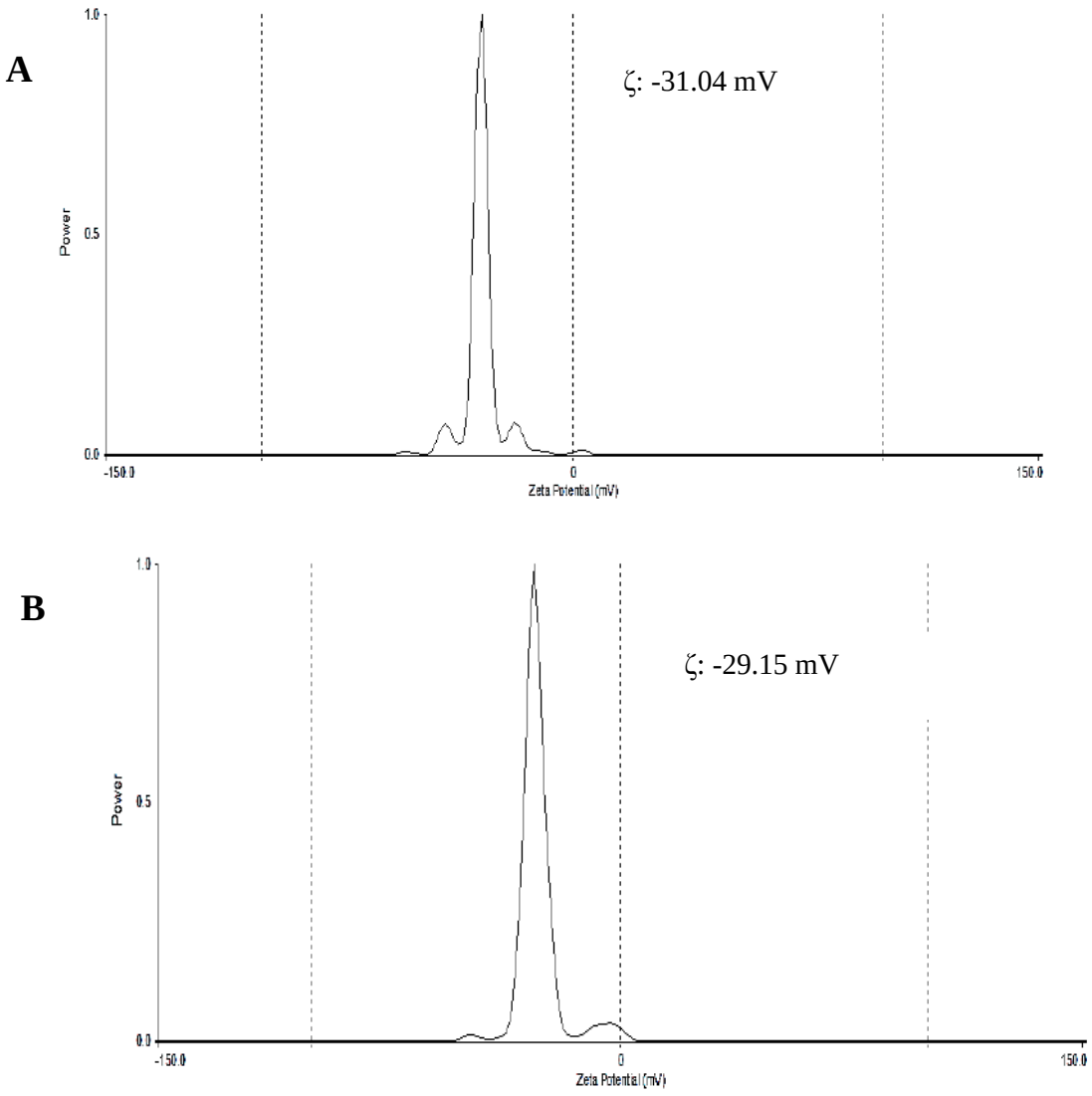

Figure III.2: Potential zeta of MNP (**A**) and amine-silanized MNP (**B**) using water as solvent.

A

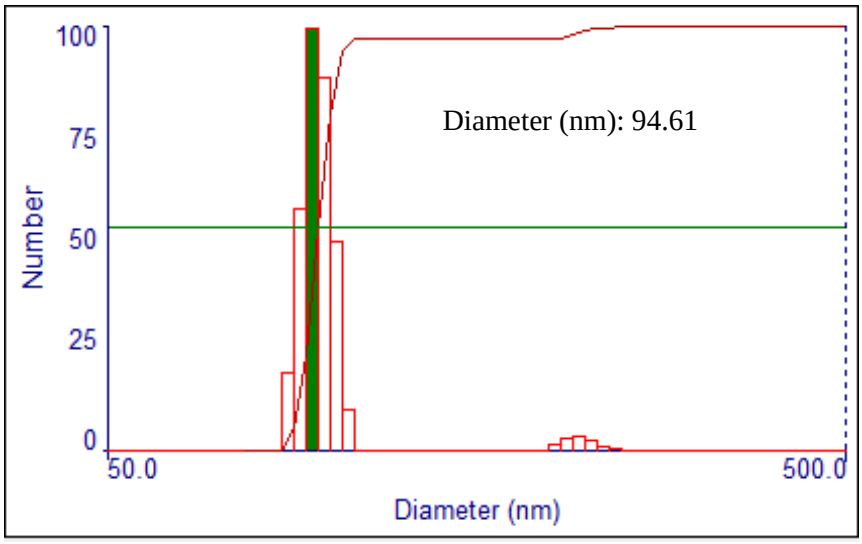

B

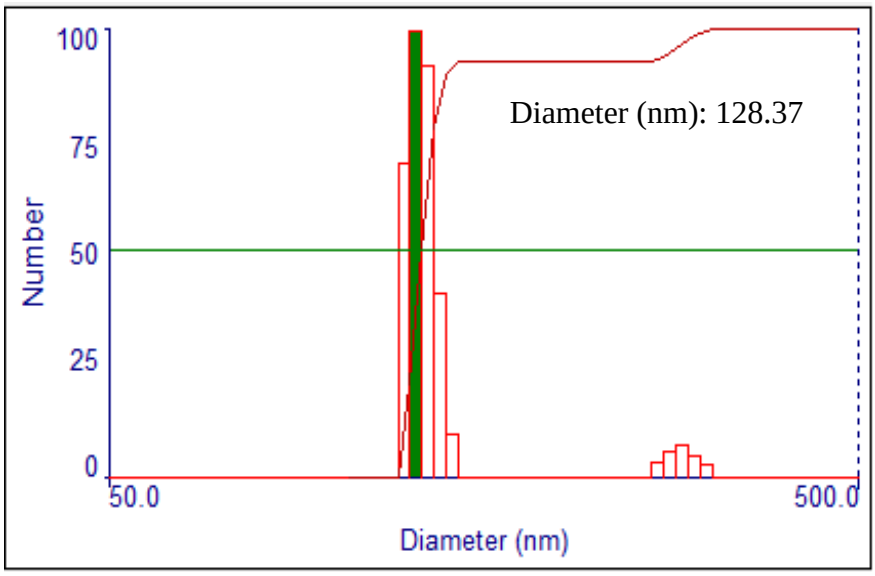

Figure III.3: Hydrodynamic diameter of MNP (**A**) and amine-silanized MNP (**B**) using water as solvent.

Amino-silanization of nanoparticles using ethanol/water as solvent.

Unlike the nanoparticles silanized with APTES-water, in this case it can be observed that the nanoparticles obtained, with and without APTES, have a positive surface charge in both cases, being higher in the nanoparticles functionalized with APTES (**Figure III.4).**

Also, **Figure III.5** shows that the size of the nanoparticles with APTES is smaller than that of the nanoparticles synthesized without APTES. This would be explained by the repulsion charges of the nanoparticles, generating a dispersion of MNPs.

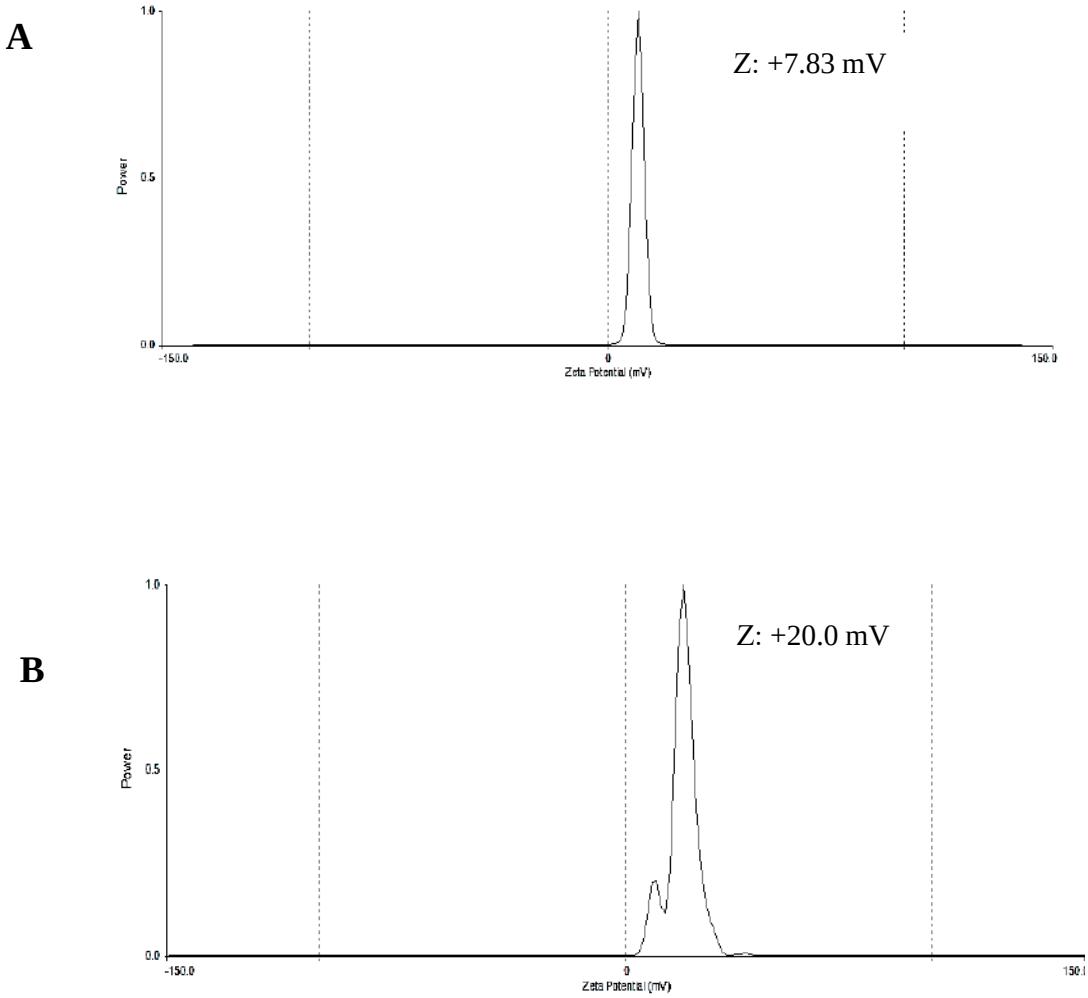

Figure III.4: Potential zeta of MNP (**A**) and amine-silanized MNP (**B**) using ethanol/water as solvent.

A

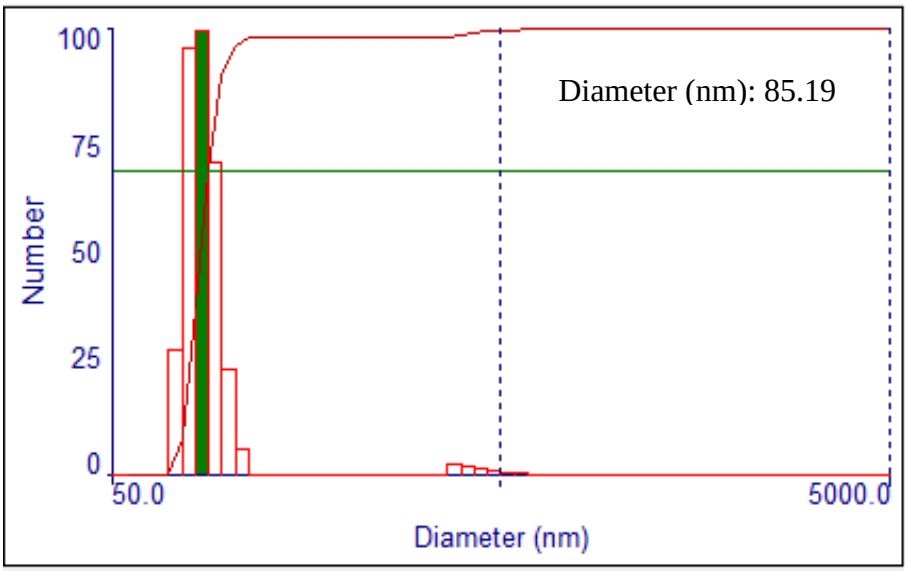

B

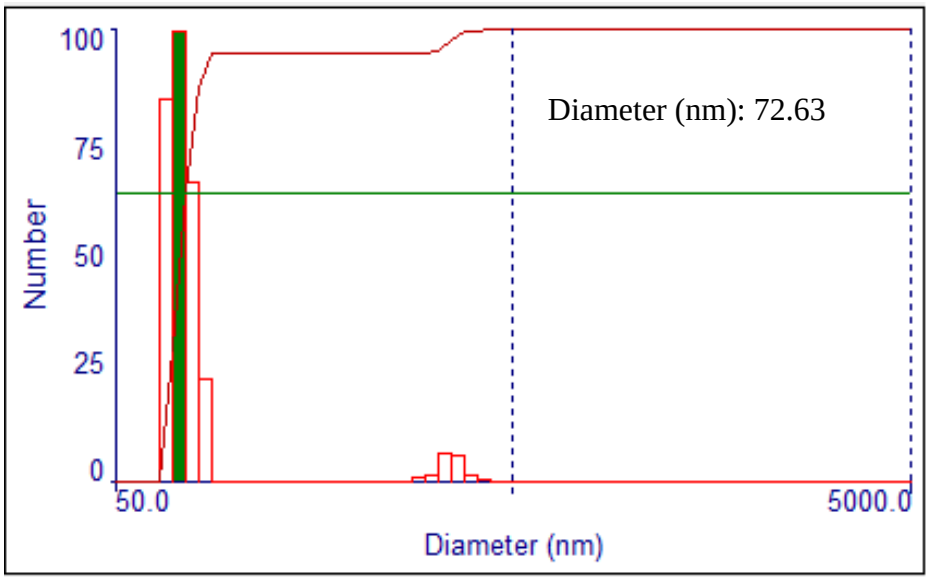

Figure III.5: Hydrodynamic diameter of MNP (**A**) and amine-silanized MNP (**B**) using ethanol/water as solvent.

Amino-silanization of nanoparticles using methanol/toluene as solvent.

Liu *et al.*, 2013 reported that the highest equilibrium grafting density, data based on TGA, was reached using toluene/methanol as solvent in the silanization process (Liu *et al.*, 2013).

Figure III.6 shows a negative charge on the surface of nanoparticles without APTES-methanol/toluene while the nanoparticles silanized with APTES-methanol/toluene presented a positive charge, indicating the amino groups from silanization process.

Figure III.7 indicates a similar hydrodynamic diameter between both nanoparticles.

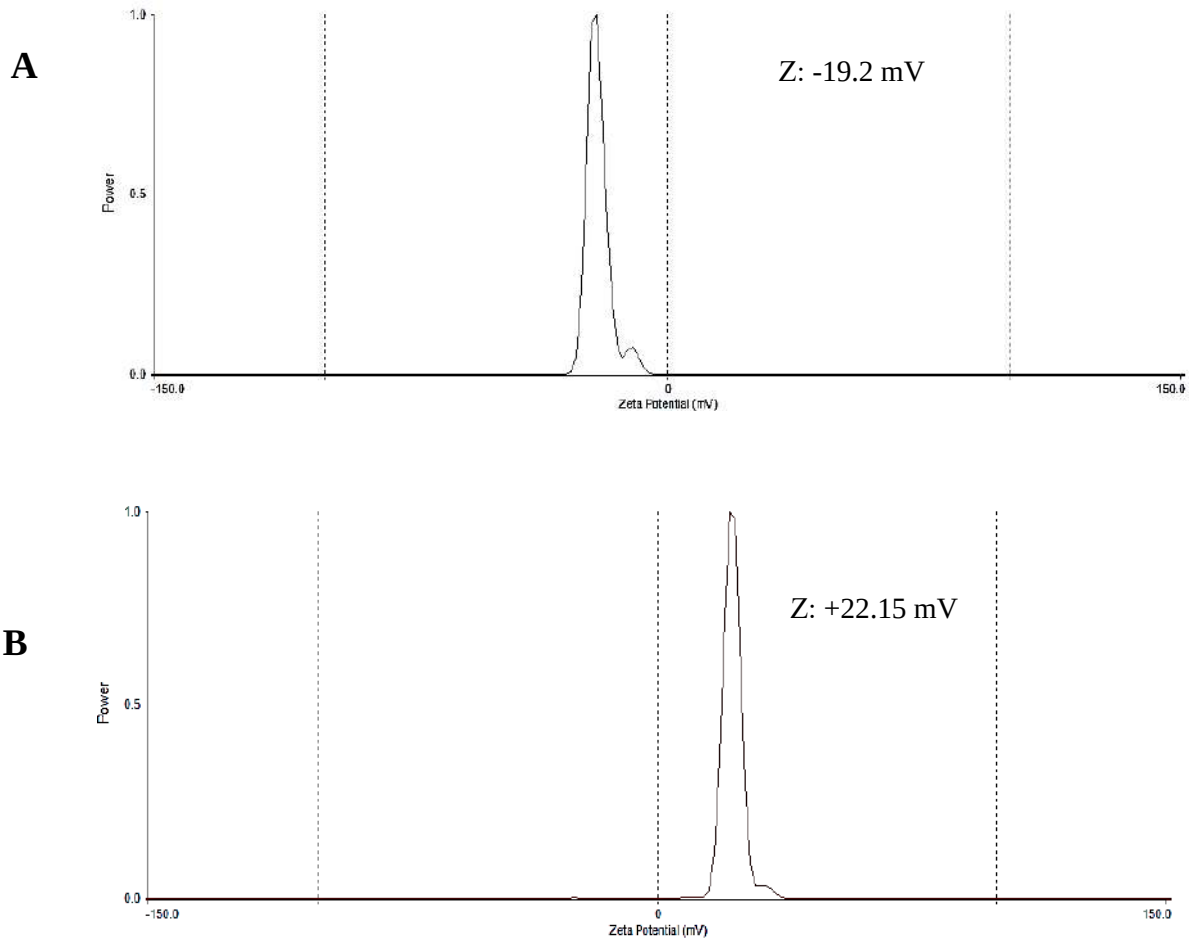

Figure III.6: Potential zeta of MNP (**A**) and amine-silanized MNP (**B**) using methanol/toluene as solvent.

A

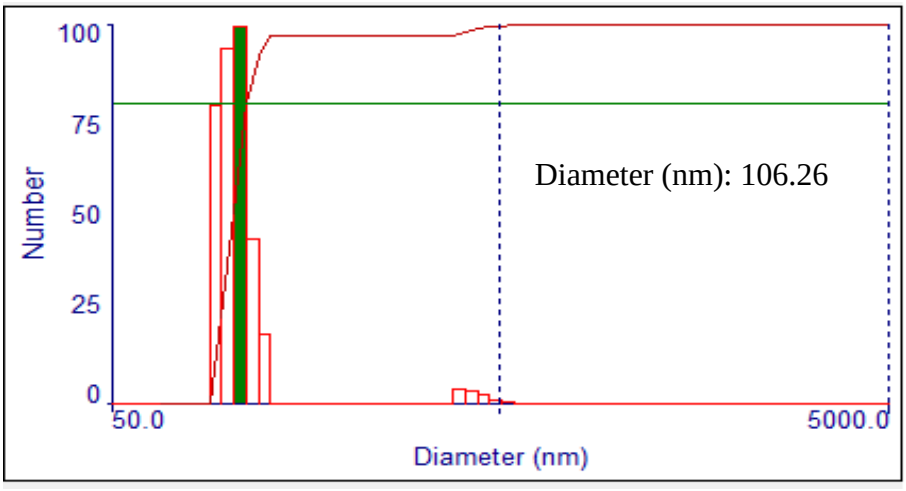

B

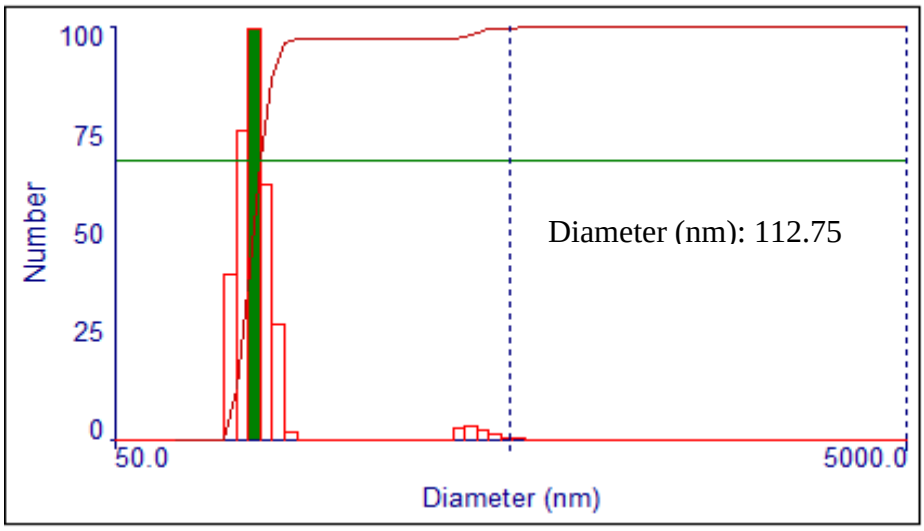

Figure III.7: Hydrodynamic diameter of MNP (**A**) and amine-silanized MNP (**B**) using methanol/toluene as solvent.

The Table III.2 summarizes the characteristics obtained from the silanized MNPs with different solvents. When the mixture methanol/toluene was used, the surface charge was higher (+22.15) compared to the other MNPs silanized with other solvents. In the case of the mixture ethanol/water the hydrodynamic diameter was lower, guaranteeing a greater dispersion in MNPs. On the other hand, the non-silanized nanoparticles with APTES-ethanol/water presented a positive surface charge (+7.83). Probably, the nanoparticles were

not washed properly until reaching a neutral pH. and a possible residues of NH_4OH, used for the co-precipitation of the nanoparticles, could have remained in the reaction.

Table III.2: characteristics of silanized MNPs with different solvents. *Negative*: indicate a reaction without APTES, and *Positive*: indicate a reaction with APTES.

Nanoparticles		**Polydispersion (%)**	**Hydrodynamic diameter (nm)**	**Z- potential**
APTES-water	Negative	13.6	94.61	-31.04
	Positive	13.3	128.37	-29.15
APTES-ethanol/water	Negative	29.1	85.19	+7.83
	Positive	27.0	72.63	+20
APTES-methanol/toluene	Negative	27.6	102.26	-19.20
	Positive	26.6	112.75	+22.15

Determination of the ability of the amine-silanized MNPs to be functionalized by biomolecules on their surface.

Because the charge of the nanoparticles silanized with the system APTES-water had a net negative charge, the reactive amino groups would not be present on the surface. Consequently, functionalization with proteins could only be generated through weak interactions and/or adsorption. In the case of nanoparticles silanized with the system APTES-ethanol/water and with the system APTES-methanol/toluene, it is observed positive surface charges in both cases, it means that there are amino groups on the surface, which are essential to generate the peptide bonds with the carboxyl groups of the proteins to be functionalized.

Table III.3 shows the amount of proteins (mg of BSA and IgG) immobilized on the surface of the silanized MNP, after 6h incubation. A higher percentage of bound BSA (10.65 %) is observed when methanol/toluene is used as solvent in the silanization process. However, in the case of antibodies (IgG), only 5.26% was fixed on the MNP surface. Despite of the promising characteristics of the silanized MNPs using the mixtures

ethanol/water and methanol/toluene, these systems were not very efficient for the immobilization of biomolecules on their surface. Consequently, other conditions and protocols for the silanization of nanoparticles were evaluated.

Table III.3: Immobilization of biomolecules (BSA and IgG) on the surface of silanized MNPs with different solvents (water, ethanol/water and methanol/toluene).

MNP-BSA	**0 h (mg)**	**6 h (mg)**	**% BSA linked**
APTES- water	36.37	37.7	0
APTES- ethanol/water	37.3	36.67	1.69
APTES-methanol/toluene	38.22	34.15	10.65
MNP-IgG	**0 h (mg)**	**6 h (mg)**	**% IgG linked**
APTES-methanol/toluene	0.39	0.36	5.26

- **Condition N° 4: MNP coating using TEOS/APTES (two steps).**

Although MNP is efficient to immobilize proteins on its surface (13.52 % of BSA and 46.15% of IgG) (**Table III.4),** the main disadvantage was the very small amount of MNPs produced. This could be due to the interference with ethylene glycol during the washing step of the nanoparticles.

Table III.4: Functionalization by BSA and IgG on the surface of the amine-silanized MNP.

MNP-TEOS/APTES	**0 h (mg)**	**16 h (mg)**	**% linked protein**
MNP-BSA	2.22	1.99	13.52
MNP-IgG	0.13	0.09	46.15

A protocol reported by Liu *et al.*, 2011 was used in the next section. MNP coating using TEOS/APTES in ethanol solvent is described. It was the most efficient method to produce modified nanoparticles capable of binding high amounts of proteins on their surface. Therefore, all experiments onwards will be performed with the MNPs described below.

III.1.2. Synthesis of MNP@Si@NH_2 by co-precipitation method.

This section presents the best protocol of synthesis and coverage of MNP, for the immobilization of proteins on its surface. Using this protocol, a greater amount of MNP was produced (grames). As in the cases previously described, the magnetic nanoparticles were synthesized successfully following a modified co-precipitation method (Liu et al., 2011). After the synthesis, to produce monodispersed particles, the MNPs were stabilized with amino-silane groups (TEOS/APTES in two steps) on the surface to avoid/reduce particle agglomeration (**Figure III.8**); which may occur during synthesis, drying or post-synthesis processing (Smit, 2018). In this way the repulsive forces between the particles increased.

The **Table III.5** shows the amount of proteins conjugated on nanoparticle surfaces (MNP@Si@NH_2). The values of linked BSA and IgG (13.88% and 44.75%, respectively) were similar to MNPs previously reported (table III.4). However, the advantage of this method is the amount of synthesized nanoparticles, because it can be measured in grams, unlike the previous one that only produced mg of MNPs. In addition, the synthesis and amino-silanization methodologies were easier and cheaper than the previous one, because ethylene glycol was not used.

Table III.5: Functionalization of biomolecules on the surface of the MNP@Si@NH_2.

MNP@Si@NH_2	0 h (mg)	16 h (mg)	% protein linked
MNP-BSA	2.35	2.07	13.88
MNP-IgG	0.15	0.10	44.75

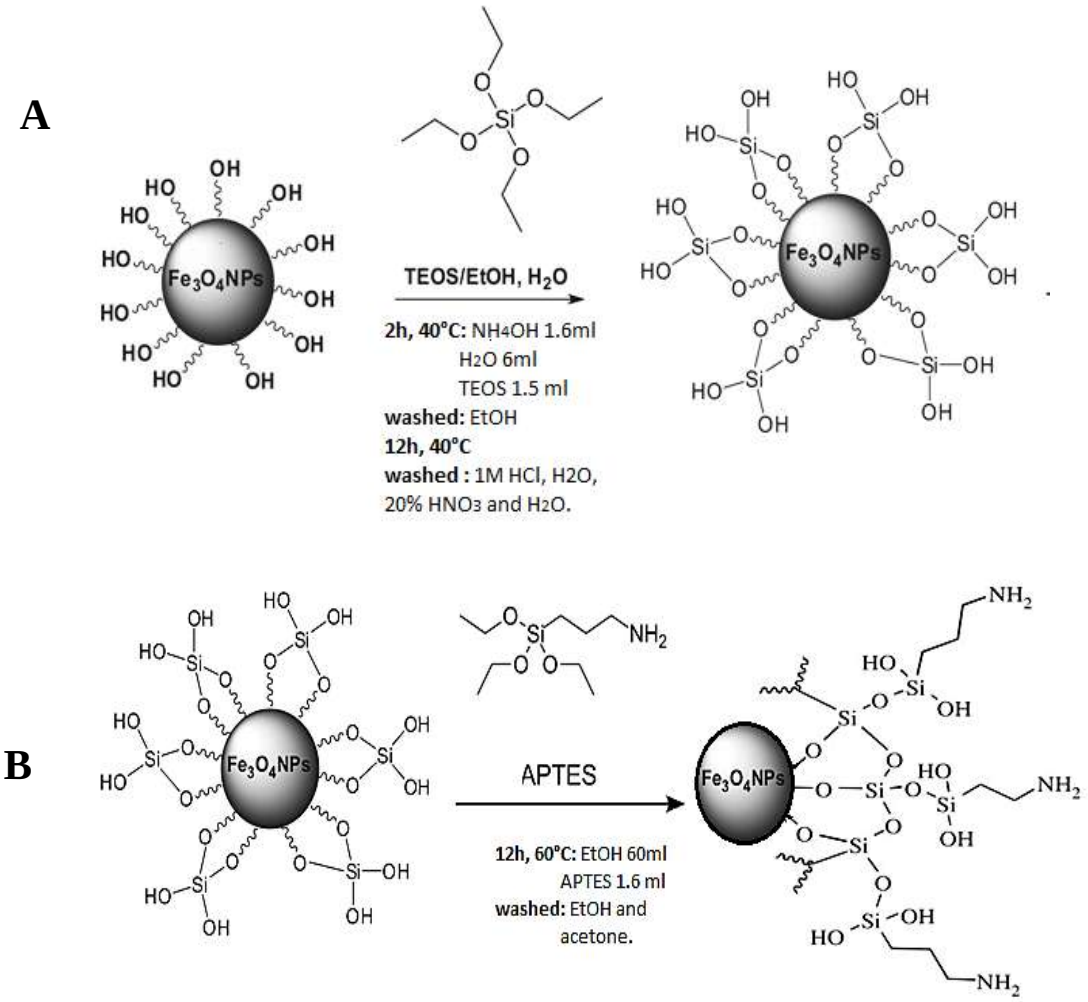

Figure III.8: Stabilization of NMPs. First silanization of the surface using TEOS (**A)** and the second amine-silanization using APTES (**B**).

III.1.3. Physical-chemical characterization of coated magnetic nanoparticles.

To determine the physical-chemical properties of the MNP@Si@NH_2 synthesized, different techniques of evaluation were used. The most important results of this characterization are described below:

The structural characterizations made **by X-Ray Diffraction (XRD)** (**Figure III.9**) showed different reflection planes corresponding to its Bragg angles, characteristic for magnetite (JCPD card N° 19-0629). According Wen *et al*. the XRD patterns of the magnetic particles have *2θ* peaks at 18.44°, 30.32°, 35.75°, 43.32°, 53.89°, 57.34° and

62.96°, which are attributed to the crystal planes of magnetite at (111), (220), (311), (400), (422), (511) and (440), respectively (Wen *et al*., 2008). Our diffraction peaks were similar to XRD pattern previously reported. XRD data shows similar peaks between bare MNP compared to MNP@Si@NH_2. In addition, XRD of MNP@Si@NH_2 showed a characteristic amorphous shoulder ($2\theta = 50.0°$) associated to amorphous silica recovering the magnetite particles. The XRD patterns of magnetite and amine-silanized magnetite were similar, indicating that Si@NH_2 groups has not effect on the crystallization process. However, the broadening analysis of diffraction peaks for MNP@Si@NH_2 and bare MNP shows different nanometric grain size, 8 nm and 12 nm, respectively. This difference in size could be due to the stabilization of nanoparticles with amino-silane groups, generating a repulsive force, consequently a lower degree of aggregation. On the other hand, in the case of naked nanoparticles, there is an attraction between them that in time can produce an aggregation of the nanoparticles.

The magnetite **XRD** pattern was identified as F d-3 m spatial group with a = b = c = 0.837 nm, cell conditions.

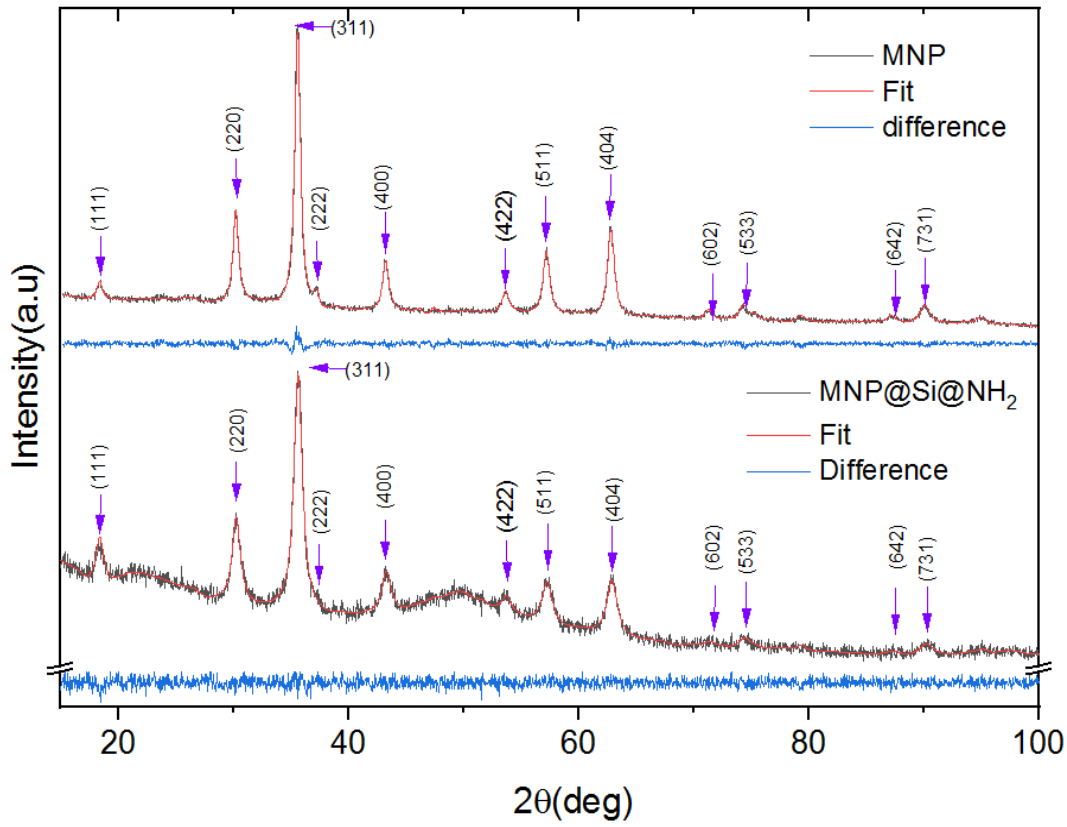

Figure III.9: XRD data showing peaks of bare MNP compared to MNP@Si@NH_2 following the crystallographic pattern of magnetite (JCPD card N° 19-0629).

Mössbauer spectra of magnetite nanoparticles and amine-silanized magnetite are shown on **Figure III.10A and III.10B**, respectively.

A

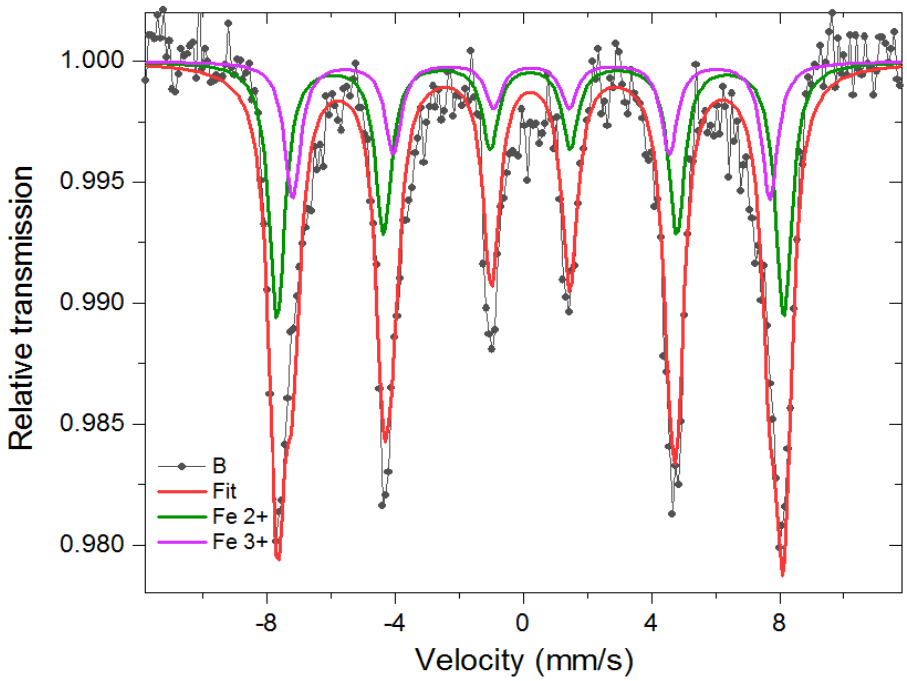

B

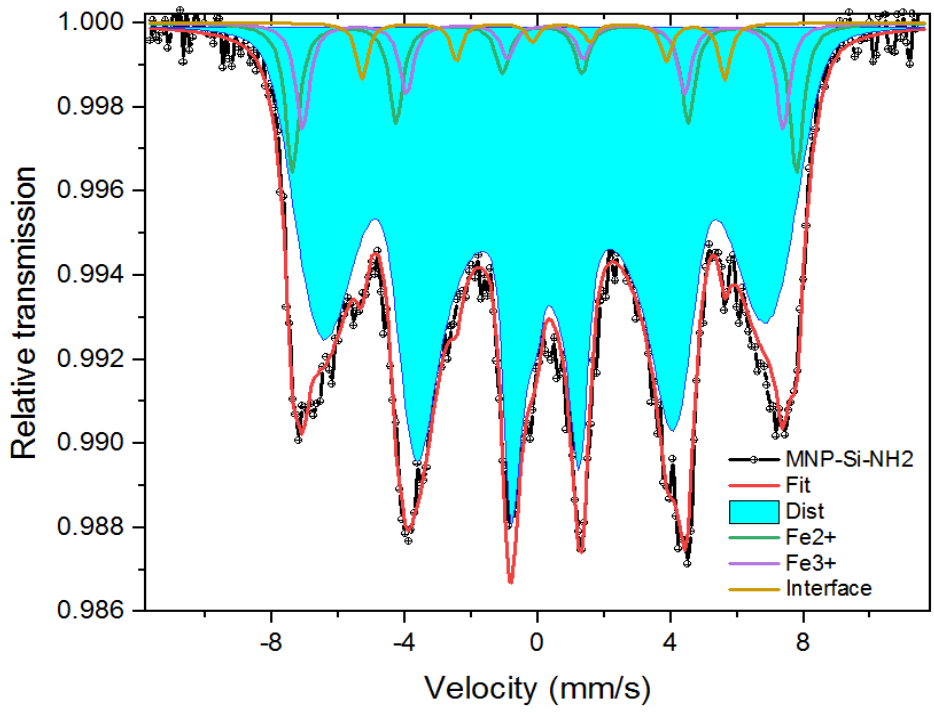

Figure III.10: Mossbauer pattern of MNP (A) and MNP@Si@NH_2 (B).

The Mössbauer spectrum for MNP was fitted using only two crystalline iron site associated to Fe^{2+} and Fe^{3+} related to octahedral and tetrahedral iron sites (Cabrera *et al.*, 2013; Wang *et al.*, 2008). However, Mössbauer spectra of amine-silanized magnetite was fitted using three crystalline iron sites and a distribution of non-equivalent iron sites fitted by a hyperfine field distribution. The hyperfine conditions of three crystalline sites were identifies as Fe^{2+}, Fe^{3+} and interfacial iron sites. While, the distribution was associated to non-equivalent iron site with nanosized grain size supported by XRD analysis. **Figure III.11** shows the hyperfine field distribution used to analyze MNP@Si@NH_2 Mössbauer spectra.

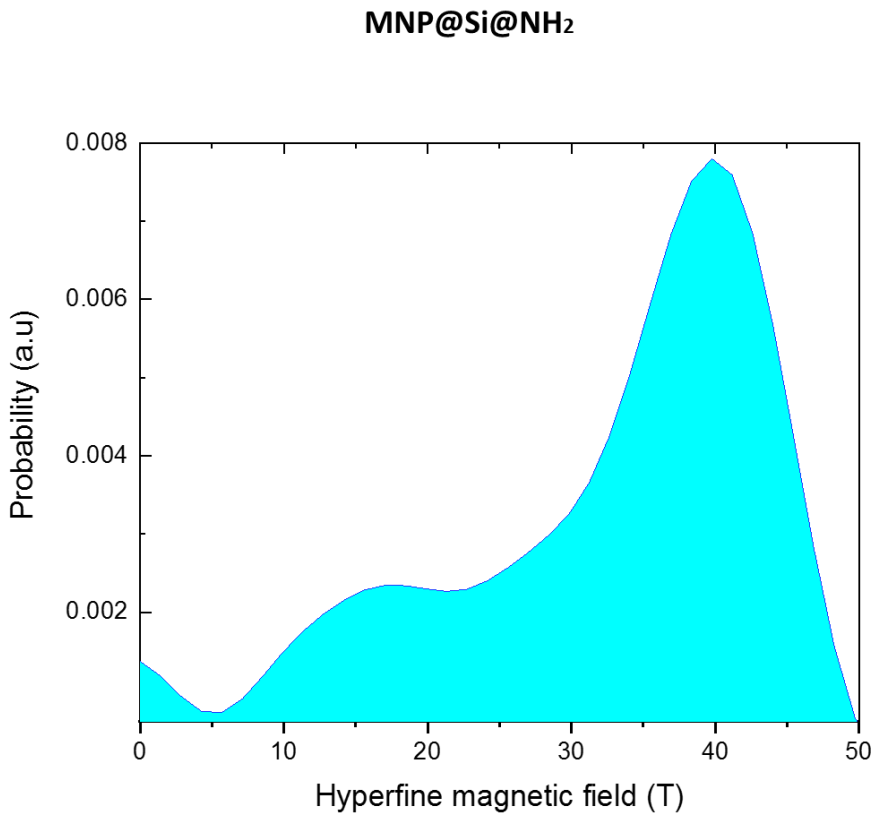

Figure III.11: Hyperfine field for MNP@Si@NH_2.

Using the **TEM** technique was observed a nanoparticle size distribution of 6.5-15 nm, with an average particle size of approximately 10.48 ± 2.56 nm. This value was similar to

that calculated through XRD (8 nm). Additionally, nanoparticles with structures similarly to spheres were observed (**Figure III.12**).

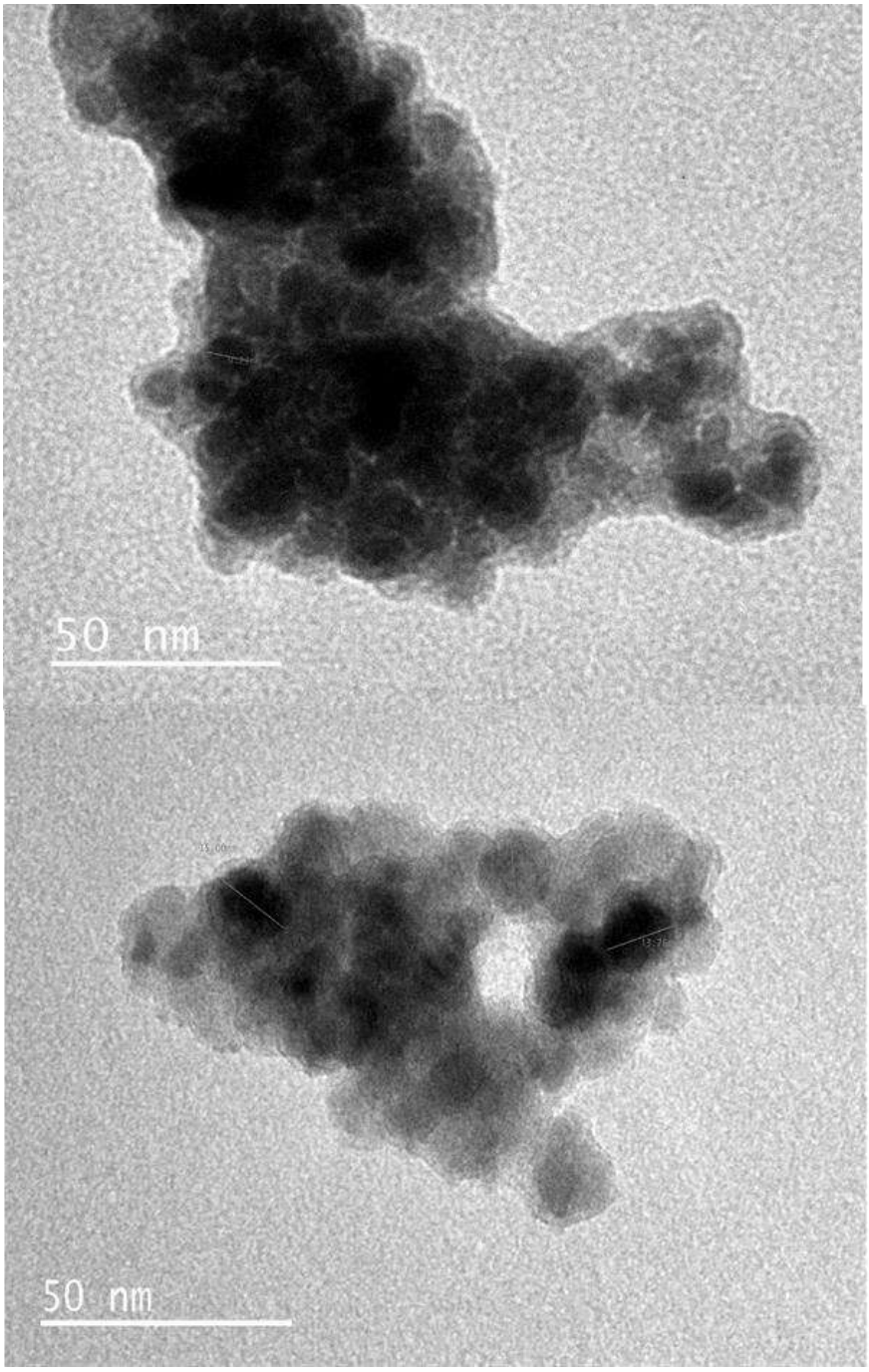

Figure III.12: TEM images of amine-silanized magnetic nanoparticles synthetized by coprecipitation method.

Magnetism results from the movement and/or rotation of unpaired electrons in an atom. The spin of an electron inside an atom, is equivalent to the force of the magnetic moment

of the electron. These electrons are organized in increasing energy orbitals, and each orbital contains a maximum of 2 electrons with opposite spins. When an orbital is full, there is no net magnetic moment (Warren, 2013).

The **magnetic properties** of synthesized magnetite nanoparticles were analyzed measuring hysteresis loop up to 2T magnetic field at RT. The hysteresis loop for MNP and MNP@Si@NH_2 are shown on **Figure III.13**. The saturation magnetization for MNP@Si@NH_2 was 37.06 emu.g^{-1} lower than the value of 55.04 emu.g^{-1} observed for MNP. This reduction of magnetism in MNP@Si@NH_2, can be attributed to the shield provided by the amine-silane layers on the surface of the nanoparticles. This generates an interference effect between the magnetic field and the magnetic domains of nanoparticles (Cabrera *et al*., 2013).

In general, both nanoparticles exhibited ferromagnetic behavior. Additionally, a coercivity (Hc) of 280.9 Oe for MNP and 87.8 Oe for MNP@Si@NH_2 were observed. The Hc value has a direct relationship with the grain size of nanoparticles. It is because, magnetite nanoparticles are strongly affected by thermal effect which decrease the magnetic moment due to missorientation of magnetic moments (Wen *et al*., 2008), resulting in a larger grain size for MNPs compared to MNP@Si@NH_2, as corroborated by XRD.

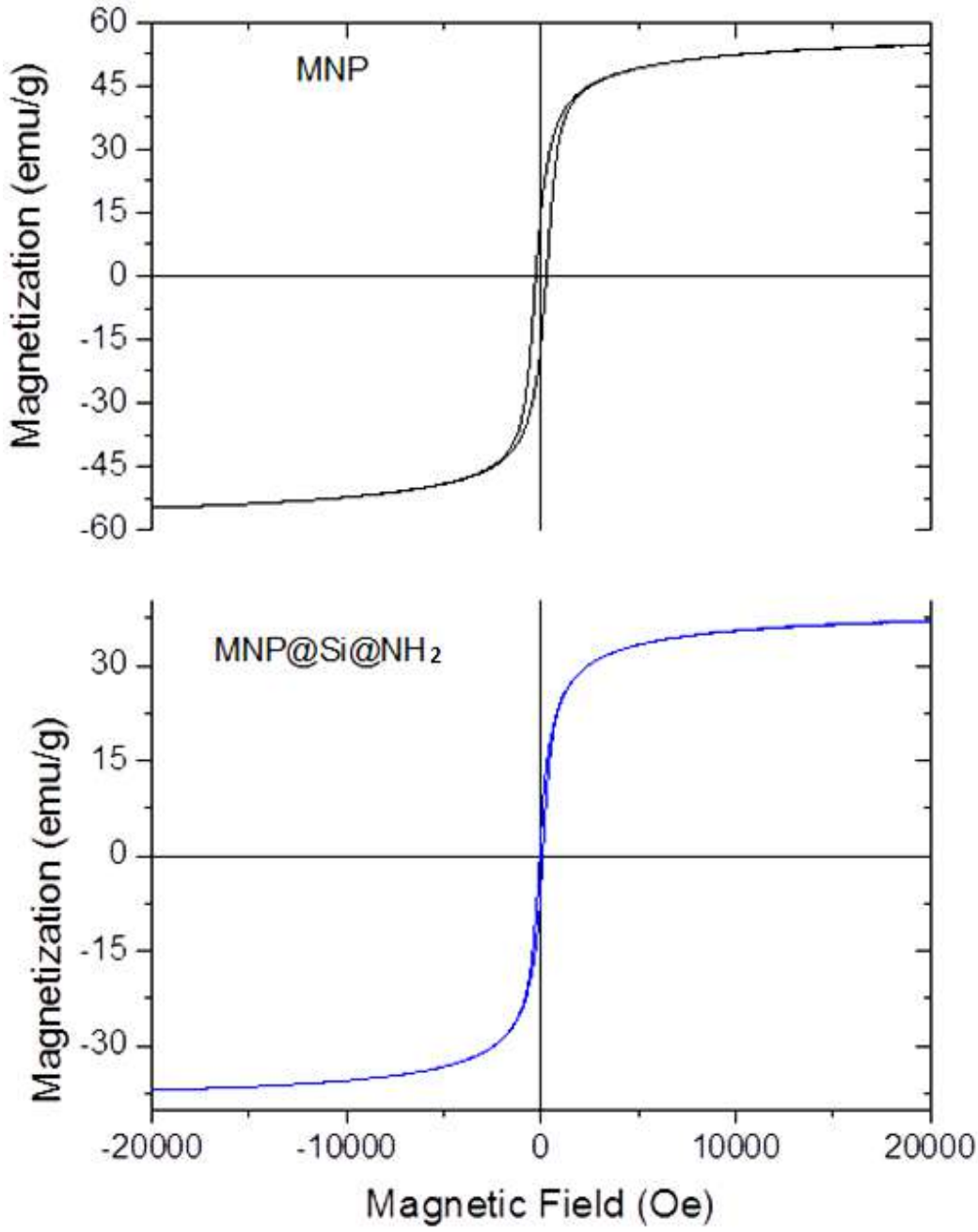

Figure III.13: Magnetic properties of bare MNP (55.04 emu.g^{-1}), and amine-silanized MNP (37.06 emu.g^{-1}).

Diffuse Reflectance Infrared Fourier Transform Spectroscopy (DRIFTS) measurements were performed to investigate the silanization and the functionalization by amino groups (APTES) of the nanoparticles surface. The infrared spectra were recorded for the bare magnetite nanoparticles (MNP), silanized nanoparticles (MNP@Si) and amino-functionalized nanoparticles (MNP@Si@NH_2) and are reported in the **Figure**

III.14 and III.15. The DRIFTS spectrum of magnetite nanoparticles **MNP** shows absorption bands related to the stretching vibrations υFe-O located in the 500-700 cm^{-1} spectral range (at about 640 and 590 cm-^{1}). The spectrum of **MNP@Si** exhibits intense vibrational modes associated with the formation of the silica shell. Among them, the characteristic modes at 1100 and 800 cm^{-1} are attributed to the stretching vibrations of the Si-O-Si linkages (antisymmetric and symmetric stretching modes, respectively) and the band at 475 cm^{-1} is related to the Si-O-Si bending vibration. The spectrum of **MNP@Si@NH_2** is also dominated by the features related to the silica layer but presents additional vibrational modes in the 1600-1400cm^{-1} range. The observed bands can be assigned to amino groups vibrations (NH_2 bending δNH_2 at 1600 cm^{-1}) and to C-H vibrations in CH_2 groups (δCH_2 at 1469 cm^{-1}) and in CH_3 groups (asymmetric bending δCH_3 at 1450 cm^{-1}). These results confirm the presence of the silica shell at the surface of the MNPs, successfully functionalized with amino groups during the synthesis process (Siurdyban *et al*., 2016; Socrates, 2001).

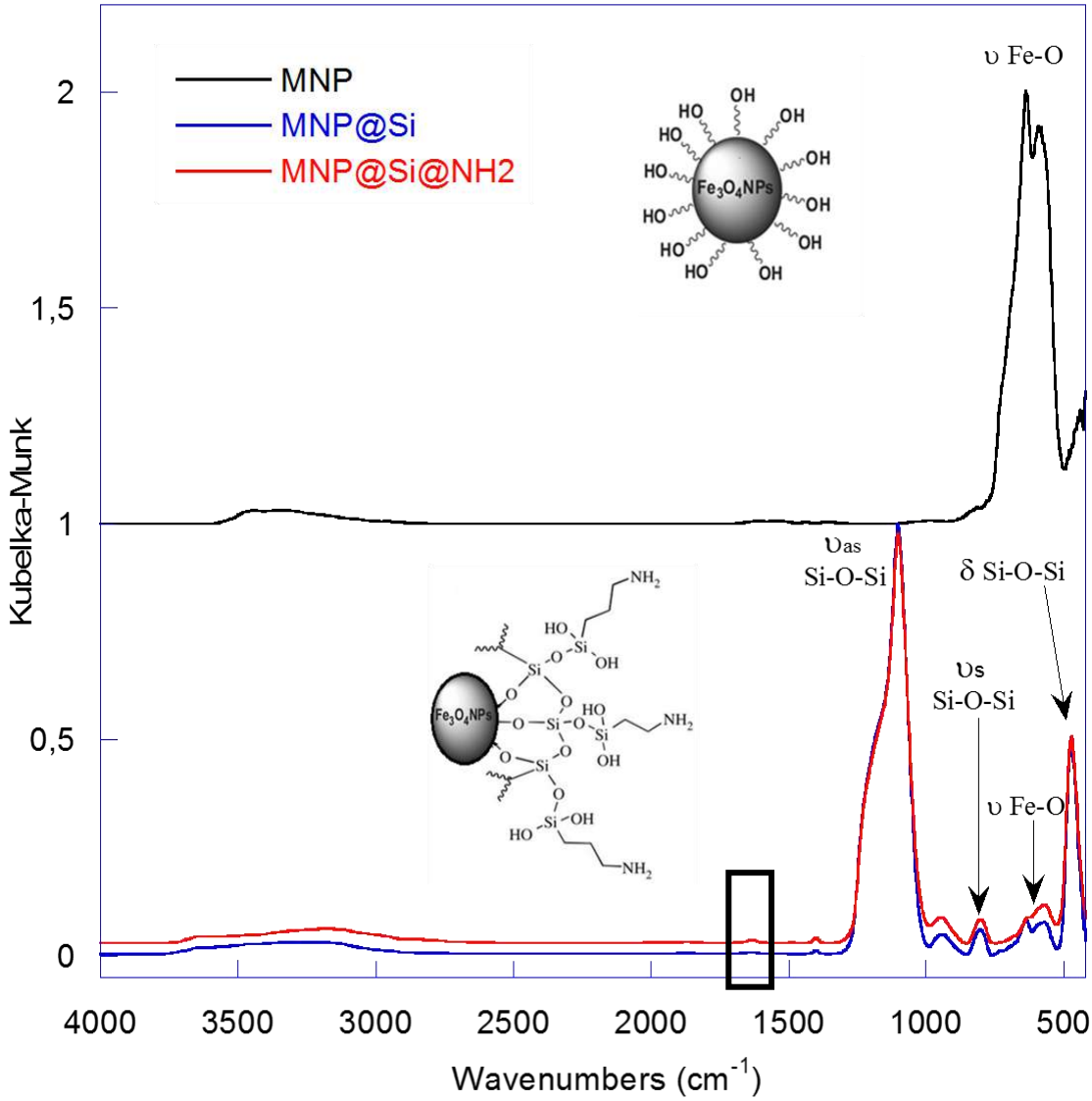

Figure III.14: DRIFTS spectra of MNP and MNP@Si@NH_2 were obtained to confirm the synthesis of amine-silanes nanoparticles. The black box shows the δNH_2 at 1600 cm^{-1} spectral peak.

Figure III.15 shows the amplified NH_2 peak for nanoparticles silanized with TEOS (MNP@Si, blue curve) and with TEOS/APTES (MNP@Si@NH_2, red curve). It is observed that the peak of δNH_2 at 1600 cm^{-1} is a slight pronunciation, different from the blue curve (MNP silanized without NH_2 groups).

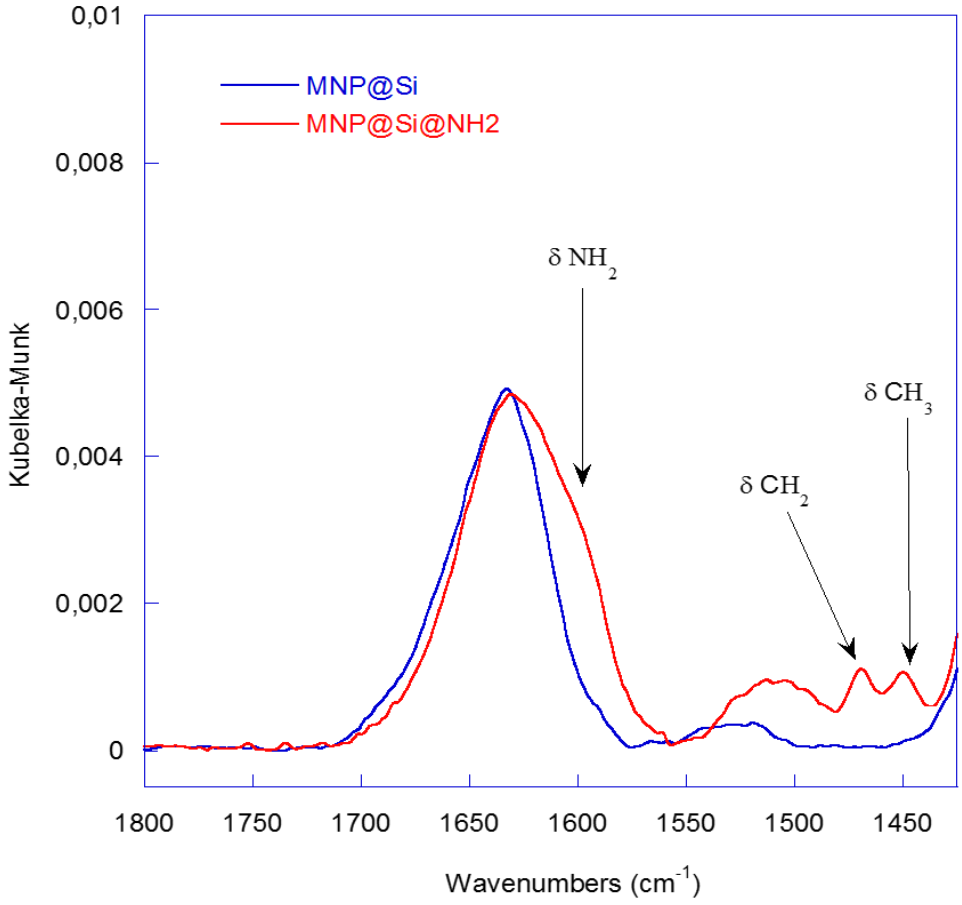

Figure III.15: DRIFTS spectra of MNP@Si and MNP@Si@NH_2 showing N-H bond confirming amine-silanization of nanoparticles.

Using **TGA,** 21.85 – 30.5 mg of nanoparticles were evaluated from 25 to 600 ° C. According to the type of the molecules coated on the surface of the MNPs, different percentages of mass loss were obtained. **Thermogravimetric plots** (**Figure III.16A and III.16B**) show the first loss of mass, attributed to water desorption, happening at temperatures lower than 150°C. At higher temperatures, amine-silanes MNP showed a loss of mass of 1.79 % (0.546 mg) at 435 °C, corresponding the loss of the Si@NH_2 layer. Despite, the amine-silanization had already been corroborated through the **DRIFTS,** an approximate quantification was achieved using TGA. Additionally, the analysis of mass loss as a function of temperature allowed us to determine that amino-silanes tend to evaporate at around 450 °C.

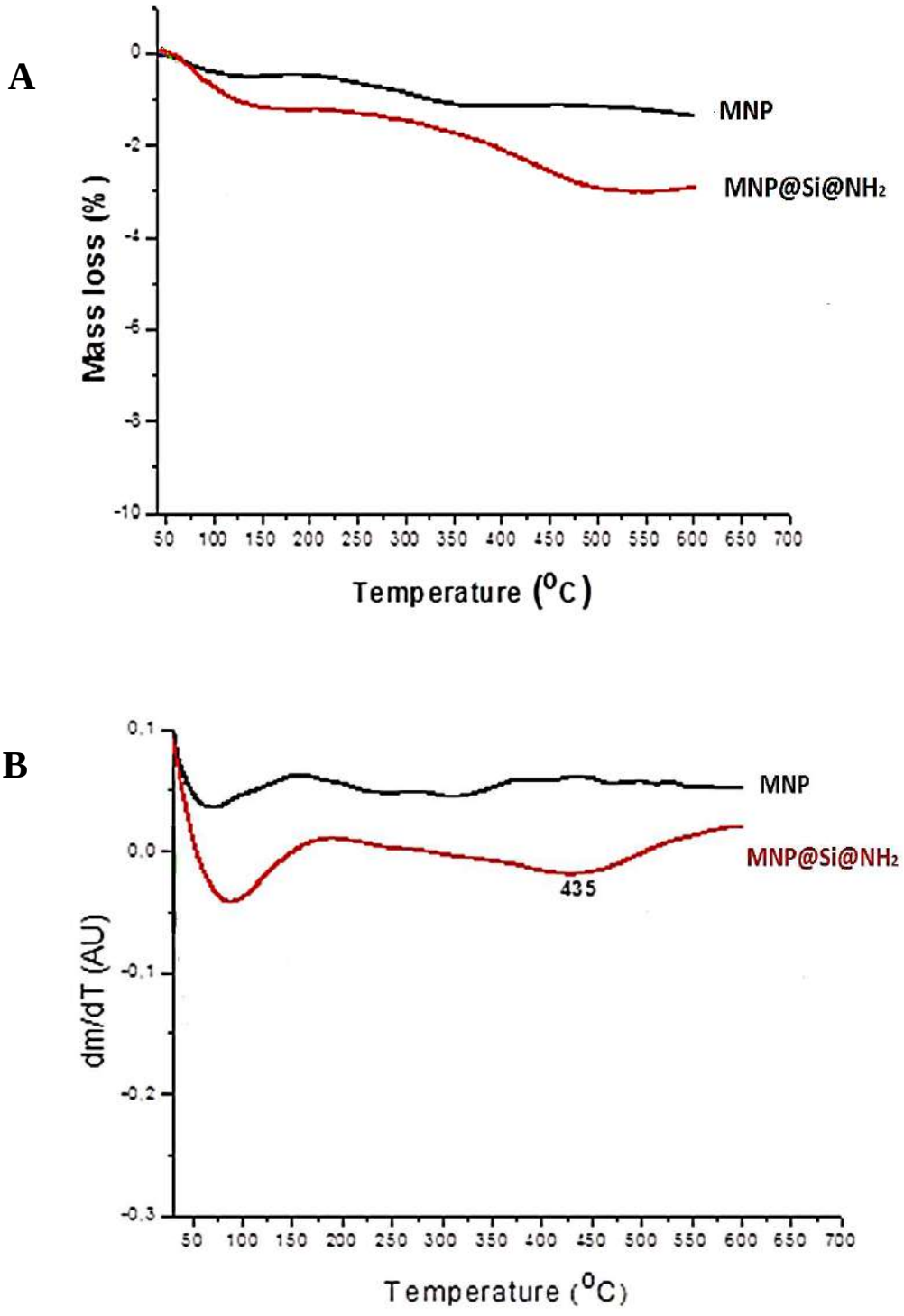

Figure III.16: Thermogravimetry of amine-silanized magnetic nanoparticles. **A)** TGA for magnetic nanoparticles (MNP) (black) and coated MNPs with amine silane groups (red). **B)** DTGA corresponding to naked and conjugated nanoparticles.

About the **surface charge**, MNP@Si@NH_2 exhibited positive charge of around **ζ: +23.57 ± 2.87 mV** (millivolt), important for an electrostatic stabilization of nanoparticles. Instead, a naked MNP (magnetite) had a negative charge due to the –OH ions at the surface. This favored the anisotropic dipolar attraction causing aggregation of particles to large clusters, resulting in the increase of the particle size (Maximilien *et al*., 2015). However, when MNPs are coated with suitable capping agent, a positive net surface charge is exhibited on amine-silanized nanoparticles. It indicates a transformation of -NH_2 groups in -NH^+_3, at neutral pH, generating an steric/electrostatic repulsion between the iron particles (Jesse *et al*., 2015; Liu *et al*., 2011; Vereda *et al*., 2007).

Using **Dynamic Light Scattering (DLS),** the hydrodynamic diameter (d_H) of magnetic nanoparticles was evaluated considering the accumulated number. In solution, the naked MNP showed a d_H of 360.97 nm (87.61 %), and MNP@Si@NH_2 a d_H of 148.32 nm (55.41 %) (**Figure III.17A and III.17 B**). Compared with the results of TEM and XRD, an increase up to 10 times of the nanoparticle diameters was observed. It happened when they were in solution. To explain this phenomenon, we have two hypotheses. First, the amino-silane layers were formed in a disordered way, on the surface of the nanoparticles (d = 10.48 ± 2.56 nm), generating greater exposure of NH_2 and OH functional groups. Depending the pH variations in the solution, these functional groups tend to be protonated or deprotonated. It generates an electrostatic attraction between the amino-silanized nanoparticles. These interactions could generate clusters of silanized nanoparticles, increasing the hydrodynamic diameter. Second, the magnetic properties of the nanoparticles (55.04 emu.g^{-1}) could have generated an aggregation of the nanoparticles before the amino-silanization. In this way, the core of the particle would be formed of a magnetite cluster, and on them the amino-silanization would have been carried out.

A

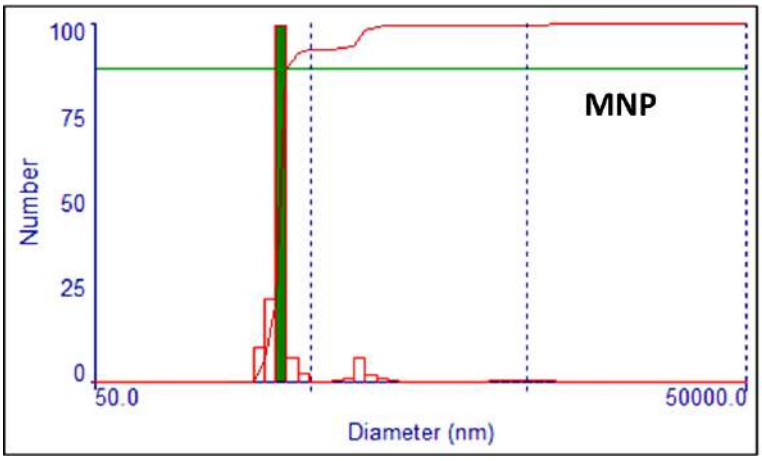

B

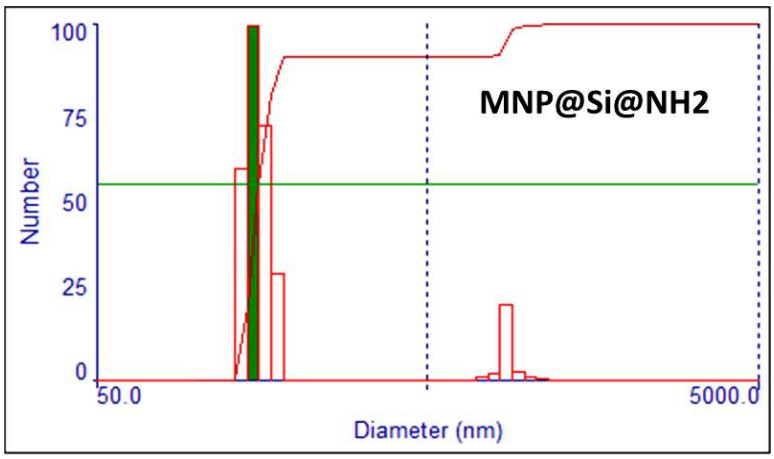

Figure III.17: Hydrodynamic diameter of functionalized magnetic nanoparticles**. A)** MNP (d_H: 360.97 nm; accumulated number: 87.61 %), **B)** MNP@Si@NH_2 (d_H: 148.32 nm; accumulated number: 55.41 %).

III.2. EXPERIMENTAL SECTION (METHODOLOGY).

Different slightly modified protocols for the synthesis and coating of magnetic nanoparticles have been evaluated (Bordbar *et al*., 2014; Han *et al*., 2010; Huynh *et al*., 1998; Jesse *et al*., 2015; Liu *et al*., 2011, 2013; Makovec *et al*., 2015; Zhang *et al*., 2013). At the same time, different solvents (water, ethanol, ethanol/water and methanol/toluene), different coating (carboxymethyl-dextran, APTES, TEOS/APTES) and reaction temperatures were used. However, not all the modified nanoparticles obtained were able to successfully immobilize the proteins on their surface. The conditions evaluated are

described below, before obtaining the best protocol for the synthesis and amino-silanization of MNPs.

III.2.1. Evaluation of conditions for coating of magnetic nanoparticles.

- **Chemicals.**

All chemical used were reagent grade. Ferrous chloride ($FeCl_2$), Ferrous chloride tetrahydrate ($FeCl_2 \cdot 4H_2O$), ferric chloride ($FeCl_3$), tetraethyl orthosilicate (TEOS), (3-aminopropyl) triethoxysilane (APTES), Carboxymethyl-dextran sodium salt (CMD, 10-20kDa), Bovine Serum Albumin (BSA) and sodium citrate ($Na_3C_6H_5O_7$) were bought from Sigma-Aldrich,Saint-Quentin-Fallavier, France. Hydrochloric acid (HCl) and ammonium hydroxide (NH_4OH, 28%) were purchased from Merck and nitric acid from Fisher Scientific India Pvt. Ltd. The antibody (IgG) used was obtained from a rabbit immunized with recombinant antigen (Hsp16.3), described in the previous chapter. Ultrapure Milli-Q water (H_2O) used in this study, was produced in Ultra-pure water purification unit for laboratory (Millipore, Massachusetts, USA). Chemical reactions were made under nitrogen gas. All glassware materials used for the synthesis of iron oxide nanoparticles, were washed with aqua regia solution freshly prepared.

- **<u>Condition N° 1</u>: MNP coating using CMD.**

Due to the numerous studies reported in biomedicine, using CMD to coat MNP, this was considered as the first organic group of interest in our study. Below protocols for the synthesis and functionalization of MNP-CMD.

Protocol 1: Under nitrogen gas, 8.125 g of $FeCl_3$ and 4.98 g of $FeCl_2.4H_2O$ were solubilized in 100 ml of deionized water (H_2O). Then 1.3 g of sodium citrate was added. The mixture was vigorously stirred at 65 °C and ammonium hydroxide (volume of 17.5 ml of NH_4OH) was added dropwise until pH 12. The mixture was stirred for 3 h at 70 °C and

washed using H_2O until neutral pH (approximately 5 times). Acidic water (adjusted to pH 3-4 with HCl) was added to the pellet. The reaction was sonicated for 30 min and stirred for 2 h at 25 °C. Then 0.2 gr of CMD was added in the mixture, and it was stirred over night at 25 °C. The MNP-CMD obtained was washed with H_2O until pH 7.0. The nanoparticles were dried in the oven at 60 ° C. In this section the protocol of Han *et al.* (2010) was slightly modified.

Note: The washes were performed by centrifugation. The pellet turned brown when the acidic water was added. The nanoparticles covered with CMD did not show to be magnetic when they were dry, but after diluting they acquired magnetism.

Protocol 2: Under nitrogen gas, 0.62 g of $FeCl_3$, 0.38 g of $FeCl_2.4H_2O$ and 550 mg of CMD were diluted in 50 ml of acidic water (pH 3-4, adjusted with HCl). The nanoparticles were evidenced when 10 ml of NH_4OH (25%) was added. The reaction was stirred at 80 °C for 2 hours, sonicated for 30 min, and incubated at 80 °C for 3 h. Using a magnet, the nanoparticles were washed with deionized water, until neutral pH. The nanoparticles were dried in the oven at 60 ° C. In this section the protocol of Makovec *et al.* (2015) was slightly modified.

Protocol 3: Under nitrogen gas, 1.95 g of $FeCl_3$ and 1.2 g of $FeCl_2.4H_2O$ were solubilized in 50 ml of deionized water. The nanoparticles were precipitated using NH_4OH (25%) dropwise until pH 11. The reaction was stirred at 80 °C for 3 hours, and black nanoparticles were washed with H_2O until neutral pH. The nanoparticles were resuspended in acidic water (adjust with HCl), and 1g of CMD was added. The mixture was stirred at 45 °C for 20 min. The nanoparticles were isolated using a magnet and adjusted until pH 5-6 with NH_4OH (25%). The pellet was washed with deionized water until neutral pH. MNP-CMD was sonicated and dried in the oven at 60 °C.

Functionalization of MNP-CMD surface with biomolecules.

Resuspended MNP-CMD (5 mg previously dispersed in MES), protein (BSA ~2.2 mg/ml or antibody 10µl/ml), EDC/NHS (5/10 mM for both cases) were mixed in a clean eppendorf tube. The reaction was incubated at room temperature, 15 rpm, overnight. The supernatants of the reactions were dialyzed with PBS at 4°C, and their concentrations were read at A280nm.

- **Condition N°2: MNP coating using APTES at RT.**

To synthesize MNP, 0.25 M $FeCl_2$ and 0.5 M $FeCl_3$ (Fe^{2+}: Fe^{3+} = 1: 2) were mixed in 20 ml of milliQ water, under N_2 gas. The reaction was incubated at 30 °C for 1 h. Then, using NH_4OH, the MNPs were precipitated at pH 12. At room temperature, the MNPs were washed to remove the hydroxide, until pH 7. Subsequently, the black pellet was sonicated and incubated in a shaker with 10 ml APTES (10%, pH 4 with glacial acetic acid) at RT for 16 hrs. Finally, the silanized MNP were washed with milliQ water until neutral pH. In this section the protocol of Jesse *et al.* (2015) was slightly modified.

- **Condition N°3: MNP coating using APTES at 70°C in different solvents.**

The following experiment was carried out according to methodology previously reported (Liu *et al*., 2013), but slightly modified.

For the synthesis of the NPM: Under nitrogen gas, 8.125 g of $FeCl_3$ and 3.175 g of $FeCl_2$ were solubilized in 100 ml of deionized water (H_2O). The mixture was vigorously stirred for 30-60 min at 30 ° C, heated until 80 ° C and then, ammonia solution (volume of 17.5 ml of NH_4OH) was added dropwise until pH 12. The reaction was stirred vigorously for 3-4h at 100 ° C.

Amino silanization using water or ethanol/water as solvents:

The total MNP obtained previously was washed with H_2O until neutral pH (approximately 5-10 times), and the pellets were sonicated for 30 min, and then 40 ml of the solvent (water or ethanol/ water) were added with 10% APTES (pH 4.0, calibrated with about 10 ml of glacial acetic acid). The reaction with APTES (Cf: 10%) was mixed vigorously, for 16 h at 70 ° C. Finally, with the help of a magnet, the nanoparticles were washed with the solvent (water or ethanol/ water) and finally with deionized water, until neutral pH. The black pellets were dried in the oven at 65 ° C.

Amino silanization using the methanol/ toluene solvent:

The MNPs were washed with H_2O until neutral pH (approximately 5 times). Subsequently, the MNPs were washed 3 times with methanol, and the pellet was sonicated for 30 min. 100 ml of methanol/toluene (v/v) was added and the reaction was connected to a distiller, and 50% of the volume was evaporated at 105 °C. Then 50 ml of methanol was added, and the volume was re-evaporated to 50%. This process was repeated 3 times to ensure that the reaction was free of water (anhydrous). Subsequently, 40 ml of methanol was added with 10% APTES (pH 4.0, calibrated with glacial acetic acid). The reaction with APTES (Cf: 4%) was mixed vigorously, for 16 h at 70 ° C. Finally, using a magnet, the nanoparticles were washed with absolute ethanol (3 times) and with deionized water, until neutral pH; and dried in the oven at 65 ° C.

Conjugation of biomolecules on amine-silanized MNPs.

To determine whether synthesized and silanized MNPs have the ability to bind proteins on their surface, a protein immobilization assay was performed. Nanoparticle reactions (6.5 and 5 mg previously dispersed in MES), protein (BSA 35mg/ml or antibody 10µl/ml), EDC/NHS (33.4/66.7 mM and 10/5 mM) in clean eppendorf tubes were prepared and incubated at room temperature, 15 rpm, with semi-circumferential movement. The

supernatants of the reactions were dialyzed, and their concentrations were read in a Nanodrop and a Nanovue at A280nm.

- **<u>Condition N° 4</u>: MNP coating using APTES/TEOS (two steps).**

Under nitrogen gas, 8.125 g of $FeCl_3$ and 4.98 g of $FeCl_2.4H_2O$ were diluted in 100 ml of ethylene glycol. It was mixed vigorously for 30 min at RT and precipitated adding dropwise ammonia solution until pH 12, at 80 °C. The reaction was incubated for 1 h at 80 °C and 2 h at 140 °C under stirring. By centrifugation, the MNPs were washed with ethanol until pH 7. The reaction was diluted with 160 ml ethanol, 40 ml water, 10 ml NH_4OH and 4 ml TEOS (dropwise), sonicated for 30 min, and incubated over night at 40 °C. After, the silane-MNPs, were sonicated for 20 min, and 6 ml of APTES was added. The reaction was incubated for 2 h at 60 °C and sonicated for 1 h. By centrifugation, the amine-silanized nanoparticles were washed with ethanol and water until pH 7.0. The black pellet was dried at 60 ° C.

Functionalization of MNP@TEOS@APTES surface with biomolecules.

5 mg of amine-silanized MNPs were resuspended with protein (BSA ~2.2 mg/ml or antibody 10µl/ml) and coupling agent EDC/NHS (5/10 mM for both cases). The reaction was mixed and incubated at RT, 15 rpm, overnight. The supernatants of the reactions were dialyzed with PBS at 4°C, and their concentrations were read at A280nm.

III.2.2. Synthesis of MNP@Si@NH2 by co-precipitation method.

Iron oxide magnetic nanoparticles coated with amine-silane groups ($MNP@Si@NH_2$), were synthesized following a slightly modified co-precipitation protocol described by Liu *et al.*, 2011 (Liu *et al.*, 2011).

- **Magnetite synthesis.**

$FeCl_2 \cdot 4H_2O$ (2.0 g) and $FeCl_3$ (3.24 g) were dissolved in hydrochloric acid solution (25 ml, 2M, HCl). Aqueous ammonium hydroxide (NH_4OH, 26.78 ml, 28%) was added drop by drop until pH 12 with vigorous stirring (600 rpm) at room temperature, to produce black magnetic nanoparticles (MNP). The reaction mixture was additionally stirred for 30 min at room temperature. MNPs were washed with acid solution (2 times using 50 ml of 2M, HCl) and H_2O (50 ml). The black pellets were then dispersed in ethanol (40 ml) and sonicated (40 min).

- **Amine-silanization of MNP surface.**

The amino-silanization of the surface of the magnetic nanoparticles was carried out in two steps, described below:

MNPs were coated with a first layer (silanization), following the next reaction: total magnetic nanoparticles were vigorously stirred for 2 h at 40°C with aqueous NH_4OH (28%, 1.6 ml), H_2O (6 ml) and TEOS (1.5 ml, 6.72 mmoles). The reaction mixture was sonicated (1h) at room temperature, MNP@Si were washed (3 times with 50 ml of ethanol) and resuspended in 40 ml of ethanol. The suspension was mixed for 12 h at 40 °C, washed with 1 M HCl (50 ml), H_2O, 20% HNO_3 (50 ml) and, finally, H_2O until neutral pH.

After, the second amine-silanization layer was coated on magnetic nanoparticles surface, such as described below: the previously MNP@Si obtained, were resuspended in 60 ml of ethanol. After sonication (30 min) at room temperature, the suspension was mixed with APTES (6 ml, 25.64 mmoles) at 60°C for 12 h. Pellets of $MNP@Si@NH_2$ were washed with ethanol (3 times with 100 ml) and acetone (3 times with 100 ml) and dried at 60°C in a stove.

Functionalization of $MNP@Si@NH_2$ surface with biomolecules.

Protein (BSA ~2.2 mg/ml or antibody 10µl/ml), EDC/NHS (5/10 mM for both cases) and 5 mg of amine-silanized MNP, were mixed and incubated at RT, 15 rpm,

overnight. The supernatants of the reactions were dialyzed with PBS at 4°C, and their concentrations were read at A280nm.

III.2.3. Characterization of synthesized magnetic nanoparticles.

Physical-chemical properties of synthesized magnetic nanoparticles were characterized using different methods. Each type of characterization of the nanoparticles was carried out as described below:

- **X-ray diffraction.**

X-ray powder diffraction (**XRD**) is a rapid analytical technique that allows to identify the phases of a crystalline material, reveal information about the chemical composition of the material, as well as provide informations about the average dimensions of the unit cells. The identification of the phases is achieved by comparing the acquired data with those of the reference databases (Garcia-Granda and Montejo-bernardo, 2013).

The XRD patterns were measured at room temperature in D8 FOCUS X-ray Diffractometer (Bruker, Karlsruhe, Germany) using CuKα radiation (λ= 1.5406 Å). The analyses of diffraction pattern were made by refining crystalline structure using the Rietveld method performed by the Fullprof software.

- **Transmission Electron Microscopy.**

The transmission electron microscopy (**TEM**) is used to view superfine samples through which electrons can pass and generate a projection image. An electron source in the upper part of a TEM emits electrons that travel through the vacuum tube of the microscope. Instead of having a glass lens, the TEM uses an electromagnetic lens that focuses the electrons in a very thin beam. In such a way that an image of the electron density of the sample is generated (Franken *et al*., 2017).

Samples for TEM were prepared by suspending powder nanoparticles in ethanol and ultrasonication for 15 min. The suspension was evaluated using the GATAN TEM JEOL 1400 (JEOL, Brussel, Belgium), equipped with an Orius SC1000 CCD Camera (GATAN),

to 60kV and 120kv. Microphotographs were taken to determine the size and structure of the amino-silanized magnetic nanoparticles.

- **Dynamic Light Scattering:**

Dynamic light scattering (DLS) is a technique used to determine the size distribution of small particles in suspension or polymers in solution. Basically, the sample is illuminated by a laser beam and the fluctuations of the scattered light are detected at a scattering angle ($\theta = 90°$) by a photon detector (NanoComposix, 2012).

For **DLS,** the MNP@Si@NH_2 were dispersed in water and measure in 90Plus Particle Size Analyzer (Brookhaven Instruments Corporation, New York, USA). To completely dilute the nanoparticles in the solution, they were sonicated for 15 minutes before the measurement.

- **Diffuse reflectance infrared Fourier transform spectroscopy**.

Diffuse reflectance infrared Fourier transform spectroscopy (**DRIFTS**) allows spectra of powdered samples to be obtained with a minimum of sample preparation required. Normally, the sample is placed on a flat surface inside a chamber with two windows, then an infrared beam is reflected and scattered on the surface of the sample. Emerging radiation leaves the sample in all directions, but with the appropriate optical settings it is directed towards the detector. The intensity of the infrared peaks is expressed in units of Kubelka-Munk, in which case the spectra are similar to the transmission spectra shown as absorbance (Mosiewicki *et al*., 2011).

DRIFTS was used to analyze the chemical modifications of the nanoparticles surface. The measurements were conducted on a Thermo Scientific Nicolet 6700 spectrometer equipped with a diffuse reflection unit (Harrick Praying Mantis™). The spectra were recorded by averaging 200 scans at a resolution of 4 cm^{-1} in the 4000 to 400 cm^{-1} spectral range. All powder samples (at a concentration of 1 weight-%) were intermixed with calcinated KBr and finely ground. The pure KBr was used as background. The spectral intensities were converted to Kubelka-Munk units.

- **Mössbauer Spectroscopy.**

Mössbauer spectroscopy **(MS)** is a non-destructive technique based on the emission and resonant absorption of gamma rays in solids. Currently, this technique allows to study the electronic structure, the binding properties, the molecular symmetry, the magnetic behavior and the phase transitions in the solid state, which constitutes the basis for identifying all types of materials, such as a "fingerprint" (Gütlich *et al*., 2012).

MS was used to determine the iron oxidation state in nanoparticle core. Mössbauer spectra were recorded at RT using a conventional Mössbauer spectrometer in transmission geometry and employing a 25 mCi, ^{57} Co/Rh source. The spectra were analyzed using the least squares method assuming Lorentzian line shapes and a hyperfine field distribution.

- **Thermogravimetric Analysis (TGA).**

The TGA measures the amount and velocity (velocity) of change in the mass of a sample as a function of temperature or time in a controlled atmosphere. Basically, when a sample is heated, its mass changes (reduces), due to decomposition, reduction or evaporation. This allows to determine the thermal or oxidative stabilities of the materials, as well as their composition properties. In the case of Derived Thermogravimetry (DTG), the speed of changes in weight of the material when heating is compared with the temperature and allows to analyze the thermogram peaks of weight versus temperature (Groenewoud, 2001).

To quantify the organic material conjugated on nanoparticle surfaces, **TGA** was carried out using Setaram Thermogravimetric Analyzer (LABSYS EVO DTA/DSC, Lyon, France). The sample weight ranged from 21.85 to 30.5 mg. Analysis was performed from 25 to 900 °C at a heating rate of 10°C/min, under argon atmosphere, with a gas flow rate of 16 mL/min. The loss mass of organic material was calculated using a derivative plot dm/dT (DTGA).

- **Zeta potential (ζ)**

The superficial charge of MNP@Si@NH_2 was determined using **zeta potential (ζ)** in a Zetasizer cell adapted to 90Plus Particle Size Analyzer. The nanoparticles were dispersed (sonication 15 min) in water and evaluated to neutral pH.

- **Vibrating Sample Magnetometer (VSM).**

Magnetization measurements were performed at RT in magnetic fields varying from 0 to 20 kOe (2.0 T) using a Vibrating Sample Magnetometer (Quantum Design Model VersaLab -3T, California, USA). The saturation magnetization was determined from the magnetization curve at maximum magnetic field.

III.3. RESULTS.

III.3.1. Evaluation of conditions for the coating of magnetic nanoparticles.

- **<u>Condition N° 1</u>: MNP coating using CMD.**

The **Table III.1** shows the main visible characteristics of the MNP-CMD after the synthesis. Iron nanoparticles are characterized by having a blackish color. In our case, we obtained brown and black MNPs. In addition, the magnetism varied according to the state of the NPM, the magnetization was faster when the black NPM was in powder (+++) and the brown (oxidized) did not show magnetization. However, a medium magnetization (++) was observed when the brown MNP was dispersed. Finally, no agglomeration of the nanoparticles was observed.

- **<u>Condition N° 2</u>: MNP coating using APTES at RT.**

The silanized MNP with APTES at RT presented a polydispersity of 29.5% in DLS measures. The hydrodynamic diameter was 285,2 nm ± 9,5 nm (**Figure III.1A**). The positive zeta potential of the MNP surface was Z: 17,66 ± 2,25 mV(**Figure III.1 B**). Additionally, the silanized MNPs showed a hysteresis of 10.87 Oe (**Figure III.1 C**).

- **<u>Condition N° 3</u>: MNP coating using APTES at 70°C using different solvents.**

The amine-silanization was made only with APTES, using the solvents water, ethanol/water and methanol/toluene. Characteristics of the nanoparticles with and without APTES were evaluated, such as the zeta potential values and the hydrodynamic diameter.

Amino-silanization of nanoparticles using the water as solvent.

Figure III.2 shows nanoparticles with and without APTES in water as solvent (APTES-water), both has a negative surface charge, ζ: -31.04 mV and ζ: -29.15 mV, respectively.

In **Figure III.3** the hydrodynamic diameter of the nanoparticles synthesized is observed. The diameter of MNP silanized with APTES-water (128.37 nm) is greater than the nanoparticles without APTES (94.61 nm).

Amino-silanization of nanoparticles using ethanol/water as solvent.

The nanoparticles obtained with and without APTES, have a positive surface charge Z: +7.83 mV and Z: +20.0 mV, respectively (**Figure III.4**).

Figure III.5 shows the hydrodynamic diameters of the nanoparticles with APTES (72.63 nm) and without APTES (85.19 nm).

Amino-silanization of nanoparticles using methanol/toluene as solvent.

Figure III.6 shows a negative charge on the surface of nanoparticles without APTES-methanol/toluene (Z: -19.2 mV) while the nanoparticles silanized with APTES-methanol/toluene presented a positive charge (Z: +22.15 mV). **Figure III.7** indicates hydrodynamic diameters, 106.26 and 112.75 nm, respectively for both nanoparticles.

The **Table III.2** summarizes the characteristics obtained from the silanized MNPs with different solvents. When the mixture methanol/toluene was used, the surface charge was higher (+22.15) compared to the other MNPs silanized with other solvents. In the case of the mixture ethanol/water the hydrodynamic diameter was lower, guaranteeing a greater dispersion in MNPs. On the other hand, the non-silanized nanoparticles with APTES-ethanol/water presented a positive surface charge (+7.83), indicating possible residues of

NH_4OH, used for the co-precipitation of the nanoparticles. Probably, the nanoparticles were not washed properly until reaching a neutral pH.

Determination of the ability of the amine-silanized MNPs to be functionalized by biomolecules on their surface.

Table III.3 shows the amount of proteins (mg of BSA and IgG) immobilized on the surface of the silanized MNP, after 6 h incubation. A higher percentage of bound BSA (10.65 %) is observed when methanol/toluene is used as solvent in the silanization process. However, in the case of antibodies (IgG), only 5.26% was fixed on the MNP surface. Despite of the promising characteristics of the silanized MNPs using the mixtures ethanol/water and methanol/toluene, these systems were not very efficient for the immobilization of biomolecules on their surface. Consequently, other conditions and protocols for the silanization of nanoparticles were evaluated.

- **Condition N° 4: MNP coating using TEOS/APTES (two steps).**

In this case the silanization was made using TEOS (first layer) and APTES (second layer. **Table III.4** shows the functionalization of BSA and IgG on the surface of the amine-silanized MNP, 13.52 % and 46.15% , respectively.

A protocol reported by Liu *et al.*, 2011, MNP coating using TEOS/APTES in ethanol solvent, was used in the next section. It demonstrated to be most efficient to produce modified nanoparticles able to bind high amounts of proteins on their surface. Therefore, all experiments onwards were performed with the MNPs described below.

III.3.2. Synthesis of MNP@Si@NH_2 by co-precipitation method.

The **Table III.5** shows the amount of proteins conjugated on nanoparticle surfaces (MNP@Si@NH_2). The values of linked BSA and IgG (13.88% and 44.75%, respectively) were similar to MNPs previously reported (table III.4).

III.3.3. Physical-chemical characterization of coated magnetic nanoparticles.

To determine the physical-chemical properties of the MNP@Si@NH_2 synthesized, different techniques of evaluation were used. The most important results of this characterization are described below:

The structural characterizations made **by XRD** (**Figure III.9**) showed different reflection planes corresponding to its Bragg angles, characteristic for magnetite (JCPD card N° 19-0629). According Wen *et al*. (2008) the XRD patterns of the magnetic particles have 2θ peaks at 18.44°, 30.32°, 35.75°, 43.32°, 53.89°, 57.34° and 62.96°, which are attributed to the crystal planes of magnetite at (111), (220), (311), (400), (422), (511) and (440), respectively (Wen *et al*., 2008). The broadening analysis of diffraction peaks for MNP@Si@NH_2 and bare MNP shows different nanometric grain size, 8 nm and 12 nm, respectively.

The magnetite **XRD** pattern was identified as F d-3 m spatial group with a = b = c = 0.837 nm, cell conditions.

Mössbauer spectra of magnetite nanoparticles and amine-silanized magnetite are shown on **Figure III.10A and III.10B**, respectively.

The Mössbauer spectrum for MNP was fitted using only two crystalline iron site associated to Fe^{2+} and Fe^{3+} related to octahedral and tetrahedral iron sites (Cabrera *et al*., 2013; Wang *et al*., 2008). However, Mössbauer spectra of amine-silanized magnetite was fitted using three crystalline iron sites and a distribution of non-equivalent iron sites fitted by a hyperfine field distribution. The hyperfine conditions of three crystalline sites were identifies as Fe^{2+}, Fe^{3+} and interfacial iron sites. While, the distribution was associated to non-equivalent iron site with nanosized grain size supported by XRD analysis. **Figure III.11** shows the hyperfine field distribution used to analyze MNP@Si@NH_2 Mössbauer spectra.

Using the **TEM** technique was observed a nanoparticle size distribution of 6.5-15 nm, with an average particle size of approximately 10.48 ± 2.56 nm. Additionally, nanoparticles with structures similarly to spheres were observed (**Figure III.12**). The **magnetic properties** of synthesized magnetite nanoparticles were analyzed measuring hysteresis loop up to 2T magnetic field at RT. The hysteresis loop for MNP and MNP@Si@NH_2 are shows on **Figure III.13**. The saturation magnetization for MNP@Si@NH_2 was 37.06 emu.g^{-1} lower than the value of 55.04 emu.g^{-1} observed for MNP.

In general, both nanoparticles exhibited ferromagnetic behavior. Additionally, a coercivity (Hc) of 280.9 Oe for MNP and 87.8 Oe for MNP@Si@NH_2 were observed.

Diffuse reflectance infrared Fourier transform spectroscopy (DRIFTS) measurements were performed to investigate the salinization and the functionalization by amino groups (APTES) of the nanoparticles surface. The infrared spectra were recorded for the bare magnetite nanoparticles (MNP), silanized nanoparticles (MNP@Si) and amino-functionalized nanoparticles (MNP@Si@NH_2) and are reported in the **Figure III.14 and III.15**.

Using **TGA** (**Figure III.16A and III.16B**), 21.85 – 30.5 mg of nanoparticles were evaluated from 25 to 600 ° C. According to the type of the molecules coated on the surface of the MNPs, different percentages of mass loss were obtained.

About the **surface charge**, MNP@Si@NH_2 exhibited positive charge of around **ʒ: +23.57 ± 2.87 mV**, important for an electrostatic stabilization of nanoparticles.

Using **DLS,** the hydrodynamic diameter (d_H) of magnetic nanoparticles was evaluated considering the accumulated number. In solution, the naked MNP

showed a d_H of 360.97 nm (87.61 %), and MNP@Si@NH_2 a d_H of 148.32 nm (55.41 %) (**Figure III.17A and III.17 B**).

III.4. DISCUSSION.

III.4.1. Evaluation of conditions for the coating of magnetic nanoparticles.

- **Condition N° 1: MNP coating using CMD.**

In our study, we evaluated three previously reported protocols: Protocol 1 (Han *et al*., 2010), protocol 2 (Makovec *et al.*, 2015) and protocol 3 (Li *et al*., 2011), where CMD was successfully coated on the surface of the MNPs. However, in our results the process of MNP coating with CMD generated nanoparticles with low magnetism, and consequently they were not efficient to immobilize proteins on their surface (data not shown).

After the synthesis, the naked MNPs must be covered for avoid degradation, aggregation and oxidation, especially with metals such as iron. A shell layer allows to increase the chemical stability and integrity of the MNP (Fields *et al*., 2016). Before choosing the amino groups for the coating of the MNPs, the CMD was evaluated, because this polymer was used in previous studies in biomedicine.

The CMD is a polysaccharide commonly used due their negative charged carboxylic groups and their hydrophilicity, avoiding the agglomeration of MNP-CMD (Li *et al*., 2011). Han *et al.*, 2010 reported a MNP-CMD conjugated to Octreotide, which is a synthetic somatostatin analogue that specifically targets somatostatin receptors, for MRI applications into pancreatic and colon cancer cells (Han *et al.*, 2010). Also, Li *et al*., 2011 reported a MNP-CMD able to conjugated covalently anti-BSA in their surface. After incubation with BSA, the antigen was efficiently dissociated and the regenerated antibody covered MNP-CMD was repeatedly used *(Li et al.*, 2011).

In our results the process of MNP coating with CMD generated nanoparticles with low magnetism, this could be explained because the CMD is a complex and large polymer, and

probably it is generating an interference between the surface and the core domains of the MNPs. In general, the CMD option was discarded to conjugate biomolecules due to its instability in its magnetization, which could be due to the interference of the CMD exerted on its surface. Consequently, amino-silane groups were used to cover the surface of the MNPs.

- **Condition N° 2: MNP coating using APTES at RT.**

Silica is a popular election for the inorganic coating of MNPs. It is because the silanization process is not complex, is effective, has low cytotoxicity, inertia to redox reactions, stability in acidic conditions and there are available a great different functional groups associated to commercial silanes (Fields *et al*., 2016). In general, the initial silanization is a very fast process, but the saturation progress is very slow, involving adsorption, chemical sorption, and chemical diffusion processes (Liu *et al.*, 2013).

Jesse *et al.*, 2016 reported a modified protocol to synthesize nanoparticles with APTES; and conjugate specific antibodies covalently for the bio-separation of begomovirus (Jesse et al., 2015). This protocol was followed because it presents a similar strategy to the one proposed in this study.

In our results, the silanized MNP with APTES at RT, presented a high polydispersity (29.5%) in DLS measures, this means that there was an heterogeneity of MNPs with different measures. The hydrodynamic diameter was elevated (285,2 nm ± 9,5 nm) compared with 25 nm (d_H) reported by Jesse *et al.*, 2015 (**Figure III.1A**).

The magnetic hysteresis is a characteristic where MNPs retain a remaining magnetism, although the magnetic field no longer exists. The hysteresis curve shows the behavior of the magnetism of a material, to different levels of magnetic intensity (Oe) applied. At certain point, the magnetization is proportional (linear zone) until reaching the point of saturation induction. This means that although a greater magnetic force is induced to the material, it will no longer magnetize (Ahmadzadeh *et al*., 2018).

Our silanized MNPs showed a hysteresis of 10.87 Oe. This is because by subjecting the silanized MNPs to an alternating magnetic field, their domains were oriented according to the sense of the magnetic field. But when the intensity of the field decreased, most of the domains returned to their initial position. However, others did not reach it, possibly due to molecular friction between them. Therefore, these domains retained part of their forced orientation, persisting a remnant magnetism that manifests as a small level of magnetic induction (**Figure III.1 C**)

The positive zeta potential demonstrated an correct silanization of the MNP surface (**Figure III.1 B**). However, previous studies reported that a high temperature for the silanization process, can improve an homogeneuos monolayer structure of the amine-silane groups on MNP surfaces.

- **<u>Condition N° 3</u>: MNP coating using APTES at 70°C using different solvents.**

The silane groups are activated by hydrolysis, subsequently a condensation between the Si-OH (silanol) and OH- (MNP surface) groups, is produced by forming stable bonds on the surface. However, the different types of solvents in the silanization process could influence the formation of homogenous or heterogeneous layers of silane groups on the MNP surfaces (Liu *et al*., 2013). This could have an impact on the immobilization of biomolecules on the surface of the nanoparticles. In this way, silanized MNPs with different solvents were identified and their effect on protein conjugation was evaluated.

Amino-silanization of nanoparticles using the water as solvent.

Figure III.2 shows nanoparticles with and without APTES in water as solvent (APTES-water), both has a negative surface charge, indicating that probably the OH groups are the predominant ones on the surface. It means that the functionalization with the amino groups is scarce or null.

In **Figure III.3** the hydrodynamic diameter of the nanoparticles synthesized is observed. The MNP silanized with APTES-water is greater than the nanoparticles without APTES, indicating that there is no stabilization of the nanoparticles by APTES.

Amino-silanization of nanoparticles using ethanol/water as solvent.

Unlike the nanoparticles silanized with APTES-water, in this case it can be observed that the nanoparticles obtained, with and without APTES, have a positive surface charge in both cases, being higher in the nanoparticles synthesized with APTES (**Figure III.4**).

Also, **Figure III.5** shows that the size of the nanoparticles with APTES is smaller than that of the nanoparticles synthesized without APTES. This would be explained by the repulsion charges of the nanoparticles, generating a dispersion of MNPs.

Amino-silanization of nanoparticles using methanol/toluene as solvent.

Liu *et al.,* 2013 reported that the highest equilibrium grafting density, data based on TGA, was reached using toluene/methanol as solvent in the silanization process (Liu *et al.,* 2013).

Figure III.6 shows a negative charge on the surface of nanoparticles without APTES-methanol/toluene while the nanoparticles silanized with APTES-methanol/toluene presented a positive charge, indicating the amino groups from silanization process. **Figure III.7** indicates a similar hydrodynamic diameter between both nanoparticles.

Determination of the ability of the amine-silanized MNPs to be functionalized by biomolecules on their surface.

Because the charge of the nanoparticles silanized with the system APTES-water had a net negative charge, the reactive amino groups would not be present on the surface. Consequently, functionalization with proteins could only be generated through weak interactions and/or absorption. In the case of nanoparticles silanized with the system APTES-ethanol/water and with the system APTES-methanol/toluene, it is observed positive surface charges in both cases, it means that there are amino groups on the surface,

which are essential to generate the peptide bonds with the carboxyl groups of the proteins to be functionalized. However, the silanized MNPs using the mixtures ethanol/water and methanol/toluene, were not very efficient for the immobilization of biomolecules on their surface.

- **Condition N° 4: MNP coating using TEOS/APTES (two steps).**

Although MNP were efficient to immobilize proteins on its surface (13.52 % of BSA and 46.15% of IgG) (**Table III.4**), the main disadvantage was the very small amount of MNPs produced. This could be due to the interference with ethylene glycol during the washing step of the nanoparticles.

III.4.2. Synthesis of MNP@Si@NH_2 by co-precipitation method.

This section presents the best protocol of synthesis and coverage of MNP, for the immobilization of proteins on its surface. Using this protocol, a greater amount of MNP was produced (grames). As in the cases previously described, the magnetic nanoparticles were synthesized successfully following a modified co-precipitation method (Liu et al., 2011). After the synthesis, to produce monodispersed particles, the MNPs were stabilized with amino-silane groups (TEOS/APTES in two steps) on the surface to avoid/reduce particle agglomeration (**Figure III.8**); which may occur during synthesis, drying or post-synthesis processing (Smit, 2018). In this way the repulsive forces between the particles increased.

The advantage of this method is the amount of synthesized nanoparticles, because it can be measured in grams, unlike the previous one that only produced mg of MNPs. In addition, the synthesis and amino-silanization methodologies were easier and cheaper than the previous one, because ethylene glycol was not used.

III.4.3. Physical-chemical characterization of coated magnetic nanoparticles.

Our diffraction peaks were similar to XRD pattern previously reported. XRD data shows similar peaks between bare MNP compared to MNP@Si@NH_2. In addition, XRD of MNP@Si@NH_2 showed a characteristic amorphous shoulder ($2\theta = 50.0°$) associated to amorphous silica recovering the magnetite particles. The XRD patterns of magnetite and amine-silanized magnetite were similar, indicating that Si@NH_2 groups has not effect on the crystallization process. However, the broadening analysis of diffraction peaks for MNP@Si@NH_2 and bare MNP shows different nanometric grain size, 8 nm and 12 nm, respectively. This difference in size could be due to the stabilization of nanoparticles with amino-silane groups, generating a repulsive force, consequently a lower degree of aggregation. On the other hand, in the case of naked nanoparticles, there is an attraction between them that in time can produce an aggregation of the nanoparticles.

Mössbauer spectra provided important information on the characteristics of the magnetic states for iron nuclei located in different regions in the nanoparticles. The diameter of MNPs (10.48 ± 2.56 nm), measured by TEM, was similar to that calculated through XRD (8 nm).

Magnetism results from the movement and/or rotation of unpaired electrons in an atom. The spin of an electron inside an atom, is equivalent to the force of the magnetic moment of the electron. These electrons are organized in increasing energy orbitals, and each orbital contains a maximum of 2 electrons with opposite spins. When an orbital is full, there is no net magnetic moment (Warren, 2013).

The saturation magnetization for MNP@Si@NH_2 was lower than for MNP. This reduction of magnetism in MNP@Si@NH_2, can be attributed to the shield provided by the amine-silane layers on the surface of the nanoparticles. This generates an interference effect between the magnetic field and the magnetic domains of nanoparticles (Cabrera *et al.*, 2013).

The Hc value has a direct relationship with the grain size of nanoparticles. It is because, magnetite nanoparticles are strongly affected by thermal effect which decrease the magnetic moment due to missorientation of magnetic moments (Wen et al., 2008). Resulting in a larger grain size for MNPs compared to MNP@Si@NH2, as corroborated by XRD.

The DRIFTS spectrum of magnetite nanoparticles **MNP** shows absorption bands related to the stretching vibrations υFe-O located in the 500-700 cm^{-1} spectral range (at about 640 and 590 cm-^{1}). The spectrum of **MNP@Si** exhibits intense vibrational modes associated with the formation of the silica shell. Among them, the characteristic modes at 1100 and 800 cm^{-1} are attributed to the stretching vibrations of the Si-O-Si linkages (antisymmetric and symmetric stretching modes, respectively) and the band at 475 cm^{-1} is related to the Si-O-Si bending vibration. The spectrum of **MNP@Si@NH_2** is also dominated by the features related to the silica layer but presents additional vibrational modes in the 1600-1400cm^{-1} range. The observed bands can be assigned to amino groups vibrations (NH_2 bending δNH_2 at 1600 cm^{-1}) and to C-H vibrations in CH_2 groups (δCH_2 at 1469 cm^{-1}) and in CH_3 groups (asymmetric bending δCH_3 at 1450 cm^{-1}). These results confirm the presence of the silica shell at the surface of the MNPs, successfully functionalized with amino groups during the synthesis process (Siurdyban *et al*., 2016; Socrates, 2001). **Figure III.15** shows the amplified NH_2 peak for nanoparticles silanized with TEOS (MNP@Si, blue curve) and with TEOS/APTES (MNP@Si@NH_2, red curve). It is observed that the peak of δNH_2 at 1600 cm^{-1} is a slight pronunciation, different from the blue curve (MNP silanized without NH_2 groups).

Thermogravimetric plots show the first loss of mass, attributed to water desorption, happens at temperatures lower than 150°C. At higher temperatures, amine-silanes MNP showed a loss of mass of 1.79 % (0.546 mg) at 435 °C, corresponding the loss of the Si@NH_2 layer. Despite, the amine-silanization had already been corroborated through the

DRIFTS, an approximate quantification was achieved using TGA. Additionally, the analysis of mass loss as a function of temperature allowed us to determine that amino-silanes tend to evaporate at around 450 °C.

About the **surface charge**, a naked MNP (magnetite) had a negative charge due to the –OH ions at the surface. This favored the anisotropic dipolar attraction causing aggregation of particles to large clusters, resulting in the increase of the particle size (Maximilien *et al*., 2015). However, when MNPs are coated with suitable capping agent, a positive net surface charge is exhibited on amine-silanized nanoparticles. It indicates a transformation of $-NH_2$ groups in $-NH_3$, at neutral pH, generating an steric/electrostatic repulsion between the iron particles (Jesse *et al*., 2015; Liu *et al*., 2011; Vereda *et al*., 2007).

Compared with the results of TEM and XRD, increase up to 10 times of the nanoparticle diameters was observed in the DLS. It happened when they were in solution. To explain this phenomenon, we have two hypotheses. First, the amino-silane layers were formed in a disordered way, on the surface of the nanoparticles ($d = 10.48 \pm 2.56$ nm). Generating greater exposure of NH_2 and OH functional groups. Depending the pH variations in the solution, these functional groups tend to be protonated or deprotonated. It generates an electrostatic attraction between the amino-silanized nanoparticles. These interactions could generate clusters of silanized nanoparticles, increasing the hydrodynamic diameter. Second, the magnetic properties of the nanoparticles (55.04 $emu.g^{-1}$) could have generated an aggregation of the nanoparticles before the amino-silanization. In this way, the core of the particle would be formed of a magnetite cluster, and on them the amino-silanization would have been carried out.

III.5. CONCLUSSION.

MNPs were successfully synthesized using the coprecipitation method. The XRD, Mössbauer spectroscopy, zeta potential, TEM and FTIR showed appropriate characteristics to functionalize biomolecules on the nanoparticle surface. A diffraction crystal diameter of ~12.5 nm (10.48 ± 2.56 nm), superficial net charge of ζ: +23.57 ± 2.87 mV, a magnetization saturation of 37.06 emu.g^{-1} and a spherical structure were observed in the silanized MNPs. For the functionalization of nanoparticle surfaces with proteins, active ester method (coupling agent EDC/NHS) were used for peptide bond formation.

Chapter IV: Biorecognition of antigens from *Mycobacterium tuberculosis* using a sandwich ELISA associated with magnetic nanoparticles.

Chapter IV

Biorecognition of antigens from *Mycobacterium tuberculosis* using a sandwich ELISA associated with magnetic nanoparticles.

Abstract:

Introduction: This chapter details the standardization of protein immobilization (bovine serum albumin and polyclonal antibodies) using the coupling agent EDC/NHS on selected MNP@Si@NH_2. Also, the chapter describe the development of a sandwich ELISA associated with functionalized magnetic nanoparticles to capture and detect MTB antigens; using recombinant proteins, negative and positive sputum pools from confirmed patients

Methodology: Parameters such as the incubation time, the initial amount of protein, and the concentration of EDC/NHS were standardized for an efficient bio-functionalization of nanoparticles with proteins. Using the nanoparticles conjugated with antibodies, a sandwich ELISA associated with magnetic nanoparticles (sELISA-MNP@Si@ab) was developed. The detection of the recombinant and native antigens of MTB were evaluated.

Results: An effective functionalization of the proteins on the surface of silanized MNPs was achieved with low concentrations of EDC/NHS, at 22 h of incubation. About sELISA-MNP@Si@ab, native ESAT6 and CFP10 antigens were better discriminated in sputum pooles from patients with TB (fold value ~ 1.8). The conventional sELISA reported in this study took about 2 days to give a result.

Discussion: The sELISA-MNP@Si@ab assay is a relatively fast method that can be performed in less than 4 h. Another advantage of sELISA-MNP@Si@ab is that the introduction of functionalized nanoparticles with specific antibodies allowed a better detection of native sputum MTB antigens. The demonstration of the sELISA-MNP@Si@ab feasibility was carried out on biological samples stored for a long period before analysis. This factor could have affected the integrity of the MTB proteins and

consequently influenced the sensibility of measurements. Nevertheless, it was possible to discriminate the positive samples from the negative ones.

Conclusion: The use of MNP@Si@ab improved the detection of MTB antigens in biological samples. Our results are encouraging, but the essay requires additional evaluations such as determining cross-reactions with sputum samples from patients with other infections, performing the test with fresh sputum of TB patients, and determining the sensitivity and specificity of the method.

NOTE:

This chapter has been divided into 4 subchapters: narrative description (**IV.1**), experimental section (methodology, **IV.2**), results (**IV.3**) and discussion (**IV.4**). The structure of narrative description - experimental section is a format widely used in the domain of chemical sciences, while the structure of methodology - results - discussion is a standard format in the area of biology. In this chapter, the narrative description shows merged results and discussion. The experimental section describes the materials and methods used in this chapter. The results and discussion sections have the same content as the previously described narrative description, but they are separated. This means that reading the narrative description - experimental section is the equivalent of reading experimental section - results - discussion.

Despite the redundancy of information between narrative section (**IV.1**) and results – discussion (**IV.3** and **IV.4**), this format is justified for easy understanding for chemists (narrative section - experimental section) and biologists (experimental section - results - discussion).

IV.1. NARRATIVE DESCRIPTION.

IV.1.1. Standardization of the immobilization of proteins on MNP@Si@NH_2 surface.

IV.1.1.1. Conjugation of Albumin on magnetic nanoparticles surfaces.

The parameters considered for an efficient bio-functionalization of nanoparticles with proteins, were: the incubation time, the initial amount of protein in the incubation, and the concentration of EDC/NHS, which can vary according to the initial amount of protein to conjugate.

The amount of protein immobilized on nanoparticle surface was calculated following the next equation:

initial mass – final mass = mass of immobilized proteins (µg) **(Eq. 1).**

To express the value of the immobilized protein in percentage (%), the following equation was used:

X% = [(mass of immobilized protein) *(100)]/(initial mass of protein) (**Eq. 2).**

The reaction **buffers** evaluated to conjugate BSA on nanoparticles surfaces, were PBS pH 7.4, Tris-HCl and buffer phosphate. However, the amounts of conjugated BSA on the MNP@Si@NH_2 surface, were similar in each case: 23.02, 22.32 and 23.05%, respectively (**Figure IV.1).** Thus, the other reactions were made with PBS.

Bordbar *et al*., 2014 reported that in a reaction where there are high concentrations of salts, an increase of ionic strength occurs. This generates a reduction of the electrostatic interactions between the BSA and the nanoparticles, decreasing the immobilization of the proteins on the surface (Bordbar *et al*., 2014). In our work, since functionalization reactions did not show significant variations when using different buffer types; it can be inferred that the salts present in the PBS did not interfere in the reaction. It is because the amount of NaCl was 0.14 M, an amount that would have no effect on the deactivation of some active sites of the nanoparticles.

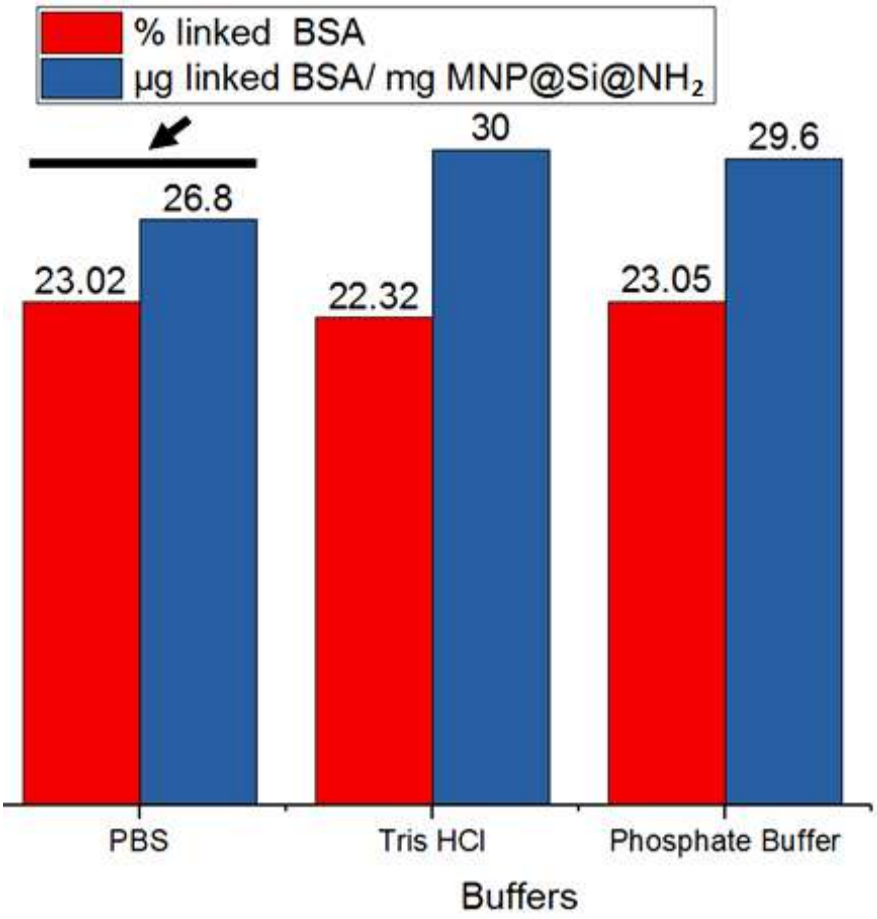

Figure IV.1: Evaluation of buffer types to functionalize nanoparticle surfaces with BSA.

About the **magnetic nanoparticles amount** required to conjugate BSA on MNP@Si@NH_2 surfaces, it is observed that more less 20% of the total BSA is conjugated to the MNP surface (10 mg). Theoretically, 22.56 µg of BSA saturate 1 mg of nanoparticles synthesized in this study (**Appendix 2.1 and 2.2, pages 294 and 295, respectively).**

The calculations were made using the magnetite unit cell parameters reported by Kokate, *et al.*, 2013 (Kokate *et al*., 2013). Our results showed that there is a high percentage of conjugated BSA when a high MNP amount is used in the reaction. However, the mass of conjugated BSA per mg of nanoparticles (µg linked BSA/mg MNP@Si@NH_2) is increased when a small amount of magnetic nanoparticles is used (**Figure IV.2).** It means that, apart from MNP surface saturation with BSA, there are other interactions between

proteins (ionic, electrostatic and hydrogen bonds), which favored the increase of conjugated BSA. So, for convenience, we consider between 1 - 5 mg of nanoparticles for bio-functionalization.

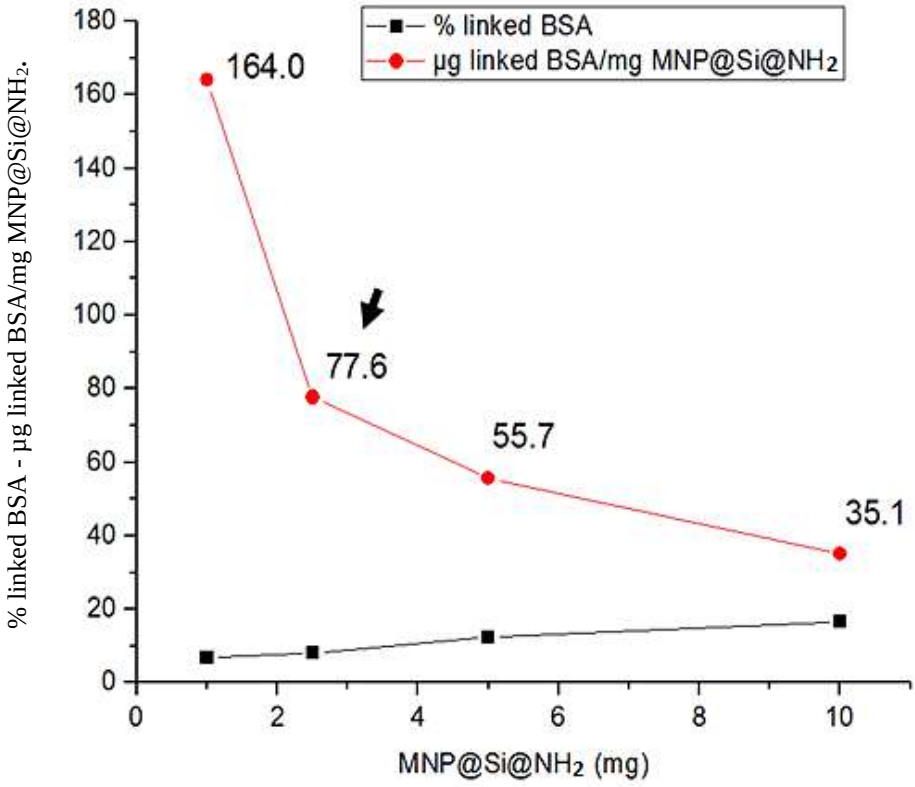

Figure IV.2: Amount of MNP@Si@NH_2 for functionalization by BSA.

In the case of the **BSA amount to saturates the magnetic nanoparticle surface**, a direct relationship is observed between the amount of initial protein and the amount of protein conjugated to nanoparticles. Around 76.25±2.05 µg of BSA saturated 1 mg of MNP@Si@NH_2, when 1 mg (15.04 nmoles) of BSA was used as initial amount (**Figure IV.3**).

Previously, Bordbar *et al* (2014) reported that the amount of BSA immobilized increases with increasing the initial value of BSA, until saturating the surface of the nanoparticles. The saturation would be directly related to the number of amino groups of the MNPs and to the activated sites of the BSA.

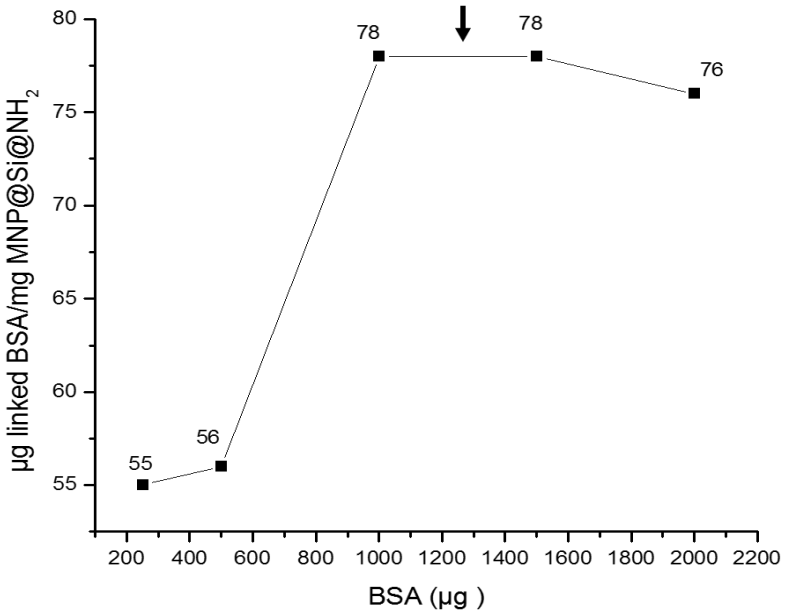

Figure IV.3: Saturation of the silanized magnetic nanoparticle surface using BSA.

About the **activation reaction**, using the coupling agent EDC/NHS, is better to follow two-step reactions performed in a non-amine or carboxylated buffer. EDC reaction is better performed at pH 4.7-6.0, and the NHS-activated molecules with primary amines is most efficient at pH 7-8. Finally, the NHS-ester reactions are usually performed in PBS at pH 7.2-7.5 (Grabarek and Gergely, 1990).

About the most **efficient coupling agent concentration**, a low amount of BSA is conjugated when a high EDC/NHS concentration is used in the reaction. Additionally, it has been determined that 1/0.5 and 0.5/1 µmoles of EDC/NHS are the most efficient concentrations to functionalize MNP surface by BSA (131 and 119.4 µg linked BSA/ mg of MNP@Si@NH_2) (**Figure IV.4**).

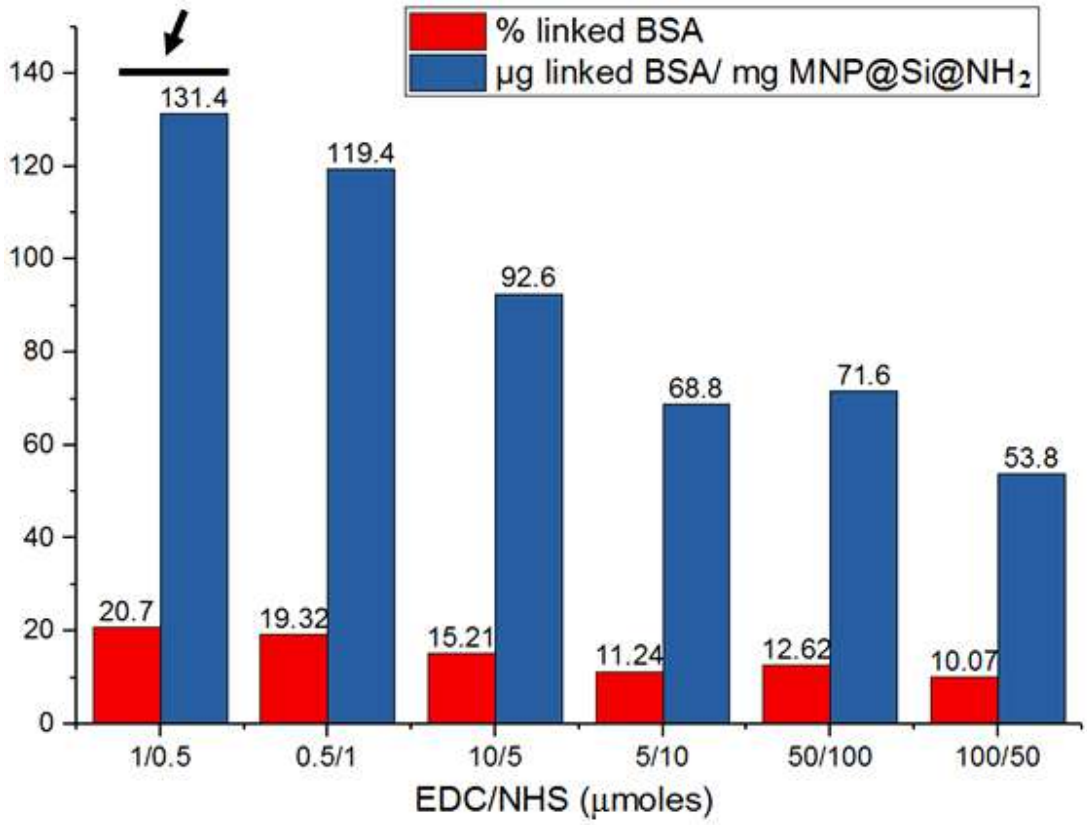

Figure IV.4: Evaluation of EDC/NHS concentration to functionalize nanoparticle surface by BSA.

In general, a high amount of EDC/NHS reduces the amount of proteins bound on the surface of the nanoparticles. It is because an excess of EDC/NHS contributes to the polymerization of the proteins, due to high number of active sites generated by the coupling agent. This phenomenon, previously described by Bartczak and Kanaras (2011), reduces the number of activated sites of binding to the amino groups of the nanoparticles. Additionally, a BSA molecule contains 100 free carboxyl groups (Saroff *et al*., 1953), indicating a high exposure of COOH. For this, is not necessary to use a high amount of EDC/NHS in the reaction.

Thermogravetric and Dynamic Light Scattering analysis of MNP@Si@BSA

To corroborate the amount of BSA bound to the surface of the nanoparticles, measured by spectrometry, a TGA assay was additionally performed. For this, the samples were

heated at elevated temperatures, until the organic layer evaporated, and the mass loss, corresponding to the evaporated BSA, was measured.

Using **TGA,** 21.85 – 30.5 mg of nanoparticles were evaluated from 25 to 600 ° C. **Thermogravimetric plots** (**Figure IV.5 A and Figure IV.5 B)** show the first loss of mass, attributed to water desorption (150°C). The released water percentage was 3% of MNP@Si@BSA mass. In drying condition (after 150 °C), the relative loss of mass of organic material of MNP@Si@BSA (330 °C and 498 °C) was 5.35 %. A percentage of 1.53 % (0.348 mg) corresponded specifically to the loss of mass of BSA, and 3.82 % would correspond to $Si@NH_2$ layer. Showing a high density of BSA in the MNP surface. Interesting, these BSA mass reduction (0.348 mg) was in accordance with the values obtained with UV-Vis spectrophotometer (loss of mass of 0.364 mg for BSA).

Additionally, the analysis of mass loss as a function of temperature allowed us to determine that around 330°C, BSA tends to evaporate; while amino-silanes are lost at around 450 °C. This temperature difference may be due to the physical-chemical properties of the compounds, or to the greater heat exposure of BSA.

A

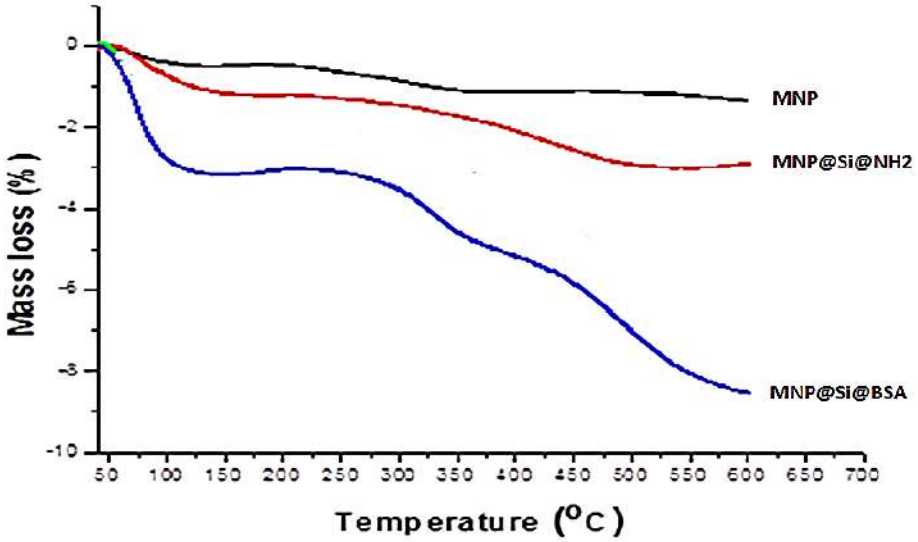

B

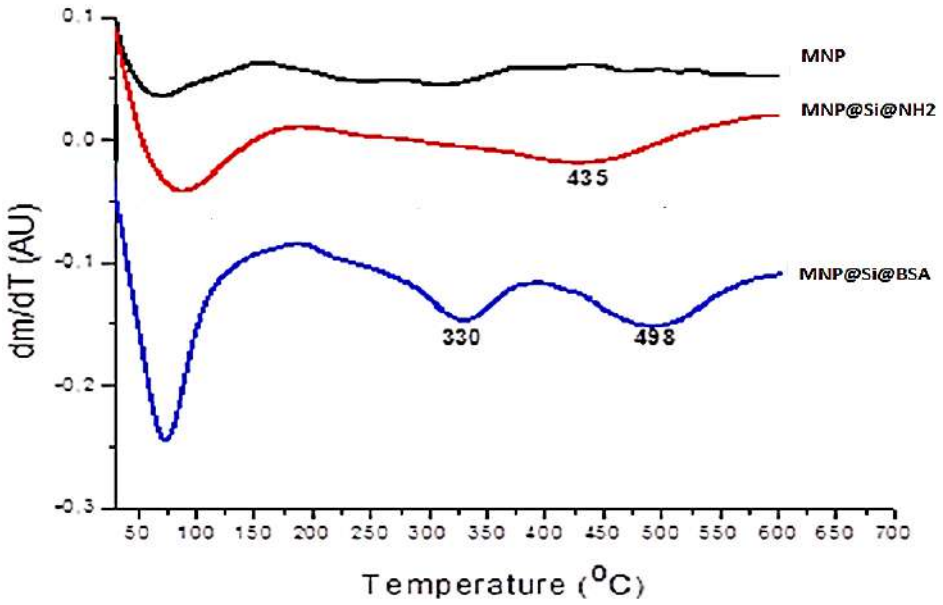

Figure IV.5: Biofunctionalization of magnetic nanoparticles using BSA. **A)** DTGA corresponding to naked and conjugated nanoparticles. MNP@Si@BSA shows two successive loss of mass rate after water desorption. **B)** TGA for MNP (Fe_3O_4) (black), coated MNPs with amine silane groups (red), and MNP conjugated with BSA (blue).

On the other hand, nanoparticles conjugated with BSA had a larger hydrodynamic diameter (d_H) than the nanoparticles that were only amine-silanized.

MNP@Si@BSA showed a d_H of 394.24 nm (52.16 %), while MNP@Si@NH_2, haved a d_H of 148.32 nm (55.41 %) (**Figure IV.6 A and Figure IV.6 B**). In summarize, the size of nanoparticles conjugated with BSA incremented drastically (d_H: 394.24) compared to bare amine-silanized nanoparticles (d_H: 148.32 nm). We hypothesized an aggregation of the conjugated proteins, due to the polymeric nature of BSA. It can cause an approximation between nanoparticles, increasing their size (Liu *et al*., 2011). Additionally, EDC/NHS coupling agent could favor this aggregation when the activated protein was incubated with the nanoparticles (Bartczak and Kanaras, 2011).

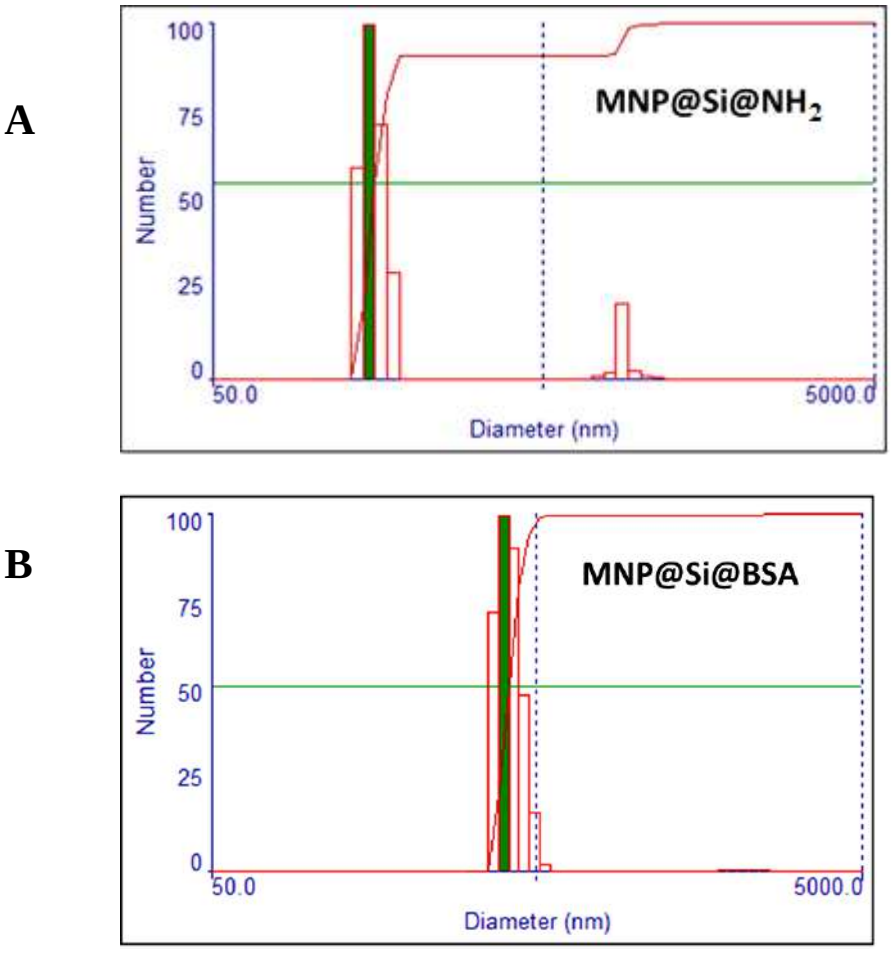

Figure IV.6: Hydrodynamic diameter of functionalized magnetic nanoparticles**. A)** MNP@Si@NH_2 (d_H: 148.32 nm; accumulated number: 55.41 %), **B)** MNP@Si@BSA (d_H: 394.24 nm; accumulated number: 52.16 %).

IV.1.1.2. Standardization of magnetic nanoparticles functionalization with specific polyclonal antibody.

Figure IV.7 shows that using PBS buffer during bio-functionalization reaction effectively contributed to the immobilization of casein, both on MNP@Si@NH_2 and in naked MNP (52.39% and 20.73%, respectively). It was calculated following **Eq. 2**.

In the first case, the presence of amino groups contributes to a greater amount of protein being bound to the surface of the nanoparticles MNP@Si@NH_2. On the second case, the immobilization of casein on the non-modified MNPs is probably due to a weak adsorption reaction and/or electrostatic interactions between the protein and the hydroxyl groups (OH) on the MNP surface (Roque *et al*., 2009). These results show that PBS is the best reaction buffer for protein conjugation.

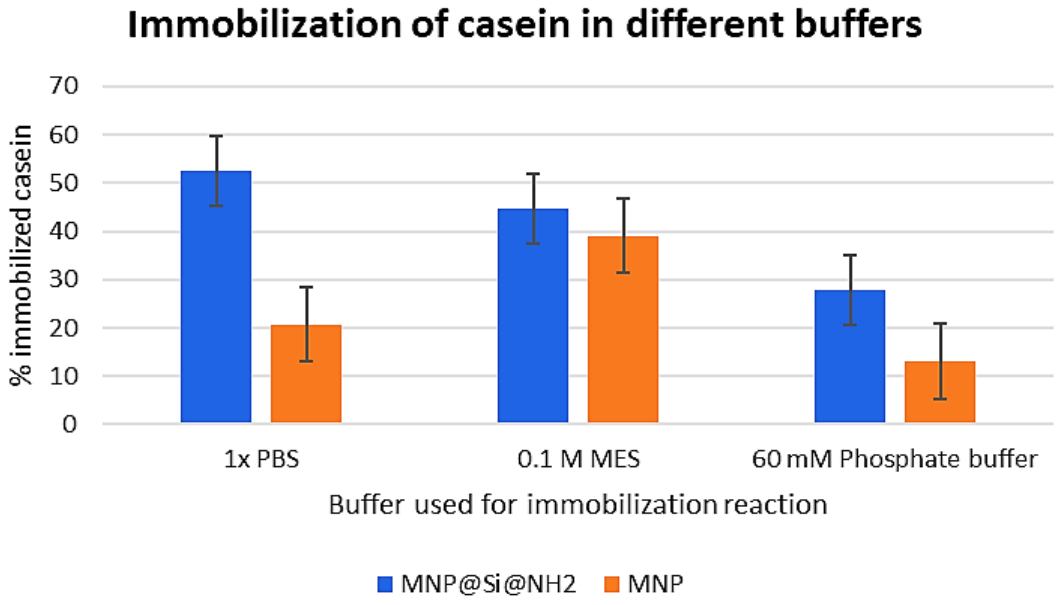

Figure IV.7: Types of reaction buffers used to functionalize modified magnetic nanoparticles with casein.

In general, an antibody (IgG) has two regions: one variable (Fab or antigen-binding fragment) and another constant (Fc or crystallizable fragment). Fab is rich in amine groups ($-NH_3^+$), while Fc has a large number of carboxyl groups (COO^-). Thus, the COOH groups of antibody Fc region were activated using EDC/NHS as coupling agent. The reaction of

activated carboxyl groups with the amine groups of silanizated nanoparticles, generated covalent (peptide) bonds. In this way, it is ensured that most of the functionalized antibodies display freely the Fab regions, favoring a greater interaction with the antigens (Jesse *et al*., 2015; Liu *et al.*, 2011).

Functionalization was performed following the conditions evaluated with BSA. The **Figure IV.8** summarizes the process of immobilization of antibodies on the nanoparticles surface.

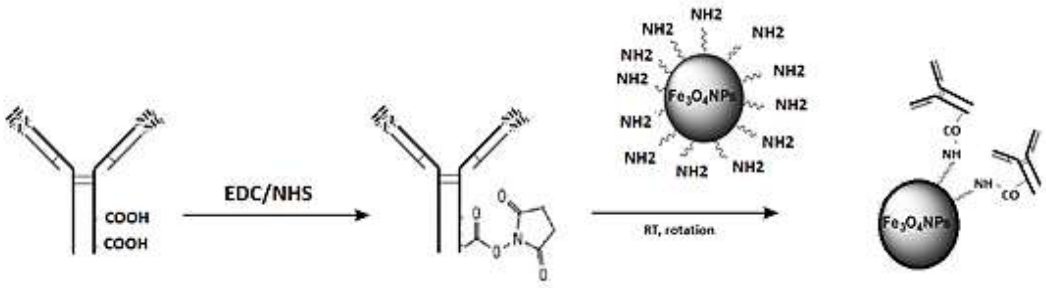

Figure IV.8: Activation of the carboxyl groups of the antibodies using EDC/NHS and functionalization of the nanoparticles with the activated antibodies.

About the parameters for an efficient immobilization of polyclonal antibodies on nanoparticle surface, we considered as determining factors: the incubation time, the initial amount of protein, and the concentration of the coupling agent EDC/NHS, which can vary according to the initial amount of protein to conjugate. The most important results are described below:

- **Time reaction for protein immobilization.**

The reaction time is a very important factor, for proteins such as BSA, it has been observed that a time of 4 hours is sufficient to saturate the nanoparticles (Bordbar *et al*., 2014). However, in the case of antibodies the time was longer for nanoparticle saturation.

Figure IV.9 shows that the amount of antibodies conjugated on the surface of the MNPs increases over time, reaching 69.85% after 22h of incubation. However, between 4

and 6 h of incubation is observed the beginning of the plateau in the curve. It means that at this time the saturation of the nanoparticles would be starting. For practical purpose, we consider an incubation of 22 h for the all reactions.

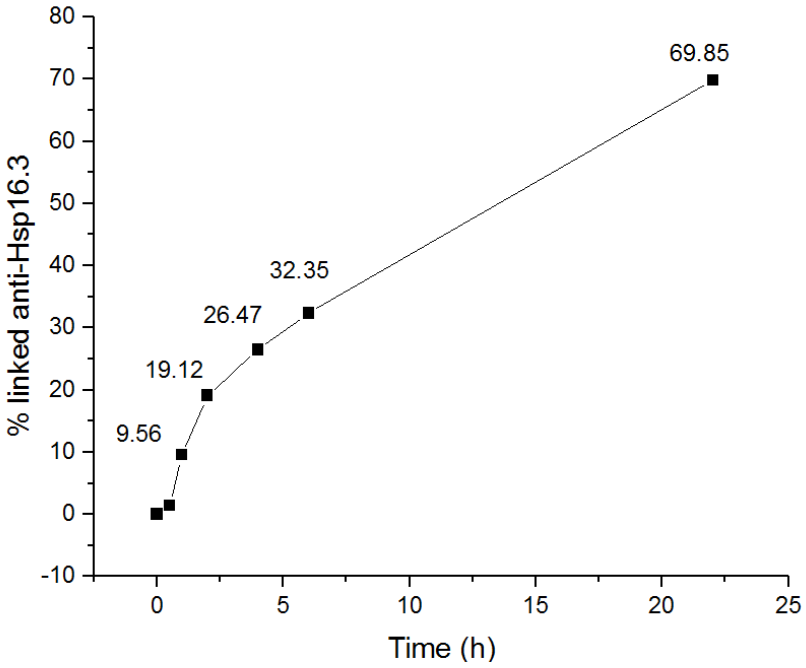

Figure IV.9: Evaluation of incubation time to functionalize nanoparticle surface with anti-Hsp16.3.

- **Saturation of magnetic nanoparticle surface.**

Similar to BSA, a direct relationship is observed between the amount of initial protein and the amount of IgG conjugated to nanoparticles. **Figure IV.10** shows a curve that reaches an equilibrium when 135 ± 2 µg of anti-Hsp16.3 saturated 1 mg of amine-silanized nanoparticles. It happens when 1.2 mg (8 nmoles) of anti-Hsp16.3 serum is used in the initial incubation.

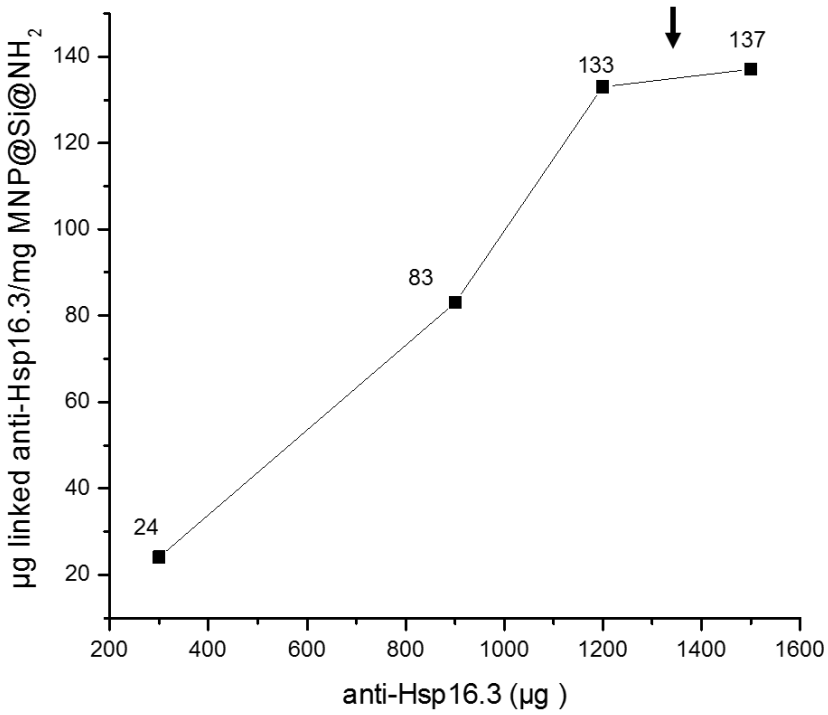

Figure IV.10: Saturation of the silanized magnetic nanoparticle surface using anti-Hsp16.3.

As previously described, Bordbar *et al.* (2014) reported a direct relationship between the initial amount of BSA in the reaction and the amount of BSA conjugated to the nanoparticles. This phenomenon has also been observed with antibodies. This means that by increasing the initial value of IgG, the amount of immobilized IgG will also be increased until the surface of the nanoparticles is saturated. The saturation would be directly related to the number of amino groups of the MNPs and with the activated sites of the antibody (Conde *et al*., 2014).

- **Efficient coupling agent concentration.**

Similar to BSA, the activation reaction in two-steps using EDC/NHS, in a non-amine or carboxylated buffer, were the best conditions. This means, activation of the carboxylic groups of the protein in the first step, and subsequently conjugation of the activated proteins

with MNPs in the second step. Among the different concentrations of EDC/NHS, so much variation was not observed. The results showed that with all EDC/NHS concentrations evaluated, more than 50% of anti-Hsp16.3 (serum) was immobilized on magnetic nanoparticle surface. In general, anti-Hsp16.3 is efficiently conjugated (62.5%) when low concentrations of EDC/NHS (0.5/1 µmoles) are used in the reaction (**Figure IV.11).** Similar to BSA, a high amount of EDC/NHS reduces the amount of proteins bound on the surface of the nanoparticles. But this reduction was not very high in our experiments. Bartczak and Kanaras (2011) reported the contribution of the EDC/NHS excess in the protein polymerization, due to high number of active sites generated by the coupling agent. This could reduce the number of binding activated sites of IgG to the amino groups of the nanoparticles.

An IgG has around 12636 free COOH groups (Huang *et al* 2017). It means that there is a high exposure of carboxyl groups, allowing the use of low EDC/NHS concentration in the reactions.

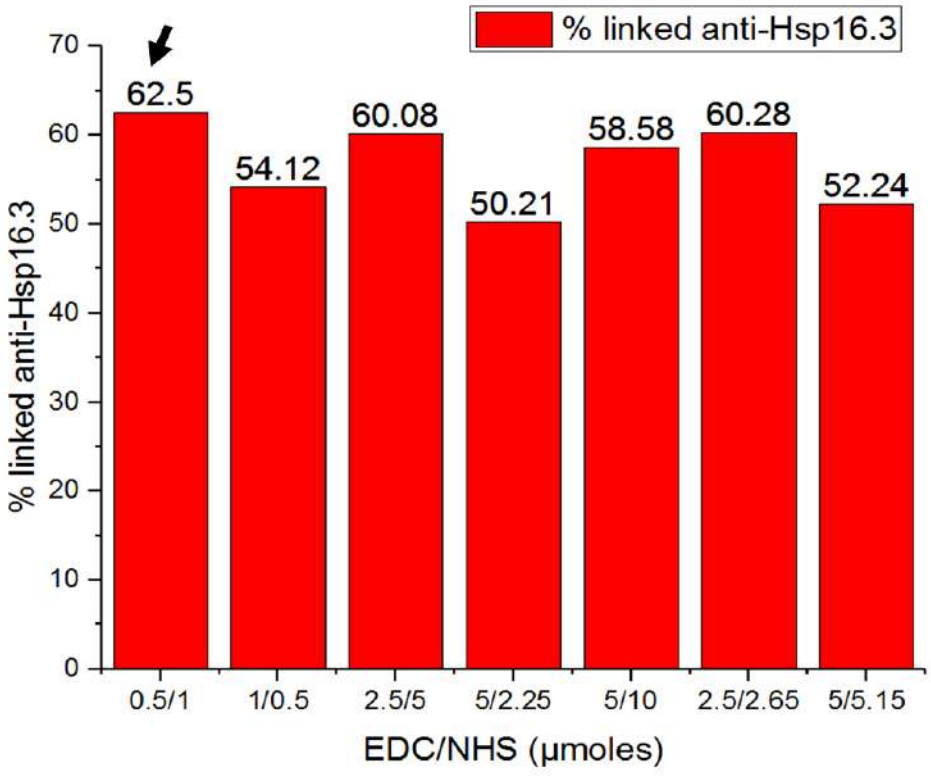

Figure IV.11: EDC/NHS concentration to functionalize nanoparticle surface with anti-Hsp16.3.

According to the results obtained from our previous experiments, it has been observed that the antibodies used directly from sera were immobilized adequately on the surface of the nanoparticles. To corroborate the above data, an experiment using purified and non-purified anti-Hsp16.3 was carried to evaluate if there is a difference in protein immobilization. The antibodies used for the reaction were: **1) non-purified** serum, **2)** serum proteins (IgG) purified by precipitation of salts (**precipitated**), and **3)** serum IgG purified by HPLC (**purified**).

The **type of antibody** (non-purified, precipitated and purified) used in the reaction, **Figure IV.12** corroborated that when more antibody is used, the amount of conjugated antibody also increases. Additionally, although the amount of conjugated anti-Hsp16.3 is lower in the case of precipitated and purified antibodies, the fold of ELISA tests in the three assays were very similar (around 3.8). This means that precipitated and purified antibodies, conjugated on nanoparticles, can efficiently detect antigens despite being in low amounts. However, the antibody purification process demands an additional cost and generates a loss in the antibody concentrations. In our case, the results show that it is possible to work with non-purified anti-Hsp16.3 and obtain the same results such as purified antibodies. For this reason, in the subsequent tests, the non-purified polyclonal antibodies were immobilized directly.

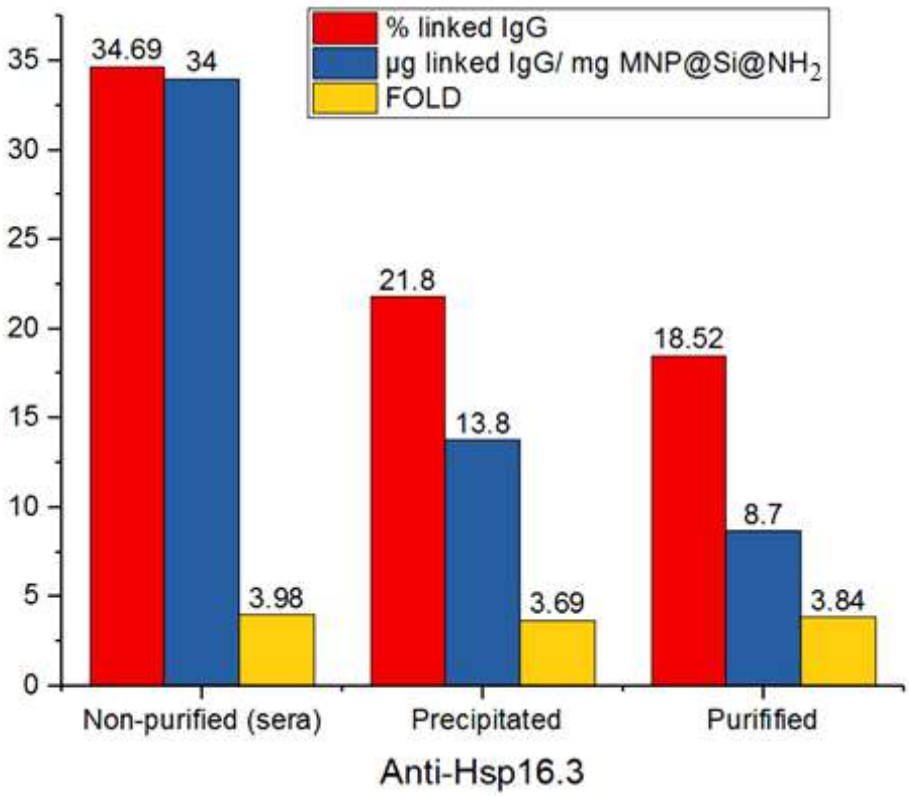

Figure IV.12: Type of antibody (non-purified, precipitated and purified) to functionalize nanoparticle surface with anti-Hsp16.3.

Thermogravetric and Dynamic Light Scattering analysis of MNP@Si@anti-Hsp16.3.

For thermogravimetry analysis, bare nanoparticles, nanoparticles functionalized only with amino-silanes and MNP@Si@anti-Hsp16.3 were used. Similar to BSA, thermogravimetric plots (**Figure IV.13)** shows the first loss of mass (< 150°C) attributed to water desorption. In a drying condition (>150 °C), the relative loss of mass of organic material of MNP@Si@anti-Hsp16.3 (320°C and 457 °C) was 3.50 %; where 0.92 % (0.201 mg) corresponded specifically to anti-Hsp16.3 loss of mass and 2.58 % corresponds to $Si@NH_2$.

In summary, the amount of immobilized antibody (0.282 mg) on MNP@Si@anti-Hsp16.3 surface, previously measured by spectrophotometry, was corroborated using TGA (mass loss of 0.201 mg). These results indicate that the methods of immobilization and indirect quantification of proteins immobilized on nanoparticle surface, are efficient.

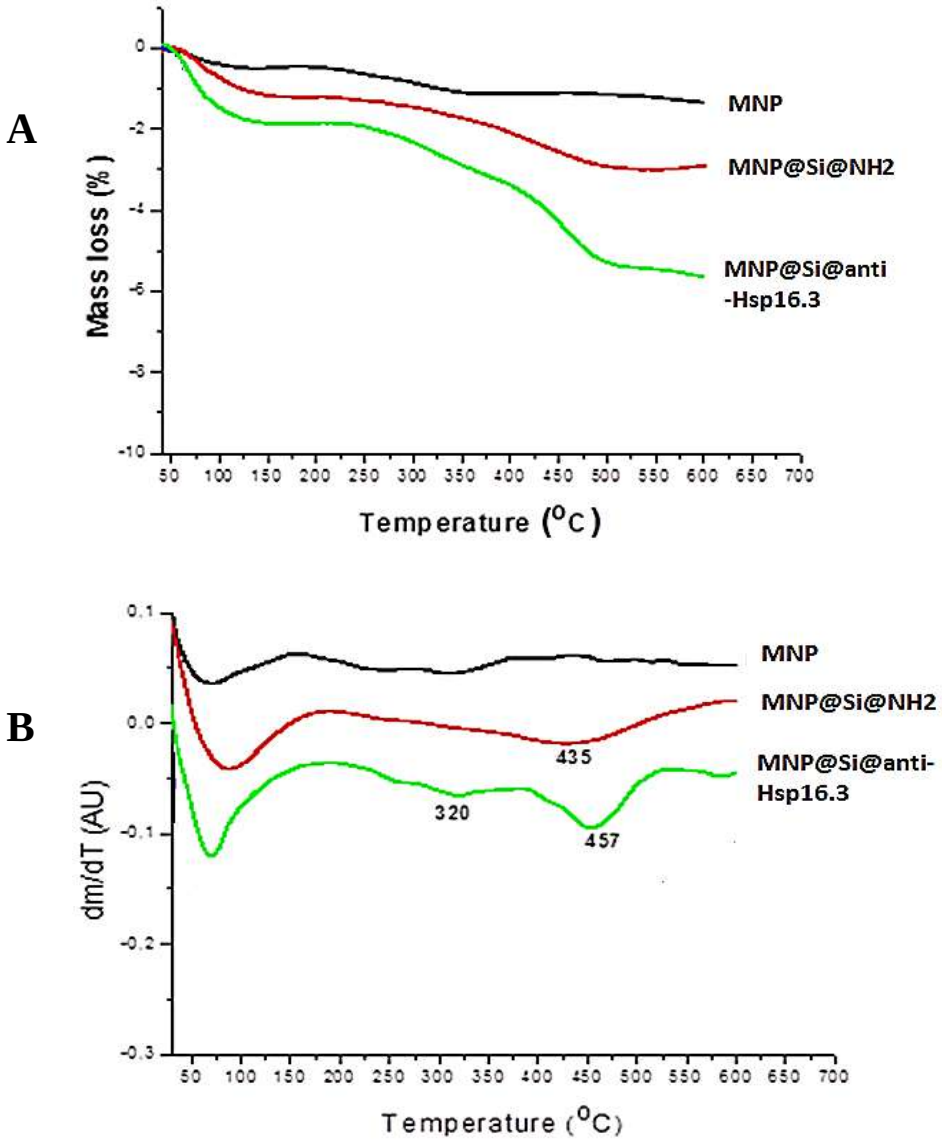

Figure IV.13: Thermogravimetry analysis of functionalized nanoparticles. **A)** DTGA corresponding to naked and conjugated nanoparticles. MNP@Si@anti-Hsp16.3 shows two successive mass loss rate after water desorption. **B)** TGA for MNP (Fe_3O_4) (black), coated MNPs with amine silane groups (red), and MNP conjugated with anti-Hsp16.3 (green).

IV.1.2. Immobilization of antibodies on modified magnetic nanoparticle surface.

Immobilization of antibodies on the nanoparticle surface was performed as described above for anti-Hsp16.3

Table IV.1 shows the amount of protein immobilized on MNP@Si@NH_2, and the values of the hydrodynamic diameters of the nanoparticles conjugated with the antibodies. The d_H of MNP@Si@NH_2 (without antibodies) is 148.32 nm. However, the range values of d_H for MNP@Si@ab is 119.61-370.93 nm. This difference of up to 2.5 times of increase in the d_H of the nanoparticles conjugated with the antibodies would be due to an aggregation of the nanoparticles. This phenomenon could have occurred during the process of immobilization of antibodies on the surface of the amino-silanized nanoparticles, through physical-chemical interactions. Further, the table shows the theorical amount of antibodies capable of saturating 2.5 mg of MNP@Si@NH_2 according to its hydrodynamic diameter (calculated in **Appendix 2.3 and 2.4, pages 295 and 296, respectively).** In all cases, the experimental amount of antibodies immobilized on the surface of the nanoparticles exceeded the theoretical value. We hypothesized that this phenomenon would be due to a protein multilayer formation on the MNP surface. Because an antibody contains both carboxyl and amine groups, during the EDC/NHS activation reaction used for the surface bio-functionalization, the interactions between these functional groups may lead to the formation of covalently interlinked antibodies that then conjugate to the MNP@Si@NH_2 surface (Smith *et al*., 2011).

Table IV.1: Amount of specific polyclonal antibodies immobilized on the surface of the amino-silanized magnetic nanoparticles.

Polyclonal antibodies	Linked IgG (µg)	Hydrodynamic diameter (d_H, nm)	Theorical saturation (IgG, µg)*	Saturation percentage (%)**	Antibody (µg) in 5 µl of MNP@Si@ab ***
Anti-38kDa	101	348.77 (70.24%)	16.0	> 100	2.53
Anti-MTC28	61	344.23 (84.61 %)	16.2	> 100	1.53
Anti-Ag85B	299	370.93 (42.11 %)	15.05	> 100	7.48
Anti-MPT64	88	355.02 (42.11 %)	15.73	> 100	2.2
Anti-MoeX	93	338.52 (65.11 %)	16.48	> 100	2.33
Anti-ESAT6	79	119.61 (26.38 %)	46.65	> 100	1.98
Anti-CFP10	70	149.27 (46.93 %)	37.38	> 100	1.75
Anti-Hsp16.3	94	358.62 (50.06 %)	15.55	> 100	2.35

* 'Theorical saturation value' represents the amount **(µg)** of IgG which cover completely an amount of 2.5 mg of modified magnetic MNPs. These values were calculated using the hydrodynamic diameter.
** 'Saturation percentage' represents what percentage of the modified MNPs are covered with IgG used in the experiment.
*** Amount of antibody immobilized in 5 µl of nanoparticles. This volume of MNP@Si@ab was used in sELISA-MNP@Si@ab, to detect recombinant and native *M. tuberculosis* antigens.

The **Figure IV.14** shows the hydrodynamic diameter of the majority of the population of nanoparticles functionalized with the anti-38kDa antibody. It is observed that more than 50% of nanoparticles (accumulated number: 70.24%) have a d_H of 348.77nm. However, there is also a very small population of nanoparticles of greater size, indicating larger aggregations in the solution. Unlike the previous case, a greater homogeneity in the nanoparticle population functionalized with anti-MTC28 is observed. Most of the population has a d_H of 344.23 in the 84.61% of MNP@Si@anti-MTC28. Similarly, the

population of MNP conjugated with anti-Ag85B, anti-MPT64 and anti-Moex did not have diameters very dispersed in the solution. The d_H observed were: 370.93 nm, 355.02 nm and 338.52 nm, respectively. This would indicate that more complex aggregates would not have formed in the reaction.

In the case of nanoparticles immobilized with anti-ESAT and and anti-CFP10, two populations of nanoparticles are clearly observed. But the largest MNP@Si@ab population is indicated in the **Figure IV.14** with d_H of 119.61 and 149.27 nm, respectively. These hydrodynamic diameters were lower than the d_H of the nanoparticles conjugated with the other antibodies. This could be explained by a better dispersion of the complexes (sonication). The second population is also significant, indicating that despite the dispersion of the nanoparticles, there is an equal aggregation of these in the solution. Finally, the nanoparticles conjugated with anti-Hsp16.3, also presented a high d_H (358.62 nm), within a homogeneous population (50.6 %).

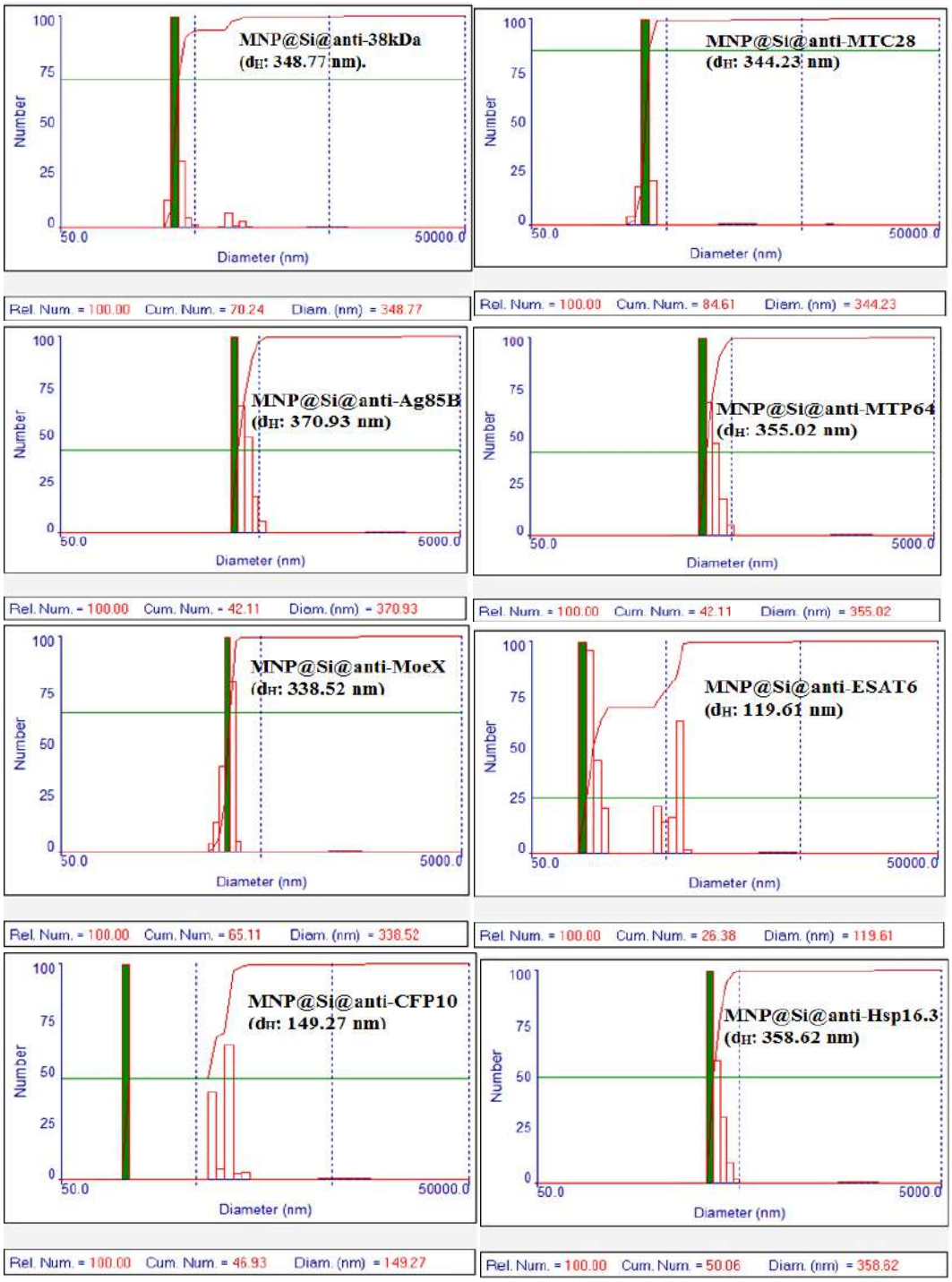

Figure IV.14: Hydrodynamic diameters of functionalized MNP@Si@ab.

IV.1.3. Detection of recombinant antigen from MTB using sandwich ELISA associated with magnetic nanoparticles.

Using the nanoparticles previously conjugated with antibodies, a sandwich ELISA associated with magnetic nanoparticles (sELISA-MNP@Si@ab) was developed (described in Experimental section). The detection of the recombinant antigens of MTB was evaluated using the antibodies produced in rabbits and mice (previously described in chapter II) in the sELISA-MNP@Si@ab assay. **Figure IV.15 and Figure IV.16** show the curves (antigen quantity in well *vs* fold values) obtained after a sandwich ELISA associated with magnetic nanoparticles. The protein rHsp16.3 was detected up to value 0.08 ng/µl (0.008 µg/well). In the case of r38kDa, rMoeX and rAg85B proteins were successfully detected up to values ≤ 0.15 ng/µl (0.015 µg/well); while in the case of the rMPT64 and rMTC28 proteins, the detection limit was raised to 0.31 ng/µl (0.031 µg/well). The rCFP10 and rESAT6 proteins required up to 1.25 ng/µl (0.125 µg/well) to give the positive response.

In the ELISA sandwich tests associated with MNP@Si@ab, the minimum recombinant antigen amount detected in the assays were 10 ng/well (0.1 ng/µl), 15.6 ng/well (0.156 ng/µl), 6 ng/well (0.06 ng/µl), 15.6 ng/well (0.156 ng/µl), 31 ng/well (0.31 ng/µl) and 31 ng/well (0.31 µng/l) for rAg85B, r38kDa, rMoeX, rHsp16.3, rMPT64 and rMTC28, respectively. In the case of the immunodetection of rESAT6, the **fold** values (sample/negative ratio = average sample OD/ average negative OD) observed are very low. It could due to protein degradation, because ESAT6 was a soluble protein that precipitated slightly over time. Using an ELISA sandwich associated with MNP@Si@anti-ESAT6 was possible to detect 125 ng/well (12.5 ng/µl) of rESAT6. At the same way, rCFP10 detection using an sELISA-MNP@Si@anti-CFP10 showed low fold values, and 125 ng/well (12.5 ng/µl) of rCFP10 was the minimum amount detected. Finally, a sMNP@Si@anti-MTC28 detected 31 ng/well (0.31 µng/l) of rMTC28. Similarly, to ESAT6 and CFP10, the fold values were low.

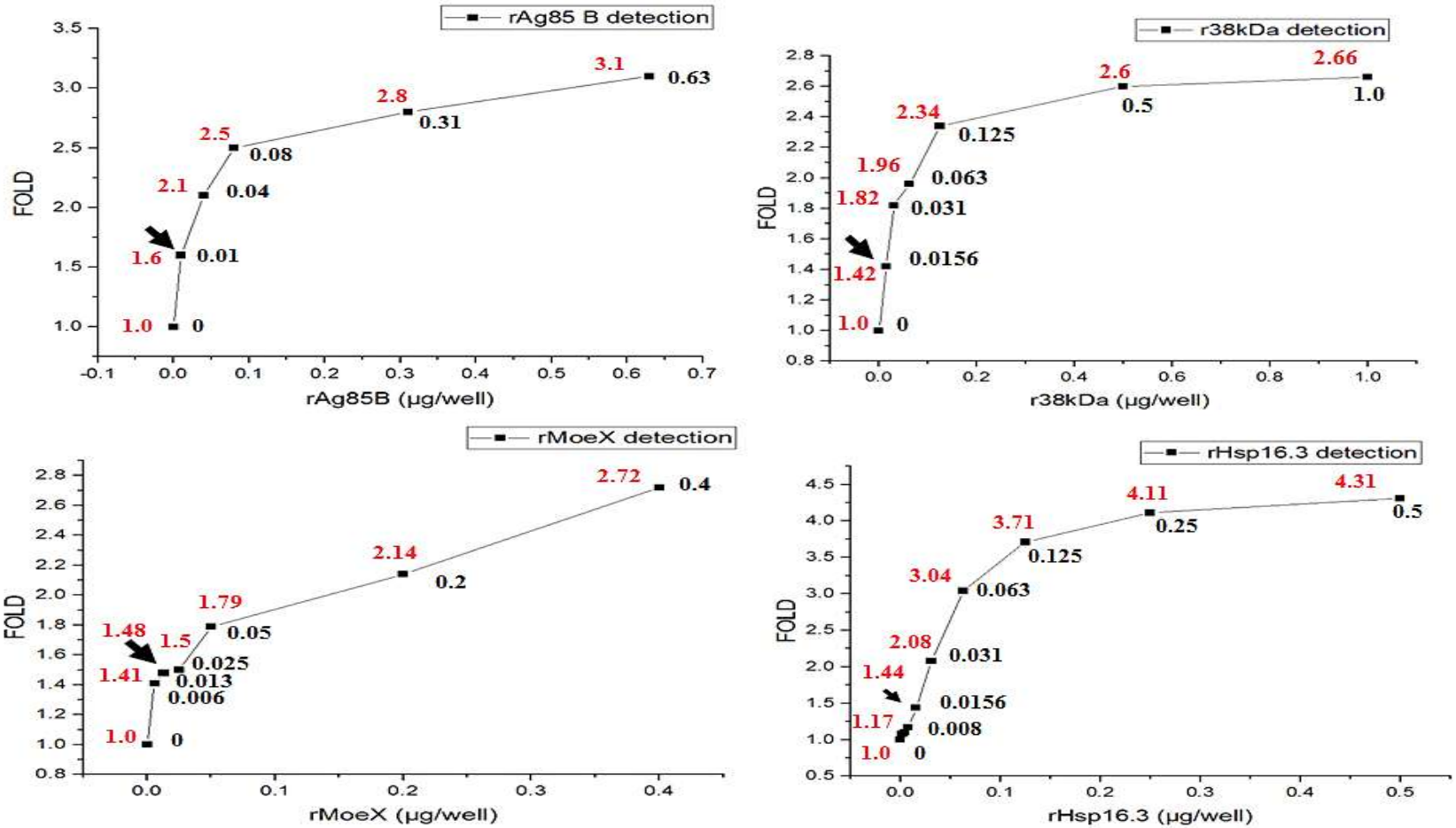

Figure IV.15: Immunodetection of recombinant antigens rAg85B, r38kDa, rMoeX and rHsp16.3 from *M. tuberculosis* using sELISA-MNP@Si@ab. In black numbers is indicated the amount of recombinant antigens used in the experiment, and in red the fold in each case. The black arrow shows the minimum amount of recombinant antigen recognized for the assay.

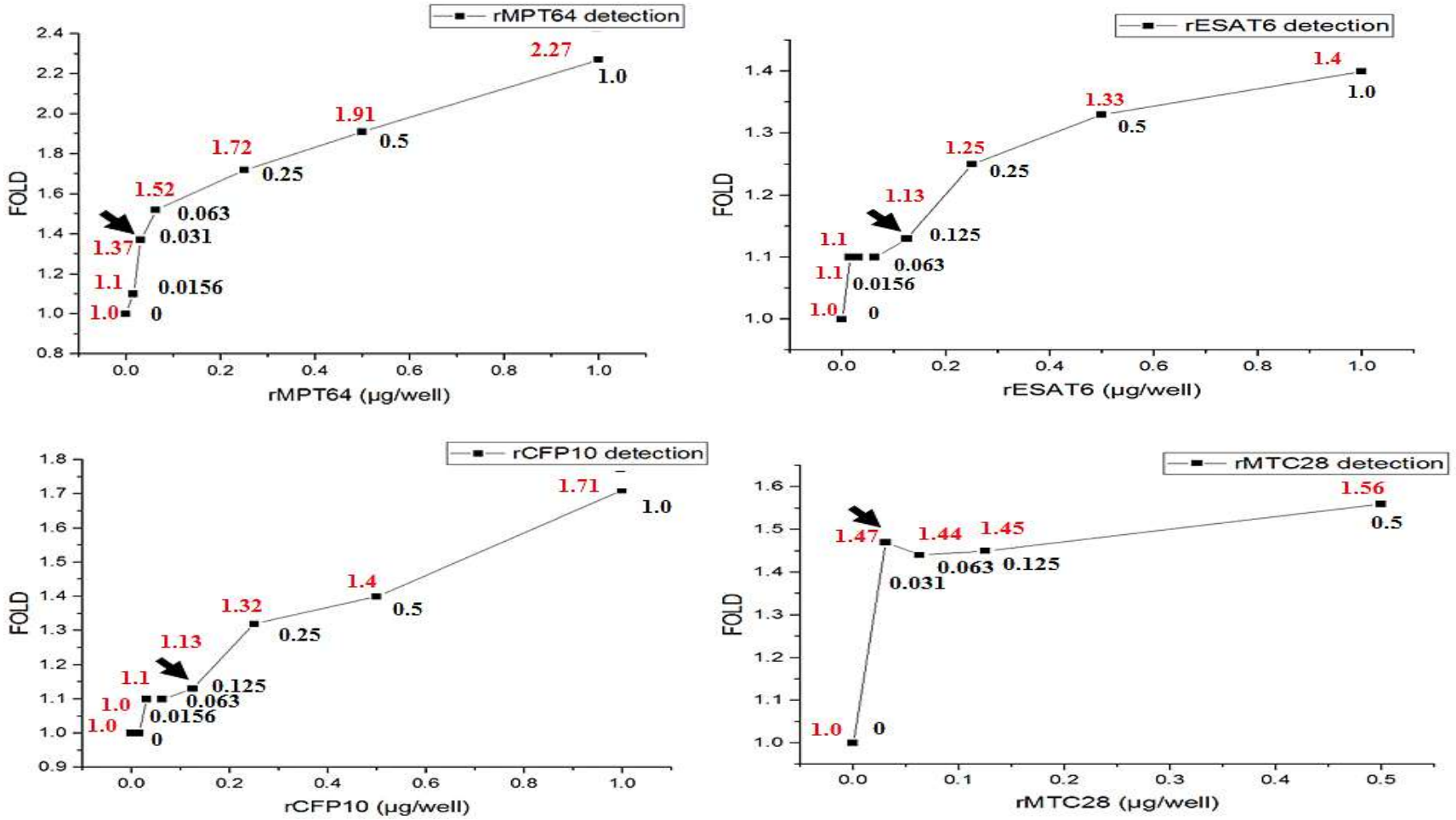

Figure IV.16: Immunodetection of recombinant antigens rMPT64, rESAT, rCFP10 and rMTC28 from *M. tuberculosis* using sELISA-MNP@Si@ab. In black numbers is indicated the amount of recombinant antigens used in the experiment, and in red the fold in each case. The black arrow shows the minimum amount of recombinant antigen recognized for the assay.

In addition, **Figure IV.17** illustrates a comparison between the conventional sELISA and the sELISA-MNP@Si@ab.

Unlike the sELISA reported in **chapter II,** this test was performed in parallel with the sELISAs associated with the nanoparticles. Therefore, the quality of the antigens and antibodies were the same, as the reagents used. The folds in this case are smaller than those previously reported (chapter II), but these data are comparable with the folds of the sELISA-MNP@Si@ab. The variation of the results could be due to the quality of the antigens or antibodies used.

In the case of rMTC28, rMPT64, rMoeX and rCFP10 proteins, it can be observed that a conventional sELISA was enough to detect recombinant *M. tuberculosis* antigens; but for rCFP10, r38kDa, and rAg85B proteins, the use of MNP@Si@ab improved the detection of these recombinant antigens.

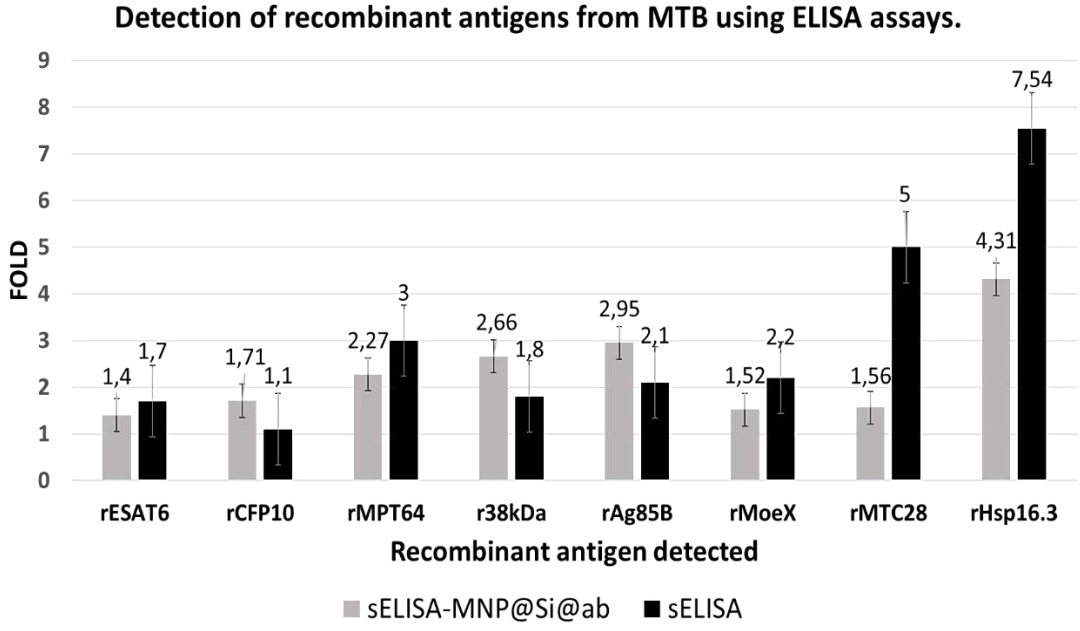

Figure IV.17: Detection of recombinant antigens (0.5 µg/well for rHsp16.3 and 1 µg/well for the other proteins) from MTB using conventional sELISA vs sELISA-MNP@Si@ab.

IV.1.4. Detection of MTB native antigen using sandwich ELISA associated with magnetic nanoparticles.

Detection of native antigens of sputum pools from positive and negative TB patients, using sELISA-MNP@Si@ab, was evaluated. Sputum samples characteristics is described in experimental section.

It is important to consider that sputum samples from TB patients used in this study, were collected approximately 12 months before being evaluated in the test. But despite this, it was possible to discriminate the native antigens of MTB.

In general, the processing of sputum samples is crucial to maximize the optimal exposition of epitopes of natives MTB antigens. Many bacteria and proteins from *M. tuberculosis* are sequestered in the viscous and mucosal complexes formed by different proteins in the sputum of the patient. To detect native MTB in this kind of biological samples is complicated, special pre-treatment is needed to disintegrate the protein aggregation. In this sense, an adequate processing of the sputum sample will allow the sample to become fluid, and thus easy to manipulate. Currently, the N-Acetyl-L-Cysteine (NALC) - sodium hydroxide (NaOH) method is used to decontaminate sputum samples from patients suspected of TB, prior to culture (Ferroni e*t al*., 2006). In our case, this method is not convenient because NaOH is a strong alkali, and it can denature our interest proteins. Pereira Arias-Bouda *et al*. (2000) found that treatment of the purified culture filtrate of *M. tuberculosis* with 0.25 M sodium hydroxide in combination with 15 mM NALC reduces by 50% the detection of LAM (Pereira Arias-Bouda *et a*l., 2000). Due to sputum samples will be used to directly TB diagnosis, it is important to keep the markers of the bacteria in the sample. Another option is a pretreatment using NALC-proteinase K method, nonetheless this chemical could affect the antigen-antibody recognition. Therefore, we use a simple mechanical homogenization to dilute the viscosity of the

complex and release the highest amount of MTB antigens, without affect the protein structure.

Figure IV.18 - Figure IV.19 shows an sELISA-MNP@Si@ab assay of seven target native MTB antigens. The best detection was for CFP10 and ESAT6 antigens with fold value of ~ 1.8. It could be explained by the high expression of ESAT6/CFP10 during the early infection. In fact, they are the most abundant secretory proteins isolated from the filtered MTB culture (Renshaw *et al*., 2005). For other proteins, the fold values were 1.4-1.5.

Specifically, in the case of **native ESAT6,** is observed different fold values for each sputum volume/well: **1.8 (100 µl),** 1.33 (25 µl) and 1.22 (6.25 µl). Similar values are observed for **native CFP10** detection: **1.83 (100 µl),** 1.35 (50 µl), 1.12 (25 µl) and 1.0 (6.25 µl). It is observed that for the detection of native proteins ESAT6 and CFP10, better results are obtained by using 100 ul of treated samples from patients with TB. However, when the sandwich ELISA associated with magnetic nanoparticles was made with the recombinant proteins, a lower fold was observed for both cases. This could confirm that rESAT and rCFP10 were in the degradation process, so they were not very useful to standardize the method.

In the case of **native 38kDa protein** detection, different fold values for each sputum volume/well were observed: **1.46 (50 µl),** 1.4 (25 µl), 1.26 (12.5 µl). and 1.0 (6.25 µl). For **native MPT64** detection, a dilution of 1/2 (50 µl of treated sample/well) presented a better result in the assay. The fold values obtained according the sputum volume/well were: **1.41 (50 µl),** 1.4 (25 µl), 1.38 (12.5 µl). and 1.1 (6.25 µl). About **native MoeX** detection, FOLDs calculated were: **1.4 (100 µl),** 1.36 (50 µl), 1.24 (25 µl) and 1.1 (12.5 µl). In the case of **native Ag85B** detection, the FOLDs observed were: **1.47 (50 µl),** 1.38 (25 µl), 1.27 (12.5 µl). and 1.1 (6.25 µl). Finally, for **native Hsp16.3** detection from sputum samples. It was better using 50 µl of treated sample/well. The Fold values varied according the sputum volume/well: **1.32 (50 µl**), 1.2 (25 µl) and 1.16 (12.5 µl).

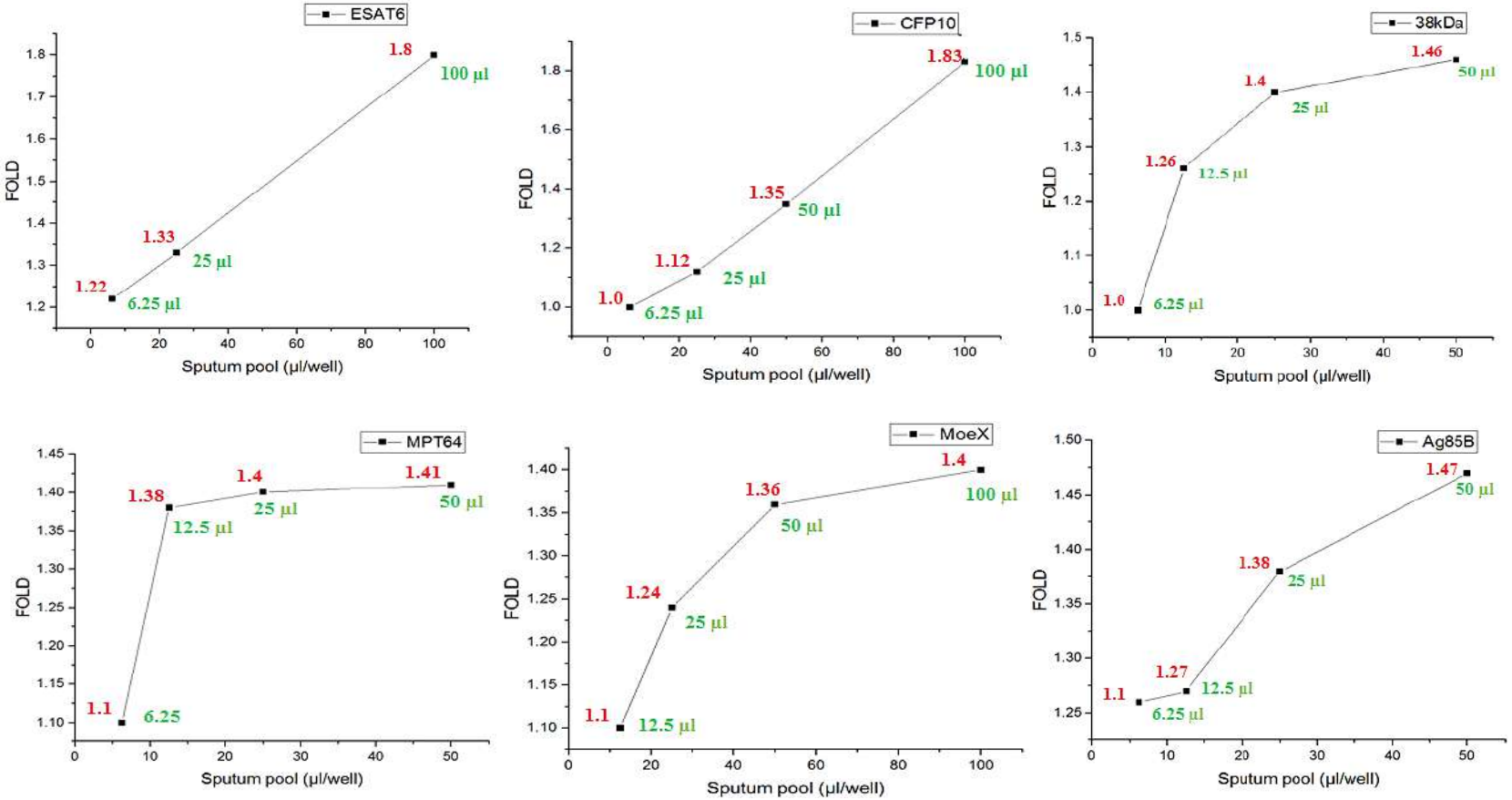

Figure IV.18: Sandwich ELISA associated with MNP@Si@anti-ab to detect the **native protein** from *M. tuberculosis*, in a pool of positive TB sputum samples. In red the fold value, and in green the volume of sputum /well. FOLD = average sample OD/ average negative OD.

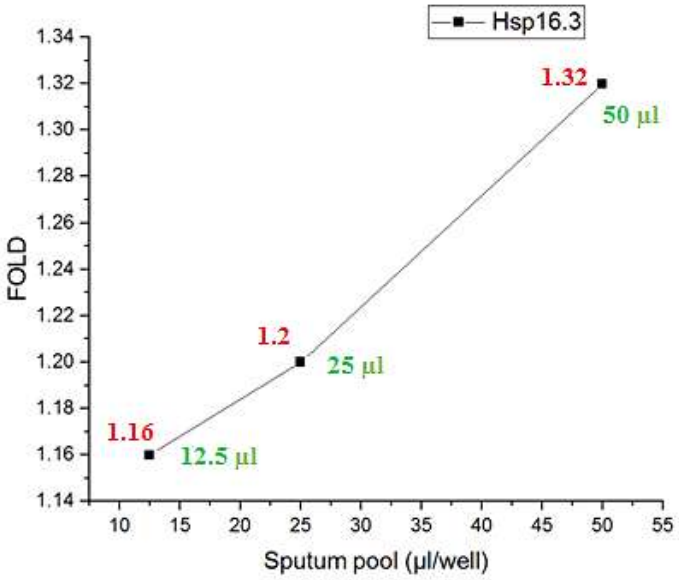

Figure IV.19: Detection of the native Hsp16.3 from *M. tuberculosis* using a sELISA-MNP@Si@ab in a pool of positive TB sputum samples. In red the fold value, and in green the volume of sputum /well. FOLD = average sample OD/ average negative OD.

Finally, the results obtained were compared between the methods of sELISA and sELISA-MNP@Si@ab, after processing the sputum pools of patients with TB.

The results showed that the detection of native antigens in real biological samples was much more efficient when magnetic nanoparticles were introduced in the assay.

Figure IV.20 shows that the conventional sELISA was not able to detect MPT64, 38kDa, Ag85B or MoeX. Also, the detection of ESAT6, CFP10, Hsp16.3 and MTC28 was very low (fold values <1.23).

On the other hand, sELISA-MNP@Si@ab was able to detect all the native MTB proteins from the sputum samples of patients, especially the antigens ESAT6 and CFP10 with a fold ≥1.8. Although this discrimination value is not very high, it should also be considered that sputum samples were kept for more than 12 months. Therefore, many antigens may have been degraded over time, although the samples were stored at -20 ° C. Therefore, consider fresh sputum samples is important.

The difference in detection efficiency between both methods could have been due to the best exposition of the antibodies conjugated with the nanoparticles, favoring the capture of the antigens from samples. In conventional sELISAs, the antibodies are randomly fixed at the base of the wells, making less efficient the specific antigen-antibody recognition. This is particularly true for sputum, where mucosal complexes are capable of sequestering the proteins of interest.

The introduction of magnetic nanoparticles in the diagnostic test, allows to expose optimally the antibodies that are on the surface of the nanoparticles, and thus capture a greater amount of antigen in the sample. In addition, the use of magnetic nanoparticles could facilitate the control of the total amount of antibodies introduced in a well and, therefore, guarantee the best reproducibility.

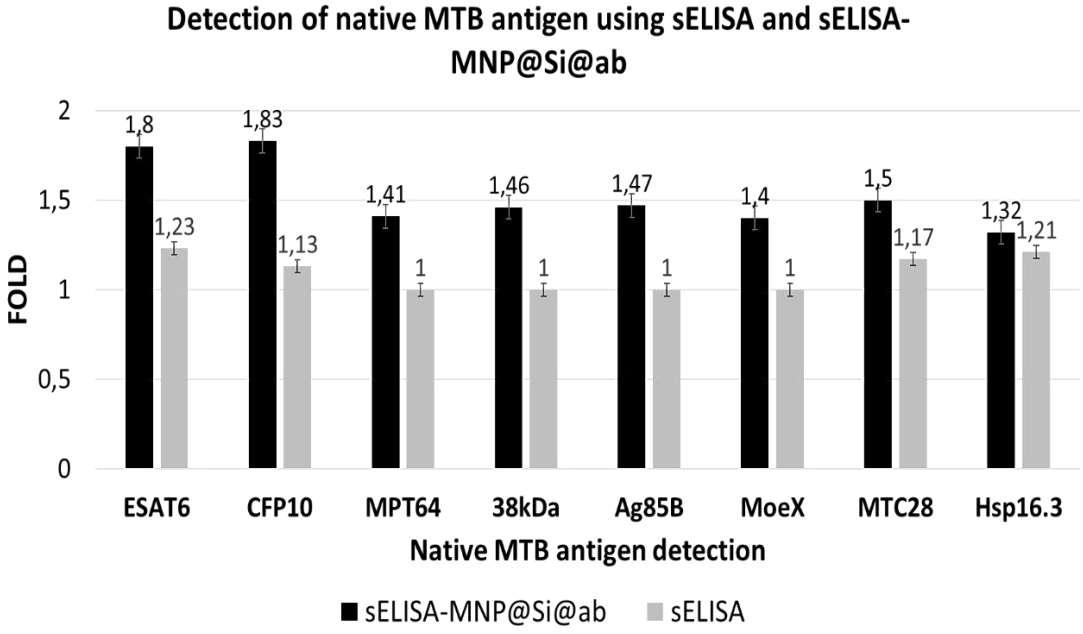

Figure IV.20: Comparisons between sELISA and sELISA-modified MNPs to detect native antigens from MTB.

In summary, the sELISA-MNP@Si@ab essay is a relatively fast method that can be performed in less than 4 h. The conventional sELISA reported in this study took about 2 days to give a result. Besides, another advantage of sELISA-MNP@Si@ab is that the

introduction of functionalized nanoparticles with specific antibodies allowed a better detection of native sputum MTB antigens. The demonstration of the sELISA-MNP@Si@ab feasibility was carried out on biological samples stored for a long period before analysis. This factor could have affected the integrity of the MTB proteins and consequently influenced the sensibility of measurements. Nevertheless, it was possible to discriminate the positive samples from the negative ones.

IV.2. EXPERIMENTAL SECTION (METHODOLOGY).

- **Chemicals and Biological materials.**

For the experiments, polyclonal antibodies produced in rabbits and mice (previously described) were used, as well as magnetic nanoparticles (MNP@Si@NH_2) synthesized and characterized in the previous chapter. N- (3-Dimethylaminopropyl) -N'-ethylcarbodiimide hydrochloride (EDC) and N-Hydroxysuccinimide (NHS) were used as the coupling agent. Bovine Albumin Serum (BSA), EDC and NHS were bought from Sigma-Aldrich, Saint-Quentin-Fallavier,

IV.2.1. Standardization of BSA immobilization on MNP@Si@NH_2 surface.

Briefly, the surface functionalization was carried out in two steps. The typical procedure was as follows: First, BSA and EDC/NHS coupling agents, in a final volume reaction of 1ml, were mixed on a rotating wheel for 1 h at room temperature. Second, MNP@Si@NH_2, 500 µL of PBS and 500 µL of activated BSA solution were incubated at room temperature overnight, rotating at 15 rpm. BSA (µg) activated only with EDC/NHS, without MNPs, was considered as a negative control (**initial value of the protein, V0**). Subsequently, in all cases the supernatant was separated using a magnet and dialyzed in Spectrum™ Spectra/Por™ 4 RC Dialysis Membrane Tubing 12,000 to 14,000 Dalton MWCO (Fisher Scientific, Madrid, Spain) against 1x PBS pH 7.4, at 4°C overnight.

Dialyzed protein concentrations were read at A280nm in UV-Vis spectrophotometer NanoVue Plus™ (Biochrom, Massachusetts, USA).

The amount of linked protein on the nanoparticle surface, was calculated as follows: subtracting the values (µg) of the dialyzed protein incubated without nanoparticles (**V0**) minus the dialyzed protein after incubation (**Vf**). It should be noted that, despite the initial amounts of BSA were exactly measured on an analytical balance, during the incubation and dialysis process, a little quantity of protein was lost. To determine precisely the amount of linked protein on MNP surface, the calculations were done using following equations:

Linked protein per mg of MNP = (V0 - Vf)/(N° mg of MNP),

and **% linked protein = [(V0 - Vf)/ V0] *100.**

The standardization of parameters for an efficient functionalization of MNP@Si@NH_2 surface with proteins, is described below.

- **Evaluation of the best type of buffer.**

Due to the influence of the salts on the immobilization of proteins on the surface of nanoparticles, different buffers were evaluated (Bordbar *et al*., 2014). 10 mM Tris-HCl, PBS (10 mM phosphate buffer, 2.7 mM potassium chloride, 140 mM sodium chloride, pH 7.4) and 10mM Buffer Phosphate, pH 7.4 were evaluated. To determine this parameter, 1 mg of BSA (15.04 nmol), 5 mg MNP@Si@NH_2 and 1/0.5 µmol of EDC/NHS were reacted in 1 ml of buffer in experimental conditions as described above.

- **Determination of nanoparticles amount.**

10, 5, 2.5 and 1 mg of magnetic nanoparticles were incubated with 2.5 of mg BSA (37.59 nmol) with 5/10 µmol of EDC/NHS, in PBS.

- **Saturation of the nanoparticle surface**.

Different amounts of BSA 250 µg (3.76 nmol), 500 µg (7.52 nmol), 1000 µg (15.04 nmol), 1500 µg (22.56 nmol) and 2000 µg (30.08 nmol) conjugated with 1 mg of magnetic nanoparticles were used, in the presence of 2/2.2 µmol of EDC/NHS, in PBS.

- **Evaluation of the most efficient coupling agent concentration**.

Different amounts of EDC/NHS were evaluated: 0.5/1, 5/10, 50/100, 1/0.5, 10/5 and 100/50 μmol. For the reaction, 5 mg of MNP@Si@NH_2 and 2.5 mg of BSA (37.59 nmol) were used in PBS.

In addition, the thermogravimetry analysis (**TGA**) and Dynamic light scattering (**DLS**) were made to quantify the organic material conjugated on nanoparticle surface and determine the hydrodynamic diameter of conjugated nanoparticles. Using TGA was possible to corroborate the BSA immobilization on MNP@Si@NH_2 surface. The physical method was carried out in a Setaram Thermogravimetric Analyzer (LABSYS EVO DTA/DSC, Lyon, France). Analysis was performed from 25 to 600 °C at a heating rate of 10°C/min, under argon atmosphere, with a gas flow rate of 16 mL/min. The loss of mass of organic material was calculated using a derivative plot dm/dT (DTGA). The **DLS** was measure in 90Plus Particle Size Analyzer (Brookhaven Instruments Corporation, New York, USA).

IV.2.2. Standardization of polyclonal antibody immobilization on MNP@Si@NH_2 surface.

To determine the type of buffer to be used in the reaction, the casein protein (2 mg/ml) was immobilized on the surface of the modified nanoparticles (2 mg/ml) using 1x PBS (10mM phosphate buffer, 2.7 mM potassium chloride, 140 mM sodium chloride, pH 7.4), buffer MES 0.1 M and 60 mM buffer phosphate. It was observed that the best reaction buffer was PBS 1x pH 7.4, immobilizing up to 52.39 % of casein. In this sense, in the following experiments PBS 1x will be used in the reactions.

Similar to BSA, the immobilization of proteins on magnetic nanoparticle surface, was carried out in two steps:

First, anti-IgG and EDC/NHS coupling agents (final volume reaction of 1ml) were mixed and incubated for 1 h, RT on rotating.

Second, washed, sonicated and resuspended MNP@Si@NH_2 (PBS 1x, 500 µL) were mixed and incubated with activated protein solution (from the first step), at RT, overnight, 15 rpm on rotating. As a negative control, protein (µg) activated only with EDC/NHS, without MNPs, was considered.

After IgG conjugation on magnetic nanoparticle surface, the supernatants were dialyzed in Spectrum™ Spectra/Por™ 4 RC Dialysis Membrane Tubing 12,000 to 14,000 Dalton MWCO (Fisher Scientific, Madrid, Spain) against PBS, at 4°C overnight. Dialyzed protein concentrations were read at A280nm in UV-Vis spectrophotometer NanoVue Plus™ (Biochrom, Massachusetts, USA). Using this method was possible to quantify the non-conjugated proteins on magnetic nanoparticles. In the case of the negative control (proteins without nanoparticles), this indicated the initial amount of protein that was used for the immobilization reaction. In this way, the amount of immobilized protein on the nanoparticle surface was calculated subtracting the initial value of protein minus the non-conjugated proteins.

For the standardization of antibodies on the surface of the MNP@Si@NH_2, anti-Hsp16.3 antibodies were used as reference.

- **Determination of the optimal incubation time.**

0, 0.5, 1, 2, 4, 6 and 22 h were evaluated. The reaction incubated was: 10 µL (272 µg or 1.81 nmol) of anti-Hsp16.3 sera mixed with 5/10 µmol of EDC/NHS and 25 mg of MNP@Si@NH_2. As a main result it was observed that in 22 h a greater amount of protein was immobilized on the nanoparticles, therefore, the other reactions were carried out in this incubation time.

- **Saturation of the magnetic nanoparticle surface.**

2 (300 µg), 6 (900 µg), 8 (1200 µg) and 10 (1500 µg) nmol of anti-Hsp16.3 (sera) were reacted with 1 mg of magnetic nanoparticles, using 5/10 µmol of EDC/NHS. This experiment showed that a large amount of protein is not required to saturate 1 mg of nanoparticles, therefore low amounts of protein were used in the following experiments.

- **Evaluation of the most efficient coupling agent concentration.**

Different amounts of EDC/NHS: 0.5/1, 1/0.5, 2.5/5, 5/2.25, 5/10, 2.5/2.65 and 5/5.15 µmol were incubated with 450 µg (3 nmol) of anti-Hsp16.3 (sera) and 2.5 mg of MNP@Si@NH_2. As the main result, it was observed that low concentrations of the coupling agent EDC/NHS is sufficient to immobilize proteins on the surface of the nanoparticles. So, to work with the other antibodies, this parameter was taken into consideration.

Additionally, to determine what type of antibodies (**whole serum or isolated antibodies**) works better in sandwich ELISA-MNP assay, antibodies were purified by physicochemical and chromatographic fractionation.

Rabbit polyclonal antibodies (anti-Hsp16.3) were used in this experience. First, to enrich and concentrate antibodies from serum, ammonium sulfate precipitation was performed. Saturated ammonium sulfate aqueous solution (1.33 mL, 100%) was added drop by drop to 1 mL of rabbit serum. The mixture was incubated for 1 h at 4°C, centrifuged (10 min x 4500 rpm at 4°C). After removal of the supernatant, the pellet was washed with 40% ammonium sulfate solution (2x2 mL), dissolved in PBS approx. 1mL and dialyzed against PBS (24 h at 4°C).

For further purification by affinity chromatography, antibodies pre-purified by precipitation were injected into a column coated with protein A (HiTrap Protein A Sepharose, Amersham Pharmacia Biotech, Germany), in a Hitachi Chromaster HPLC System (Interlink Scientific Services Limited, Kent, United Kingdom). After fixation of antibodies on stationary phase and washing at neutral pH (PBS, pH 7.4), the desorption of immobilized IgG was made with acid solution (0.1 M citrate-NaOH buffer pH 3.0). The renaturation of isolated antibodies was achieved by adding 1/10th volume of 1M Tris-HCl (pH 9). Finally, the antibodies were dialyzed against PBS (24 h at 4 °C) and quantified at A280nm.

Separately, these different anti-Hsp16.3 preparations and whole rabbit serum were conjugated to the MNP@Si@NH_2 surface as previously described 400 µg (2.67 nmol) of

non-purified **serum,** 300 µg (2.0 nmol) of **precipitated serum proteins by salts,** and 250 µg (1.67 nmol) of **purified antibodies by affinity chromatography**, were conjugated to 2 mg of magnetic nanoparticles. Supernatants were dialyzed and measured at A280nm. The nanoparticles functionalized with antibodies (MNP@Si@anti-Hsp16.3) were washed with PBS and dispersed in 200 µl of buffer. The most important result of this experiment was that the unpurified anti-hsp16.3 serum was immobilized on the nanoparticles in greater quantity than the rest, so it was decided to work with unpurified sera for the other antibodies.

Finally, the **TGA** was made to quantify the organic material conjugated on nanoparticle surface. This allowed to corroborate the immobilization of the antibodies on the surface of the nanoparticles. The physical method was carried out in a in the same machine where MNP conjugated with BSA was evaluated, and under the same conditions.

IV.2.3. Immobilization of polyclonal antibodies on MNP@Si@NH_2 surface.

The immobilization of polyclonal antibodies is described below, considering the previous standardization carried out on the anti-Hsp16.3 antibody (sera).

In general, MNP@Si@NH_2 were dispersed in 1x PBS by sonication for 20 minutes. Specific antibodies, produced in rabbits and diluted in sera (**initial amount**), were incubated with EDC/NHS at room temperature for 1h. Subsequently, the previous reaction was mixed with dispersed nanoparticles, rotating at 15 rpm, overnight. Supernatants from the reactions were separated and dialyzed in dialysis membrane (12,000 to 14,000 Dalton) against PBS, at 4 °C, overnight. The amount of protein recovered after dialysis (**final amount**) was determined by absorbance reading at A_{280nm}. The amount of protein immobilized on nanoparticle surface was calculated following the next equation:

initial mass – final mass= amount of immobilized proteins (µg) **(Eq. 1).**

To express the value of the immobilized protein in percentage (%), the following equation was used:

X% = [(amount of immobilized protein) *(100)]/(initial amount of protein) (**Eq. 2).**

Finally, the bio-functionnalized nanoparticles MNP@Si@ab were washed with buffer and resuspended in a volume of 200 µl PBS (final concentration of nanoparticles was 12.5 mg/ml). For the assays of sELISA associated with nanoparticles, 5 µl of MNP@Si@ab were used for each well.

According of the antibody characteristics, different concentrations of nanoparticles and EDC/NHS were used in the reaction (**Table IV.2**). To determine the size of the MNP@Si@ab, their hydrodynamic diameters were evaluated using Dinamic Light Scatering. For **DLS**, the MNP@Si@ab were dispersed in water and measured in the same conditions as the MNP conjugated with BSA.

The theoretical amount of antibodies that can saturate 1 mg of nanoparticles was calculated considering d_H data. Additionally, certain parameters were assumed for the calculations: a nanoparticle has the shape of a sphere, the internal structure of the nanoparticle is composed of Fe_3O_4, the nanoparticles are coated homogeneously by amine-silane groups forming a monolayer; and a molecule of hydrated IgG has a structure similar to an ellipsoid (a=13.7 nm, b=8.4 nm, stokes radius= 6.4 nm) (Karlsson *et al*., 2002).

Table IV.2: Immobilization of antibodies on 2.5 mg of amine-silanized magnetic nanoparticle surface (MNP@Si@NH_2), using EDC/NHS as coupling reagents.

Antibodies specific for MTB antigens	Initial amount (µg)	EDC/NHS (µmoles)
Anti-38kDa	263	2/4
Anti-MTC28	227	2/4
Anti-Ag85B	394	3.4/6.8
Anti-MPT64	336	5/10
Anti-MoeX	255	2/4
Anti-ESAT6	223	2/4
Anti-CFP10	255	2/4
Anti-Hsp6.3	255	2/4

IV.2.4. Conventional sandwich ELISA and sELISA associated with magnetic nanoparticles to detect recombinant MTB antigens.

A **conventional sandwich ELISA** (sELISA) assay was developed to detect *M. tuberculosis* antigens. Specific polyclonal antibodies produced in rabbits, were fixed in wells of Nunc MaxiSorp ELISA plates (Sigma-Aldrich, St Louis, USA) overnight at 4 °C. Free space's wells were blocked with Blocker™ Casein in PBS (Thermo Fisher Scientific, Rockford, USA) for 1h at 37 °C. Subsequently 1 µg/well of recombinant antigen (ag) from *M. tuberculosis* was used for their recognition (except for rHsp16.3, where 0.5 µg/well was used). A sandwich complex was formed with polyclonal antibodies produced in mice, overnight at 4 °C. Dilutions of rabbits sera were 1/250 to 1/1600, and for mice sera were 1/50 to 1/400 (**Table IV.3**). The complex formation was recognized by 1/1500 dilution of goat anti-mouse IgG (H+L) secondary antibody, HRP (Thermo Fisher Scientific, Rockford,

USA) incubated for 1h at 37 °C, and revealed with OPD substrate. The reaction was stopped with 0.5 M HCl and OD was read at a wavelength of 450 nm.

Table IV.3: Titers of sera used for the sandwich ELISA (sELISA) and for the ELISA sandwich associated with magnetic nanoparticles (sELISA-MNP@Si@ab). A volume of 5µl of nanoparticles associated with immobilized rabbit serum, was used in each well.

	sELISA		**sELISA@MNP@ab**
Protein	**rabbit serum**	**mouse serum**	**mouse serum**
rESAT6	1/250	1/400	1/100
rCFP10	1/200	1/50	1/100
rMPT64	1/1600	1/200	1/100
r38kDa	1/1600	1/200	1/100
rAg85B	1/400	1/100	1/200
rMoeX	1/1600	1/200	1/200
rMTC28	1/400	1/150	1/100

On the other hand, **a sandwich ELISA assay associated with magnetic nanoparticles** (sELISA-MNP@Si@ab) was evaluated. Polyclonal antibodies previously immobilized in magnetic nanoparticle surfaces (5 µl) were incubated with recombinant antigens (1.0 - 0.006 µg/well) from *M. tuberculosis* for 1 h at 37°C. Then, using a magnet, the MNP@Si@ab-ag were washed (3 times) with PBS 1x pH 7.4. The immune-complex formed by functionalized nanoparticles and captured antigens, was detected by corresponding polyclonal antibodies produced in mice (1/100). This reaction was incubated 1h at 37°C. Subsequently, the nanoparticles were again washed. Finally, to recognize the final sandwich immune complex built on the surface of magnetic nanoparticles, the 1/1500 dilution of goat anti-mouse IgG (H+L) secondary antibody tagged with HRP and OPD were

added and incubated for 1h at 37 °C. After the incubation, the nanoparticles were washed. A colorimetric reaction was revealed using OPD (1mg/ml), stopped with HCl 0.5 M and read at 450 nm (OD) in an ELISA plate reader.

IV.2.5. Sandwich ELISA associated with magnetic nanoparticles to detect native MTB antigens.

To evaluate both types of ELISA assays with patient samples (n=20), pools using positive (13) and negative (7) sputum for TB, were prepared. The biological samples came from Peruvian population from the project "*Unraveling the resistance mechanism of pyrazinamide, the unique - sterilizing drug against tuberculosis of the Wellcome Trust*", approved by the ethics committee from the Universidad Peruana Cayetano Heredia. Previously, the positive and negative samples for TB (**Table IV.4)** were placed in sterile tubes with screw cap, and mechanically homogenized using a vortex and zirconium beads. Subsequently, the samples were inactivated at 80 °C for 20 min. The biological samples were stored at -20 °C for ~12 months.

The conventional sELISA and sELISA-MNP@Si@ab were performed following the protocols previously described. Different volumes (100 - 6.25 µl/well) of thawed sputum pools (diluted in PBS) from patients with TB were used. Both sELISAs, with and without nanoparticles, were evaluated in duplicate, in different days to determine the reproducibility of the methods.

Table IV.4: Laboratory results of patients positive for TB. The sputum samples from confirmed patients (13) were collected, processed and stored at -20 ° C until their use. Also, sputum samples from patients suspected for TB (7), but with negative laboratory diagnosis, were also considered as negative control (data not shown).

Sample information*		**MODS****		**Wayne*****	**Culture*****	
COD	**Date collected**	**Isoniazid (0.4µg/ml)**	**Rifampicin (1µg/ml)**	**Result**	**Result**	**colonies number**
TBN 03	Feb, 2017	sensible	sensible	Positive	positive	4
TBN 05	Feb, 2017	sensible	sensible	Positive	positive	-
TBN 07	Feb, 2017	Resistant	Resistant	Positive	positive	2
TBN 23	Mar, 2017	Resistant	Resistant	Positive	positive	-
TBN 42	Mar, 2017	sensible	sensible	Positive	positive	2
TBN 52	Mar, 2017	sensible	sensible	Negative	positive	-
TBN 55	May, 2017	sensible	sensible	Positive	positive	-
TBN 61	May, 2017	sensible	sensible	Positive	positive	3
TBN 64	May, 2017	Resistant	Resistant	Positive	positive	1
TBN 65	May, 2017	Resistant	Resistant	Positive	positive	1
TBN 66	May, 2017	sensible	sensible	Positive	positive	2
TBN 67	May, 2017	sensible	sensible	Positive	positive	3
TBN 74	May, 2017	sensible	sensible	Positive	positive	-

*Sample information indicates the laboratory code of the sample (COD) and the date of collection of the sputum..

** Using the Microscopic-Observation Drug-Susceptibility method (MODS), bacterial growth and the susceptibility and/or resistance of *M. tuberculosis* to the drugs isoniazid and rifampicin (commonly used in the TB treatment) were evaluated.

*** Using the Wayne method (pyrazinamidase test), the susceptibility of the bacteria to the drug pyrazinamide (also used in the treatment of TB patients) was determined.

****The culture of *M. tuberculosis* is the ‘gold standard’ method to diagnose TB. The culture was performed on a solid Ogawa medium, and the growth of the bacteria was evaluated (result: positive or negative), as well as the number of colonies that grew in the medium.

IV.3. RESULTS.

IV.3.1. Standardization of proteins on MNP@Si@NH_2 surfaces.

IV.3.1.1. Conjugation of Albumin on magnetic nanoparticles surfaces.

The amount of protein immobilized on nanoparticle surface was calculated following the next equation:

initial mass – final mass = mass of immobilized proteins (μg) **(Eq. 1).**

To express the value of the immobilized protein in percentage (%), the following equation was used:

X% = [(mass of immobilized protein) *(100)]/(initial mass of protein) (**Eq. 2).**

The reaction **buffers** evaluated to conjugate BSA on nanoparticles surfaces, were PBS pH 7.4, Tris-HCl and buffer phosphate. However, the amounts of conjugated BSA on the MNP@Si@NH_2 surface, were similar in each case: 23.02, 22.32 and 23.05%, respectively (**Figure IV.1).** Thus, the other reactions were made with PBS.

About the **magnetic nanoparticles amount** required to conjugate BSA on MNP@Si@NH_2 surfaces, it is observed that less than 20% of the total BSA is conjugated to the MNP surface (10 mg). Theoretically, 22.56 μg of BSA saturate 1 mg of nanoparticles synthesized in this study (**Appendix 2.1 and 2.2, pages 294 and 295, respectively).** The calculations were made using the magnetite unit cell parameters reported by Kokate, *et al.*, 2013 (Kokate *et al*., 2013).

Our results showed that there is a high percentage of conjugated BSA when a high MNP amount is used in the reaction. However, the mass of conjugated BSA per mg of nanoparticles (μg linked BSA/mg MNP@Si@NH_2) is increased when a small amount of magnetic nanoparticles is used (**Figure IV.2**). So, for convenience between 1 - 5 mg of nanoparticles for bio-functionalization we considered.

In the case of the **BSA amount to saturates the magnetic nanoparticle surface**, around 76.25±2.05 μg of BSA saturated 1 mg of MNP@Si@NH_2, when 1 mg (15.04 nmoles) of BSA was used as initial amount (**Figure IV.3**).

About the most **efficient coupling agent concentration**, a low amount of BSA is conjugated when a high EDC/NHS concentration is used in the reaction. Additionally, it has been determined that 1/0.5 and 0.5/1 μmoles of EDC/NHS are the most efficient concentrations to functionalize MNP surface by BSA (131 and 119.4 μg linked BSA/ mg of MNP@Si@NH_2) (**Figure IV.4**).

Thermogravetric and Dynamic Light Scattering analysis of MNP@Si@BSA

To corroborate the amount of BSA bound to the surface of the nanoparticles, measured by spectrometry, a TGA assay was additionally performed. For this, the samples were heated at elevated temperatures, until the organic layer evaporated, and the mass loss corresponding to the evaporated BSA was measured.

Using **TGA,** 21.85 – 30.5 mg of nanoparticles were evaluated from 25 to 600 ° C. **Thermogravimetric plots** (**Figure IV.5 A and Figure IV.5 B**) show the first loss of mass, attributed to water desorption (150°C). The released water percentage was 3% of MNP@Si@BSA mass. In drying condition (after 150 °C), the relative loss of mass of organic material of MNP@Si@BSA (330 °C and 498 °C) was 5.35 %. Additionally, the analysis of mass loss as a function of temperature allowed us to determine that around 330°C, BSA tends to evaporate; while amino-silanes are lost at around 450 °C.

About the **DLS** measures, MNP@Si@BSA showed a d_H of 394.24 nm (52.16 %), while MNP@Si@NH_2, haved a d_H of 148.32 nm (55.41 %) (**Figure IV.6 A and Figure IV.6 B**). In summarize, the size of nanoparticles conjugated with BSA incremented drastically (d_H: 394.24) compared with bare amine-silanized nanoparticles (d_H: 148.32 nm).

IV.3.1.2. Standardization of magnetic nanoparticles functionalization with specific polyclonal antibody.

Figure IV.7 shows that using PBS buffer during bio-functionalization reaction effectively contributed to the immobilization of casein, both in MNP@Si@NH_2 and in naked MNP (52.39% and 20.73%, respectively). It was calculated following **Eq. 2**. These results corroborate that PBS is the best reaction buffer, as previously described for BSA conjugation.

Functionalization of polyclonal antibodies was performed following the conditions evaluated with BSA. The **Figure IV.8** summarizes the process of immobilization of antibodies on the nanoparticles surface. About the parameters for an efficient immobilization of polyclonal antibodies on nanoparticle surface, we considered as determining factors: the incubation time, the initial amount of protein, and the concentration of the coupling agent EDC/NHS, which can vary according to the initial amount of protein to conjugate. The most important results are described below:

- **Time reaction for protein immobilization.**

Figure IV.9 shows that the amount of antibodies conjugated on the surface of the MNPs increases over time, reaching 69.85% after 22h of incubation. However, between 4 and 6 h of incubation is observed the beginning of the plateau in the curve. It means that at this time the saturation of the nanoparticles would be starting. For practical purpose, we consider an incubation of 22 h for the all reactions.

- **Saturation of magnetic nanoparticle surface.**

Figure IV.10 shows a curve that reaches an equilibrium when 135 ± 2 μg of anti-Hsp16.3 saturated 1 mg of amine-silanized nanoparticles. It happens when 1.2 mg (8 nmoles) of anti-Hsp16.3 serum is used in the initial incubation. However, it is important to consider that the half of the reaction is used to functionalize the nanoparticles (second step). Therefore, only 600 μg (4 nmoles) of anti-Hsp16.3 were really used for the conjugation of IgG on the surface of the nanoparticles.

- **Efficient coupling agent concentration.**

Similar to BSA, the activation reaction in two-steps using EDC/NHS, in a non-amine or carboxylated buffer, were the best conditions. The results showed that with all EDC/NHS concentrations evaluated, more than 50% of anti-Hsp16.3 (sera) was immobilized on magnetic nanoparticle surface. In general, anti-Hsp16.3 is efficiently conjugated (62.5%) when low concentrations of EDC/NHS (0.5/1 μmoles) are used in the reaction (**Figure IV.11).**

According to the results obtained from our previous experiments, it has been observed that the antibodies used directly from sera were immobilized adequately on the surface of the nanoparticles. To corroborate the above data, an experiment using purified and non-purified anti-Hsp16.3 was carried to evaluate if there is a difference in protein immobilization. The antibodies used for the reaction were: **1) non-purified** serum, **2)** serum proteins (IgG) purified by precipitation of salts (**precipitated**), and **3)** serum IgG purified by HPLC (**purified**).

The **type of antibody** (non-purified, precipitated and purified) used in the reaction, **Figure IV.12** corroborated that when more antibody is used, the amount of conjugated antibody also increases. Additionally, although the amount of conjugated anti-Hsp16.3 is lower in the case of precipitated and purified antibodies, the fold of ELISA tests in the three assays were very similar (around 3.8). This means that precipitated and purified antibodies, conjugated on nanoparticles, can efficiently detect antigens despite being in low amounts. However, the antibody purification process demands an additional cost and generates a loss in the antibody concentrations. In our case, the results show that it is possible to work with non-purified anti-Hsp16.3 and obtain the same results such as purified antibodies. For this reason, in the subsequent tests, the polyclonal antibodies were immobilized directly from the sera.

Thermogravetric and Dynamic Light Scattering analysis of MNP@Si@anti-Hsp16.3.

For thermogravimetry analysis, bare nanoparticles, nanoparticles functionalized only with amino-silanes and MNP@Si@anti-Hsp16.3 were used. Similar to BSA, thermogravimetric plots (**Figure IV.13)** shows the first loss of mass (< 150°C) attributed to water desorption. In a drying condition (>150 °C), the relative loss of mass of organic material of MNP@Si@anti-Hsp16.3 (320°C and 457 °C) was 3.50 %; where 0.92 % (0.201 mg) corresponded specifically to anti-Hsp16.3 loss of mass and 2.58 % corresponds to Si@NH_2.

IV.3.2. Immobilization of antibodies on modified magnetic nanoparticle surface.

Immobilization of antibodies on the nanoparticle surface was performed as described above for anti-Hsp16.3

Table IV.1 shows the amount of protein immobilized on MNP@Si@NH_2, and the values of the hydrodynamic diameters of the nanoparticles conjugated with the antibodies. The d_H of MNP@Si@NH_2 (without antibodies) is 148.32 nm. However, the range values of d_H for MNP@Si@ab is 119.61-370.93 nm. Further, the table shows the theorical amount of antibodies capable of saturating 2.5 mg of MNP@Si@NH_2 according to its hydrodynamic diameter (calculated in **Appendix 2.3 and 2.4, page 295 and 296, respectively).** The **Figure IV.14** shows the hydrodynamic diameter of the majority of the population of nanoparticles functionalized with the anti-38kDa antibody. It is observed that more than 50% of nanoparticles (accumulated number: 70.24%) have a d_H of 348.77nm. However, there is also a very small population of nanoparticles of greater size, indicating larger aggregations in the solution. Unlike the previous case, a greater homogeneity in the nanoparticle population functionalized with anti-MTC28 is observed. Most of the population has a d_H of 344.23 in the 84.61% of MNP@Si@anti-MTC28. Similarly, the

population of MNP conjugated with anti-Ag85B, anti-MPT64 and anti-Moex did not have diameters very dispersed in the solution. The d_H observed were: 370.93 nm, 355.02 nm and 338.52 nm, respectively.

In the case of nanoparticles immobilized with anti-ESAT and and anti-CFP10, two populations of nanoparticles are clearly observed. But the largest MNP@Si@ab population is indicated in the **Figure IV.14** with d_H of 119.61 and 149.27 nm, respectively. These hydrodynamic diameters were lower than the d_H of the nanoparticles conjugated with the other antibodies. This could be explained by a better dispersion of the complexes (sonication). The second population is also significant, indicating that despite the dispersion of the nanoparticles, there is an equal aggregation of these in the solution. Finally, the nanoparticles conjugated with anti-Hsp16.3, also presented a high d_H (358.62 nm), within a homogeneous population (50.6 %).

IV.3.3. Detection of recombinant antigen from MTB using sandwich ELISA associated with magnetic nanoparticles.

Using the nanoparticles previously conjugated with antibodies, a sandwich ELISA associated with magnetic nanoparticles (sELISA-MNP@Si@ab) was developed (described in Experimental section). The detection of the recombinant antigens of MTB was evaluated, using the antibodies produced in rabbits and mice (previously described in chapter II) in the sELISA-MNP@Si@ab assay.

Figure IV.15 Figure IV.16 show the curves (antigen quantity in well *vs* fold values) obtained after a sandwich ELISA associated with magnetic nanoparticles. The protein rHsp16.3 was detected up to value 0.08 ng/µl (0.008 µg/well). In the case of r38kDa, rMoeX and rAg85B proteins were successfully detected up to values ≤ 0.15 ng/µl (0.015 µg/well); while in the case of the rMPT64 and rMTC28 proteins, the detection limit was

raised to 0.31 ng/µl (0.031 µg/well). The rCFP10 and rESAT6 proteins required up to 1.25 ng/µl (0.125 µg/well) to give the positive response.

In the ELISA sandwich tests associated with MNP@Si@ab, the minimum recombinant antigen amount detected in the assays were 10 ng/well (0.1 ng/µl), 15.6 ng/well (0.156 ng/µl), 6 ng/well (0.06 ng/µl), 15.6 ng/well (0.156 ng/µl), 31 ng/well (0.31 ng/µl) and 31 ng/well (0.31 µng/l) for rAg85B, r38kDa, rMoeX, rHsp16.3, rMPT64 and rMTC28, respectively.

In the case of the immunodetection of rESAT6, the **fold** values (sample/negative ratio = average positive OD/ average negative OD) observed are very low. It could due to protein degradation, because ESAT6 was a soluble protein that precipitated slightly over time. Using an ELISA sandwich associated with MNP@Si@anti-ESAT6 was possible to detect 125 ng/well (12.5 ng/µl) of rESAT6. At the same way, rCFP10 detection using an sELISA-MNP@Si@anti-CFP10 showed low fold values, and 125 ng/well (12.5 ng/µl) of rCFP10 was the minimum amount detected.

Finally, a sMNP@Si@anti-MTC28 detected 31 ng/well (0.31 µng/l) of rMTC28. Similarly, to ESAT6 and CFP10, the fold values were low.

In addition, **Figure IV.17** illustrates a comparison between the conventional sELISA and the sELISA-MNP@Si@ab. In the case of rMTC28, rMPT64, rMoeX and rCFP10 proteins, it can be observed that a conventional sELISA was sufficient to detect recombinant *M. tuberculosis* antigens; but for rCFP10, r38kDa, and rAg85B proteins, the use of MNP@Si@ab improved the detection of these recombinant antigens. Unlike the sELISA reported in **chapter II**, this test was performed in parallel with the sELISAs associated with the nanoparticles. Therefore, the quality of the antigens and antibodies were the same, as the reagents used. The folds in this case are smaller than those previously reported (chapter II), but these data are comparable with the folds of the sELISA-MNP@Si@ab. The variation of the results could be due to the quality of the antigens or antibodies used.

IV.3.4. Detection of MTB native antigen using sandwich ELISA associated with magnetic nanoparticles.

Detection of native antigens from sputum pooles of positive and negative TB patients, using sELISA-MNP@Si@ab, was evaluated. Sputum samples characteristics is described in experimental section.

It is important to consider that sputum samples from TB patients used in this study, were collected approximately 12 months before being evaluated in the test. But despite this, it was possible to discriminate the native antigens of MTB.

Figure IV.18 - Figure IV.19 shows an sELISA-MNP@Si@ab assay of seven target native MTB antigens. The best detection was for CFP10 and ESAT6 antigens with fold value of ~ 1.8.

Specifically, in the case of **native ESAT6,** is observed different fold values for each sputum volume/well: **1.8 (100 µl),** 1.33 (25 µl) and 1.22 (6.25 µl). Similar values are observed for **native CFP10** detection: **1.83 (100 µl),** 1.35 (50 µl), 1.12 (25 µl) and 1.0 (6.25 µl).

It is observed that for the detection of native proteins ESAT6 and CFP10, better results are obtained by using 100 ul of treated samples from patients with TB. However, when the sandwich ELISA associated with magnetic nanoparticles was made with the recombinant proteins, a lower fold was observed for both cases. This could confirm that rESAT and rCFP10 were in the degradation process, so they were not very useful to standardize the method.

In the case of **native 38kDa protein** detection, different fold values for each sputum volume/well were observed: **1.46 (50 µl),** 1.4 (25 µl), 1.26 (12.5 µl). and 1.0 (6.25 µl). For **native MPT64** detection, a dilution of 1/2 (50 µl of treated sample/well) presented a better result in the assay. The fold values obtained according the sputum volume/well were: **1.41 (50 µl),** 1.4 (25 µl), 1.38 (12.5 µl). and 1.1 (6.25 µl). About **native MoeX** detection, FOLDs

calculated were: **1.4 (100 µl),** 1.36 (50 µl), 1.24 (25 µl) and 1.1 (12.5 µl). In the case of **native Ag85B** detection, the FOLDs observed were: **1.47 (50 µl),** 1.38 (25 µl), 1.27 (12.5 µl). and 1.1 (6.25 µl). Finally, for **native Hsp16.3** detection from sputum samples. It was better using 50 µl of treated sample/well. The Folds values, varied according the sputum volume/well: **1.32 (50 µl**), 1.2 (25 µl) and 1.16 (12.5 µl).

Finally, the results obtained were compared between the methods of sELISA and sELISA-MNP@Si@ab, after processing the sputum pools of patients with TB. **Figure IV.20** shows that the conventional sELISA was not able to detect MPT64, 38kDa, Ag85B or MoeX. Also, the detection of ESAT6, CFP10, Hsp16.3 and MTC28 was very low (fold values <1.23).

IV.4. DISCUSSION.

IV.4.1. Standardization of proteins on MNP@Si@NH_2 surfaces.

IV.4.1.1. Conjugation of Albumin on magnetic nanoparticles surfaces.

About the parameters for an efficient bio-functionalization of nanoparticles with proteins, we considered as determining factors: the incubation time, the initial amount of protein in the incubation, and the concentration of EDC/NHS, which can vary according to the initial amount of protein to conjugate.

Bordbar *et al*., 2014 reported that in a reaction where there are high concentrations of salts, an increase of ionic strength occurs. This generates a reduction of the electrostatic interactions between the BSA and the nanoparticles, decreasing the immobilization of the proteins on the surface (Bordbar *et al*., 2014). In our work, since functionalization reactions did not show significant variations when using different buffer types; it can be inferred that the salts present in the PBS did not interfere in the reaction. It is because the amount of NaCl was 0.14 M, an amount that would have no effect on the deactivation of some active sites of the nanoparticles.

We observed that the mass of conjugated BSA per mg of nanoparticles is increased when a small amount of magnetic nanoparticles is used. It means that, apart from MNP surface saturation with BSA, there are other interactions between proteins (ionic, electrostatic and hydrogen bonds), which favored the increase of conjugated BSA.

In the case of the **BSA amount to saturates the magnetic nanoparticle surface**, a direct relationship is observed between the amount of initial protein and the amount of protein conjugated to nanoparticles. Previously, Bordbar *et al* (2014) reported that the amount of BSA immobilized increases with increasing the initial value of BSA, until saturating the surface of the nanoparticles. The saturation would be directly related to the number of amino groups of the MNPs and to the activated sites of the BSA.

About the **activation reaction**, using the coupling agent EDC/NHS, is better to follow two-step reactions performed in a non-amine or carboxylated buffer. EDC reaction is better performed at pH 4.7-6.0, and the NHS-activated molecules with primary amines is most efficient at pH 7-8. Finally, the NHS-ester reactions are usually performed in PBS at pH 7.2-7.5 (Grabarek and Gergely, 1990).

About the most **efficient coupling agent concentration**, a high amount of EDC/NHS reduces the amount of proteins bound on the surface of the nanoparticles. It is because an excess of EDC/NHS contributes to the polymerization of the proteins, due to high number of active sites generated by the coupling agent. This phenomenon, previously described by Bartczak and Kanaras (2011), reduces the number of activated sites of binding to the amino groups of the nanoparticles. Additionally, a BSA molecule contains 100 free carboxyl groups (Saroff *et al*., 1953), indicating a high exposure of COOH. For this, is not necessary to use a high amount of EDC/NHS in the reaction.

Thermogravetric and Dynamic Light Scattering analysis of MNP@Si@BSA

In the **thermogravimetric plots, a** percentage of 1.53 % (0.348 mg) corresponded specifically to the loss of mass of BSA, and 3.82 % would correspond to Si@NH_2 layer.

Showing a high density of BSA in the MNP surface. Interesting, these BSA mass reduction (0.348 mg) was in accordance with the values obtained with UV-Vis spectrophotometer (loss of mass of 0.364 mg for BSA).

Additionally, the analysis of mass loss as a function of temperature allowed us to determine that around 330°C, BSA tends to evaporate; while amino-silanes are lost at around 450 °C. The differences in evaporation temperatures between the BSA and the amino-silane groups could be due to the physical-chemical properties of the compounds, or to the greater heat exposure of BSA.

On the other hand, nanoparticles conjugated with BSA had a larger hydrodynamic diameter (d_H) than the nanoparticles that were only amine-silanized. We hypothesized an aggregation of the conjugated proteins, due to the polymeric nature of BSA. It can cause an approximation between nanoparticles, increasing their size (Liu *et al*., 2011). Additionally, we believe that EDC/NHS coupling agent could favor this aggregation when the activated protein was incubated with the nanoparticles (Bartczak and Kanaras, 2011).

IV.4.1.2. Standardization of magnetic nanoparticles functionalization with specific polyclonal antibody.

In the immobilization of casein, the presence of amino groups contributed to a greater amount of protein bound to the surface of the nanoparticles MNP@Si@NH_2. In naked MNPs, the immobilization of casein on the non-modified MNPs is probably due to a weak adsorption reaction and/or electrostatic interactions between the protein and the hydroxyl groups (OH) on the MNP surface (Roque *et al*., 2009).

In general, an antibody (IgG) has two regions: one variable (Fab or antigen-binding fragment) and another constant (Fc or crystallizable fragment). Fab is rich in amine groups ($-NH_3^+$), while Fc has a large number of carboxyl groups (COO^-). Thus, the COOH groups of antibody Fc region were activated using EDC/NHS as coupling agent. The reaction of activated carboxyl groups with the amine groups of silanizated nanoparticles, generated

covalent (peptide) bonds. In this way, it is ensured that most of the functionalized antibodies display freely the Fab regions, favoring a greater interaction with the antigens (Jesse *et al*., 2015; Liu *et al.*, 2011). Different parameters for an efficient immobilization of polyclonal antibodies on nanoparticle surface were considered.

- **Time reaction for protein immobilization.**

The reaction time is a very important factor, for proteins such as BSA, it has been observed that a time of 4 hours is sufficient to saturate the nanoparticles (Bordbar *et al*., 2014). However, in the case of antibodies the time was longer (22 h) for nanoparticle saturation.

- **Saturation of magnetic nanoparticle surface.**

Similar to BSA, a direct relationship is observed between the amount of initial protein and the amount of IgG conjugated to nanoparticles.

As previously described, Bordbar *et al.* (2014) reported a direct relationship between the initial amount of BSA in the reaction and the amount of BSA conjugated to the nanoparticles. This phenomenon has also been observed with antibodies. This means that by increasing the initial value of IgG, the amount of immobilized IgG will also be increased until the surface of the nanoparticles is saturated. The saturation would be directly related to the number of amino groups of the MNPs and with the activated sites of the anti-Hsp16.3.

- **Efficient coupling agent concentration.**

Activation reaction in two-steps using EDC/NHS, in a non-amine or carboxylated buffer, were the best conditions. This means, activation of the carboxylic groups of the protein in the first step, and subsequently conjugation of the activated proteins with MNPs in the second step. Among the different concentrations of EDC/NHS, so much variation was not observed.

Similar to BSA, a high amount of EDC/NHS reduces the amount of proteins bound on the surface of the nanoparticles. But this reduction was not dramatically in our experiments. Bartczak and Kanaras (2011) reported the contribution of the EDC/NHS excess in the

protein polymerization, due to high number of active sites generated by the coupling agent. This could reduce the number of binding activated sites of IgG to the amino groups of the nanoparticles.

An IgG has around 12636 free COOH groups (Huang *et al.*, 2017). It means that there is a high exposure of carboxyl groups, allowing the use of low EDC/NHS concentration in the reactions.

About the **type of antibody,** non-purified and purified antibodies, conjugated on nanoparticles, detected efficiently the antigens.

Thermogravetric and Dynamic Light Scattering analysis of MNP@Si@anti-Hsp16.3.

For thermogravimetry analysis, the amount of immobilized antibody (0.282 mg) on MNP@Si@anti-Hsp16.3 surface, previously measured by spectrophotometry, was corroborated using TGA (mass loss of 0.201 mg). These results indicate that the methods of immobilization and indirect quantification of proteins immobilized on nanoparticle surface, wereefficient.

IV.4.2. Immobilization of antibodies on modified magnetic nanoparticle surface.

The range values of d_H for MNP@Si@ab was 119.61-370.93 nm. The difference of up to 2.5 times of increase in the d_H of the nanoparticles conjugated with the antibodies would be due to an aggregation of the nanoparticles. This phenomenon could have occurred during the process of immobilization of antibodies on the surface of the amino-silanized nanoparticles, through physical-chemical interactions.

On the other hand, the amount of protein fixed on the surface of the MNPs is much greater than the calculated value. We hypothesized that this phenomenon would be due to a protein multilayer formation on the MNP surface. Because an antibody contains both

carboxyl and amine groups, during the EDC/NHS activation reaction used for the surface bio-functionalization, the interactions between these functional groups may lead to the formation of covalently interlinked antibodies that then conjugate to the MNP@Si@NH_2 surface (Smith *et al*., 2011).

On the other hand, the diameter of the antibody-associated nanoparticles was high, indicating an aggregation between them.

IV.4.3. Detection of MTB native antigen using sandwich ELISA associated with magnetic nanoparticles.

In general, the processing of sputum samples is crucial to maximize the optimal exposition of epitopes of natives MTB antigens. Many bacteria and proteins from *M. tuberculosis* are sequestered in the viscous and mucosal complexes formed by different proteins in the sputum of the patient. To detect native MTB in this kind of biological samples is complicated, special pre-treatment is needed to disintegrate the protein aggregation. In this sense, an adequate processing of the sputum sample will allow the sample to become fluid, and thus easy to manipulate. Currently, the N-Acetyl-L-Cysteine (NALC) - sodium hydroxide (NaOH) method is used to decontaminate sputum samples from patients suspected of TB, prior to culture (Ferroni e*t al*., 2006). In our case, this method is not convenient because NaOH is a strong alkali, and it can denature our interest proteins. Pereira Arias-Bouda *et al*. (2000) found that treatment of the purified culture filtrate of *M. tuberculosis* with 0.25 M sodium hydroxide in combination with 15 mM NALC reduces by 50% the detection of LAM (Pereira Arias-Bouda *et a*l., 2000). Due to sputum samples will be used to directly TB diagnosis, it is important to keep the markers of the bacteria in the sample. Another option is a pretreatment using NALC-proteinase K method, nonetheless this chemical could affect the antigen-antibody recognition.

Therefore, we use a simple mechanical homogenization to break the viscosity of the complex and release the MTB antigens, without affect the protein structure.

In the sELISA-MNP@Si@ab assay of seven target native MTB antigens, the best detection was for CFP10 and ESAT6 antigens with fold value of ~ 1.8. It could be explained by the high expression of ESAT6/CFP10 during the early infection. In fact, they are the most abundant secretory proteins isolated from the filtered MTB culture (Renshaw *et al*., 2005). For other proteins, the fold values were 1.4-1.5.

The folds obtained of sELISA and sELISA-MNP@Si@ab, after processing the sputum pools of patients with TB, were compared. The results showed that the detection of native antigens in real biological samples was much more efficient when magnetic nanoparticles were introduced in the assay.

On the other hand, sELISA-MNP@Si@ab was able to detect all the native MTB proteins from the sputum samples of patients, especially the antigens ESAT6 and CFP10 with a fold ≥1.8. Although this discrimination value is not very high, it should also be considered that sputum samples were kept for more than 12 months. Therefore, many antigens may have been degraded over time, although the samples were stored at -20 ° C. Therefore, consider fresh sputum samples is important.

The difference in detection efficiency between both methods could have been due to the best exposition of the antibodies conjugated with the nanoparticles, favoring the capture of the antigens from samples. In conventional sELISAs, the antibodies are randomly fixed at the base of the wells, making less efficient the specific antigen-antibody recognition. This is particularly true for sputum, where mucosal complexes are capable of sequestering the proteins of interest.

The introduction of magnetic nanoparticles in the diagnostic test, allows to expose optimally the antibodies that are on the surface of the nanoparticles, and thus capture a greater amount of antigen in the sample. In addition, the use of magnetic nanoparticles

could facilitate the control of the total amount of antibodies introduced in a well and, therefore, guarantee the best reproducibility.

IV.5. CONCLUSION.

The sELISA-MNP@Si@ab essay is a relatively fast method that can be performed in less than 4 h. The conventional sELISA reported in this study took about 2 days to give a result. Besides, another advantage of sELISA-MNP@Si@ab is that the introduction of functionalized nanoparticles with specific antibodies allowed a better detection of native sputum MTB antigens. The demonstration of the sELISA-MNP@Si@ab feasibility was carried out on biological samples stored for a long period before analysis. This factor could have affected the integrity of the MTB proteins and consequently influenced the sensibility of measurements. Nevertheless, it was possible to discriminate the positive samples from the negative ones.

General conclusion and Perspectives.

General conclusion and Perspectives.

Conclusion.

Tuberculosis is a serious problem in worldwide public health, because hundreds of thousands of people die annually due to this disease. Different diagnostic strategies have been developed, but many of them are often expensive or difficult to implement in areas of low economic resources. Consequently, until now, methods that have limitations in the rapid diagnosis of TB continue to be used. Therefore, development of fast, efficient and low-cost methods remains a challenge.

In this study, a sandwich ELISA assay associated with magnetic nanoparticles has been successfully developed to detect native antigens from sputum from TB patients. For this purpose, a multidisciplinary study was carried out, whose objectives were reached in the different chapters described.

In the biological domain, recombinant MTB antigens from MTB (rESAT6, rCFP10, rMPT64, rMTC28, rMoeX, r38kDa, rAg85B and rHsp16.3) were successfully cloned and expressed into the *E. coli* bacterial system. These proteins proved to be highly immunogenic, since they efficiently activated the production of polyclonal antibodies in the experimental animal models of New Zeland rabbits and BALB/C mice. Likewise, high values of FOLD were observed when evaluating the production of antibodies in the ELISA assays.

In the chemistry domain, magnetic nanoparticles were successfully synthesized through the co-precipitation method. Different parameters were evaluated for the synthesis, and it was observed that although many of the nanoparticles produced have adequate physical characteristics, some did not have sufficient capacity to adequately conjugate proteins on their surface. The nanoparticles that proved to be efficient to immobilize proteins were completely characterized. It was observed a spherical shape and the chemical

bonds Fe-O-Fe, Si-O-Si and N-H on nanoparticle surfaces. This result corroborated an adequate functionalization of the nanoparticles with the amine-silane groups. About the magnetic properties, it was observed that the covering polymer ($Si@NH_2$) slightly reduced the magnetic properties of nanoparticles, which has been previously reported in other studies. The mass of $Si@NH_2$ present on the surface of the MNPs was corroborated and quantified using TGA. Using XRD and TEM, the nanometric scale size of the amino-silanized nanoparticles was verified, however when it was resuspended in water, an aggregation of the nanoparticles was observed, and this was corroborated by DLS.

Integrating the biological and chemical results, proteins (BSA and IgG) were successfully immobilized on nanoparticle surface. Parameters for the bio-functionalization of the magnetic nanoparticles with BSA and IgG were efficiently carried out, where the incubation time and EDC/NHS concentration were important parameters for an effective immobilization of proteins on $MNP@Si@NH_2$ surface. Also, the conjugation of proteins was corroborated by different methods (spectrophotometry and TGA). The antibody-conjugated nanoparticles (MNP@Si@ab) were effectively integrated in a colorimetric immunoassay ELISA. So, a sandwich ELISA associated with MNP@Si@ab was successfully developed to detect antigens from MTB. Both recombinant and native antigens were evaluated in a conventional sandwich ELISA (sELISA) and in sandwich ELISA tests associated to magnetic nanoparticles. According our results, the introduction of MNP@Si@ab improved the detection of native MTB antigens in sputum samples of TB patients. The ESAT6 and CFP10 proteins were better discriminated, obtaining a fold of ~ 1.8.

Although the synthesis of the magnetic nanoparticles (MNP) was carried out under nitrogen gas, a slight oxidation of the nanoparticles was observed. So, it is recommended to work in a glovebox with constant nitrogen gas flow, to guarantee that the environmental oxygen does not react with the iron oxide of the nanoparticles.

On the other hand, a nanometric size of the nanoparticles (corroborated by TEM and XDR) has been determined. However, the aggregation of MNPs was observed when nanoparticles were resuspended in water; so that other organic and/or inorganic layers could be evaluated to cover the nanoparticle surface. In this way to reduce the aggregation of nanoparticles. In our study, dextran, TEOS and TEOS/APTES were used; and it was observed that the last functionalized organic layer improved the protein immobilization.

Although, MNP@Si@NH_2 was aggregated, it does not decrease their efficiency to immobilized proteins (BSA and antibodies) on their surface. The antigen epitopes were exposed and recognized for the antibodies. But in our assays, the discrimination values between a positive and a negative samples for TB were relatively low. This could be due to the age of the sample, because it was collected a year ago. Therefore, it is recommended to use fresh samples from TB patients.

Perspectives.

As previously described, an ELISA assay associated with magnetic nanoparticles has been successfully developed to improve the detection of MTB antigens, from sputum samples from TB patients. The effectiveness of the test was demonstrated using recombinant proteins and pools of infected patients. As next steps of the investigation. the sensitivity and specificity of the test will be evaluated using many individual patient samples. Cross-reactions with other mycobacteria belonging to the MTB complex will also be determined. A complete validation of the clinical parameters, as well as the statistical analyzes must be carried out, but with a significant biological samples from patients.

On the other hand, other types of biological samples (serum and urine) of patients with TB will be evaluated, which are easier to manipulate in this type of assays. In the case of sputum samples, the proteins that form the mucous tend to sequester a percentage of the MNPs used in the assay.

Additionally, the concentration and detection of the antigens from liquid cultures of MTB, at different incubation times, will be evaluated in order to determine if the MNP@Si@ab is able to detect MTB in initial cultures. In this way, MTB can be identified, in a shorter incubation time, also allowing a fast confirmation.

Finally, other assays associated with the MNP@Si@ab used in this study, will be evaluated. For example, immunochromatography is a practical method, in which the nanoparticles characterized, could be adapted to develop a rapid commercial test.

Appendix

Appendix 1

Cloning and expression of MTB antigens.

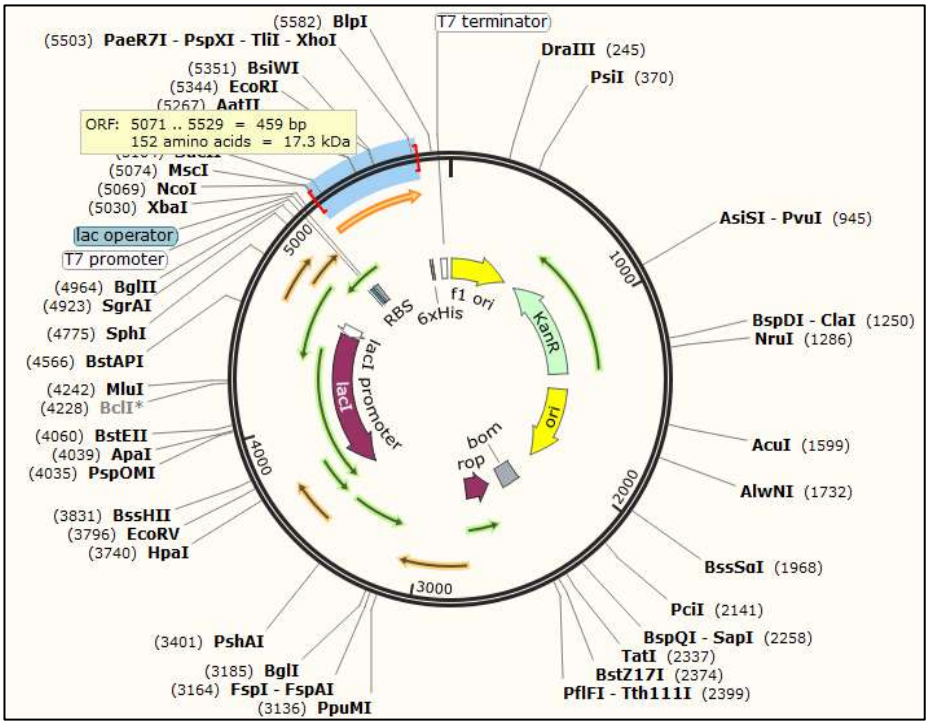

Appendix 1.1: *In silico* ligation of Hsp16.3 in pET28a plasmid.

```
Hsp16_3_pET28_-_clona_2     TTTAACTTTAAGAAGGAGATATA-CATGGCCACCACCCTTCCCGTTCAGCGCCACCCGCG
Hsp16_3_pET28_-_clona_1     ----ACTTTAAGAAGGAGATATACCATGGCCACCACCCTTCCCGTTCAGCGCCACCCGCG
Hsp16.3                     -------------------------ATGGCCACCACCCTTCCCGTTCAGCGCCACCCGCG
                                                      **********************************

Hsp16_3_pET28_-_clona_2     GTCCCTCTTCCCCGAGTTTTCTGAGCTGTTCGCGGCCTTCCCGTCATTCGCCGGACTCCG
Hsp16_3_pET28_-_clona_1     GTCCCTCTTCCCCGAGTTTTCTGAGCTGTTCGCGGCCTTCCCGTCATTCGCCGGACTCCG
Hsp16.3                     GTCCCTCTTCCCCGAGTTTTCTGAGCTGTTCGCGGCCTTCCCGTCATTCGCCGGACTCCG
                            ************************************************************

Hsp16_3_pET28_-_clona_2     GCCCACCTTCGACACCCGGTTGATGCGGCTGGAAGACGAGATGAAAGAGGGGCGCTACGA
Hsp16_3_pET28_-_clona_1     GCCCACCTTCGACACCCGGTTGATGCGGCTGGAAGACGAGATGAAAGAGGGGCGCTACGA
Hsp16.3                     GCCCACCTTCGACACCCGGTTGATGCGGCTGGAAGACGAGATGAAAGAGGGGCGCTACGA
                            ************************************************************

Hsp16_3_pET28_-_clona_2     GGTACGCGCGGAGCTTCCCGGGGTCGACCCCGACAAGGACGTCGACATTATGGTCCGCGA
Hsp16_3_pET28_-_clona_1     GGTACGCGCGGAGCTTCCCGGGGTCGACCCCGACAAGGACGTCGACATTATGGTCCGCGA
Hsp16.3                     GGTACGCGCGGAGCTTCCCGGGGTCGACCCCGACAAGGACGTCGACATTATGGTCCGCGA
                            ************************************************************

Hsp16_3_pET28_-_clona_2     TGGTCAGCTGACCATCAAGGCCGAGCGCACCGAGCAGAAGGACTTCGACGGTCGCTCGGA
Hsp16_3_pET28_-_clona_1     TGGTCAGCTGACCATCAAGGCCGAGCGCACCGAGCAGAAGGACTTCGACGGTCGCTCGGA
Hsp16.3                     TGGTCAGCTGACCATCAAGGCCGAGCGCACCGAGCAGAAGGACTTCGACGGTCGCTCGGA
                            ************************************************************

Hsp16_3_pET28_-_clona_2     ATTCGCGTACGGTTCCTTCGTTCGCACGGTGTCGCTGCCGGTAGGTGCTGACGAGGACGA
Hsp16_3_pET28_-_clona_1     ATTCGCGTACGGTTCCTTCGTTCGCACGGTGTCGCTGCCGGTAGGTGCTGACGAGGACGA
Hsp16.3                     ATTCGCGTACGGTTCCTTCGTTCGCACGGTGTCGCTGCCGGTAGGTGCTGACGAGGACGA
                            ************************************************************

Hsp16_3_pET28_-_clona_2     CATTAAGGCCACCTACGACAAGGGCATTCTTACTGTGTCGGTGGCGGTTTCGGAAGGGAA
```

```
Hsp16_3_pET28_-_clona_1      CATTAAGGCCACCTACGACAAGGGCATTCTTACTGTGTCGGTGGCGGTTTCGGAAGGGAA
Hsp16.3                      CATTAAGGCCACCTACGACAAGGGCATTCTTACTGTGTCGGTGGCGGTTTCGGAAGGGAA
                             ************************************************************

Hsp16_3_pET28_-_clona_2      GCCAACCGAAAAGCACATTCAGATCCGGTCCACCAACCTCGAGCACCCG
Hsp16_3_pET28_-_clona_1      GCCAACCGAAAAGCACATTCAGATCCGGTCCACCAACCTCGAGCACC--
Hsp16.3                      GCCAACCGAAAAGCACATTCAGATCCGGTCCACCAAC------------
                             ************************************
```

Appendix 1.2: Alignment of clones pET28a-Hsp16.3 obtained by sequencing (Macrogen), with the theoretical sequence Hsp16.3 (purple) (**Accession number: Rv2031c**), using CLUSTAL multiple sequence alignment in MUSCLE 3.8 (http://www.ebi.ac.uk/Tools/msa/muscle/).

```
hypothetical_protein_M_xenopi_WP     --TTLAIQRHPRSLFPEFSELFTAFPSFTGLHPIFDARLMRLEDEKKEGRYEVRAEIPGV
hypothetical_protein_M_angelicum     --STVPAQRASRSLFPEFPDLFAAFPSFAGLRPVIDTRAMRLEDEMKDGRYEVRAEIPGV
hypothetical_protein_M_shimoidei     --TAVQVQHQPRPLFPEISELFTAFPSFAGLRPVFDTRLMRLEDEMKDGRYEVRAEIPGV
hypothetical_protein_M_shinjukue     --TTLPVQRQMRSLFPEFSELFAAFPSFAGIRPAFDTRIMRLEDEMKEGRYLVRAEIPGV
hypothetical_protein_M_              --TALPVQRQPRSRFREFSELFAAFPSFAGLRPVFDTRLMRLEDEMKEGRYEVRAELPGV
HspX_MTB_RGTB327_AFE16906.1          MATTLPVQRHPRSLFPEFSELFAAFPSFAGLRPTFDTRLMRLEDEMKEGRYEVRAELPGV
hypothetical_protein_MTB_WP_0573     MATTLPVQRHPRSLFPEFSELFAAFPSFAGLRPTFDTRLMRLEDEMKEGRYEVRAELPGV
hspX_MTB_str.Haarlem/NITR202_AGL     MATTLPVQRHPRSLFPEFSELFAAFPSFAGLRPTFDTRLMRLXDEMKEGRYEVRAELPGV
hypothetical_protein_MTB_WP_0571     MAATLPVQRHPRSLFPEFSELFAAFPSFAGLRPTFDTRLMRLEDEMKEGRYEVRAELPGV
hypothetical_protein_M_canettii_     MATTLPVQRHPRSLFPEFSELFAAFPSFAGLRPTFDTRLMRLEDEMKEGRYEVRAELPGV
antigen_MTB_WP_031729373.1           MATTLPAQRHPRSLFPEFSELFAAFPSFAGLRPTFDTRLMRLEDEMKEGRYEVRAELPGV
hspX_MTB_SUMu002_EFP15883.1          MATTLPVQRYPRSLFPEFSELFAAFPSFAGLRPTFDTRLMRLEDEMKEGRYEVRAELPGV
Hsp16.3_rec_MTB.                     MATTLPVQRHPRSLFPEFSELFAAFPSFAGLRPTFDTRLMRLEDEMKEGRYEVRAELPGV
alpha-crystallin_MTB_complex         MATTLPVQRHPRSLFPEFSELFAAFPSFAGLRPTFDTRLMRLEDEMKEGRYEVRAELPGV
hspX_MTB_                            MATTLPVQRHPRSLFPEFSELFAAFPSFAGLRPTFDTRLMRLEDEMKEGRYEVRAELPGV
19kda_major_membrane_protein_MTB     -ATTLPVQRHPRSLFPEFSELFAAFPSFAGLRPTFDTRLMRLEDEMKEGRYEVRAELPGV
AGZ53357.1                           MMTTLPVKREQHSLFPEFSDLFTAFPSFAGLRPMFDTRLMRLEDEMAEGRYEVRAEMPGI
WP_036413084.1                       --TTLPVKREPHSLFPEFSDLFSAFPSFAGLRPMFDTRLMRLEDEMAEGRYVVRAEMPGI
hypothetical_protein_M_mantenii_     MTTTLPATQKPRSLLPEFSDFFAAFPSFAGIRPLFDTRLMRLEDEMAEGRYEVRAEIPGI
hypothetical_protein_M_lacus_WP_     --TTLPVSRRPRSLFPEFSEFFSAFPSFAGVRPLFDTRLMRLEDEMTDGRYEVRAEIPGI
hypothetical_protein_M_mantenii_     --STVSLRRRPMSLFPEFSELFAGFPSLAGLRPAFDTRVMRLEDEMKDGRYVVRAEMPGV
antigen_M_nebraskense_WP_0461860     --TILPV-RRPRSLFPEFSDLFAGFPALTGLRPVFDTRMMRLEDEMKEGRYVVRAEIPGV
                                       : :   .   . : *:.::*:.**:::*:.* :*:* *** **  :*** ****:**:

hypothetical_protein_M_xenopi_WP     DPAKDIDITVRDGQLTIKAERREKKEFNGRSEFSYGSFARTVSLPAGANEDDVKATYDNG
hypothetical_protein_M_angelicum     DPAKDIDITVRDGQLTIKAERSEKKDFDGRSEFSYGSFVRTLSLPDGADDGDIKATYDKG
hypothetical_protein_M_shimoidei     DPAENIDVTVHDGQLTIKAERSEKKDFDGRSEFNYGSFVRTVSLPAGADEDDVKATYDKG
hypothetical_protein_M_shinjukue     DPTKDIDITVRDGQLTIKAERSEKKEFDGRSEFTYGTFVRTVSLPAGADEDTIEATYDQG
hypothetical_protein_M_              DPTKDVDITVRDGQLTIKAERSEKKDFDGRSEFSYGSFVRTVTLPPGADEDDVKATYDKG
HspX_MTB_RGTB327_AFE16906.1          DPDKDVDIMVRDGQLTIKAERTEQKDFDGRSEFAYGSFVRTVSLPVGADEDDIKATYDKG
hypothetical_protein_MTB_WP_0573     DPDKDVDIMVRDGQLTIKAERTEQKDFDGRSEFAYGSFVRTVSLPVGADEDDIKATYDKG
hspX_MTB_str.Haarlem/NITR202_AGL     DPDKDVDIMVRDGQLTIKAERTEQKDFDGRSEFAYGSFVRTVSLPVGADEDDIKATYDKG
hypothetical_protein_MTB_WP_0571     DPDKDVDIMVRDGQLTIKAERTEQKDFDGRSEFAYGSFVRTVSLPVGADEDDIKATYDKG
hypothetical_protein_M_canettii_     DPDKDVDIMVRDGQLTIKAERTEQKDFDGRSEFAYGSFVRTVSLPVGADEDDIKATYDKG
antigen_MTB_WP_031729373.1           DPDKDVDIMVRDGQLTIKAERTEQKDFDGRSEFAYGSFVRTVSLPVGADEDDIKATYDKG
hspX_MTB_SUMu002_EFP15883.1          DPDKDVDIMVRDGQLTIKAERTEQKDFDGRSEFAYGSFVRTVSLPVGADEDDIKATYDKG
Hsp16.3_rec_MTB.                     DPDKDVDIMVRDGQLTIKAERTEQKDFDGRSEFAYGSFVRTVSLPVGADEDDIKATYDKG
alpha-crystallin_MTB_complex         DPDKDVDIMVRDGQLTIKAERTEQKDFDGRSEFAYGSFVRTVSLPVGADEDDIKATYDKG
hspX_MTB_                            DPDKDVDIMVRDGQLTIKAERTEQKDFDGRSEFAYGSFVRTVSLPVGADEDDIKATYDKG
19kda_major_membrane_protein_MTB     DPDKDVDIMVRDGQLTIKAERTEQKDFDGRSEFAYGSFVRTVSLPVGADEDDIKATYDKG
AGZ53357.1                           DPAKDVDITVRNGQLTIKAERTEKKEFEGRSEFSYGSFVRTVSLPDGADEDDIKATYDKG
WP_036413084.1                       DPAKDVDITVRNGQLTIKAERTEKKEFEGRSEFSYGSFVRTVSLPEGADEDDIKATYDKG
hypothetical_protein_M_mantenii_     DPDKDVDVTVRDGQLTIKAERSEKKEFDGRSEFSYGSFVRTVSLPAGADEDDIRATYDKG
hypothetical_protein_M_lacus_WP_     DPAKDVDITVHNGQLTIKAERSEKKEFDGRSEFSYGSFVRTVSLPAGANEDDIKATYDKG
hypothetical_protein_M_mantenii_     DPAKDIDITVRDGHLTIKAERSERKDFDGRSEFSYGTFVRSVSLPAGADEGSIEATYDKG
antigen_M_nebraskense_WP_0461860     DPAKNLDVTVRDGQLTIKAERSEKKDFDGRSEFSYGSFIRTVALPAGADEENIEANYDKG
                                     ** :::*: *.:*:******* *.*:*:***** **:* *:::** **::  : *.**:*

hypothetical_protein_M_xenopi_WP     ILTVSVAVTEATPTEKHVPISS--
hypothetical_protein_M_angelicum     ILTISVAVAQKKPAERRVQIQSPN
hypothetical_protein_M_shimoidei     ILVVSVGISESKPPEKHVPITVAN
hypothetical_protein_M_shinjukue     ILTVAVAVAEPKPAERHVQVHSVN
hypothetical_protein_M_              ILTISVAVSESKPAEKHVPIAAAS
HspX_MTB_RGTB327_AFE16906.1          ILTLC-------------------
hypothetical_protein_MTB_WP_0573     ILTVSVAVSEGKPNEKHIQIRSTN
hspX_MTB_str.Haarlem/NITR202_AGL     ILTVSVAVSEGKPTEKHIQIRSTN
hypothetical_protein_MTB_WP_0571     ILTVSVAVSEGKPTEKHIQIRSTN
hypothetical_protein_M_canettii_     ILTVSVAVSEGRPTEKHIQIRSTN
antigen_MTB_WP_031729373.1           ILTVSVAVSEGKPTEKHIQIRSTN
hspX_MTB_SUMu002_EFP15883.1          ILTVSVAVSEGKPTEKHIQIRSTN
Hsp16.3_rec_MTB.                     ILTVSVAVSEGKPTEKHIQIRSTN
alpha-crystallin_MTB_complex         ILTVSVAVSEGKPTEKHIQIRSTN
hspX_MTB_                            ILTVSVAVSEGKPTEKHIQIRSTN
```

```
19kda_major_membrane_protein_MTB      ILTVSVAVSEGKPTEKHIQIRSTN
AGZ53357.1                            ILTVSVGVSEPAKPEKHIQVATN-
WP_036413084.1                        ILTVSVGVSEPAKPEKHIQV----
hypothetical_protein_M_mantenii_      ILTVSVKVSEPASAEKHVQV----
hypothetical_protein_M_lacus_WP_      ILAVSVGVSESAPAEKHVQITTN-
hypothetical_protein_M_mantenii_      ILTVAVAVSEAKPAERHIEVQSAN
antigen_M_nebraskense_WP_0461860      ILTVSVAVSEAKPAERHVQVQSN-
                                      **.:.
```

Appendix 1.3: Alignment of Hsp16.3 from MTB sequences with other Mycobacteria (http://www.ebi.ac.uk/Tools/msa/clustalw2/).

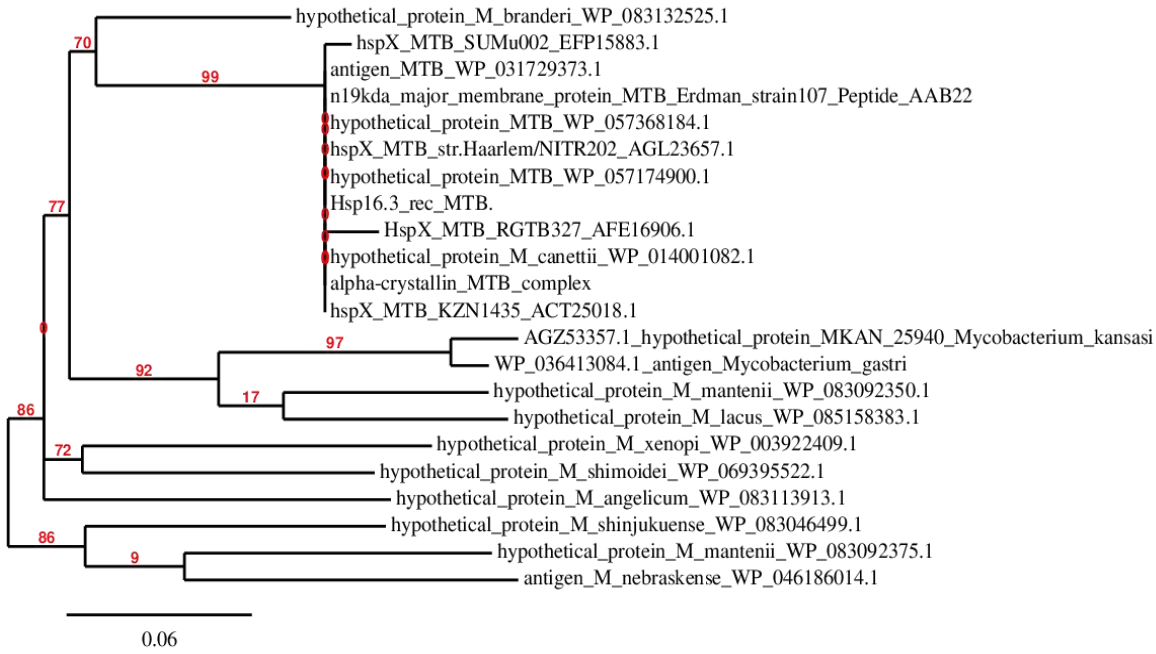

Appendix 1.4: Phylogenetic tree of the amino acid sequence of recombinant Hsp16.3 from MTB, compared with Hsp16.3 from other Mycobacteria. In red it indicates the percentage of support of the branches of the tree.

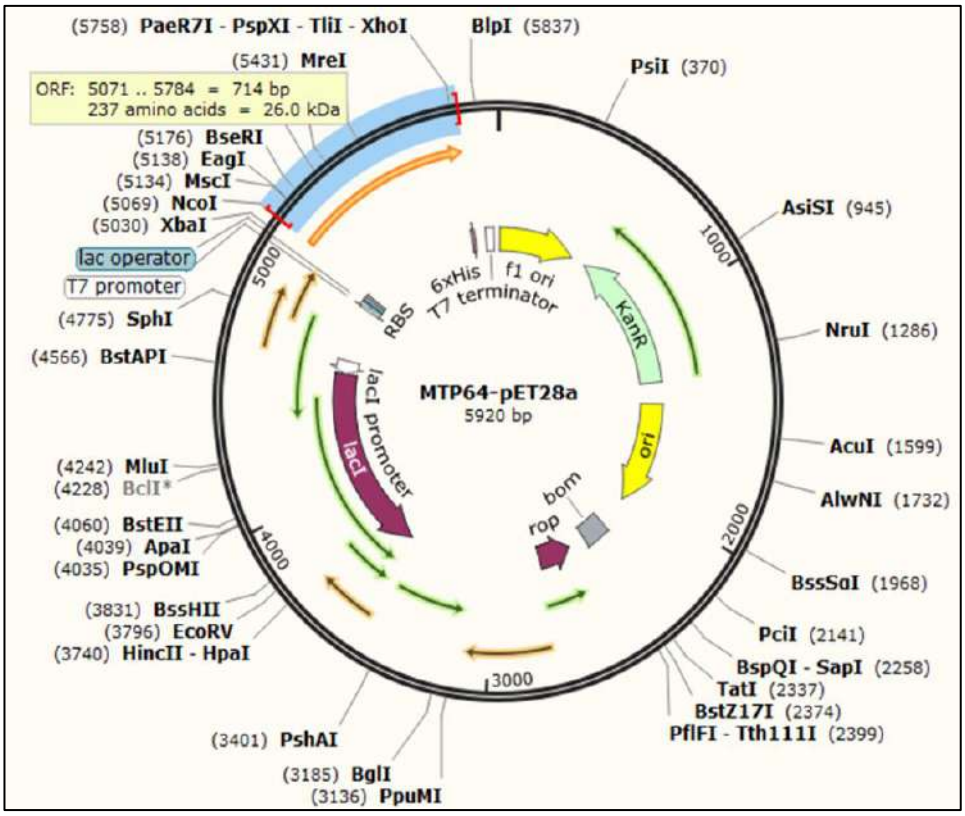

Appendix 1.5: *In silico* ligation of MPT64 in pET28a (+).

```
MPT64                                   ------------------------------------ATGGTGCGCATCAAGATCTTCATG
MPT64_pET28_-clona_1_promoter           -----ATTTTGTTTAACTTTAAGAAGGAGATATACCATGGTGCGCATCAAGATCTTCATG
MPT64_pET28_-_clona_1_terminator        AAATAATTTTGTTTAACTTTAAGAAGGAGATATACCATGGTGCGCATCAAGATCTTCATG
                                                                             ************************

MPT64                                   CTGGTCACGGCTGTCGTTTTGCTCTGTTGTTCGGGTGTGGCCACGGCCGCGCCCAAGACC
MPT64_pET28_-clona_1_promoter           CTGGTCACGGCTGTCGTTTTGCTCTGTTGTTCGGGTGTGGCCACGGCCGCGCCCAAGACC
MPT64_pET28_-_clona_1_terminator        CTGGTCACGGCTGTCGTTTTGCTCTGTTGTTCGGGTGTGGCCACGGCCGCGCCCAAGACC
                                        ************************************************************

MPT64                                   TACTGCGAGGAGTTGAAAGGCACCGATACCGGCCAGGCGTGCCAGATTCAAATGTCCGAC
MPT64_pET28_-clona_1_promoter           TACTGCGAGGAGTTGAAAGGCACCGATACCGGCCAGGCGTGCCAGATTCAAATGTCCGAC
MPT64_pET28_-_clona_1_terminator        TACTGCGAGGAGTTGAAAGGCACCGATACCGGCCAGGCGTGCCAGATTCAAATGTCCGAC
                                        ************************************************************

MPT64                                   CCGGCCTACAACATCAACATCAGCCTGCCCAGTTACTACCCCGACCAGAAGTCGCTGGAA
MPT64_pET28_-clona_1_promoter           CCGGCCTACAACATCAACATCAGCCTGCCCAGTTACTACCCCGACCAGAAGTCGCTGGAA
MPT64_pET28_-_clona_1_terminator        CCGGCCTACAACATCAACATCAGCCTGCCCAGTTACTACCCCGACCAGAAGTCGCTGGAA
                                        ************************************************************

MPT64                                   AATTACATCGCCCAGACGCGCGACAAGTTCCTCAGCGCGGCCACATCGTCCACTCCACGC
MPT64_pET28_-clona_1_promoter           AATTACATCGCCCAGACGCGCGACAAGTTCCTCAGCGCGGCCACATCGTCCACTCCACGC
MPT64_pET28_-_clona_1_terminator        AATTACATCGCCCAGACGCGCGACAAGTTCCTCAGCGCGGCCACATCGTCCACTCCACGC
                                        ************************************************************

MPT64                                   GAAGCCCCCTACGAATTGAATATCACCTCGGCCACATACCAGTCCGCGATACCGCCGCGT
MPT64_pET28_-clona_1_promoter           GAAGCCCCCTACGAATTGAATATCACCTCGGCCACATACCAGTCCGCGATACCGCCGCGT
MPT64_pET28_-_clona_1_terminator        GAAGCCCCCTACGAATTGAATATCACCTCGGCCACATACCAGTCCGCGATACCGCCGCGT
                                        ************************************************************

MPT64                                   GGTACGCAGGCCGTGGTGCTCAAGGTCTACCAGAACGCCGGCGGCACGCACCCAACGACC
MPT64_pET28_-clona_1_promoter           GGTACGCAGGCCGTGGTGCTCAAGGTCTACCAGAACGCCGGCGGCACGCACCCAACGACC
MPT64_pET28_-_clona_1_terminator        GGTACGCAGGCCGTGGTGCTCAAGGTCTACCAGAACGCCGGCGGCACGCACCCAACGACC
                                        ************************************************************

MPT64                                   ACGTACAAGGCCTTCGATTGGGACCAGGCCTATCGCAAGCCAATCACCTATGACACGCTG
MPT64_pET28_-clona_1_promoter           ACGTACAAGGCCTTCGATTGGGACCAGGCCTATCGCAAGCCAATCACCTATGACACGCTG
MPT64_pET28_-_clona_1_terminator        ACGTACAAGGCCTTCGATTGGGACCAGGCCTATCGCAAGCCAATCACCTATGACACGCTG
```

```
                                    ************************************************************

MPT64                               TGGCAGGCTGACACCGATCCGCTGCCAGTCGTCTTCCCCATTGTGCAAGGTGAACTGAGC
MPT64_pET28_-clona_1_promoter       TGGCAGGCTGACACCGATCCGCTGCCAGTCGTCTTCCCCATTGTGCAAGGTGAACTGAGC
MPT64_pET28_-_clona_1_terminator    TGGCAGGCTGACACCGATCCGCTGCCAGTCGTCTTCCCCATTGTGCAAGGTGAACTGAGC
                                    ************************************************************

MPT64                               AAGCAGACCGGACAACAGGTATCGATAGCGCCGAATGCCGGCTTGGACCCGGTGAATTAT
MPT64_pET28_-clona_1_promoter       AAGCAGACCGGACAACAGGTATCGATAGCGCCGAATGCCGGCTTGGACCCGGTGAATTAT
MPT64_pET28_-_clona_1_terminator    AAGCAGACCGGACAACAGGTATCGATAGCGCCGAATGCCGGCTTGGACCCGGTGAATTAT
                                    ************************************************************

MPT64                               CAGAACTTCGCAGTCACGAACGACGGGGTGATTTTCTTCTTCAACCCGGGGGAGTTGCTG
MPT64_pET28_-clona_1_promoter       CAGAACTTCGCAGTCACGAACGACGGGGTGATTTTCTTCTTCAACCCGGGGGAGTTGCTG
MPT64_pET28_-_clona_1_terminator    CAGAACTTCGCAGTCACGAACGACGGGGTGATTTTCTTCTTCAACCCGGGGGAGTTGCTG
                                    ************************************************************

MPT64                               CCCGAAGCAGCCGGCCCAACCCAGGTATTGGTCCCACGTTCCGCGATCGACTCGATGCTG
MPT64_pET28_-clona_1_promoter       CCCGAAGCAGCCGGCCCAACCCAGGTATTGGTCCCACGTTCCGCGATCGACTCGATGCTG
MPT64_pET28_-_clona_1_terminator    CCCGAAGCAGCCGGCCCAACCCAGGTATTGGTCCCACGTTCCGCGATCGACTCGATGCTG
                                    ************************************************************

MPT64                               GCC--------------------------
MPT64_pET28_-clona_1_promoter       GCCCTCGAGCACCACCACCACCACCACTG
MPT64_pET28_-_clona_1_terminator    GCCCTCGAGCACCACCACCACCACCACTG
                                    ***
```

Appendix 1.6: Alignment of the theoretical sequence MPT64 and the promoter and terminator sequences of clone pET28a-MPT64 obtained by sequencing (Macrogen). The alignment was performed in CLUSTAL multiple sequence alignment by MUSCLE 3.8 (http://www.ebi.ac.uk/Tools/msa/muscle/).

```
WP_036416207.1_DUF3298_domain-      -MRITVPLLVLAVVTLGSPAVAAAAP-KTYCDELKGTTTGQVCQIQISDP
WP_083153218.1_DUF3298_domain-      -MRITAPLVVLAVVALGSPAIAAAAP-KTYCDELKGATTGQVCQIQVSDP
ORB83212.1_MPB64_M_kansasii         -MRIKVPLLVLAVVALGSPAVAAAAP-KTYCDELKGTVAGQVCQIQMSDP
Mpt64_rec_MTB                       -VRIKIFMLVTAVVLLCCSGVATAAP-KTYCEELKGTDTGQACQIQMSDP
AAK46307.1_MPB64/MPT64_CDC1551      -VRIKIFMLVTAVVLLCCSGVATAAP-KTYCEELKGTDTGQACQIQMSDP
WP_003409954.1_hypothetical_pr      -MRIKIFMLVTAVVLLCCSGVATAAP-KTYCEELKGTDTGQACQIQMSDP
WP_079367536.1_DUF3298_domain-      -MRIKIFMLVTAVVLLCCSGVATAAP-KTYCEELKGTDTGQACQIQMSDP
AGL23606.1_hypothetical_protei      -MRIKIFMLVTAVVLLCCSGVATAAP-KTYCEELKGTDTGQACQIQMSDP
WP_014001044.1_DUF3298_domain-      -MRIKIFMLVTAVVLLCCSGVATAAP-KTYCEELKGTDTGQACQIQTSDP
WP_085250794.1_DUF3298_domain-       MRIVKIAMLITAVVLIGCPAVAAAAP-KSYCENLNGTVNGQTCQIQVSDP
WP_020727003.1_DUF3298_domain-       MRHIMMFVLVTFATLFGSTGLAAAAPPKSYCDELKGTTTGEVCKIQMTEP
WP_047315949.1_DUF3298_domain-      -MRITVAVLVAASVLFGCPGVAAAAP-KTFCDELKGVIAGQVCQIQITDP
OBF81347.1_MPB64_Mycobacterium      -------MLVAAAAIVGSNGVAGAAP-KDYCADLKGGNTGKTCEIQLSDP
                                           :::   . . . .:* *** * :* :*:*   *:.*:** ::*

WP_036416207.1_DUF3298_domain-      AYNVNISLPSNYPDQKSLQSYVAQTRDDFLNVAKSSAPREAPYQLEITST
WP_083153218.1_DUF3298_domain-      AYTINISLPSNYPDQKSLQSYVAQTRDDFLNVAKSSAPRDAPYQLEITST
ORB83212.1_MPB64_M_kansasii         GYTINISLPSNYPDQKSLQSYVEQTRDDFLNVAKSSAPRDAPYQLEITSA
Mpt64_rec_MTB                       AYNINISLPSYYPDQKSLENYIAQTRDKFLSAATSSTPREAPYELNITSA
AAK46307.1_MPB64/MPT64_CDC1551      AYNINISLPSYYPDQKSLENYIAQTRDKFLSAATSSTPREAPYELNITSA
WP_003409954.1_hypothetical_pr      AYNINISLPSYYPDQKSLENYIAQTRDKFLSAATSSTPREAPYELNITSA
WP_079367536.1_DUF3298_domain-      AYNINISLPSYYPDQKSLENYIAQTRDKFLSAATSSTPREAPYELNITSA
AGL23606.1_hypothetical_protei      AYNINISLPSYYPDQKSLENYIAQTRDKFLSAATSSTPREAPYELNITSA
WP_014001044.1_DUF3298_domain-      AYNINISLPSYYPDQKSLENYIAQTRDKFLSAATSSTPREAPYELNITSA
WP_085250794.1_DUF3298_domain-      AYNIQITLPSYYPDQKSLETYVTQTRDTFLSTAKSSTPREHPYELDITST
WP_020727003.1_DUF3298_domain-      GYTVDISLPSNYPDGKSLESFVRETGEHFLDKAKSSTARDAPYELDITST
WP_047315949.1_DUF3298_domain-      AYKIDISLPSFYPDQKALQDYVAQTRDGFVNAAKSAPPRDVPNELDITSA
OBF81347.1_MPB64_Mycobacterium      GYRVDISIPLDYPDQKSVADYISQTRDGFLNVAKSGAPRDTPYELTIKPT
                                    .* ::*::*  *** *::  :: :* : *:. *.*...*: * :* *..:

WP_036416207.1_DUF3298_domain-      NYESAIPPRGTQSLVLKVVQNVGNGQPTTKYKAFNWDQGYRKPITYDTLW
WP_083153218.1_DUF3298_domain-      NYESAIPPRGTQSLVLKVVQNVGSGQPTTKYKAFNWDQGYRKPITYDTLW
ORB83212.1_MPB64_M_kansasii         TYESAIPPRGTQSLVLKVVQNVGSGQPTTKYKAFNWDQGYRKPITYDTLW
Mpt64_rec_MTB                       TYQSAIPPRGTQAVVLKVYQNAGGTHPTTTYKAFDWDQAYRKPITYDTLW
AAK46307.1_MPB64/MPT64_CDC1551      TYQSAIPPRGTQAVVLKVYQNAGGTHPTTTYKAFDWDQAYRKPITYDTLW
WP_003409954.1_hypothetical_pr      TYQSAIPPRGTQAVVLKVYQNAGGTHPTTTYKAFDWDQAYRKPITYDTLW
WP_079367536.1_DUF3298_domain-      TYQSAIPPRGTQAVVLKVYQNAGSTHPTTTYKAFDWDQAYRKPITYDTLW
```

```
AGL23606.1_hypothetical_protei      TYQSAIPPRGTQAVVLKVYQNAGGTHPTTTYKAFDWDQAYRKPITYDTLW
WP_014001044.1_DUF3298_domain-      TYQSAIPPRGTQAVVLKVYQNAGGTHPTTTYKAFDWDQAYRKPITYDTLW
WP_085250794.1_DUF3298_domain-      DYGSAIPPRGTQAVVLKVYQNLGGAHPQISYKAFNWDQAYRKAITFDTLW
WP_020727003.1_DUF3298_domain-      NYESAIPPRGTQSVVLKIYQNVGGPRPQTTYKAFNWDQAYRKPITWDKLW
WP_047315949.1_DUF3298_domain-      PYGSAVPPRGTQSLVLKIYQTVGDAPPQTSYKAFNWDQGYRKPITYTTLW
OBF81347.1_MPB64_Mycobacterium      EYNSAIPPRGTQAVVFKVYQNVGGAHPQTTFKAFNWDQTYRKAITYTAAS
                                     * **:******:*:*:*: *. *.  *  .:***:*** ***.**:

WP_036416207.1_DUF3298_domain-      QPK--------TDPLPTVFPIVQTVLQKQTG-------------------
WP_083153218.1_DUF3298_domain-      QPK--------TDPLPIVFPIVQTALQKQTG-------------------
ORB83212.1_MPB64_M_kansasii         QPK--------TDPLPTVFPIVQTALQKQTG-------------------
Mpt64_rec_MTB                       QAD--------TDPLPVVFPIVQGELSKQTG-------------------
AAK46307.1_MPB64/MPT64_CDC1551      QAD--------TDPLPVVFPIVQGELSKQTG-------------------
WP_003409954.1_hypothetical_pr      QAD--------TDPLPVVFPIVQGELSKQTG-------------------
WP_079367536.1_DUF3298_domain-      QAD--------TDPLPVVFPIVQGELSKQTG-------------------
AGL23606.1_hypothetical_protei      QAD--------TDPLPVVFPVQG-ELSKQTG-------------------
WP_014001044.1_DUF3298_domain-      QAD--------TDPLPVVFPIVQGELSKQTG-------------------
WP_085250794.1_DUF3298_domain-      KPD--------TDPLPVVFPIVQAELQKQTG-------------------
WP_020727003.1_DUF3298_domain-      QPE--------TDPLKVVFPIVESELSKQSE-------------------
WP_047315949.1_DUF3298_domain-      KPD--------TDPLPAVFPIVQAELQKQTG-------------------
OBF81347.1_MPB64_Mycobacterium      DDKEHTPLWRVDDPLKTVAPIVQAELQKQLAPTPPPAQPGQPATATPTPA
                                    . .         ***  * *:    *.**

WP_036416207.1_DUF3298_domain-      QQV--APAAGLDPANYQNFAITNDGVTFFFNPGELLPESAGPTQASVPRS
WP_083153218.1_DUF3298_domain-      QQV--APAAGLDPANYQNFAITNDGVTFFFNPGELLPESAGPTQASVPRS
ORB83212.1_MPB64_M_kansasii         QQI--ATTAGLDPANYQNFAVTNDGVTFFFNPGELLPESAGPLQVSVPRS
Mpt64_rec_MTB                       QQVSIAPNAGLDPVNYQNFAVTNDGVIFFFNPGELLPEAAGPTQVLVPRS
AAK46307.1_MPB64/MPT64_CDC1551      QQVSIAPNAGLDPVNYQNFAVTNDGVIFFFNPGELLPEAAGPTQVLVPRS
WP_003409954.1_hypothetical_pr      QQVSIAPNAGLDPVNYQNFAVTNDGVIFFFNPGELLPEAAGPTQVLVPRS
WP_079367536.1_DUF3298_domain-      QQVSIAPNAGLDPVNYQNFAVTNDGVIFFFNPGELLPEAAGPTQVLVPRS
AGL23606.1_hypothetical_protei      QQVSIAPNAGLDPXBYQXFAVTNDGVIFFFNPGELLPEAAGPTQVLVPRS
WP_014001044.1_DUF3298_domain-      QQVSIAPNAGLDPVNYQNFAVTNDGVIFFFNPGELLPEAAGPTQVLVPRS
WP_085250794.1_DUF3298_domain-      QQVSIAPAAGLDPTNYQNFAITNDGVIFFFSQGGLLPESAGATQALVPRT
WP_020727003.1_DUF3298_domain-      EQVVIASSAGLDPKNYQNFAISNDGITFFFSPGELLPEAAGARQVLVPRA
WP_047315949.1_DUF3298_domain-      QPVAIAPDVGLDPANYQNFAITNDGLIFFFSQGQLLPAAVGATQAVVPRS
OBF81347.1_MPB64_Mycobacterium      PPLPIAQPALYNPANYQNFAVVNDGVIFFFDQGVLLPDSFGALQVLVPRS
                                      :  *  .  :*  ** **: ***: ***. * *** : *. *. ***:

WP_036416207.1_DUF3298_domain-      AIDSMLA
WP_083153218.1_DUF3298_domain-      AIDSMLA
ORB83212.1_MPB64_M_kansasii         AIDSMLA
Mpt64_rec_MTB                       AIDSMLA
AAK46307.1_MPB64/MPT64_CDC1551      AIDSMLA
WP_003409954.1_hypothetical_pr      AIDSMLA
WP_079367536.1_DUF3298_domain-      AIDSMLA
AGL23606.1_hypothetical_protei      AIDSMLA
WP_014001044.1_DUF3298_domain-      AIDSMLA
WP_085250794.1_DUF3298_domain-      AIDPMLA
WP_020727003.1_DUF3298_domain-      AVDPMLA
WP_047315949.1_DUF3298_domain-      VVDPMLA
OBF81347.1_MPB64_Mycobacterium      AIDPMLA
                                    .:*.***
```

Appendix 1.7: Alignment of MPT64 from MTB sequences with other Mycobacteria (http://www.ebi.ac.uk/Tools/msa/clustalw2/).

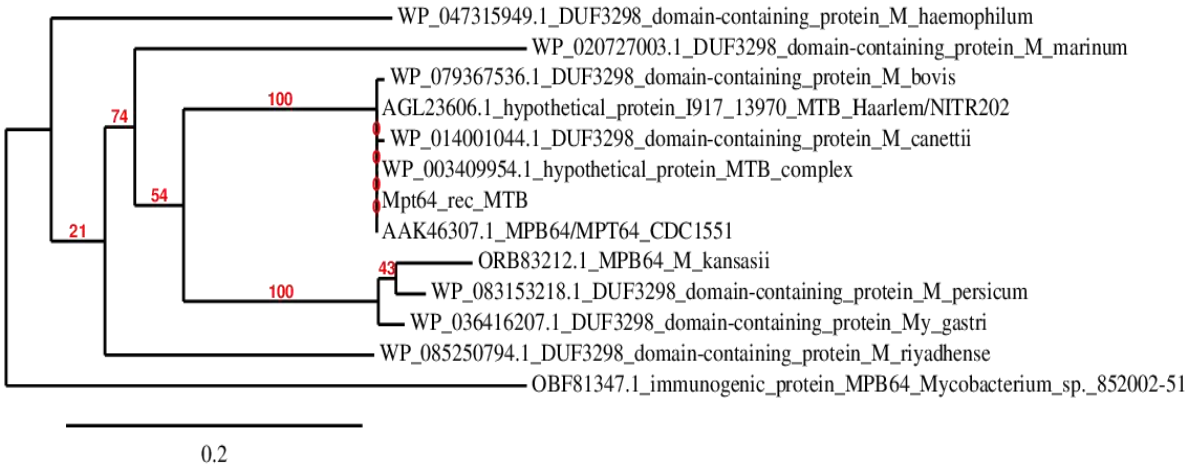

Appendix 1.8: Phylogenetic tree of the amino acid sequence of recombinant MPT64 from MTB, compared with MPT64/MBP64 and DUF3298 from other Mycobacteria. In red it indicates the percentage of support of the branches of the tree.

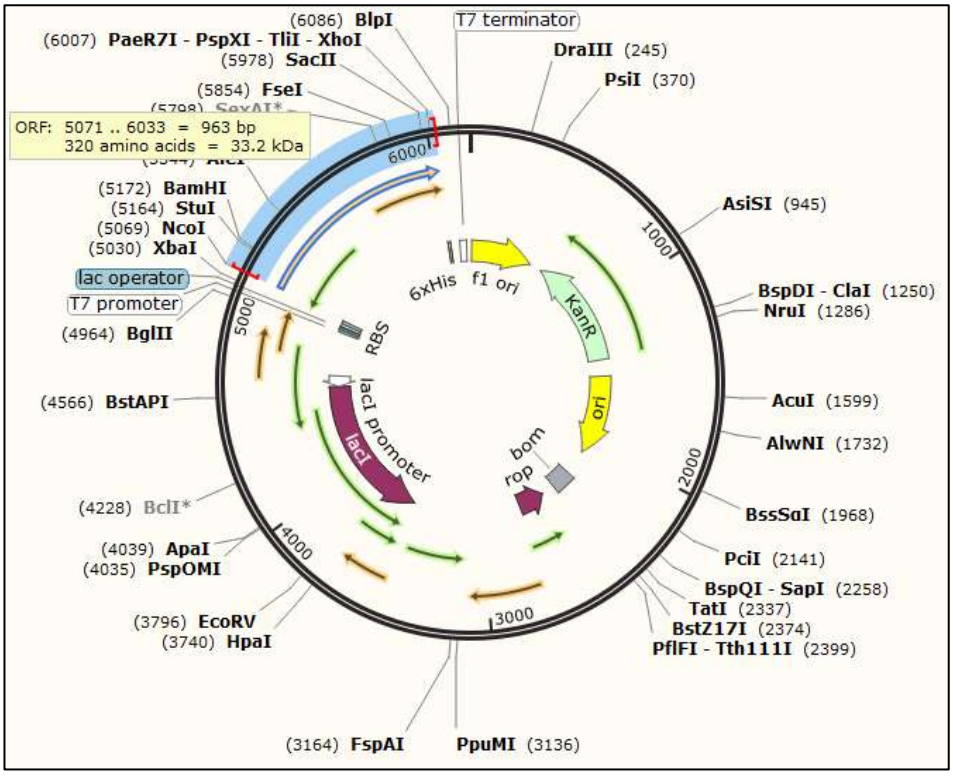

Appendix 1.9: *In silico* linkage of MTC28 in pET28a (+).

```
MTC28_pET28_-clona_5      ATACCATGGGGATGATCCAGATCGCGCGCACCTGGCGGGTCTTCGCAGGCGGCATGGCCA
MTC28                     ----------ATGATCCAGATCGCGCGCACCTGGCGGGTCTTCGCAGGCGGCATGGCCA
MTC28_pET28_-clona_6      ATACCATGGGGATGATCCAGATCGCGCGCACCTGGCGGGTCTTCGCAGGCGGCATGGCCA
                                  **********************************************

MTC28_pET28_-clona_5      CCGGTTTCATCGGCGTGGTGCTGGTCACCGCCGGGAAGGCCTCACCGGATCCCCTGCTAC
MTC28                     CCGGTTTCATCGGCGTGGTGCTGGTCACCGCCGGGAAGGCCTCAGCGGATCCCCTGCTGC
MTC28_pET28_-clona_6      CCGGTTTCATCGGCGTGGTGCTGGTCACCGCCGGGAAGGCCTCAGCGGATCCCCTGCTGC
                          ****************************************** ************ *

MTC28_pET28_-clona_5      CACCNNCGCCTATCCCTGCCCCAGTCTCGGCGCCGGCAACAGTCCCGCCCGTGCAGAACC
MTC28                     CACCGCCGCCTATCCCTGCCCCAGTCTCGGCGCCGGCAACAGTCCCGCCCGTGCAGAACC
MTC28_pET28_-clona_6      CACCGCCGCCTATCCCTGCCCCAGTCTCGGCGCCGGCAACAGTCCCGCCCGTGCAGAACC
                          ****  **************************************************

MTC28_pET28_-clona_5      TCACGGCGCTTCCGGNCNNGANNAGCAACNNNTTNTNACCGGCGCCAGCANCCGCACCGA
MTC28                     TCACGGCGCTTCCGGGCGGGAGCAGCAACAGGTTCTCACCGGCGCCAGCACCCGCACCGA
MTC28_pET28_-clona_6      TCACGGCGCTTCCGGGCGGGAGCAGCAACAGGTTCTCACCGGCGCCAGCACCCGCACCGA
                          *************** *  **  ******   ** * ************ *********

MTC28_pET28_-clona_5      TCGAGTNGCCGATTCCGGTCGGAGCACCCGGGTCCACCGCTGTGCCCCCGCTGCCGCCGC
MTC28                     TCGCGTCGCCGATTCCGGTCGGAGCACCCGGGTCCACCGCTGTGCCCCCGCTGCCGCCGC
MTC28_pET28_-clona_6      TCGCGTCGCCGATTCCGGTCGGAGCACCCGGGTCCACCGCTGTGCCCCCGCTGCCGCCGC
                          *** ** **************************************************

MTC28_pET28_-clona_5      CAGTGACTCCCGCGATCAGCGGCACACTTCGGGACCACCTCCGGGAGAAGGGCGTCAAGC
MTC28                     CAGTGACTCCCGCGATCAGCGGCACACTTCGGGACCACCTCCGGGAGAAGGGCGTCAAGC
MTC28_pET28_-clona_6      CAGTGACTCCCGCGATCANCGGCACACTTCGGGACCACCTCCGGGAGAAGGGCGTCAAGC
                          ****************** ****************************************

MTC28_pET28_-clona_5      TGGAGGCACAGCGACCGCACGGATTCAAGGCGCTCGACATCACACTGCCCATGCCGCCGC
MTC28                     TGGAGGCACAGCGACCGCACGGATTCAAGGCGCTCGACATCACACTGCCCATGCCGCCGC
MTC28_pET28_-clona_6      TGGAGGCACAGCGACCGCACGGATTCAAGGCGCTCGACATCACACTGCCCATGCCGCCGC
                          ************************************************************

MTC28_pET28_-clona_5      GCTGGACTCAGGTGCCCGACCCCAACGTGCCCGACGCGTTCGTGGTGATCGCCGACCGGT
MTC28                     GCTGGACTCAGGTGCCCGACCCCAACGTGCCCGACGCGTTCGTGGTGATCGCCGACCGGT
MTC28_pET28_-clona_6      GCTGGACTCAGGTGCCCGACCCCAACGTGCCCGACGCGTTCGTGGTGATCGCCGACCGGT
                          ************************************************************

MTC28_pET28_-clona_5      TGGGCAACAGCGTCTACACGTCGAATGCGCAGCTGGTGGTGTATAGGCTGATCGGTGACT
MTC28                     TGGGCAACAGCGTCTACACGTCGAATGCGCAGCTGGTGGTGTATAGGCTGATCGGTGACT
MTC28_pET28_-clona_6      TGGGCAACAGCGTCTACACGTCGAATGCGCAGCTGGTGGTGTATAGGCTGATCGGTGACT
                          ************************************************************

MTC28_pET28_-clona_5      TCGATCCCGCTGAGGCCATCACACACGGCTACATTGACAGCCAGAAATTGCTCGCATGGC
MTC28                     TCGATCCCGCTGAGGCCATCACACACGGCTACATTGACAGCCAGAAATTGCTCGCATGGC
MTC28_pET28_-clona_6      TCGATCCCGCTGAGGCCATCACACACGGCTACATTGACAGCCAGAAATTGCTCGCATGGC
                          ************************************************************

MTC28_pET28_-clona_5      AGACCACAAACGCCTCGATGGCCAATTTCGACGGCTTTCCGTCATCAATCATCGAGGGCA
MTC28                     AGACCACAAACGCCTCGATGGCCAATTTCGACGGCTTTCCGTCATCAATCATCGAGGGCA
MTC28_pET28_-clona_6      AGACCACAAACGCCTCGATGGCCAATTTCGACGGCTTTCCGTCATCAATCATCGAGGGCA
                          ************************************************************

MTC28_pET28_-clona_5      CCTACCGCGAAAACGACATGACCCTCAACACCTCCCGGCGCCACGTCATCGCCACCTCCG
MTC28                     CCTACCGCGAAAACGACATGACCCTCAACACCTCCCGGCGCCACGTCATCGCCACCTCCG
MTC28_pET28_-clona_6      CCTACCGCGAAAACGACATGACCCTCAACACCTCCCGGCGCCACGTCATCGCCACCTCCG
                          ************************************************************

MTC28_pET28_-clona_5      GAGCCGACAAGTACCTGGTTTCGCTGTCGGTGACCACCGCGCTGTCGCAGGCGGTCACCG
MTC28                     GAGCCGACAAGTACCTGGTTTCGCTGTCGGTGACCACCGCGCTGTCGCAGGCGGTCACCG
MTC28_pET28_-clona_6      GAGCCGACAAGTACCTGGTTTCGCTGTCGGTGACCACCGCGCTGTCGCAGGCGGTCACCG
                          ************************************************************

MTC28_pET28_-clona_5      ACGGGCCGGCCACCGATGCGATTGTCAACGGATTCCAAGTGGTTGCGCATGCGGCGCCCG
MTC28                     ACGGGCCGGCCACCGATGCGATTGTCAACGGATTCCAAGTGGTTGCGCATGCGGCGCCCG
MTC28_pET28_-clona_6      ACGGGCCGGCCACCGATGCGATTGTCAACGGATTCCAAGTGGTTGCGCATGCGGCGCCCG
                          ************************************************************

MTC28_pET28_-clona_5      CTCAGGCGCCTGCCCCGGCACCCGGTTCGGCACCGGTGGGACTACCCGGGCAGGCGCCTG
```

```
MTC28                   CTCAGGCGCCTGCCCCGGCACCCGGTTCGGCACCGGTGGGACTACCCGGGCAGGCGCCTG
MTC28_pET28_-clona_6    CTCAGGCGCCTGCCCCGGCACCCGGTTCGGCACCGGTGGGACTACCCGGGCAGGCGCCTG
                        ************************************************************

MTC28_pET28_-clona_5    GGTATCCGCCCGCGGGCACCCTGACACCAGTCCCGCCGCGCCTCGAGCACCACCACCACC
MTC28                   GGTATCCGCCCGCGGGCACCCTGACACCAGTCCCGCCGCGC------------------
MTC28_pET28_-clona_6    GGTATCCGCCCGCGGGCACCCTGACACCAGTCCCGCCGCGCCTCGAGCACCACCACCACC
                        ****************************************

MTC28_pET28_-clona_5    ACCACTGA
mtc28                   --------
MTC28_pET28_-clona_6    ACCACTGA
```

Appendix 1.10: Nucleotide alignment of the theoretical sequence MTC28 (red) with the sequences of clones pET28a-MTC28 obtained by sequencing (Macrogen). The analysis was made using CLUSTAL multiple sequence alignment by MUSCLE 3.8 (http://www.ebi.ac.uk/Tools/msa/muscle/).

```
Mycobacterium_haemophilum           WPMFQFAQT-WRVLAGGLAAGAIGVTAFAGGTASADPSPPAPPPAIPGVPAVLPPASLPP
Mycobacterium_lacus_WP_085163097    --MTHIARTSWRVFAGGIVTGFIGVMLFAGGRAAADPVFPPPPFPAP----GPAQAPAPP
Mycobacterium_bovis_AIO11216.1      ----------------------------------DPLLPPPPIPAP----VSAPATVPP
Mycobacterium_mungi                 WPMIQIART-WRVFAGGMATGFIGVVLVTAGKASADPLLPQPPIPAP----VSAPATVPP
Mycobacterium_tuberculosis          WPMIQIART-WRVFAGGMATGFIGVVLVTAGKASADPLLPPPPIPAP----VSAPATVPP
Mycobacterium_canettii              --MIQIART-WRVFAGGMATGFIGVVLVTAGKASADPLLPPPPIPAP----VSAPATVPP
Mtc28_rec_MTB                       --MIQIART-WRVFAGGMATGFIGVVLVTAGKASADPLLPPPPIPAP----VSAPATVPP
Mycobacterium                       --MIQIART-WRVFAGGMATGFIGVVLVTAGKASADPLLPPPPIPAP----VSAPATVPP
Mycobacterium_marinum               WPMIHIART-WRGFAGCMAAGFVGVTLIASGTASADPLYPQPPSPAP----APAQAAVPP
Mycobacterium_ulcerans_WP_011738    --MIHIART-WRGFAGCMAAGFVGVTLIASGTASADPLYPQPPSPAP----APAQAAVPP
Mycobacterium_kansasii_WP_075544    ----------------------VGVVLIAGGKASAEPLYPQPPLPAP----VSVHPAAPP
Mycobacterium_gastris_WP_0364150    --MIHIART-WRVFAGGMAAGFVGVVLIAGGKASAEPLYPLPPLPAP----VPVQPAAPP
Mycobacterium_szulgai               WPMIQIARN-WRVFAGGVAAGFVGVVLITSGTASADPLYPPPAIPAP----GPSQAAVPP
Mycobacterium_kubicae_WP_0850744    --MIQIARN-WRVFAGGVAAGFVGVVLITSGTASADPLYPPPAIPAP----GPSQAAVPP
Mycobacterium_riyadhense_WP_0852    ------------------------------------------------APAPATSPL
Mycobacterium_shinjukuense_WP_08    --MHQYVPT-RRLFAAGMATGFIGVMLIAGGRASADPLFPPPPNPVP----VPTQAAAPP
                                                                                        .. *

Mycobacterium_haemophilum           IQNVTAVPGGITTNNRFVATPQ-------------APGPAA-------------------
Mycobacterium_lacus_WP_085163097    VQNLTALPGAV-N-NRLAPAAPPALAPA--PAPIASPNPATV-----------LAAGPAP
Mycobacterium_bovis_AIO11216.1      VQNLTALPGGS-S-NRFSPAPAPA--PIASPIPVGAPGSTA-------------------
Mycobacterium_mungi                 VQNLTALPGGS-S-NRFSPAPAPA--PIASPIPVGAPGSTA-------------------
Mycobacterium_tuberculosis          VQNLTSLPGGS-S-NRFSPAPAPA--PIASPIPVGAPGSTA-------------------
Mycobacterium_canettii              VQNLTALPGGS-S-NRFSPAPAPA--PIASPIPVGAPGSTA-------------------
Mtc28_rec_MTB                       VQNLTALPGGS-S-NRFSPAPAPA--PIASPIPVGAPGSTA-------------------
Mycobacterium                       VQNLTALPGGS-S-NRFSPAPAPA--PIASPIPVGAPGSTA-------------------
Mycobacterium_marinum               VQNLNASPGSI-T-NRFAPVPAQVPAPMQVPAATAAPVPAAIPATGQMPAAGQVPAAGQL
Mycobacterium_ulcerans_WP_011738    VQNLNASPGSI-T-NRFAPAPAQVPAPMQVPAATAAPVPAAIPATGQMPAAGQVPAAGQL
Mycobacterium_kansasii_WP_075544    VQNLTAVPGGV-S-NRFAPVPAQA--PAPAPVVSALP-PAA-------------------
Mycobacterium_gastris_WP_0364150    VQNLTAVPGGA-S-NRFAPVPAQA--PAPAPVVSALP-PVA-------------------
Mycobacterium_szulgai               AQNLTVYPGGV-T-NRFAPAPAQTVPPVQLPAPIASPVPAA------------VPAAGAG
Mycobacterium_kubicae_WP_0850744    AQNLTVYPGGV-T-NRFAPAPAQAVPPVQLPAPIASPVPAA------------VPAAGAG
Mycobacterium_riyadhense_WP_0852    A------PTGIGT------APAAA-----------------------------------
Mycobacterium_shinjukuense_WP_08    VQNLTASPGGVAA-NRFAPAPAPA--PAQAPALVASPIPAT-------------AAAAAP
                                           * .         ..

Mycobacterium_haemophilum           --LGPTPPTVAAPVAGTLRDYFKAKDVKLVAQKPQGFKALDITLPVPTRWTQVPDPNVPD
Mycobacterium_lacus_WP_085163097    TAVAPMPPPVTPATTGTLRDYLTGKGVKLEPQRAQGFNALDITLPMPPRWTRVPDPNVPD
Mycobacterium_bovis_AIO11216.1      --VPPLPPPVTPAISGTLRDHLREKGVKLEAQRPHGFKALDITLPMPPRWTQVPDPNVPD
Mycobacterium_mungi                 --VPPLPPPVTPAISGTLRDHLREKGVKLEAQRPHGFKALDITLPMPPRWTQVPDPNVPD
Mycobacterium_tuberculosis          --VPPLPPPVTPAISGTLRDHLREKGVKLEAQRPHGFKALDITLPMPPRWTQVPDPNVPD
Mycobacterium_canettii              --VPPLPPPVTPAISGTLRDHLREKGVKLEAERPHGFKALDITLPMPPRWTQVPDPNVPD
Mtc28_rec_MTB                       --VPPLPPPVTPAISGTLRDHLREKGVKLEAQRPHGFKALDITLPMPPRWTQVPDPNVPD
Mycobacterium                       --VPPLPPPVTPAISGTLRDHLREKGVKLEAQRPHGFKALDITLPMPPRWTQVADPNVPD
Mycobacterium_marinum               PVAAPVAPAITPAATGTVRDYLNGKGVKLEAQRPQGFNALEITLPMPPRWTSVPDPNVPD
Mycobacterium_ulcerans_WP_011738    PVAAPVAPAITPAVTGTVRDYLNGKGVKLEAQRPQGFNALEITLPMPPRWTQVPDPNVPD
Mycobacterium_kansasii_WP_075544    --VAPTPPAVTPAVAGTLREFLQGKGVKFEPQRSQGFKALDVTLPLPPRWTPVPDPNVPD
Mycobacterium_gastris_WP_0364150    --VVPTPPAVTPAVAGTLREFLQGKGVKLEPQRSPGFKALDVTLPMPPRWTPVPDPNVPD
Mycobacterium_szulgai               AVAAPTPPAATPAVSGTLRDYLRAKGVKLEAQRAQGFKALDITLPVPPRWTQVPDPNVPD
Mycobacterium_kubicae_WP_0850744    AVAAPTPPAATPAVSGTLRDYLRAKGVKLEAQRAQGFKALDITLPVPPRWTQVPDPNVPD
Mycobacterium_riyadhense_WP_0852    ----PMPPTMTPAITGTLRDYLHAKGVKLEAQRPQGFKALDITLPMPPRWTHVPDPNVPD
Mycobacterium_shinjukuense_WP_08    TVVAPMPPTMTPLVTGTLREYLQAQGVKLEAQRPQGFQALDITLPMPPRWTHVPDPNVPD
                                        * .*. :.  :**:*:.:  :.**: .:.. **:**::***:*.*** *.******
```

```
Mycobacterium_haemophilum           AFAVIADRL-GNSLYTSNAQVVVYQLVGNFDPKEAITHGFVDAQQLFAWQTTNASQADFE
Mycobacterium_lacus_WP_085163097    AFVVIADRVGGNSVYTSNAQVVVYKLIGEFDPAEAITHGYVDSQQLLAWQTTNASMANFG
Mycobacterium_bovis_AIO11216.1      AFVVIADRL-GNSVYTSNAQLVVYRLIGDFDPAEAITHGYIDSQKLLAWQTTNASMANFD
Mycobacterium_mungi                 AFVVIADRL-GNSVYTSNAQLVVYRLIGDFDPAEAITHGYIDSQKLLAWQTTNASMANFD
Mycobacterium_tuberculosis          AFVVIADRL-GNSVYTSNAQLVVYRLIGDFDPAEAITHGYIDSQKLLAWQTTNASMANFD
Mycobacterium_canettii              AFVVIADRL-GNSVYTSNAQLVVYKLIGDFDPAEAITHGYIDSQKLLAWQTTNASMANFD
Mtc28_rec_MTB                       AFVVIADRL-GNSVYTSNAQLVVYRLIGDFDPAEAITHGYIDSQKLLAWQTTNASMANFD
Mycobacterium                       AFVVIADRL-GNSVYTSNAQLVVYRLIGDFDPAEAITHGYIDSQKLLAWQTTNASMANFD
Mycobacterium_marinum               AFAVIADRVGGNSVYTSNAQVVVYKLVGDLDPAEAISHGFVDSQNLLAWRTTNASMAEFG
Mycobacterium_ulcerans_WP_011738    AFAVIADRVGGNSVYTSNAQVVVYKLVGDLDPAEAISHGFVDSQNLLAWRTTNASMAEFG
Mycobacterium_kansasii_WP_075544    AFLVIADRVGGNSVYTSNAQVVVYKLVGDFDPAEAITHGFVDSQKLLAWRTTNSSMADFN
Mycobacterium_gastris_WP_0364150    AFLVIADRVGGNSVYTSNAQVVVYKLVGGFDPAEAITHGFVDSQKLLAWRTTNSSMADFN
Mycobacterium_szulgai               AFVVIADRVGGNSIYTSNAQIVVYKLVGDFDPAEAISHGYVDSQQLLGWQTTNASMANLG
Mycobacterium_kubicae_WP_0850744    AFVVIADRVGGNSIYTSNAQIVVYKLVGDFDPAEAISHGYVDSQQLLGWQTTNASMANLG
Mycobacterium_riyadhense_WP_0852    AFAVIADRVGGTSIYTSNAQVVVYKLVGDFDPAEAITHGYVDSQQLLAWQTTNASMANLG
Mycobacterium_shinjukuense_WP_08    AFVVIADRL-GNSVYTSNAQVVVYKLVGNFDPAEAITHGYVDSQRLLAWQTTNASLANFC
                                    ** *****: *.*:******:***.*:* :** ***:**::*:*.*:.*.***:* *::

Mycobacterium_haemophilum           GFPSSIIEGTYRENDMTLNTSRRHVIASSGPDKYLVSLSVTTALSQAVADAPATNAISNG
Mycobacterium_lacus_WP_085163097    GFPSSIIEGTYRENDMTLNTSRRHVIATSGKNKYLVSLAVTTAASQAVADAPATDAIING
Mycobacterium_bovis_AIO11216.1      GFPSSIIEGTYRENDKTLNTSRRHVIAASGADKYLVSLSVTTALSQAVTDGPATDAIVNG
Mycobacterium_mungi                 GFPSSIIEGTYRENDMTLNTSRRHVIATSGADKYLVSLSVTTALSQAVTDGPATDAIVNG
Mycobacterium_tuberculosis          GFPSSIIEGTYRENDMTLNTSRRHVIATSGADKYLVSLSVTTALSQAVTDGPATDAIVNG
Mycobacterium_canettii              GFPSSIIEGTYRENDMTLNTSRRHVIATSGADKYLVSLSVTTALSQAVTDGPATDAIVNG
Mtc28_rec_MTB                       GFPSSIIEGTYRENDMTLNTSRRHVIATSGADKYLVSLSVTTALSQAVTDGPATDAIVNG
Mycobacterium                       GFPSSIIEGTYRENDMTLNTSRRHVIATSGADKYLVSLSVTTALSQAVTDGPATDAIVNG
Mycobacterium_marinum               GFPSSVIEGTYRENDMTLNTSRRHVIATSGSENYLVSLSVTTAQSQAVADAPATDAIING
Mycobacterium_ulcerans_WP_011738    GFPSSVIEGTYRENDMTLNTSRRHVIAASGSENYLVSLSVTTAQSQAVADAPATDAIING
Mycobacterium_kansasii_WP_075544    GFPSSIIEGTYRENDMTLNTSRRHVLASSGADKYLVSLSVTTAASQAIADAPATDAIVNG
Mycobacterium_gastris_WP_0364150    GFPSSVIEGTYRENDMTLNTSRRHVLATSGADKYLVSLSVTTAASQAIADAPATDAIVNG
Mycobacterium_szulgai               NFPSSVIEGTYRENDMTLNTSRRHVIATAGNEKYLVSLSVTTAASQAVSDAPATDAIVNG
Mycobacterium_kubicae_WP_0850744    NFPSSVIEGTYRENDMTLNTSRRHVIATAGNEKYLVSLSVTTAASQAVSDAPATDAIVNG
Mycobacterium_riyadhense_WP_0852    SFPSSVIEGTYRENDMTLNTSRRHVIASSGPDKYLVSLSVTTAASQAVADAPATDAIING
Mycobacterium_shinjukuense_WP_08    GFPSSIIEGTYRENDMTLNTSRRHVIATSGPDRYLVSLSVTTALSQAVADGPATDAIING
                                    .****:********* *********:*::* :.*****:**** ***::*.***:** **

Mycobacterium_haemophilum           FRVSAPTASAPAPTQRPGSTPVGLTGPAPLPGMPPGQPPAPNL---------
Mycobacterium_lacus_WP_085163097    FRVTAPAGTAPPPVAAP--APLGRSGQASLPSPSPAPQPLPNLLTLVPGMPP
Mycobacterium_bovis_AIO11216.1      FQVVAHAAPAQAPAPAPGSAPVGLPGQAPGYPPAGTLIPVPPR---------
Mycobacterium_mungi                 FQVVAHAAPAQAPAPAPGSAPVGLPGQAPGYPPAGTLTPVPPR---------
Mycobacterium_tuberculosis          FQVVAHAAPAQAPAPAPGSAPVGLPGQAPGYPPAGTLTPVPPR---------
Mycobacterium_canettii              FQVVAHAAPAQAPAPAPGSAPVGLPGQAPGYPPAGTLTPVPPR---------
Mtc28_rec_MTB                       FQVVAHAAPAQAPAPAPGSAPVGLPGQAPGYPPAGTLTPVPPR---------
Mycobacterium                       FQVVAHAAPAQAPAPAPGSAPVGLPGQAPGYPPAGTLTPVPPR---------
Mycobacterium_marinum               FRV-------------------------------------------------
Mycobacterium_ulcerans_WP_011738    FRVATPTAAGHTP----------------------------------------
Mycobacterium_kansasii_WP_075544    FRV-------------------------------------------------
Mycobacterium_gastris_WP_0364150    FRV-------------------------------------------------
Mycobacterium_szulgai               FRV-------------------------------------------------
Mycobacterium_kubicae_WP_0850744    FRVTA-----------------------------------------------
Mycobacterium_riyadhense_WP_0852    FGVAAPAAGARSPARVTAPTAPAQVPATPSHPAPLALPGQQP----------
Mycobacterium_shinjukuense_WP_08    FRV-------------------------------------------------
                                    * *
```

Appendix 1.11: Alignment of MTC28 from MTB with other sequences of Mycobacteria (http://www.ebi.ac.uk/Tools/msa/clustalw2/).

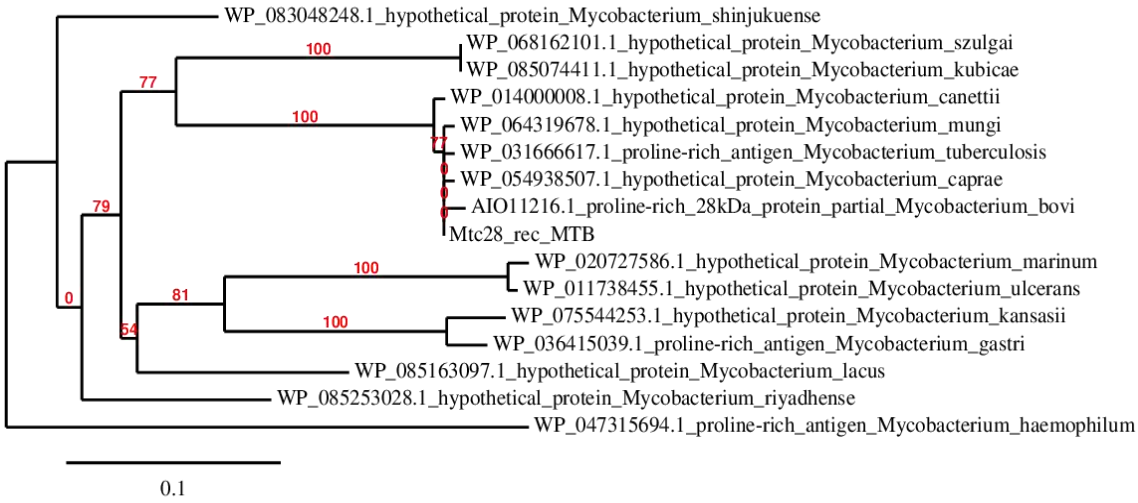

Appendix 1.12: Phylogenetic tree of the amino acid sequence of recombinant MTC28 from MTB, compared with other Mycobacteria sequences. In red it indicates the percentage of support of the branches of the tree.

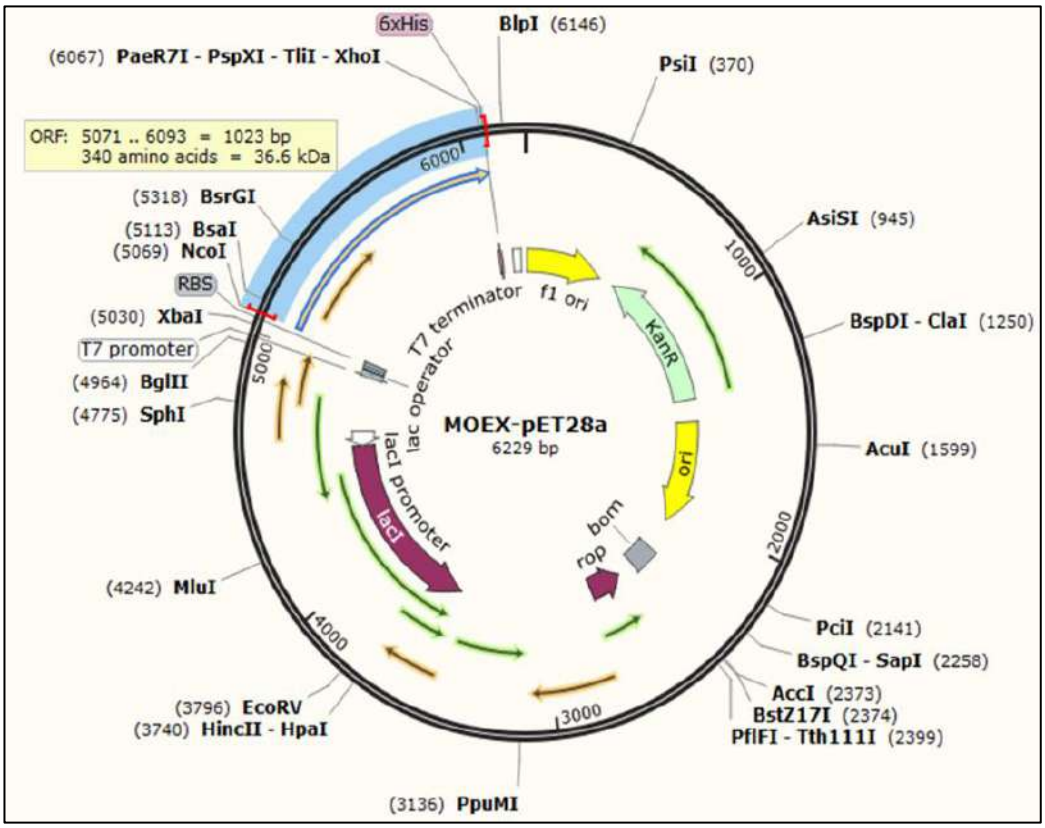

Appendix 1.13: In silico pET28a-MoeX.

```
MoeX_pET28_-_clona_1      TTTAAGAAGGAGATATACCATGGGGATGATCATAGAGCTGATGCGCCGGGTGGTAGGTCT
MoeX                      ------------------------ATGATCATAGAGCTGATGCGCCGGGTGGTAGGTCT
MoeX_pET28_-_clona_3      TTTAAGAAGGAGATATACCATGGGGATGATCATAGAGCTGATGCGCCGGGTGGTAGGTCT
                                                   **********************************

MoeX_pET28_-_clona_1      CGCACAGGGAGCTACCGCCGAGGTCGCCGTCTATGGCGACCGAGATCGTGATCTCGCGGA
MoeX                      CGCACAGGGAGCTACCGCCGAGGTCGCCGTCTATGGCGACCGAGATCGTGATCTCGCGGA
MoeX_pET28_-_clona_3      CGCACAGGGAGCTACCGCCGAGGTCGCCGTCTATGGCGACCGAGATCGTGATCTCGCGGA
                          ************************************************************

MoeX_pET28_-_clona_1      GCGATGGTGCGCGAACACCGGAAACACCCTGGTGCGCGCCGACGTGGACCAGACCGGCGT
MoeX                      GCGATGGTGCGCGAACACCGGAAACACCCTGGTGCGCGCCGACGTGGACCAGACCGGCGT
MoeX_pET28_-_clona_3      GCGATGGTGCGCGAACACCGGAAACACCCTGGTGCGCGCCGACGTGGACCAGACCGGCGT
                          ************************************************************

MoeX_pET28_-_clona_1      CGGCACCCTGGTGGTGCGCCGCGGCCATCCGCCTGACCCGGCAAGCGTGTTGGGCCCCGA
MoeX                      CGGCACCCTGGTGGTGCGCCGCGGCCATCCGCCTGACCCGGCAAGCGTGTTGGGCCCCGA
MoeX_pET28_-_clona_3      CGGCACCCTGGTGGTGCGCCGCGGCCATCCGCCTGACCCGGCAAGCGTGTTGGGCCCCGA
                          ************************************************************

MoeX_pET28_-_clona_1      CCGGCTACCCGGGGTCCGGTTGTGGCTGTACACCAACTTCCACTGCAACCTGTGCTGCGA
MoeX                      CCGGCTACCCGGGGTCCGGTTGTGGCTGTACACCAACTTCCACTGCAACCTGTGCTGCGA
MoeX_pET28_-_clona_3      CCGGCTACCCGGGGTCCGGTTGTGGCTGTACACCAACTTCCACTGCAACCTGTGCTGCGA
                          ************************************************************

MoeX_pET28_-_clona_1      CTACTGCTGCGTCTCGTCGTCACCAAGCACCCCGCATCGCGAACTGGGGGCGGAGCGGAT
MoeX                      CTACTGCTGCGTCTCGTCGTCACCAAGCACCCCGCATCGCGAACTGGGGGCGGAGCGGAT
MoeX_pET28_-_clona_3      CTACTGCTGCGTCTCGTCGTCACCAAGCACCCCGCATCGCGAACTGGGGGCGGAGCGGAT
                          ************************************************************

MoeX_pET28_-_clona_1      CGGCCGAATCGTCGGTGAAGCGGCGCGCTGGGGAGTGCGCGAACTGTTCCTCACCGGCGG
MoeX                      CGGCCGAATCGTCGGTGAAGCGGCGCGCTGGGGAGTGCGCGAACTGTTCCTCACCGGCGG
MoeX_pET28_-_clona_3      CGGCCGAATCGTCGGTGAAGCGGCGCGCTGGGGAGTGCGCGAACTGTTCCTCACCGGCGG
                          ************************************************************

MoeX_pET28_-_clona_1      TGAGCCGTTCCTGCTGCCCGACATCGACACGATCATCGCGACCTGTGTGAAGCAGTTGCC
MoeX                      TGAGCCGTTCCTGCTGCCCGACATCGACACGATCATCGCGACCTGTGTGAAGCAGTTGCC
MoeX_pET28_-_clona_3      TGAGCCGTTCCTGCTGCCCGACATCGACACGATCATCGCGACCTGTGTGAAGCAGTTGCC
                          ************************************************************

MoeX_pET28_-_clona_1      CACCACCGTCCTCACCAACGGCATGGTGTTCAAAGGGCGGGGTCGGCGCGCGCTGGAATC
MoeX                      CACCACCGTCCTCACCAACGGCATGGTGTTCAAAGGGCGGGGTCGGCGCGCGCTGGAATC
MoeX_pET28_-_clona_3      CACCACCGTCCTCACCAACGGCATGGTGTTCAAAGGGCGGGGTCGGCGCGCGCTGGAATC
                          ************************************************************

MoeX_pET28_-_clona_1      CCTACCTAGAGGGCTCGCCTTGCAGATCAGCCTGGACTCGGCCACCCCGGAGCTGCACGA
MoeX                      CCTACCTAGAGGGCTCGCCTTGCAGATCAGCCTGGACTCGGCCACCCCGGAGCTGCACGA
MoeX_pET28_-_clona_3      CCTACCTAGAGGGCTCGCCTTGCAGATCAGCCTGGACTCGGCCACCCCGGAGCTGCACGA
                          ************************************************************

MoeX_pET28_-_clona_1      TGCGCACCGCGGCGCGGGGACGTGGGTCAAGGCAGTAGCTGGTATCCGGTTGGCGCTCTC
MoeX                      TGCGCACCGCGGCGCGGGGACGTGGGTCAAGGCAGTAGCTGGTATCCGGTTGGCGCTCTC
MoeX_pET28_-_clona_3      TGCGCACCGCGGCGCGGGGACGTGGGTCAAGGCAGTAGCTGGTATCCGGTTGGCGCTCTC
                          ************************************************************

MoeX_pET28_-_clona_1      ACTTGGCTTCCGGGTGCGGGTGGCCGCGACGGTTGCCAGCCCCGCACCTGGCGAGCTGAC
MoeX                      ACTTGGCTTCCGGGTGCGGGTGGCCGCGACGGTTGCCAGCCCCGCACCTGGCGAGCTGAC
MoeX_pET28_-_clona_3      ACTTGGCTTCCGGGTGCGGGTGGCCGCGACGGTTGCCAGCCCCGCACCTGGCGAGCTGAC
                          ************************************************************

MoeX_pET28_-_clona_1      GGCGTTTCACGACTTCCTCGACGGGCTTGGCATCGCACCCGGGGATCAGCTGGTCCGGCC
MoeX                      GGCGTTTCACGACTTCCTCGACGGGCTTGGCATCGCACCCGGGGATCAGCTGGTCCGGCC
MoeX_pET28_-_clona_3      GGCGTTTCACGACTTCCTCGACGGGCTTGGCATCGCACCCGGGGATCAGCTGGTCCGGCC
                          ************************************************************

MoeX_pET28_-_clona_1      GATCGCGCTGGAGGGCGCCGCGTCGCAAGGGGTGGCGCTCACCCGCGAATCGCTGGTTCC
MoeX                      GATCGCGCTGGAGGGCGCCGCGTCGCAAGGGGTGGCGCTCACCCGCGAATCGCTGGTTCC
MoeX_pET28_-_clona_3      GATCGCGCTGGAGGGCGCCGCGTCGCAAGGGGTGGCGCTCACCCGCGAATCGCTGGTTCC
                          ************************************************************
```

```
MoeX_pET28_-_clona_1      CGAGGTGACCGTCACCGCCGACGGCGTGTACTGGCACCCAGTGGCCGCCACCGACGAGCG
MoeX                      CGAGGTGACCGTCACCGCCGACGGCGTGTACTGGCACCCAGTGGCCGCCACCGACGAGCG
MoeX_pET28_-_clona_3      CGAGGTGACCGTCACCGCCGACGGCGTGTACTGGCACCCAGTGGCCGCCACCGACGAGCG
                          ************************************************************

MoeX_pET28_-_clona_1      CGCCCTGGTCACCCGTACCGTCGAACCCTTGACCCCGGCGCTGGACATGGTAAGCCGGCT
MoeX                      CGCCCTGGTCACCCGTACCGTCGAACCCTTGACCCCGGCGCTGGACATGGTAAGCCGGCT
MoeX_pET28_-_clona_3      CGCCCTGGTCACCCGTACCGTCGAACCCTTGACCCCGGCGCTGGACATGGTAAGCCGGCT
                          ************************************************************

MoeX_pET28_-_clona_1      ATTCGCCGAACAGTGGACACGAGCCGCCGAAGANGCCGCGTTGTTCCCGTGTGCGCTCGA
MoeX                      ATTCGCCGAACAGTGGACACGAGCCGCCGAAGAGGCCGCGTTGTTCCCGTGTGCG-----
MoeX_pET28_-_clona_3      ATTCGCCGAACAGTGGACACGAGCCGCCGAAGAGGCCGCGTTGTTCCCGTGTGCGCTCGA
                          ********************************* ********************

MoeX_pET28_-_clona_1      GCACCACCACCACCACCACTGAC
MoeX                      -----------------------
MoeX_pET28_-_clona_3      GCACCACCACCACCACCACT---
```

Appendix 1.14: Alignment of the sequences of clones pET28a-MoeX obtained by sequencing (Macrogen) with the theoretical MoeX sequence (blue), using CLUSTAL multiple sequence alignment by MUSCLE 3.8 (http://www.ebi.ac.uk/Tools/msa/muscle/).

```
4Fe-4S_single_cluster_domain-con      -MVVMALMRTVEQLAEGDTAEFPVASASELDLVRRWCAKTGNTVVSTMMVEQDAGYVTVG
radical_SAM_protein_Rhodococcus_      --MILDLMRLMTGLPDGGTGEVAIGSAEDLVLARRWCAHSGNTIVRENVDATDTGTLVVR
radical_SAM_protein_M._austroafr      -MVILDLMRLMATLADGAIGEIAVASVAERETAEKWCARSGNTVVQADLDETGAGTLTVR
radical_SAM_protein_My._vanbaale      -MVILDLMRLMATLADGAVGEIAVASVAERETAEKWCARSGNTVVQADLDETGAGTLTVR
radical_SAM_protein_Gordonia_rhi      -MVILELMRTLGGVPVGTTVEIPIGSAADRDLAQRWCERNGNSVVRADVDETGEGTLTVR
radical_SAM_protein_M._tusciae_W      -MVIIDLMRVMGGIADGMLAEVTIQSAADHELADRWCARTGNTIVRADVDDAGVGTLVVR
MoeX_MTB_BTB09-091_KCP25895.1         --MIIELMRRVVGLAQGATAEVAVYGDRDRDLAERWCANTGNTLVRADVDQTGVGTLVVR
radical_SAM_protein_MTB_TRS29_AQ      -MVIIELMRRVVGLAQGATAEVAVYGDRDCDLAERWCANTGNTLVRADVDQTGVGTLVVR
MoeX_M._microti_AMC59290.1            -MVIIELMRRVVGLAQGATAEVAVYGDRDRDLAERWCANTGNTLVRADVDQTGVGTLVVR
moeX_MTB_SGC82502.1                   -MVIIELMRRVVGLAQGATAEVAVYGDRDRDLAERWCANTGNTLVRADVDQTGVGTLVVR
radical_SAM_protein_Mycobacteriu      --MIIELMRRVVGLAQGATAEVAVYGDRDRDLAERWCANTGNTLVRADVDQTGVGTLVVR
Moex_MTB_KT-0089_KCG92103.1           --MIIELMRRVVGLAQGATAEVAVYGDRDRDLAERWCANTGNTLVRADVDQTGVGTLVVR
Moex_recombinante_MTB                 MGMIIELMRRVVGLAQGATAEVAVYGDRDRDLAERWCANTGNTLVRADVDQTGVGTLVVR
radical_SAM_protein_M._persicum_      --MILDLMRQVSGLAQGATVEVAVSSHRDRELAEKWCARTGNTLVRADLDEVGVGTVVVR
radical_SAM_protein_M._kansasii_      -MVILDLMRQVGGLAQGATVEVAVSSPGDRELAEKWCARTGNTLVRADLDEAGAGTVIVR
radical_SAM_protein_M._gastri_WP      -MVILDLMRQVGGLAQGATVEVAVSSPRDRELAEKWCARTGNTLVRADLDETGAGTVVVR
radical_SAM_protein_M._shinjukue      -MVILDLMRRVGGLAQGATAEVPVCCHRDRELAERWCARTGNTLVRADVDQAGVGTVVVR
radical_SAM_protein_M._lacus_WP_      -MVILDLMRRVGGLAQGATAEVAVRSERDRELAERWCARTGNTLVRADVDQGGAGTLVVR
radical_SAM_protein_M._riyadhens      -MVILDLMRRVGGLAQGATAEVAVSGDRDRELAERWCAQTGNTVVRAEVDQAGVGTLVVR
                                        ::: *** :  :. *   *..:    :   . .** ..**::*   :   . * : *

4Fe-4S_single_cluster_domain-con      RGRPRNPATMIPADRMPGARLWLYTNFHCNLACDYCCVASSPRADPRLLGIETIEALVAE
radical_SAM_protein_Rhodococcus_      RGHAPDPRDALGPDRMPGARLWLYTNFHCNLACDYCCVSSSPHAPRRELGVERIARLVTE
radical_SAM_protein_M._austroafr      RGRPPDPLLVLGPERMPGARLWMYTNFHCNLACDYCCVESSPQAPRRELGADRIARLARE
radical_SAM_protein_My._vanbaale      RGRPPDPLLVLGPERMPGARLWMYTNFHCNLACDYCCVESSPQAPRRELGADRIARLARE
radical_SAM_protein_Gordonia_rhi      RGRPPDPATVIGADRLPGMRLWLYTNFHCNLSCDYCCVASSPRAPRRELGAQRIARLIRE
radical_SAM_protein_M._tusciae_W      RGRPADPAVDLGRDRIPGARLWLYTNFHCNLACDYCCVASSPQAPRRELGSERIARLVTE
MoeX_MTB_BTB09-091_KCP25895.1         RGHPPDPASVLGPDRLPGVRLWLYTNFHCNLCCDYCCVSSSPSTPHRELGAERIGRIVGE
radical_SAM_protein_MTB_TRS29_AQ      RGHPPDPASVLGPDRLPGVRLWLYTNFHCNLCCDYCCVSSSPSTPHRELGAERIGRIVGE
MoeX_M._microti_AMC59290.1            RGHPPDPASVLGPDRLPGVRLWLYTNFHCNLCCDYCCVSSSPSTPHRELGAERIGRIVGE
moeX_MTB_SGC82502.1                   RGHPPDPASVLGPDRLPGVRLWLYTNFHCNLCCDYCCVSSSPSTPHRELGAERIGRIVGE
radical_SAM_protein_Mycobacteriu      RGHPPDPASVLGPDRLPGVRLWLYTNFHCNLCCDYCCVSSSPSTPHRELGAERIGRIVGE
Moex_MTB_KT-0089_KCG92103.1           RGHPPDPASVLGPDRLPGVRLWLYTNFHCNLCCDYCCVSSSPSTPHRELGAERIGRIVGE
Moex_recombinante_MTB                 RGHPPDPASVLGPDRLPGVRLWLYTNFHCNLCCDYCCVSSSPSTPHRELGAERIGRIVGE
radical_SAM_protein_M._persicum_      RGHPPDPAEVLGVDRLPGVRLWLYTNFHCNLSCDYCCVSSSPQAPHRELGAERIGRIVGE
radical_SAM_protein_M._kansasii_      RGHPPDPAEVLGADRLPGVRLWLYTNFHCNLSCDYCCVSSSPQAAHRELGAERIGRIVGE
radical_SAM_protein_M._gastri_WP      RGHPPDPAVVLGADRLPGVRLWLYTNFHCNLSCDYCCVSSSPQAAHRELGAERIGRIVGE
radical_SAM_protein_M._shinjukue      RGHPPDPASVLGADRLPGVRLWLYTNFHCNLSCDYCCVSSSPTAPRRELGAERIARIVRE
radical_SAM_protein_M._lacus_WP_      RGRPPDPASVLGADRLPGVRLWLYTNFHCNLSCDYCCVSSSPSAPHRELGAERIGRLVRE
radical_SAM_protein_M._riyadhens      RGRPPDPASVLGADRLPGVRLWLYTNFHCNLSCDYCCVASSPQAPHRELGAERIARIVRE
                                      **.. :*   :  :*:** ***:********.****** *** :  * ** : *  :  *

4Fe-4S_single_cluster_domain-con      AAAWGVRELYLTGGEPFLLPDIDAIVRSCVDRLPTTLLTNGMLFRGQGLRKLQAMPRAGF
radical_SAM_protein_Rhodococcus_      AAEWGVGEIYLTGGEPFLLPDIDTIVRTCMDVLPTTVLTNAMVFKGRGLRALESLPREGL
radical_SAM_protein_M._austroafr      AADWGVREVFLTGGEPFLLSDIGTIVRSCAALLPTTVLTNGMVFRGRGLRELDTIPRDNV
radical_SAM_protein_My._vanbaale      AADWGVREVFLTGGEPFLLSDIGTIVRSCAALLPTTVLTNGMVFRGRGLRELDAIPRDNV
radical_SAM_protein_Gordonia_rhi      AADWGAAELFLTGGEPFLLPDIGEIIADCVTVLPTTVLTNGMVFRGRGLRALEALPRTGL
radical_SAM_protein_M._tusciae_W      AAAWGVRELYLTGGEPFLLTDIDTIVRTCVDALPTTVLTNGMVFRGRGRRALESMPRKGL
MoeX_MTB_BTB09-091_KCP25895.1         AARWGVRELFLTGGEPFLLPDIDTIIATCVKQLPTTVLTNGMVFKGRGRRALESLPR-GL
```

```
radical_SAM_protein_MTB_TRS29_AQ      AARWGVRELFLTGGEPFLLPDIDTIIATCVKQLPTTVLTNGMVFKGRGRRALESLPR-GL
MoeX_M._microti_AMC59290.1            AARWGVRELFLTGGEPFLLPDIDTIIATCVKQLPTTVLTNGMVFKGRGRRALESLPR-GL
moeX_MTB_SGC82502.1                   AARWGVRELFLTGGEPFLLPDIDTIIATCVKQLPTTVLTNGMVFKGRGRRALESLPR-GL
radical_SAM_protein_Mycobacteriu      AARWGVRELFLTGGEPFLLPDIDTIIATCVKQLPTTVLTNGMVFKGRGRRALESLPR-GL
Moex_MTB_KT-0089_KCG92103.1           AARWGVRELFLTGGEPFLLPDIDTIIATCVKQLPTTVLTNGMVFKGRGRRALESLPR-GL
Moex_recombinante_MTB                 AARWGVRELFLTGGEPFLLPDIDTIIATCVKQLPTTVLTNGMVFKGRGRRALESLPR-GL
radical_SAM_protein_M._persicum_      AARWGVRELFLTGGEPFLLPDIDTIISACAQTLPTTVLTNGMVFKGRARRALESLPRDGL
radical_SAM_protein_M._kansasii_      AARWGVRELFLTGGEPFLLPDIATIISTCVETLPTTVLTNGMVFKGRARRALESLPRDGL
radical_SAM_protein_M._gastri_WP      AARWGVRELFLTGGEPFLLPDIATIISACVQTLPTTVLTNAMVFKGRARRALESLPRDGL
radical_SAM_protein_M._shinjukue      AANWGVRELFLTGGEPFLLPDIDTIIGSCVDTLPTTVLTNGMVFKGRARQALESLPRDGL
radical_SAM_protein_M._lacus_WP_      AAAWGVRELFLTGGEPFLLPDIGTIIRSCLDTLPTTVLTNGMVFKGRGLRALESLPRTGL
radical_SAM_protein_M._riyadhens      AADWGVRELFLTGGEPFLLTDIDTIIESCVDTLPTTVLTNGMVFKGRALRALESLPRTGL
                                      ** **. *::*********.**  *:  *   ****:***.*:*.*.. . *:::** ..

4Fe-4S_single_cluster_domain-con      ALQISVDSPTAEVHDSHRGVGSWKRALAGIRVALDEGFTVRVAATISAHDDPALDELHAL
radical_SAM_protein_Rhodococcus_      ALQISLDSATPGLHDSHRGAGSWARAVAGIRLARQLGFRVRIAATIASPGPGTITALHDF
radical_SAM_protein_M._austroafr      ALQISLDSATPELHDSHRGHGSWARAVEGIRVARGLGFRVRVAATVAAPVPGELKAFHEF
radical_SAM_protein_My._vanbaale      ALQISLDSATSELHDSHRGHGSWARAVEGIRVARGLGFRVRVAATVAAPVPGELKAFHDF
radical_SAM_protein_Gordonia_rhi      ALQISLDSSTPDLHDSHRGAGSWKRAVAGIRLAISLGFRVRVAATIADPAPGELDKFHTF
radical_SAM_protein_M._tusciae_W      ALQISLDSATPRLHDAHRGPGSWQKAVDGIRLACSLGFRVRVAATVAAPAPGQLDDFHKF
MoeX_MTB_BTB09-091_KCP25895.1         ALQISLDSATPELHDAHRGAGTWVKAVAGIRLALSLGFRVRVAATVASPAPGELTAFHDF
radical_SAM_protein_MTB_TRS29_AQ      ALQISLDSATPELHDAHRGAGTWVKAVAGIRLALSLGFRVRVAATVASPAPGELTAFHDF
MoeX_M._microti_AMC59290.1            ALQISLDSATPELHDAHRGAGTWVKAVAGIRLALSLGFRVRVAATVASPAPGELTAFHDF
moeX_MTB_SGC82502.1                   ALQISLDSATPELHDAHRGAGTWVKAVAGIRLALSLGFRVRVAATVASPAPGELTAFHDF
radical_SAM_protein_Mycobacteriu      ALQISLDSATPELHDAHRGAGTWVKAVAGIRLALSLGFRVRVAATVASPAPGELTALHDF
Moex_MTB_KT-0089_KCG92103.1           ALQISLDSATPELHDAHRGAGTWVKAVAGIRLALSLGFRVRVAATVASPAPGELTAFHDF
Moex_recombinante_MTB                 ALQISLDSATPELHDAHRGAGTWVKAVAGIRLALSLGFRVRVAATVASPAPGELTAFHDF
radical_SAM_protein_M._persicum_      ALQISLDSATPDLHDSHRGRGSWEKAVAGIRFALSLGFRVRVAATVAAPAPGELAAFHEF
radical_SAM_protein_M._kansasii_      ALQISLDSATPELHDLHRGAGTWEKAVAGIRFALSLGFRVRVAATVAAPGPGELAAFHEF
radical_SAM_protein_M._gastri_WP      ALQISLDSATPDLHDAHRGAGSWEKAVAGIRFALSLGFRVRVAATVAAPAPGELAAFHEF
radical_SAM_protein_M._shinjukue      VLQISLDSATPELHDSHRGAGTWAKAVAGIRLALSLGFRVRVAATVASPGPGELAAFHDF
radical_SAM_protein_M._lacus_WP_      ALQISLDSATPDLHDSHRGAGTWAKAVAGIRVALSLGFRVRVAATVAAPGPGELAAFHDF
radical_SAM_protein_M._riyadhens      ALQISLDSATPDLHDSHRGVGTWAKAVTGIGLALSLGFRVRVAATIAAPAPGELAAFHDF
                                      .****:**.*. :** *** *:* .*: ** .*   ** **:***::      :  :* :

4Fe-4S_single_cluster_domain-con      FDGLGIPRADQVIRPIALQGVADEGFAFSRESLIPEVTVTADGIYWHPVAALDEDALVSR
radical_SAM_protein_Rhodococcus_      CDQLGIERGDQLIRPIARQGAAVKGLVLTPESLVPEVTVTAEGVYWHPVAATDDRALVTR
radical_SAM_protein_M._austroafr      LDELGIAQDDQVVRPVAREGSAADGVQITRASLVPEVAVTADGVYWHPVAAIDDDALVTR
radical_SAM_protein_My._vanbaale      LDELGIAQDDQVVRPVAREGSAADGVQITRASLVPEVAVTAEGVYWHPVAAIDDDALVTR
radical_SAM_protein_Gordonia_rhi      LDDLGIARDDQVIRPIAREGVADVGQTLSRESLVPEVTVTAEGVYWHPVTATDEQALVTP
radical_SAM_protein_M._tusciae_W      LDELGIASDDQVIRPIAAEGIATNGVVLTRETLVPEVTVTADGVYWHPVAAIDQNALVSP
MoeX_MTB_BTB09-091_KCP25895.1         LDGLGIAPGDQLVRPIALEGAASQGVALTRESLIPEVTVAADGVYWHPVAATDERALVTR
radical_SAM_protein_MTB_TRS29_AQ      LDGLGIAPGDQLVRPIALEGAASQGVALTRESLVPEVTVTADGVYWHPVAATDERALVTR
MoeX_M._microti_AMC59290.1            LDGLGIAPGDQLVRPIALEGAASQGVALTRESLVPEVTVTADGVYWHPVAATDERALVTR
moeX_MTB_SGC82502.1                   LDGLGIAPGDQLVRPIALEGAASQGVALTRESLVPEVTVTADGVYWHPVAATDERALVTR
radical_SAM_protein_Mycobacteriu      LDGLGIAPGDQLVRPIALEGAASQGVALTRESLVPEVTVTADGVYWHPVAATDERALVTR
Moex_MTB_KT-0089_KCG92103.1           LDGLGTAPGDQLVRPIALEGAASQGVALTRESLVPEVTVTADGVYWHPVAATDERALVTR
Moex_recombinante_MTB                 LDGLGIAPGDQLVRPIALEGAASQGVALTRESLVPEVTVTADGVYWHPVAATDERALVTR
radical_SAM_protein_M._persicum_      LNALGIAGEDQLVRPIALEGVASEGLSLRRESLVPEVTVTADGVYWHPVAATDERALVSR
radical_SAM_protein_M._kansasii_      LDALGIAGEDQLVRPIALEGVASKGLSLRRESLVPEVTVTADGVYWHPVAATDERALVSR
radical_SAM_protein_M._gastri_WP      LDALGIAGEDQLVRPIALEGVASEGLSLRRESLVPEVTVTADGVYWHPVAATDERALVSR
radical_SAM_protein_M._shinjukue      LDQLGIARPDQLVRPIALEGVASQGVALTRESLVPEVTVTADGVYWHPVAAIDERALVSR
radical_SAM_protein_M._lacus_WP_      LDGLGIARADQLVRPIALEGVASEGLALARESLVPEVTVTADGVYWHPVAATDQRALVTR
radical_SAM_protein_M._riyadhens      LDELGIARADQLVRPIALEGVASEGLALSRESLVPEVTVTADGVYWHPVAAIDERALVSR
                                       : **    **:::**:* :* *  *  :   :*:***:*:*:*:*****:* *: ***:

4Fe-4S_single_cluster_domain-con      QILPLAPSLDRVSDLFAEQWSSMTAASTLFACA
radical_SAM_protein_Rhodococcus_      QVEPLRPALDEIYERFTRQWAVAATAAALFPCA
radical_SAM_protein_M._austroafr      QIEPLAPALDEIAHAFAELWARKANAAQLFPCA
radical_SAM_protein_My._vanbaale      QIEPLAPALDEIAHAFAELWARKANAAQLFPCA
radical_SAM_protein_Gordonia_rhi      TIEPLTPALETIKLQFAEQWARASESASLFPCA
radical_SAM_protein_M._tusciae_W      RIEPLTPALDEIARLFAEQWAKASTAAALFPCA
MoeX_MTB_BTB09-091_KCP25895.1         TVEPLTPALDMVSRLFAEQWTRAAEEAALFPCA
radical_SAM_protein_MTB_TRS29_AQ      TVEPLTPALDMVSRLFAEQWTRAAEEAALFPCA
MoeX_M._microti_AMC59290.1            TVEPLTPALDMVSWLFAEQWTRAAEEAALFPCA
moeX_MTB_SGC82502.1                   TVEPLTPALDMVSRLFAEQWTRAAEEAALFPCA
radical_SAM_protein_Mycobacteriu      TVEPLTPALDMVSRLFAEQWTRAAEEAALFPCA
Moex_MTB_KT-0089_KCG92103.1           TVEPLTPALDMVSRLFAEQWTRAAEEAALFPCA
Moex_recombinante_MTB                 TVEPLTPALDMVSRLFAEQWTRAAEEAALFPCA
radical_SAM_protein_M._persicum_      TIEPLTPALDAVSRLFAEQWAQAAEAAALFPCA
radical_SAM_protein_M._kansasii_      TIEPLTPALDAVSRLFTEQWARAAEAAALFPCA
radical_SAM_protein_M._gastri_WP      TIEPLTPALDAVSGLFAEQWAQAAEAAALFPCA
radical_SAM_protein_M._shinjukue      TVEPLTPALDTISKLFAEQWAQAAEAAALFPCA
radical_SAM_protein_M._lacus_WP_      TIEPLTPALDEVSRLFAEQWARAADAAALFPCA
radical_SAM_protein_M._riyadhens      AIEPLAPALDKVNRLFAEQWARAAEAAALFPCA
                                       : ** *:*: :   *:  *:  :  : **.**
```

Appendix 1.15: Alignment of MTB MoeX and SAM sequences with other Mycobacteria (http://www.ebi.ac.uk/Tools/msa/clustalw2/).

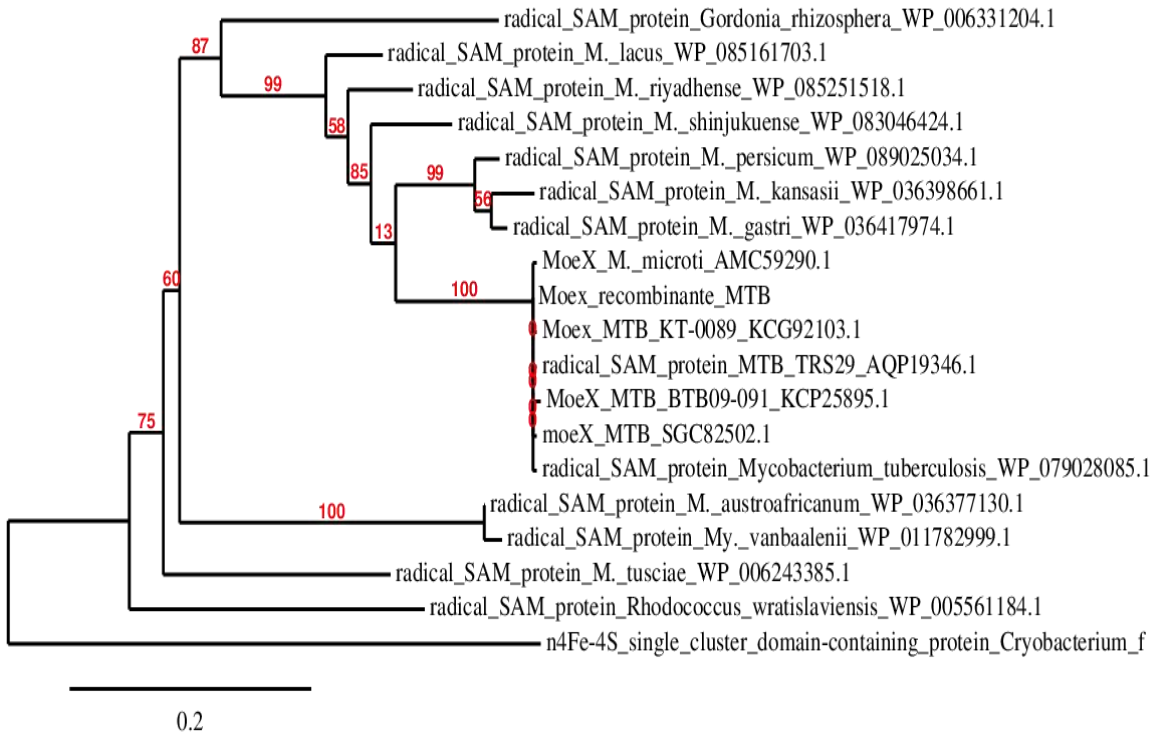

Appendix 1.16: Phylogenetic tree of the amino acid sequence of recombinant MoeX from MTB, compared with MoeX and SAM from other Mycobacteria. In red it indicates the percentage of support of the branches of the tree.

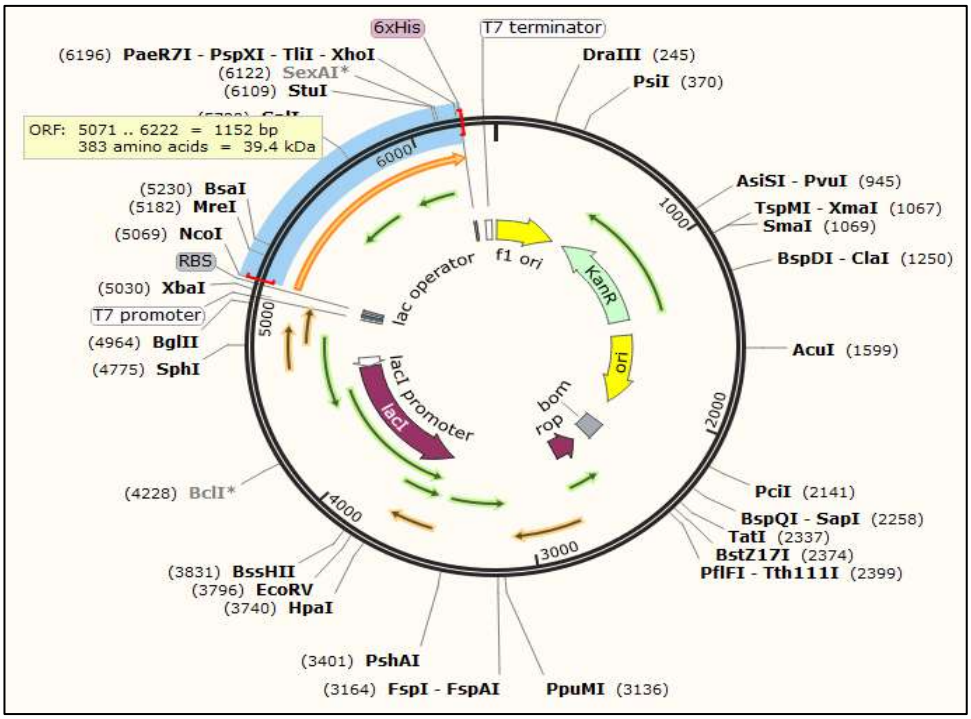

Appendix 1.17: *In silico* pET28a-38kDa.

```
38_kDa_pET28_clona_1      TTTAACTTTAAGAAGGAGATATACCATGGTGAAAATTCGTTTGCATACGCTGTTGGCCGT
38_kDa_pET28_clona_2      TTTAACTTTAAGAAGGAGATATACCATGGTGAAAATTCGTTTGCATACGCTGTTGGCCGT
38kDa                     ------------------------ATGGTGAAAATTCGTTTGCATACGCTGTTGGCCGT
                                                   *********************************

38_kDa_pET28_clona_1      GTTGACCGCTGCGCCGCTGCTGCTAGCAGCGGCGGGCTGTGGCTCGAAACCACCGAGCGG
38_kDa_pET28_clona_2      GTTGACCGCTGCGCCGCTGCTGCTAGCAGCGGCGGGCTGTGGCTCGAAACCACCGAGCGG
38kDa                     GTTGACCGCTGCGCCGCTGCTGCTAGCAGCGGCGGGCTGTGGCTCGAAACCACCGAGCGG
                          ************************************************************

38_kDa_pET28_clona_1      TTCGCCTGAAACGGGCGCCGGCGCCGGTACTGTCGCGACTACCCCCGCGTCGTCGCCGGT
38_kDa_pET28_clona_2      TTCGCCTGAAACGGGCGCCGGCGCCGGTACTGTCGCGACTACCCCCGCGTCGTCGCCGGT
338kDa                    TTCGCCTGAAACGGGCGCCGGCGCCGGTACTGTCGCGACTACCCCCGCGTCGTCGCCGGT
                          ************************************************************

38_kDa_pET28_clona_1      GACGTTGGCGGAGACCGGTAGCACGCTGCTCTACCCGCTGTTCAACCTGTGGGGTCCGGC
38_kDa_pET28_clona_2      GACGTTGGCGGAGACCGGTAGCACGCTGCTCTACCCGCTGTTCAACCTGTGGGGTCCGGC
38kDa                     GACGTTGGCGGAGACCGGTAGCACGCTGCTCTACCCGCTGTTCAACCTGTGGGGTCCGGC
                          ************************************************************

38_kDa_pET28_clona_1      CTTTCACGAGAGGTATCCGAACGTCACGATCACCGCTCAGGGCACCGGTTCTGGTGCCGG
38_kDa_pET28_clona_2      CTTTCACGAGAGGTATCCGAACGTCACGATCACCGCTCAGGGCACCGGTTCTGGTGCCGG
38kDa                     CTTTCACGAGAGGTATCCGAACGTCACGATCACCGCTCAGGGCACCGGTTCTGGTGCCGG
                          ************************************************************

38_kDa_pET28_clona_1      GATCGCGCAGGCCGCCGCCGGGACGGTCAACATTGGGGCCTCCGACGCCTATCTGTCGGA
38_kDa_pET28_clona_2      GATCGCGCAGGCCGCCGCCGGGACGGTCAACATTGGGGCCTCCGACGCCTATCTGTCGGA
38kDa                     GATCGCGCAGGCCGCCGCCGGGACGGTCAACATTGGGGCCTCCGACGCCTATCTGTCGGA
                          ************************************************************

38_kDa_pET28_clona_1      AGGTGATATGGCCGCGCACAAGGGGCTGATGAACATCGCGCTAGCCATCTCCGCTCAGCA
38_kDa_pET28_clona_2      AGGTGATATGGCCGCGCACAAGGGGCTGATGAACATCGCGCTAGCCATCTCCGCTCAGCA
38kDa                     AGGTGATATGGCCGCGCACAAGGGGCTGATGAACATCGCGCTAGCCATCTCCGCTCAGCA
                          ************************************************************

38_kDa_pET28_clona_1      GGTCAACTACAACCTGCCCGGAGTGAGCGAGCACCTCAAGCTGAACGGAAAAGTCCTGGC
38_kDa_pET28_clona_2      GGTCAACTACAACCTGCCCGGAGTGAGCGAGCACCTCAAGCTGAACGGAAAAGTCCTGGC
38kDa                     GGTCAACTACAACCTGCCCGGAGTGAGCGAGCACCTCAAGCTGAACGGAAAAGTCCTGGC
                          ************************************************************

38_kDa_pET28_clona_1      GGCCATGTACCAGGGCACCATCAAAACCTGGGACGACCCGCAGATCGCTGCGCTCAACCC
38_kDa_pET28_clona_2      GGCCATGTACCAGGGCACCATCAAAACCTGGGACGACCCGCAGATCGCTGCGCTCAACCC
38kDa                     GGCCATGTACCAGGGCACCATCAAAACCTGGGACGACCCGCAGATCGCTGCGCTCAACCC
                          ************************************************************

38_kDa_pET28_clona_1      CGGCGTGAACCTGCCCGGCACCGCGGTAGTTCCGCTGCACCGCTCCGACGGGTCCGGTGA
38_kDa_pET28_clona_2      CGGCGTGAACCTGCCCGGCACCGCGGTAGTTCCGCTGCACCGCTCCGACGGGTCCGGTGA
38kDa                     CGGCGTGAACCTGCCCGGCACCGCGGTAGTTCCGCTGCACCGCTCCGACGGGTCCGGTGA
                          ************************************************************

38_kDa_pET28_clona_1      CACCTTCTTGTTCACCCAGTACCTGTCCAAGCAAGATCCCGAGGGCTGGGGCAAGTCGCC
38_kDa_pET28_clona_2      CACCTTCTTGTTCACCCAGTACCTGTCCAAGCAAGATCCCGAGGGCTGGGGCAAGTCGCC
38kDa                     CACCTTCTTGTTCACCCAGTACCTGTCCAAGCAAGATCCCGAGGGCTGGGGCAAGTCGCC
                          ************************************************************

38_kDa_pET28_clona_1      CGGCTTCGGCACCACCGTCGACTTCCCGGCGGTGCCGGGTGCGCTGGGTGAGAACGGCAA
38_kDa_pET28_clona_2      CGGCTTCGGCACCACCGTCGACTTCCCGGCGGTGCCGGGTGCGCTGGGTGAGAACGGCAA
338kDa                    CGGCTTCGGCACCACCGTCGACTTCCCGGCGGTGCCGGGTGCGCTGGGTGAGAACGGCAA
                          ************************************************************

38_kDa_pET28_clona_1      CGGCGGCATGGTGACCGGTTGCGCCGAGACACCGGGCTGCGTGGCCTATATCGGCATCAG
38_kDa_pET28_clona_2      CGGCGGCATGGTGACCGGTTGCGCCGAGACACCGGGCTGCGTGGCCTATATCGGCATCAG
38kDa                     CGGCGGCATGGTGACCGGTTGCGCCGAGACACCGGGCTGCGTGGCCTATATCGGCATCAG
                          ************************************************************

38_kDa_pET28_clona_1      CTTCCTCGACCAGGCCAGTCAACGGGGACTCGGCGAGGCCCAACTAGGCAATAGCTCTGG
38_kDa_pET28_clona_2      CTTCCTCGACCAGGCCAGTCAACGGGGACTCGGCGAGGCCCAACTAGGCAATAGCTCTGG
38kDa                     CTTCCTCGACCAGGCCAGTCAACGGGGACTCGGCGAGGCCCAACTAGGCAATAGCTCTGG
                          ************************************************************

38_kDa_pET28_clona_1      CAATTTCTTGTTGCCCGACGCGCAAAGCATTCAGGCCGCGGCGGCTGGCTTCGCATCGAA
```

```
38_kDa_pET28_clona_2      CAATTTCTTGTTGCCCGACGCGCAAAGCATTCAGGCCGCGGCGGCTGGCTTCGCATCGAA
38kDa                     CAATTTCTTGTTGCCCGACGCGCAAAGCATTCAGGCCGCGGCGGCTGGCTTCGCATCGAA
                          ************************************************************

38_kDa_pET28_clona_1      AACCCCGGCGAACCAGGCGATTTCGATGATCGACGGGCCCGCCCCGGACGGCTACCCGAT
38_kDa_pET28_clona_2      AACCCCGGCGAACCAGGCGATTTCGATGATCGACGGGCCCGCCCCGGACGGCTACCCGAT
38kDa                     AACCCCGGCGAACCAGGCGATTTCGATGATCGACGGGCCCGCCCCGGACGGCTACCCGAT
                          ************************************************************

38_kDa_pET28_clona_1      CATCAACTACGAGTACGCCATCGTCAACAACCGGCAAAAGGACGCCGCCACCGCGCAGAC
38_kDa_pET28_clona_2      CATCAACTACGAGTACGCCATCGTCAACAACCGGCAAAAGGACGCCGCCACCGCGCAGAC
38kDa                     CATCAACTACGAGTACGCCATCGTCAACAACCGGCAAAAGGACGCCGCCACCGCGCAGAC
                          ************************************************************

38_kDa_pET28_clona_1      CTTGCAGGCATTTCTGCACTGGGCGATCACCGACGGCAACAAGGCCTCGTTCCTCGACCA
38_kDa_pET28_clona_2      CTTGCAGGCATTTCTGCACTGGGCGATCACCGACGGCAACAAGGCCTCGTTCCTCGACCA
38kDa                     CTTGCAGGCATTTCTGCACTGGGCGATCACCGACGGCAACAAGGCCTCGTTCCTCGACCA
                          ************************************************************

38_kDa_pET28_clona_1      GGTTCATTTCCAGCCGCTGCCGCCCGCGGTGGTGAAGTTGTCTGACGCGTTGATCGCGAC
38_kDa_pET28_clona_2      GGTTCATTTCCAGCCGCTGCCGCCCGCGGTGGTGAAGTTGTCTGACGCGTTGATCGCGAC
38kDa                     GGTTCATTTCCAGCCGCTGCCGCCCGCGGTGGTGAAGTTGTCTGACGCGTTGATCGCGAC
                          ************************************************************

38_kDa_pET28_clona_1      GATTTCCAGCCTCGAGCACCACCACCACCACCACTGAG
38_kDa_pET28_clona_2      GATTTCCAGCCTCGAGCACCACCACCACCACCACTGAG
38kDa                     GATTTCCAGCCTCGAG----------------------
                          ****************
```

Appendix 1.18: Alignment of the sequences of clones pET28a-38kDa obtained by sequencing (Macrogen) with the theoretical 38kDa sequence (green), using CLUSTAL multiple sequence alignment by MUSCLE 3.8 (http://www.ebi.ac.uk/Tools/msa/muscle/).

```
PstS_Mycobacteriumsp_TBL1200985_      LYPLFNLWGPAFHQKYPNVTITTQGTGSGTGIAQAAAGTVNIGASDAYLSEGDMAAHKGL
PstS_M_canettii_WP_015289424.1        LYPLFNLWGPAFHEKYPNVTITAQGTGSGAGIAQAAAGTVNIGASDAYLSEGDMAAHKGL
PstS_M_bovis_WP_047709742.1           LYPLFSLWGPAFHERYPNVTITAQGTGSGAGIAQAAAGTVNIGASDAYLSEGDMAAHKGL
PstS_M_caprae_WP_075744482.1          LYPLFNLWGPAFHERYPNVTITAQGTGSGAGIAQAAAGTVNIGASDAYLSEGDMAAHKGL
PstS_                                 LYPLFNLWGPAFHERYPNVTITAQGTGSGAGIAQAAAGTVNIGASDAYLSEGDMAAHKGL
phosphate-binding_protein_MTB_WP      LYPLFNLWGPAFHERYPNITITAQGTGSGAGIAQAAAGTVNIGASDAYLSEGDMAAHKGL
PstS_MTB_WP_075963977.1               LYPLFNLWGPAFHERYPNVTITAQGTGSGAGIAQAAAGTVNIGASDAYLSEGDMAAHKGL
PstS_38kDa_rec_MTB                    LYPLFNLWGPAFHERYPNVTITAQGTGSGAGIAQAAAGTVNIGASDAYLSEGDMAAHKGL
PstS1_MTB_UT0088_KBL59748.1           LYPLFNLWGPAFHERYPNVTITAQGTGSGAGIAQAAAGTVNIGASDAYLSEGDMAAHKGL
                                      *****.*******:.***:***:******:******************************

PstS_Mycobacteriumsp_TBL1200985_      MNIALAISAQQVNYNLPGVTEHLKLNGKVLAAMYQGTVKTWNDPQIAGLNPGVNLPDTPV
PstS_M_canettii_WP_015289424.1        MNIALAISAQQVNYNLPGVSEHLKLNGKVLAAMYQGTIKTWDDPQIAALNPGVNLPGTAV
PstS_M_bovis_WP_047709742.1           MNIALAISAQQVNYNLPGVSEHLKLNGKVLAAMYQGTIKTWDDPQIAALNPGVNLPGTAV
PstS_M_caprae_WP_075744482.1          MNIALAISAQQVNYNLPGVSEHLKLNGKVLAAMYQGTIKTWDDPQIAALNPGVNLPGTAV
PstS_                                 MNIALAISAQQVNYNLPGVSEHLKLNGKVLAAMYQGTIKTWDDPQIAALNPGVNLPGTAV
phosphate-binding_protein_MTB_WP      MNIALAISAQQVNYNLPGVSEHLKLNGKVLAAMYQGTIKTWDDPQIAALNPGVNLPGTAV
PstS_MTB_WP_075963977.1               MNIALAISAQQVNYNLPGVSEHLKMNGKVLAAMYQGTIKTWDDPQIAALNPGVNLPGTAV
PstS_38kDa_rec_MTB                    MNIALAISAQQVNYNLPGVSEHLKLNGKVLAAMYQGTIKTWDDPQIAALNPGVNLPGTAV
PstS1_MTB_UT0088_KBL59748.1           MNIALAISAQQVNYNLPGVSEHLKLNGKVLAAMYQGTIKTWDDPQIAALNPGVNLPGTAV
                                      ******************:****:***********:***:*****.********.*.*

PstS_Mycobacteriumsp_TBL1200985_      VPLHRSDGSGDTFLFTQYLSKQDPDGWGKSPGFGTTVDFPAVPGALGENGNGGMVTGCAE
PstS_M_canettii_WP_015289424.1        VPLHRSDGSGDTFLFTQYLSKQDPDGWGKSPGFGTTVDFPAVPGALGENGNGGMVTGCAE
PstS_M_bovis_WP_047709742.1           VPLHRSDGSGDTFLFTQYLSKQDPEGWGKSPGFGTTVDFPAVPGALGENGNGGMVTGCAE
PstS_M_caprae_WP_075744482.1          VPLHRSDGSGDTFLFTQYLSKQDPEGWGKSPGFGTTVDFPAVPGALGENGNGGMVTGCAE
PstS_                                 VPLHRSDGSGDTFLFTQYLSKQDPEGWGKSPGFGTTVDFPAVPGALGENGNGGMVTGCAE
phosphate-binding_protein_MTB_WP      VPLHRSDGSGDTFLFTQYLSKQDPEGWGKSPGFGTTVDFPAVPGALGENGNGGMVTGCAE
PstS_MTB_WP_075963977.1               VPLHRSDGSGDTFLFTQYLSKQDPEGWGKSPGFGTTVDFPAVPGALGENGNGGMVTGCAE
PstS_38kDa_rec_MTB                    VPLHRSDGSGDTFLFTQYLSKQDPEGWGKSPGFGTTVDFPAVPGALGENGNGGMVTGCAE
PstS1_MTB_UT0088_KBL59748.1           VPLHRSDGSGDTFLFTQYLSKQDPEGWGKSPGFGTTVDFPAVPGALGENGNGGMVTGCAE
                                      ************************:**********************************

PstS_Mycobacteriumsp_TBL1200985_      TPGCVAYIGISFLDQAKQRGLGEAQLGNSSGNFLLPDAQSIKAGAAGFASKTPANQAISM
PstS_M_canettii_WP_015289424.1        TPGCVAYIGISFLDQASQRGLGEAQLGNSSGNFLLPDAQSIQAAAAGFASKTPANQAISM
PstS_M_bovis_WP_047709742.1           TPGCVAYIGISFLDQASQRGLGEAQLGNSSGNFLLPDAQSIQAAAAGFASKTPANQAISM
PstS_M_caprae_WP_075744482.1          TPGCVAYIGISFLDQASQRGLGEAQLGNSSGNFLLPDAQSIQAAAAGFASKTPANQAISM
PstS_                                 TPGCVAYIGISFLDQASQRGLGEAQLGNSSGNFLLPDAQSIQAAAAGFASKTPANQAISM
phosphate-binding_protein_MTB_WP      TPGCVAYIGISFLDQASQRGLGEAQLGNSSGNFLLPDAQSIQAAAAGFASKTPANQAISM
PstS_MTB_WP_075963977.1               TPGCVAYIGISFLDQASQRGLGEAQLGNSSGNFLLPDAQSIQAAAAGFASKTPANQAISM
```

```
PstS_38kDa_rec_MTB                  TPGCVAYIGISFLDQASQRGLGEAQLGNSSGNFLLPDAQSIQAAAAGFASKTPANQAISM
PstS1_MTB_UT0088_KBL59748.1         TPGCVAYIGISFLDQASQRGLGEAQLGNSSGNFLLPDAQSIQAAAAGFASKTPANQAISM
                                    ***************.***********************:*.***************

PstS_Mycobacteriumsp_TBL1200985_    IDGPAPDGYPIINYEYAIVSNRQKDAATAQTVQAFLHWAITDGNNASFLDQVHFQPLPPE
PstS_M_canettii_WP_015289424.1      IDGPAPDGYPIINYEYAIVNNRQKDAATAQTLQAFLHWAITEGNDASFLDQVHFQPLPPA
PstS_M_bovis_WP_047709742.1         IDGPAPDGYPIINYEYAIVNNRQKDAATAQTLQAFLHWAITDGNKASFLDQAHFQPLPPA
PstS_M_caprae_WP_075744482.1        IDGPAPDGYPIINYEYAIVNNRQKDAATAQTLQAFLHWAITDGNKASFLDQAHFQPLPPA
PstS_                               IDGPAPDGYPIINYEYAIVNNRQKDAATAQTLQAFLHWAITDGNKASFLDQAHFQPLPPA
phosphate-binding_protein_MTB_WP    IDGPAPDGYPIINYEYAIVNNRQKDAATAQTLQAFLHWAITDGNKASFLDQVHFQPLPPA
PstS_MTB_WP_075963977.1             IDGPAPDGYPIINYEYAIVNNRQKDAATAQTLQAFLHWAITDGNKASFLDQVHFQPLPPA
PstS_38kDa_rec_MTB                  IDGPAPDGYPIINYEYAIVNNRQKDAATAQTLQAFLHWAITDGNKASFLDQVHFQPLPPA
PstS1_MTB_UT0088_KBL59748.1         IDGPAPDGYPIINYEYAIVNNRQKDAATAQTLQAFLHWAITDGNKASFLDQVHFQPLPPA
                                    ******************.**********:*********:**.******.*******

PstS_Mycobacteriumsp_TBL1200985_    VVKLSDAQIATISS
PstS_M_canettii_WP_015289424.1      VVKLSDALIATISS
PstS_M_bovis_WP_047709742.1         VVKLSDALIATISS
PstS_M_caprae_WP_075744482.1        VVKLSDALIATISS
PstS_                               VVKLSDALIATISS
phosphate-binding_protein_MTB_WP    VVKLSDALIATISS
PstS_MTB_WP_075963977.1             VVKLSDALIATISS
PstS_38kDa_rec_MTB                  VVKLSDALIATISS
PstS1_MTB_UT0088_KBL59748.1         VVKLSDALIATISS
                                    ******* ******
```

Appendix 1.19: Alignment of 38kDa from MTB with other sequences of Mycobacteria (http://www.ebi.ac.uk/Tools/msa/clustalw2/).

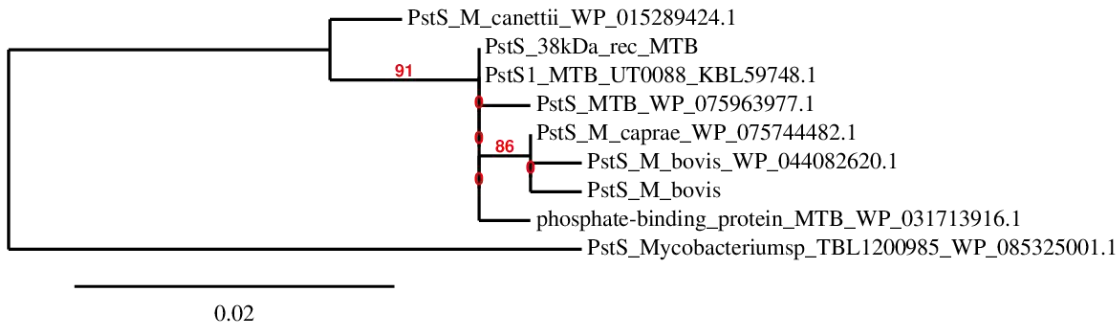

Appendix 1.20: Phylogenetic tree of the amino acid sequence of recombinant 38kDa from MTB, compared with other Mycobacteria sequences. In red it indicates the percentage of support of the branches of the tree.

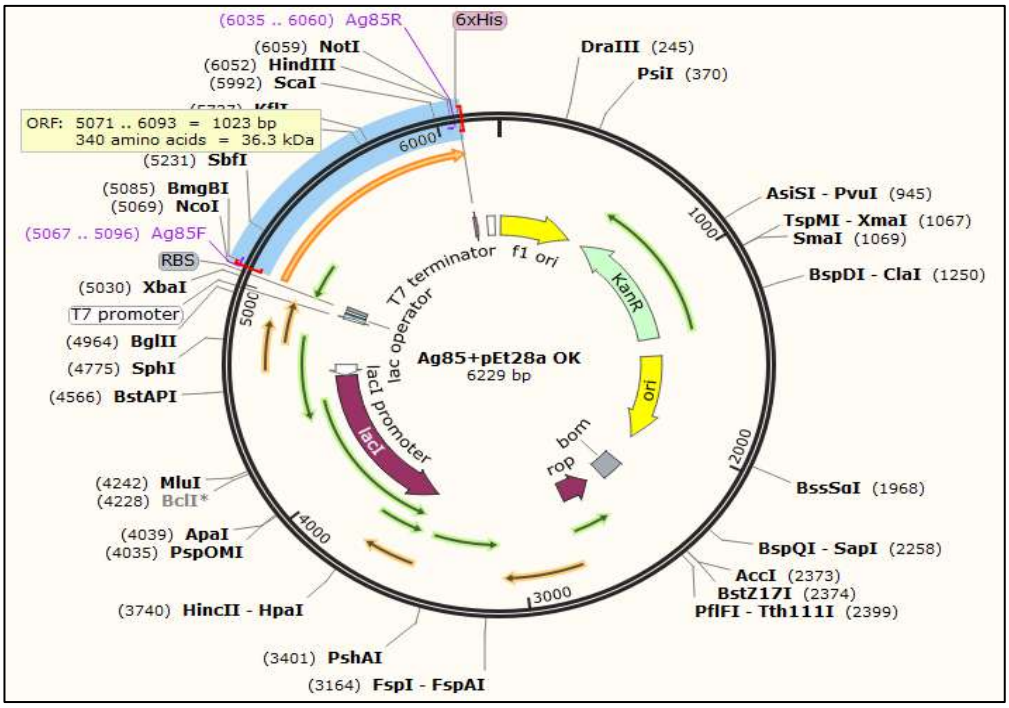

Appendix 1.21: *In silico* pET28a-Ag85B.

```
Ag85B_pET28_clona_1     TTTAACTTTAAGAAGGAGATATACCATGGGCATGACAGACGTGAGCCGAAAGATTCGAGC
Ag85B                   ------------------------------ATGACAGACGTGAGCCGAAAGATTCGAGC
Ag85B_pET28_clona_2     TTTAACTTTAAGAAGGAGATATACCATGGGCATGACAGACGTGAGCCGAAAGATTCGAGC
                                                       ****************************

Ag85B_pET28_clona_1     TTGGGGACGCCGATTGATGATCGGCACGGCAGCGGCTGTAGTCCTTCCGGGCCTGGTGGG
Ag85B                   TTGGGGACGCCGATTGATGATCGGCACGGCAGCGGCTGTAGTCCTTCCGGGCCTGGTGGG
Ag85B_pET28_clona_2     TTGGGGACGCCGATTGATGATCGGCACGGCAGCGGCTGTAGTCCTTCCGGGCCTGGTGGG
                        ************************************************************

Ag85B_pET28_clona_1     GCTTGCCGGCGGAGCGGCAACCGCGGGCGCGTTCTCCCGGCCGGGGCTGCCGGTCGAGTA
Ag85B                   GCTTGCCGGCGGAGCGGCAACCGCGGGCGCGTTCTCCCGGCCGGGGCTGCCGGTCGAGTA
Ag85B_pET28_clona_2     GCTTGCCGGCGGAGCGGCAACCGCGGGCGCGTTCTCCCGGCCGGGGCTGCCGGTCGAGTA
                        ************************************************************

Ag85B_pET28_clona_1     CCTGCAGGTGCCGTCGCCGTCGATGGGCCGCGACATCAAGGTTCAGTTCCAGAGCGGTGG
Ag85B                   CCTGCAGGTGCCGTCGCCGTCGATGGGCCGCGACATCAAGGTTCAGTTCCAGAGCGGTGG
Ag85B_pET28_clona_2     CCTGCAGGTGCCGTCGCCGTCGATGGGCCGCGACATCAAGGTTCAGTTCCAGAGCGGTGG
                        ************************************************************

Ag85B_pET28_clona_1     GAACAACTCACCTGCGGTTTATCTGCTCGACGGCCTGCGCGCCCAAGACGACTACAACGG
Ag85B                   GAACAACTCACCTGCGGTTTATCTGCTCGACGGCCTGCGCGCCCAAGACGACTACAACGG
Ag85B_pET28_clona_2     GAACAACTCACCTGCGGTTTATCTGCTCGACGGCCTGCGCGCCCAAGACGACTACAACGG
                        ************************************************************

Ag85B_pET28_clona_1     CTGGGATATCAACACCCCGGCGTTCGAGTGGTACTACCAGTCGGGACTGTCGATAGTCAT
Ag85B                   CTGGGATATCAACACCCCGGCGTTCGAGTGGTACTACCAGTCGGGACTGTCGATAGTCAT
Ag85B_pET28_clona_2     CTGGGATATCAACACCCCGGCGTTCGAGTGGTACTACCAGTCGGGACTGTCGATAGTCAT
                        ************************************************************

Ag85B_pET28_clona_1     GCCGGTCGGCGGGCAGTCCAGCTTCTACAGCGACTGGTACAGCCCGGCCTGCGGTAAGGC
Ag85B                   GCCGGTCGGCGGGCAGTCCAGCTTCTACAGCGACTGGTACAGCCCGGCCTGCGGTAAGGC
Ag85B_pET28_clona_2     GCCGGTCGGCGGGCAGTCCAGCTTCTACAGCGACTGGTACAGCCCGGCCTGCGGTAAGGC
                        ************************************************************

Ag85B_pET28_clona_1     TGGCTGCCAGACTTACAAGTGGGAAACCTTCCTGACCAGCGAGCTGCCGCAATGGTTGTC
Ag85B                   TGGCTGCCAGACTTACAAGTGGGAAACCTTCCTGACCAGCGAGCTGCCGCAATGGTTGTC
Ag85B_pET28_clona_2     TGGCTGCCAGACTTACAAGTGGGAAACCTTCCTGACCAGCGAGCTGCCGCAATGGTTGTC
                        ************************************************************
```

```
Ag85B_pET28_clona_1      CGCCAACAGGGCCGTGAAGCCCACCGGCAGCGCTGCAATCGGCTTGTCGATGGCCGGCTC
Ag85B                    CGCCAACAGGGCCGTGAAGCCCACCGGCAGCGCTGCAATCGGCTTGTCGATGGCCGGCTC
Ag85B_pET28_clona_2      CGCCAACAGGGCCGTGAAGCCCACCGGCAGCGCTGCAATCGGCTTGTCGATGGCCGGCTC
                         ************************************************************

Ag85B_pET28_clona_1      GTCGGCAATGATCTTGGCCGCCTACCACCCCCAGCAGTTCATCTACGCCGGCTCGCTGTC
Ag85B                    GTCGGCAATGATCTTGGCCGCCTACCACCCCCAGCAGTTCATCTACGCCGGCTCGCTGTC
Ag85B_pET28_clona_2      GTCGGCAATGATCTTGGCCGCCTACCACCCCCAGCAGTTCATCTACGCCGGCTCGCTGTC
                         ************************************************************

Ag85B_pET28_clona_1      GGCCCTGCTGGACCCCTCTCAGGGGATGGGGCCTAGCCTGATCGGCCTCGCGATGGGTGA
Ag85B                    GGCCCTGCTGGACCCCTCTCAGGGGATGGGGCCTAGCCTGATCGGCCTCGCGATGGGTGA
Ag85B_pET28_clona_2      GGCCCTGCTGGACCCCTCTCAGGGGATGGGGCCTAGCCTGATCGGCCTCGCGATGGGTGA
                         ************************************************************

Ag85B_pET28_clona_1      CGCCGGCGGTTACAAGGCCGCAGACATGTGGGGTCCCTCGAGTGACCCGGCATGGGAGCG
Ag85B                    CGCCGGCGGTTACAAGGCCGCAGACATGTGGGGTCCCTCGAGTGACCCGGCATGGGAGCG
Ag85B_pET28_clona_2      CGCCGGCGGTTACAAGGCCGCAGACATGTGGGGTCCCTCGAGTGACCCGGCATGGGAGCG
                         ************************************************************

Ag85B_pET28_clona_1      CAACGACCCTACGCAGCAGATCCCCAAGCTGGTCGCAAACAACACCCGGCTATGGGTTTA
Ag85B                    CAACGACCCTACGCAGCAGATCCCCAAGCTGGTCGCAAACAACACCCGGCTATGGGTTTA
Ag85B_pET28_clona_2      CAACGACCCTACGCAGCAGATCCCCAAGCTGGTCGCAAACAACACCCGGCTATGGGTTTA
                         ************************************************************

Ag85B_pET28_clona_1      TTGCGGGAACGGCACCCCGAACGAGTTGGGCGGTGCCAACATACCCGCCGAGTTCTTGGA
Ag85B                    TTGCGGGAACGGCACCCCGAACGAGTTGGGCGGTGCCAACATACCCGCCGAGTTCTTGGA
Ag85B_pET28_clona_2      TTGCGGGAACGGCACCCCGAACGAGTTGGGCGGTGCCAACATACCCGCCGAGTTCTTGGA
                         ************************************************************

Ag85B_pET28_clona_1      GAACTTCGTTCGTAGCAGCAACCTGAAGTTCCAGGATGCGTACAACGCCGCGGGCGGGCA
Ag85B                    GAACTTCGTTCGTAGCAGCAACCTGAAGTTCCAGGATGCGTACAACGCCGCGGGCGGGCA
Ag85B_pET28_clona_2      GAACTTCGTTCGTAGCAGCAACCTGAAGTTCCAGGATGCGTACAACGCCGCGGGCGGGCA
                         ************************************************************

Ag85B_pET28_clona_1      CAACGCCGTGTTCAACTTCCCGCCCAACGGCACGCACAGCTGGGAGTACTGGGGCGCTCA
Ag85B                    CAACGCCGTGTTCAACTTCCCGCCCAACGGCACGCACAGCTGGGAGTACTGGGGCGCTCA
Ag85B_pET28_clona_2      CAACGCCGTGTTCAACTTCCCGCCCAACGGCACGCACAGCTGGGAGTACTGGGGCGCTCA
                         ************************************************************

Ag85B_pET28_clona_1      GCTCAACGCCATGAAGGGTGACCTGCAGAGTTCGTTAGGCGCCGGCAAGCTTGCGGCCGC
Ag85B                    GCTCAACGCCATGAAGGGTGACCTGCAGAGTTCGTTAGGCGCCGGC--------------
Ag85B_pET28_clona_2      GCTCAACGCCATGAAGGGTGACCTGCAGAGTTCGTTAGGCGCCGGCAAGCTTGCGGCCGC
                         *******************************************

Ag85B_pET28_clona_1      ACTCGAGCACCACCACCACCACCACTG-
Ag85B                    ----------------------------
Ag85B_pET28_clona_2      ACTCGAGCACCACCACCACCACCACTGN
```

Appendix 1.22: Alignment of the sequences of clones pET28a-Ag85B obtained by sequencing (Macrogen) with the theoretical Ag85B sequence, using CLUSTAL multiple sequence alignment by MUSCLE 3.8 (http://www.ebi.ac.uk/Tools/msa/muscle/).

```
esterase_family_M_nebraskense_WP     MTDLSKKVRAWGRRLLVGTAAAVTLPGLIGLAGGAPTAGAFSRPGLPVEYLQVPSAGMGR
esterase_family_M_paraffinicum_W     MTEVREKVRAWGRRLLVGAAAAVTLPGLIGLAGGAPTAGAFSRPGLPVEYLQVPSAGMGR
esterase_family_M_marinum_WP_012     MTDVSGKIRTWGRRLLIGAAAAITLPGLVGLAGGAPAAKAFSRPGLPVEYLQVPSAAMGR
esterase_family_M_ulcerans_WP_01     MTDVSGKIRTWGRRLLIGAAAAITLPGLVGVAGGAPAAKAFSRPGLPVEYLQVPSAAMGR
Ag85A_M_shinjukuense_WP_08304901     MTDVSGKMRAWGRRLLVGAAAAVTLPGLVGLAGGAATAGAFSRPGLPVEYLQVPSAAMGR
Ag85B_MTB_Haarlem/NITR202_AGL235     MTDVSRKIRAWGRRXMIGTAAAVVLPGLVGLAGGAATAGAFSRPGLPVEYLQVPSPSMGR
Ag85A_MTB_WP_055371452.1             MTDVSRKIRAWGRRLMIGTAAAVVLPGLVGLAGGAATAGAFSRPGLPVDYLQVPSPSMGR
Ag85B_rec__MTB                       MTDVSRKIRAWGRRLMIGTAAAVVLPGLVGLAGGAATAGAFSRPGLPVEYLQVPSPSMGR
Ag85B_MTB_CDC1551_AAK46207.1         MTDVSRKIRAWGRRLMIGTAAAVVLPGLVGLAGGAATAGAFSRPGLPVEYLQVPSPSMGR
esterase_family_protein_M_bovis_     MTDVSRKIRAWGRRLMIGTAAAVVLPGLVGLAGGAATAGAFSRPGLPVEYLQVPSPSMGR
Ag85B_M_bovis_BCG_AKO24924.1         ---MSRKIRAWGRRLMIGTAAAVVLPGLVGLAGGAATAGAFSRPGLPVEYLQVPSPSMGR
Ag85B_MTB_SUMu003_EFP19521.1         ---MSRKIRAWGRRLMIGTAAAVVLPGLVGLAGGAATAGAFSRPGLPVEYLQVPSPSMGR
                                        :  *:*:**** ::*:***:.****:*:****.:* *********:******..***
```

```
esterase_family_M_nebraskense_WP      NIKVQFQSGGNGSPAVYLLDGLRAQDDYNGWDINTPAFEWYYQSGLSIVMPVGGQSSFYS
esterase_family_M_paraffinicum_W      NIKVQFQSGGNNSPAVYLLDGLRAQDDYNGWDINTPAFEWYYQSGLSIIMPVGGQSSFYS
esterase_family_M_marinum_WP_012      SIKVQFQSGGDNSPAVYLLDGLRAQDDYNGWDINTPAFEWYYQSGLSVIMPVGGQSSFYA
esterase_family_M_ulcerans_WP_01      SIKVQFQSGGDNSPAVYLLDGLRAQDDYNGWDINTPAFEWYYQSGLSVIMPVGGQSSFYA
Ag85A_M_shinjukuense_WP_08304901      SIKVQFQSGGDNSPAVYLLDGLRAQDDYNGWDINTPAFEWYYQSGLSIVMPVGGQSSFYS
Ag85B_MTB_Haarlem/NITR202_AGL235      DIKVQFQSGGNNSPAVYLLDGLRAQDDYNGWXINTPAFEWYYQSGLSIVMPVGGQSSFYS
Ag85A_MTB_WP_055371452.1              DIKVQFQSGGNNSPAVYLLDGLRAQDDYNGWDINTPAFEWYYQSGLSIVMPVGGQSSFYS
Ag85B_rec__MTB                        DIKVQFQSGGNNSPAVYLLDGLRAQDDYNGWDINTPAFEWYYQSGLSIVMPVGGQSSFYS
Ag85B_MTB_CDC1551_AAK46207.1          DIKVQFQSGGNNSPAVYLLDGLRAQDDYNGWDINTPAFEWYYQSGLSIVMPVGGQSSFYS
esterase_family_protein_M_bovis_      DIKVQFQSGGNNSPAVYLLDGLRAQDDYNGWDINTPAFEWYYQSGLSIVMPVGGQSSFYS
Ag85B_M_bovis_BCG_AKO24924.1          DIKVQFQSGGNNSPAVYLLDGLRAQDDYNGWDINTPAFEWYYQSGLSIVMPVGGQSSFYS
Ag85B_MTB_SUMu003_EFP19521.1          DIKVQFQSGGNNSPAVYLLDGLRAQDDYNGWDINTPAFEWYYQSGLSIVMPVGGQSSFYS
                                      .*********:.****************** ***************::**********:

esterase_family_M_nebraskense_WP      DWYSPACGKAGCSTYKWETFVTSELPQYLASNKSVKSTGSAAVGISMAGSSALILAAYHP
esterase_family_M_paraffinicum_W      DWYSPACGKAGCSTYKWETFLTSELPQYLASNKSVKSTGSAAVGISMAGSSALILAAYHP
esterase_family_M_marinum_WP_012      NWYQPACGKAGCSTYKWETFLTSELPEWLSANRSVKPTGSAAVGISMSGSSAMILAVYHP
esterase_family_M_ulcerans_WP_01      NWYQPACGKSGCSTYKWETFLTSELPEWLSANRSVKPTGSAAIGISMSGSSAMILAVYHP
Ag85A_M_shinjukuense_WP_08304901      DWYSPACGKAGCSTYKWETFLTSELPQWLSANRGVKPTGSAAVGLSMAGSSALILAAYHP
Ag85B_MTB_Haarlem/NITR202_AGL235      DWYSPACGKAGCQTYKWEXFLXSELPQWLSANRAVKPTGSAAIGXSMAGSSAMILAAYHP
Ag85A_MTB_WP_055371452.1              DWYSPACGKAGCQTYKWETFLTSELPQWLSANRAVKPTGSAAIGLSMAGSSAMILAAYHP
Ag85B_rec__MTB                        DWYSPACGKAGCQTYKWETFLTSELPQWLSANRAVKPTGSAAIGLSMAGSSAMILAAYHP
Ag85B_MTB_CDC1551_AAK46207.1          DWYSPACGKAGCQTYKWETFLTSELPQWLSANRAVKPTGSAAIGLSMAGSSAMILAAYHP
esterase_family_protein_M_bovis_      DWYSPACGKAGCQTYKWETFLTSKLPQWLSANRAVKPTGSAAIGLSMAGSSAMILAAYHP
Ag85B_M_bovis_BCG_AKO24924.1          DWYSPACGKAGCQTYKWETLLTSELPQWLSANRAVKPTGSAAIGLSMAGSSAMILAAYHP
Ag85B_MTB_SUMu003_EFP19521.1          DWYSPACGKAGCQTYKWETFLTSELPQWLSANRAVKPTGSAAIGLSMAGSSAMILAAYHP
                                      :**.*****:**.***** :: *:**::*::*..**.*****:* **:****:***.***

esterase_family_M_nebraskense_WP      NQFIYAGSLSALMDPSQGMGPSLIGLAMGDAGGYKANDMWGPSSDPAWQRNDPSLQIPKL
esterase_family_M_paraffinicum_W      NQFVYAGSLSALMDPSQGMGPSLIGLAMGDAGGYKASDMWGPSSDPAWQRNDPTLQIPKL
esterase_family_M_marinum_WP_012      QQFVYAGSLSALLDPSQGMGPSLIGLAMGDAGGYKAGDMWGPSSDPAWQRNDPTIQIPAL
esterase_family_M_ulcerans_WP_01      QQFVYAGSLSALLDPSQGMGPFLIGLAMGDAGGYKAGDMWGPSSDPAWQRNDPTIQIPAL
Ag85A_M_shinjukuense_WP_08304901      QQFIYAGSLSALMDPSSGMGPTLIGLAMGDAGGYKAADMWGPSSDPAWQRNDPTVQIPLL
Ag85B_MTB_Haarlem/NITR202_AGL235      QQFIYAGSLSALLDPSQGMGPSLIGLAMGDAGGYKAADMWGPSSDPAWERNDPTQQIPKL
Ag85A_MTB_WP_055371452.1              QQFIYAGSLSALLDPSQGMGPSLIGLAMGDAGGYKAADMWGPSSDPAWERNDPTQQIPKL
Ag85B_rec__MTB                        QQFIYAGSLSALLDPSQGMGPSLIGLAMGDAGGYKAADMWGPSSDPAWERNDPTQQIPKL
Ag85B_MTB_CDC1551_AAK46207.1          QQFIYAGSLSALLDPSQGMGPSLIGLAMGDAGGYKAADMWGPSSDPAWERNDPTQQIPKL
esterase_family_protein_M_bovis_      QQFIYAGSLSALLDPSQGMGPSLIGLAMGDAGGYKAADMWGPSSDPAWERNDPTQQIPKL
Ag85B_M_bovis_BCG_AKO24924.1          QQFIYAGSLSALLDPSQGMGPSLIGLAMGDAGGYKAADMWGPSSDPAWERNDPTQQIPKL
Ag85B_MTB_SUMu003_EFP19521.1          QQFIYAGSLSALLDPSQGMGPSLIGLAMGDAGGYKAADMWGPSSDPAWERNDPTQQIPKL
                                      :**:********:***.**** ************* ***********:****: *** *

esterase_family_M_nebraskense_WP      VGNNTRLWIYCGNGTPSELGGANMPAEFLENFVRSSNLKFQDAYNAAGGHNAVFNFNANG
esterase_family_M_paraffinicum_W      VGNNTRLWVYCGNGTPSELGGANMPAEFLENFVRSSNLKFQDQYNAAGGHNAVFNFNANG
esterase_family_M_marinum_WP_012      VSNNTRLWVYCGNGTPSELGGANLPAEFLENFVRSSNLKFQDAYNAAGGHNAVFNFNDNG
esterase_family_M_ulcerans_WP_01      VSNNTRLWVYCGNGTPSELGGASLPAEFLENFVRSSNLKFQDAYNAAGGHNAVFNFNDNG
Ag85A_M_shinjukuense_WP_08304901      VANNTRLWVYCGNGTPTELGGANIPAEFLENFVRSSNIKFQDAYNAAGGHNAVFNFPPNG
Ag85B_MTB_Haarlem/NITR202_AGL235      VANNTRLWVYCGNGTPNELGGANIPAEFLENFVRSSNLKFQDAYNAAGGHNAVFNFPPNG
Ag85A_MTB_WP_055371452.1              VANNTRLWVYCGNGTPNELGGANIPAEFLENFVRSSNLKFQDAYNAAGGHNAVFNFPPNG
Ag85B_rec__MTB                        VANNTRLWVYCGNGTPNELGGANIPAEFLENFVRSSNLKFQDAYNAAGGHNAVFNFPPNG
Ag85B_MTB_CDC1551_AAK46207.1          VANNTRLWVYCGNGTPNELGGANIPAEFLENFVRSSNLKFQDAYNAAGGHNAVFNFPPNG
esterase_family_protein_M_bovis_      VANNTRLWVYCGNGTPNELGGANIPAEFLENFVRSSNLKFQDAYNAAGGHNAVFNFPPNG
Ag85B_M_bovis_BCG_AKO24924.1          VANNTRLWVYCGNGTPNELGGANIPAEFLENFVRSSNLKFQDAYNAAGGHNAVFNFPPNG
Ag85B_MTB_SUMu003_EFP19521.1          VANNTRLWVYCGNGTPNELGGANIPAEFLENFVRSSNLKFQDAYNAAGGHNAVFNFPPNG
                                      *.******:*******.*****.:*************:**** *************  **

esterase_family_M_nebraskense_WP      THSWEYWGAQLNAMKGDLQGTLGA-
esterase_family_M_paraffinicum_W      THSWEYWGAQLNAMKPDLQGTLGA-
esterase_family_M_marinum_WP_012      THSWEYWGAQLNAMKGDLQASLGA-
esterase_family_M_ulcerans_WP_01      THSWEYWGAQLNAMKGDLQTSLGA-
Ag85A_M_shinjukuense_WP_08304901      THSWEYWGAQLNAMKGDLQGSLGA-
Ag85B_MTB_Haarlem/NITR202_AGL235      THSWEYWGAQLNAMKGDLQSSLGAG
Ag85A_MTB_WP_055371452.1              THSWEYWGAQLNAMKGDLQSSLGAG
Ag85B_rec__MTB                        THSWEYWGAQLNAMKGDLQSSLGAG
Ag85B_MTB_CDC1551_AAK46207.1          THSWEYWGAQLNAMKGDLQSSLGAG
esterase_family_protein_M_bovis_      THSWEYWGAQLNAMKGDLQSSLGAG
Ag85B_M_bovis_BCG_AKO24924.1          THSWEYWGAQLNAMKGDLQSSLGAG
Ag85B_MTB_SUMu003_EFP19521.1          THSWEYWGAQLNAMKGDLQSSLGAG
                                      *************** *** :***
```

Appendix 1.23: Alignment of Ag85B from MTB with other sequences of Mycobacteria (http://www.ebi.ac.uk/Tools/msa/clustalw2/).

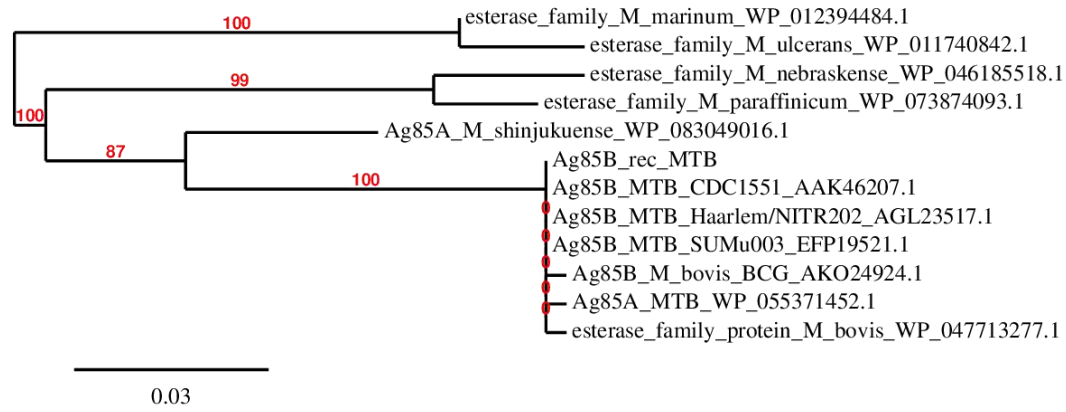

Appendix 1.24: Phylogenetic tree of the amino acid sequence of recombinant Ag85B from MTB, compared with other Mycobacteria sequences. In red it indicates the percentage of support of the branches of the tree.

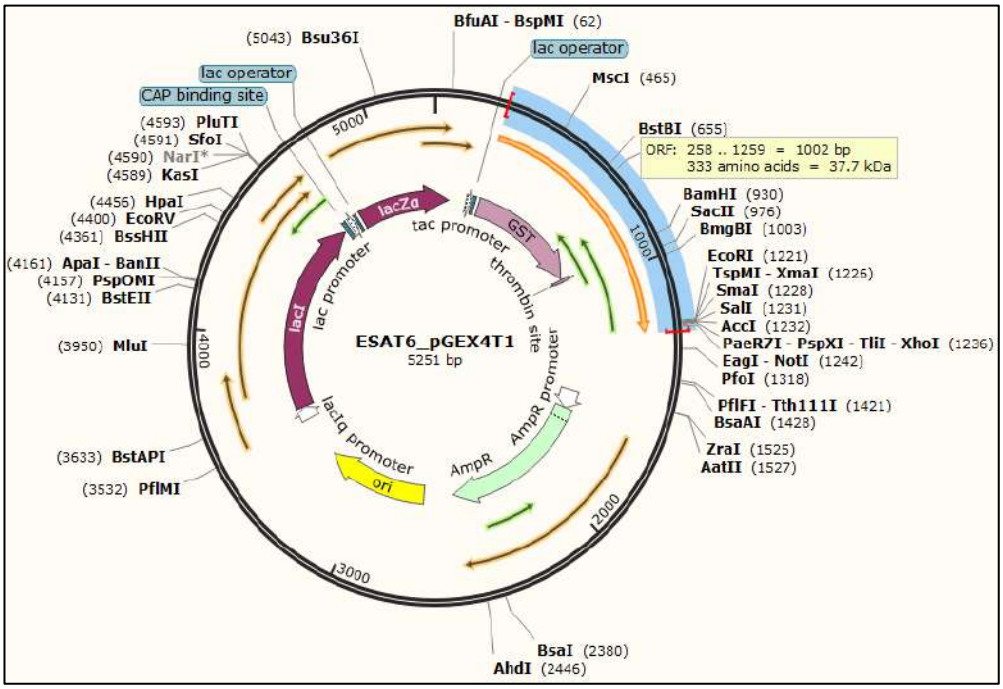

Appendix 1.25: *In silico* pGEX4T1-ESAT6.

```
ESAT_pGEX_clona_6       ATCGGATCTGGTTCGCGTGGATCCATGACAGAGCAGGAGTGGAATTTCGCGGGTATCGAG
ESAT6                   ------------------------ATGACAGAGCAGCAGTGGAATTTCGCGGGTATCGAG
                                                 *********** **********************

ESAT_pGEX_ clona_6      GCCGCGGCAAGCGCAATCCAGGGAAATGTCACGTCCATTCATTCCCTCCTTGACGAGGGG
ESAT6                   GCCGCGGCAAGCGCAATCCAGGGAAATGTCACGTCCATTCATTCCCTCCTTGACGAGGGG
                        ************************************************************

ESAT_pGEX_clona_6       AAGCAGTCCCTGACCAAGCTCGCAGCGGCCTGGGGCGGTAGCGGTTCGGAGGCGTACCAG
ESAT6                   AAGCAGTCCCTGACCAAGCTCGCAGCGGCCTGGGGCGGTAGCGGTTCGGAGGCGTACCAG
                        ************************************************************

ESAT_pGEX_clona_6       GGTGTCCAGCAAAAATGGGACGCCACGGCTACCGAGCTGAACAACGCGCTGCAGAACCTG
ESAT6                   GGTGTCCAGCAAAAATGGGACGCCACGGCTACCGAGCTGAACAACGCGCTGCAGAACCTG
                        ************************************************************
```

```
ESAT_pGEX_clona_6       GCGCGGACGATCAGCGAAGCCGGTCAGGCAATGGCTTCGACCGAAGGCAACGTCACTGGG
ESAT6                   GCGCGGACGATCAGCGAAGCCGGTCAGGCAATGGCTTCGACCGAAGGCAACGTCACTGGG
                        ************************************************************

ESAT_pGEX_clona_6       ATGTTCGCAGAATTCCCGGGTCGACTCA
ESAT6                   ATGTTCGCAGAATTCGCA----------
                        ************** *
```

Appendix 1.26: Alignment of the sequences of clones pGEX4T1-ESAT6 obtained by sequencing (Macrogen) with the theoretical ESAT6 sequence, using CLUSTAL multiple sequence alignment by MUSCLE 3.8 (http://www.ebi.ac.uk/Tools/msa/muscle/).

```
WXG100_family_M_gordonae_WP_0694     MTEQQWNFAGIEAAASTIQGNVSSIHSLLDEGKQSLTKLAAAWGGSGSESYQSVQQKWDG
WXG100_family_M_gordonae_WP_0555     MTEQQWNFAGIEAAASTIQGNVSSIHSLLDEGKQSLTKLAAAWGGSGSESYQAVQQKWDG
WXG100_family_M_asiaticum_WP_036     MTEQQWNFAGIEAAASTIQGNVTTIHSLLDEGKQSLTKLSAAWGGSGSEAYQGVQQKWDA
WXG100_family_M_liflandii_WP_015     MTEQQWNFAGIEAASSSIGGNVGSIHSLLDEGKQSLHKLAAAWGGSGSEAYQGVQQKWDS
WXG100_family_M_marinum_WP_01239     MTEQQWNFAGIEAASSAIQGNVTSIHSLLDEGKQSLHKLAAAWGGSGSEAYRGVQQNWDS
WXG100_family_M_marinum_WP_02072     MTEQQWNFAGIEAASSAIQGNVTSIHSLLDEGKQSLHKLAAAWGGSGSEAYQGVQQKWDS
WXG100_family_M_kansasii_WP_0364     MTEQQWNFAGIEAAASAIQGNVTSIHSLLDEGKQSLTKLAAAWGGSGSEAYQGVQQKWDA
WXG100_family_M_lacus_WP_0851626     MTEQQWNFAGIEAAASAIQGNVTSIHSLLDEGKQSLTKLAAAWGGSGSDAYQGVQQKWDA
WXG100_family_Mycobacteriumsp_14     MTEQQWNFAGIEAAASSIQGNVTSIHSLLDEGKQSLTKLAAAWGGSGSEAYQGVQQKWDA
WXG100_family_M_kansasii_ORB8566     MTEQQWNFAGIEAASSAIQGNVTSIHSLLDEGKQSLTKLAAAWGGSGSEAYQGVQQKWDA
WXG100_family_M_riyadhense_WP_08     MTEQQWNFAGIEAASSAIQGNVTSIHSLLDEGKQSLTKLAAAWGGSGSEAYQGVQQKWDA
Esat6_M_riyadhense_AEP68522.1        ----QWNFAGIEAASSAIQGNVTSIHSLLDEGKQSLTKLAAAWGGSGSEAYQGVQQKWDA
WXG100_family_M_shinjukuense_WP_     MTEQQWNFAGIEAAASAIQGNVTSIHSLLDEGKQSLTKLAAAWGGSGSEAYQGVQQKWDA
WXG100_family_M_bovis_WP_0233498     MTEQQWNFAGIEAAASAIQGNVTSIHSLLDEGKQSLTKLAAAWGGSGSEAYQGVQQKWDA
Esat6_rec_MTB                        MTEQQWNFAGIEAAASAIQGNVTSIHSLLDEGKQSLTKLAAAWGGSGSEAYQGVQQKWDA
WXG100_family_MTB_WP_031657339.1     MTEQQWNFAGIEAAASAIQGNVTSIHSLLDEGKQSLTKLAAAWGGSGSEAYQGVQQKWDA
Esat6_M_tuberculosis_RGTB327_AFE     -------------------NVTSIHSLLDEGKQSLTKLAAAWGGSGSEAYQGVQQKWDA
WXG100_family_M_boenickei_WP_077     MTEQVWNFAGIEGGASEIQGAVSTTAGLLDEGKGSLASLASAWGGSGSEAYQAVQTRWDS
WXG100_family_M_celatum_WP_06253     MSEQVWNFAGIEGGASDIQGAVQTTHGLLDEGKGSLASLAAVWGGSGSEAYQAVQQRWDN
WXG100_family_M_kyorinense_WP_04     MSEQVWNFAGIEGGASDIQGAVQTTHGLLDEGKGSLASLAAVWGGSGSEAYQAVQQRWDN
                                                          * :  .****** ** .*::.******::*..** .**

WXG100_family_M_gordonae_WP_0694     TAQELNTSLQNLARTISEASQAMQSTEGSVTGLFA
WXG100_family_M_gordonae_WP_0555     TAQELNNSLQNLARTISEASQAMQSTEGSVTGLFA
WXG100_family_M_asiaticum_WP_036     TAQELNNSLQNLARTISEAGQAMQSTEGSVTGMFA
WXG100_family_M_liflandii_WP_015     TAQELNNALQNLARTISEAGQAMSSTEGNVTGMFA
WXG100_family_M_marinum_WP_01239     TAQELNNSLQNLARTISEAGQAMSSTEGNVTGMFA
WXG100_family_M_marinum_WP_02072     TAQELNNALQNLARTISEAGQAMSSTEGNVTGMFA
WXG100_family_M_kansasii_WP_0364     TAQELNSALQNLSRTISEAGQAMASTEGNVTGMFA
WXG100_family_M_lacus_WP_0851626     TAQELNNALQNLARTISEAGQAMASTEGNVTGMFA
WXG100_family_Mycobacteriumsp_14     TAQELNNALQNLARTISEAGQAMQSTEGNVTGMFA
WXG100_family_M_kansasii_ORB8566     TAQELNNALQNLARTISEAGQAMASTEGNVTGMFA
WXG100_family_M_riyadhense_WP_08     TAQELNNALQNLARTISEAGQAMQSTEGNVTGMFA
Esat6_M_riyadhense_AEP68522.1        TAQELNNALQNLARTISEAGQAMQSTEGNVTG---
WXG100_family_M_shinjukuense_WP_     TATELNNALQNLARTISEAGQAMQSTEG-------
WXG100_family_M_bovis_WP_0233498     TAAELNNALQNLARTISEAGQAMASTEGNVTGMFA
Esat6_rec_MTB                        TATELNNALQNLARTISEAGQAMASTEGNVTGMFA
WXG100_family_MTB_WP_031657339.1     TATELNNALQNLARTISEAGQAMASTEGNVTGMFA
Esat6_M_tuberculosis_RGTB327_AFE     TATELNNALQNLARTISEAGQAMASTEGNVTGMFA
WXG100_family_M_boenickei_WP_077     TANELNSALQNLAQTISEAGQTMSQTEAGVTGMFA
WXG100_family_M_celatum_WP_06253     TAMELNTALQNLAQTISEAGQTMGQTEAGVTGMFA
WXG100_family_M_kyorinense_WP_04     TAAELNMALQNLAQTISEAGQTMGQTEAGVTGMFA
                                     ** *** :****:.*****.*:* .**.
```

Appendix 1.27: Alignment of ESAT6 from MTB with other sequences of Mycobacteria (http://www.ebi.ac.uk/Tools/msa/clustalw2/).

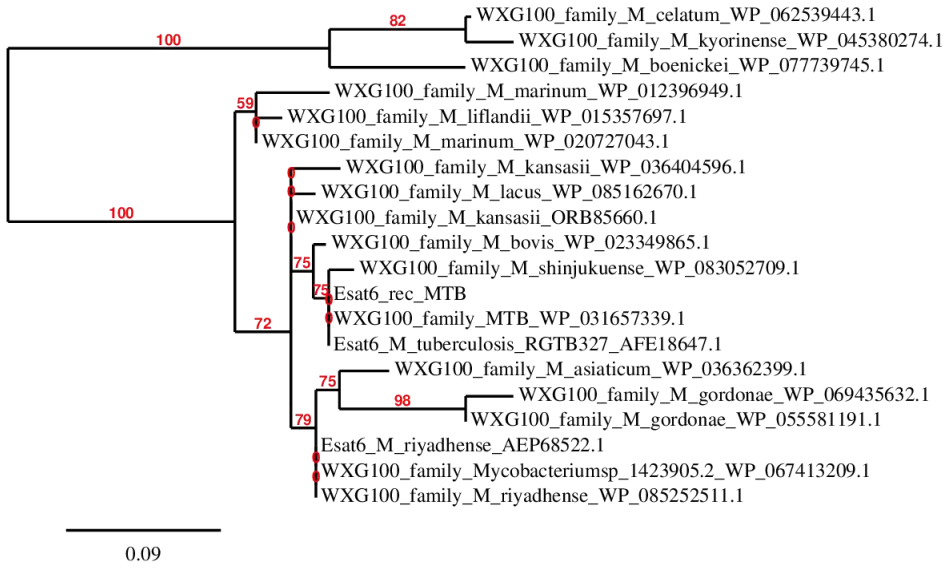

Appendix 1.28: Phylogenetic tree of the amino acid sequence of recombinant ESAT6 from MTB, compared with other Mycobacteria sequences. In red it indicates the percentage of support of the branches of the tree.

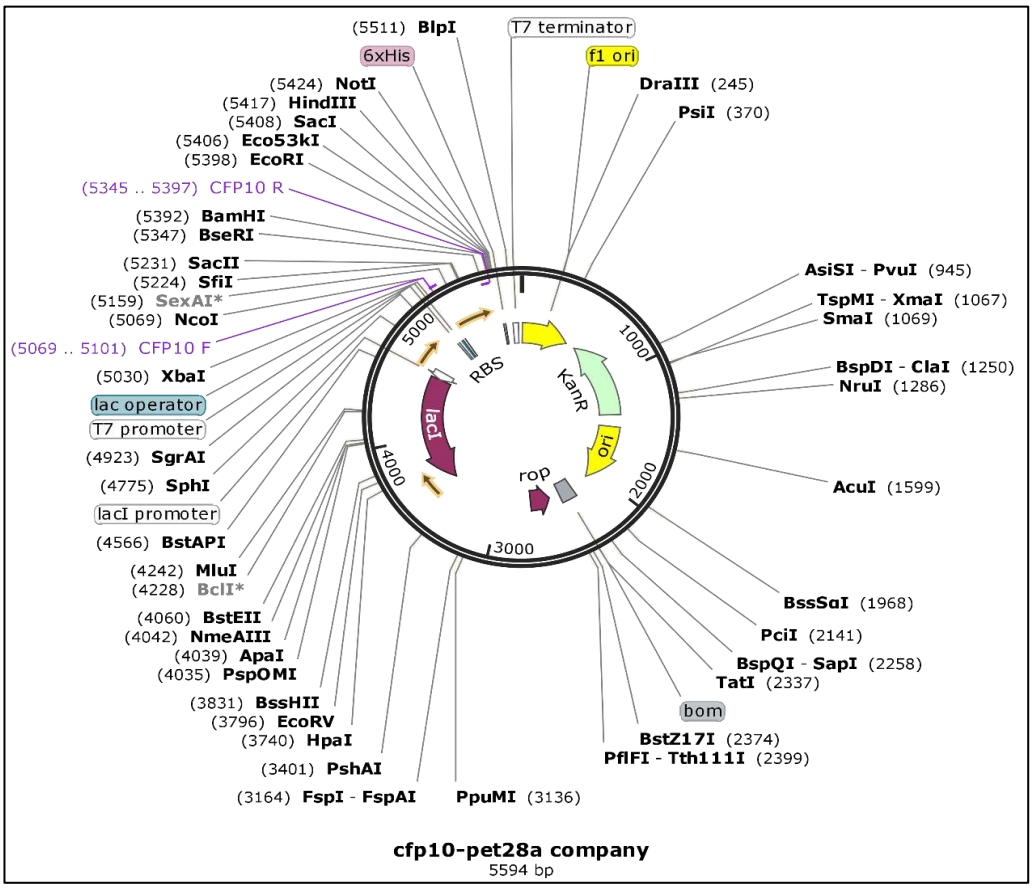

Appendix 1.29: *In silico* pET28a-CFP10.

```
type_VII_secretion_target_M_trip      MAEMKTDASTLSAEAGNFDRIGGELQGVIKGVEHTGGELASHWTGQAGSAAQSALQRFQE
type_VII_secretion_target_Mycoba      MAEMKTDAATLSAEAGNFDRISGELQRVIATVESTGGELAGHWRGQAGAAAQQALARFHE
EsxB_M_shigaense_BAX95048.1           MAEMRTDAATLSAEAANFDRISGELQRVISGVEQTGGELASHMVGQAGTATQQALQRFHE
EsxB_M_gordonae_WP_055581190.1        MAEMKTDAAALAQEAGNFERISSDLKTQIDQIESTAGSLQGQWRGVAGQAAQAAVVRFQE
Cfp10_MTB_Haarlem/NITR202_AGL254      MAEMKTXAATLAQEAGNFERISGDLKTQIDQVESTAGSLQGQWRGAAGTAAQAAVVRFQE
EsxB_MTB_WP_052632688.1               MAEMKTDAATLAQEAGNFERISGDLKTQIDQVESTAGSLQGQWRGAAGTAAQAAVVRFKE
ESAT-6-like_EsxB_MTB_WP_00390077      MAEMKTDAATLAQEAGNFERISGDLKTQIDQVESTAGSLQGQWRGAAGTAAQAAVVRFQE
Cfp10_rec_MTB                         MAEMKTDAATLAQEAGNFERISGDLKTQIDQVESTAGSLQGQWRGAAGTAAQAAVVRFQE
Cfp10-esat6_MTB_pdb|3FAV|A            MAEMKTDAATLAQEAGNFERISGDLKTQIDQVESTAGSLQGQWRGAAGTAAQAAVVRFQE
Cfp10_M_bovis_AEQ02359.1              -AEMKTDAATLAQEAGNFERISGDLKTQIDQVESTAGSLQGQWRGAAGTAAQAAVVRFQE
CFP_M_marinum_MB2_EPQ70954.1          ---MKTDAATLAQEAGNFERISGDLKTQIDQVESTAGSLQAQWRGAAGTAAQAAVVRFQE
CFP-10_M_ulcerans_AAW68021.1          ---LKNDAATLAQEAGNFERISGDLKTQIDQVESTAGSLQAQWRGAAGTAAQAAVVRFQE
Cfp-10_My_liflandii_AAX20067.1        ----------------FERISGDLKTQIDQVESTAGSLQAQWRGAAGTAAQAAVVRFQE
esxB_M_kansasii_OOK71084.1            ---MKTDAATLAQEAGNFERISGDLKTQIDQVESTAASLQAQWRGAAGTAAQAAVVRFQE
esxB_M_kansasii_OOK75781.1            ---MKTDAATLAQEAGNFERISGDMKTQIDQVESTAASLQAQWRGAAGAAAQAAVVRFQE
EsxB_M_asiaticum_WP_065144405.1       MAEMKTDAAALAQEAGNFERISGDLKTQIDQVESTAASLQGQWQGAAGQAAQAAVVRFQE
type_VII_secretion_target_M_riya      MAEMKTDAATLAQEAGNFERISGDLKTQIDQVESTAATLQSQWQGAAGQAAQAAVVRFQE
Cfp10_M_riyadhense_ACB41411.1         MAEMKTDAATLAQEAGNFERISGDLKTQIDQVESTAATLQSQWQGAAGQAAQAAVVRFQE
EsxB_M_celatum_WP_062539444.1         MAQMQTDAAVLAKEASNFERISGELKGVIAHVESVAGSLAPQFQGQAGSAAQAALMRFQE
EsxB_M_rhodesiae_WP_014210298.1       ---MNTDVAVLAKEAANFERISGELTAVIAQVEATAGALASHMVGQAGTAAQQALIRFHE
EsxB_M_septicum_WP_044514397.1        MAQMNTDAAVLAKEAANFERISGELKSVIAQVESTGGTLAAQMQGQAGTAAQAALLRFHE
                                                  *:**..::   *  :* ... *  :  * ** *:* *: **:*

type_VII_secretion_target_M_trip      AGNAQIKALTDIHEKISQAGVQYQRANEEQASNLQSTAGNMGF
type_VII_secretion_target_Mycoba      AGQAQIKALSEISQNIHGAGAQYSSADEEQASSLSS---QMNF
EsxB_M_shigaense_BAX95048.1           AGTAQIKALGDISHSVSQAGIHYQRADEEQASSLSS---QMNF
EsxB_M_gordonae_WP_055581190.1        AANKQKAELDEISTNIRQAGVQYQRADEEQQQALSS---QMGF
Cfp10_MTB_Haarlem/NITR202_AGL254      AANKQKQELDEISTNIRQAGVQYSRADEEQQQALSS---QMGF
EsxB_MTB_WP_052632688.1               AANKQKQELDEISTNIRQAGVQYSRADEEQQQALSS---QMGF
ESAT-6-like_EsxB_MTB_WP_00390077      AANKQKQKLDEISTNIRQAGVQYSRADEEQQQALSS---QMGF
Cfp10_rec_MTB                         AANKQKQELDEISTNIRQAGVQYSRADEEQQQALSS---QMGF
Cfp10-esat6_MTB_pdb|3FAV|A            AANKQKQELDEISTNIRQAGVQYSRADEEQQQALSS---QMGF
Cfp10_M_bovis_AEQ02359.1              AANKQKQELDEISTNIRQAGVQYSRADEEQQQALSS---QMGF
CFP_M_marinum_MB2_EPQ70954.1          AANKQKAELDEISTNIRQAGVQYSRADDEQQQALSS---QMGF
CFP-10_M_ulcerans_AAW68021.1          AANKQKAELDEISTNIR-------------------------
Cfp-10_My_liflandii_AAX20067.1        AANKQKAELDEISTNIR-------------------------
esxB_M_kansasii_OOK71084.1            AANKQKAELEEISTNIRQAGVQYSKADEEQQQALSS---QMGF
esxB_M_kansasii_OOK75781.1            AANKQKAELEEISTNIRQAGVQYSKADEEQQQALSS---QMGF
EsxB_M_asiaticum_WP_065144405.1       AANKQKAELDEISTNIRQAGVQYSRADEEQQQALSS---QMGF
type_VII_secretion_target_M_riya      AANKQKAELDEISTNIRQAGVQYSKADEEQQQALSS---QMGF
Cfp10_M_riyadhense_ACB41411.1         AANKQKAELDEISTNIRQAGV----------------------
EsxB_M_celatum_WP_062539444.1         AANQQIQELNDISSNIHTAGAHYTSTDEEQHSALSQ---AMG-
EsxB_M_rhodesiae_WP_014210298.1       AAAQQTKQLDDISANIHTSGVQYTSTDDDQASAFSS---AMNI
EsxB_M_septicum_WP_044514397.1        AADKQIQELNEISTNIHTSGTQYSSTDDDQAGNLAS---SM--
                                      *.  *   * :*  .:
```

Appendix 1.30: Alignment of CFP10 from MTB with other sequences of Mycobacteria (http://www.ebi.ac.uk/Tools/msa/clustalw2/).

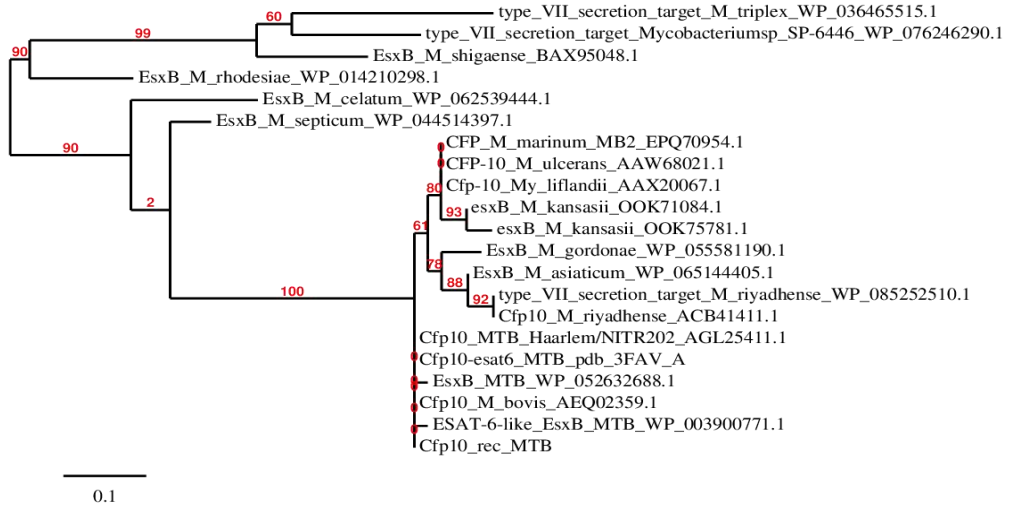

Appendix 1.31: Phylogenetic tree of the amino acid sequence of recombinant CFP10 from MTB, compared with other Mycobacteria sequences. In red it indicates the percentage of support of the branches of the tree.

Appendix 2

Immobilization of proteins on MNP@Si@NH_2 surfaces.

Appendix 2.1: Calculations of N° MNP@Si@NH_2 in 1 mg of nanoparticles.

Considering that:

- A nanoparticle has the shape of a sphere.
- 100% of the surface of each nanoparticle is silanized.
- All the nanoparticles are silanized.
- 100% of the internal structure of the nanoparticle is Fe_3O_4.
- A hydrated TEOS/APTES molecule has a globular structure

Previously, data from the magnetite and proteíns.

- **Unit cell of 8Fe_3O_4** is a=b=c=8.39 amstrong (Å) → 1 Fe_3O_4 has the measures of a=b=c=4.195 Å or **0.4195 nm**.
- MW **Fe_3O_4= 231.535 g/mol**
- BSA: Stokes $radius_{BSA}$= 3.48 nm, MW=66500 Da or 66500 g/mol
- Antibody IgG : Stokes $radius_{IgG}$= 6.4 nm, MW=150000 Da or 150000 gr/mol
- Avogadro's Number (N_A) = $6.022*10^{23}$, π=3.1416.
- M : mass, V : volume, MNP: magnetic nanoparticle

Formulas:

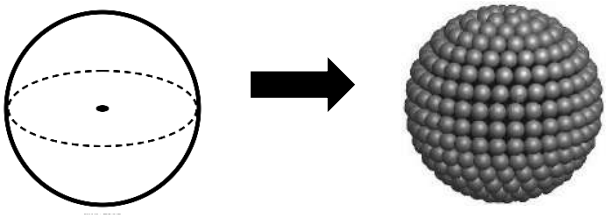

1 nanoparticle

Molecules of Fe_3O_4 in 1

$A_o = \pi*R^2$	$S_{esf} = 4\pi*R^2$	$N°_{molecules} = M*N_A/MW$
$V_{esf} = 4\ (\pi*R^3)/3$	$R_h = (3\rho*MW/10\pi*N_A)^{1/3}$ in cm.	

First:

N° $_{molecules}$ Fe_3O_4/1MNP = V_{MNP}/VFe_3O_4 = 23142106.8

Where **VFe_3O_4=** $(0.4195\ nm)^3 = 0.073823715\ nm^3$

V_{MNP}= $4\ (\pi*R^3)/3 = 1708436.29\ nm^3$

Second:

Mass of 1 molecule of Fe_3O_4= ($1*231.35g/mol)/(6.022*10^{23}) = 3.84175*10^{-22}$ g.

Mass of 1 MNP= (mass of 1 molecule of Fe_3O_4)*(N° $_{molecules}$ Fe_3O_4/ 1MNP)= $8.8906*10^{-15}$ g.

N° MNPs in 1 mg= 0.001g/mass of 1 MNP = 0.001/8.8906*10^{-15} **= 1.1248*10^{11}**

MNP	**d_H (nm)**	**R_H (nm)**	**N° $_{molecules}$ Fe_3O_4/ 1MNP**	**Mass of 1 MNP (g)**	**N° MNPs /1mg**
MNP@Si@NH_2	148.32	74.16	23142106.8	8.8906*10^{-15}	1.1248*10^{11}

Appendix 2.2: Calculations of N° molecules of BSA in 1 mg of MNP@Si@NH_2.

Surface of a silanized nanoparticle is: $\mathbf{S_{MNP@Si@NH2} = 4\pi*(R_h)^2}$
The area occupied by 1 molecule of BSA on the surface of the nanoparticle is:

$$\mathbf{A_{oBSA} = \pi*R^2 = 3.1416*(3.48\ nm)^2 = 38.05\ nm^2}$$

So:

$$\mathbf{N°_{molecules}BSA/1\ MNP} = S_{MNP@Si@NH2}/A_{oBSA} = \mathbf{1816.52319}$$

After:

$$\mathbf{Mass\ 1\ molecule\ of\ BSA} = (1*66500)/(6.022*10^{23}) = \mathbf{1.10428*10^{-19}}$$

Mass of BSA in 1mg of MNP = (mass of 1 molecule BSA)*(N° molecules BSA in 1MNP)*(N° MNP in 1 mg) = 22.56*10^{-6} g =**22.56 µg**

MNP	**R_H (nm)**	**MW (Da)**	**N°$_{molecules}$BSA/ 1 MNP**	**Mass 1 molecule of BSA (g)**	**Mass of BSA in 1mg of MNP**
MNP@Si@BSA	3.48	66500	1816.52319	1.10428*10^{-19}	22.56 µg

Appendix 2.3: Calculations of N° molecules of IgG in 1 mg of MNP@Si@NH_2.

Surface of a silanized nanoparticle is: $\mathbf{S_{MNP@Si@NH2} = 4\pi*(R_h)^2}$
The area occupied by 1 molecule of IgG on the nanoparticle surface is:

$$\mathbf{A_{oIgG} = \pi*R^2 = 3.1416*(6.4\ nm)^2 = 128.68\ nm^2}$$

So:

$$\mathbf{N°_{molecules}IgG/\ 1\ MNP} = S_{MNP@Si@NH2}/A_{oIgG} = 537.060625$$

After:

$$\mathbf{Mass\ 1\ molecule\ of\ IgG} = (1*150000)/(6.022*10^{23}) = \mathbf{2.49087*10^{-19}\ g.}$$

Mass of IgG in 1mg of MNP = (mass of 1 molecule IgG)*(N° molecules IgG in 1MNP)*(N° MNP in 1mg) = 15.047*10^{-6} g =**15.047 µg.**

MNP	**R_H IgG (nm)**	**MW (Da)**	**N°$_{molecules}$IgG/ 1 MNP**	**Mass of 1 molecule of IgG (g)**	**Mass of IgG in 1mg of MNP**
MNP@Si@IgG	6.4	150000	537.060625	2.49087*10^{-19}	15.047 µg

Appendix 2.4: Calculations of theorical antibody amounts to saturate 2.5 mg of MNP@Si@NH_2 according to its hydrodynamic diameter.

Antibodies specific for MTB antigens	Hydrodynamic diameter (d_H, nm)	R_H (nm)	N° MNPs / 1 mg	Theorical mass of IgG in 1mg of MNPs	Theorical IgG mass in 2.5 mg MNPs
Anti-38kDa	348.77 (70.24%)	174.36	8654399459	6.4 µg	16 µg
Anti-MTC28	344.23 (84.61 %)	172.115	8997489622	6.48 µg	16.2 µg
Anti-Ag85B	370.93 (42.11 %)	185.465	7191038706	6.02 µg	15.05 µg
Anti-MPT64	355.02 (42.11 %)	177.51	8201797566	6.29 µg	15.73 µg
Anti-MoeX	338.52 (65.11 %)	169.26	9460509112	6.59 µg	16.48 µg
Anti-ESAT6	119.61 (26.38 %)	59.805	$2.1447*10^{11}$	18.66 µg	46.65 µg
Anti-CFP10	149.27 (46.93 %)	74.635	$1.1034*10^{11}$	14.95 µg	37.38 µg
Anti-Hsp16.3	358.62 (50.06 %)	179.31	7957268018	6.22 µg	15.55 µg

References.

REFERENCES.

Acres, R.G., Ellis, A. V, Alvino, J., Lenahan, C.E., Khodakov, D.A., Metha, G.F., Andersson, G.G., 2012. Molecular Structure of 3-Aminopropyltriethoxysilane Layers Formed on Silanol-Terminated Silicon Surfaces. J. Phys. Chem. 116, 6289–6297.

Ahmadzadeh, M., Romero, C., Mccloy, J., 2018. Magnetic analysis of commercial hematite, magnetite, and their mixtures. AIP Adv. 8, 055815. https://doi.org/10.1063/1.5006474

Akbarzadeh, A., Samiei, M., Davaran, S., 2012. Magnetic nanoparticles : preparation , physical properties, and applications in biomedicine. Nanoscale Res. Lett. 7, 144. https://doi.org/10.1186/1556-276X-7-144

Albuquerque YM, Lima AL, Lins AK, Magalhães M, Magalhães V, 2014. Quantitative real-time PCR (q-PCR) for sputum smear diagnosis of pulmonary tuberculosis among people with HIV/AIDS. Rev Inst Med Trop Sao Paulo.56(2):139-42. doi: 10.1590/S0036-46652014000200009.

Ali, A., 2014. *Mycobacterium tuberculosis* and Molecular Epidemiology : An Overview. J. Microbiol. Res. 4, 25–31. https://doi.org/10.5923/s.microbiology.201401.04

Ali, A., Zafar, H., Zia, M., ul Haq, I., Phull, A.R., Ali, J.S., Hussain, A., 2016. Synthesis, characterization, applications, and challenges of iron oxide nanoparticles. Nanotechnol. Sci. Appl. 9, 49–67. https://doi.org/10.2147/NSA.S99986

Anderson, D.H., Harth, G., Horwitz, M.A., Eisenberg, D., 2001. An interfacial mechanism and a class of inhibitors inferred from two crystal structures of the *Mycobacterium tuberculosis* 30 kda major secretory protein (antigen 85B), a mycolyl transferase11Edited by I. A. Wilson. J. Mol. Biol. 307, 671–681. https://doi.org/10.1006/jmbi.2001.4461

Armitige, L.Y., Jagannath, C., Wanger, A.R., Norris, S.J., 2000. Disruption of the genes encoding antigen 85A and antigen 85B of *Mycobacterium tuberculosis* H37Rv: Effect on growth in culture and in macrophages. Infect. Immun. 68, 767–778. https://doi.org/10.1128/IAI.68.2.767-778.2000

Baba, K., Dyrhol-Riise, A.M., Sviland, L., Langeland, N., Hoosen, A.A., Wiker, H.G., Mustafa, T., 2008. Rapid and Specific Diagnosis of Tuberculous Pleuritis With Immunohistochemistry by Detecting *Mycobacterium Tuberculosis* Complex Specific Antigen MPT64 in Patients From a HIV Endemic Area. Appl. Immunohistochem. Mol. Morphol. 16, 554–561. https://doi.org/10.1097/PAI.0b013e31816c3f79

Barnakov, Y.A., Yu, M.H., Rosenzweig, Z., 2005. Manipulation of the Magnetic Properties of Magnetite - Silica Nanocomposite Materials by Controlled Stober Synthesis. Langmuir 21, 7524–7527.

Bartczak, D., Kanaras, A.G., 2011. Preparation of Peptide-Functionalized Gold Nanoparticles Using One Pot EDC/Sulfo-NHS Coupling. Langmur 27, 10119–10123. https://doi.org/10.1021/la2022177

Behrouzkia Z, Joveini Z, Keshavarzi B, Eyvazzadeh N, Aghdam RZ, 2016. Hyperthermia: How Can It Be Used?. Oman Med J.31(2):89-97. doi: 10.5001/omj.2016.19.

Bekmurzayeva, A., Sypabekova, M., Kanayeva, D., 2013. Tuberculosis diagnosis using immunodominant, secreted antigens of *Mycobacterium tuberculosis*. Tuberculosis 93, 381–388. https://doi.org/10.1016/j.tube.2013.03.003

Belisle, J.T., Vissa, V.D., Sievert, T., Takayama, K., Patrick, J., Belisle, J.T., Vissa, V.D., Sievert, T., Takayama, K., Brennan, P.J., Besra, G.S., 2016. Role of the Major Antigen of *Mycobacterium tuberculosis* in Cell Wall Biogenesis Brennan and Gurdyal S . Besra Published by : American Association for the Advancement of Science Stable URL : http://www.jstor.org/stable/2892814 JSTOR is a not-for-profit ser. Science (80-.). 276, 1420–1422.

Bentley-hibbert, S.I., Quan, X., Newman, T., Godfrey, H.P., Quan, X.I.N., Huygen, K., 1999. Pathophysiology of Antigen 85 in Patients with Active Tuberculosis : Antigen 85 Circulates as Complexes with Fibronectin and Immunoglobulin G Pathophysiology of Antigen 85 in Patients with Active Tuberculosis : Antigen 85 Circulates as Complexes with Fibr. Infect. Immun. 67, 581–588.

Bhalla N, Jolly P, Formisano N, Estrela P, 2016. Introduction to biosensors. Essays Biochem.60(1):1-8. doi: 10.1042/EBC20150001.

Bhavesh, R., Lechuga-vieco, A. V, Ruiz-cabello, J., Herranz, F., 2015. T1-MRI Fluorescent Iron Oxide Nanoparticles by Microwave Assisted Synthesis. Nanomaterials 5, 1880–1890. https://doi.org/10.3390/nano5041880

Bhusal, N., Shrestha, S., Pote, N., Alocilja, E., 2019. Nanoparticle-Based Biosensing of Tuberculosis , an Affordable and Practical Alternative to Current Methods. Biosensors 9, 1–11. https://doi.org/10.3390/bios9010001

Bonilla, C., 2008. Situación de la Tuberculosis en el Perú. Acta Médica Peru. 25, 163–170.

Bordbar, A.K., Rastegari, A.A., Amiri, R., Ranjbakhsh, E., Abbasi, M., Khosropour, A.R., 2014. Characterization of Modified Magnetite Nanoparticles for Albumin Immobilization. Biotechnol. Res. Int. 2014. https://doi.org/doi.org/10.1155/2014/705068 Research

Bottai, D., Batoni, G., Esin, S., Maisetta, G., Pardini, M., Florio, W., Rindi, L., Garzelli, C., Campa, M., 2003. Expression of SA5K, a secretion antigen of *Mycobacterium tuberculosis*, inside human macrophages and in sputum from tuberculosis patients. FEMS Microbiol. Lett. 226, 229–235. https://doi.org/10.1016/S0378-1097(03)00602-5

Bozzano, F., Marras, F., De Maria, A., 2014. Immunology of Tuberculosis. Mediterr. J. Hematol. Infect. Dis. 6, 2014027. https://doi.org/10.4084/mjhid.2014.027

Cabrera, M., Quispe-marcatoma, J., Maciel, J., Pandey, B., Neri, D., Soria, F., Baggio-saitovitch, E., De Carvalho Jr, L., 2013. Magnetic composites from minerals: study of the iron phases in clay and diatomite using Mössbauer spectroscopy, magnetic measurements and XRD. Hyperfine Interact. https://doi.org/10.1007/s10751-013-0858-x

Caccamo, N., Guggino, G., Joosten, S.A., Gelsomino, G., Di Carlo, P.D., Titone, L., Galati, D., Bocchino, M., Matarese, A., Salerno, A., Sanduzzi, A., Franken, W.P.J., Ottenhoff, T., Dieli, F., 2010. Multifunctional CD4+ T cells correlate with active *Mycobacterium tuberculosis* infection. Eur. J. Immunol. 40, 2211–2220. https://doi.org/10.1002/eji.201040455

Cambier CJ, Takaki KK, Larson RP, Hernandez RE, Tobin DM, Urdahl KB, et al ., 2017. Mycobacteria manipulate macrophage recruitment through coordinated use of membrane lipids. Nature 10, 4173–4183. https://doi.org/10.1021/acsnano.5b07425.Molecular

Cambier, F., 2006. Production of catalysts with an inductive atmospheric plasma torch. Elsevier 243–250. https://doi.org/10.1016/S0167-2991(06)80913-4

Cave, M.D., Eisenach, K.D., McDermott, P.F., Bates, J.H., Crawford, J.T., 1991. IS6110: Conservation of sequence in the *Mycobacterium tuberculosis* complex and its utilization in DNA fingerprinting. Mol. Cell. Probes 5, 73–80. https://doi.org/10.1016/0890-8508(91)90040-Q

Caviedes, L., Lee, T., Gilman, R.H., Sheen, P., Spellman, E., Lee, E.H., Berg, D.E., Montenegro-James, S., 2000. Rapid, efficient detection and drug susceptibility testing of *Mycobacterium tuberculosis* in sputum by microscopic observation of broth cultures. J. Clin. Microbiol. 38, 1203–1208.

Chamé, K., 2013. Síntesis y Caracterización de Nanopartículas Magnéticas.

Chang, Z., Choudhary, A., Lathigra, R., Quiocho, F., 1994. The Immunodominant 38-kDa Lipoprotein Antigen of *Mycobacterium tuberculosis* is a phosphate-binding protein. J. Biol. Chem. 269, 1988–1990.

Chaudhary, M., Gupta, S., Khare, S., Lal, S., 2010. Diagnosis of tuberculosis in an era of HIV pandemic: A review of current status and future prospects. Indian J. Med. Microbiol. 28, 281. https://doi.org/10.4103/0255-0857.71805

Cheng, k K., Chan, S.P., Fan, S., Kwan, M.S., Yeung, L.K., Wáng, Y.-X.J., Chow, L., Wu, E.X., Baum, L., 2015. Biomaterials Curcumin-conjugated magnetic nanoparticles for detecting amyloid plaques in Alzheimer ' s disease mice using magnetic resonance imaging (MRI). Biomaterials 44, 155–172. https://doi.org/10.1016/j.biomaterials.2014.12.005

Cheon, H.J., Lee, S.M., Kim, S., Shin, H.Y., Seo, Y.H., Cho, Y.K., Lee, S.P., Kim, M. Il, 2019. Colorimetric Detection of MPT64 Antibody Based on an Aptamer Adsorbed Magnetic Nanoparticles for Diagnosis of Tuberculosis. J. Nanosci. Nanotechnol. 19, 622–626. https://doi.org/10.1166/jnn.2019.15905

Choudhary, A., Vyas, M., Vyas, N., Chang, Z., Quiocho, F.A., 1994. Crystallization and preliminary X-ray crystallographic analysis of the 38-kDa immunodominant antigen of *Mycobacterium tuberculosis*. Protein Sci. 45, 2450–2451.

Chu, T.P.J., Yuann, J.M.P., 2011. Expression, purification, and characterization of protective MPT64 antigen protein and identification of its multimers isolated from nontoxic *Mycobacterium tuberculosis* H37Ra. Biotechnol. Appl. Biochem. 58, 185–189. https://doi.org/10.1002/bab.26

Conde J, Dias JT, Grazú V, Moros M, Baptista PV, de la Fuente JM, 2014. Revisiting 30 years of biofunctionalization and surface chemistry of inorganic nanoparticles for nanomedicine. Front Chem.2:48. doi: 10.3389/fchem.2014.00048.

Conroy, S., Lee, J.S.H., Zhanga, M., 2008. Magnetic Nanoparticles in MR Imaging and Drug Delivery. Adv. Drug Deliv. Rev. 60, 1252–1265. https://doi.org/10.1016/j.addr.2008.03.018.Magnetic

Cousins DV, Bastida R, Cataldi A, Quse V, Redrobe S, Dow S, et al. 2003. Tuberculosis in seals caused by a novel member of the *Mycobacterium tuberculosis* complex: Mycobacterium pinnipedii sp. nov. Int J Syst Evol Microbiol.53:1305-14.

Daniel, T.M., Debanne, S.M., 1987. The serodiagnosis of tuberculosis and other mycobacterial diseases by enzyme-linked immunosorbent assay. Am. Rev. Respir. Dis. 135, 1137–1151.

Davis JM and Ramakrishnan, 2011. The Role of the Granuloma in Expansion and Dissemination of Early Tuberculous Infection. Cell 136, 37–49. https://doi.org/10.1016/j.cell.2008.11.014.The

Demin, A.M., Krasnov, V.P., Charushin, V.N., 2013. Covalent surface modification of Fe3O4 magnetic nanoparticles with alkoxy silanes and amino acids. Mendeleev Commun. 23, 14–16. https://doi.org/10.1016/j.mencom.2013.

Diouani, M.F., Ouerghi, O., Refai, A., Belgacem, K., Tlili, C., Laouini, D., Essafi, M., 2017. Detection of ESAT-6 by a label free miniature immuno-electrochemical biosensor as a diagnostic tool for tuberculosis. Mater. Sci. Eng. C 74, 465–470. https://doi.org/10.1016/j.msec.2016.12.051

Druszczynska M, Wawrocki S, Szewczyk R, Rudnicka W, 2017. Mycobacteria-derived biomarkers for tuberculosis diagnosis. Indian J Med Res.146(6):700-707. doi: 10.4103/ijmr.IJMR_1441_16.

Farzam B, Imani Fooladi AA, Izadi M, Hossaini HM, Feizabadi MM, 2015. Comparison of cyp141 and IS6110 for detection of *Mycobacterium tuberculosis* from clinical specimens by PCR. J Infect Public Health. 8(1):32-6. doi: 10.1016/j.jiph.2014.08.005.

Feng, X., Xiu, B., Chen, K., Yang, X., Zhang, H., Yue, J., Tan, Y., Li, H., Nicholson, R.A., Tam, A.W., Zhao, P., Zhang, L., Liu, J., Song, X., Wang, G., Zhang, H., 2013. Enhanced serodiagnostic utility of novel *Mycobacterium tuberculosis* polyproteins. J. Infect. 66, 366–375. https://doi.org/10.1016/j.jinf.2012.10.029

Ferroni, A., Vu-thien, H., Lanotte, P., Bourgeois, M. Le, Sermet-gaudelus, I., Fauroux, B., Marchand, S., Varaigne, F., Berche, P., Gaillard, J., Offredo, C., 2006. Value of the Chlorhexidine Decontamination Method for Recovery of Nontuberculous Mycobacteria from Sputum Samples of Patients with Cystic Fibrosis. J. Clin. Microbiol. 44, 2237–2239. https://doi.org/10.1128/JCM.00285-06

Fields, C., Li, P., Mahony, J.J.O., Lee, G.U., 2016. Advances in Affinity Ligand-Functionalized Nanomaterials for Biomagnetic Separation. Biotechnol. Bioeng. 113, 11–25. https://doi.org/10.1002/bit.25665

Fogel, N., 2015. Tuberculosis: A disease without boundaries. Tuberculosis 95, 527–531. https://doi.org/10.1016/j.tube.2015.05.017

Forrellad, M.A., Klepp, L.I., Gioffré, A., Sabio, J., Morbidoni, H.R., De, M., Santangelo, P., Cataldi, A.A., Bigi, F., 2013. Virulence factors of the *Mycobacterium tuberculosis* complex. Virulence 3–66.

Franken, L.E., Boekema, E.J., Stuart, M.C.A., 2017. Transmission Electron Microscopy as a Tool for the Characterization of Soft Materials: Application and Interpretation. Adv. Sci. 4, 1–9. https://doi.org/10.1002/advs.201600476

Fujita, Y., Ogata, H., Yano, I., 2005. Clinical evaluation of serodiagnosis of active tuberculosis by multiple-antigen ELISA using lipids from Mycobacterium bovis BCG Tokyo 172. Clin. Chem. Lab. Med. 43, 1253–1262. https://doi.org/10.1515/CCLM.2005.216

Garcia-Granda, S., Montejo-bernardo, J.M., 2013. X-RAY ABSORPTION AND DIFFRACTION | X-Ray Diffraction | Powder, in: Reference Module in Chemistry, Molecular Sciences and Chemical Engineering. Elsevier Inc., pp. 1–10. https://doi.org/10.1016/B978-0-12-409547-2.00577-1

García-Romo, G.S., Pedroza-González, A., Aguilar-León, Di., Orozco-Estevez, H., Lambrecht, B.N., Estrada-Garcia, I., Flores-Romo, L., Hernández-Pando, R., 2004. Airways infection with virulent *Mycobacterium tuberculosis* delays the influx of dendritic cells and the expression of costimulatory molecules in mediastinal lymph nodes. Immunology 112, 661–668. https://doi.org/10.1046/j.1365-2567.2004.01904.x

Gatoo MA, Naseem S, Arfat MY, Dar AM, Qasim K, Zubair S, 2014. Physicochemical properties of nanomaterials: implication in associated toxic manifestations. Biomed Res Int. 2014:498420. doi: 10.1155/2014/498420.

Grabarek, Z., Gergely, J., 1990. Zero-length crosslinking procedure with the use of active esters. Anal. Biochem. 185, 131–135. https://doi.org/10.1016/0003-2697(90)90267-d

Groenewoud, W., 2001. Thermogravimetry., in: Characterisation of Polymers by Thermal Analysis. pp. 61–76.

Gupta, A.K., Naregalkar, R., Vaidya, V.D., Gupta, M., 2007. Recent advances on surface engineering of magnetic iron oxide nanoparticles and their biomedical applications. Nanomedicine 2, 23–39.

Gütlich, P., Schroder, C., Schünemann, V., 2012. Mössbauer spectroscopy — an indispensable tool in solid state research. SpectroscopyEurope 24, 21–32.

Han, G., Ouyang, Y., Long, X., Zhou, Y., Li, M., Liu, Y.-N., Kraatz, H.-B., 2010. (Carboxymethyl – Dextran) -Modified Magnetic Nanoparticles Conjugated to Octreotide for MRI Applications. Eur. J. Chem. 5455–5461. https://doi.org/10.1002/ejic.201000715

Harboe, M., Wiker, H.G., 1992. The 38-kDa Protein of *Mycobacterium tuberculosis* : A Review. J. Infect. Dis. 166, 874–884.

He, F., Xiong, Y., Liu, J., Tong, F., Yan, D., 2016. Construction of Au-IDE/CFP10-ESAT6 aptamer/DNA-AuNPs MSPQC for rapid detection of *Mycobacterium tuberculosis.* Biosens. Bioelectron. 77, 799–804. https://doi.org/10.1016/j.bios.2015.10.054

He, H., Zhong, Y., Liang, X., Tan, W., Zhu, J., Wang, C.Y., 2015. Natural Magnetite : an efficient catalyst for the degradation of organic contaminant. Sci. Rep. https://doi.org/10.1038/srep10139

Hernandez-Pando, R., Orozco, H., Mancilla, R., 1995. T-cell lung granulomas induced by sepharose-coupled *Mycobacterium tuberculosis* protein antigens: immunosuppressive phenomena reversed with cyclophosphamide and indomethacin. Immunology 86, 506–511.

Herranz, F., Salinas, B., Groult, H., Pellico, J., Lechuga-Vieco, A., Bhavesh, R., Cabello-Ruiz, J., 2014. Superparamagnetic Nanoparticles for Atherosclerosis Imaging. Nanomaterials 4, 408–438. https://doi.org/10.3390/nano4020408

Hira, F., Kyo-seon, K., 2017. Magnetic nanoparticles for bioseparation. Korean J. Chem. Eng. 34, 589–590. https://doi.org/10.1007/s11814-016-0349-2

Hong, S.C., Lee, J., Shin, H.C., Kim, C.M., Park, J.Y., Koh, K., Kim, H.J., Chang, C.L., Lee, J., 2011. Clinical immunosensing of tuberculosis CFP-10 in patient urine by surface plasmon resonance spectroscopy. Sensors Actuators, B Chem. 160, 1434–1438.

https://doi.org/10.1016/j.snb.2011.10.006

Huang, Z., Raghuwanshi, V.S., Garnier, G., 2017. Functionality of immunoglobulin g and immunoglobulin M antibody Physisorbed on cellulosic Films. Front. Bioeng. Biotechnol. 5, 1–10. https://doi.org/10.3389/fbioe.2017.00041

Huynh, R., Chaubet, F., Jozefonvicz, J., 1998. Carboxymethylation of dextran in aqueous alcohol as the first step of the preparation of derivatized dextrans. Die Angew. Makromol. Chemie 254, 61–65.

Hwang, S.H., Kim, D.E., Sung, H., Park, B.M., Cho, M.J., Yoon, O.J., Lee, D.H., Neyrolles, O., 2015. Simple detection of the IS6110 sequence of *Mycobacterium tuberculosis* complex in sputum, based on PCR with graphene oxide. PLoS One 10, 2–9. https://doi.org/10.1371/journal.pone.0136954

Ito, A., Shinkai, M., Honda, H., Kobayashi, T., 2005. Medical application of functionalized magnetic nanoparticles. J. Biosci. Bioeng. 100, 1–11. https://doi.org/10.1263/jbb.100.1

Jesse, M., Raman, S., Duraisamy, N., Muthuramalingam, R., Riyaz, M., Gunasekaran, D., Krishnan, K., 2015. Preparation, characterization and application of antibody-conjugated magnetic nanoparticles in the purification of begomovirus. RSC Adv. 5, 99820–99831. https://doi.org/10.1039/C5RA17982C

Ji, M., Cho, B., Cho, Y.S., Park, S.Y., Cho, S.N., Jeon, B.Y., Yoon, B.S., 2014. Development of a quantitative sandwich enzyme-linked immunosorbent assay for detecting the MPT64 antigen of *Mycobacterium tuberculosis.* Yonsei Med. J. 55, 746–752. https://doi.org/10.3349/ymj.2014.55.3.746

Kaplan G, Post FA, Moreira AL, Wainwright H, Kreiswirth BN, Tanverdi M, Mathema B, Ramaswamy SV, Walther G, Steyn LM, Barry III CE, d B.L., 2003. *Mycobacterium tuberculosis* Growth at the Cavity Surface: a Microenvironment with Failed Immunity. Infect. Immun. 71, 7099–7108. https://doi.org/10.1128/IAI.71.12.7099

Karlsson, D., Zacchi, G., Axelsson, A., 2002. Electronic Speckle Pattern Interferometry : A Tool for Determining Diffusion and Partition Coefficients for Proteins in Gels. Biotechnol. Prog. 18, 1423–1430.

Katia Caamaño, 2016. Síntesis, Caracterización Y Funcionalización de Nanopartículas Magnéticas para Detección de Patógenos. Estudio de la Funcionalización con SiO2 Mesoporoso. Universidad de Coruña.

Kaufmann, S.H.E., Cole, S.T., Mizrahi, V., Rubin, E., Nathan, C., 2005. *Mycobacterium tuberculosis* and the host response. J. Exp. Med. 201, 1693–1697. https://doi.org/10.1084/jem.20050842

Kennaway, C.K., Benesch, J.L.P., Gohlke, U., Wang, L., Robinson, C. V, Orlova, E. V, Saibi,

H.R., Keep, N.H., 2005. Dodecameric Structure of the Small Heat Shock Protein Acr1 from *Mycobacterium tuberculosis*. J. Biol. Chem. 280, 33419–33425. https://doi.org/10.1074/jbc.M504263200

Kim, E.J., Kim, E.B., Lee, S.W., Cheon, S.A., Kim, H.J., Lee, J., Lee, M.K., Ko, S., Park, T.J., 2017. An easy and sensitive sandwich assay for detection of *Mycobacterium tuberculosis* Ag85B antigen using quantum dots and gold nanorods. Biosens. Bioelectron. 87, 150–156. https://doi.org/10.1016/j.bios.2016.08.034

Kim, J., Lee, K., Kim, E.B., Paik, S., Chang, C.L., Park, T.J., Kim, H., Lee, J., Kim, J., Lee, K., Kim, E.B., Paik, S., Chang, C.L., Park, T.J., Kim, H., Lee, J., 2017. Early detection of the growth of *Mycobacterium tuberculosis* using magnetophoretic immunoassay in liquid culture. Biosens. Bioelectron. S0956-5663, 30273–7. https://doi.org/10.1016/j.bios.2017.04.025

Kim, J., Park, S., Lee, J.E., Jin, S.M., Lee, J.H., Lee, I.S., Yang, I., Kim, J., Kim, S.K., Cho, M., Hyeon, T., 2006. Designed fabrication of multifunctional magnetic gold nanoshells and their application to magnetic resonance imaging and photothermal therapy. Nanomedicine 118, 7918–7922. https://doi.org/10.1002/ange.200602471

Kirby, A.C., Coles, M.C., Kaye, P.M., 2013. Europe PMC Funders Group Alveolar macrophages transport pathogens to lung draining 183, 1983–1989. https://doi.org/10.4049/jimmunol.0901089.Alveolar

Kokate, M., Garadkar, K., Gole, A., 2013. One pot synthesis of magnetite-silica nanocomposites: Applications as tags, entrapment matrix and in water purification. J. Mater. Chem. A 1, 2022–2029. https://doi.org/10.1039/c2ta00951j

Krishnan, N., Robertson, B.D., Thwaites, G., 2010. The mechanisms and consequences of the extra-pulmonary dissemination of *Mycobacterium tuberculosis*. Tuberculosis 90, 361–366. https://doi.org/10.1016/j.tube.2010.08.005

Kruh, N.A., Troudt, J., Izzo, A., Prenni, J., Dobos, K.M., 2010. Portrait of a pathogen: The *Mycobacterium tuberculosis* proteome In vivo. PLoS One 5, 1–13. https://doi.org/10.1371/journal.pone.0013938

Kumar VG, Urs TA, Ranganath RR, 2011. MPT 64 Antigen detection for Rapid confirmation of *M. tuberculosis* isolates. BMC Res Notes. 4:79. doi: 10.1186/1756-0500-4-79.

Kundu, P., Biswas, R., Mukherjee, S., Reinhard, L., Dutta, A., Mueller-Dieckmann, J., Weiss, M.S., Pal, N.K., Das, A.K., 2016. Structure-based epitope mapping of *Mycobacterium tuberculosis* secretary antigen MTC28. J. Biol. Chem. 291, 13943–13954. https://doi.org/10.1074/jbc.M116.726422

LaMer, V., Dinegar, H., 1950. Theory, Production and Mechanism of Fromation of

Monodispersed Hydrosols. J. Am. Chem. Soc. 72, 4847–4854.

Laszlo, A., 1999. Tuberculosis: 7. Laboratory aspects of diagnosis. Cmaj 160, 1725–1729.

Laverdiere, M., Poirier, L., Weiss, K., Béliveau, C., Bédard, L., Desnoyers, D., 2000. Comparative evaluation of the MB/BacT and BACTEC 460 TB systems for the detection of mycobacteria from clinical specimens: Clinical relevance of higher recovery rates from broth-based detection systems. Diagn. Microbiol. Infect. Dis. 36, 1–5. https://doi.org/10.1016/S0732-8893(99)00103-0

Lawn, S.D., 2015. Advances in Diagnostic Assays for Tuberculosis., in: Cold Spring Harbor Perspectives in Medicine. pp. 1–17.

Lee, J., Paik, T., Yoo, Y., Lee, J., Shin, A., Song, C., Jo, E., Kim, H., Park, J., 2006. Purification of Native Ag85 Complex, 38-kDa and MTB12 Protein Antigens from the Culture Filtrate of *Mycobacterium tuberculosis.* J. Bacteriol. Virol. 36, 211–220.

Li, J., Li, J., Zhou, Y., Li, M., Xia, N., Huang, Q., 2011. Carboxymethylated Dextran-Coated Magnetic Iron Oxide Nanoparticles for Regenerable Bioseparation Carboxymethylated Dextran-Coated Magnetic Iron Oxide Nanoparticles for Regenerable Bioseparation. J. Nanosci. Nanotechnol. 11, 10187–10192. https://doi.org/10.1166/jnn.2011.5002

Lin, J., Zhou, W., Kumbhar, A., Wiemann, J., Fang, J., Carpenter, E.E., O'Connor, C.J., 2001. Gold-Coated Iron (Fe@Au) Nanoparticles : Synthesis , Characterization , and Magnetic Field-Induced Self-Assembly. J. Solid State Chem. 159, 26–31. https://doi.org/10.1006/jssc.2001.9117

Lim, E.N.G.M., Rauzier, J., Timm, J., Torrea, G., Murray, A., Gicquel, B., Portnoi, D., 1995. Identification of *Mycobacterium tuberculosis* DNA Sequences Encoding Exported Proteins by Using phoA Gene Fusions. J. Bacteriol. 177, 59–65.

Liu, H., Tang, J., Guo, L., Xie, J., Wang, Y., 2011. Galactose-functionalized Magnetic Iron-oxide Nanoparticles for Enrichment and Detection of Ricin Toxin. Anal. Sci. 27, 19–24. https://doi.org/10.2116/analsci.27.19

Liu, Y., Li, Y., Li, X., He, T., 2013. Kinetics of (3-Aminopropyl)triethoxylsilane (APTES) Silanization of Superparamagnetic Iron Oxide Nanoparticles. ACS 29, 15275–15282. https://doi.org/10.1021/la403269u

Liu, Z.H., Qin, L.H., Feng, Y.H., Bi, A.X., Yang, H., Ding, Y.., Z-L, C., R-L, J., R-J, Z., Z-Y, H., 2009. Identification of the *Mycobacterium tuberculosis* complex by detecting recombinant secretory protein MPT64. Chin J Tuber Respir Dis 32, 608e12.

López-Hernández, Y., Patiño-Rodríguez, O., García-Orta, S.T., Pinos-Rodríguez, J.M., 2016. Mass spectrometry applied to the identification of *Mycobacterium tuberculosis* and biomarker discovery. J. Appl. Microbiol. 121, 1485–1497.

https://doi.org/10.1111/jam.13323

López, Y., Yero, D., Falero-Diaz, G., Olivares, N., Sarmiento, M.E., Sifontes, S., Solis, R.L., Barrios, J.A., Aguilar, D., Hernández-Pando, R., Acosta, A., 2009. Induction of a protective response with an IgA monoclonal antibody against *Mycobacterium tuberculosis* 16 kDa protein in a model of progressive pulmonary infection. Int. J. Med. Microbiol. 299, 447–452. https://doi.org/10.1016/j.ijmm.2008.10.007

Luo, Y., Suliman, S., Asgari, S., Amariuta, T., Calderon, R., Lecca, L., León, S., Jimenez, J., Yataco, R., Contreras, C., Galea, J., Becerra, M., Nejentsev, S., Martinez-Bonet, M., Nigrovic, P., Moody, D., Murray, M., Raychaudhuri, S., 2018. Progression of recent *Mycobacterium tuberculosis* exposure to active tuberculosis is a highly heritable complex trait driven by 3q23 in Peruvians. bioRxiv.

Mahmoudi, S., Mamishi, S., Ghazi, M., Hosseinpour Sadeghi, R., Pourakbari, B., 2013. Cloning, expression and purification of *Mycobacterium tuberculosis* ESAT-6 and CFP-10 antigens. Iran. J. Microbiol. 5, 374–378.

Makovec, D., Gyergyek, S., Primc, D., Plantan, I., 2015. The formation of magnetic carboxymethyl-dextrane-coated iron-oxide nanoparticles using precipitation from an aqueous solution. Mater. Chem. Phys. 153, 376–383. https://doi.org/10.1016/j.matchemphys.2015.01.028

Manca, C., Lyashchenko, K., Colangeli, R., Gennaro, M.L., 1997. MTC28, a novel 28-kilodalton proline-rich secreted antigen specific for the *Mycobacterium tuberculosis* complex. Infect. Immun. 65, 4951–4957.

Mao, X., Xu, J., Cui, H., 2017. Functional Nanoparticles for Magnetic Resonance Imaging. Wiley Interdiscip Rev Nanomed Nanobiotechnol. 8, 814–841. https://doi.org/10.1002/wnan.1400.Functional

Marín, P.A., Botero, L.E., Robledo, J.A., Murillo, A.M., Torres, R.A., Montagut, Y.J., Pabón, E., 2015. Purificación del antígeno 38 kDa de *Mycobacterium tuberculosis* mediante immunosensores piezoeléctricos. Mycobacterium 38 kDa Antigen Purification and Potential Diagnostic Use by Piezoelectric Immunosensors. Acta Biológica Colomb. 20, 129–139.

Maximilien, J., Beyazit, S., Rossi, C., Haupt, K., Tse Sum Bui, B., 2015. Nanoparticles in Biomedical Applications, in: Chemistry and Materials Science. https://doi.org/5. 10.1007/11663_2015_12.

McMurray, D.N., 2003. Hematogenous reseeding of the lung in low-dose, aerosol-infected guinea pigs: Unique features of the host-pathogen interface in secondary tubercles. Tuberculosis 83, 131–134. https://doi.org/10.1016/S1472-9792(02)00079-3

McNerney, R., Wondafrash, B.A., Amena, K., Tesfaye, A., McCash, E.M., Murray, N.J., 2010. Field test of a novel detection device for *Mycobacterium tuberculosis* antigen in cough. BMC Infect. Dis. 10, 161. https://doi.org/10.1186/1471-2334-10-161

Meier NR, Jacobsen M, Ottenhoff THM, Ritz N, 2018. A Systematic Review on Novel *Mycobacterium tuberculosis* Antigens and Their Discriminatory Potential for the Diagnosis of Latent and Active Tuberculosis. Front Immunol. 9:2476. doi: 10.3389/fimmu.2018.02476.

Meng QL, Liu F, Yang XY, Liu XM, Zhang X, Zhang C, Zhang ZD, 2014. Identification of latent tuberculosis infection-related microRNAs in human U937 macrophages expressing *Mycobacterium tuberculosis* Hsp16.3. BMC Microbiol. 14:37. doi: 10.1186/1471-2180-14-37.

Minion, J., Leung, E., Menzies, D., Pai, M., 2010. Microscopic-observation drug susceptibility and thin layer agar assays for the detection of drug resistant tuberculosis: A systematic review and meta-analysis. Lancet Infect. Dis. 10, 688–698. https://doi.org/10.1016/S1473-3099(10)70165-1

Moore, D.A.J., Evans, C.A.W., Gilman, R.H., Caviedes, L., Coronel, J., Vivar, A., Sanchez, E., Piñedo, Y., Saravia, J.C., Salazar, C., Oberhelman, R., Maria-Graciela, H.-D., LaChira, D., Escombe, A.R., Friedland, J.S., 2006. Microscopic Observation Drug-Susceptibility Assay for the Diagnosis of TB. N. Engl. J. Med. 335, 1539–1550. https://doi.org/10.1056/NEJMoa055524.Microscopic-Observation

Mosiewicki, M., Marcovich, N., Aranguren, M., 2011. Characterization of fiber surface treatments in natural fiber composites by infrared and Raman spectroscopy., in: Interface Engineering of Natural Fibre Composites. pp. 117–145. https://doi.org/10.1533/9780857092281.1.117

Mukundan, H., Kumar, S., Price, D.N., Ray, S.M., Lee, Y.-J., Min, S., Eum, S., Sutherland, J.K., Resnick, J.M., Grace, W.K., Anderson, A.S., Hwang, S.H., Cho, S.N., Via, L.E., Barry III, C., Sakamuri, R., Swanson, B.I., 2012. Rapid Detection of *Mycobacterium tuberculosis* Biomarkers using a Waveguide-based Biosensor. Tuberculosis 92, 407–416. https://doi.org/10.1021/nl061786n.Core-Shell

Murray, E.J., Bond, V.A., Marais, B.J., Godfrey-Faussett, P., Ayles, H.M., Beyers, N., 2013. High levels of vulnerability and anticipated stigma reduce the impetus for tuberculosis diagnosis in Cape Town, South Africa. Health Policy Plan. 28, 410–418. https://doi.org/10.1093/heapol/czs072

NanoComposix, 2012. NanoComposix's Guide to Dynamic Light Scattering measurement and analysis.

Narasimhan P, Wood J, Macintyre CR, Mathai D, 2013. Risk factors for tuberculosis. Pulm Med. 2013:828939. doi: 10.1155/2013/828939.

Ottenhoff TH, 2012. New pathways of protective and pathological host defense to mycobacteria. Trends Microbiol. 20(9):419-28.

Pai, M., Behr, M.A., Dowdy, D., Dheda, K., Divangahi, M., Boehme, C.C., Ginsberg, A., Swaminathan, S., Spigelman, M., Getahun, H., Menzies, D., Raviglione, M., 2016. Tuberculosis. Dis. Prim. 2, 1–23. https://doi.org/10.1038/nrdp.2016.76

Pereira Arias-Bouda, L.M., Nguyen, L.N., Ho, L.M., Kuijper, S., Jansen, H.M., Kolk, A.H., 2000. Development of antigen detection assay for diagnosis of tuberculosis using sputum samples. J. Clin. Microbiol. 38, 2278–83.

Peter, J.G., Cashmore, T.J., Meldau, R., Theron, G., Van Zyl-Smit, R., Dheda, K., 2012. Diagnostic accuracy of induced sputum LAM ELISA for tuberculosis diagnosis in sputum-scarce patients. Int. J. Tuberc. Lung Dis. 16, 1108–1112. https://doi.org/10.5588/ijtld.11.0614

Piccini, P., Chiappini, E., Tortoli, E., de Martino, M., Galli, L., 2014. Clinical peculiarities of tuberculosis. BMC Infect. Dis. 14, S4. https://doi.org/10.1186/1471-2334-14-S1-S4

Pollock, N.R., Macovei, L., Kanunfre, K., Dhiman, R., Restrepo, B.I., Zarate, I., Pino, P.A., Mora-Guzman, F., Fujiwara, R.T., Michel, G., Kashino, S.S., Campos-Neto, A., 2013. Validation of *Mycobacterium tuberculosis* Rv1681 protein as a diagnostic marker of active pulmonary tuberculosis. J. Clin. Microbiol. 51, 1367–1373. https://doi.org/10.1128/JCM.03192-12

Purohit M, Mustafa T, Wiker H, Morkve O, Sviland L, 2007. Immunohistochemical diagnosis of abdominal and lymph node tuberculosis by detecting *Mycobacterium tuberculosis* complex specific antigen MPT64. Diagn Pathol.2. http://dx.doi.org/10.1186/1746-1596-2-36.

Ramos-Vara JA, 2005. Technical aspects of immunohistochemistry. Vet Pathol. 42:405e26. http://dx.doi.org/10.1354/vp.42-4-405

Reji, P., Aga, G., Abebe, G., 2013. The role of AFB microscopy training in improving the performance of laboratory professionals: analysis of pre and post training evaluation scores. BMC Health Serv. Res. 13, 1. https://doi.org/10.1186/1472-6963-13-392

Renshaw, P.S., Lightbody, K.L., Veverka, V., Muskett, F.W., Kelly, G., Frenkiel, T.A., Gordon, S. V, Hewinson, R.G., Burke, B., Norman, J., Williamson, R.A., Carr, M.D., 2005. Structure and function of the complex formed by the tuberculosis virulence factors CFP-10 and ESAT-6. EMBO J. 24, 2491–2498. https://doi.org/10.1038/sj.emboj.7600732

Roche, P.W., Feng, C.G., Britton, W.J., 1996. Human T-cell epitopes on the *Mycobacterium*

tuberculosis secreted protein MPT64. Scand. J. Immunol. 43, 662–670.

Roche, P.W., Winter, N., TriccasS, J.A., Feng, C.G., Britton, W.J., 1996. Expression of *Mycobacterium tuberculosis* MPT64 in recombinant Myco. smegmatis: purification, immunogenicity and application to skin tests for tuberculosis. Clin. Exp. Immunol. 103, 226–232. https://doi.org/10.1046/j.1365-2249.1996.d01-613.x

Rockenberger, J., Scher, E.C., Alivisatos, A.P., 1999. A New Nonhydrolytic Single-Precursor Approach to Surfactant-Capped Nanocrystals of Transition Metal Oxides. J. Am. Chem. Sco. 121, 11595–11596.

Rodríguez, B.S., 2014. Síntesis y funcionalización covalente de nanopartículas superparamagnéticas para imagen biomédica. Universidad Complutense de Madrid.

Rodriguez, L., Alva, A., Coronel, J., Caviedes, L., Mendoza-Ticona, A., Gilman, R., Sheen, P., Zimic, M., 2014. Implementation of a telediagnostic system for tuberculosis and determination of multi-drug resistance based in the MODS method in Trujillo, Peru. Rev Peru Med Exp Salud Publica 31, 445–453.

Roque, A.C.A., Bispo, S., Pinheiro, A.R.N., Antunes, J.M.A., Goncalves, D., Ferreira, H., 2009. Antibody immobilization on magnetic particles. J. Mol. Recognit. 22, 77–82. https://doi.org/10.1002/jmr.913

Sánchez Paradinas, S., 2013. Nanopartículas como herramientas en procesos bio-químicos. Síntesis, caracterización, funcionalización y aplicaciones. Universidad de Salamanca.

Sarkar, P., Biswas, D., Sindhwani, G., Rawat, J., Kotwal, A., Kakati, B., 2014. Application of lipoarabinomannan antigen in tuberculosis diagnostics: current evidence. Postgrad. Med. J. 90, 155–63. https://doi.org/10.1136/postgradmedj-2013-132053

Scherrer S, Landolt P, Friedel U, Stephan R, 2019. Distribution and expression of esat-6 and cfp-10 in non-tuberculous mycobacteria isolated from lymph nodes of slaughtered cattle in Switzerland. J Vet Diagn Invest. 31(2):217-221. doi: 10.1177/1040638718824074.

Sethi, S., Yadav, R., Mewara, A., Dhatwalia, S.K., Sharma, M., Gupta, D., 2012. Evaluation of in-house mpt64 real-time PCR for rapid detection of *Mycobacterium tuberculosis* in pulmonary and extra-pulmonary specimens. Brazilian J. Infect. Dis. 16, 493–494. https://doi.org/10.1016/j.bjid.2012.08.010

Shaw, D., 1992. Colloid And Surface Chemistry., Fourth Edi. ed. Oxford.

Siurdyban, E., Brotin, T., Talaga, D., Heuzé, K., Vellutini, L., T., B., 2016. Immobilization of Cryptophane Derivatives onto γ-Fe2O3 Core−Shell Magnetic Nanoparticles. J. Phys. Chem. C 120, 6583–6590.

Slim-Saidi, L., Mehiri-Zeghal, E., Ghariani, A., Tritar, F., 2015. Nouvelles méthodes de diagnostic de la tuberculose. Rev. Pneumol. Clin. 71, 110–121.

https://doi.org/10.1016/j.pneumo.2015.02.002

Smit, M., 2018. Polymer-coated magnetic nanoparticles and modified polymer nanofibers for the efficient capture of *Mycobacterium tuberculosis* (Mtb) by Marica Smit. Stellenbosch University.

Smith, J., Sapsford, K., Tan, W., Ligler, F., 2011. Optimization of antibody-conjugated magnetic nanoparticles for target preconcentration and immunoassays. Anal Biochem 410, 124–132. https://doi.org/10.1016/j.ab.2010.11.005.Smith

Socrates, G., 2001. Infrared and Raman characteristic group frequencies. Tables and chart.

Solari, L., Gutierrez, A., Suarez, C., Jave, O., Castillo, E., Yale, G., Ascencios, L., Quispe, N., Valencia, E., Suarez, V., 2011. [Cost analysis of rapid methods for diagnosis of multidrug resistant tuberculosis in different epidemiologic groups in Peru]. Anal. costos los Metod. rapidos para diagnostico Tuberc. multidrogorresistente en Difer. Grup. Epidemiol. del Peru. 28, 426–431.

Soo, P.C., Horng, Y.T., Chen, A.T., Yang, S.C., Chang, K.C., Lee, J.J., Peng, W.P., 2015. Validation of nanodiamond-extracted CFP-10 antigen as a biomarker in clinical isolates of *Mycobacterium tuberculosis* complex in broth culture media. Tuberculosis 95, 620–624. https://doi.org/10.1016/j.tube.2015.05.008

Steingart, K.R., Henry, M., Laal, S., Hopewell, P.C., Ramsay, A., Menzies, D., Cunningham, J., Weldingh, K., Pai, M., 2007. Commercial serological antibody detection tests for the diagnosis of pulmonary tuberculosis: A systematic review. PLoS Med. 4, 1041–1060. https://doi.org/10.1371/journal.pmed.0040202

Steingart KR, Flores LL, Dendukuri N, Schiller I, Laal S, Ramsay A, Hopewell PC, Pai M, 2011. Commercial serological tests for the diagnosis of active pulmonary and extrapulmonary tuberculosis: an updated systematic review and meta-analysis. PLoS Med.8(8):e1001062. doi: 10.1371/journal.pmed.1001062.

Sutherland JS, Lalor MK, Black GF, Ambrose LR, Loxton AG, Chegou NN, Kassa D, Mihret A, Howe R, Mayanja-Kizza H, Gomez MP, Donkor S, Franken K, Hanekom W, Klein MR, Parida SK, Boom WH, Thiel BA, Crampin AC, Ota M, Walzl G, Ottenhoff TH, Dockrell HM, Kaufmann SH; GCGH Biomarkers for TB consortium, 2013. Analysis of host responses to *Mycobacterium tuberculosis* antigens in a multi-site study of subjects with different TB and HIV infection states in sub-Saharan Africa. PLoS One.8(9):e74080. doi: 10.1371/journal.pone.0074080.

Tamura, H., Tanaka, A., Mita, K., Furuichi, R., 1999. Surface Hydroxyl Site Densities on Metal Oxides as a Measure for the Ion-Exchange Capacity. J. Colloid. Interface Sci. 209, 225–231.

Thabet, S., Souissi, N., 2017. Transposition mechanism, molecular characterization and evolution of IS6110, the specific evolutionary marker of *Mycobacterium tuberculosis* complex. Mol. Biol. Rep. 44, 25–34. https://doi.org/10.1007/s11033-016-4084-x

Thapa, D., Palkar, V.R., Kurup, M.B., Malik, S.K., 2004. Properties of magnetite nanoparticles synthesized through a novel chemical route. Mater. Lett. 58, 2692–2694. https://doi.org/10.1016/j.matlet.2004.03.045

Thierry D, Cave MD, Eisenach KD, Crawford JT, Bates JH, Gicquel B, Guesdon JL, 1990. IS6110, an IS-like element of Mycobacterium tuberculosis complex. Nucleic Acids Res. 18(1):188. DOI: 10.1093/nar/18.1.188

Tiwari, D., Tiwari, R.P., Chandra, R., Bisen, P.S., Haque, S., 2014. Efficient ELISA for diagnosis of active tuberculosis employing a cocktail of secretory proteins of *Mycobacterium tuberculosis.* Folia Biol. (Czech Republic) 60, 10–20.

Tsai, T.-T., Shen, S.-W., Cheng, C.-M., Chen, C.-F., 2013. Paper-based tuberculosis diagnostic devices with colorimetric gold nanoparticles. Sci. Technol. Adv. Mater. 14, 044404. https://doi.org/10.1088/1468-6996/14/4/044404

Ugarte-Gil, C., Ponce Alvarez, M., Moore, D. a J., 2008. Pruebas de sensibilidad para *Mycobacterium tuberculosis.* Acta Médica Peru. 25, 171–175. https://doi.org/10.17843/rpmesp.2016.332.2169

Unsoy, G., Gunduz, U., Oprea, O., Ficai, D., Sonmez, M., Radulescu, M., Alexie, M., Ficai, A., 2015. Magnetite: From Synthesis to Applications. Curr. Top. Med. Chem. 15, 1622–1640. https://doi.org/10.2174/1568026615666150414153928

Vereda, F., De Vicente, J., Hidalgo-Álvarez, R., 2007. Influence of a magnetic field on the formation of magnetite particles via two precipitation methods. Langmuir 23, 3581–3589. https://doi.org/10.1021/la0633583

Volkman, H.E., Clay, H., Beery, D., Chang, J.C.W., Sherman, D.R., Ramakrishnan, L., 2004. Tuberculous granuloma formation is enhanced by a Mycobacterium virulence determinant. PLoS Biol. 2. https://doi.org/10.1371/journal.pbio.0020367

Wang, J., Wu, H.-Y., Yang, C.-Q., Lin, Y.-L., 2008. Room temperature Mössbauer characterization of ferrites with spinel structure. Mater. Charact. 59, 1716–1720. https://doi.org/10.1016/j.matchar.2008.03.013

Wang, Z., Potter, B.M., Gray, A.M., Sacksteder, K.A., Geisbrecht, B. V, Laity, J.H., 2007. The Solution Structure of Antigen MPT64 from *Mycobacterium tuberculosis* Defines a New Family of Beta-Grasp Proteins. J. Mol. Biol. 366, 375–381. https://doi.org/10.1016/j.jmb.2006.11.039

Warren, C., 2013. Synthesis , Characterization , and Functionalization of Magnetic Iron

Nanoparticles for Enhanced Biological Applications. Virginia Commonwealth University.

Wen, X., Yang, J., He, B., Gu, Z., 2008. Preparation of monodisperse magnetite nanoparticles under mild conditions 8, 535–541. https://doi.org/10.1016/j.cap.2007.09.003

WHO, 2018. Global Tuberculosis Report 2018. Geneva.

WHO, 2016. Global Tuberculosis Report 2016, Cdc 2016. https://doi.org/ISBN 978 92 4 156539 4

Wu, X., Yang, Y., Zhang, J., Li, B., Liang, Y., Zhang, C., Dong, M., 2010. Comparison of antibody responses to seventeen antigens from *Mycobacterium tuberculosis.* Clin. Chim. Acta 411, 1520–1528. https://doi.org/10.1016/j.cca.2010.06.014

Yallapu, M., Othman, S., Curtis, E.T., Bauer, N.A., Chauhan, N., Kumar, D., Jaggi, M., Chauhan, S., 2012. Curcumin-loaded magnetic nanoparticles for breast cancer therapeutics and imaging applications. Int. J. Nanomedicine. 7, 1761–1779.

Yamaguchi, R., Matsuo, K., Yamazaki, A., Abe, C., Nagal, S., Terasaka, K., Yamada, T., 1989. Cloning and Characterization of the Gene for Immunogenic Protein MPB64 of Mycobacterium bovis BCG. Infect. an Inmmunity 57, 283–288.

Zarif, R., Sankian, M., Gholubi, A., Farshadzadeh, Z., Soleimanpour, S., Youssefi, F., Karamoddini, M.K., Ghazvini, K., Varasteh, A.R., 2013. Cloning and expression of *Mycobacterium tuberculosis* major secreted protein antigen 85B (Ag85B) in Escherichia coli. Jundishapur J. Microbiol. 6, 112–116. https://doi.org/10.5812/jjm.4701

Zhang, C., Song, X., Zhao, Y., Zhang, H., Zhao, S., Mao, F., Bai, B., Wu, S., Shi, C., 2015. *Mycobacterium tuberculosis* Secreted Proteins As Potential Biomarkers for the Diagnosis of Active Tuberculosis and Latent Tuberculosis Infection. J. Clin. Lab. Anal. 29, 375–382. https://doi.org/10.1002/jcla.21782

Zhang, H., Fu, X., Jiao, W., Zhang, X., Liu, C., Chang, Z., 2005. The association of small heat shock protein Hsp16.3 with the plasma membrane of *Mycobacterium tuberculosis*: Dissociation of oligomers is a prerequisite. Biochem. Biophys. Res. Commun. 330, 1055–1061. https://doi.org/10.1016/j.bbrc.2005.03.092

Zhang, X., Su, Z., Zhang, X., Hu, C., Yu, J., Gao, Q., Wang, H., 2013. Generation of *Mycobacterium tuberculosis*-specific recombinant antigens and evaluation of the clinical value of antibody detection for serological diagnosis of pulmonary tuberculosis. Int. J. Mol. Med. 31, 751–757. https://doi.org/10.3892/ijmm.2013.1254

Zhang, Y., Kuang, M., Zhang, L., Yang, P., Lu, H., 2013. An accessible protocol for solid-phase extraction of N-linked glycopeptides through reductive amination by amine-functionalized magnetic nanoparticles. Anal. Chem. 85, 5535–5541. https://doi.org/10.1021/ac400733y